ACTIVE RESERVOIR MANAGEMENT ENGINEERING AND EVALUATION SUMMARY – BRINE EXTRACTION AND STORAGE TEST PHASE II FINAL REPORT – VOLUME 1

Brine Extraction and Storage Test Phase II Final Report
Task 6.0 Deliverable 5 (D5)

Prepared for:

AAD Document Control

National Energy Technology Laboratory
U.S. Department of Energy
626 Cochrans Mill Road
PO Box 10940, MS 921-107
Pittsburgh, PA 15236-0940

Project Period: Phase I (BP1): September 1, 2015 – July 6, 2016
Phase II (BP2–BP4): July 7, 2016 – May 31, 2024
Cooperative Agreement No. DE-FE0026160
DUNS No. 102280781

Prepared by:

Agustinus Zandy
Cody B. Williamson
Todd Jiang
Timothy M. Shenk
Xue Yu
Ryan J. Klapperich
Lonny L. Jacobson
Lawrence J. Pekot
Nicholas S. Kalenze
Marc D. Kurz
John A. Hamling

Energy & Environmental Research Center
University of North Dakota
15 North 23rd Street, Stop 9018
Grand Forks, ND 58202-9018
Phone (701) 777-5278; Fax (701) 777-5181
mkurz@undeerc.org

Marc D. Kurz, Principal Investigator

2024-EERC-04-02 April 5, 2024

EERC DISCLAIMER

LEGAL NOTICE This research report was prepared by the Energy & Environmental Research Center of the University of North Dakota (UND EERC) as an account of work sponsored by the U.S. Department of Energy (DOE) National Energy Technology Laboratory. (SPONSOR). Because of the research nature of the work performed, neither UND EERC nor any of its employees makes any warranty, express or implied, or assumes any legal liability or responsibility for the accuracy, completeness, or usefulness of any information, apparatus, product, or process disclosed, or represents that its use would not infringe privately owned rights. Reference herein to any specific commercial product, process, or service by trade name, trademark, manufacturer, or otherwise does not necessarily constitute or imply its endorsement or recommendation by UND EERC. SPONSOR understands and accepts that this research report and any associated deliverables are intended for a specific project. Any modifications of the report or of any associated deliverables or use or reuse other than for the intended project is at the sole risk of the SPONSOR and without liability or legal exposure to UND EERC or to its directors, officers, or employees.

DOE DISCLAIMER

This report was prepared as an account of work sponsored by an agency of the United States Government. Neither the United States Government, nor any agency thereof, nor any of their employees, makes any warranty, express or implied, or assumes any legal liability or responsibility for the accuracy, completeness, or usefulness of any information, apparatus, product, or process disclosed, or represents that its use would not infringe privately owned rights. Reference herein to any specific commercial product, process, or service by trade name, trademark, manufacturer, or otherwise does not necessarily constitute or imply its endorsement, recommendation, or favoring by the United States Government or any agency thereof. The views and opinions of authors expressed herein do not necessarily state or reflect those of the United States Government or any agency thereof.

TABLE OF CONTENTS

LIST OF FIGURES iii

LIST OF TABLES vi

EXECUTIVE SUMMARY viiii

INTRODUCTION 1

FIELD ACTIVITIES 3
- Well Drilling and Completion 3
- Injection Well 3
- Extraction Well 7
- Rink Wells 7
- Additional Information 11

BOREHOLE-TO-SURFACE ELECTROMAGNETIC SURVEY 11
- BSEM Baseline Operation 11
- BSEM Data Analysis 12
- BSEM Repeat Operation 14

ARM OPERATION 15
- Stage 1 16
- Tracer Injection and Analysis 19
- Stage 2 22

DATA COLLECTION AND PROCESSING 23
- Analytical Approach 26
- Model Development 27
- ML Analysis 28
- Pressure Response When Well Is Closed 28
- Pressure Response at the Injection Well 29
- Data-Processing Discussion 33
- Data-Processing Conclusions 34

EVALUATION OF ARM ACTIVITIES 35
- Geologic Model 35
- History Matching 36
- CO_2 ARM Simulation 44
- CO_2 ARM Simulation Results 45
  - Geosteering 48
  - Linear Geosteering 49
  - Water Injection Over CO_2 50

Continued . . .

TABLE OF CONTENTS (continued)

Discussion 51
Scaled-Up Model 52
Expanded CO_2 ARM Simulations 54
Scenario Matrix 1-mile Separation 56
Scenario Matrix 3-mile Separation 59
Linear and Staggered Well Placement 62
Constrained Injection Rate 63

CONCLUSIONS 66

SYNERGISTIC ACTIVITY 67
Assessment of Carbonated Brine Injection Feasibility 67

REFERENCES 68

ADDITIONAL FIELD ACTIVITIES ..... Appendix A

WELL DRILLING AND COMPLETION ..... Appendix B

ESP PUMP SPECIFICATIONS ..... Appendix C

ASSESSMENT OF CARBONATED BRINE INJECTION AS LOW-RISK STRATEGY FOR GEOLOGIC CARBON STORAGE ..... Appendix D

LIST OF FIGURES

1 Integrated and iterative approach to project management 3

2 Location and layout of BEST project site, illustrating the location of the existing SWD wells and the new project wells and other supporting infrastructure 4

3 BEST-I1 wellbore schematic postcompletion 5

4 Field photographs of the 4-in. core collected in BEST-I1 well: a) sandstone from the Inyan Kara Formation, b) shale from the Opeche Formation, c) sandstone from the Broom Creek Formation, and d) shale with interbedded siltstone from the Amsden Formation 6

5 BEST-E1 well schematic post-ESP removal 8

6 Rink SWD #1 wellbore schematic with suspended pressure/temperature gauge 9

7 Rink SWD #2 wellbore schematic with suspended pressure/temperature gauge 10

8 Map of the BSEM survey area 12

9 Lateral slice of the inverted resistivity model at a depth of 5347 ft 13

10 Additional feasibility modeling showing the percent difference of BSEM data compared to baseline measurements because of changes in reservoir parameters caused by changes in injected fluid properties and survey options 15

11 BHP profile 19

12 Rink SWD #1 tracer results 21

13 Rink SWD #2 tracer results 22

14 Locations of the two injection wells and the brine extraction well, showing the distance in feet between each well 24

15 Raw data and moving average smoothed clean data of the dependent variables and independent variables 25

16 Time series data for a portion of the data record showing injection well Rink SWD #1 BHP and flow during brine production from extraction well BEST-E1 27

Continued . . .

LIST OF FIGURES (continued)

17 General pattern of BHP response at the injection and production wells when the corresponding wells were closed 29

18 XGBoost modeling performance for predicting Rink SWD #1 BHP and variable importance 30

19 Partial dependence analysis of the flow rates at the three wells in predicting Rink SWD #1 BHP 31

20 Time series of the partial dependence effects of injection at Rink SWD #1 well and production/injection ratio at BEST-E1 well on the BHPs in Rink SWD #1 32

21 Effects of BEST-E1 production on the BHPs in the injection well at different stationary injection rates of 1000, 3000, and 5000 bbl/day 33

22 3D view of the simulation model and 2D aerial view of the top horizontal layer of the Inyan Kara Formation 36

23 BEST-E1 sensitivity analysis results 39

24 Rink SWD #1 sensitivity analysis results 40

25 Rink SWD #2 sensitivity analysis results 41

26 BEST-E1 BHP responses 42

27 Rink SWD #1 BHP responses 42

28 Rink SWD #2 BHP responses 43

29 Relative permeability curve for the common occurrence of sandstone in the Inyan Kara Formation 44

30 Average reservoir pressure trend of the entire simulation model during 25 years of CO_2 injection 45

31 Average reservoir pressure response to 1:1 injection-to-production ratio at the five different distances 46

32 CO_2 mass injection rate over 25 years of injection for cases with a 10,000-bpd extraction rate from the injection well 47

33 CO_2 plume migration viewed as gas per unit are total in all vertical layers 48

Continued . . .

LIST OF FIGURES (continued)

34 CO_2 plume migration viewed as gas per unit are total in all vertical layers 49

35 2D cross-sectional view of well placement pattern for the water-over-CO_2 injection simulation tests 50

36 CO_2 plume migration viewed as gas per unit are total in all vertical layers 51

37 Trapped CO_2 over time 51

38 2D 6-mile × 6-mile model and 2D 30-mile × 30-mile model arial view comparison of the two simulations 53

39 Square well placement pattern, 3-mile separation of four production wells located in the center of the injection well simulation with a centrally located water production well..... 57

40 Cumulative CO_2 injection totals using 1-mile well spacing and varied production 57

41 Water production rates using 1-mile spacing 58

42 CO_2 plume after 20 years with no production and CO_2 plume after 20 years using 80,000-bbl/day production rate..... 59

43 Cumulative CO_2 injection totals using 3-mile well spacing and varied production rates... 59

44 Water production rates in the 3-mile well separation simulations 60

45 CO_2 plume after 20 years with no production and CO_2 plume after 20 years using an 80,000-bbl/day production rate 61

46 Cumulative CO_2 injection totals using three well placement patterns at 1-mile separation 62

47 Cumulative CO_2 injection totals using three well placement patterns at 3-mile separation 62

48 CO_2 plume after 20 years in a linear well placement pattern, CO_2 plume after 20 years in a staggered well placement pattern, and CO_2 plume after 20 years in a square well placement pattern 63

49 Average reservoir pressure within 1 mile of the injection wells..... 64

Continued . . .

LIST OF FIGURES (continued)

50 Extraction/injection ratio of different production rates and a constant combined 4-MMt/yr injection rate 64

51 Reservoir volumetrics of CO_2 injection rates versus volumetric brine production rate representing a 1:1 extraction/production ratio 65

52 Average reservoir pressure increases with varied production rates 65

53 Graphical representation of CBI compared to traditional free-phase CO_2 injection and standard produced water disposal 68

LIST OF TABLES

1 BEST-I1 and BEST-E1 Surface Locations and Well Information 4

2 Core Collection from BEST-I1 Well 6

3 Reservoir Characteristics at the Rink SWD #1, Rink SWD #2, and BEST-E1 Wells 16

4 Planned Rate vs. Actual Rate During Stage 1 18

5 BEST Tracer Survey Injection Details 19

6 BEST Tracer Survey Water Sample Analysis Summary Showing Concentrations of Measured Tracer in parts per trillion 20

7 Planned Rates vs. Actual Rates for Stage 2 23

8 Data Categorization Based on Well 24

9 Descriptive Statistics of BHP and Flow at the Two Injection Wells and One Production Well 26

10 Hyperparameters for the XGBoost Algorithm 27

11 Sensitivity Analysis Parameters 37

12 Sensitivity Analysis Parameters with Optimal History Match Solution 43

13 Summary of Reservoir Properties in the Simulation Model 44

14 Simulation Cases with Cumulative Injected CO_2 Results and Percentage Increase of Total CO_2 Compared to the Simulation Without Any Extraction 47

15 Summary of Changes in Geologic Properties 53

16 Summary of Reservoir Properties in the Expanded Simulation Model 54

17 Summary Simulation Cases 55

18 Additional Summary Simulation Cases 56

19 Injection Results Using 1-mile Well Spacing and Varied Brine Extraction Rates 58

20 Injection Results Using 3-mile Well Spacing and Varied Brine Extraction Rates 60

21 Injection Results Using Different Well Placement Strategies and Well Separation Distances 63

ACTIVE RESERVOIR MANAGEMENT ENGINEERING AND EVALUATION SUMMARY – BRINE EXTRACTION AND STORAGE TEST PHASE II FINAL REPORT – VOLUME 1

EXECUTIVE SUMMARY

The Energy & Environmental Research Center (EERC) conducted a multiyear program over two phases to perform a field study of the potential efficacy of formation water extraction during carbon dioxide (CO_2) injection for CO_2 storage as a means of improving efficiency and/or effectiveness. Phase I was a 2-year study on potential methodologies for a field study of pressure management, culminating in site selection and experimental and site design. Phase II was a 7-year effort that involved constructing site facilities, conducting experiments, and evaluating collected field data. The experimental portion was split into two collaborative components, one for the active reservoir management (ARM) experiment and a second component to host and demonstrate potential water treatment technologies appropriate for high-saline brine at the project site. The results of the overall project are expected to benefit future saline storage projects through validation of techniques that may reduce stress on sealing formations, increase storage capacity, and reduce area of review. The following report focuses on the Phase II ARM experimental implementation and results. A second companion report summarizes the results of the high-saline brine demonstrations.

The EERC's Brine Extraction and Storage Test (BEST) was sited on a location with active oilfield saltwater brine disposal occurring in two existing wells injecting into a regionally expansive brine formation (the Inyan Kara Formation). These two injection wells provided the pressure pulse that acted as a proxy for CO_2 injected for storage and enabled the field-testing of various pressure management and plume control strategies without the added complications of injecting a separate CO_2 plume. A new formation water extraction well was installed downgradient of the two brine water disposal wells as the experimental pressure reduction well, and a second new well was installed into a deeper saline formation to allow disposal of the extracted formation water without the added interference of reinjecting extracted water into the Inyan Kara Formation. The experiment's host site is operated by project partner Landtech Enterprises, LLC, a subsidiary of Select Water (formerly Nuverra Environmental Solutions). Drilling of the new wells and installation of the supporting infrastructure (oil water separator, tanks, flowlines, pumps, downhole pressure sensors, and sensors for safety and control, etc.) and subsequent equipment testing and debugging were conducted over the course of approximately 3 years.

A vast quantity of data were collected over the course of the roughly 2-year injection–extraction experiment. The interactions between the two injection wells and the extraction well resulted in a complex, nonstationary dataset that is a reflection of the dynamic pressure behaviors likely to be encountered by other similar tests and CO_2 storage projects. Machine learning methods of data processing proved to be the most effective. Water extraction activities were shown to have the ability to alleviate pressure buildup in proximity to the extraction well, as verified by pressure gauges installed in offset injection wells. Up to a 50-psi pressure reduction was observed for the highest extraction rate tested. However, the relatively small size of the project site (approximately 1400-ft offset between wells) required modeling to extrapolate the results for applicability to CO_2 storage operations.

The first round of modeling focused on larger volumes and timescales by simulating injection of up to 1 million tonnes (MMt) of CO_2/yr over 25 years into a history-matched model

of the BEST site. Multiple volumetric extraction ratios (volume extracted to volume injected) were tested: 1:1 or equivalent volumes extracted and injected, 3:4, 1:2, and 1:4 over a range of extraction/injection well offset distances out to 2.5 miles. The extraction wells were shut in when CO_2 breakthrough occurred. Under these conditions, water extraction was shown to have a modest impact on reducing reservoir pressure buildup from injection and demonstrated how short-term and long-term effectiveness of extraction can be influenced by well placement. Closer extraction wells resulted in improved CO_2 injection rates, but over a short operating period, whereas more distant wells showed a more prolonged improvement for CO_2 injection, but ultimately a limited total impact.

Evaluations of the potential for injected plume geosteering (using pressure to influence plume growth or dispersal) demonstrated the influence of reservoir heterogeneity on such designs. Existing zones of higher reservoir permeability need to be aligned with the desired geosteering objective to be effective. An alternate method of geosteering, termed "water over injection," focused on maximizing CO_2 trapping in the reservoir as an effective application of geosteering. In this method, water is withdrawn from the reservoir outside of the plume area and reinjected directly above the CO_2 injection point. The injected water enhances mixing and dissolution interactions of the reservoir fluids, leading to more rapidly dissolved CO_2 in the reservoir and a more diffuse plume of free-phase CO_2.

A second round of modeling was conducted using an expanded model to better represent commercial-scale CO_2 injection operations, reservoir volumes and distances, and a variety of potential operating scenarios. The simulations provided a more comprehensive study of the interwell-spacing analysis, encompassing simulations performed at 1-mile, 2-mile, and 3-mile well distances and at a constant injection rate of 1 MMt of CO_2/yr. This approach enabled an in-depth investigation into the expanded maximum CO_2 storage potential and a more substantial analysis of the impact that brine production wells and well placement strategies have on optimizing the CO_2 storage resource. These revised simulations demonstrated that for water extraction to significantly enhance CO_2 storage resource or fully mitigate reservoir overpressurization, the rate of brine production must be sufficiently high to maintain an extraction-to-injection ratio near or above 1:1. Results indicate that optimizing extraction well placement alone could have a >5% impact on storage efficiency, or more if replacement extraction wells are installed after breakthrough. However, it is acknowledged that the volume of extracted water must be handled through reinjection or treatment and beneficial use. Smaller extraction-to-injection ratios can be effective at reducing the pressurization from CO_2 injection in certain conditions, such as in closed reservoir systems, already overpressurized regions, or to allow for incremental CO_2 storage at existing storages sites.

The inherent heterogeneity of subsurface reservoir models poses a significant challenge when attempting to recommend a generalized approach for well placement and extraction/injection ratios for CO_2 storage. As a result, the optimal placement and optimal design of extraction wells are highly dependent on the unique characteristics of a given reservoir, and nonconforming patterns are often necessary to account for the permeability heterogeneity and to effectively influence the CO_2 plume. Effective CO_2 storage plume and pressure management demands a highly nuanced understanding of reservoir heterogeneity as well as a sophisticated approach to well placement and production management. Achieving optimal outcomes in this context requires a willingness to embrace dynamic, site-specific strategies that account for the unique complexities of each subsurface reservoir.

ACTIVE RESERVOIR MANAGEMENT ENGINEERING AND EVALUATION SUMMARY – PHASE II BRINE EXTRACTION AND STORAGE TEST FINAL REPORT – VOLUME 1

INTRODUCTION

The Energy & Environmental Research Center (EERC) conducted the second phase (Phase II) of a project entitled "Developing and Validating Pressure Management and Plume Control Strategies in the Williston Basin Through a Brine Extraction and Storage Test (BEST)." During the previous Phase I activities, an engineering design plan was developed that specified the protocols and procedures to be used in installing site infrastructure and designing and conducting a field implementation plan (FIP). The main objective was to utilize ongoing brine injection activities at a saltwater disposal (SWD) facility, coupled with downgradient on-site extraction, as a proxy study for understanding effects of the application of engineering controls on carbon dioxide (CO_2) injection, sequestration, and storage. This enables the field testing of various pressure management and plume control strategies without the added complications of injecting a separate CO_2 plume. The ongoing saltwater injection provides the pressure and fluid plume to which management strategies can be applied.

Phase II was conducted over 5 years and focused on the development and implementation of the FIP and validation of engineering strategies for managing formation pressure as well as predicting and monitoring differential pressure plume movement in the subsurface and validating differential pressure plume predictions through monitoring and simulation. The results of the overall project were expected to benefit future saline storage projects through validation of techniques that reduce stress on sealing formations and consequently reduce risk of breaching sealing formations, reduce risk of brine and CO_2 intrusion into other formations, increase storage capacity, and reduce area of review (AOR). The field validation also provided a test bed platform for evaluation of brine treatment technologies that have the potential of treating high-total-dissolved-solids (TDS) extracted water for beneficial use as a means of managing and reducing extracted-brine disposal volumes.

Deep saline formations (DSFs) constitute the most prominent potential global resource for geologic storage of CO_2 (Intergovernmental Panel on Climate Change, 2005, 2014; International Energy Agency Greenhouse Gas R&D Programme, 2008). Active reservoir management (ARM), the process of pumping formation fluids from a geologic reservoir as a means of reducing reservoir pressure or otherwise altering the direction of flow of fluids withing the reservoir, has been postulated as a means to improve injectivity and manage CO_2 plume migration through pressure management via strategic formation water extraction (Davidson and others, 2014; Birkholzer and others, 2015; Cihan and others, 2015). Treatment of the extracted formation water can provide an alternate source of water and potential salable products for a variety of beneficial uses. These products may provide additional economic incentives or cost offsets for ARM (Klapperich and others, 2013). ARM strategies may also be used to mitigate concerns of overpressurization within a reservoir and interference from other CO_2 injection projects or other injection wells (Birkholzer and Zhou, 2009; Buscheck and others, 2011, 2014; Court and others, 2011; Zhou and Birkholzer, 2011; Klapperich and others, 2013).

The scope and scale of monitoring activities for carbon capture and storage (CCS) sites are dependent on the project's AOR. As defined by the U.S. Environmental Protection Agency (EPA), AOR is the maximum extent of the pressure plume (resulting from CO_2 injection activities) which contains enough head pressure to lift fluid from the storage reservoir to an underground source of drinking water (U.S. Environmental Protection Agency, 2013). AOR delineates the region in which all potential natural and artificial conduits to the surface must be located and evaluated by a CCS site operator. If necessary, the operator is obligated to undertake corrective actions to remediate identified vertical migration pathways. Any reductions in the footprint of the pressure plume through ARM will likely result in reducing the number of conduits characterized and designated for corrective action. This corresponds to reduced costs and the scope of required monitoring. In regions with a large number of wells, such as the Williston Basin, this can be a substantial cost reduction.

The EERC developed the components of a field project to successfully execute a BEST evaluation at an active SWD facility in western North Dakota, an active saltwater injection facility. This site had optimal geology, geography, and existing permits and infrastructure for conducting a BEST evaluation. This BEST Phase II topical report describes the steps which were taken to develop the BEST FIP, collect and process field implementation data, and evaluate ARM operations. These steps consisted of performing the following:

- Drilling two new wells
- Data collection for formation characteristics
- ARM schema through reservoir simulation
- Site infrastructure and monitoring
- ARM field implementation, monitoring, and data collection
- Data processing and ARM evaluation
- Site decommissioning

The EERC developed a FIP that integrated site characterization; modeling and simulation; risk assessment; and monitoring, verification, and accounting (MVA) strategies into an iterative process to produce meaningful results for commercial subsurface injection and/or production operations (Figure 1) (Ayash and others, 2017). Elements of any of these activities are crucial for understanding or developing the other activities. For example, new knowledge gained from site characterization reduces a given amount of uncertainty in geologic reservoir properties. This reduced uncertainty can then propagate through modeling, risk assessment, and MVA efforts. This approach has been applied in Phase I of the BEST project to develop a tailored technical design that enabled the achievement of the project's objectives while minimizing risk. This approach was also implemented in the BEST Phase II efforts.

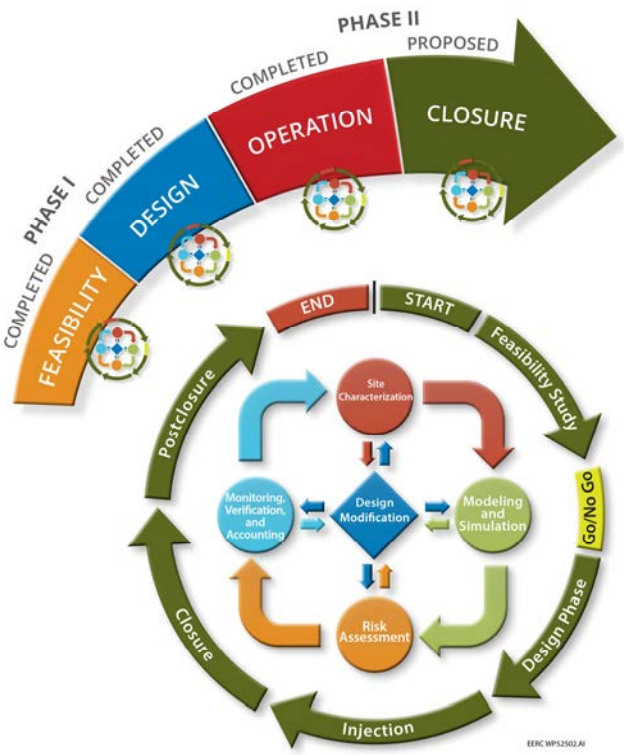


Figure 1. Integrated and iterative approach to project management. Each of these elements feeds into another, iteratively improving results and efficiency of evaluation during each project phase.

FIELD ACTIVITIES

Well Drilling and Completion

The BEST-I1 permit to drill was submitted to the North Dakota Industrial Commission (NDIC) on January 27, 2017, and approved on July 28, 2017, as a vertical disposal well, while the BEST-E1 permit to drill was submitted on January 27, 2017, and approved on August 2, 2017, as a water source well. The BEST-I1 and BEST-E1 wells are located in McKenzie County, North Dakota, near Johnson's Corner (Figure 2). Site survey data and well information for BEST-I1 and BEST-E1 are compiled in Table 1.

Injection Well (BEST-I1)

The injection well, BEST-I1, was drilled and completed in 2018. The well was constructed with a surface casing set at 1868 ft and a long-string casing at 7955 ft. The well was configured as a Class I non-hazardous waste disposal well by installing 13Cr-80 casing (7235–7955 ft) to cover the target injection zones, the Broom Creek and Amsden Formations, which are part of the Minnelusa Group stratigraphic unit. The Broom Creek and Amsden Formations were perforated as the target injection zone from 7478 to 7703 ft. Figure 3 shows the as-completed wellbore schematic of BEST-I1.

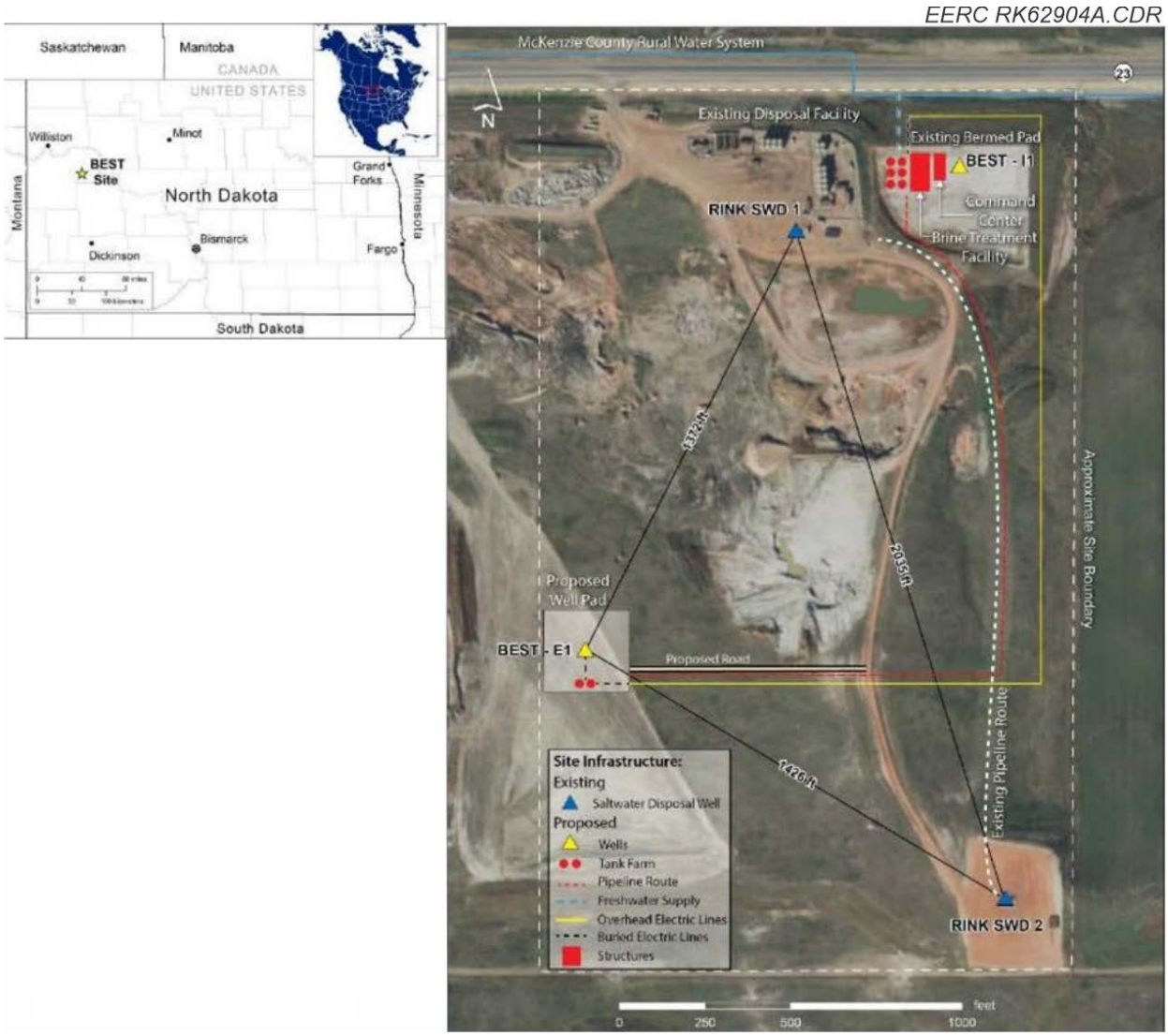


Figure 2. Location and layout of BEST project site, illustrating the location of the existing SWD wells (blue) and the new project wells (yellow) and other supporting infrastructure.

Table 1. BEST-I1 and BEST-E1 Surface Locations and Well Information

Well Name:	BEST-I1	BEST-E1
NDIC Well File No.	90383	90384
Latitude	N47° 48' 11.66"	N47° 47' 58.37"
Longitude	W102° 58' 28.81"	W102° 58' 44.39"
Location	NENW Sec 21, T150N, R96W	SENW Sec 21, T150N, R96W
County	McKenzie	McKenzie
Field	Pershing	Pershing
Spud Date	22-Apr-18	16-May-18
Formation	Broom Creek	Inyan Kara
Total Depth	7960 ft	5688 ft

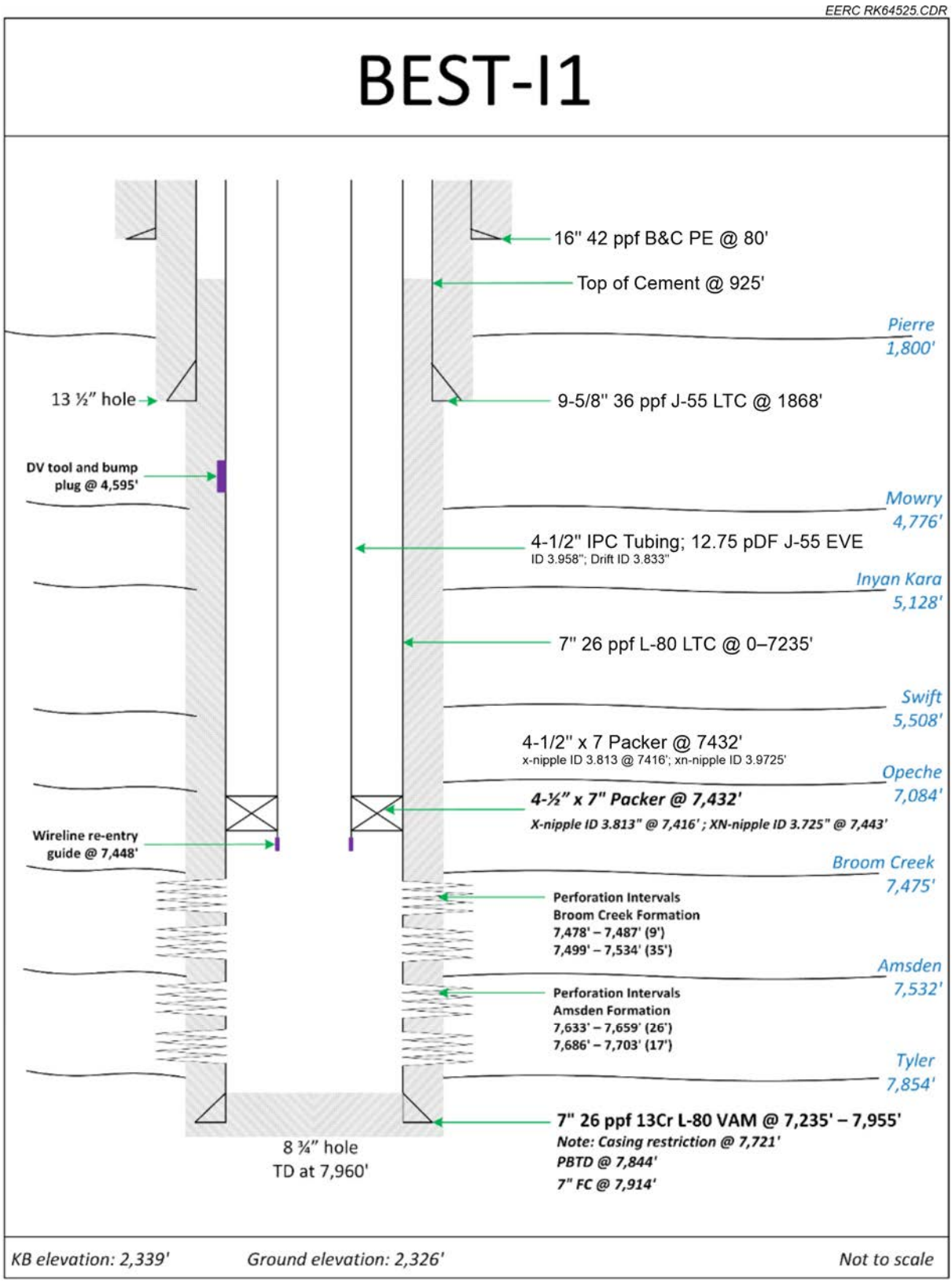


Figure 3. BEST-I1 wellbore schematic postcompletion.

A set of formation characterization activities were performed on the BEST-I1 well, including core, geophysical logs, downhole testing, and fluid sampling in the Inyan Kara and Broom Creek and associated confining layers. 4-in. whole core samples were collected from the Inyan Kara and Broom Creek Formations, with the cored interval summarized in Table 2.

Figure 4 shows photographs of the 4-in. core of the target and sealing formations. The Inyan Kara serves as the ARM target formation, the Opeche is a low-permeability confining layer directly over the Broom Creek, while the Broom Creek and Amsden are the deeper disposal formations.

Table 2. Core Collection from BEST-I1 Well

Formation	Cored Interval, ft	Recovered Core Length, ft
Inyan Kara–Opeche	5271–5371	100.6
Broom Creek–Amsden	7435–7535	90.1

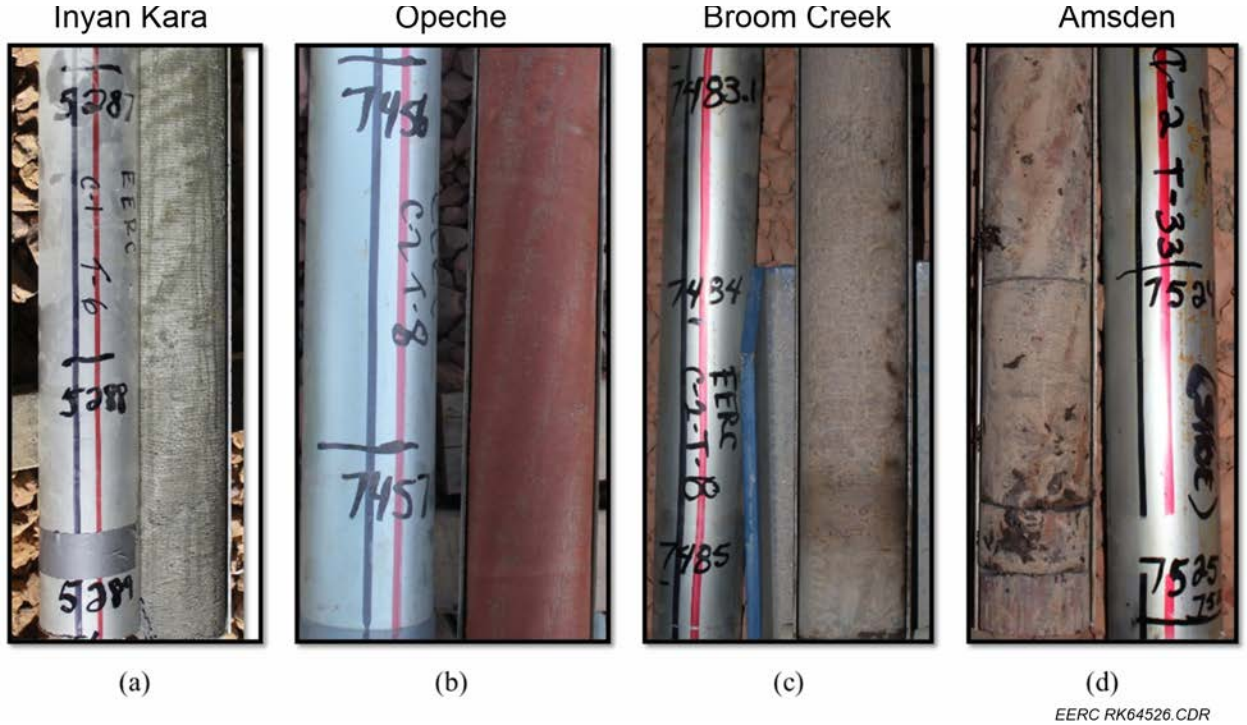


Figure 4. Field photographs of the 4-in. core collected in BEST-I1 well: a) sandstone from the Inyan Kara Formation, b) shale from the Opeche Formation, c) sandstone from the Broom Creek Formation, and d) shale with interbedded siltstone from the Amsden Formation.

Extraction Well (BEST-E1)

The extraction well, BEST-E1, was drilled and completed in 2018. The well was constructed with a surface casing set at 1855 ft and a long-string casing at 5683 ft. A casing-conveyed PROMORE gauge was installed at 5243 ft to monitor bottomhole pressure (BHP) during ARM operation. The Inyan Kara Formation was perforated at 5290–5506 ft as the target extraction zone.

A step rate test was performed to determine the fracture pressure of the Inyan Kara Formation. The test successfully determined the fracture pressure at a rate of 3 barrels per minute (bpm), with the calculated fracture gradient of 0.72 psi/ft. Acid stimulation using 178.5 bbl of hydrochloric acid was performed to improve reservoir near-wellbore permeability, allowing consistent inflow from the reservoir. The injected acid had a noticeable pressure response. A 4½-in. internal plastic-coated tubing and an electrical submersible pump (ESP) were installed as the extraction string. The ESP consisted of two 538 S4000N pumps with 56 and 66 stages, respectively; a 562 Maximus F120 motor (450 hp) was landed at 5228 ft, with the intake at 5180 ft. The initial flow test suggested the well was capable of 50,000 barrels per day (bpd), estimated to meet the FIP maximum extraction rate of 5000 bpd.

Upon completion of initial field testing, it was determined that the ESP could not produce the required volumes as the native pressure enabled the well to naturally flow well in excess of 5000 bpd. The elevated downhole pressure that enabled these artesian conditions also hindered the ESP's ability to function as designed. The end result was that the ESP created a choke point in the wellbore and actually restricted flow from BEST-E1. A reservoir simulation was performed and verified that the reservoir was capable of producing 5000 bpd continuously for more than 12 months. Based on these results and the possibility that the ESP could get stuck, the EERC decided to remove the ESP on February 14, 2020. The well was completed with 4½-in. tubing and packer string, as shown in Figure 5. The well was thereafter able to produce at the volumes required by the project via flow resulting from the elevated local pressure induced by injection from the Rink wells.

Rink Wells

The existing wells, Rink SWD #1 and Rink SWD #2, were part of the ARM project and served as injection wells. These wells are operated by Landtech Enterprises, LLC, the project partner and an operating subsidiary of Select Water (formerly Nuverra Environmental Solutions). A PROMORE suspended pressure and temperature gauge was installed below the end of the tubing to monitor BHP and temperature in each well. The gauge was connected to the supervisory control and data acquisition (SCADA) system to enable real-time monitoring and record data for evaluation. Figures 6 and 7 illustrate the Rink SWD #1 and Rink SWD #2 wellbore schematics, respectively.

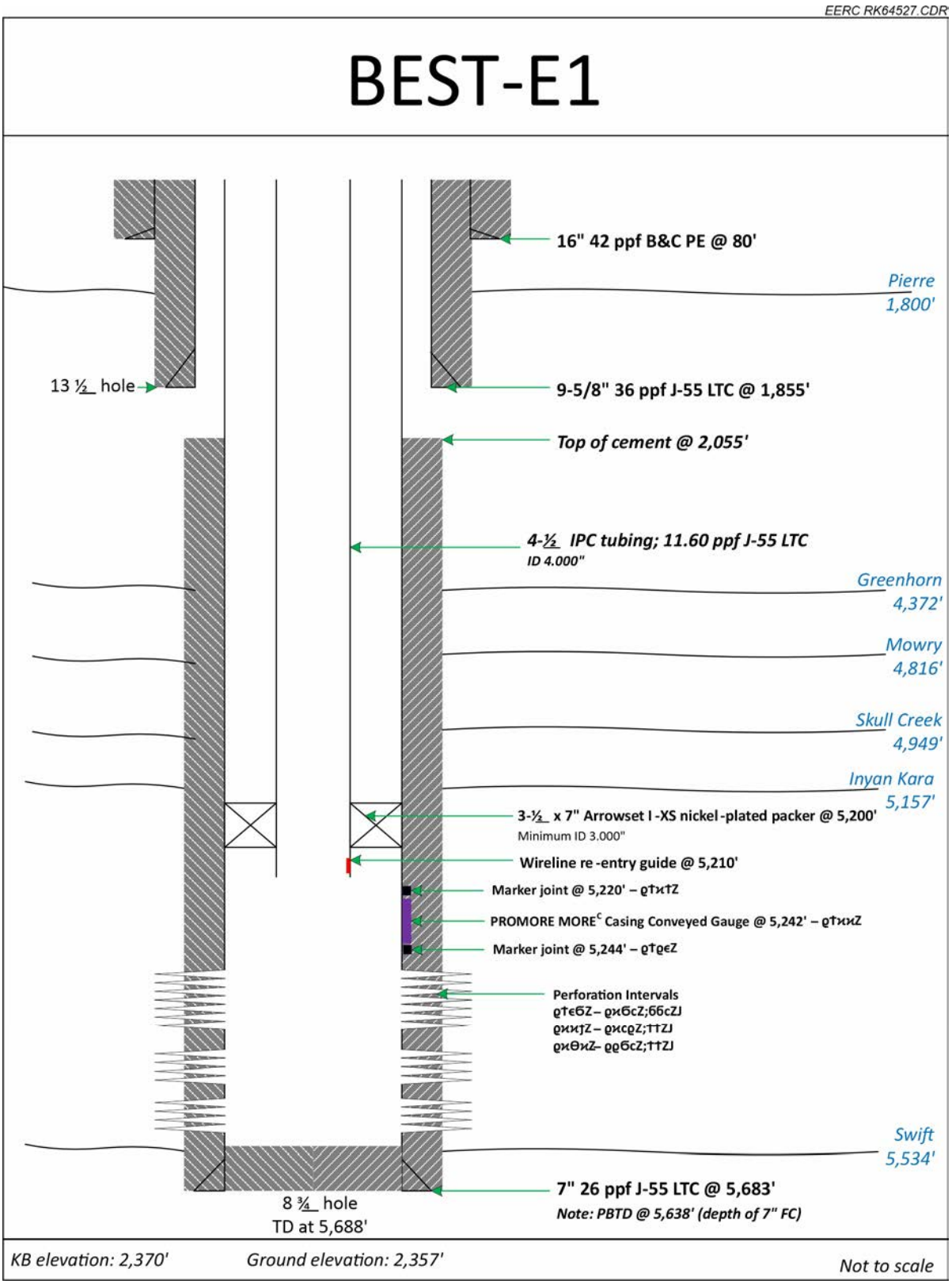


Figure 5. BEST-E1 well schematic post-ESP removal.

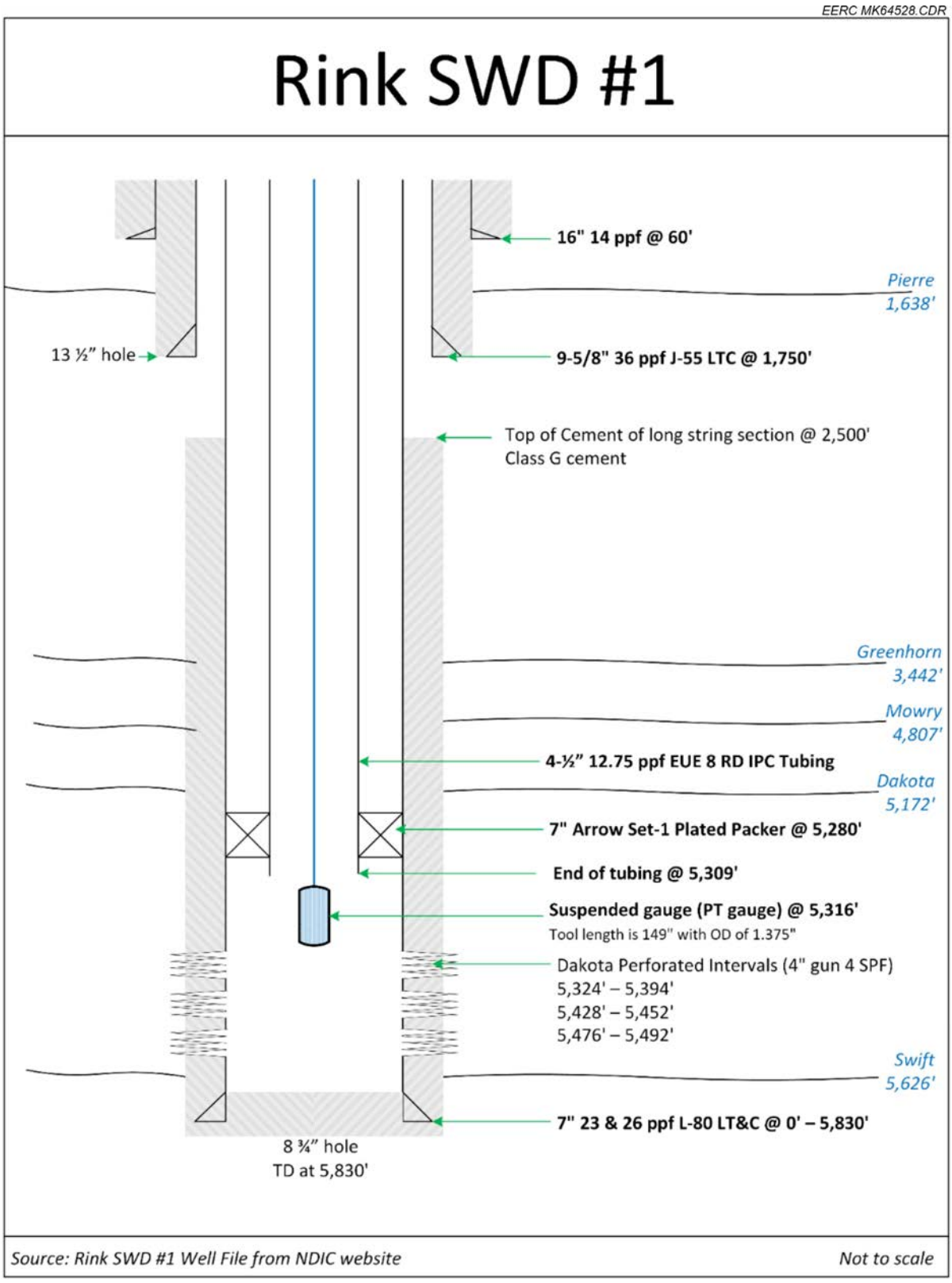


Figure 6. Rink SWD #1 wellbore schematic with suspended pressure/temperature gauge.

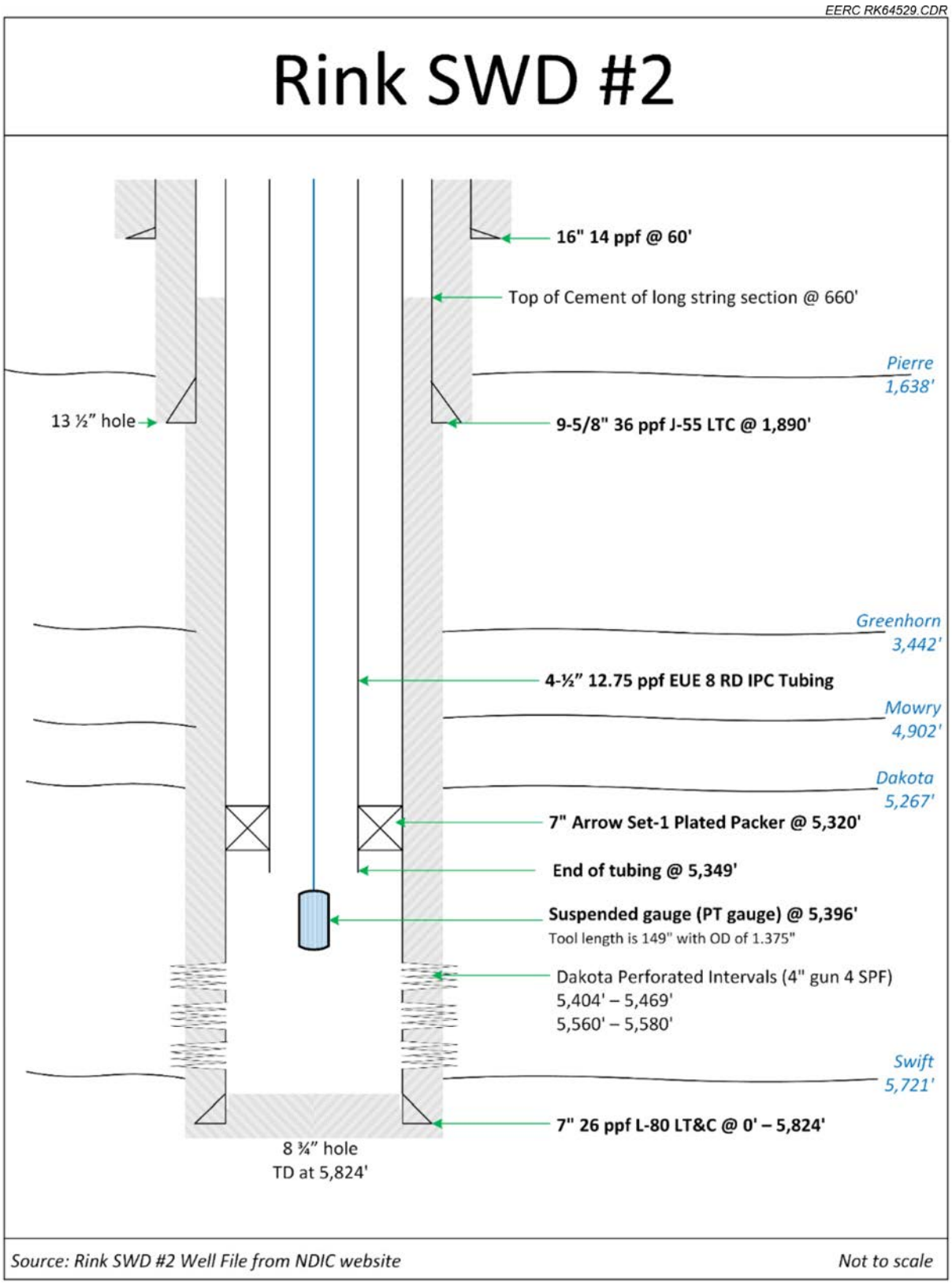


Figure 7. Rink SWD #2 wellbore schematic with suspended pressure/temperature gauge.

Additional Information

Additional details and information regarding the field installations, well drilling and completion activities, and ESP can be found in Appendixes A, B, and C.

BOREHOLE-TO-SURFACE ELECTROMAGNETIC SURVEY

A borehole-to-surface electromagnetic (BSEM) survey was acquired at the site in 2018, prior to the start of the extraction experiment, to serve as a baseline survey for time-lapse monitoring of changes in the Inyan Kara Formation due to extraction operations. The goal was to obtain data that would support validation of the input geologic model used as the basis for the predictive simulations. The shape of the injected high-salinity brine plume and salinity distribution are measurable representations of the actual reservoir geologic character that can be used to improve the statistically derived geologic model. By injecting electric current into the reservoir formation and monitoring its return at the surface, the resistivity profile in the reservoir can be mapped in three dimensions and can be used to derive an image of the brine plume. A repeat ("monitor") BSEM survey was planned for the end of the active extraction operations to determine the shape and distribution of the site's injected brine plumes after extraction operations ceased. These data would provide validation for simulation predictions and an assessment of the validity of BSEM for tracking injected fluid plumes under ARM conditions.

BSEM Baseline Operation

In a BSEM survey, an electrical connection is made to a metal well casing, either at the top of the casing or at some depth within the casing. An electrical current is generated, and this current flows along the length of the casing and out into the subsurface rock formations and back up to the surface, eventually completing a circuit at a distantly placed electrode. The path that the current takes as it flows through the subsurface depends on the resistivity of the material it encounters – solid rock and hydrocarbons, as well as CO_2, are more resistive and impede current flow, while brine or saline fluids are less resistive (or equivalently, more conductive, where conductivity is the reciprocal of resistivity) and allow current to flow more easily. As the current moves, it creates electric fields, which will propagate through the subsurface and can be measured at the surface using sensitive electrode receivers. By placing an array of these receivers across the survey area and using multiple locations of source wells and return electrodes, as well as multiple depths within the wells, a model of the resistivity distribution within the subsurface can be obtained. At the BEST site, the low-resistivity areas of this 3D model at the depth of the Inyan Kara Formation should correlate with the presence of the injected brine.

The baseline BSEM survey was carried out by GroundMetrics, Inc., at the project site over the course of 4 days, September 8–11, 2018. Acquisition of the BSEM data consisted of laying out a network of surface receivers and return electrodes across the site, electrically connecting to BEST-I1 and Rink SWD #2, and generating electrical currents at multiple frequencies. The electrical source was connected to the two wells both at the surface and at multiple depths within the well using a downhole tool. Receiver systems were deployed in arrays throughout the site area during each day, and the source current was turned on to collect measurements overnight. In total, 58 receiver locations collected data over 3 nights.

The data were collected and processed to remove noise and poor-quality measurements. The output of the processing step was a series of electric field values for each receiver and well source pair at a given frequency. These data were then inverted to generate a 3D resistivity volume using prior information about the salinity and porosity generated as part of the geologic model and served as a baseline of preinjection conditions.

BSEM Data Analysis

The inversion focused on imaging the resistivity of the Inyan Kara within the lateral extent, shown in Figure 8 by the white circles, which surrounds the wells of interest. A horizontal slice of the 3D resistivity model in this region at a depth of 5347 ft is shown in Figure 9 and is representative of the inversion results within the Inyan Kara. The model shows a general west-to-east increase in resistivity within the layer, with very low values of resistivity around Rink SWD #1 and BEST-E1. There is also a low-resistivity blob near Rink SWD #2. These low-resistivity areas may represent the presence of injected brine.

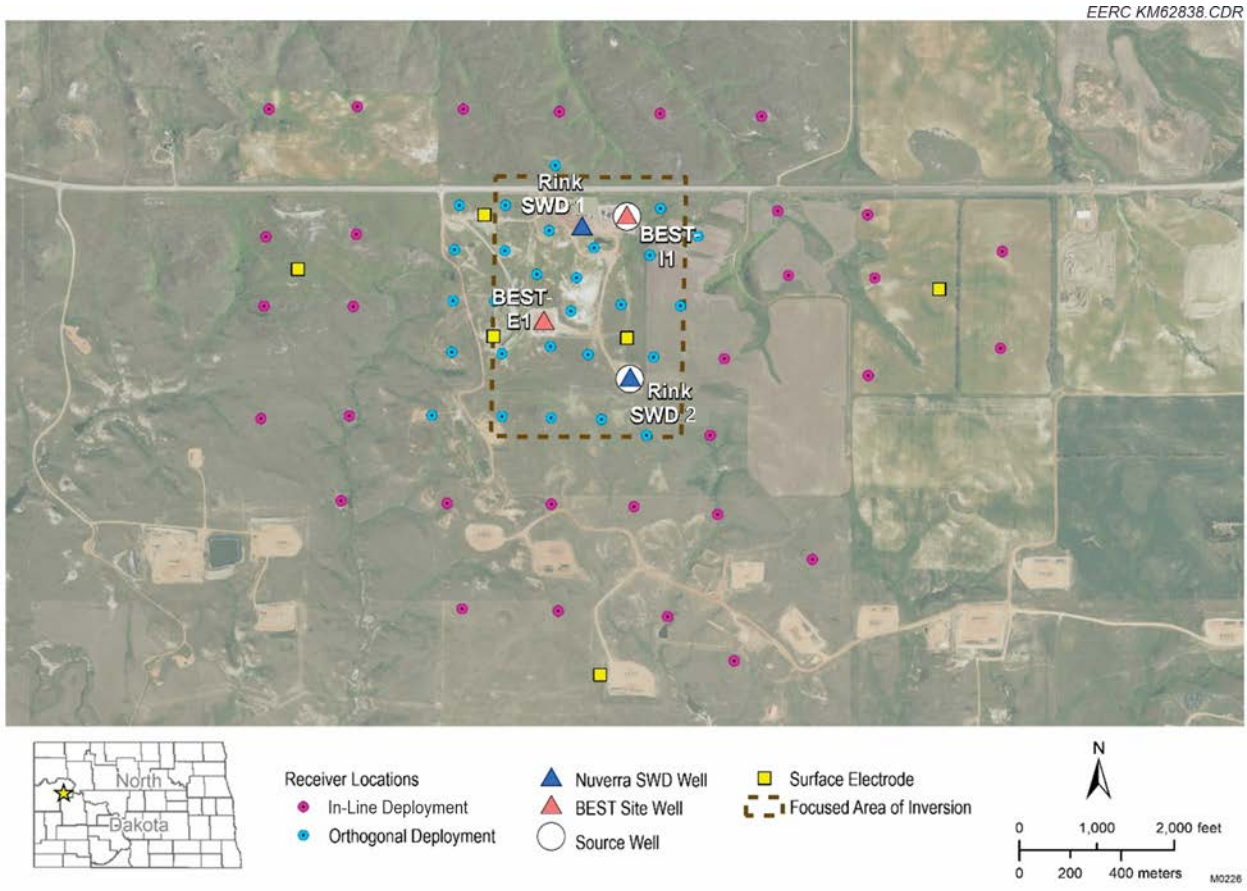


Figure 8. Map of the BSEM survey area. Dots indicate receiver locations, with colors indicating either “inline” (pink) or “orthogonal” (blue) deployment. Yellow squares indicate the location of surface electrodes. White circles identify the location of source wells. The brown dotted line represents the area of focus for inversion results.

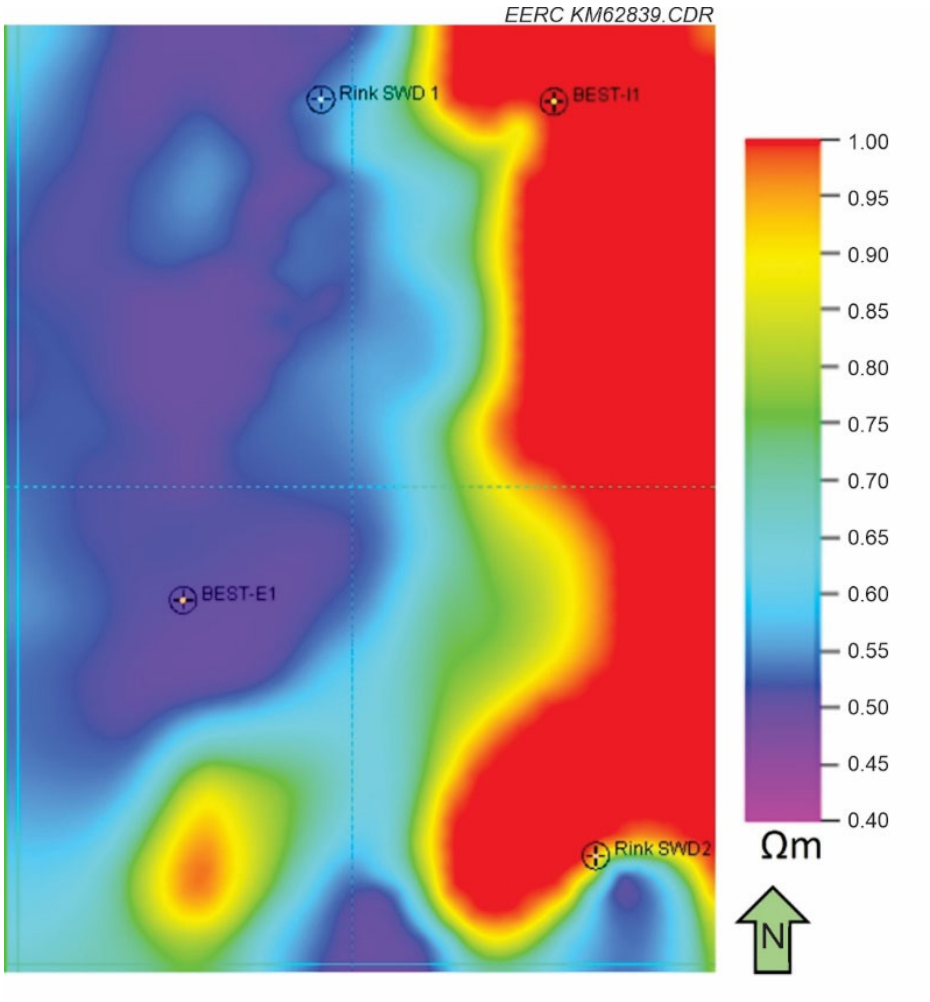


Figure 9. Lateral (X.Y.) slice of the inverted resistivity model at a depth of 5347 ft. There is a general west–east trend of increasing resistivity that correlates with a porosity pinch-out in this direction. Low-resistivity values are seen around the extraction well, BEST-E1, that match values calculated directly from water samples.

These results correlate well with prior information. The lithology within the reservoir gradually changes moving from west to east as the porosity pinches out, correlating with the resistivity trend seen in the inversion. Further, the resistivity values from the inversion around the BEST-E1 extraction well agreed with resistivity estimates calculated using salinity values taken directly from the extracted formation water. These were calculated using Archie's law, which relates the bulk resistivity of a formation $\boldsymbol{R_t}$ to the resistivity of the pore fluid $\boldsymbol{R_w}$ (itself a function of salinity and temperature), the water saturation $\boldsymbol{S_w}$, and the porosity of the formation $\boldsymbol{\Phi}$. The inversion results represent a useful update of the 3D resistivity structure within the Inyan Kara from the values derived from the initial porosity model (Equation 1).

$$\mathcal{R}_t = a\phi^{-m} S_w^{-n} \mathcal{R}_w \qquad \text{[Eq. 1]}$$

BSEM Repeat Operation

A repeat BSEM survey was originally scheduled to occur at the end of active extraction operations, with the goal to determine the shape and distribution of the site's brine injection plumes after extraction operations ceased. Unfortunately, in 2020, the EERC was notified by GroundMetrics that it would not be able to acquire a repeat BSEM survey. While alternative options (such as the EERC conducting the repeat survey using GroundMetrics equipment or hiring an alternative survey provider) were investigated, these options were deemed to be non-cost-effective and/or had additional technical risks that might have impacted the repeatability of the dataset.

In addition, less brine was injected into the Inyan Kara by the end of active extraction than initially predicted, potentially impacting the detectability of changes within the reservoir. The EERC conducted an additional feasibility study to determine if this reduced amount of brine would still be imageable using BSEM, as the lower amount of brine present resulted in a lower-resistivity contrast within the reservoir than originally estimated by nearly an order of magnitude. The new feasibility results indicated a difference between the predicted and baseline BSEM data of less than 2%, as shown in Figure 10. This low probability of a repeat BSEM survey successfully detecting a difference with the most likely distribution of brine plume parameters within the reservoir suggested it would be challenging to use the repeat BSEM survey results for calibration of the reservoir fluid model. Given these results, as well as the limited options for conducting a repeat survey, the EERC decided to not pursue a repeat BSEM survey.

In place of the repeat BSEM survey, the EERC conducted a sensitivity study of the time-lapse BSEM method. Previous BSEM feasibility work studied only the ability of the method to detect and image the injected brine within the reservoir. The BSEM time-lapse sensitivity study focused on the repeatability aspects of such a survey and the most influential factors in obtaining an accurate image of the injected brine in the reservoir over time. The study (MacLennan and others, 2022) found that variations in salinity and plume volume and pattern can alter the ability of an inversion to image a saline plume successfully. Incorporating various possible simulations of brine flooding into presurvey forward modeling is an important technique to cut down on the uncertainty within the inversion results. Currently, conditions at the field site are not optimal for a repeat survey to have a high chance of success in imaging a saline plume, but potential scenarios where the BSEM method would return a positive result with confidence are possible. Initial analysis shows that care must be taken with receiver and source position when differencing time-lapse BSEM data directly, but ultimately the understanding gained of the inversion parameters and changes within the model may be the most crucial factor toward validating changes within the reservoir over time. MacLennan and others (2022) contains more information on the methods applied and results.

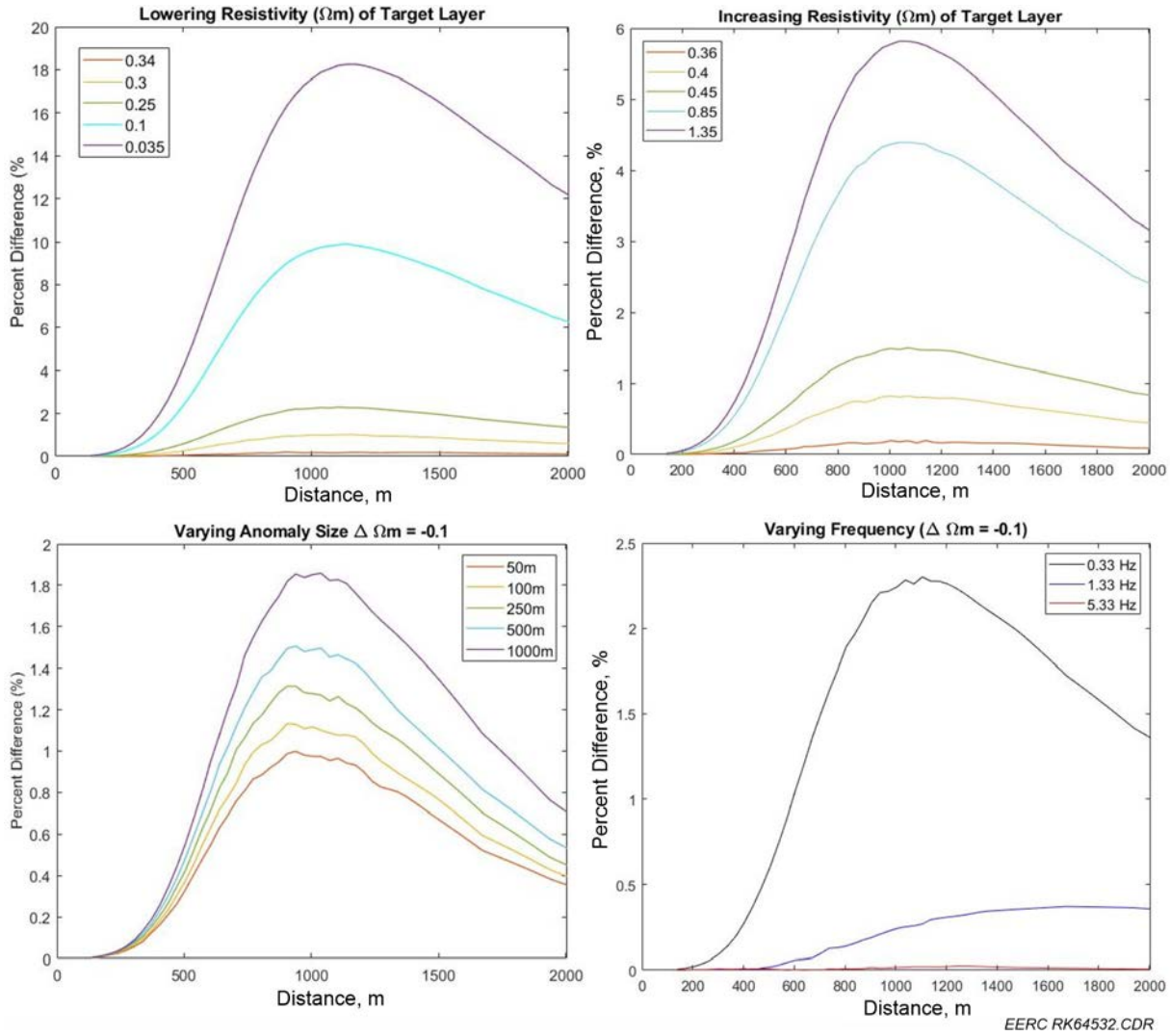


Figure 10. Additional feasibility modeling showing the percent difference of BSEM data compared to baseline measurements because of changes in reservoir parameters caused by changes in injected fluid properties and survey options. These include making the reservoir less resistive (increased salinity) or more resistive (less saline), varying the size of the saline anomaly, and measuring at different source frequencies. Likely changes within the reservoir resulted in a 2% difference or less, which would be difficult to detect in a repeat BSEM survey at this time.

ARM OPERATION

ARM is the management of the reservoir through means of production, injection, and monitoring. ARM is a potential method to improve reservoir storage capacity, steer pressure plume migration, and manage reservoir pressure to maximize the utility of DSFs for CO_2 storage and thereby reduce some of the associated costs and impacts. The BEST project was designed to demonstrate ARM operations using previously drilled SWD wells operated by Landtech Enterprises, LLC, in the Inyan Kara Formation and the two newly drilled wellsto serve as an

extraction well (BEST-E1) from the Inyan Kara Formation and an injector well (BEST-I1) to dispose of the extracted fluid into the Broom Creek Formation.

The Inyan Kara is a regionally extensive DSF previously identified as a potential target for commercial-scale CO_2 storage because of its promising geologic properties, see Table 3. This, combined with the fact that current brine injection operations at the Johnson's Corner site emulate commercial-scale CO_2 storage (volumetrically equivalent to >250,000 tons/yr CO_2), means the results of ARM in the Inyan Kara will be directly applicable to widespread adoption in CCS projects.

Table 3. Reservoir Characteristics at the Rink SWD #1, Rink SWD #2, and BEST-E1 Wells

Reservoir Description		
Target Formation		Inyan Kara
Lithology		Sandstone and shale
Porosity		20%
Water Saturation		100%
Formation Thickness	Rink SWD #1 and Rink SWD #2	~170 ft
	BEST-E1	~215 ft
Permeability	Rink SWD #1 and Rink SWD #2	75 mD
	BEST-E1	150 mD
Interwell Distance	Rink SWD #1 to BEST-E1	0.27 mile (1426 ft)
	Rink SWD #2 to BEST-E1	0.25 mile (1320 ft)
	Rink SWD #1 to Rink SWD #2	0.42 miles (2218 ft)

Operations at the Johnson's Corner site are ideally suited for conducting a BEST. Long-term operations at the site have created a differential pressure plume that can be modified through ARM, and the established injection history allows for confident simulated predictions. The four-well design—the Rink SWD #1 and Rink SWD #2 injection wells, the BEST-E1 extraction well, and the BEST-I1 injection well—provides operational flexibility and monitoring capability to test ARM scenarios through a range of injection and extraction rates. The injection can be independently controlled into both SWD wells, and the extraction rate can be varied.

This project is divided into two FIP stages. The first stage was intended to probe the reservoir and well responses to a specific sequence of injection and extraction tests to determine the level of performance interference among the wells and the system's capabilities. The second stage was performed to verify the repeatability of the ARM operations.

Stage 1

During the first stage of the scenario, the BEST-E1 well alternated between extraction and shut-in cycles, called the interference test. This test was designed to provide enough time for the monitoring wells to see a pressure response because of extraction/shut-in cycles. Multiple extraction/injection rate ratios were performed during the first stage. The data from each well were

recorded through the SCADA system and stored for ARM performance evaluation. In addition, chemical tracers were injected into injection wells Rink SWD #1 and Rink SWD #2 to verify well connectivity. The tracer evaluation is discussed in the Tracer Survey section. Fluid sampling from BEST-E1 was performed periodically to track tracer production. Table 4 provides the actual and planned ARM FIP for Stage 1.

SCADA data were downloaded periodically and examined. The data collected were then used as inputs for the reservoir simulation to evaluate ARM performance and its impact on the reservoir. Figure 11 provides data collected during test Steps 2–4, which show the reservoir pressure response during extraction/shut-in.

Table 4. Planned Rate vs. Actual Rate During Stage 1

BEST ARM FIP											
Test Details				Planned Rate, bwpd*				Actual Rate, bwpd			
Test	Duration, days	Start Date	End Date	BEST-E1	BEST-I1	Rink SWD #1	Rink SWD #2	BEST-E1	BEST-I1	Rink SWD #1	Rink SWD #2
Stage One											
1	59	1-Jan-19	13-Jun-19	–	–	7100	7400	–	–	7750	7650
2	11	13-Jun-19	25-Jun-19	–5000	5000	7100	7400	−3600	3600	7000	6825
3	22	25-Jun-19	16-Jul-19	–	–	7100	7400	–	–	7550	6875
4	10	16-Jul-19	26-Jul-19	–5000	5000	7100	7400	−4975	4975	7250	6850
5	20	26-Jul-19	15-Aug-19	–	–	7100	7400	–	–	6900	6850
6	12	15-Aug-19	27-Aug-19	–	2000	5100	7400	–	1680	5450	6900
7	20	27-Aug-19	16-Sep-19	–3000	5000	5100	7400	−3000	4350	5775	6900
8	20	16-Sep-19	6-Oct-19	–	2000	5100	7400	–	–	7150	6900
9	11	6-Oct-19	17-Oct-19	–	2000	7100	5400	–	–	7100	6900
10	21	17-Oct-19	7-Nov-19	–3000	5000	7100	5400	−2627	3540	3729	5225
11	20	7-Nov-19	27-Nov-19	–	2000	7100	5400	–	–	4838	2763

* Barrels of water per day.

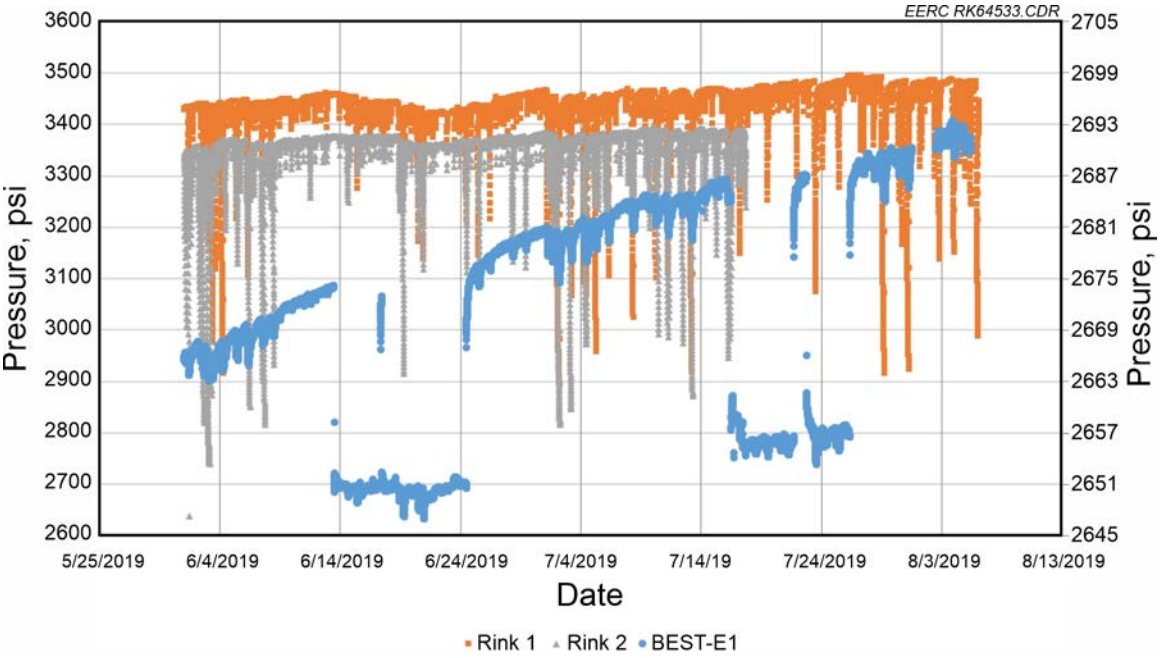


Figure 11. BHP profile. X-axis represents date from June 1 through August 7, 2019. Left Y-axis represents BHP for Rink SWD #1 (orange dots) and Rink SWD #2 (gray dots). Right Y-axis represents BHP for BEST-E1 as producer or observer well. The lower pressures, seen through the blue dots representing BEST-E1, were recorded during extraction intervals.

Tracer Injection and Analysis

A tracer survey was conducted as part of the BEST project to characterize reservoir connectivity further and validate brine plume growth predicted by the reservoir simulation. Tracer surveys utilize uniquely identifiable materials injected into two injection wells, then the offset producing well is monitored for the appearance and concentration of the tracers. This process allows for direct measurement of breakthrough time between injectors and producers to provide additional qualitative data such as reservoir connectivity.

Two water-based tracers were used. One was injected into Rink SWD #1 and the other into Rink SWD #2 on the same day. Samples were collected from the BEST-E1 well. The sampling frequency recommendation of the tracer company, ProTechnics, was followed. The tracer details are included in Table 5.

Table 5. BEST Tracer Survey Injection Details

Tracer Name	IWT 1900	IWT 2200
Injection Well	Rink SWD #1	Rink SWD #2
Injection Date	June 25, 2019	June 25, 2019
Injected Tracer Mass, kg	2	3

The recommended sampling frequency was weekly for the first 2 months, once every 2 weeks for Months 3–6, and monthly from Month 7 and beyond. The recommended frequency was exceeded, with a plan to collect three samples per week on Tuesdays, Thursdays, and Saturdays during the first 2 months and two samples per week from Month 3 onward. The specific days of the week were identified to space sampling evenly across each week. This exact schedule was not always met because of operational variability associated with ARM activities as well as general SWD operations. However, efforts were made to ensure that the sampling schedule remained as close to the plan as possible. Samples collected were then retained until a subset was selected for analysis. The results of each tested sample batch informed the selection of each subsequent batch of the preceding analyses. The analyzed samples and results are shown in Table 6 and plotted in Figure 12 for the Rink SWD #1 tracer and Figure 13 for the Rink SWD #2 tracer.

Table 6. BEST Tracer Survey Water Sample Analysis Summary Showing Concentrations of Measured Tracer in parts per trillion (ppt). Any measurement under 50 ppt is under the reliable detection limit and is classified as no detection (ND). One sample was determined to be contaminated (CS).

Sample Date	Days Since Injection	Analysis Date	Rink SWD #1	Rink SWD #2
7/16/2019	22	7/23/2021	ND	ND
7/25/2019	31	10/8/2019	ND	ND
9/1/2019	69	4/22/2020	ND	ND
9/6/2019	73	10/8/2019	63	ND
9/12/2019	79	4/22/2020	ND	ND
9/16/2019	83	4/22/2020	ND	ND
10/19/2019	116	3/24/2020	ND	54
10/22/2019	119	4/22/2020	ND	ND
11/5/2019	133	4/22/2020	ND	ND
1/10/2020	199	4/22/2020	ND	ND
3/1/2020	251	7/21/2020	ND	ND
4/28/2020	308	7/21/2020	ND	ND
6/15/2020	356	5/10/2021	ND	ND
6/29/2020	370	5/11/2021	ND	51
7/18/2020	389	6/11/2021	ND	80
8/17/2020	419	4/27/2021	ND	69
10/16/2020	479	4/20/2021	ND	55
10/26/2020	489	11/5/2021	ND	ND
6/4/2021	710	11/5/2021	CS	CS
8/11/2021	778	NA[1]	ND	55

[1] Not applicable.

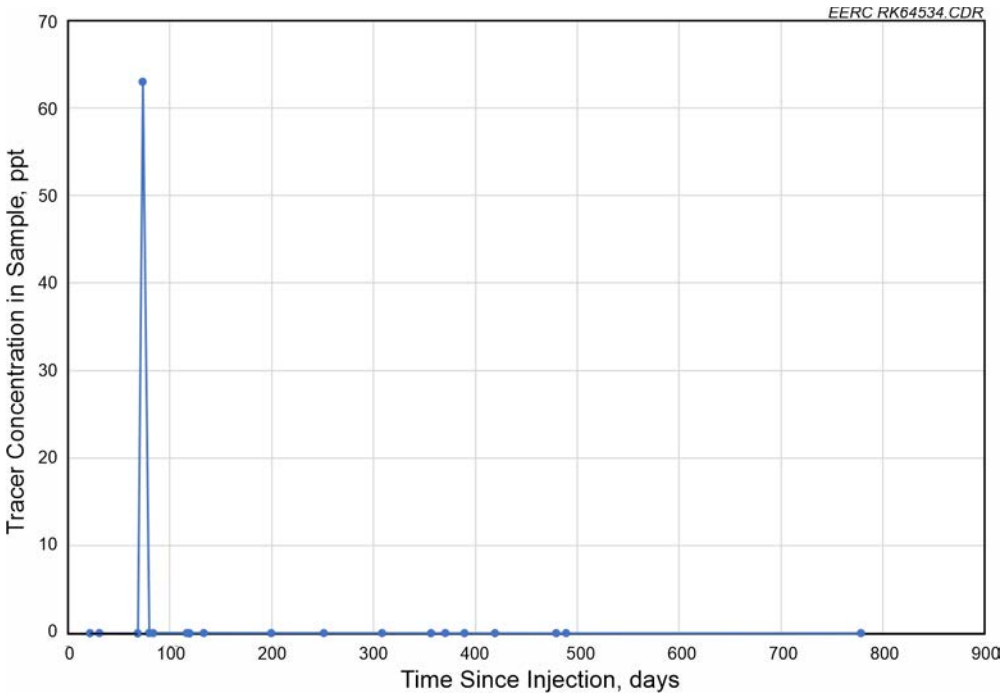


Figure 12. Rink SWD #1 tracer results.

The results for Rink SWD #1 in Figure 12 clearly indicate no obvious or sustained breakthrough of the tracer, while the results for Rink SWD #2 in Figure 13 may appear more compelling at first glance. However, all of the detections were only slightly above the reportable threshold. The tracer survey vendor, ProTechnics, stated the minimum detection threshold was 10 ppt, and anything under 50 ppt is reported as "no detection" because of likely interference to the apparatus during sample analysis. Further, the amount of tracer injected into each well was designed such that concentrations at BEST-E1 should read in the 1000s or 10,000s once the front breaks through. Subsurface reservoirs often exhibit varying levels of heterogeneity, which can result in injected media traveling in a preferred direction or path of least resistance. No tracer detected was determined because of the natural heterogeneity and geologic features of the Inyan Kara, which resulted in the tracers traveling in a direction other than BEST-E1.

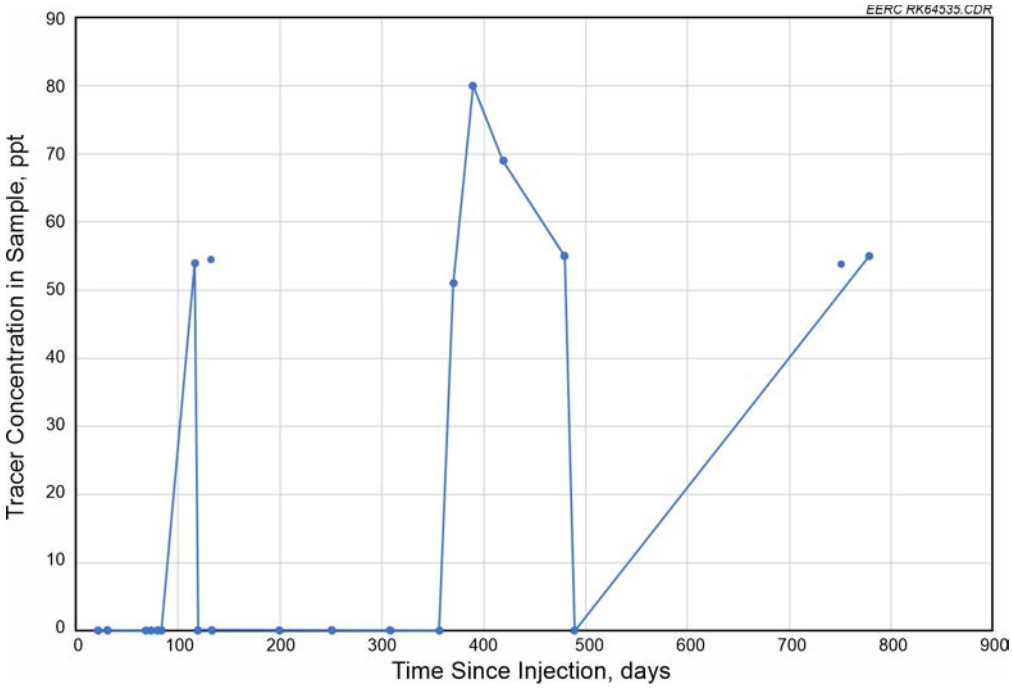


Figure 13. Rink SWD #2 tracer results.

Stage 2

As this project progressed, the data were entered into simulation and history matching to refine model performance prior to Stage 2 operating periods. Table 7 shows actual rates versus planned rates. Stage 2 was used to verify the results from Stage 1 and the repeatability of the ARM operations. The Stage 2 objective was to find through ARM if there is a potential for maximizing the reservoir's storage, reducing cap rock exposure, and aiding in the management of pressure plume migration.

Regional oil production decreased, resulting in reduced injection rates from Rink SWD #1 and Rink SWD #2 from ~15,000 bpd in fall 2019 to ~1000 bpd in spring 2020. This shift in injection activity allowed the unique opportunity to:

1. Increase the ratio of the extraction-to-injection rate compared to the original FIP.
2. Evaluate ARM performance through an extended range of operation parameters.
3. Increase ARM response to improve the signal to noise in pressure results.

On July 7, 2021, the completion of ARM operations was satisfied. With the conclusion of testing, data were gathered and used to evaluate the efficacy of ARM for various implementation scenarios.

Table 7. Planned Rates vs. Actual Rates for Stage 2 (negative rates mean extraction, while positive rates mean injection)

BEST ARM FIP									
Test Details		Planned Rate, bwpd				Actual Rate, bwpd			
Test	Duration, days	BEST-E1	BEST-I1	Rink SWD #1	Rink SWD #2	BEST-E1	BEST-I1	Rink SWD #1	Rink SWD #2
Stage Two									
12	69	−5000	5000	7100	7400	−407	1200	3145	1189
13	90	−2500	2500	7100	7400	−5000	6000	2451	2044
14	29	–	–	7100	7400	−4153	5100	536	85
15	5	–	1000	7100	6400	–	–	562	–
16	26	−4000	5000	7100	6400	−4569	5200	1224	139
17	9	–	1000	7100	6400	−193	500	1320	2494
18	111	−4000	1000	6100	7400	−3790	4800	1433	2370
19	92	–	5000	6100	7400	–	–	2005	1270
20	75	–	1000	6100	7400	–	–	1500	1800
21	35	−4000	0	7100	7400	−4500	5500	–	2500

DATA COLLECTION AND PROCESSING

In this study, machine learning (ML)-assisted data analytics was used to fill knowledge gaps by evaluating the effects of injection/extraction on in situ reservoir pressure based on field measurements. The extraction well is located nearly the same distance from both injection wells, approximately 1426 ft from Rink SWD #1 and 1320 ft from Rink SWD #2 (Figure 14). The measurements included interrogator pressure (BHP) and flow rate and were acquired at approximately 5- or 2-minute intervals over the study period.

The wells were periodically shut in and reopened, which created discontinuities in the time series data record. Eight cases were defined to describe the data, which capture the combinations of Rink SWD #1, Rink SWD #2, and BEST-E1 being either open (on) or closed (off) (Table 8). Therefore, only cases where BEST-E1 was open and there were flowing BHP values were considered in this analysis. Consequently, the first three cases were the primary focus of the calculations and ML efforts.

Missing values in the data were attributed to either well shut-ins or periods with no measurements and were not included in the analysis. Outliers in the dataset (i.e., extremely low or high values relative to the other measurements) were detected and removed based on visual inspection using sliding time windows. The sliding time windows sequentially identified potential outliers along windows of weeks or months depending on the progression of the records, and these points were manually removed if they were determined to be outliers in relation to the other measurements. To reduce the effect of irregularities (noise) in the data, daily averages were calculated for all variables to smooth the data from 2- to 5-minute frequency to daily frequency prior to ML analysis. The data gaps (missing values) in the scale of days were not filled to preserve the original hydrogeologic dynamics of the injection and production processes. Results of the processed data showing daily averages and missing values for the dependent variables (BHPs at Rink SWD #1, Rink SWD #2, and BEST-E1) and independent variables (flow rates at the three wells) are illustrated in Figure 15.

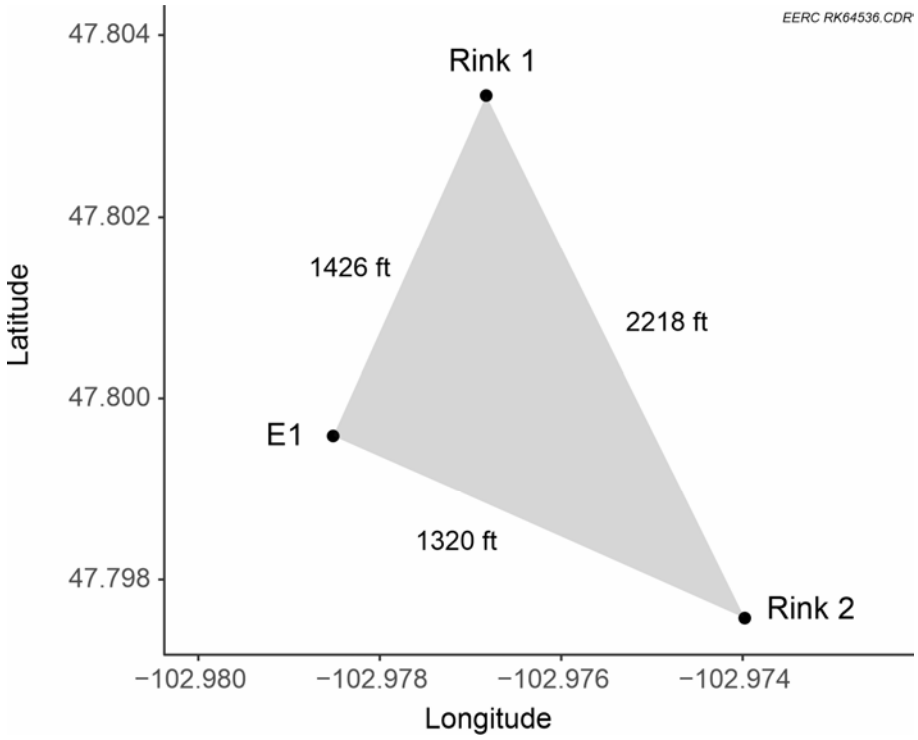


Figure 14. Locations of the two injection wells (Rink SWD #1 and Rink SWD #2) and the brine extraction well (BEST-E1), showing the distance in feet between each well.

Table 8. Data Categorization Based on Well Operational Status

Case	Rink SWD #1	Rink SWD #2	BEST-E1
Case 1	On	On	On
Case 2	On	Off	On
Case 3	Off	On	On
Case 4	Off	Off	On
Case 5	Off	Off	Off
Case 6	On	Off	Off
Case 7	Off	On	Off
Case 8	On	On	Off

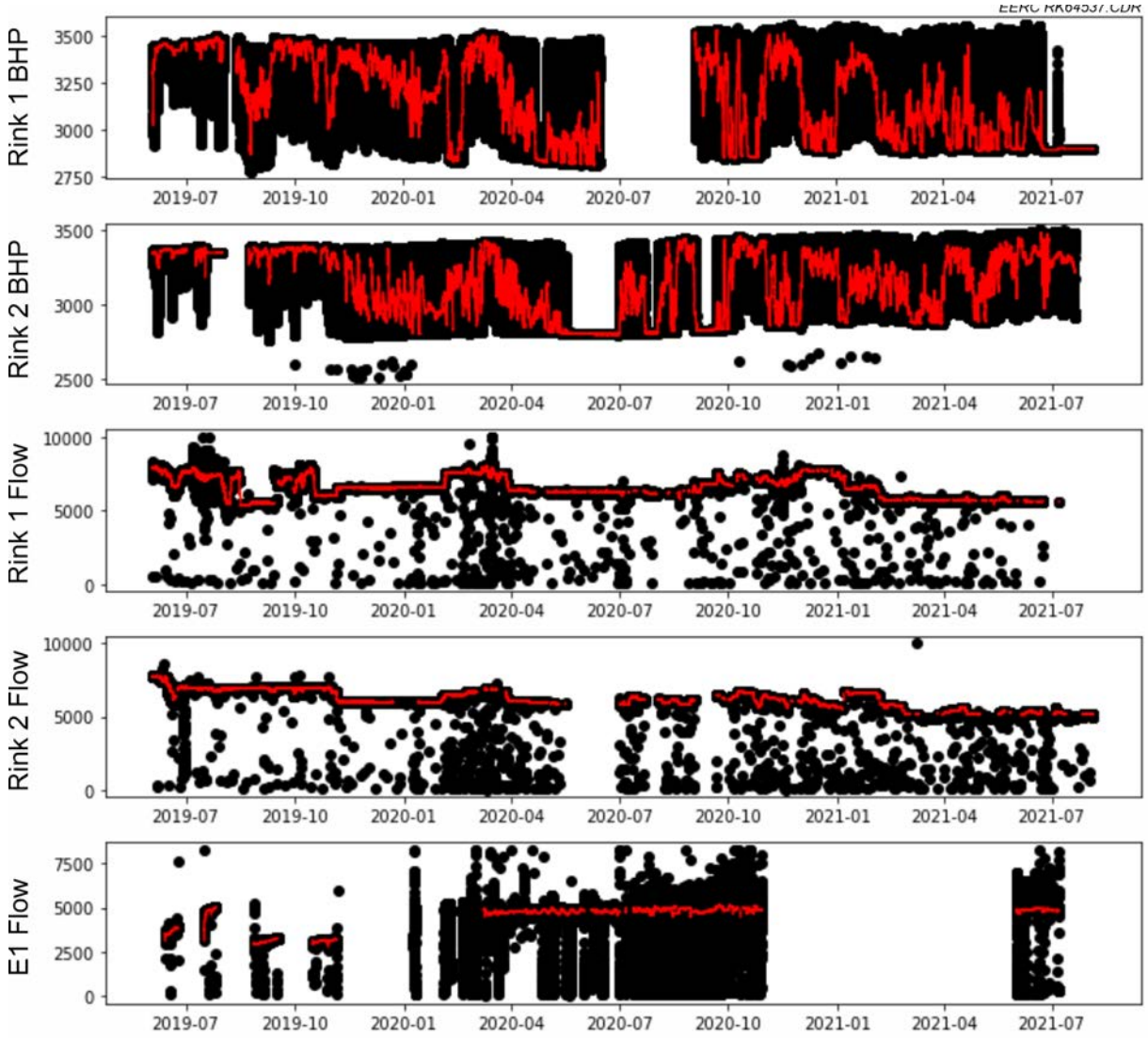


Figure 15. Raw data (black points) and moving average smoothed clean data (red line) of the dependent variables (Rink SWD #1 and Rink SWD #2 BHPs) and independent variables (flow rates at the three wells).

Descriptive statistics of pressure and flow rate data for the three wells are summarized in Table 9. The data show that more fluid is injected than fluid produced. For example, the ratio of extraction/injection for Rink SWD #1 is 0.629 (1.32 MMbbl/2.10 MMbbl); for Rink SWD #2, it is 0.632 (1.32 MMbbl/2.09 MMbbl); and for the combined Rink wells, it is 0.315 (1.32 MMbbl/4.19 MMbbl). Therefore, the Rink SWD #1 and Rink SWD #2 wells injected more than three times greater fluid than was extracted from BEST-E1, which provided challenges for data analysis to discriminate signal (effects on BHP) from noise (variation in the injection rates and time series data attributable to normal operating procedures).

Table 9. Descriptive Statistics of BHP and Flow at the Two Injection Wells (Rink #1 and Rink #2) and One Production Well (BEST-E1)

	Pressure, psi		Flow Rate, bbl/day		Cumulative Flow, MMbbl
	Mean	SD[1]	Mean	SD	
Rink SWD #1	3162	210	2648	2579	2.10
Rink SWD #2	3140	201	2633	2440	2.09
BEST-E1	2916	305	1681	2074	1.32

[1] Standard deviation.

A new variable representing the instantaneous extraction ratio was created from the raw measurements, where the total flow rate at the two Rink wells was used as the denominator and the flow rate at the production well as the numerator. Specifically, the extraction ratio can be represented as follows in Equation 2:

$$Extraction\ Ratio = \frac{Flow\ rate_{E1}}{Flow\ rate_{RinkSWD\#1} + Flow\ rate_{RinkSWD\#2}} \quad \text{[Eq. 2]}$$

Where:
$Flow\ rate_{E1}$ is the observed flow rate for the extraction well.
$Flow\ rate_{RinkSWD\#1}$ and $Flow\ rate_{RinkSWD\#2}$ are the observed flow rates for injection wells.
Extraction Ratio is the new variable normalized to the injection well flow rates. These ratios were calculated for each combination of wells.

Analytical Approach

The pressures at the injection wells show the aggregate effects of available reservoir storage, brine propagation because of injection, and brine production. Figure 16 shows a portion of the time series data record during brine production from BEST-E1. The results show that the BHPs at the Rink wells are directly responding to the injection rates at the same well (i.e., Rink SWD #1 BHP increases when Rink SWD #1 injection increases and vice versa), while the BHPs at the Rink wells do not show clear correlations with the production flow rates at BEST-E1. In other words, the top panel in Figure 16 contains a signal from the middle panel, and this overprint obscures effects that the bottom panel may exert on Rink SWD #1 BHP. Simmenes and others (2013) observed similar correlation patterns of BHP response to CO_2 injection at the microscale, where pressure gradually builds after injection. Figure 16 also shows that Rink SWD #1 BHP continues to decline when injection stops until rapidly building up again when injection restarts. Untangling these relationships to estimate the net effect of BEST-E1 flow (extraction) on Rink SWD #1 and Rink SWD #2 BHP was a major focus of the ML approach. Based on the close relationship between BHPs and flow rates from the same well, the BHPs were analyzed separately based on the operational status of the wells. Therefore, the data were divided into scenarios of 1) injection well closed, 2) injection well open, 3) production well closed, and 4) production well open. ML models were developed separately for each data scenario.

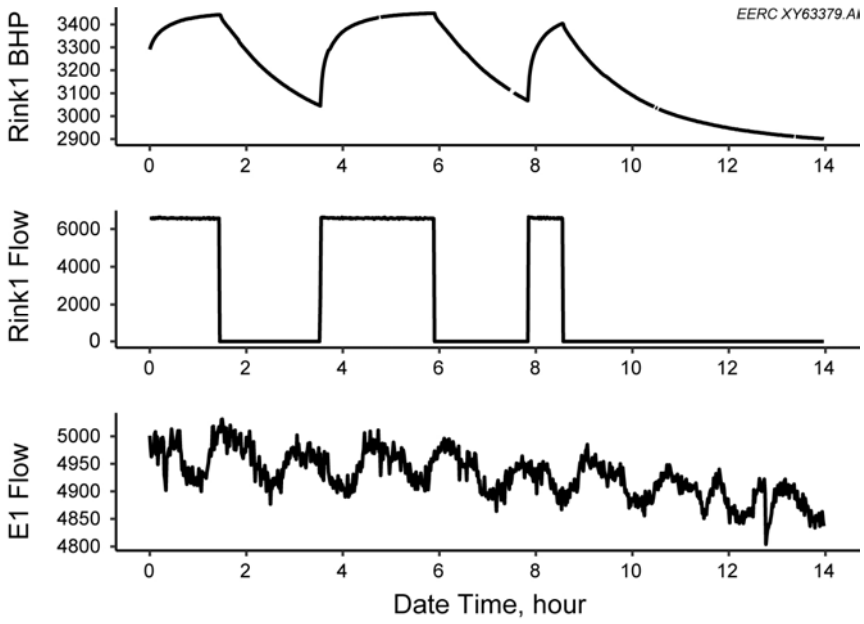


Figure 16. Time series data for a portion of the data record (January 9–10, 2022) showing injection well Rink SWD #1 BHP (top) and flow (middle) during brine production from extraction well BEST-E1 (bottom).

Model Development

For each case, the data were randomly divided into training and testing datasets by the ratio of 0.8:0.2. The training data were used to develop the ML model, and the testing data were used to evaluate the developed model. Extreme Gradient Boosting (XGBoost) algorithm was used in this study to develop the ML model. XGBoost is a boosting ensemble learning algorithm that integrates predictions of "weak" tree models to achieve a "strong" tree model via a sequential process (Chen and Guestrin, 2016). The algorithm works by building a sequential list of decision trees, and in each successive round, the decision tree uses the residuals from the prior decision tree as the target variable. The loss function, or the errors between the predicted and actual values, are minimized using the gradient descent approach to estimate the coefficients within the XGBoost model. There are seven hyperparameters to tune, and the optimal values were tuned by k-fold cross-validation (Table 10).

Table 10. Hyperparameters for the XGBoost Algorithm

Parameter	Description
nrounds	Maximum number of iterations
max_depth	Maximum depth of the tree
gamma	Regularization coefficient
min_child_weight	Minimum number of instances required in a child node
eta	Learning rate
subsample	Number of samples supplied to a tree
colsample_bytree	Number of features (variables) supplied to a tree

Two indicators were used to evaluate the model goodness-of-fit performance on the training and testing sets: 1) R-squared (R^2) values and 2) relative root-mean-squared-error (rRMSE). The R^2 value measures the proportion of the variance in the target variable (BHPs) that can be explained by the predictor variables and the XGBoost model. The R^2 value is a well-known, easy-to-use, and easy-to-interpret score to evaluate the performance of a predictive model. R^2 is bounded between 0 (no predictive value) and 1 (perfect prediction). Root-mean-squared-error (RMSE) is the standard deviation of the residuals, which measures the spread (variation) of the residuals – the difference between the predicted and observed values of the target variable. To standardize the scale of RMSE values for easier modeling performance comparisons between different cases, rRMSE was used which was defined as the value of RMSE divided by the mean value of that variable. Hence, rRMSE is unitless. In general, a good predictive model will have a value of R^2 that approaches 1 and a value of rRMSE that approaches 0.

ML Analysis

The R^2 and rRMSE values of the modeling performance for both training and testing datasets in the three cases were presented in Table 10. Results from the R^2 values and rRMSE values showed that all the developed XGBoost models have good performance in predicting the Rink well BHPs.

To understand these relationships and "open the box," partial dependence analysis calculates the marginal effect from one or several features on the predicted outcome of an ML model. The calculations of the partial dependence relationship are generalized in the following steps:

1. Hold the variable of interest (x) at a constant value and append it to the other variables' space in the training dataset.

2. Make predictions on the above-created data using the developed XGBoost model, and the average of the predictions is the marginal output of the variable x at this constant value.

3. Repeat Steps 1 and 2 with other values of the interest variable's distribution space. A list of average predictions and corresponding variable x will be generated.

4. Plot the list of x values and the average marginal predictions to visualize the partial dependence relationship between x and output.

Results of the partial dependence analysis will be illustrated using a customized partial dependence plot.

Pressure Response When Well Is Closed

The time series of BHPs when the wells were closed are presented in Figure 17. For the injection wells (Rink SWD #1 and Rink SWD #2), the BHPs exhibited limited fluctuations when the corresponding well was closed. The limited changes in the BHPs at the injection wells suggest that the perturbation activities at nearby locations have a small effect on the BHPs over the 2-year operating period. The results also suggest that the ambient pressure at the location of Rink SWD #1 was around 2900 psi and at Rink SWD #2 was around 2800 psi when there was no

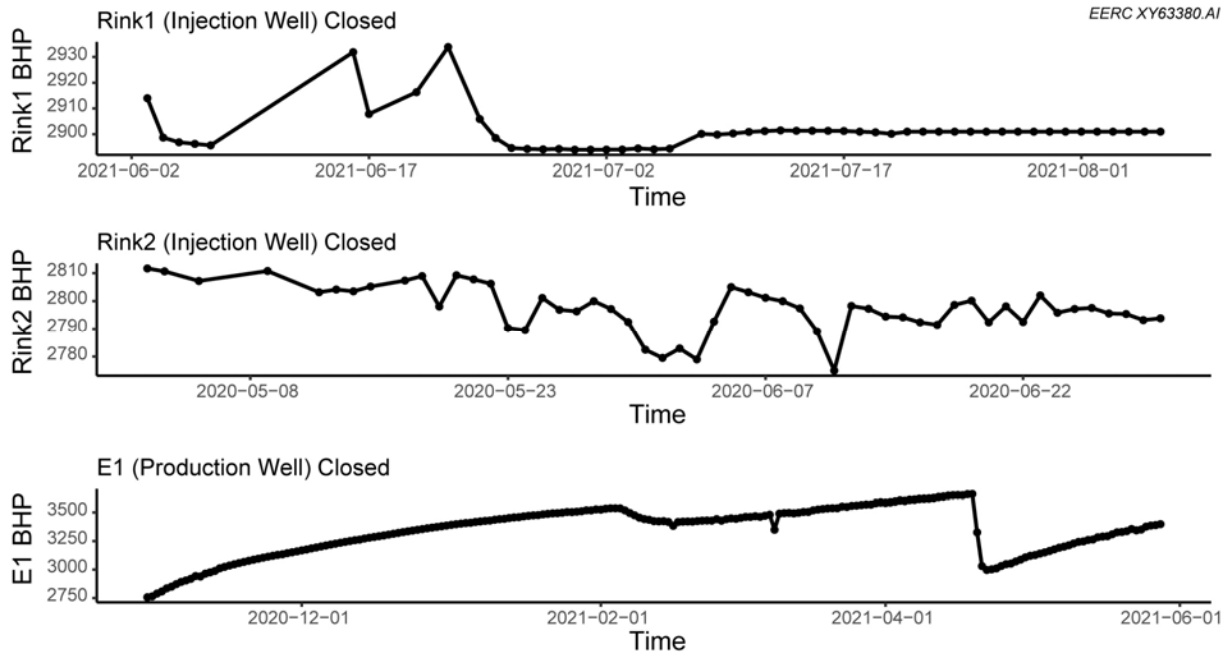


Figure 17. General pattern of BHP response at the injection and production wells when the corresponding wells were closed.

injection or production activities in the reservoir. At the production well (BEST-E1), the BHPs increased steadily when the production well was closed, which suggests that the injection activities at the nearby wells indeed influenced the ambient pressures in the reservoir. The sudden 500-psi drop in mid-April 2021 was caused by the sudden shut-ins of both Rink wells when there was no production at BEST-E1. At this point, BEST-E1 BHPs were close to the stabilized bottomhole shut-in pressure (BHSIP).

Modeling results using the XGBoost algorithm showed that BHPs at BEST-E1 were predominantly influenced by the amount of cumulative injected fluid (with r^2 values for the training and testing datasets of 0.99 and 0.96 and rRMSE values of 0 and 0.0123).

Pressure Response at the Injection Well

Because the patterns of the BHP responses at the two injection wells were similar, the analytics described here focused on the Rink SWD #1 well to illustrate the approach. An XGBoost model to predict Rink SWD #1 BHP was constructed using variables of Rink SWD #1 injection rate, Rink SWD #2 injection rate, the ratio of production rate and the total injection rate (sum of injection rates at both Rink wells), and the number of days. The modeling performance is presented in Figure 18. The r^2 values for the training and testing datasets are 1.00 and 0.95, and the rRMSE values are 0 and 0.0128, respectively. As expected, the variable importance plot shows that BHPs at Rink SWD #1 were predominantly influenced by the injection flow rates at the same well (Rink SWD #1 flow) and only slightly influenced by the injection rate at the nearby well

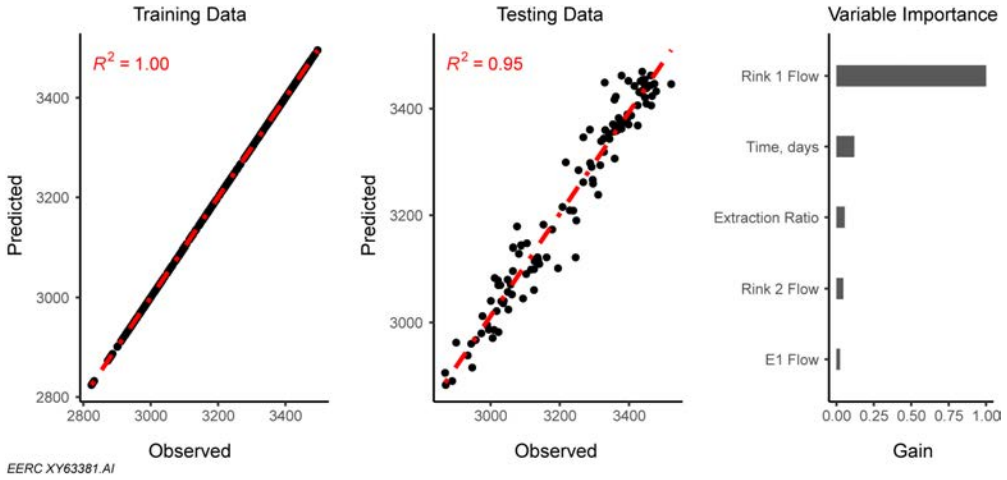


Figure 18. XGBoost modeling performance for predicting Rink SWD #1 BHP (left two panels) and variable importance (right panel).

(Rink SWD #2). The extraction ratio moderately influenced Rink SWD #1 BHPs, while the production rate of BEST-E1 had the least impact on Rink SWD #1. Rink SWD #1 BHPs also showed modest correlation with the number of days, which indicates that Rink SWD #1 BHPs increased over time throughout the testing period.

The partial dependence diagrams of the input variables with output variable (partially predicted Rink SWD #1 BHPs) are illustrated in Figure 19. The Rink SWD #1 flow rate can predict a range of Rink SWD #1 BHPs of 500 psi (from 2900 to 3400 psi), while the other variables can only predict a range of BHPs less than 50 psi, which suggests that the injection activity is the main driver of BHPs of the same well, while nearby well injection or production activities only have a minor effect in influencing the injection well BHPs. The injection rate of Rink SWD #1 exhibited a high positive correlation with BHPs at Rink SWD #1, as evidenced by the increasing curvilinear relationship between the Rink SWD #1 injection rate from 0 to 8000 bbl/day and Rink #1 BHP from 2900 to 3400 psi. The partial dependence plot between the Rink SWD #2 injection rate and Rink SWD #1 BHPs showed that the injection activity at nearby wells only had minor or slightly negative effect on the pressures at Rink SWD #1. The variations of Rink SWD #2 injection rates only result in approximately 15 psi (from 3215 to 3230 psi) variations in Rink SWD #1 BHPs. It should be noted that the total injection rate was relatively consistent throughout the operating period: lower Rink SWD #2 injection rates will correspond to relatively higher Rink SWD #1 injection rates, which corresponds to relatively higher Rink SWD #1 BHPs; therefore, Rink SWD #2 injection rates have a slightly negative correlation with Rink SWD #1 BHPs. For example, over the range of Rink SWD #2 flow rates from 4000 to 6000 bbl/day, the associated Rink SWD #1 BHP varied only from 3215 to 3225 psi – an effect of about 10 psi.

The production flow rate at BEST-E1 did not show correlation with Rink SWD #1 BHPs, with Rink SWD #1 BHPs only varying by 6 psi (from 3225 to 3231 psi). It should be noted that a lower spike of Rink SWD #1 BHPs relative to BEST-E1 flow rates was caused by relatively fewer data points at this range. The extraction ratio (BEST-E1 production/total injection) showed a negative correlation with Rink SWD #1 BHPs, and the range of the partially predicted Rink SWD #1 BHPs is about 30 psi (a decrease from 3230 to 3200 psi).

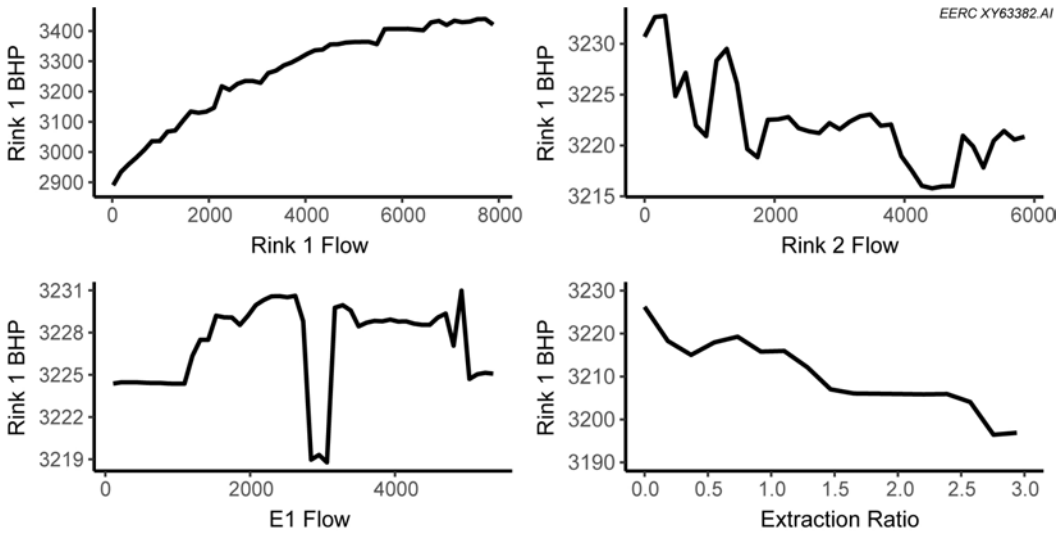


Figure 19. Partial dependence analysis of the flow rates at the three wells in predicting Rink SWD #1 (injection well) BHP.

The time series partial dependence relationships between injection and production activities on Rink SWD #1 BHPs are illustrated in Figure 20. For all scenarios of injection and production, the Rink SWD #1 BHP values increased steadily over time. The larger magnitude of injection corresponds to higher levels of BHP in the time series. The observation that Rink SWD #1 BHPs increased over time regardless of the extraction ratio suggests that the on-site injection activities dominate the BHPs and not the nearby production activities. The increase in BHPs for all scenarios of injection were approximately 100 psi. For example, in the top panel in Figure 20, the red line representing 1000 bbl/day ranges from approximately 2970 to 3075 psi, or a difference of about 105 psi over the 700-day period, while the magenta line representing 7000 bbl/day ranges from approximately 3150 to 3250 psi, or a difference of about 100 psi over the 700-day period. It should be noted that BHPs increased by a similar amount at ~100 psi for all scenarios of brine injection rates during the 2-year operating period. However, the similar amount of BHP increase does not mean that more brine injection has no effect on pressure buildup. Higher injection will result in consistently higher Rink SWD #1 BHPs, and lower injection will result in consistently lower Rink SWD #1 BHPs, while the BHP increase rates remain similar.

The increase for all scenarios of extraction ratio is approximately 50 psi. For example, in the bottom panel in Figure 20, the red line representing an extraction ratio of 0.03 ranges from 3167 to 3216 psi, or a difference of 49 psi over the 700-day period, while the magenta line representing an extraction ratio of 8 ranges from approximately 3126 to 3172 psi, or a difference of 46 psi over the 700-day period. A higher extraction ratio (i.e., greater extraction relative to injection) corresponds to generally lower BHPs, which suggests that production activities had some measurable effect on reducing pressure buildup. It should be noted that when the extraction ratio reaches 8:1 (magenta line in the bottom panel of Figure 20), the temporal pattern of Rink SWD #1 BHPs eventually showed a leveling trend (asymptote), which suggests that the larger relative magnitude of production is more effective in relieving pressure buildup, and there is a time lag for the brine production activity to have major effect on injection well pressures. Similarly, the

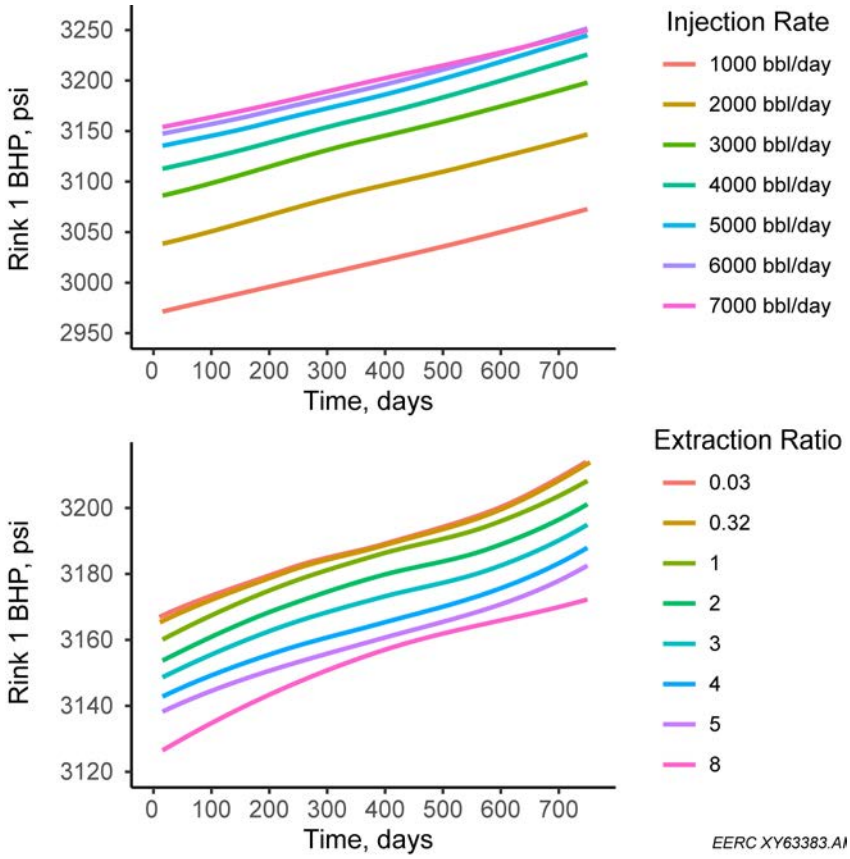


Figure 20. Time series of the partial dependence effects of injection at Rink SWD #1 well and production/injection ratio at BEST-E1 well on the BHPs in Rink SWD #1. Results showed that higher injection corresponds to higher BHPs, while higher production tends to lower BHPs.

Rink SWD #1 BHPs increased by a similar amount at ~50 psi for all scenarios of extraction rates. However, Rink SWD #1 BHPs of a lower extraction rate scenario were consistently higher than those of the higher production/injection rate, which clearly indicates that production has an effect in reducing pressure buildup.

The effects of relative extraction ratio at BEST-E1 on Rink SWD #1 BHPs were on the initial pressure change at the beginning of the test period (Figure 21). A larger extraction ratio corresponds to noticeably lower initial on-site pressures, which suggests that the more water extracted from the reservoir, the larger the impact on the entire reservoir pressure. As would be expected, the greater the injection rate, the larger the increase in the time series of BHPs regardless of the extraction ratio. However, the BHPs at Rink SWD #1 decreased about 50 psi when the extraction ratio increased from 0.5 to 8. For example, when the Rink SWD #1 injection rate was 3000 bbl/day (middle panel in Figure 21), at 400 days into the observed data record, the estimated Rink SWD #1 BHP when the extraction ratio was 0.5 was around 3150 psi. However, at that same point in time, when the extraction ratio was 8, the estimated Rink SWD #1 BHP was around 3090 psi, for a difference of nearly 60 psi after accounting for the effects of Rink SWD #1 and Rink SWD #2 injection.

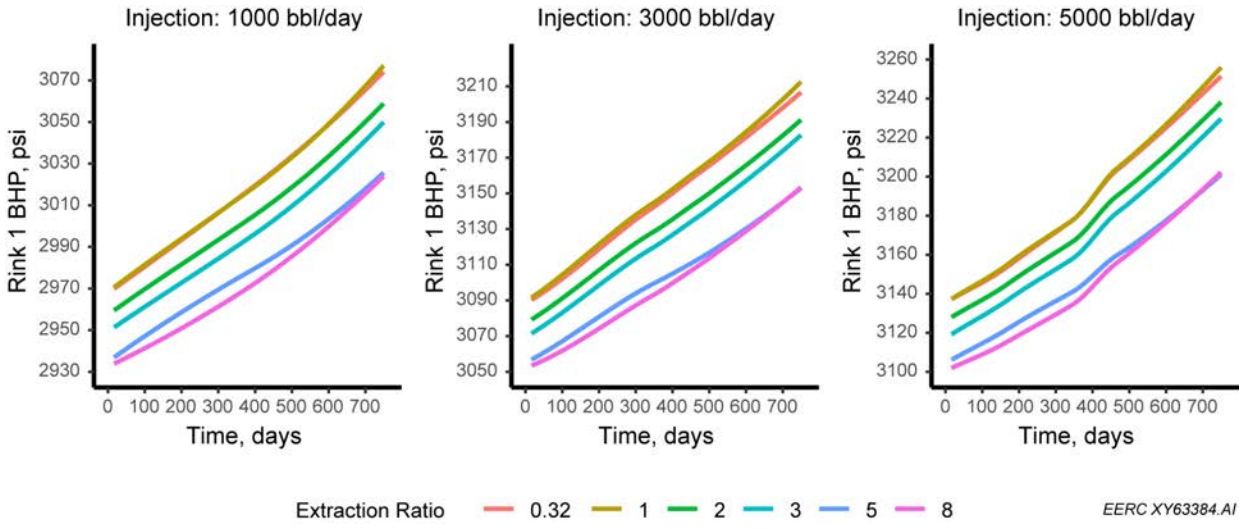


Figure 21. Effects of BEST-E1 production (expressed as extraction ratio) on the BHPs in the injection well at different stationary injection rates of 1000, 3000, and 5000 bbl/day.

Data-Processing Discussion

A large-scale geologic CCS project requires reservoir storage capacity, and the storage largely comes from the pore space in the reservoir and some minor effects from other parameters, including 1) pore size distribution including geometry and connectivity (Kashif and others, 2019); 2) dissolution of CO_2 into the native formation water (brine); 3) compressibility of the rock matrix (pore dilation); and 4) previous injectants such as CO_2 or brine. During the CCS injection activities, pressure increases can cause negative effects such as pore expansion, fluid compression (CO_2 and brine), and/or displacement of native brine into neighboring formations (Birkholzer and others, 2012). Many studies have been conducted to investigate brine extraction as an ARM approach for pressure reduction to enhance CCS efficiency (Birkholzer and others, 2012; Buscheck and others, 2014; Pongtepupathum and others, 2017). However, most of these studies focused on using reservoir simulations to simulate pressure responses and largely ignored the nuances of pressure perturbations from the nonstationary flow rates at both injection and production wells. The field monitoring data in this study provided a unique opportunity to evaluate the dynamics of pressure changes during the processes of injection and brine extraction to monitor pressure buildup. At the injection location, the reservoir pressure is directly related to the injection activities, while the other nearby injection/production activities showed only moderate impacts on the injection well BHP. Simmenes and others (2013) interpreted the increase of BHPs at the injection site as that the injected fluid cannot efficiently be displaced laterally instead of as having a storage space shortage. The bigger the plume is, the higher the required injection pressure to continue to push the pressure front farther away in an infinite reservoir. This interpretation can be further confirmed by the field observation at the BEST site that when there is no injection, the BHSIP remains at ~2900 psi over the 2-year period regardless of nearby injection/production activities. When there is injection, the BHPs at the same injection well increased steadily (about 100-psi increase) during the 2-year period. The overall time series of BHPs increased commensurately with the increase of injection

rates (about 30 psi per 1000 bbl/day, Figure 20), which suggests that the reservoir storage capacity has not been reached during operation time. The responses of the BHPs are more attributed to the propagation of brine flows.

The active production activities at a nearby location illustrate the concept of using brine extraction to reduce pressure buildup at the injection wells. In this study, an ML approach successfully determines injection pressure differences with and without extraction from a nearby production well based on field data, whereas simulation alone would have had a difficult time quantifying these relationships. The effect of production at a well around 400 m away can reduce the overall BHP at the injection well, and the magnitude of BHP reduction depends on the extraction ratio and the magnitude of injection rate. In this study, a 100-psi BHSIP increase during the life of the project was limited to only 50–70 psi by a production/extraction ratio of only 0.32. Starting at an ambient pressure of about 2900 psi, for an injection rate of 7000 bbl/day and no BEST-E1 production, the operating injection pressure would rise 90 psi, from 3160 to approximately 3250 psi, during the 2-year test period. If an extraction ratio of 1 were applied, the pressure would have risen only 55 psi to 3215 psi. Thus the extraction ratio of 1 successfully removed approximately 40% of the reservoir pressure increase. In the literature, pressure reduction as an effect of well production can be more evident because of a larger magnitude of extraction and a longer extraction time. Buscheck and others (2014) used a reservoir simulation approach to evaluate brine production effect on pressure relief and demonstrated that a brine producer can reduce two orders of magnitudes of pressure buildup during a time scale of 1000 years (from ~10,000 to ~100 psi). Gonzaléz-Nicolás and others (2019) suggested that adaptive ARM strategies by changing the frequencies of extraction ratio over time are more effective for pressure reduction than a static constant extraction ratio. In that study, limiting a pressure buildup to around 60 psi (0.4 MPa) via optimized injection rate updates could shorten the needed extraction time from 30 years to around 10 years.

Characterizing reservoir pressure using a reservoir modeling approach is often hindered by a lack of geologic data, variability of the hydrogeologic parameters such as permeability across the injection/production project area (Mohamed and others, 2011), and complex historical field operations data. In this work, an ML-assisted approach was employed to analyze the complex field monitoring data, and relationships of individual variables with the target variable BHPs were quantified using XGBoost models. ML models have the advantage of ignoring complex physical mechanisms during the injection/production processes while solely utilizing data to establish relationships. An ML approach can be employed to assimilate all available data for a 3D reservoir pressure forecast (Tang and others, 2022), as CCS projects often come with spatially sparse measurements because of high drilling costs. In future work, state-of-the-art ML approaches such as a U-Net convolutional neural network and a generative adversarial network can be leveraged with limited reservoir-modeling efforts to predict 3D pressure response and injectant plume by data assimilation and a surrogate modeling effort.

Data-Processing Conclusions

Based on ML prediction and data analysis, the following results were derived:

1. The time series of the flow rates and BHPs of the three wells (two injection wells and one production well) are highly nonstationary, which reveals the complex reservoir pressure behaviors under complicated injection and production processes.

2. ML models such as XGBoost can be used to make highly satisfactory predictions of BHPs based solely on the injection/production flow rates (with r^2 values in the training and testing datasets greater than 0.95).

3. Injection is the dominant variable to influence BHPs at injection wells. With injection activities, reservoir pressures at the two injection locations increase steadily, with an average pressure increase of 100 psi in the 2-year period.

4. Production activities have the ability to alleviate pressure buildup. Pressures can be reduced by around 30–50 psi for the injection well depending on different levels of extraction ratios, which is about 30% to 50% of the pressure buildup if there is no extraction.

5. An ML approach can be used to characterize and forecast reservoir pressure and help design an optimum ARM strategy to enhance CCS projects.

EVALUATION OF ARM ACTIVITIES

Geologic Model

A 6-mile × 6-mile geologic model of the site was developed to provide a basis for both interpreting collected field data and conducting predictive simulation analysis under a variety of test cases. The model was developed with Computer Modelling Group Ltd.'s (CMG's) GEM software (Computer Modelling Group Ltd., 2019) and incorporated both publicly available data and data collected from the site during the installation of BEST-E1 and BEST-I1 (Figure 22). Structural features of the Inyan Kara Formation were interpreted from local and offset well log interpretations, and a facies property was developed and distributed. Porosity, permeability, and other relevant reservoir data were derived from available core and log data from the site and offset wells and incorporated into the modeled facies (Hamling and others, 2016). Open model boundaries were used to emulate the excellent regional permeability and porosity of the Inyan Kara Formation.

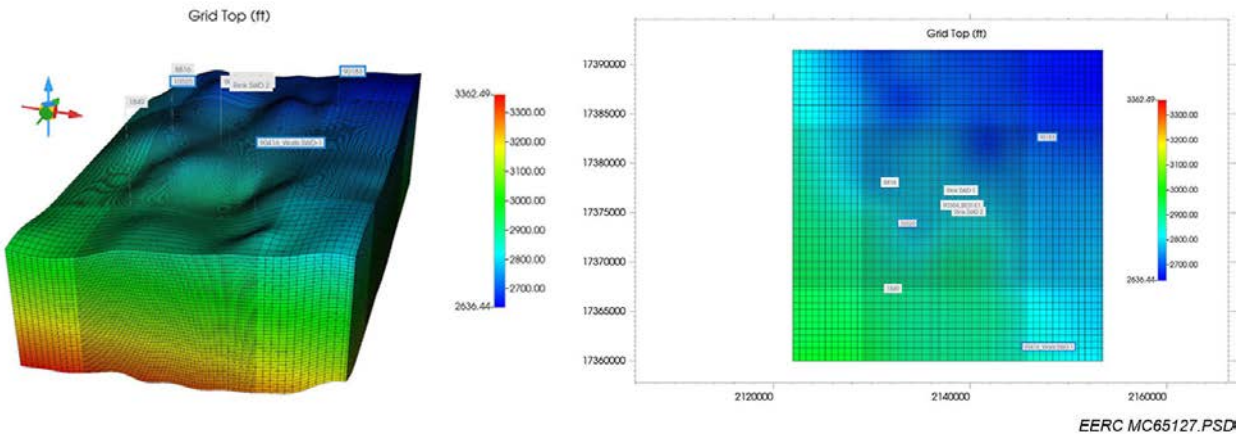


Figure 22. 3D view of the simulation model (top) and 2D aerial view of the top horizontal layer (bottom) of the Inyan Kara Formation.

History Matching

Long-term injection and production operations were conducted from November 13, 2020, to June 28, 2021. The purpose was to closely monitor the interaction between the two injection wells (Rink SWD #1 and Rink SWD #2) and the production well (BEST-E1) to evaluate any well connectivity. Daily and instantaneous rates were downloaded from the SCADA system. The gathered data were compiled and processed into a simulation-friendly input format for the purpose of history-matching the simulation model to reproduce pressures and flow rates recorded from the field.

The process of converting the SCADA data involved compiling each month's SCADA data into a single spreadsheet. BHP and flow rate data were recorded at 1-second intervals. Trying to history-match the data to the degree of every few seconds would be very difficult because of how "noisy" the data are at that scale. The daily averages were calculated and imported into CMG GEM as a field history files (.fhf). The finalized field history file contained the water rate (bbl/day) at surface conditions, BHP (psi), and on-time fraction to account for wells not operating a full 24 hours for Rink SWD #1, Rink SWD #2, and BEST-E1. The gathered data used for history-matching covered the operation period of June 3, 2019, through April 23, 2021. The operational period occurred through June 2021, but to history-match to such detail because of the highly varied injection schedule proved too difficult. The data were instead analyzed using XGBoost.

In the process of importing the field history files and verifying the simulation model, an additional nearby injection well was identified. Well #10525 was initially drilled as a production well in the Madison group, but failure to produce after the early 1990s led to the well being temporarily abandoned. In 2012, the well was converted into a SWD well in the Inyan Kara and started injecting wastewater in July 2013. Early attempts to history-match BEST-E1's BHP from the acquired field data failed to provide a match within the acceptable margin of a 5% global history match error. Updating the model with Well #10525's injection history provided the necessary pressure influence to achieve an acceptable BHP match. Because only monthly injection

totals were available from public data sources, there are still some uncertainties about the daily injection schedule, thus providing additional challenges when finding the optimal simulation solution.

The process of history-matching the simulation model with the updated field model involved running a sensitivity analysis to identify the most significant parameters on the BHPs of the three wells, Rink SWD #1, Rink SWD #2, and BEST-E1. Table 11 shows all the varied parameters and their multipliers used to observe the potential impacts on BHP responses.

In Table 11, BEST-E1, Rink SWD #1, and Rink SWD #2 Perm Mod represents the modification to the local permeability in the surrounding cells. The BEST-E1 well additionally varied the size at which the permeability modification was applied. North, south, east, and west boundary volume modifications are the boundary conditions that determine if the reservoir is infinite acting in a given direction or if the formation may pinch out, thus having limited aquifer support. It also controls the influence of water influx from the externally acting aquifer on the modeled area.

Table 11. Sensitivity Analysis Parameters

Parameter Name	Default Multiplier Value	Lower Limit	Upper Limit
BEST-E1 Perm Mod	2.8	1	4
BEST-E1 Max Perm Mod in I Direction	70	60	69
BEST-E1 Min Perm Mod in I Direction	50	51	60
BEST-E1 Max Perm Mod in J Direction	70	60	69
BEST-E1 Min Perm Mod in J Direction	50	51	60
Well #10525 Perm Mod	0.45	0.1	0.9
Rink SWD #1 Perm Mod	2.8	2	4
Rink SWD #2 Perm Mod	0.45	0.1	0.9
North Boundary Volume Mod	100	75	125
South Boundary Volume Mod	30	22.5	37.5
East Boundary Volume Mod	50	37.5	62.5
West Boundary Volume Mod	100	75	125

The sensitivity analysis results using the range of parameters in Table 11 show that volume modifiers along the southern and western boundaries have the most significant impact on BEST-E1's BHP (Figure 23). The permeability modification to the cells surrounding Rink SWD #2 has the third most significant impact on the BHP response in BEST-E1. The permeability modifier for Well #10525 "NewWell" also has a noticeable impact on BEST-E1's BHP, explained by the difficulties in history-matching when Well #10525 was not included. Increasing the area of the permeability modification surrounding BEST-E1 to the north and west had some minor influence. The remaining parameters that were varied in the sensitivity analysis ultimately have a negligible impact on BHP response.

Figure 23 shows that modifications to cells south and west of BEST-E1 have a stronger influence, suggesting that these cell regions have increased connectivity and are impacted by water injection/production operations, specifically Rink SWD #2 injection.

For the areas surrounding Rink SWD #1 and Rink SWD #2, results show that the permeability modifiers have the two largest impacts on BHP response on Rink SWD #1 (Figure 24), increasing the modified area around BEST-E1 further north and the volume modifier along the western model boundary. Additionally, the actual permeability modification of the BEST-E1 well has a noticeable impact. The remaining parameters have negligible influence on the BHP of the Rink SWD #1 well.

The Rink SWD #2 sensitivity analysis results show that this Rink SWD #2 is less impacted by the specified parameters (Figure 25). Largely, varying permeability surrounding Rink SWD #2 has the strongest impact, followed by the permeability surrounding Well #10525 "NewWell." Like the other two wells, the volume modifier for the western boundary has a significant influence.

Together, Figures 23–25 demonstrate that there is well connectivity among these four wells, BEST E1, Rink SWD #1, Rink SWD #2, and Well #10525.

After specifying the lower and upper value limits, as shown in Table 11, CMOST generated 91 unique simulation combinations to find the best set of parameters that generate BHP responses as accurately to the pressures gathered from the field gauges. A global history match error of 5% was applied to the BHPs of the three wells to force the central processing unit to calculate more accurate solutions that will be acceptable as a match.

From the 91 unique simulations, CMOST was able to solve the right combination of parameters that provided the best match solution, with a global history match error of less than 5%. Figure 26 illustrates BHP responses of the BEST-E1 well observed from altering all of the specified parameters.

Figures 27 and 28 show BHP response observed throughout the history-matching process. Constant shutting in and opening of the wells and lack of daily data for Well #10525 resulted in difficulties in capturing their behaviors precisely, but the global history match error of 5% for each of the wells still provides an acceptable match for further analysis.

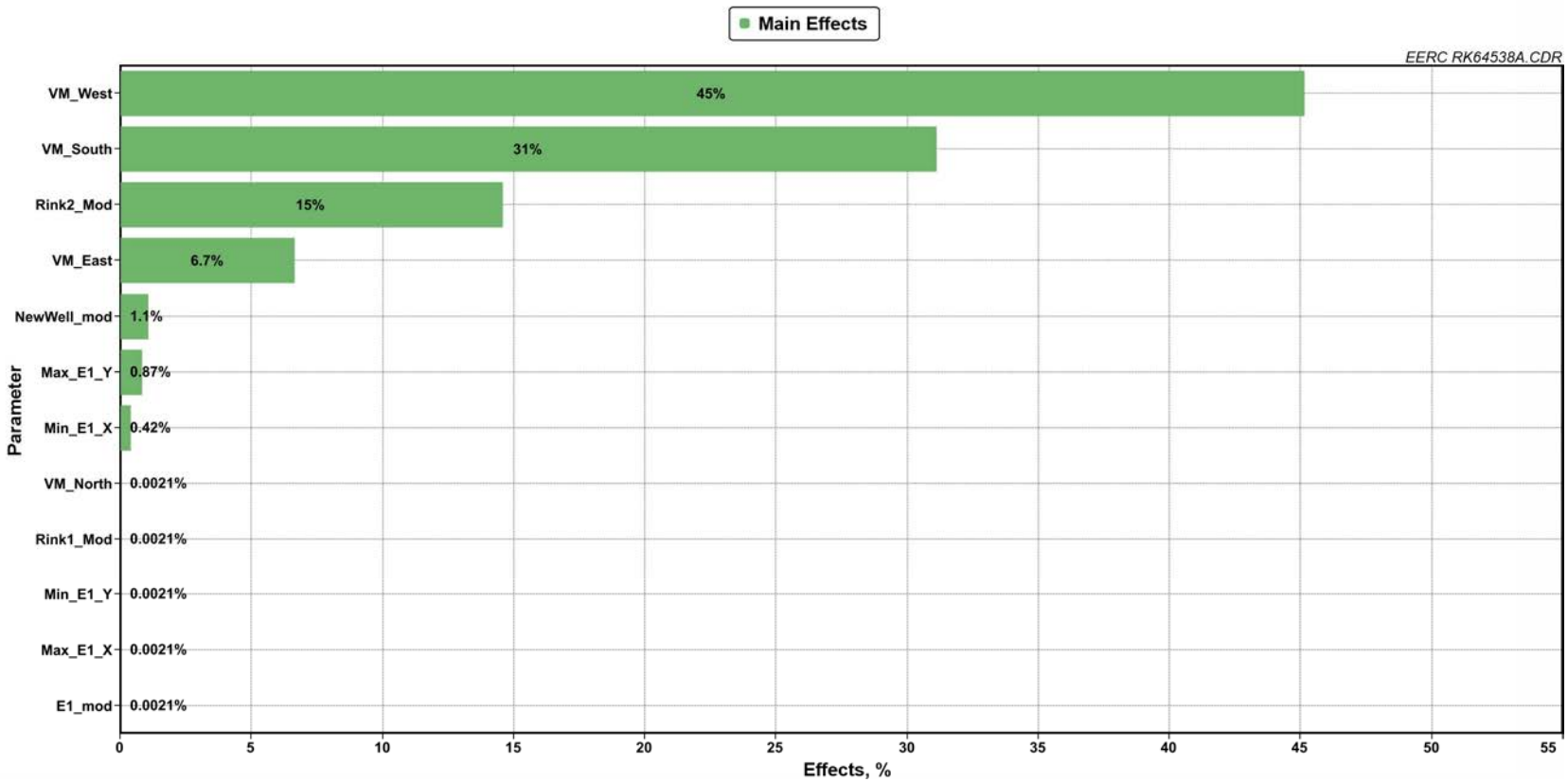


Figure 23. BEST-E1 sensitivity analysis results.

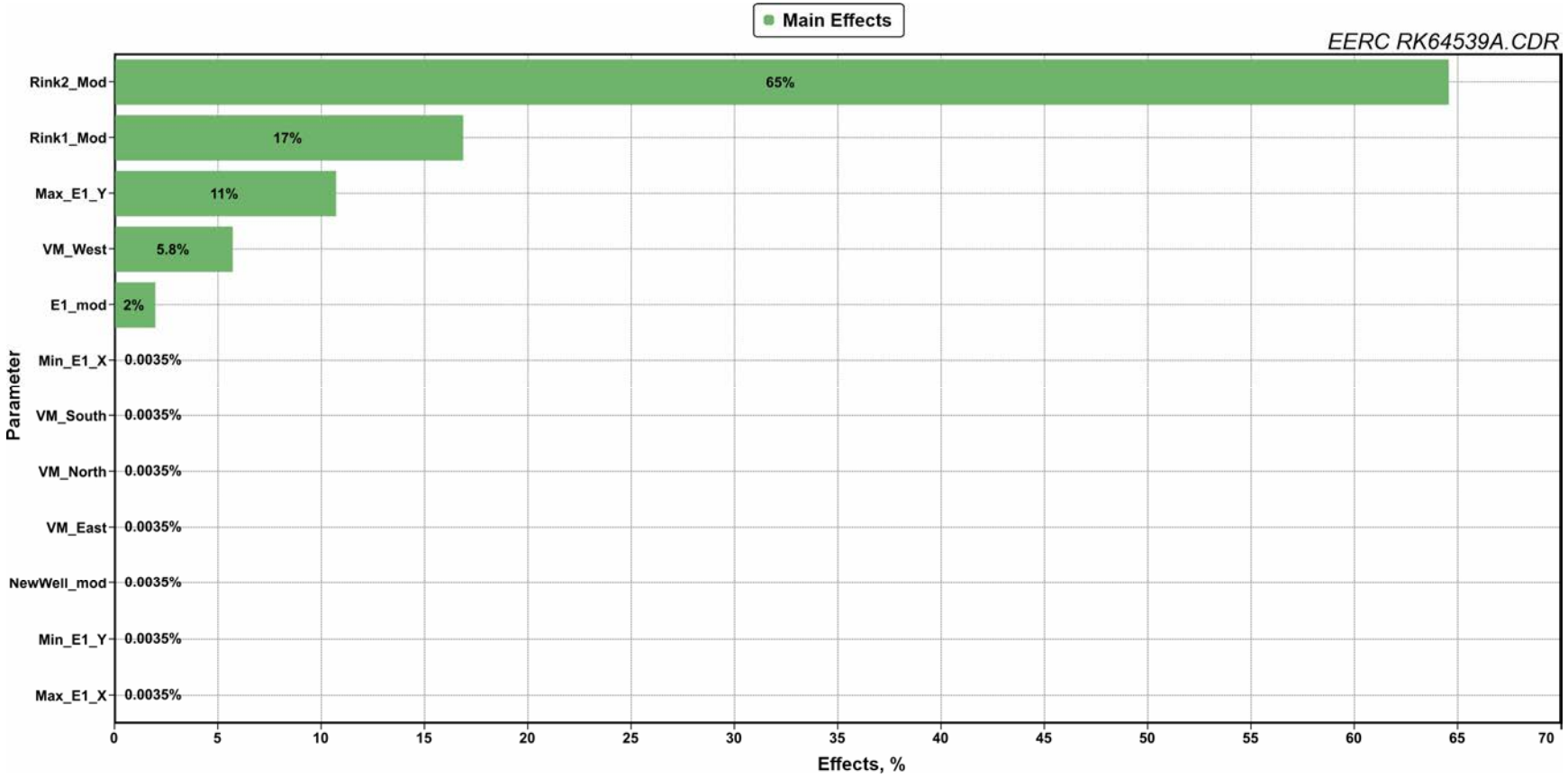


Figure 24. Rink SWD #1 sensitivity analysis results.

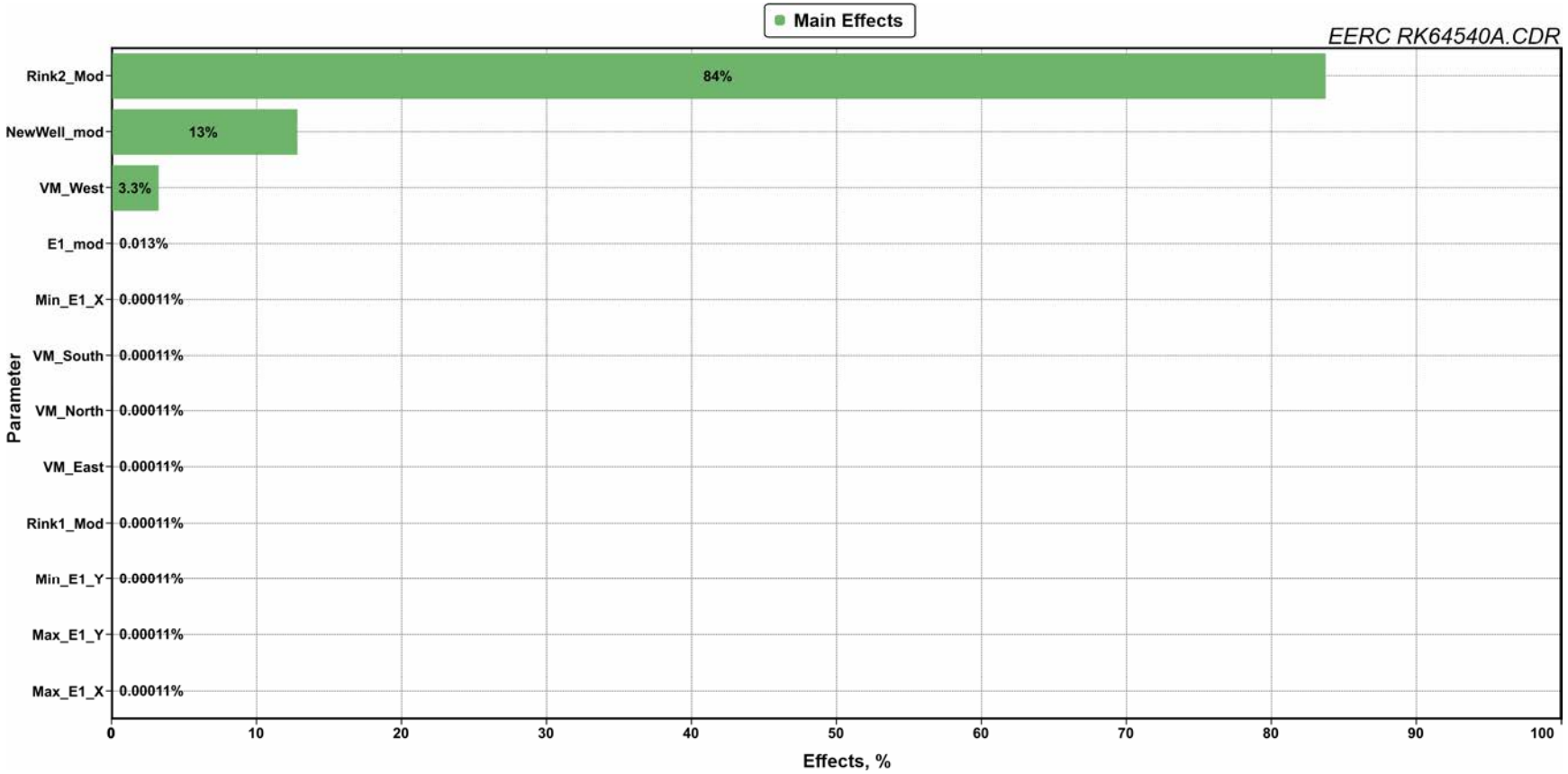


Figure 25. Rink SWD #2 sensitivity analysis results.

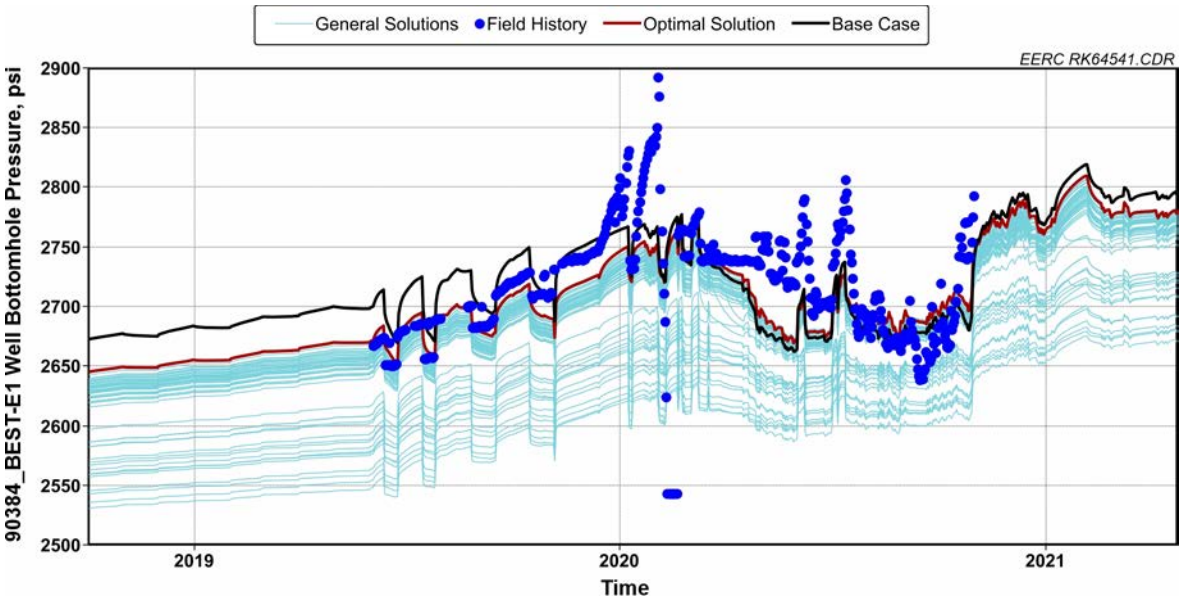


Figure 26. BEST-E1 BHP responses. Blue circles represent calculated daily averages gathered from the field. Black line represents initial simulation case for remaining cases to be modeled. Light blue lines represent all 91 unique simulations, with red line highlighting best match.

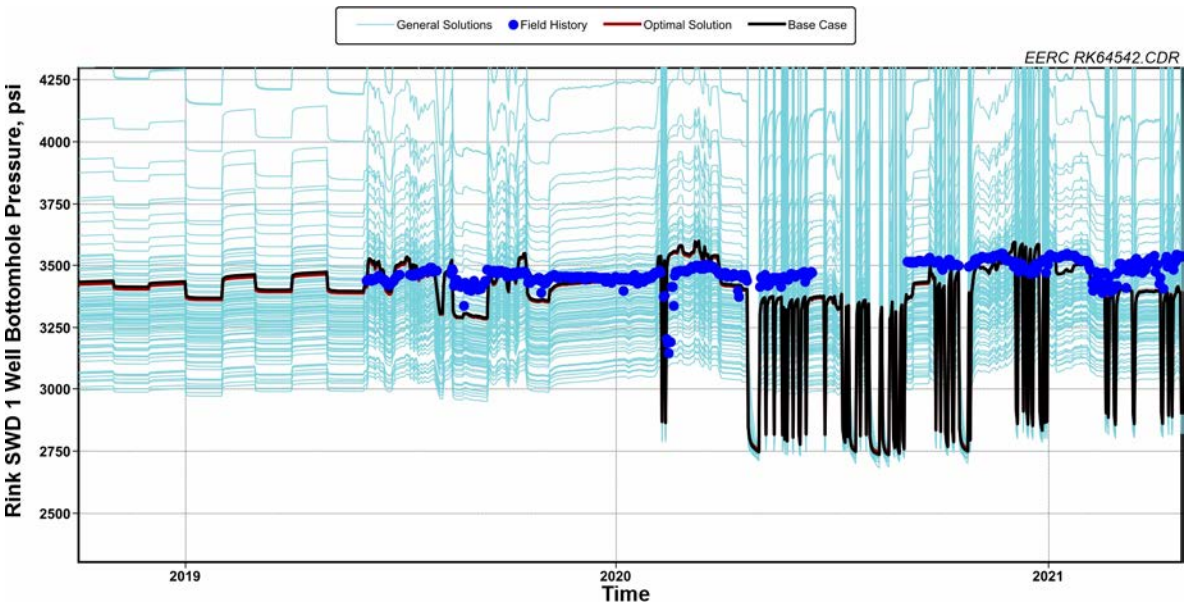


Figure 27. Rink SWD #1 BHP responses. Blue circles represent calculated daily averages gathered from the field. Black line represents initial simulation case for remaining cases to be modeled. Light blue lines represent all 91 unique simulations, with red line highlighting best match.

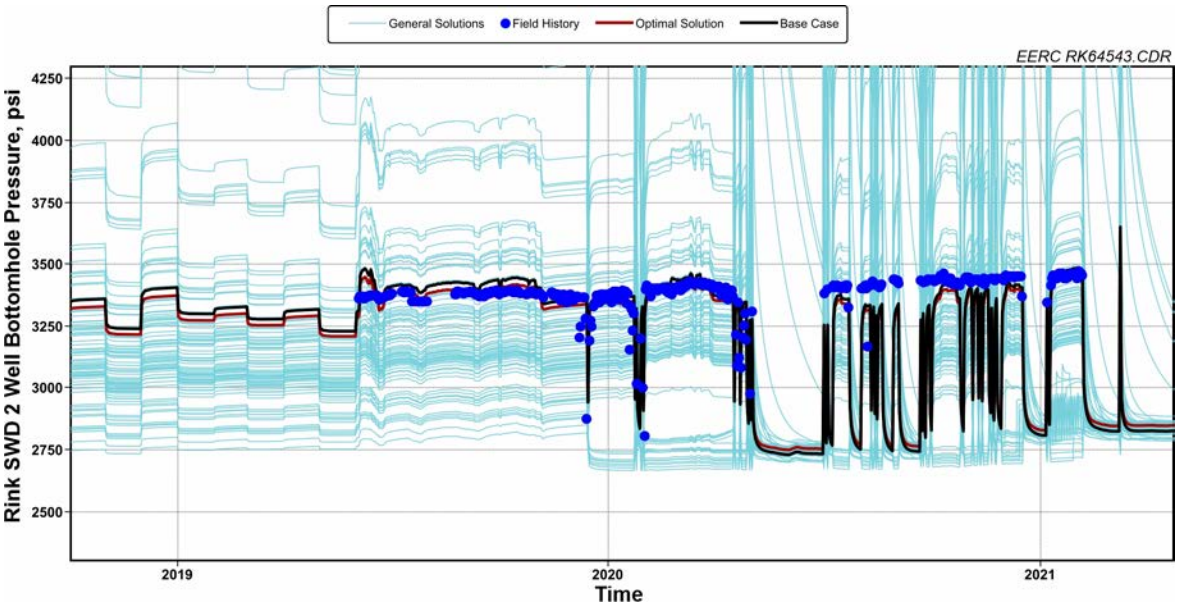


Figure 28. Rink SWD #2 BHP responses. Blue circles represent calculated daily averages gathered from the field. Black line represents initial simulation case for remaining cases to be modeled. Light blue lines represent all 91 unique simulations, with red line highlighting best match.

Case ID No. 51 out of 91 was determined by CMOST to be the optimal solution to history-matching all three wells' BHPs to what was gathered and converted in daily averages from the field using the imported production and injection daily average rates. From the initial set of parameters defined for the history-matching process (Table 11), the optimal set of parameters are shown in Table 12.

Table 12. Sensitivity Analysis Parameters with Optimal History Match Solution

Parameter Name	Default Multiplier Value	Lower Limit	Upper Limit	Optimal Multiplier Solution
BEST-E1 Perm Mod	2.8	1	4	3.775
BEST-E1 Max Perm Mod in I Direction	70	60	69	63
BEST-E1 Min Perm Mod in I Direction	50	51	60	53
BEST-E1 Max Perm Mod in J Direction	70	60	69	64
BEST-E1 Min Perm Mod in J Direction	50	51	60	59
Well #10525 Perm Mod	0.45	0.1	0.9	0.292
Rink SWD #1 Perm Mod	2.8	2	4	2.73
Rink SWD #2 Perm Mod	0.45	0.1	0.9	0.464
North Boundary Volume Mod	100	75	125	107.75
South Boundary Volume Mod	30	22.5	37.5	25.275
East Boundary Volume Mod	50	37.5	62.5	40.25
West Boundary Volume Mod	100	75	125	102

CO_2 ARM Simulation

Taking the lessons learned from ARM in an SWD simulation and the updated geological simulation model, CO_2 simulation scenarios were created to analyze the applicability of ARM in CO_2 storage using a simulation model that is history-matched to an occurring SWD operation. The main objectives were to 1) increase the total amount of CO_2 injected and 2) geosteer/contain the CO_2 plume.

The simulation model was updated with a relative permeability curve to account for the two-phase simulations caused by CO_2 injection. The rock property represents a typical sandstone that is referenced from literature (Figure 29).

Table 13 shows the general properties of the best history-matched numerical reservoir simulation that was modified to study CO_2 ARM practices.

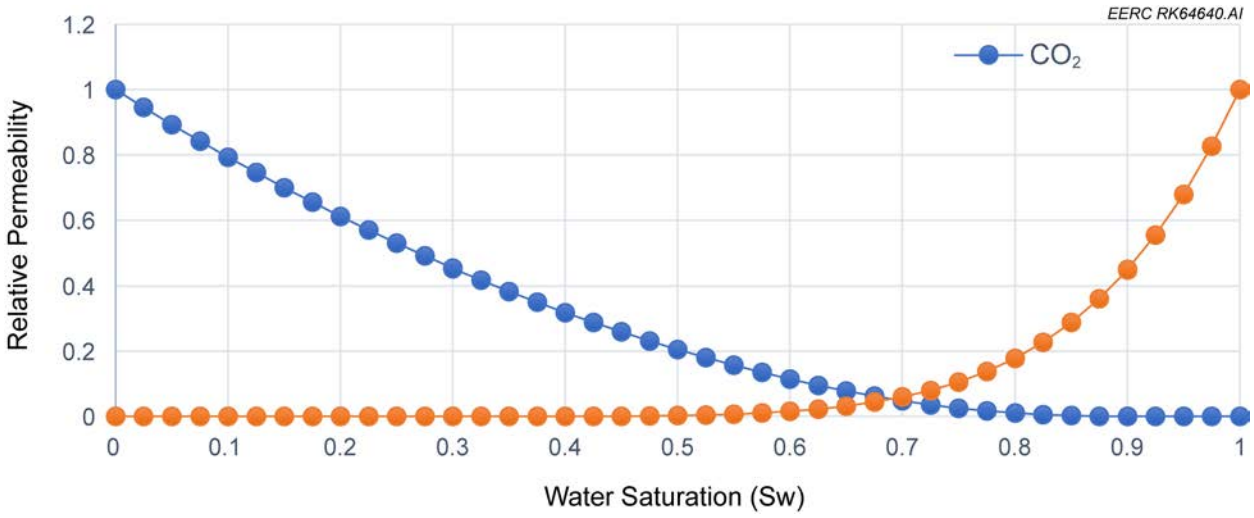


Figure 29. Relative permeability curve for the common occurrence of sandstone in the Inyan Kara Formation.

Table 13. Summary of Reservoir Properties in the Simulation Model

Average Permeability, mD	Average Porosity, %	Initial Pressure, P_i, psi	Salinity, ppm	Boundary Condition
Inyan Kara: ~293.40	Inyan Kara: ~23.53	~2335 (at 3000 ft TVDSS[1])	10,000	Open

[1] True vertical depth subsea.

CO_2 ARM Simulation Results

The field-derived, history-matched model was used to simulate and test a variety of hypothetical CO_2 injection scenarios on the site. The evaluation focused on how formation fluid extraction can increase total CO_2 storage capacity, prolong increased storage performance, geosteer injected fluids, and enhance CO_2 dissolution and storage. The initial set of simulations was used to ascertain the scale of impact that brine extraction can have on CCS performance in relation to positioning of extraction wells relative to injection wells and injection/extraction rates. Parameters that proved most influential on BHP response included permeability near extraction and injection wells, influence of the offset injection well, and modeled boundary conditions and permeability modifiers.

Simulated injection rates were set equivalent to 1 MMt/yr of CO_2 injected at reservoir conditions. Volumetric extraction ratios (volume extracted to volume injected) of 1:1, 3:4, 1:2, and 1:4 were evaluated using two simulated injection wells with one extraction well. (The ratio of injection to production volume is calculated from the volume of 1 MMt of CO_2 at initial reservoir conditions and its equivalent volume of water.) The offset distances for the extraction wells were varied in half-mile increments from 0.5 to 2.5 miles, and the extraction wells were shut in when breakthrough was observed. This resulted in 20 test cases for evaluation.

Figure 30 illustrates how the production well, when producing at a 1:1 ratio, can completely offset the pressure increase because of the CO_2 being injected. Wells that are less than 2 miles from the injection wells can offset the pressure increase for a short time, but once CO_2 breakthrough occurs and the well shuts in, the reservoir pressure increases at the same rate as if there were no extraction operations. Wells that are 2 and 2.5 miles away are able to maintain a 1:1 extraction ratio without CO_2 breakthrough occurring but are still close enough to offset the reservoir pressure increase from CO_2 injection.

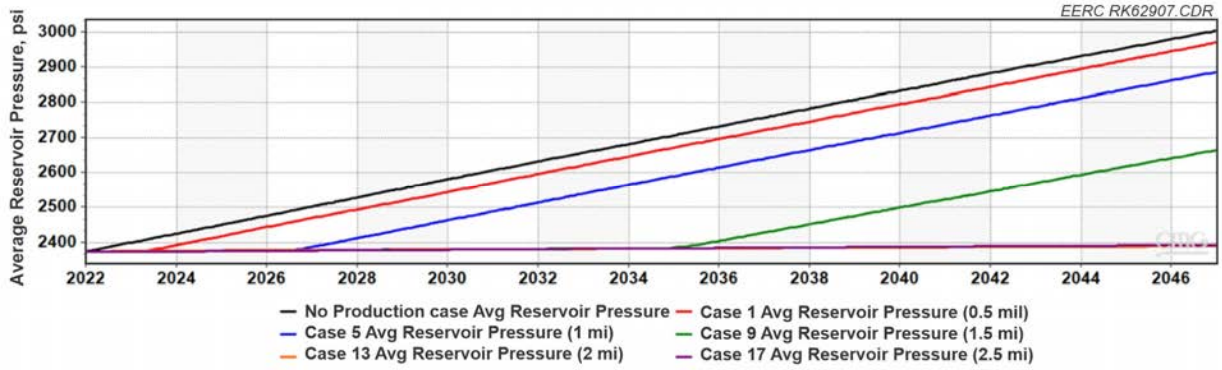


Figure 30. Average reservoir pressure trend of the entire simulation model during 25 years of CO_2 injection. Kickoff points where pressure begins to increase indicate the point of CO_2 breakthrough in the production well and the shut-in of the well.

If the evaluation is adjusted to maximize the injection rates (by setting injection to run at <90% of downhole fracture pressure), a clearer trend can be observed. The extraction and injection rate constraints are set at surface conditions. Once again, the extraction well was set to shut in once CO_2 was detected. Simulation was set for 25 years with 1 MMt of CO_2 injected per year split between the two injection wells.

Injection and extraction rates maintain constant flow throughout the 25-year simulation because they are set at surface conditions. This means there is no observed increased CO_2 injection as it is a constant 1 MMt at the surface for all the cases. There were no observed cases where the injection wells shut in because of the reservoir pressure exceeding the maximum BHP constraint. Reservoir pressure increases are significantly lower as a result of extracted water alleviating some of the reservoir pressure increase from the CO_2 injection. Figure 31 shows that in the simulation cases where well separation is at 2.5 miles, with a 1:1 extraction-to-injection mass ratio at surface conditions, the overall average reservoir pressure increase can be reduced by 16%.

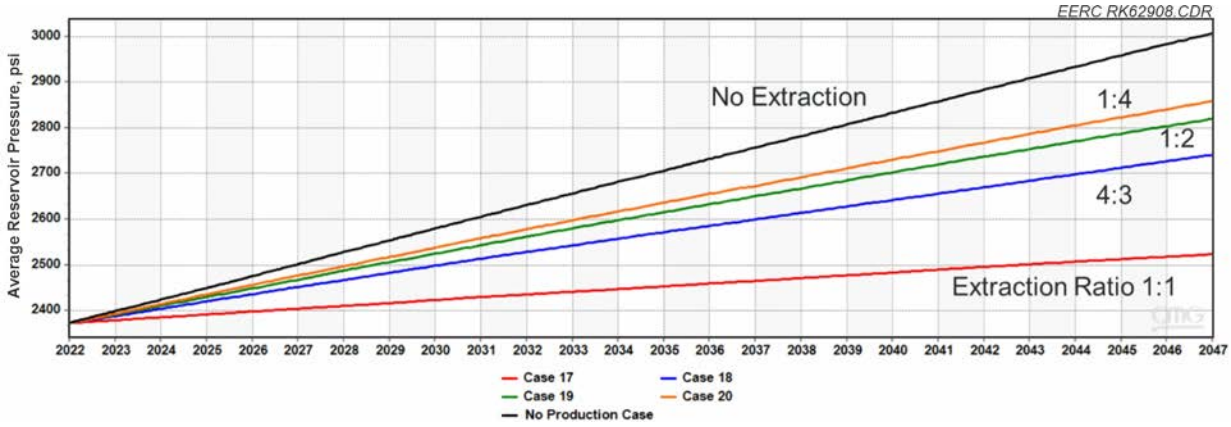


Figure 31. Average reservoir pressure response to 1:1 injection-to-production ratio at the five different distances.

When considering extraction well spacing, wells within a half-mile have a consistently strong impact on the amount of CO_2 that can be injected, as their close proximity allows for early pressure relief that translates into increased storage potential post-CO_2 breakthrough (Table 14).

The most optimal solution for this model was a single extraction well extracting 10,000 bpd located 2 miles between two injection wells. The 2-mile separation is highly sensitive to the production rates, as a 7500-bpd difference can have a 20% impact on the cumulative total of CO_2 that is stored over the 25-year simulation span. Once the distance between the wells is 2.5 miles or more, the influence begins to decline, resulting in less efficient injection/production until ultimately production has no impact on injection behavior. Figure 32 shows the diminishing influence when the distance between the injection wells and production wells is increased while maintaining the same constant 10,000-bpd extraction rate.

Table 14. Simulation Cases with Cumulative Injected CO_2 Results and Percentage Increase of Total CO_2 Compared to the Simulation Without Any Extraction

Case No.	Extraction Rate, bpd	Distance, miles	Cumulative CO_2, MMt	Increased CO_2 Injection, %
1	2500	½	52.9	114
2	5000		53	114
3	7500		53.2	115
4	10,000		52.3	116
5	2500	1	52.53	112
6	5000		52.43	112
7	7500		52.61	113
8	10,000		52.64	113
9	2500	1.5	51.3	108
10	5000		51.9	110
11	7500		52.75	113
12	10,000		50.33	104
13	2500	2	49.85	102
14	5000		51.76	109
15	7500		53.56	117
16	10,000		54.92	122
17	2500	2.5	42.23	71
18	5000		43.65	77
19	7500		45.33	83
20	10,000		46.58	88

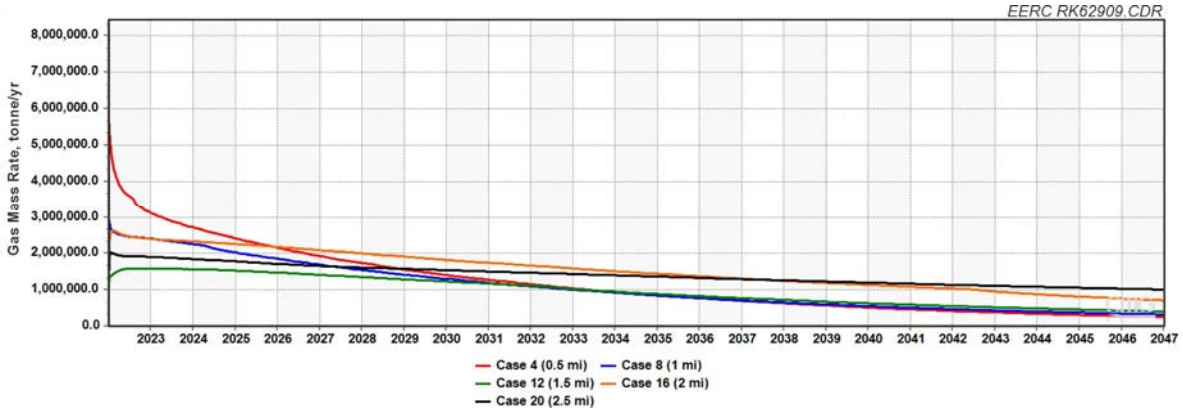


Figure 32. CO_2 mass injection rate over 25 years of injection for cases with a 10,000-bpd extraction rate from the injection well.

Cases that have the wells closer together see greater initial injection rates during the first several years. Over 25 years of injection, these cases have a larger change in injection rates, making them highly varied and dependent on when CO_2 breakthrough occurs. For cases that are further out, a steadier injection rate is observed, as the impact from the extraction wells is not as swift.

Hence, changes in extraction gradually affect injection behavior, resulting in a more manageable injection schedule.

Geosteering

Conceptual tests of geosteering were conducted by first applying a five-spot production well pattern to the model with one central injection well, constrained to a 1-MMt/yr injection rate with a maximum BHP of <90% fracture propagation pressure. The four production wells were located diagonally 1 mile and 2 miles from the injection well, and simulations were run for 25 years. Water production rates varied for the different cases, and production wells were shut in once CO_2 breakthrough occurred. Extraction ratios were set to 1:4, 1:2, 1:1.3, and 1:1 of the equivalent injected CO_2 at surface conditions.

All cases were able to inject 1 MMt/yr for 25 years without issue. All cases run with 1-mile well spacing showed CO_2 breakthrough ranging from 4.5 to 15 years. Cases with 2-mile separation did not show any CO_2 breakthrough in the 25 years of simulation. At 2 miles of distance, water extraction needed to be increased to 3 to 4 times CO_2 injection rates to trigger breakthrough and shut-in during the 25-year simulation.

Figure 33 illustrates a maximum case of production well effect on geosteering plume migration compared to the simulation without production. CO_2 is observed to migrate toward all four extraction wells, reducing the overall concentration of the plume as it spreads faster because of the increased hydrodynamic flow within the reservoir. This process increases plume mixing and reduces cap rock stress (by reducing reservoir pressure). At lower extraction rates, the CO_2 plume shows movement toward the naturally higher permeability zones present in the southwest and northwest quarters of the model.

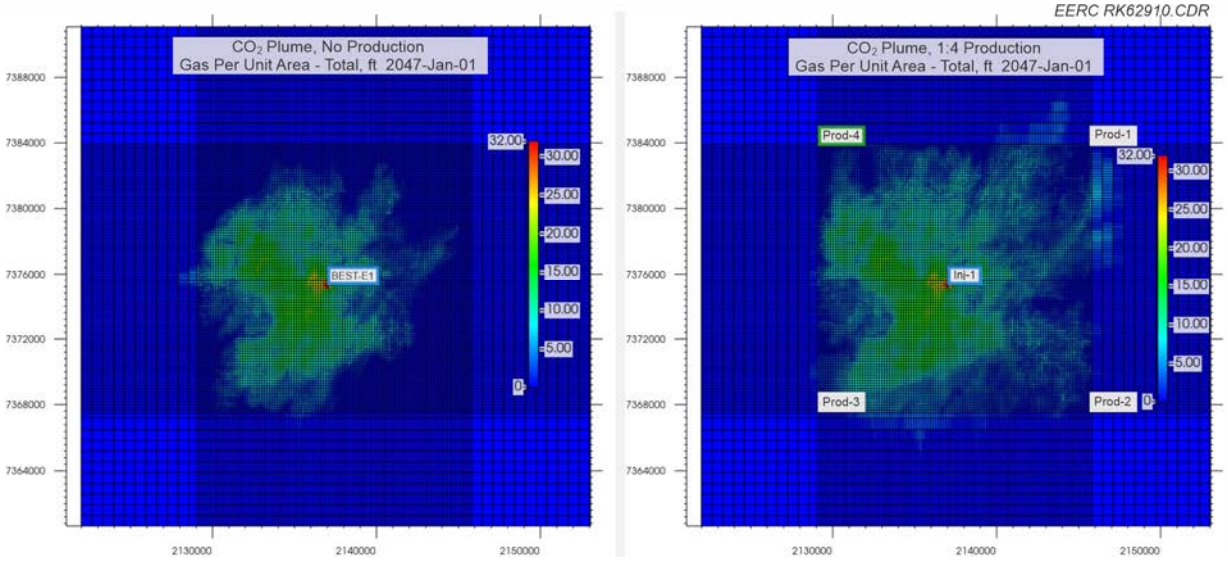


Figure 33. CO_2 plume migration viewed as gas per unit are total in all vertical layers. Left: simulation without production. Right: simulation with 4:1 ratio of extraction to injection.

Five-spot pattern extraction could also be applied in instances where reservoir pressure is a factor limiting injection capacity. Even the lowest tested extraction rate in the five-spot pattern (a 1:4 extraction ratio) showed a ~50-psi drop at the injection wellbore. Several-hundred-psi drops were achieved with aggressive extraction ratios.

Linear Geosteering

To take advantage of the high-permeability zone in the southwest quarter of the modeled area, a linear well placement pattern for geosteering was developed. Two extraction wells were placed in a line diagonally away from the injection well. One extraction well was placed 1 mile away, while the second extraction well was placed 2 miles away. The closest extraction well will immediately influence the CO_2 plume during the first few years until CO_2 breakthrough occurs. The second extraction well will continue to draw CO_2 toward the southwest after the first extraction well shuts in.

The injection well was able to maintain a rate of 1 MMt/yr throughout all iterations of this test. Breakthrough was observed in the near extraction well (1-mile distance) within the first 2–4 years of operation. For the second extraction well, 2 miles away, breakthrough occurred in 14 years under a 2:1 extraction ratio and 20 years under a 1:1 extraction ratio. As a result of the extraction wells placed in the same direction, the CO_2 plume was pulled further along in the southwest direction (Figure 34). Unlike the five-spot pattern scenario, CO_2 did not further distribute within the modeled area. The linear pattern channeled the CO_2 along the line of extraction wells, while the other portions of the plume are minimally impacted compared to the nonextraction base case.

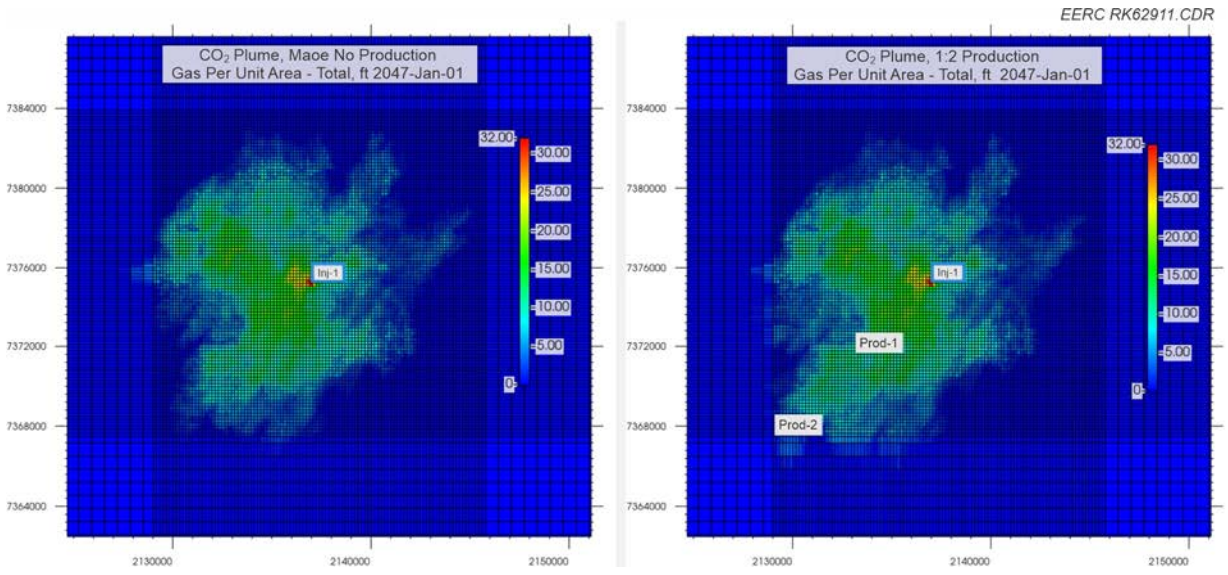


Figure 34. CO_2 plume migration viewed as gas per unit are total in all vertical layers. Left: simulation without production. Right: simulation with 1:2 ratio of injection to production.

Water Injection Over CO_2

An interesting special case of extraction testing is the use of water injection to enhance mixing and dissolution of injected CO_2 by injecting water directly above the CO_2 (Figure 35). The injected water is produced from an offset production well outside the extent of the CO_2 plume. This helps mitigate the additional pressure buildup from the water being injected above and along with the CO_2. The offset extraction also acts as the source of water for the system.

Results show that water injection over CO_2 spreads out the CO_2; the gas concentration within the larger plume is significantly lower than the cases without any water injection/production (Figure 36). The added benefit of injecting water over CO_2 is the trapping mechanisms. The added water enhances geochemical interactions that permanently trap the CO_2 and prevent additional migration of free-phase CO_2. Figure 37 shows a slight increase in the amount of CO_2 that is trapped during injection and leads to a significant increase during the postinjection phase.

The resulting CO_2 plume from a water-over-CO_2 injection scenario is significantly more diffuse than the base case and could be demonstrated to have a lower risk profile during injection. Furthermore, such a plume could be able to reach long-term stability in a much shorter time than a typical CO_2 injection program, illustrated by the base case plume. These changes could significantly reduce monitoring and site operations costs for a CO_2 storage operator. However, the added water injection causes an increase in the reservoir pressure locally around the site of injection compared to the base case without water injection, a factor that would need to be considered before pursuing this option.

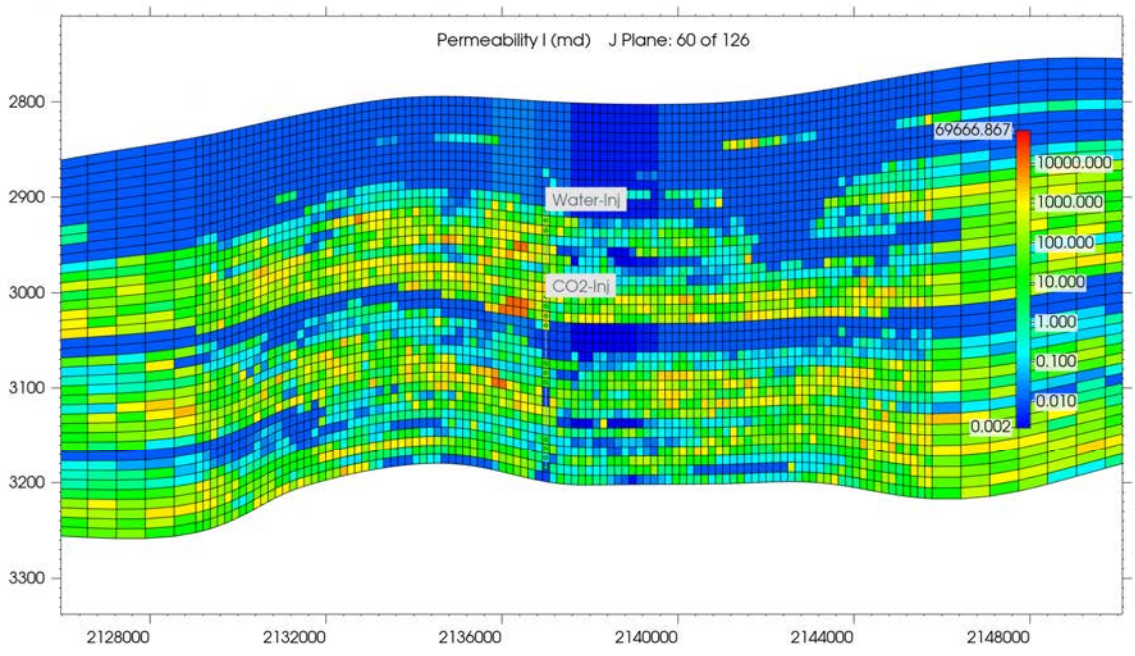


Figure 35. 2D cross-sectional view of well placement pattern for the water-over-CO_2 injection simulation tests.

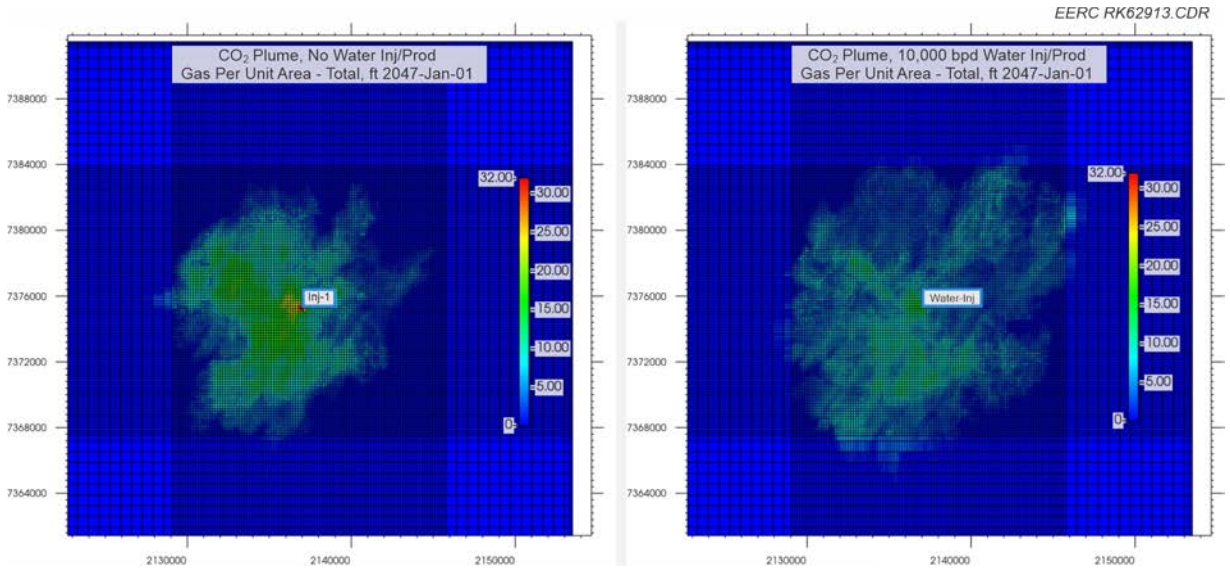


Figure 36. CO_2 plume migration viewed as gas per unit are total in all vertical layers. Left: simulation without water injection/extraction. Right: simulation with 10,000-bpd water injection/extraction.

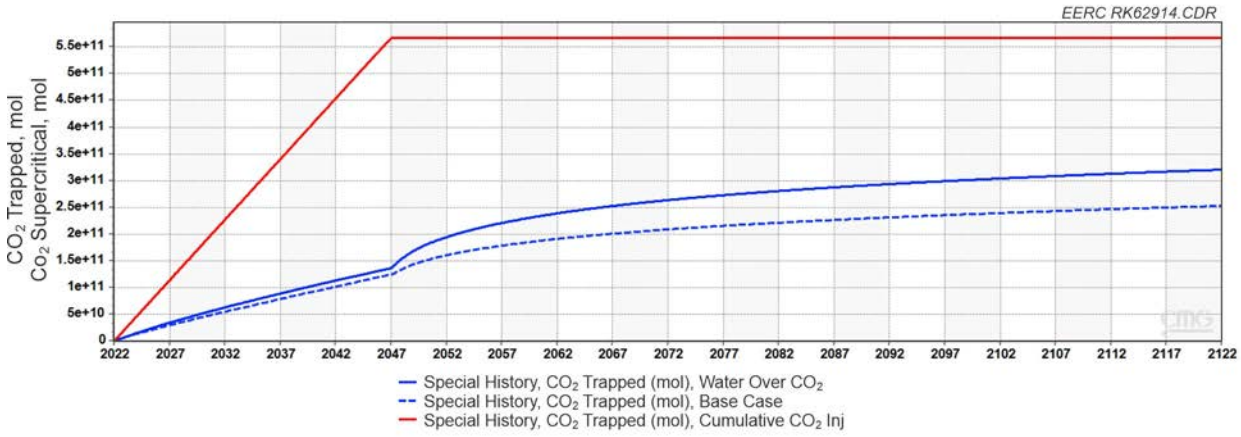


Figure 37. Trapped CO_2 over time. Red line represents cumulative total of CO_2 injected. Blue lines represent trapped CO_2. The difference between the red and blue lines is the amount of mobile CO_2.

Discussion

Water extraction has an effect on CO_2 injection. The main effect it has on the reservoir is offsetting the increased pressure as a result of CO_2 injection. This is useful in overpressurized reservoirs or if future pressurization could cause problems, water production can help alleviate a significant amount of pressure.

Geosteering can be observed but is influenced by several factors. Boundary conditions are one factor that must be considered as they have a large influence on the simulation. Because the model contains open boundaries, aquifers beyond the modeled area resupply portions of the produced water, offsetting some of the effectiveness the production wells have on geosteering. This shows that low production rates have minimal effect on the plume and not until significantly larger production are more noticeable changes observed. Additionally, because the model is not homogeneous, permeability distributions affect the flow of CO_2, as observed with the low permeabilities to the northeast and higher permeability to the southwest of the model, and that is where the CO_2 plume migrates. Permeability distribution is also important because the influence from a single production well propagates radially and must be channeled in a single direction to be more effective.

Ultimately, the heterogeneity of the model results in difficulties in trying to use a generalized approach with set well placement patterns or set injection/production ratios. Production wells must be placed in nonconforming patterns to work around the heterogeneity of the permeabilities to be in the most optimized position to steer the CO_2 plume. A project must also be willing to produce large amounts of water to see the significant influence on the plume.

Injecting water over CO_2 provides a safer method that limits the amount of mobile CO_2 and leads to quicker trapping of CO_2. The addition of a brine production well provides a water source for the water injection well and allows for active reservoir pressure management, resulting in an increase in CO_2 storage capacity. Without the brine production well, BHP of the injection wells will quickly reach the maximum BHP constraints, limiting the total amount of CO_2 which may be injected. The water injection directly above the CO_2 injection site provides a barrier between the cap rock and the CO_2 plume, protecting against any possible unintended vertical CO_2 migration where the pressure is the greatest.

Scaled-Up Model

The original geologic model underwent a significant expansion, resulting in an augmentation of the modeled area dimensions from a 6-mile × 6-mile grid to a 30-mile × 30-mile grid (Figure 38). The objective of this modification was to facilitate the implementation of more wells at higher injection rates, a task unattainable within the confines of the smaller model. The enhanced size of the model provided greater volumetric capacity for the pressure buildup from CO_2 injection, thereby increasing the maximum achievable injection rate.

The facies distribution within the reservoir underwent an extension by adhering to the same training image pattern utilized in the initial 6-mile × 6-mile model while incorporating supplementary well logs to encompass the expanded area. In terms of petrophysics, all settings, variogram lengths, and other parameters remained identical to those employed in the original model. However, it should be noted that slight discrepancies exist in the permeability and porosity properties. These variations are essential to account for the amplified geologic coverage spanned by the model. The enlargement of the study area introduces potential alterations in geologic characteristics such as rock type, lithology, and depositional environment, thereby impacting the

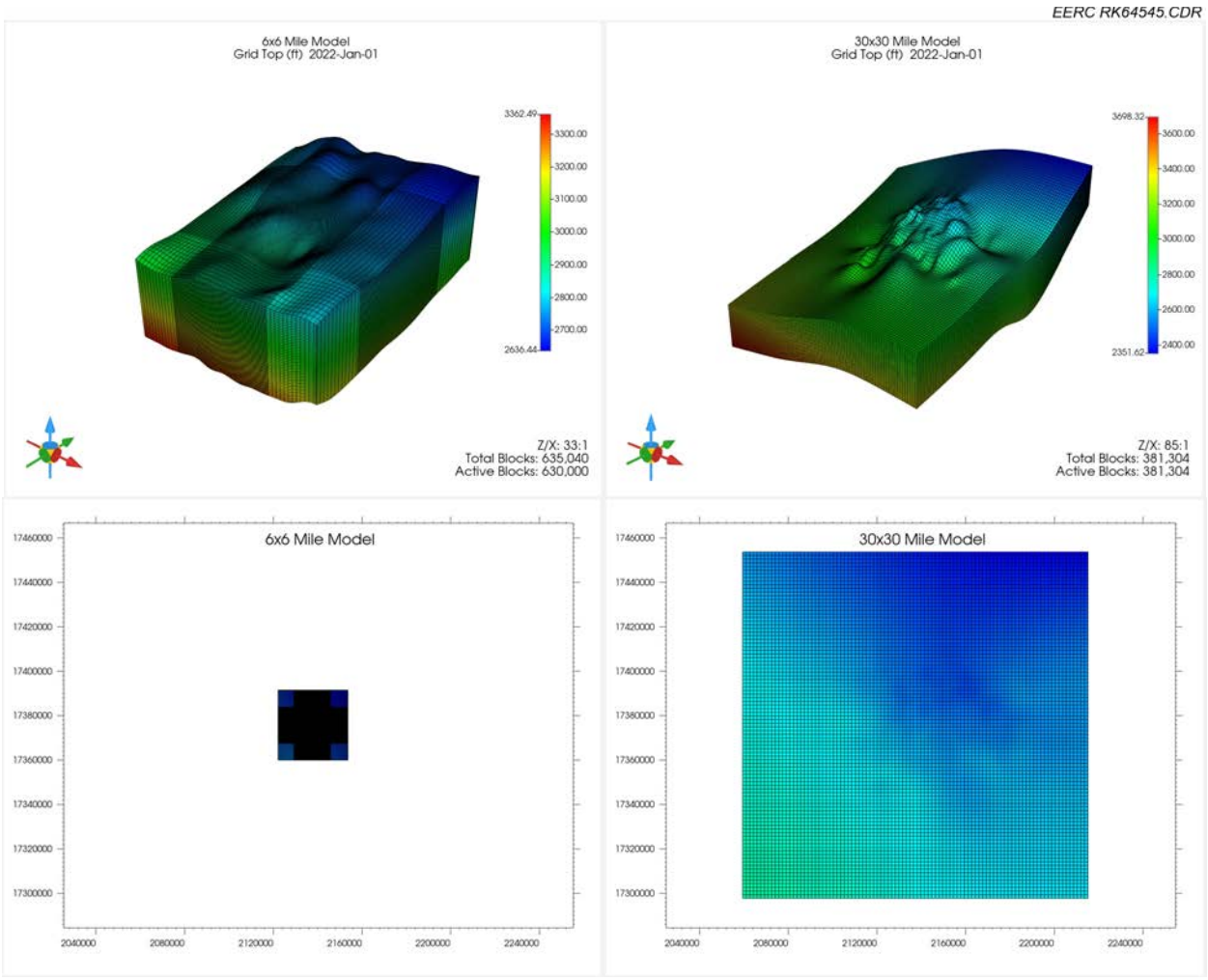


Figure 38. 2D 6-mile × 6-mile model (left) and 2D 30-mile × 30-mile model (right) arial view comparison of the two simulations.

permeability and porosity of the formations. Incorporating additional well logs from the expanded area, the property distribution of the permeably and porosity averages vary slightly from the additional data beyond the original 6-mile × 6-mile modeled region. Table 15 compares the changes in the geologic properties of the two models. Table 16 displays the reservoir simulation properties used in the 30-mile × 30-mile model.

Table 15. Summary of Changes in Geologic Properties

Model Size, mile	Number of Cells	Cell Dimensions	Geomean Permeability	Average Porosity
6 × 6	635,040	164–656 ft	Inyan Kara: ~293.40 mD	Inyan Kara: ~23.53%
30 × 30	398,700	1000 ft	Inyan Kara: ~1330.67 mD	Inyan Kara: ~15.04%

Table 16. Summary of Reservoir Properties in the Expanded Simulation Model

Geomean Permeability	Average Porosity	Rock Compressibility	Initial Pressure	Salinity	Boundary Condition
~1330.67 mD	~15.04%	5e-06 1/psi	~2335 psi (at 3000 ft TVDSS)	10,000 ppm	Infinite

Expanded CO_2 ARM Simulations

Expanding upon the prior ARM simulation performed within the smaller 6-mile × 6-mile model, the upscaled model expanded the number of injection wells and interwell-spacing options while integrating brine production wells in select simulations. The principal objective involved emulating anticipated larger CO_2 injection rates that could be seen in future CCS projects. The expanded modeled region also allows for the expanded study of well interference and how brine extraction can increase CO_2 storage capacity.

Taking insights derived from prior ARM simulations conducted in the smaller geologic model, CO_2 simulation scenarios were formulated to analyze the impacts of CO_2 injection rates encompassing a greater square mileage and assessing an extended CO_2 plume area. The primary goals were to 1) increase the total amount of CO_2 injected and 2) geosteer/contain the CO_2 plume to reduce the overall footprint of a storage project and 3) mitigate and minimize the CO_2 storage injection-induced reservoir pressure increase to prevent an overpressurized reservoir.

The expanded simulation model retained the sandstone relative permeability curve used in the two-phase simulations of the 6-mile × 6-mile model. The rock property curve emulates the typical sandstone found within the Inyan Kara and draws reference from pertinent literature.

Simulation cases were extrapolated from the 6-mile × 6-mile simulation model but were scaled up. The simulations progressed with a more comprehensive study of the interwell-spacing analysis, encompassing simulations performed at 1-mile, 2-mile, and 3-mile well distances. Such an approach enables an in-depth investigation into the expanded maximum CO_2 storage potential and a more substantial analysis of the impact that brine production wells and well placement strategies have on optimizing CO_2 storage capacity. Several well patterns were studied, composed of a linear layout of injection wells, a staggered arrangement of injection wells, and a square configuration, some encompassing centralized brine production wells. These simulations featured an evaluation of the maximum CO_2 injection rates to examine the increase in maximum CO_2 storage quantities. Furthermore, simulations were conducted at a constant injection rate of 1 MMt/yr per well to evaluate the strategies for reservoir pressure management. Table 17 highlights a comprehensive list of the extensive range of simulations conducted for this expanded study.

Table 17. Summary Simulation Cases

Case No.	Injection Rate, MMt/yr	Production Rate, bpd	Well Placement Pattern	Distance, mile
1	No injection constraint	None	Square	1
2	No injection constraint	1000	Square	1
3	No injection constraint	5000	Square	1
4	No injection constraint	10,000	Square	1
5	No injection constraint	20,000	Square	1
6	No injection constraint	40,000	Square	1
7	No injection constraint	60,000	Square	1
8	No injection constraint	80,000	Square	1
9	No injection constraint	None	Square	2
10	No injection constraint	1000	Square	2
11	No injection constraint	5000	Square	2
12	No injection constraint	10,000	Square	2
13	No injection constraint	20,000	Square	2
14	No injection constraint	40,000	Square	2
15	No injection constraint	60,000	Square	2
16	No injection constraint	80,000	Square	2
17	No injection constraint	None	Square	3
18	No injection constraint	1000	Square	3
19	No injection constraint	5000	Square	3
20	No injection constraint	10,000	Square	3
21	No injection constraint	20,000	Square	3
22	No injection constraint	40,000	Square	3
23	No injection constraint	60,000	Square	3
24	No injection constraint	80,000	Square	3
25	No injection constraint	None	Linear	1
26	No injection constraint	None	Linear	2
27	No injection constraint	None	Linear	3
28	No injection constraint	None	Staggered	1
29	No injection constraint	None	Staggered	2
30	No injection constraint	None	Staggered	3
31	4	None	Square	1
32	4	1000	Square	1
33	4	5000	Square	1
34	4	10,000	Square	1
35	4	20,000	Square	1
36	4	40,000	Square	1
37	4	60,000	Square	1
38	4	80,000	Square	1
39	4	None	Square	2
40	4	1000	Square	2
41	4	5000	Square	2
42	4	10,000	Square	2
43	4	20,000	Square	2
44	4	40,000	Square	2
45	4	60,000	Square	2
46	4	80,000	Square	2
47	4	None	Square	3
48	4	1000	Square	3

Continued . . .

Table 17. Summary Simulation Cases (continued)

Case No.	Injection Rate, MMt/yr	Production Rate, bpd	Well Placement Pattern	Distance, mile
49	4	5000	Square	3
50	4	10,000	Square	3
51	4	20,000	Square	3
52	4	40,000	Square	3
53	4	60,000	Square	3
54	4	80,000	Square	3
55	4	None	Linear	1
56	4	None	Linear	2
57	4	None	Linear	3
58	4	None	Staggered	1
59	4	None	Staggered	2
60	4	None	Staggered	3

Scenario Matrix 1-mile Separation

Scenario Matrix 1 involves the systematic observation of the square well placement pattern strategy, each well separated by a distance of 1 mile from the other. To test the robustness of this pattern, additional simulations were also conducted at distances of 2 and 3 miles apart. This enables the examination of optimal well placement, which maximizes the amount of stored CO_2 while minimizing the CO_2 plume area, ensuring optimal storage efficiency. The injection wells were subject to strict constraints, including a 3710-psi maximum BHP, which was <90% of the assumed fracture propagation pressure. Additionally, the wellhead pressure (WHP) was confined to 2000 psi. Injection rates were also limited to 1 MMt/yr per well and 4 MMt/yr combined. Additional simulations incorporated unconstrained injection rates for studying maximum CO_2 storage potential (Table 18).

Figure 39 shows the construction of the square well placement pattern. A local grid refinement (LGR) was placed at the perforated cells as well as the adjacent grid cells, reducing the grid cell size from 1000 ft down to 200 ft. Numerical simulations were done over a 20-year injection period, with varied injection rates, well spacing, and production rates.

Looking at Figures 40 and 41, results show that production has minimal impact on increasing CO_2 storage protentional because of the injection and production wells being close to each other, which results in rapid CO_2 breakthrough, making production ineffective at freeing up void space.

Table 18. Additional Summary Simulation Cases

Case No.	Injection Rate, MMt/yr	Number of Injection Wells	Production Rate, bpd	Number of Production Wells	Well Placement Pattern	Distance, mile
1–8	No injection constraint	4	0–80,000	4	Square	1

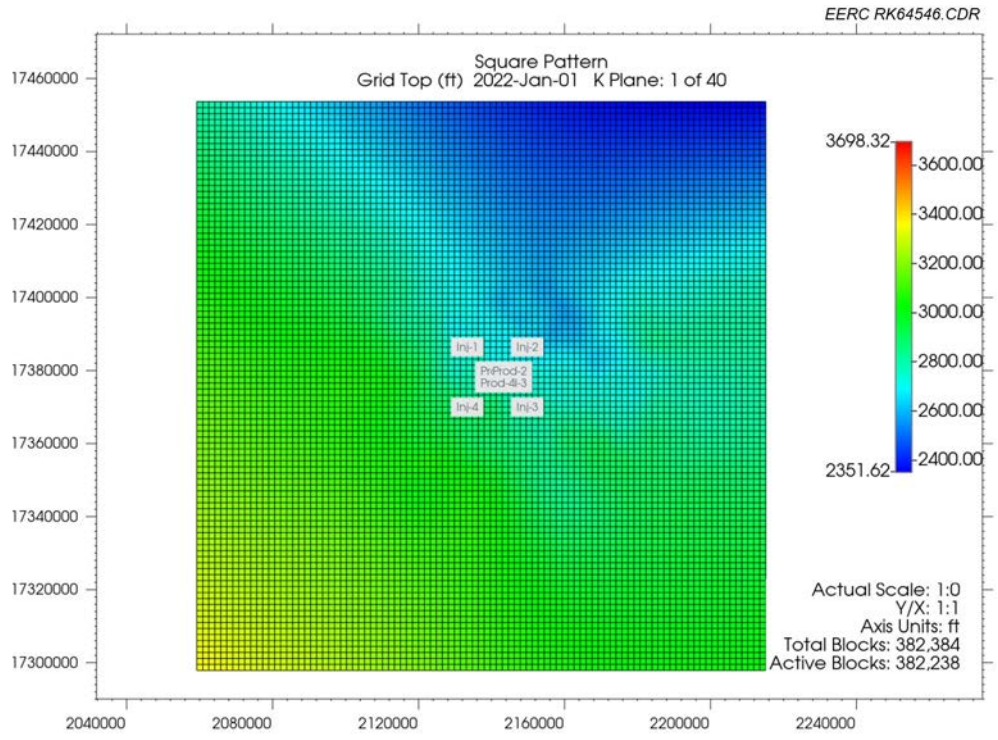


Figure 39. Square well placement pattern, 3-mile separation of four production wells located in the center of the injection well simulation with a centrally located water production well.

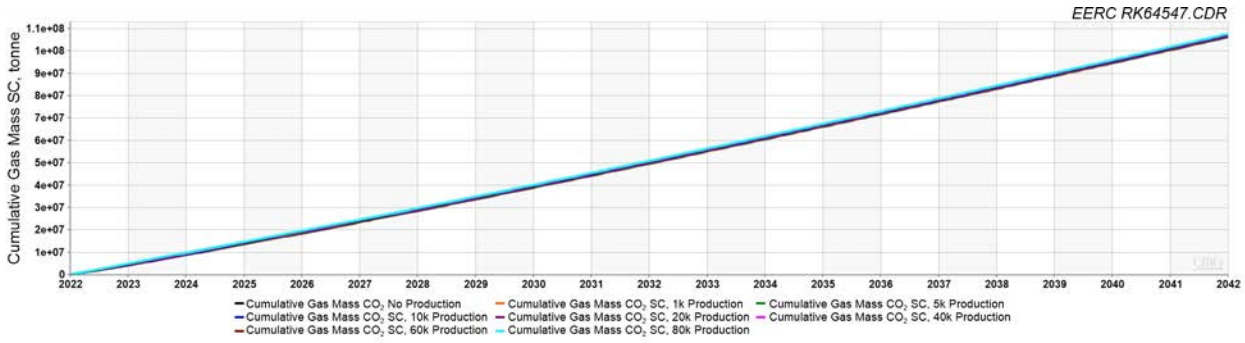


Figure 40. Cumulative CO_2 injection totals using 1-mile well spacing and varied production. rates.

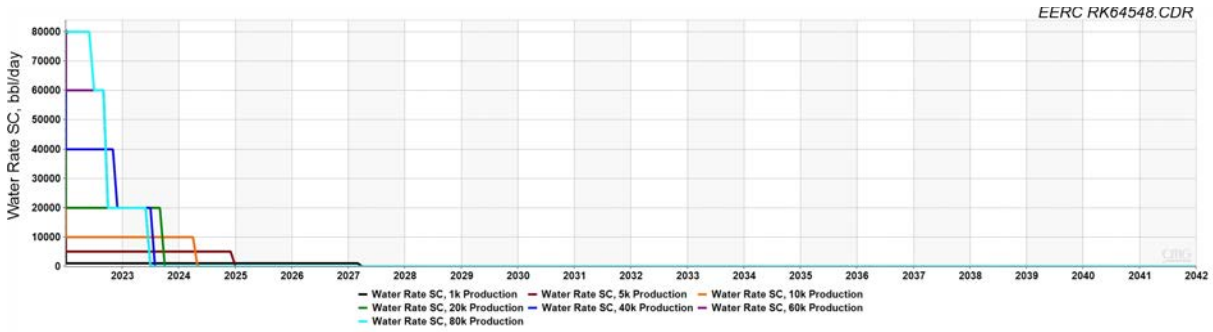


Figure 41. Water production rates using 1-mile spacing. Each drop-off in production rate represents a CO_2 breakthrough in one of the production wells.

The injection rates are compared in Table 19, which shows how small of an increase in CO_2 storage there is with the various brine extraction rates. With maximum injection in the range of 100 MMt, the maximum CO_2 increased injection only represents 1% of the original injected amount without production.

As a result of no more than an observed 1% improvement in injection capacity, the CO_2 plume remains unaltered when compared to the case of the 80,000-bbl/day production rate (Figure 42).

Table 19. Injection Results Using 1-mile Well Spacing and Varied Brine Extraction Rates

Brine Extraction Rate, bbl/day	Cumulative CO_2 Injected, MMt	CO_2 Injection Improvement, MMt
None	106,295,760	
1000	106,459,336	163,576
5000	106,697,968	402,208
10,000	106,836,512	540,752
20,000	107,103,952	808,192
40,000	107,331,744	1,035,984
60,000	107,501,608	1,205,848
80,000	107,691,976	1,396,216

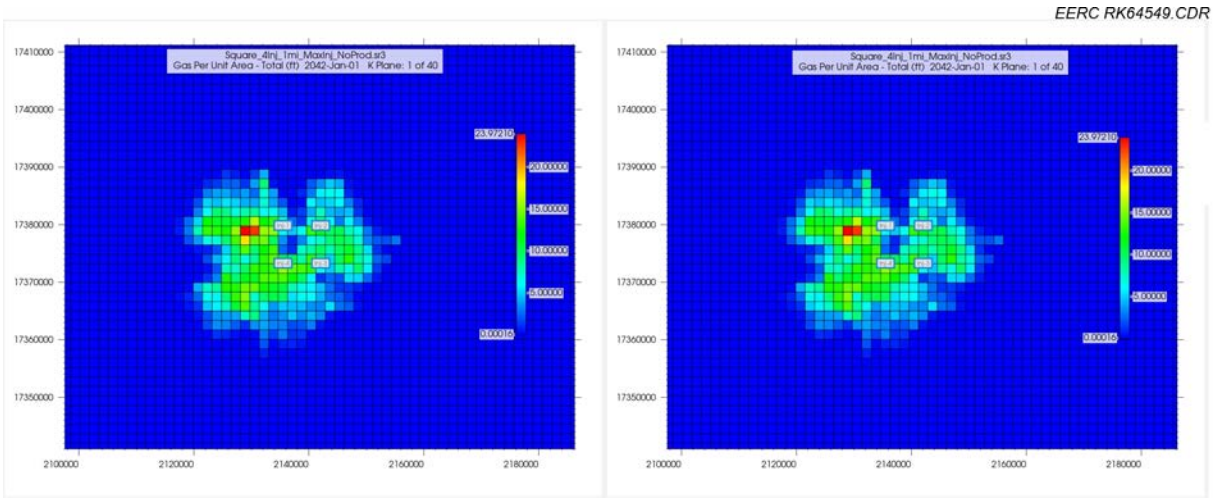


Figure 42. CO_2 plume after 20 years with no production (left) and CO_2 plume after 20 years using 80,000-bbl/day production rate (right). There are no noticeable changes to the CO_2 shape with brine extraction wells being involved.

Scenario Matrix 3-mile Separation

Looking at the results of when the wells are spaced far enough apart, results show that brine extraction can improve CO_2 storage potential as well as some geosteering of the CO_2 plume. Figure 43 and Table 20 illustrate a more noticeable increase in CO_2 storage potential. This is a result of the wells being spaced far enough apart to reduce pressure interference and allow for production wells to be much more effective by having delayed CO_2 breakthrough. Thus greater amounts of brine could be extracted to free up space for the injected CO_2.

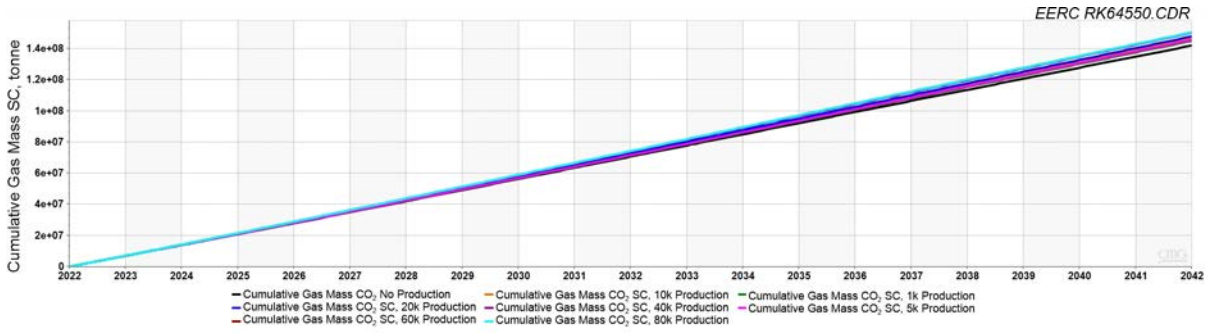


Figure 43. Cumulative CO_2 injection totals using 3-mile well spacing and varied production rates.

Table 20. Injection Results Using 3-mile Well Spacing and Varied Brine Extraction Rates

Brine Extraction Rate, bbl/day	Cumulative CO_2 Injected, MMt	CO_2 Injection Improvement, MMt
None	141,934,768	
1000	144,931,408	2,996,640
5000	145,567,952	3,633,184
10,000	146,373,648	4,438,880
20,000	147,832,368	5,897,600
40,000	150,124,816	8,190,048
60,000	150,392,992	8,458,224
80,000	150,392,992	8,458,224

Table 20 shows the greater improvement in CO_2 storage resource when the well spacing is great enough to delay CO_2 breakthrough, maximizing the volume of brine that can be extracted over a larger pore space area. The injection rates of the 60,000- and 80,000-bbl/day extraction scenarios show no improvement as the four brine extraction wells are unable to produce a combined 50,000 bbl/day.

Figure 44 illustrates how production rates are unable to exceed 50,000 bbl/day, and the sudden drop in production rates represent a CO_2 breakthrough in one of the four production wells. With adequate spacing for the production well to effectively extract displaced brine, with high enough extraction rates, the CO_2 plume can be pulled toward the center of the four wells that was otherwise an area of centralized pressure interference from brine being displaced toward the center, resulting in an increase in reservoir pressure (Figure 45).

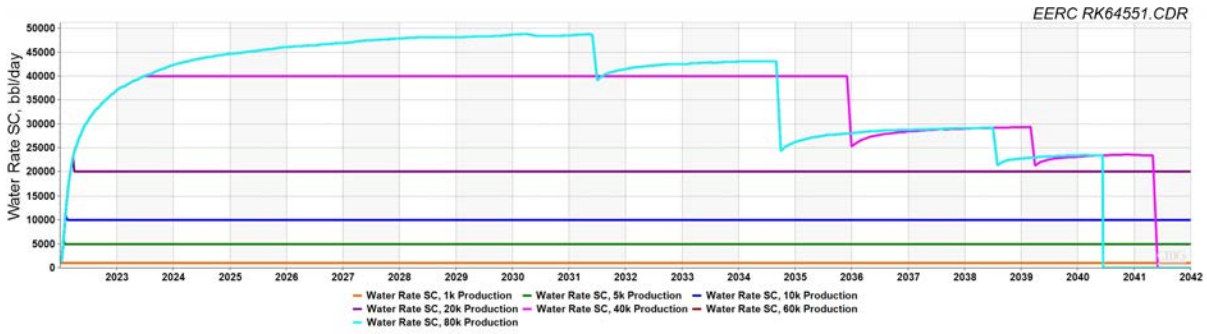


Figure 44. Water production rates in the 3-mile well separation simulations. A drop in extraction represents a CO_2 breakthrough in one of the four production wells and results in it getting shut in.

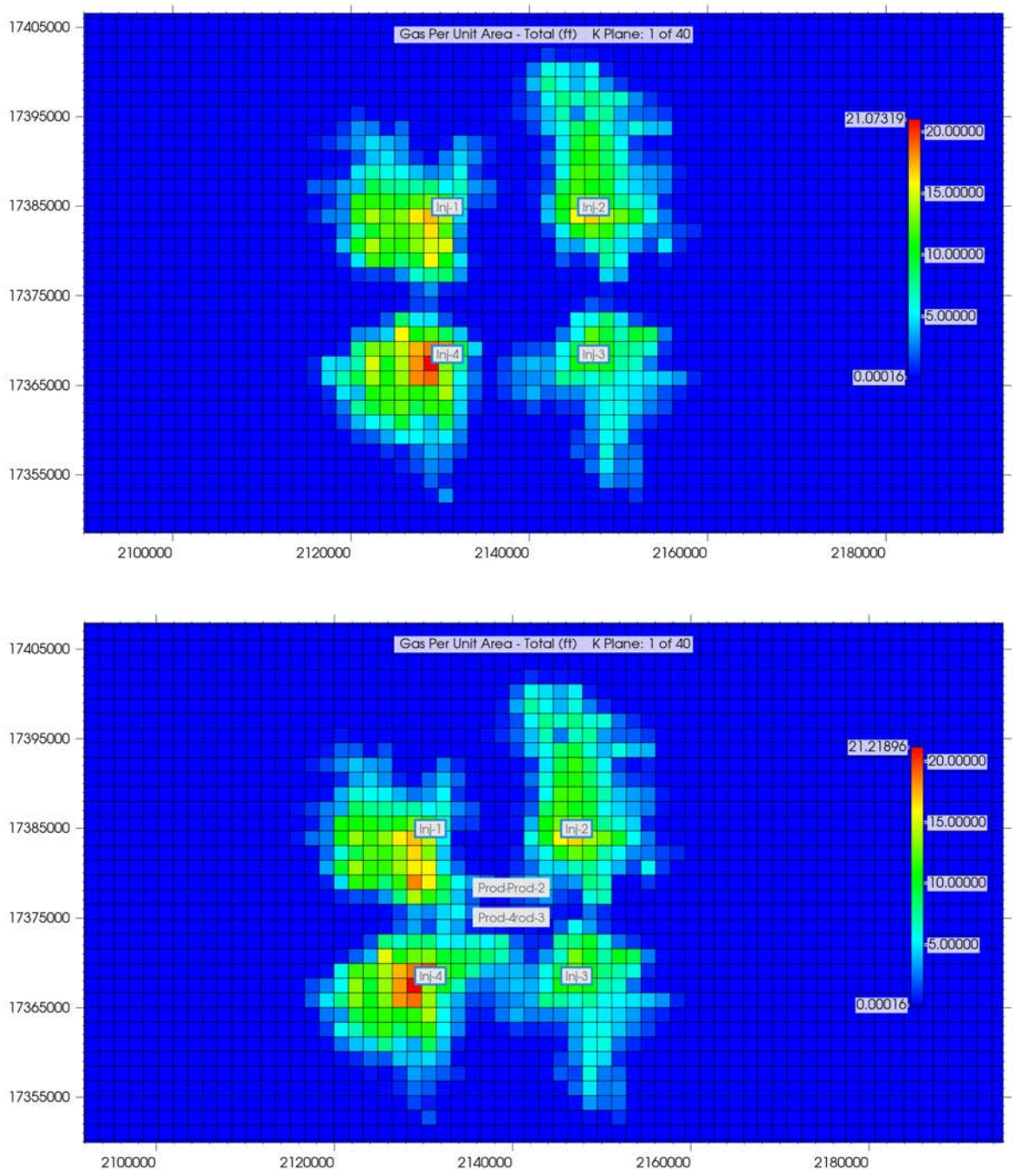


Figure 45. CO_2 plume after 20 years with no production (top) and CO_2 plume after 20 years using an 80,000-bbl/day production rate (bottom). Increased CO_2 plume migration inward with an increased CO_2 injection volume is noticeable.

Linear and Staggered Well Placement

Simulations were conducted to investigate varying well placement strategies to avoid creating a centralized pressure interference from the trapping displaced water. These methods also provide the potential advantage of increasing CO_2 injection volumes without the added costs of extraction of well-produced brine and having to deal with disposal elsewhere.

When well placements are close to each other, linear and staggered have an advantage over a square pattern (Figure 46). However, as the well separation increases, linear remains favorable, but a square pattern becomes slightly more favorable over a staggered pattern (Figure 47). Table 21 breaks down the comparison of maximum CO_2 capacity using the three different placement patterns.

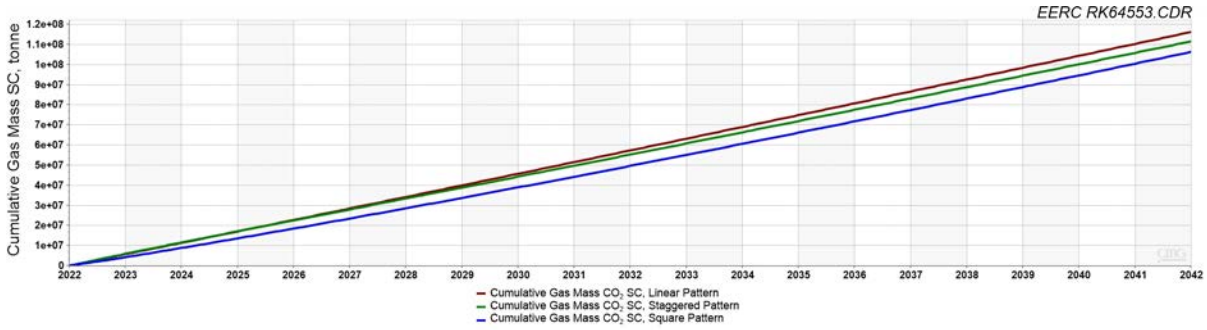


Figure 46. Cumulative CO_2 injection totals using three well placement patterns at 1-mile separation.

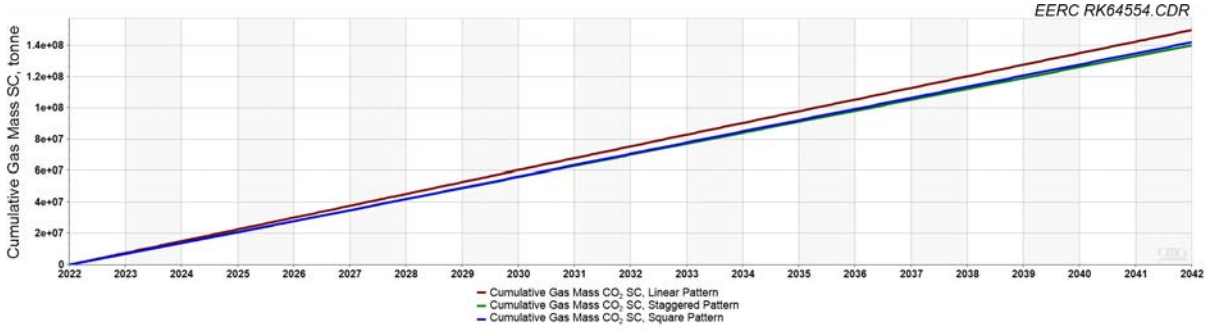


Figure 47. Cumulative CO_2 injection totals using three well placement patterns at 3-mile separation.

Table 21. Injection Results Using Different Well Placement Strategies and Well Separation Distances

Well Pattern	Well Separation, miles	Cumulative CO_2 Injected, MMt
Linear	1	116,210,232
Staggered	1	111,542,568
Square	1	106,295,760
Linear	2	126,533,168
Staggered	2	112,543,840
Square	2	122,866,496
Linear	3	149,759,792
Staggered	3	140,052,032
Square	3	141,934,768

Figure 48 shows how the CO_2 plumes compare when using different well placement patterns. Looking at a linear pattern, it requires more surface area but reduces well interference, leading to increased CO_2 injection at the cost of requiring more land in a linear line. A staggered well pattern better allows for the CO_2 to come together as one plume but has slightly more well interference than a square pattern, resulting in a slightly lower storage capacity than the square pattern. The square pattern continues to illustrate the dead zone that forms in the center of the four wells, resulting in plume migration outward.

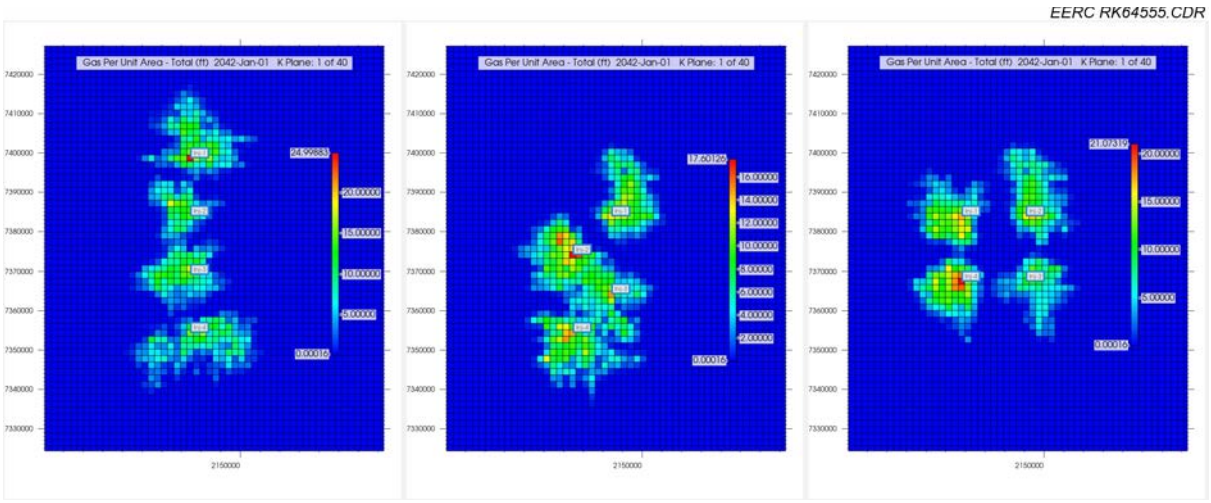


Figure 48. CO_2 plume after 20 years in a linear well placement pattern (left), CO_2 plume after 20 years in a staggered well placement pattern (center), and CO_2 plume after 20 years in a square well placement pattern (right).

Constrained Injection Rate

Constraining the injection rate allows for a closer study of the impact brine production has on minimizing the reservoir pressurization because of CO_2 storage. Simulations were performed

using a square well pattern with Wells 1, 2, and 3 miles apart. Four brine extraction wells were placed in the center of the square pattern. Four wells were used to ensure that a 1:1 ratio of the volume of CO_2 being injected and the volume of brine being extracted were equal. The injection wells were subject to strict constraints, including a 3710-psi maximum BHP, which is <90% of the assumed fracture propagation pressure. Additionally, the WHP was confined to 2000 psi. Injection rates were also limited to 1 MMt/yr per well and 4 MMt/yr combined.

Looking at a 3-mile well separation, results demonstrate high enough extraction rates to offset the volume of CO_2 being injected can minimize or negate reservoir pressure increases as the extraction/injection ratio gets closer to a 1:1 ratio of volume being injected into the formation versus volume being taken out of the formation (Figures 49 and 50). The role of extraction/production ratios in optimizing the efficiency of production wells in CO_2 sequestration can be highlighted by examining the impact of varying production rates. For instance, by increasing production rates to 100,000 bbl/day across four production wells (as depicted in Figure 49), it is possible to assess the resulting impact on the efficiency of the process. Notably, this production rate equates to the volume of water being extracted which is just slightly higher

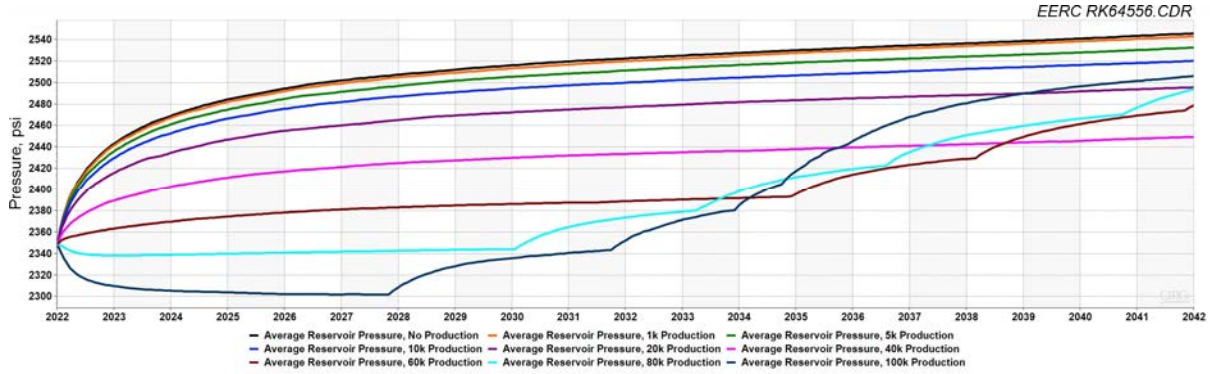


Figure 49. Average reservoir pressure within 1 mile of the injection wells.

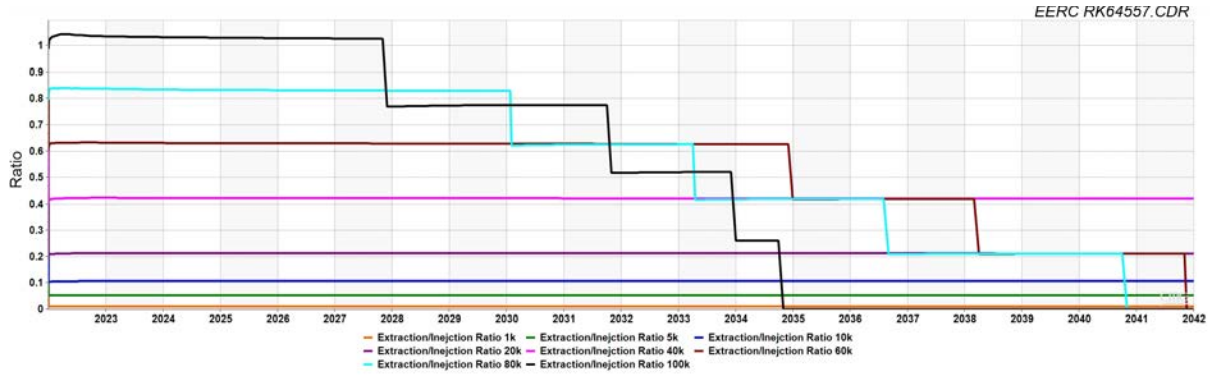


Figure 50. Extraction/injection ratio of different production rates and a constant combined 4-MMt/yr injection rate.

than the volume of 1 MMt CO_2 per well being injected at reservoir conditions. As shown, higher production rates lead to faster CO_2 breakthrough, resulting in production wells becoming shut in. These shut-in production wells can be converted into CO_2 injection wells to increase the well's lifespan once CO_2 breakthrough occurs.

The concept of a 1:1 extraction/production ratio takes on particular importance in the context of limited CO_2 injection rates. For example, when the four injection wells are set to a combined 1 MMt/yr (as depicted in Figure 51), maintaining a 1:1 ratio of extraction to production represents the ideal conditions to maintain by extracting an equivalent volume of water as the CO_2 that is injected. Such an equilibrium ensures that the pressure increase resulting from CO_2 injection is effectively offset, and during postinjection, the pressure returns to the initial conditions with no overpressurization of the reservoir, as illustrated in Figure 52.

Such an analysis underscores the importance of maintaining balanced extraction/production ratios in maximizing the effectiveness of production wells. Failure to achieve this balance can lead to a host of issues, including rapid CO_2 breakthrough, reduced injection capacity, and increased pressure interference between injection wells. Ultimately, achieving an optimal extraction/ production ratio requires careful consideration of a range of factors, including well spacing, injection and production rates, and reservoir characteristics.

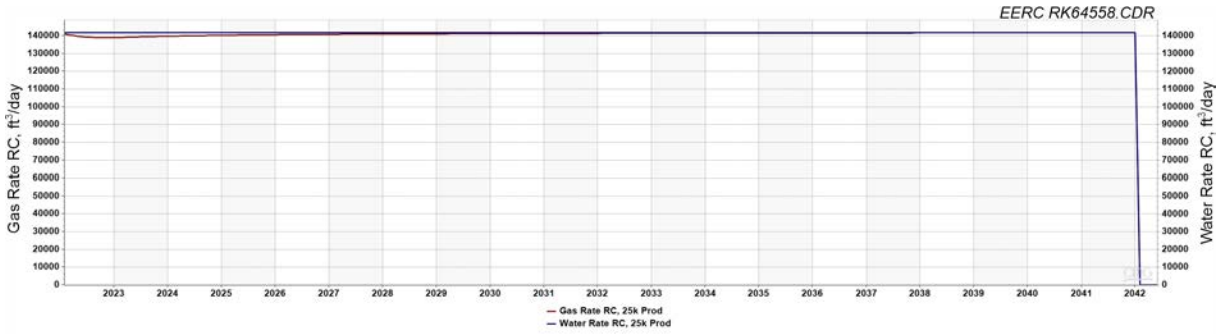


Figure 51. Reservoir volumetrics of CO_2 injection rates versus volumetric brine production rate representing a 1:1 extraction/production ratio.



Figure 52. Average reservoir pressure increases with varied production rates.

CONCLUSIONS

For reservoir conditions investigated at the BEST project site, the process of water extraction can play a crucial role in determining the efficacy of CO_2 injection in a reservoir. Specifically, it serves to counteract the elevation in pressure levels caused by the CO_2 injection if the volume of water being extracted is close to the volume of CO_2 being injected. This mechanism is particularly advantageous in reservoirs that are prone to overpressurization or where there is a risk of future pressurization-related issues. It is important to note that for the water extraction to significantly enhance the CO_2 storage resource or fully mitigate overpressurization, the rate of brine production must be sufficiently high to maintain an extraction-to-production ratio of 1:1. Smaller extraction-to-production ratios are still effective at reducing the pressurization from CO_2 injection, which can be beneficial in overpressurized regions or to allow for further potential CO_2 storage around any existing storages sites. However, this requirement also implies an escalation in the amount of produced water, especially in scenarios involving high CO_2 injection rates. For instance, a CO_2 injection rate of 4 MMt/yr necessitates the extraction of nearly 80,000 bbl/day of brine to effectively offset the volume of CO_2 injected into the reservoir.

Geosteering of CO_2 plumes can be observed but is influenced by several factors. Boundary conditions are one factor that must be considered as they have a large influence on the simulation. Because the model contains open boundaries, aquifers beyond the modeled area resupply portions of the produced water offsetting some of the effectiveness the production wells have on geosteering. It is shown that low production rates have minimal effect on the plume and not until significantly larger production is applied are more noticeable changes observed. Additionally, because the model is not homogeneous, permeability distributions affect the flow of CO_2 as observed with the lower permeabilities to the northeast and higher permeability to the southwest of the model, the direction the CO_2 plume migrates. Permeability distribution is also important because it influences the propagation of the pressure pulse from a production well, making the well placement important to be effective and not producing water that is not beneficial to increasing CO_2 storage capacity.

The positioning of wells is a critical factor that determines the direction of the CO_2 plume evolution in each reservoir. Wells that are near each other can significantly reduce the footprint of CO_2, but this placement limits the potential injection rates because of pressure interference. This closer spacing also reduces the area for displaced brine to cause a centralized pressure interference, which can negatively impact injection. In contrast, placing the wells further apart can facilitate higher injection rates, but this wider spacing also results in a larger CO_2 footprint for the project and a more extensive area of centralized pressure interference from a larger volume of displaced brine. In such instances, production wells can remove the trapped water, but if the wells are positioned too closely, rapid CO_2 breakthrough can occur. Conversely, if the wells are too far apart, water production wells may not have a significant impact on the injectors.

The inherent heterogeneity of subsurface reservoir models poses a significant challenge when attempting to implement a generalized approach to well placement and injection/production ratios for CO_2 sequestration. Specifically, the variability in permeability across the reservoir makes it challenging to identify fixed patterns or ratios that can be applied uniformly across the reservoir. As a result, the optimal placement of production wells is highly dependent on the unique

characteristics of the reservoir, and nonconforming patterns are often necessary to account for the permeability heterogeneity and steer the CO_2 plume effectively. Furthermore, achieving the desired level of plume control may require the willingness to produce significant volumes of water, which must be handled and disposed of, to offset the injected CO_2 effectively.

Effective CO_2 storage plume and pressure management demands a highly nuanced understanding of the reservoir's heterogeneity as well as a sophisticated approach to well placement and production management. Achieving optimal outcomes in this context requires a willingness to embrace dynamic, site-specific strategies that account for the unique complexities of each subsurface reservoir.

SYNERGISTIC ACTIVITY

Assessment of Carbonated Brine Injection Feasibility

The EERC participated in a Leidos-sponsored research effort, directed by the U.S. Department of Energy's National Energy Technology Laboratory, to conduct a modeling and simulation feasibility assessment of the injection of carbonated brine into the subsurface. In this study, carbonated brine injection (CBI) was investigated as a low-risk CO_2 storage strategy, whereby CO_2 is first dissolved into oilfield produced waters being injected into existing Class II SWD wells. Since the CO_2 is mixed with the produced water prior to subsurface injection, the benefits were predicted to include no migration of free-phase CO_2 and negligible pressure increase when compared to standard SWD injection. A visualization of the different injection approaches is shown in Figure 53. This study used the reservoir conditions and characteristics present in the Class II brine disposal wells found in the North Dakota Bakken play, which predominantly injects into a regionally extensive brine formation, the Inyan Kara Formation.

Data obtained as part of the BEST ARM task, including stratigraphy, formation pressures, hydraulic gradients, permeability, porosity, etc., were used to populate specific components of the geologic and simulation models used for the CBI evaluation. Three simulation studies were conducted to investigate 1) CO_2 phases at different conditions, 2) wellbore compatibility, and 3) long-term storage fate in the reservoir. Simple reservoir model and injection simulations were created using data to represent the BEST site, an operational SWD facility located near Watford City, North Dakota.

Simulations of CBI at small CO_2 molality (0.2 mol/kg) were found to show no perceivable increases in reservoir pressure or impacts to brine viscosity or density due to the dissolved CO_2. When compared specifically to standard produced water disposal operations, pressure-driven risks such as leakage, induced seismicity, cap rock failure, and migration do not increase with the inclusion of dissolved CO_2 in the brine injection stream. Evaluation of wellbore corrosion rates showed minimal change with the inclusion of dissolved CO_2 in the brine injection, enabling CBI operations for years. Finally, the carbonated brine was found to be denser than the reservoir brine, such that the CO_2-laden brine sinks to the bottom of the reservoir instead of migrating upward due to buoyancy forces, which typically happens during injection of dense-phase CO_2 for geologic storage.

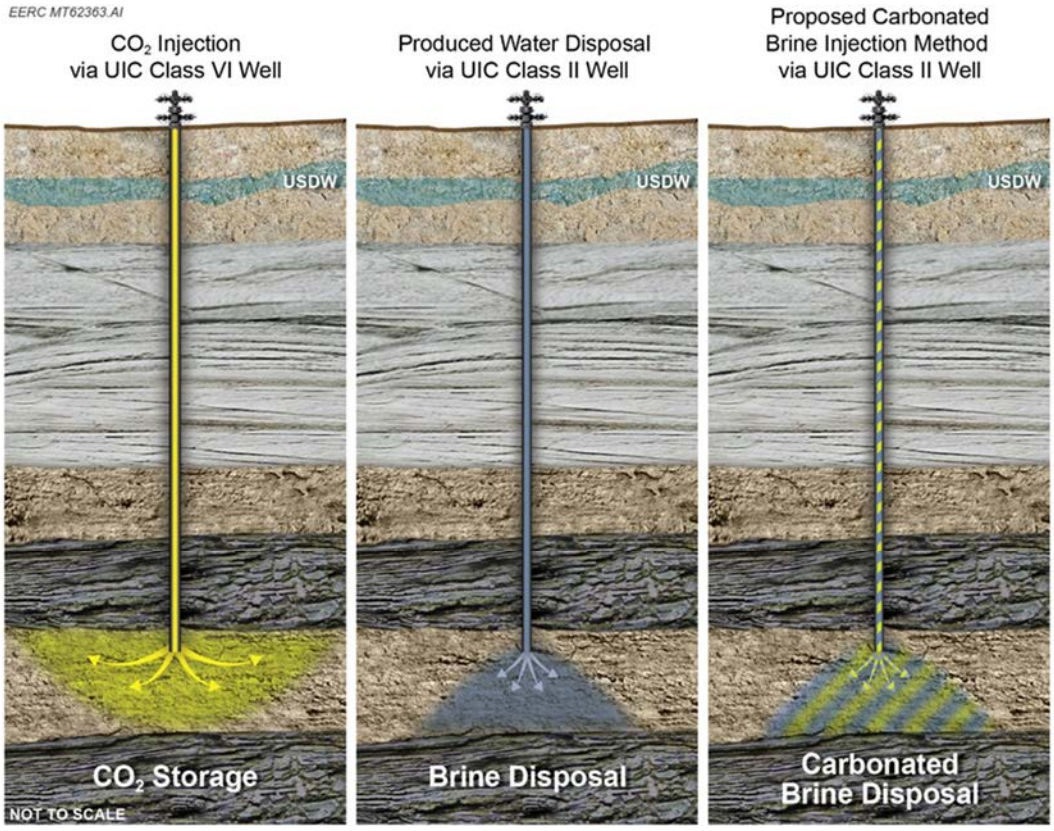


Figure 53. Graphical representation of CBI compared to traditional free-phase CO_2 injection and standard produced water (brine) disposal.

Overall, CBI and storage in North Dakota's Inyan Kara Formation appear to be a low-risk geologic sequestration strategy. CBI does not appear to result in any increased risks when compared to standard produced water disposal operations and is beneficial in its ability to use existing well infrastructure in comparison to new carbon capture, utilization, and storage (CCUS) projects. The full report on the CBI assessment can be found in Appendix D.

REFERENCES

Ayash, S. C., Nakles, D. V., Wildgust, N., Peck, W. D., Sorensen, J. A., Glazewski, K. A., Aulich, T. R., Klapperich, R. J., Azzolina, N. A., and Gorecki, C. D., 2017, Best Practice for the Commercial Deployment of Carbon Dioxide Geologic Storage: Adaptive Management Approach. United States: N. p. Web. doi:10.2172/1874353.

Birkholzer, J.T., and Zhou, Q., 2009, Basin-scale hydrogeologic impacts of CO_2 storage—capacity and regulatory implications: International Journal of Greenhouse Gas Control, v. 3, p. 745–756.

Birkholzer, J.T., Cihan, A., and Zhou, Q., 2012, Impact-driven pressure management via targeted brine extraction—conceptual studies of CO_2 storage in saline formations: International Journal of Greenhouse Gas Control, v. **7**, p. 168–180.

Birkholzer, J.T., Oldenburg, C.M., and Zhou, Q., 2015, CO_2 migration and pressure evolution in deep saline aquifers: International Journal of Greenhouse Gas Control, DOI: 10.1016/ j.ijggc.2015.03.022.

Buscheck, T.A., Sun, Y., Wolery, T.J., Bourcier, W., Tompson, F.B., Jones, E.D., Friedmann, S.J., and Aines, R.D., 2011, Combining brine extraction, desalination, and residual-brine with CO_2 storage in saline formations—implications for pressure management, capacity, and risk mitigation: Energy Procedia, v. 4, p. 4283–4290.

Buscheck, T.A., White, J.A., Chen, M., Sun, Y., Hao, Y., Aines, R.D., Bourcier, W.L., Bielicki, J.M., 2014, Pre-injection brine production for managing pressure in compartmentalized CO_2 storage reservoirs: Energy Procedia, v. 63, p. 5333–5340.

Chen, T., and Guestrin, C., 2016, XGBoost—a scalable tree boosting system: Proceedings of the 22nd ACM SIGKDD International Conference on Knowledge Discovery and Data Mining, p. 784–794.

Cihan, A., Birkholzer J.T., and Bianchi, M., 2015, Optimal well placement and brine extraction for pressure management during CO_2 sequestration: International Journal of Greenhouse Gas Control, v. 42, November, p. 175–187.

Computer Modelling Group Ltd., 2019, GEM user guide.

Court, B., Celia, M.A., Nordbotten, J.M., and Elliot, T.R., 2011, Active and integrated management of water resources throughout CO_2 capture and sequestration operations: Energy Procedia, v. 4, p. 4221–4229.

Davidson, C.L., Watson, D.J., Dooley, J.J., and Dahowski, R.T., 2014, Benefits and costs of brine extraction for increasing injection efficiency in geologic CO_2 sequestration: Energy Procedia, v. 63, p. 4745–4749.

Gonzaléz-Nicolás, A., Cihan, A., Retrusak, R., Zhou, Q., Trautz, R., Riestenberg, D., Godec, M., Birkholzer, J.T., 2019, Pressure management via brine extraction in geological CO_2 storage—adaptive optimization strategies under poorly characterized reservoir conditions: International Journal of Greenhouse Gas Control, v. 83, p. 176–185.

Hamling, J.A., Klapperich, R.J., Stepan, D.J., Sorensen, J.A., Pekot, L.J., Peck, W.D., Jacobson, L.L., Bosshart, N.W., Hurley, J.P., Wilson IV, W.I., Kurz, M.D., Burnison, S.A., Salako, O., Musich, M.A., Botnen, B.W., Kalenze, N.S., Ayash, S.C., Ge, J., Jiang, T., Dalkhaa, C., Oster, B.S., Peterson, K.J., Feole, I.K., Gorecki, C.D., and Steadman, E.N., 2016, Field implementation plan for a Williston Basin brine extraction and storage test: Phase I topical report for U.S. Department of Energy National Energy Technology Laboratory Cooperative

Agreement No. DE-FE0026160, Grand Forks, North Dakota, Energy & Environmental Research Center, April.

International Energy Agency Greenhouse Gas R&D Programme, 2008, CO_2 capture and storage—a key carbon abatement option: IEA/OECD, Paris.

Intergovernmental Panel on Climate Change, 2005, IPCC special report on carbon dioxide capture and storage: Prepared by Working Group III of the Intergovernmental Panel on Climate Change, Metz, B., Davidson, O., de Coninck, H.C., Loos, M., and Meyer, L.A., eds., Cambridge, United Kingdom, and New York, Cambridge University Press, p. 442.

Intergovernmental Panel on Climate Change, 2014. Climate change 2014—synthesis report: Contribution of Working Groups I, II and III to the Fifth Assessment Report of the Intergovernmental Panel on Climate Change, Core Writing Team Pachauri, R.K., and Meyer, L.A. eds., Geneva, Switzerland, Intergovernmental Panel on Climate Change, p. 151.

Kashif, M., Cao, Y., Yuan, G., Asif, M., Javd, K., Nicanor, M., Khan, D., Miruo, L., 2019, Pore size distribution, their geometry and connectivity in deeply buried Paleogene Es1 sandstone reservoir, Nanpu Sag, East China: Petroleum Science, v. 16, p. 981–1000.

Klapperich, R.J., Cowan, R.M., Gorecki, C.D., Liu, G., Bremer, J.M., Holubnyak, Y.I., Kalenze, N.S., Knudsen, D.J., Saini, D., Botnen, L.S., LaBonte, J.L., Stepan, D.J., Steadman, E.N., Harju, J.A., Basava-Reddi, L., and McNemar, A., 2013, IEAGHG investigation of extraction of formation water from CO_2 storage: Energy Procedia, v. 37, p. 2479–2486.

MacLennan, K., Barajas-Olalde, C., Jiang, T., Williamson, C. and Livers-Douglas, A., Klapperich, R.J., and Hamling, J.A., 2022. Assessing the borehole-to-surface electromagnetic (BSEM) method as a tool for active reservoir management (ARM) for geologic CO_2 storage: Proceedings of the 16th Greenhouse Gas Control Technologies Conference (GHGT-16) 23–24 October 2022, https://ssrn.com/abstract=4277024 or http://dx.doi.org/10.2139/ssrn.4277024 (accessed July 2023).

Mohamed, I.M., He, J., and Nasr-El-Din, A., 2011, Permeability change during CO_2 injection in carbonate aquifers—experimental study: Paper presented at the SPE Americas E&P Health, Safety, Security, and Environmental Conference, Houston, Texas, SPE-140979-MS.

Pongtepupathum, W., Williams, J., Krevor, S., Agada, S., and Williams, G., 2017, Optimising brine production for pressure management during CO_2 sequestration in the Bunter sandstone of the UK Southern North Sea: Society of Petroleum Engineers, https://doi.org/10.2118/185804-MS (accessed July 2023).

Simmenes, T., Hansen, O.R., Eiken, O., Teige, G.M.G., Hermanrud, C., Johansen, S., Nordgaard B., Hege M., and Hilde, H., 2013, Importance of pressure management in CO_2 storage: Paper presented at the Offshore Technology Conference, Houston, Texas, May 2013, doi: https://doi.org/10.4043/23961-MS (accessed July 2023).

Tang, H., Fu, P., Jo, H., Jiang, S., Sherman, C.S., Hamon, F., Azzolina, N.A., and Morris, J.P., 2022, Deep learning-accelerated 3D carbon storage reservoir pressure forecasting based on data assimilation using surface displacement from InSAR: International Journal of Greenhouse Gas Control, v. 120, p. 103765.

U.S. Environmental Protection Agency, 2013, Geologic sequestration of carbon dioxide—underground injection control (UIC) program Class VI well area of review evaluation and corrective action guidance: http://water.epa.gov/type/groundwater/uic/class6/upload/epa816r13005.pdf (accessed March 23, 2016).

Zhou, Q., and Birkholzer, J.T., 2011, On scale and magnitude of pressure build-up induced by large-scale geologic storage of CO_2—greenhouse gases: Science and Technology, v. 1, no. 1, p. 11–20.

APPENDIX A

ADDITIONAL FIELD ACTIVITIES

ADDITIONAL FIELD ACTIVITIES

Flow Line Selection and Installation

The class of flow line material initially evaluated for use in transporting extracted formation water from BEST-E1 to BEST-I1 was a spoolable reinforced plastic pipe, which is the preferred pipe class for transporting saline and produced waters in the Williston Basin. Within the spoolable reinforced plastic pipe class, two-line pipes were considered for use in the proposed demonstration, FlexSteel and Flexpipe. They exhibit excellent chemical resistance and pressure ratings and superior qualities related to the ease of installation. An evaluation of 4-in.-diameter pipe rated for 1500 psi and 155°F was based on water characteristics, as shown in Table A-1.

Table A-1. Flow Line Material Selection

Parameters	Requirement
Temperature	155°F maximum
Pressure	1500 psi maximum
Total Dissolved Solids	150,000 mg/L maximum
Possibility of H_2S	Yes, but at low concentrations
Possibility of Hydrocarbon	Yes
Pumping Method	Centrifugal or triplex

Flexsteel consists of a steel reinforcing layer between an inner and outer high-density polyethylene (HDPE) layer, while Flexpipe comprises an inner and outer HDPE layer with a dry fiberglass reinforcing layer. Both pipes employ a hydraulic process for installing fittings and couplings. A summary of pertinent pipe characteristics of the FlexSteel and Flexpipe line pipe are shown in Table A-2.

Table A-2. Summary of Line Pipe Characteristics

Parameter	FlexSteel (4-1500-HTB)	Flexpipe (FP601 HT)
ANSI Class	600	600
Nominal Diameter, in.	4	4
Inside Diameter, in.	3.669	3.9
Outside Diameter, in.	4.688	5.1
Reel Length, ft	2264	1870
Maximum Operating Temperature, °F	180	180
Maximum Operating Pressure, psi	1500	1500
Reinforcing Material	Helically wound steel	Helically wound dry fiberglass
Fitting Installation Method	Hydraulically swaged	Hydraulically compressed

A dual pipe system, or a pipe-in-a-pipe system, was selected for this project considering the safety related to flow line releases. The Flexpipe dual system consisted of a 4-in. pipe (FP601 HT) inside an 8-in. SDR11 HDPE outer pipe. An approximately 2600-ft flow line was installed from BEST-E1 to BEST-I1 in the route shown in Figure A-1. In addition, the Flexpipe system utilized strategically placed concrete vaults placed typically at topographical low points along the flow line. In this project, the concrete vaults are located at each end of the pipes. The 4-in. pipe continues through the vault while the 8-in. pipe terminates at the vault (Figures A-2 and A-3), allowing any fluid from a leak in the 4-in. pipe to be carried to the vault and activating an alarm. The alarm would activate a SCADA (supervisory control and data acquisition) signal to shut extraction/injection operation down as the precaution to minimize/eliminate any leak.

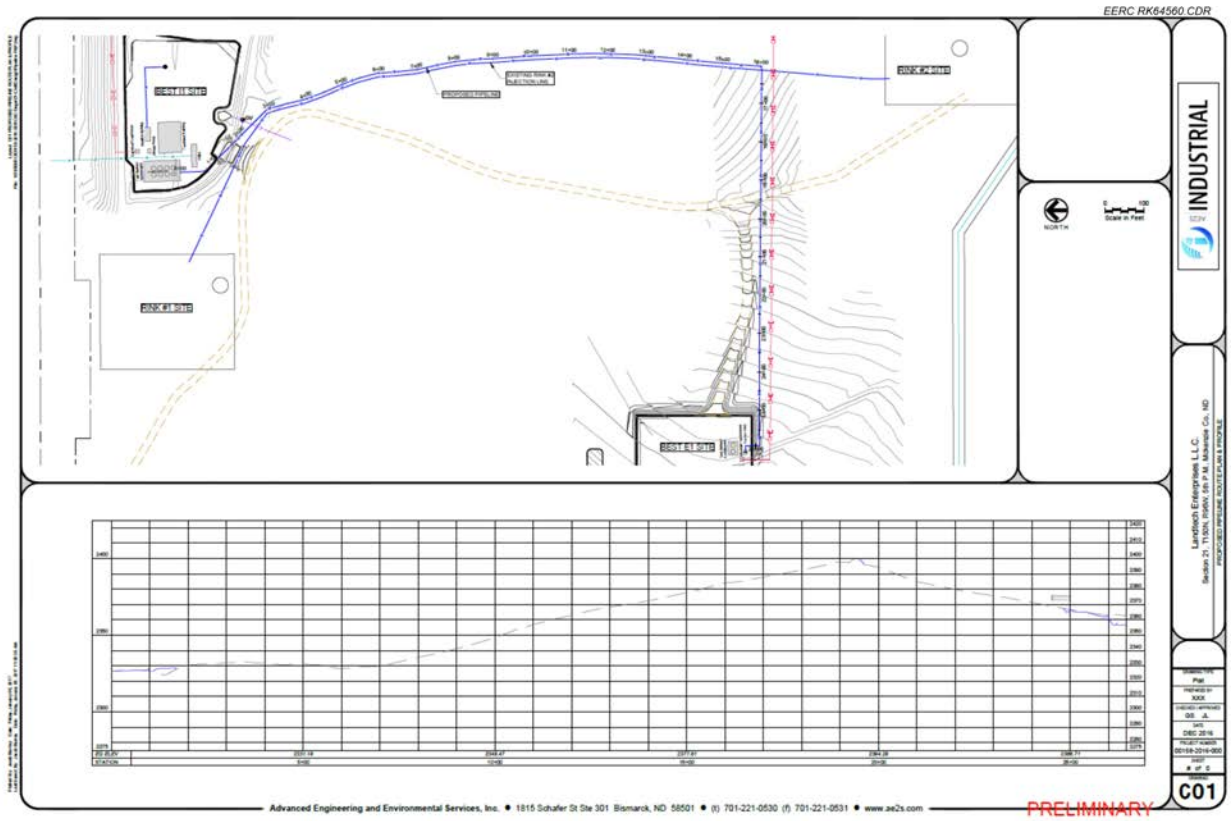


Figure A-1. Plan/profile drawing of flow line route from the BEST-E1 location to the BEST-I1 location.



Figure A-2. 4-in. inner flow line passing through containment vault.



Figure A-3. 8-in. outer flow line terminating at containment vault.

Excavation

Initially, the topsoil was stripped and stockpiled separately from other excavated material to allow topsoil to be replaced as a final step of the backfilling process. With the topsoil removed, the trench was excavated, with attention paid to maintaining a level, undisturbed bottom to allow for solid, uniform pipe support. The trench was excavated to a depth that a minimum of 6 ft of ground cover is maintained over the top-of-pipe, while the trench width was excavated to assure sufficient sidewall clearance for proper backfilling (minimum of 6 in.). Based on observed soil conditions during trench excavation, the sidewalls were constructed to minimize sloughing of material into the trench. Prior to placement of the bedding material, a visual inspection was performed of the entire trench to assure the trench was free of rocks, debris, and other foreign material.

Given the length of the flow line, a single joint was required in the inner (fluid-carrying) pipe. To maximize leak protection, the joint was placed in the concrete containment vault located at the south end of the site (Figure A-4). All end fittings and joints were installed by the pipe manufacturer.



Figure A-4. 4-in. pipe joint in the concrete containment vault (prior to connection of the inner pipe). Inner fluid-carrying pipe is white; 8-in. outer flow line (black pipe) can be seen terminating at containment vault.

Flowline Integrity Testing

Upon completion of the flow line installation and backfilling, the Energy & Environmental Research Center's (EERC's) general contractor performed a flow line integrity test on September 20, 2018. The flow line integrity test consisted of pressuring the flow line up with air in two steps, first to approximately 1300 psi for 16 hours and 35 minutes, then approximately 1800 psi for 8 hours and 5 minutes. Figure A-5 shows a graph of the pressure and temperature during the flow line integrity test.

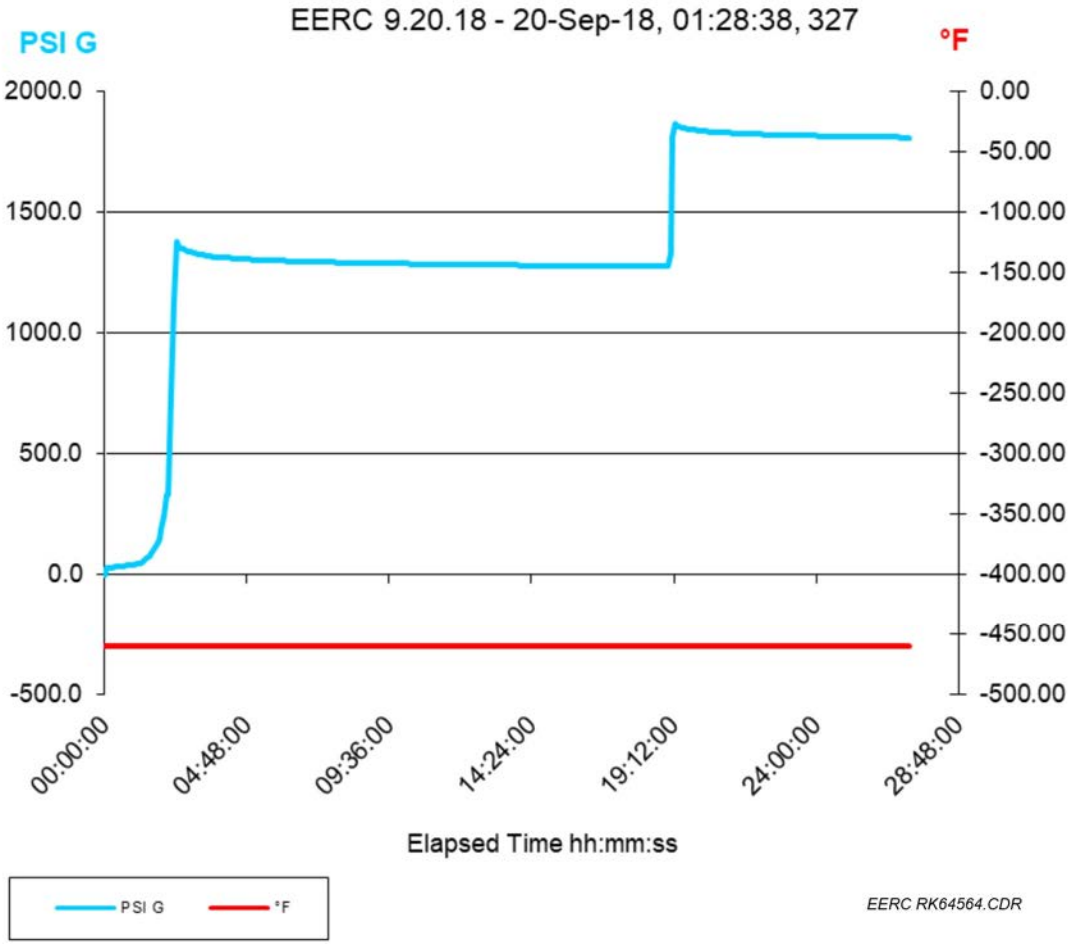


Figure A-5. Pressure data collected during flow line integrity test.

Reclamation

Once the flow line integrity testing was complete and satisfactory results observed and documented, the flow line right-of-way (ROW) was reclaimed to its original condition (or as close as possible). The ground surface was recontoured to the original grade with stockpiled topsoil, and the ROW was reseeded with appropriate vegetation. Figure A-6 shows the flow line ROW after final earthwork, prior to reseeding.



Figure A-6. Regraded ROW with flowlines buried below (prior to reseeding).

Site Infrastructure

Sites for BEST-E1 and BEST-I1 were selected, and dirt work began on November 29, 2017. The dirt work was suspended in December because of winter conditions and picked up in spring 2018. Site-specific infrastructure started to be placed on June 4, 2018. This included tanks, injection pump, flowlines, and other fluid-handling materials. Individual specifications will be stated for each site.

BEST-E1

The BEST-E1 site consists of a facility to treat the fluid produced from the BEST-E1 well. The infrastructure consisted of a producing wellhead, a two-phase separator, two 500-bbl storage tanks, and an inline transfer pump. Water would be extracted from the BEST-E1 well and directed to a two-phase separator to separate gas associated with formation water production. Produced water exits the two-phase separator and moves down the flow line to two 500-bbl, heat-traced, and insulated tanks that were valved together. These tanks provide solids settling prior to entering the flow line to BEST-I1 and provide buffer capacity between the producing well and flow line. The tanks were constantly monitored using a float and radar system that allowed the charge pump to pump the water to the BEST-I1 tank farm. The BEST-E1 process flow diagram (PFD) is provided in Figure A-7, and the facilities are pictured in Figure A-8.

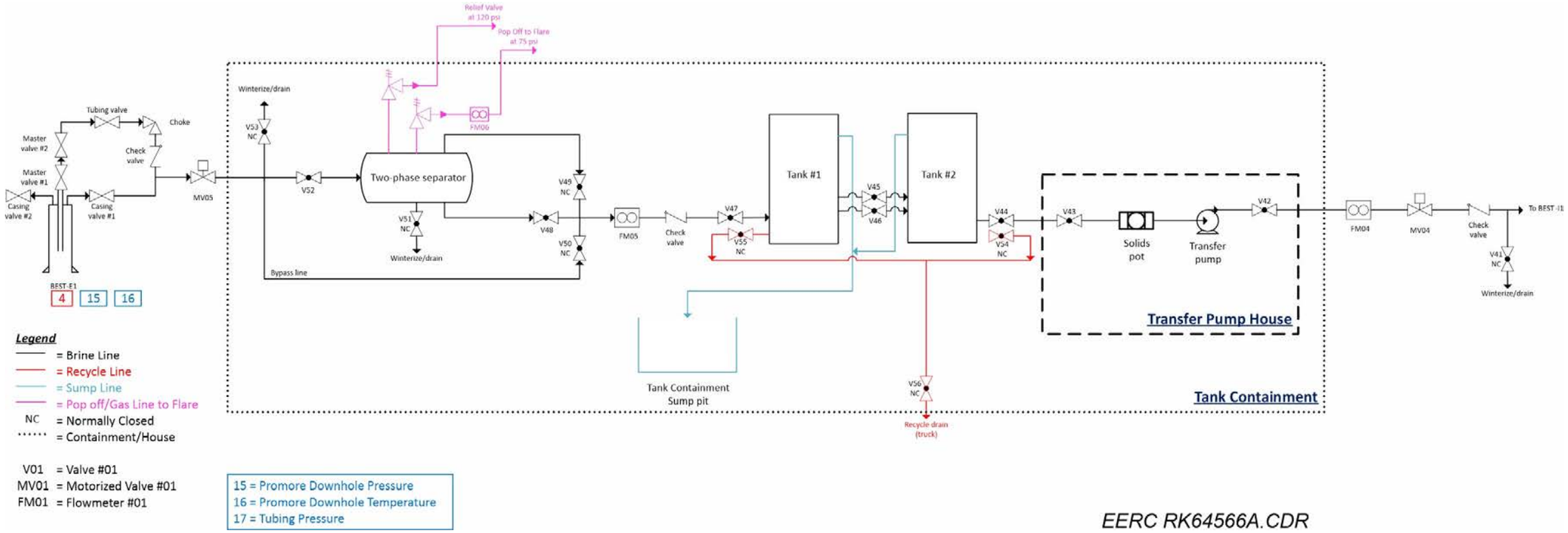


Figure A-7. BEST-E1 PFD.



Figure A-8. BEST-E1 brine-handling tank farm (right) and charge pump house (left). The charge pump sends fluid from the BEST-E1 tanks down the pipeline to the BEST-I1 well pad (note EERC personnel for scale).

The transfer pump house is an insulated enclosure that incorporates a 300-µm filter pot and a charge pump to transfer the water from the BEST-E1 to BEST-I1 site through the underground flow line. The charge pump was outfitted with high-pressure, low-pressure, and low-tank-level switches and a high-tank-level activation switch. These redundances were used to prevent spill/overflow safety and environment risk mitigation. The charge pump was a Goulds 3657 centrifugal pump capable of over 5000 bpd at 90 psi. This satisfied the estimated maximum rate for testing at 5000 bpd. All digital data (casing pressure, tubing pressure, flowmeter data, fluid density data, bottomhole pressure [BHP], bottomhole temperature [BHT], tank level, flow line, and flow line monitoring data, etc.) were tied into a real-time remote monitoring and data-logging system (SCADA). The BEST-E1 site was operational on November 24, 2018.

Rink SWD #1 and Rink SWD #2

Rink SWD #1 and Rink SWD #2 are commercial water injection sites operated by Landtech Enterprises, LLC. The site has surface handling facilities set up and was operating at upward of 14,000 bpd at the inception of this project. The installed infrastructure includes tank farms, two charge pumps, and two injection pumps. These injection pumps were approved for maximum rates of 9500 and 7500 bpd and pressures of 1450 and 1400 psi, respectively. Table A-3 provides more information on injection pumps.

Table A-3. Landtech Rink SWD #1 and Rink SWD #2 Disposal Pump Parameters

Parameters	Rink SWD #1	Rink SWD #2
Surface Pump		
Pump Type	National J-165 pump	National J-165 pump
Plunger Size, in.	3¾	3¾
Maximum Pumping Rate, blpd	9250	7500
Maximum Pumping Pressure, psig	760	1180
Approved Permit		
Maximum Injection Rate, blpd	9500	7500
Maximum Surface Injection pressure, psig	1450	1400
Current Injection Parameters		
Injection Rate, blpd	7115	6638
Surface Injection Pressure, psig	880	870

Additions to the existing Rink SWD #1 and Rink SWD #2 include digital pressure sensors on both tubing and casing, a density meter on the flow line, PROMORE suspended bottomhole pressure and temperature (BHP/T)gauges, and additional flow line from the charge pump to the BEST-I1 facility. Rink SWD #1 and Rink SWD #2 had wireline install PROMORE suspended BHT/P gauge that was completed in November 2018. Figures A-9 and A-10 show the installation process and wellbore diagram with BHP/T. Figure A-11 provides the technical drawing of the wellhead pack-off that allows the real-time reading of the gauge but still maintains the wellhead isolation.



Figure A-9. Installing the suspended BHT/P gauge at Rink SWD #1.

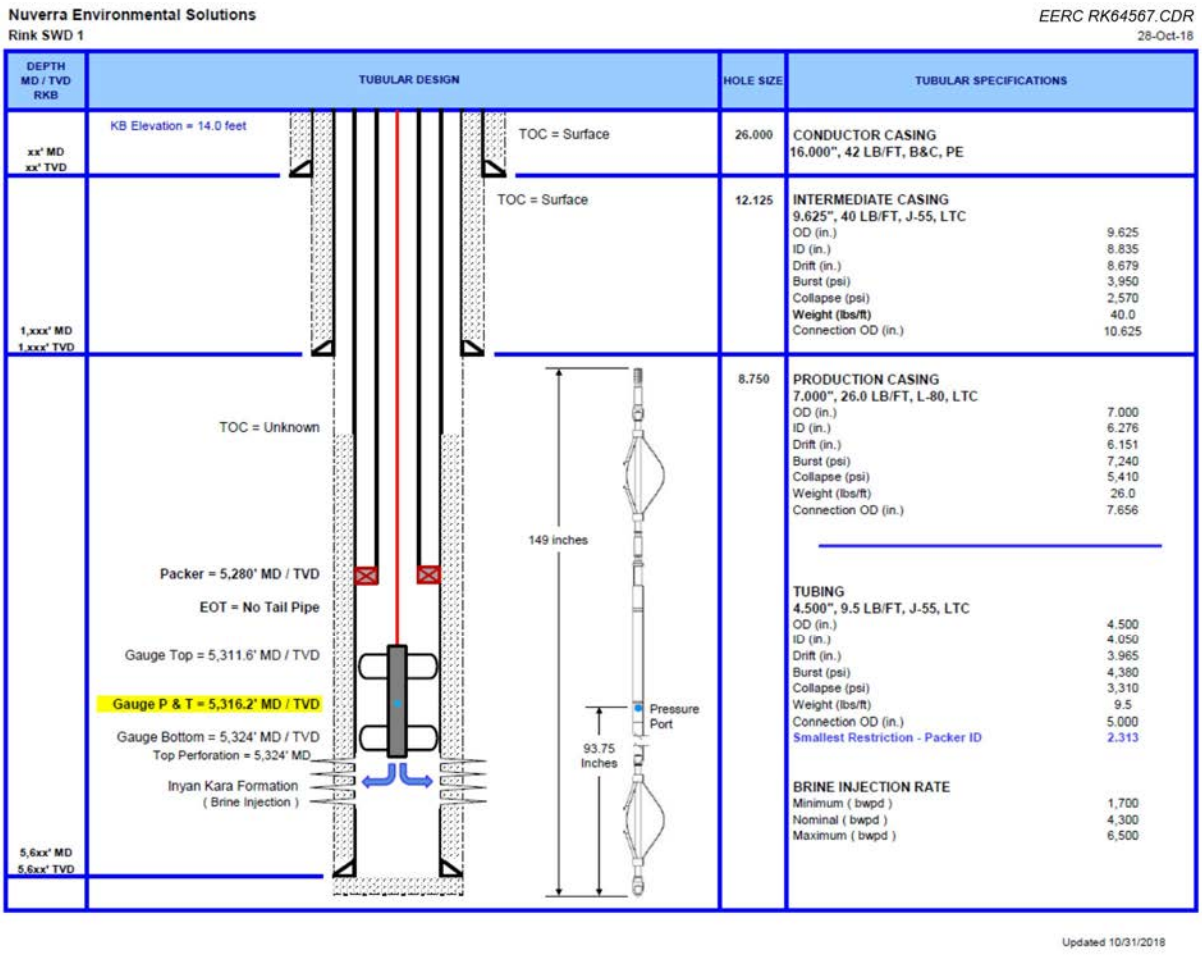


Figure A-10. Rink SWD #1 wellbore diagram with BHP/T gauge install.

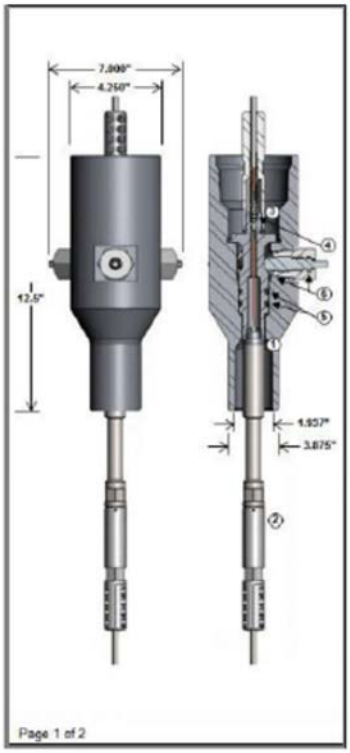
EERC RK64568.CDR

PROMORE
Core Lab

Design Specifications and Manufacturing Notes

QF-24, Rev. 0, Nov. 2004 — Page 1 of 1

Description: *Wellhead Hanger - WHSA-5000* — *Part Number:* *FG-106904*



OVERALL DIMENSIONAL DATA	
Overall Length	12.5 inch
Maximum Outside Diameter	7.000 inch
Overall Weight	Approximately 43 lbs

WELLHEAD SUSPENSION ASSEMBLY	
Length	12.5 inch
Outside Diameter - Maximum	7.000 inch
Outside Diameter - Body	4.250 inch
Inside Diameter - Minimum	1.901 inch
Thread Connection - Box	3.5 inch EUE
Thread Connection - Pin	2.875 inch EUE - Threaded to Top of Wellhead
Metallurgy	4140 QT NACE MR01-75
Weight	40 lbs

SUSPENSION CABLEHEAD SPECIFICATIONS	
Length	15 inch
Maximum Outside Diameter	1.375 inch
Primary External Seals [1]	Hermetically Sealed (Welded)
Primary Internal Seals [2]	20,000 psi Elastomer Boot Assembly
Cablehead Anchor Pull-Out Strength	1,327 lbs (80% of Cable Breaking Strength)
Service Conditions	Mild H_2S, Mild CO_2
Wetted Part Material	4140 QT NACE MR01-75
Non-Wetted Material	4140 QT NACE MR01-75
Non-Critical Material	4140 QT NACE MR01-75

HANGER INSERT SPECIFICATIONS	
Metallurgy	4140 QT NACE MR01-75
Electrical Bulkhead Connector	Kemlon / 1 Pin / Inconel / Welded / 20,000 psi
Primary Seal on Bulkhead Connector [3]	Hermetically Sealed (Welded)
Secondary Seal on Bulkhead Connector [4]	Dual O-Rings (Viton 90 Durometer)
Primary Seals on Hanger Inset [5]	Dual O-Rings (Viton 90 Durometer)
Primary Seals on Lag Bolts [6]	Dual O-Rings (Viton 90 Durometer)

TAPPED BULL PLUG *(See Page 2)*	
Model	3.5 inch EUE Male x 0.750 inch NPT Female
Pressure Rating	5,000 psi
Weight	3 lbs

Figure A-11. PROMORE wellhead suspended specification.

BEST-I1

BEST-I1 was located on a previously unoccupied 3-acre bermed pad located on the northeast corner of the Johnson's Corner site (Figure A-12). After the well was completed, brine-handling facilities, infrastructure, command center, and water treatment facilities were installed on the pad. The facilities include flowlines, six 500-bbl fiberglass tanks, transfer pumps, injection pumps, and water treatment facilities to inject extracted fluid into the BEST-I1 wellbore. The injection facility at the BEST-I1 site duplicated the setup of Rink SWD #1 and Rink SWD #2. The BEST-I1 location allows the project to obtain the water supply from the BEST-E1 site and the Rink facility to supply water to the brine treatment test bed facilities and dispose to the BEST-I1 well. The flow line outfitted with digital density, pressure, and flowmeters will connect the BEST-I1 wellhead to the 500-bbl fiberglass production tank farm. Extracted water from BEST-E1 was sent through the flow line to six 500-bbl (12-ft × 25-ft) heat-traced and insulated tanks connected in series. These tanks provide solids settling before entering the charge pump and buffer capacity between extraction and injection rates. The tanks were constantly monitored using a float and radar system. This would allow the charge pump to kick on and push water to the injection pump for BEST-I1. Multiple flowmeters were installed throughout the flow line on both the upstream and downstream



Figure A-12. Overview of the BEST-I1 brine-handling tank farm, looking north. The flow line enters the tank farm at the lower-left corner and is allowed to distribute through five of the six tall brine-handling tanks. Every tank is valved such that it can be isolated for maintenance. An environmental enclosure (foreground) contains a charge pump that is able to move fluids to and from each tank as necessary. The tanks are enclosed in a steel primary spill containment system (short wall visible around the tanks). The brine treatment test bed facility is the large building on the right. The BEST-I1 injection pump is located north of the test bed facility and is not visible.

sides of injection and transfer pumps to monitor and verify fluid volumes. Figure A-13 provides the PFD of the BEST-I1 facility (Figure A-12). The injection pump is a National J-165T-5 triplex positive displacement pump with a 2¾-in. plunger (Figure A-14). This pump was selected for fitting within the maximum operating pressure of 1590 psi with injection rates up to 5292 bpd.

Downhole monitoring equipment installed in the project wells was connected to data loggers and other supporting equipment at the surface (Figure A-15). This equipment was subsequently connected to the site's SCADA system. Prior to its removal, the driver system for the ESP was also connected to the SCADA system (Figure A-16).

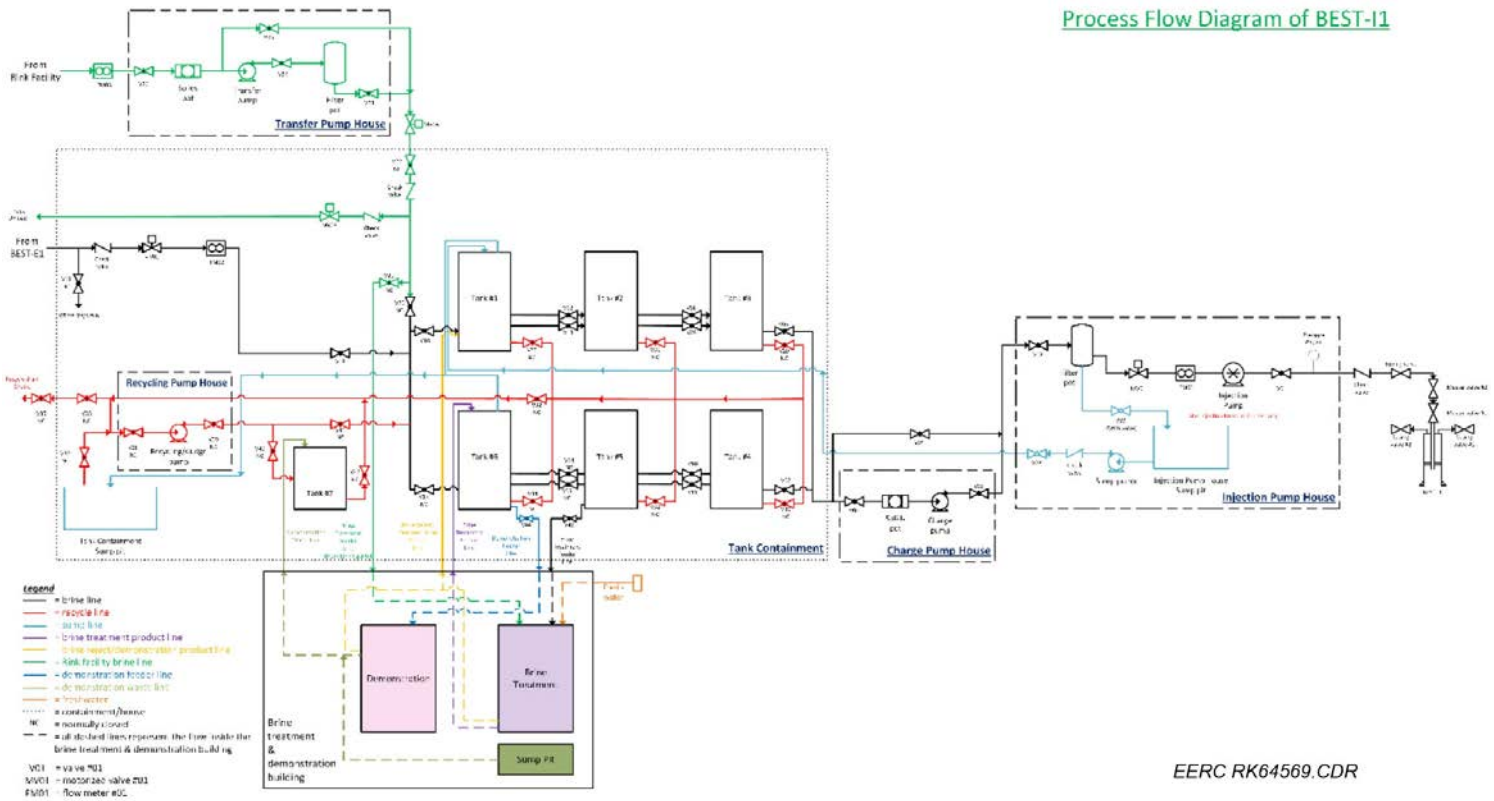


Figure A-13. PFD of BEST-I1.



Figure A-14. National J-165T-5 field photo.



Figure A-15. View of the BEST-E1 wellhead and monitoring equipment. The flow line at the top of the wellhead carried fluid pumped up the tubing by the electric submersible pump (ESP), prior to its removal. The flow line at the bottom of the wellhead carries fluid that is able to naturally flow up the casing of the well. Both lines then lead to the two-phase separator and tanks on the BEST-E1 well pad.



Figure A-16. The variable-speed driver (consisting of power and controlling equipment) is located adjacent to the BEST-E1 wellhead. The driver could be controlled on-site or remotely through the EERC's SCADA system. The driver system was removed from the site when the ESP was removed in 2020.

SCADA System

Data Acquisition System

The brine extraction and storage test (BEST) data acquisition requirements were defined by specifications given by the engineering firm AE2S, a partner in developing this system. This engineering road map constructed the system to record the BEST operation data from the extraction well to the injection well. The project of data acquisition was divided into three tasks:

1. Collect data from BEST E1 and BEST-I1.
2. Monitor and collect data from Rink SWD #1 and Rink SWD #2.
3. Create a safety-monitoring system for the flow line and extraction and injection sites.

A local area network was needed to enable the ability to seamlessly connect the extraction and injection wells over a distance of 4000 ft. The distance between the BEST-E1 site and the designated control room and line of site eliminated the possibility of radio data transmission. This left fiber-optic cable as the best means of communication between sites. Fiber-optic cable and

power cable were installed in the same trench as the flow line from the BEST-E1 to BEST-I1 site. This carried the required power for the data systems on BEST-E1's remote site.

The main data acquisition system in the control room at the BEST-I1 site contains a module capable of connecting to more signals. The program is divided into multiple programs called visual interfaces (VIs), representing different areas of the entire system (Figures A-17 and A-18). The Rink site, BEST-E1, and BEST-I1 subsystems are all independent, which allows one or more of the subsystems to be offline while the other subsystems still collect data and are functioning. The Data Save VI is used to collect the data at a user-specified rate and has seamless data file change routines to ensure that no data are lost, in addition to having the system run a RAD1 mirroring process to create duplication and backup of the hard drive. This setup allowed for continuous monitoring from June 2019 to the present. The system is visible from any remote site, with Internet access using RealVNC software. The system was reliable and required little if any maintenance.

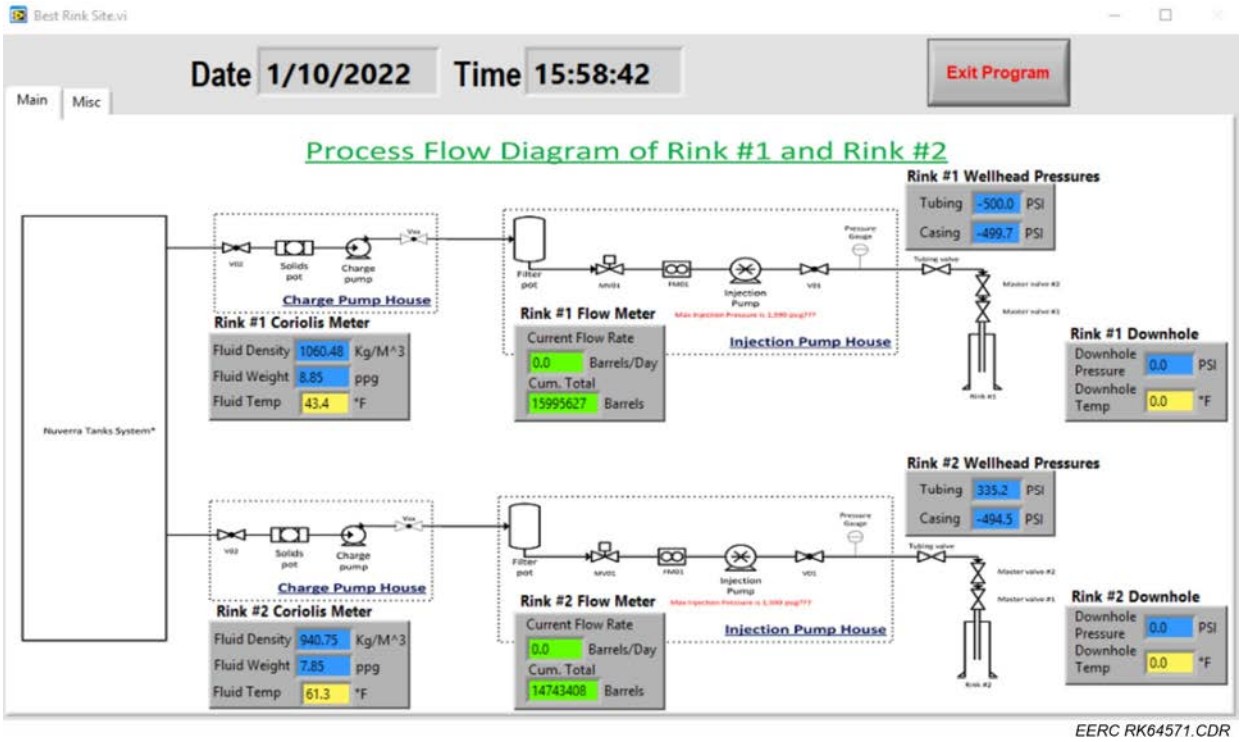


Figure A-17. VI for Rink SWD #1 and #2 injection system.

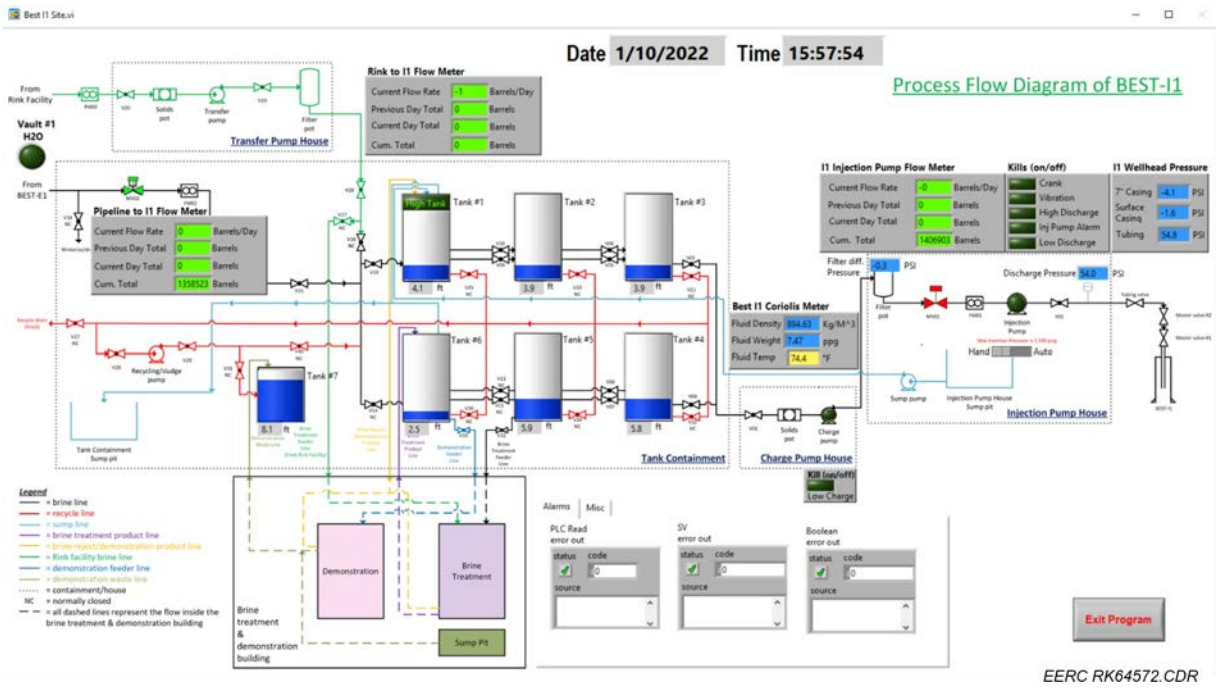


Figure A-18. VI for BEST-I1 facility.

Troubleshooting

Site Infrastructure

All volumes injected in Rink SWD #1 and Rink SWD #2 are controlled by Nuverra. Injection rates were previously agreed upon not to interfere with commercial operation. Near the end of the testing period of Phase I, oil prices fell sharply. This reduced the number of new wells being brought online in the area and caused many wells to become shut in or file for temporary abandonment. Because of this, the amount of fluid that was being commercially disposed of in this area decreased. The rates were adjusted for Phase II.

One issue that arose during the project was a higher-than-anticipated downhole temperature within BEST-E1. The industry-standard techniques for this area of the Williston Basin were used to estimate the Inyan Kara fluid temperature (155°F). These were inadequate for the area after the high temperatures were observed (180°F). The high temperatures threatened to damage surface infrastructure with long-term exposure. Multiple options were investigated, with the option of replacing items with appropriate temperature ratings selected. The selected items included some surface pumps, fittings, and piping. Figures A-19 and A-20 show initial polyvinyl chloride line install versus fiberglass replacement. Additionally, Nuverra agreed to increase retention time by increasing the tank's level from 9 to 15 ft, thus decreasing the fluid's temperature by increasing the cooling time during the winter months. The maximum extraction rate was planned in Phase II during the winter months to take advantage of the cold external temperatures.



Figure A-19. BEST-I1 T-section of poly pipe flow line was removed to replace fiberglass flowlines and associated fittings (photo June 4, 2020).



Figure A-20. High-temperature flow line was replaced by yellow fiberglass piping to allow for high-temperature fluid flow throughout active reservoir management (ARM) infrastructure. The flow line was replaced from surface holding tanks to the BEST-I1 charge pump (photo June 4, 2020). North Dakota temperatures drastically decrease during the winter months, with average temperatures between 2° and 40°F from December through

March. These temperatures have been known to cause issues with flow lines and valves during these times. The BEST facilities' complete winterization was implemented and fulfilled in November 2019 to eliminate the risk of any damage created by stationary fluid. This included heat-traced and insulated select surface flow lines and valves. Figure A-21 shows insulation and heat traces installed onto flow lines and bottom of tanks.



Figure A-21. Heat trace located on lines into and between brine storage tanks.

ESP Removal (BEST-E1)

Multiple well tests were performed to optimize the extraction rate of BEST-E1. The well test evaluation results provided that the ESP was unable to deliver the required rate of 5000 blpd and performed as a downhole choke. The summary of well tests is provided in Table A-4.

According to the test results, the BEST-E1 absolute open flow (AOF) is ~200,000 bpd generated using an inflow performance relationship (IPR) curve shown in Figure A-22. AOF is the maximum production rate when producing with a BHP of 0 psi. The IPR curve shows that the well would flow with the desired maximum rate of 5000 bpd naturally or without an ESP. Optimization was performed in October 2018 to remove the ESP since the BEST-E1 well can produce naturally at the target rate.

Table A-4. Results from Flow Test in May 2019

Test	Casing	Tubing Choke	ESP, Hz	Casing Pressure, avg. psi	Pressure Diff. (initial flowing), avg. psi	Average Rate, bpd	Time, hour:min
1	Open	Close	Off	43	NA	3312	1:00
2	Open	22	45	54	35	4050	1:00
3	Open	22	55	59	70	4512	1:00
4	Open	22	65	63	173	4406	1:00
5	Open	28	65	70	72	4512	0:30
6	Open	30	65	74	33	4752	0:10
7	Closed	30	65	63	32	1944	0:22
8	Closed	Open	Off	Closed	–89	960	0:15

The well test data provided in Table A-4 were used to generate an IPR curve of BEST-E1 (Figure A-22). This curve suggested, in concurrence, with SLB that the ESP was acting as a downhole choke in the flow path. The resulting AOF is ~200,000 bpd. AOF is the value of maximum production rate of a well when producing with a BHP of 0 psi. This curve helps to identify the well capability to extract fluid. The IPR curve shows that the well would be able to flow with desired maximum rate of 5000 bpd naturally or without an ESP.

According to the inflow–outflow performance relationship curve, BEST-E1 is capable of producing 5000 bpd by maintaining the wellhead pressure at 30 psi. This will generate a flowing BHP of 2608 psi. A reservoir simulation was performed and verified that the reservoir is capable of producing 5000 bpd continuously for more than 12 months. Based on these results and having a possibility of the ESP getting stuck, the EERC decided to remove the ESP on February 14, 2020. The well was completed with 4½-in. tubing and packer string, as shown in Figure A-23.

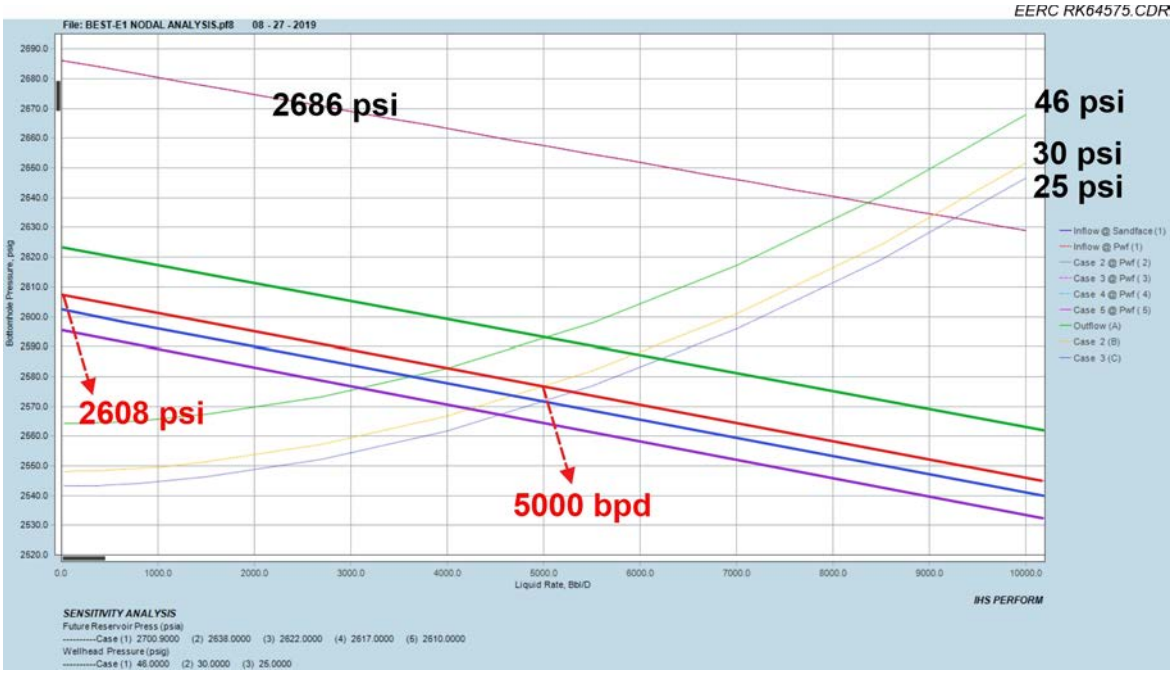


Figure A-22. IPR curve.

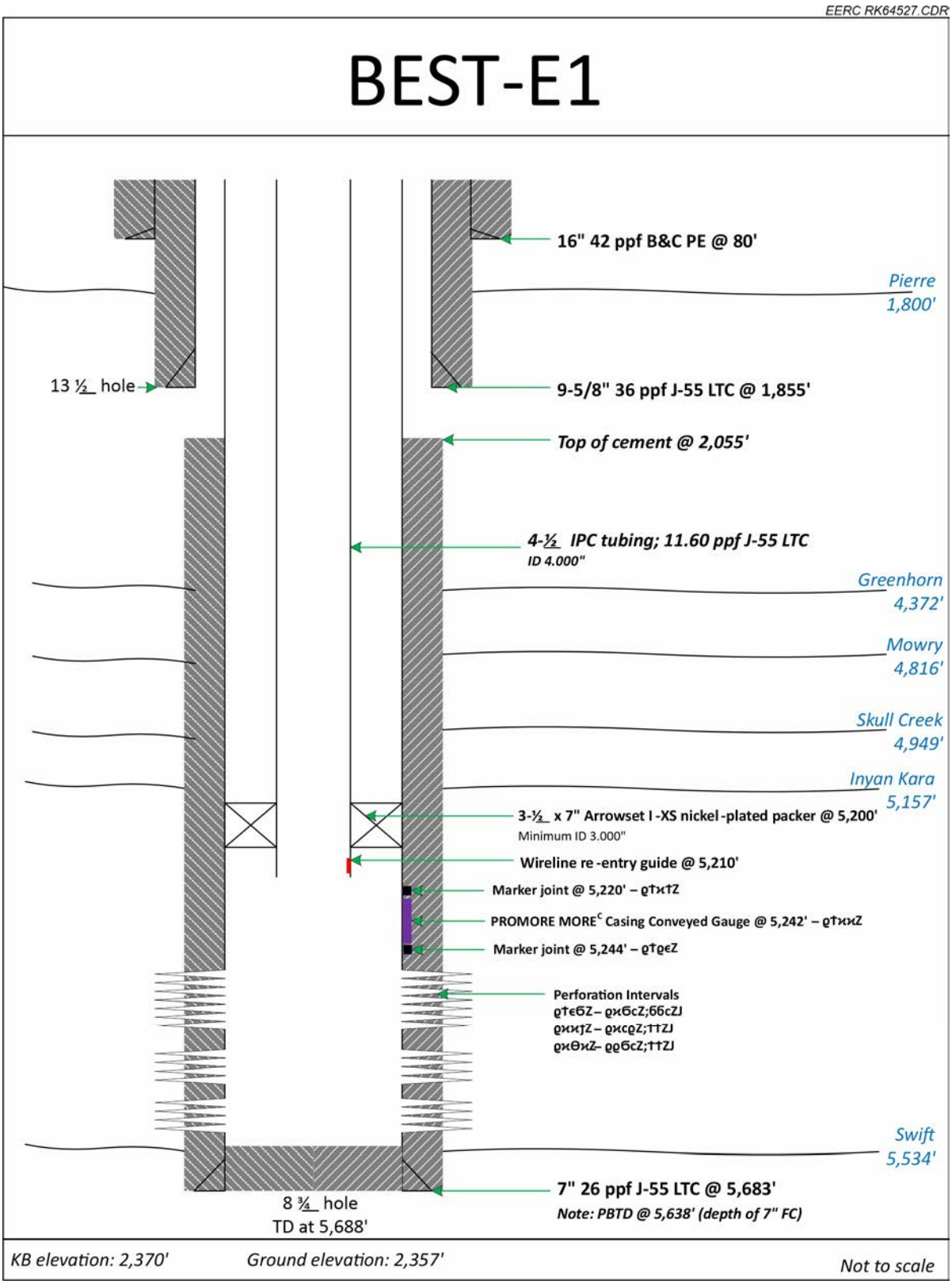


Figure A-23. BEST-E1 well schematic post-ESP removal.

APPENDIX B

WELL DRILLING AND COMPLETION

WELL DRILLING AND COMPLETION

The BEST-I1 well was spud on April 22, 2018. The 13½-in. surface section was drilled with freshwater to 1879 ft. The surface casing (9⅝ in.; J-55; 36 ppf) was set at 1868 ft and cemented with Class G cement.

The 8½-in. long-string section of the well was drilled with a saltwater gel mud system. Four-in. whole core was collected in the Inyan Kara and Broom Creek Formations and the respective confining layers. Reservoir Group, the coring company, cut 200 ft of core and recovered 190.7 ft for 95.35% overall core recovery. Table B-1 provides the core footage from the Inyan Kara and Broom Creek Formations of BEST-I1. The core barrel length on all runs was 100 ft. Reservoir Group used 20-ft-long, aluminum, half-moon sleeves to house the core. The half-moon sleeves enable performing core interpretation on-site. BEST-I1 reached a total depth of 7960 ft MD on May 10, 2018. After reaching bottom, the well was logged using triple combo log, spectral gamma ray, and a sonic scanner.

The long-string casing (7 in.; J-55; 26 ppf) was set at 7955 ft and cemented with Class G cement. A set of formation characterization activities was performed in BEST-I1 well that included core, geophysical logs, downhole testing, and sampling in Inyan Kara and Broom Creek and associated confining layers.

Table B-1 Core Collection from BEST-I1 Well

Formation	Cored Interval, ft	Recovered Core Length, ft
Inyan Kara	5271–5371	100.6
Opeche Broom Creek Amsden	7435–7535	90.1

The BEST-I1 well was completed in November 2018 as a water disposal Class I well. BEST-I1 was logged to verify top of cement at 2055 ft. The Broom Creek and Amsden Formations were perforated from 7478 to 7534 ft and 7633 to 7703 ft, respectively, using 1919-gramharges at 6 spf and 60^{o} phasing. A step rate test was performed in both the Amsden and Broom Creek. No fracture gradient was found while pumping in either. The maximum rate observed was 8.0 bpm at 4000 psi in the Amsden Formation and 7.5 bpm at 3770 psi in the Broom Creek Formation. Stimulation using hydrochloric acid was performed in each formation to improve reservoir injectivity; 178.5 and 180 bbl were used in the Amsden and Broom Creek, respectively. Pressure reduction was noticed in each treatment. The poststimulation injectivity index was 3.4 bpm at1500 psi for the Broom Creek Formation and 4.6 bpm at 1440–1780 psi for the Amsden Formation. The completion of both formations indicated that BEST-I1 is capable of injecting up to 10,500 bpd. This rate is greater than the field implementation program (FIP) target of 5000 bpd. 4½-in. internal plastic coated (IPC) tubing and a permanent packer were installed as the injection string. Figure B-1 provides the wellbore schematic of BEST-I1 postcompletion.

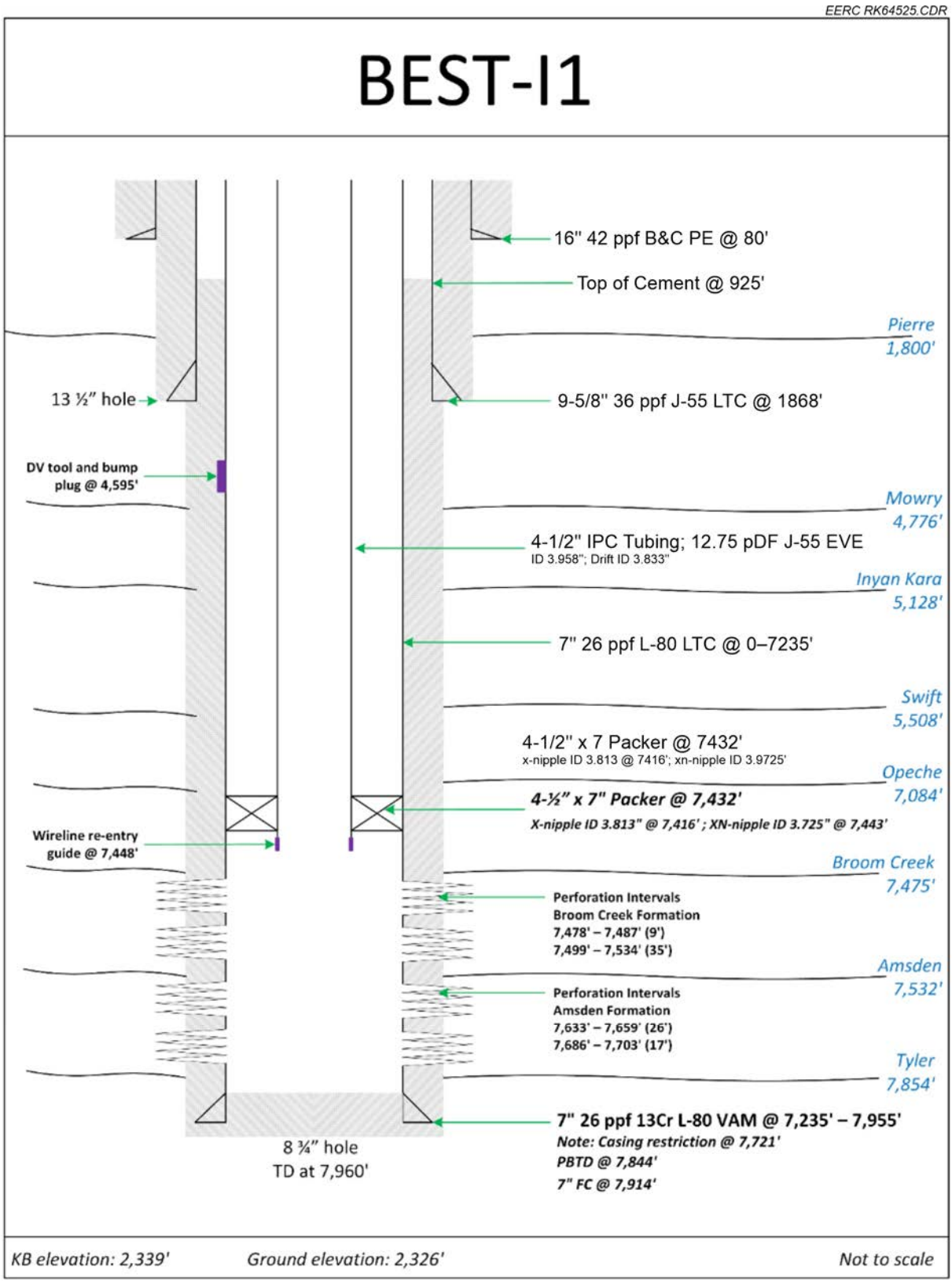


Figure B-1. BEST-I1 wellbore schematic post-well completion.

The drilling rig moved in from the BEST-I1 site to spud the BEST-E1 well on May 16, 2018. The 13½-in. surface section was drilled with freshwater to 1865 ft. The surface casing (9⅝ in.; J-55; 36 ppf) was set at 1855 ft and cemented with Class G cement The 8½-in. long-string section of the well was drilled with a saltwater gel mud system. BEST-E1 reached a total depth of 5688 ft MD on May 22, 2018. A triple combo was performed for formation characterization prior to running the casing. The long-string casing (7 in.; J-55; 26 ppf) was set at 5683 ft and cemented with Class G cement. A casing-conveyed PROMORE gauge was installed at 5243 ft to monitor bottomhole pressure response during active reservoir management (ARM) operation.

The BEST-E1 well was completed on October 24, 2018, as the extraction well. The Inyan Kara Formation was perforated with 4 spf with 90° phasing with 19-gram charges, from 5290 to 5506 ft. A step rate test was performed to determine the fracture pressure of the Inyan Kara Formation. The calculated fracture gradient is 0.72 psi/ft.

Stimulation using 178.5 bbl of hydrochloric acid was performed to improve the reservoir near-wellbore permeability. This allows consistent inflow from the reservoir. The injected acid had a noticeable pressure response. 4½-in. IPC tubing and an electrical submersible pump (ESP) were installed as the extraction string. The ESP landed at 5228 ft, with the intake at 5180 ft. The initial flow test suggested the well is capable of 50,000 bpd. This is estimated to meet the FIP maximum extraction rate of 5000 bpd.

Wellbore cleanout was performed using a 6⅛-in. scraper mill prior to perforating the Inyan Kara extraction intervals, 5290–5506 ft.

According to the initial well design, an ESP was needed to achieve the target extraction rate of 5000 bpd. The SLB ESP was installed on October 29, 2018, with the following specifications: two 538 S4000N pumps; 56 and 66 stages, respectively; with 562 Maximus F120 motor (450 hp). Appendix D provides information on the pump and motor installed. The ESP was installed with 4½-in. tubing as the extraction string. Figure B-2 provides the postcompletion wellbore schematic of BEST-E1 with ESP installed. The ESP was subsequently removed from the well.

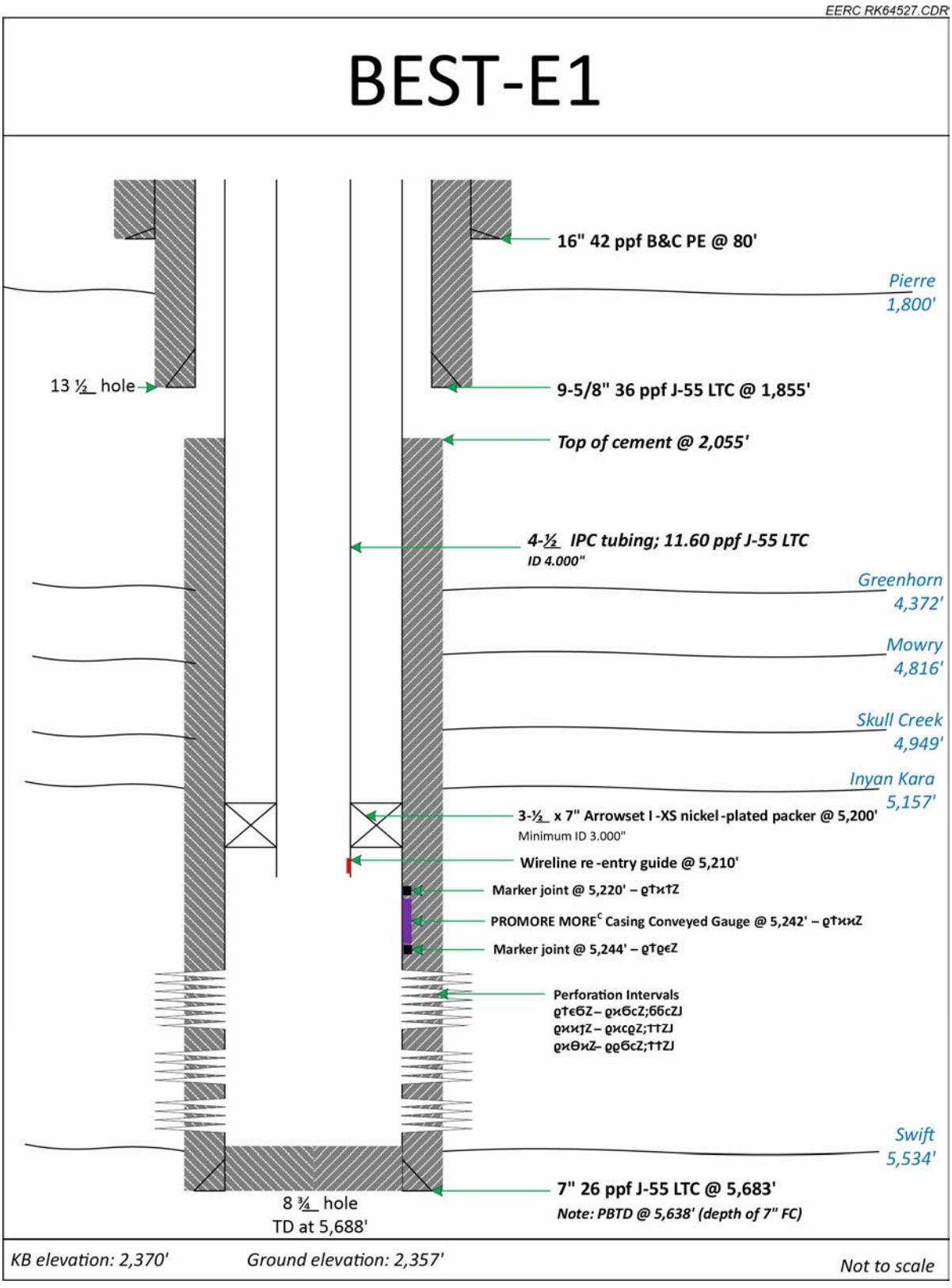


Figure B-2. BEST-E1 wellbore schematic with ESP installed.

APPENDIX C

ESP PUMP SPECIFICATIONS

ESP PUMP SPECIFICATIONS

General Report

Schlumberger

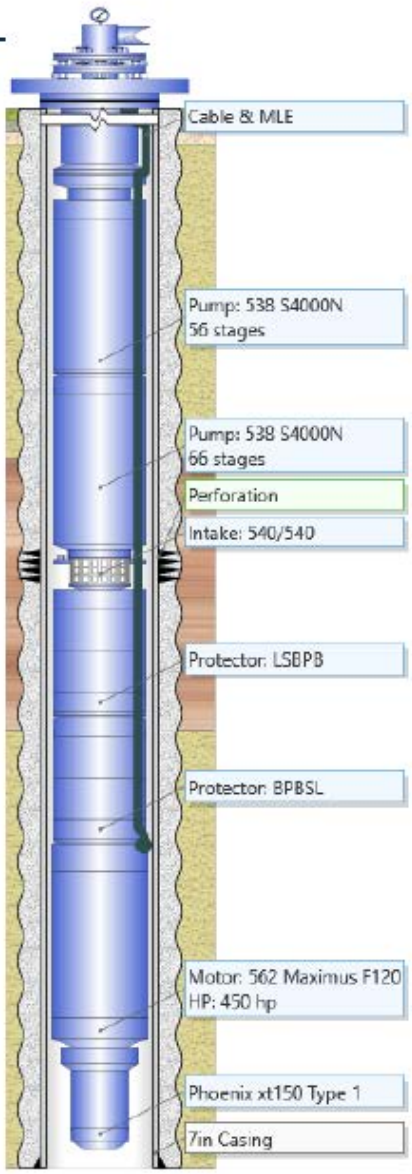
Company:	Landtech	**Project:**	ESP Design
Engineer:	Josh Geist	**Date:**	9/26/2018

Technical Design

General Information

Contact Details

Project	*ESP Design*
Prepared by	*Josh Geist*
Date	*9/26/2018 12:00:00 AM*
Corporate	*Landtech*
Customer	
Well Name	*Best E1 - EERC Project*



Company:	Landtech	**Project:**	ESP Design
Engineer:	Josh Geist	**Date:**	9/26/2018

Input Data and Information

Production and Fluid Data

Oil Gravity	*30*	*°API*	Water Specific Gravity	*1.07*	
Water Cut	*100*	*%*	Gas Specific Gravity	*0.65*	
GOR	*0*	*SCF/STB*	Bubble Point	*0*	*psig*

Wellbore Information

Wellhead Temperature	*80*	*°F*	Bottom Hole Temperature	*165*	*°F*
Perforation Depth	*5400*	*ft*			

Casing	Length (ft)	OD (in)	ID (in)	Roughness (in)	Flow Type
1	*5688*	*7*	*6.276*	*0.00065*	*TUBULAR*

Tubing	Length (ft)	OD (in)	ID (in)	Roughness (in)	Flow Type
1	*5364.4*	*4.5*	*3.958*	*0.00065*	*TUBULAR*

Desired Operating Conditions

Pump Depth	*5400*	*ft*	Frequency	*47*	*Hz*
Design Rate	*4500*	*STB/d*	Wellhead Pressure	*1000*	*psig*
Pump Speed	*2714.5*	*RPM*			

Company:	Landtech	**Project:**	ESP Design
Engineer:	Josh Geist	**Date:**	9/26/2018

Equipment and Results

Pumping Conditions

Production Rate	5146.5	STB/d	TDH	1920.93	ft
Intake Pressure	2628.3	psig	Fluid Level		
Discharge Pressure	3507.6	psig	Pump Speed	2714.5	RPM
Mixture Gradient	0.457	psi/ft	Separation Efficiency	8.25	%

Pump Information

Device Information	REDA 538 S4000N		
Stages	122		
Staging Configuration	CR-CT	Staging Type	ARZ

Pump Intake

Device Information	REDA 540/540 540/540	Power	0 hp

Motor Nameplate Information

Device Information	REDA 562 Maximus F120				
Volts	1738	Volts	Power	450	hp
Speed	2714.5	RPM	Amp	157	Amps
Rating Factor	100	%	Winding Number	F120	
Instrument Tube OD					

Motor Lead Extension

Type	KELB		Connection Type	PLUG-IN (MAXLOK-400)	
Length	100	ft	KV	5	
Minor Armor OD	0.517	in	Major Armor OD	1.302	in
Conductor Size	4	AWG	Material/Armor	M	

Cable Information

Type	ELB	
Conductor Size	2	
Length	5500	ft
KV	5	kV
Temperature Rating	450	°F

Protector

Thrust Bearing Type	540 Maximus HL	Oil Type	REDA OIL #5
Number of Seals	5		
Configuration	LSBPB BPBSL		
Number of Chambers	6		
Components	TANDEM		

Sensor

Device Information	Phoenix xt150 Type 1

VSD

Device Information	NEMA-3/R Enclosure				
Manufacturer	SCHLUMBERGER		Type	SpeedStar SWD	
Pulse	6		Nameplate Output Current	623	Amps
KVA Rating @480V 60HZ	518		KVA Rating @380V 50Hz	410	
Actual KVA	502.46		Current @ Run Frequency	604.3	Amps
Base Frequency	47	Hz	Run Frequency	47	Hz

Step Up Transformer

Device Information	3-Phase VSDRated StepUp				
Manufacturer	SWE		Description	FACTIII, OISC	
Frequency	60	Hz	KVA	520	
Primary Delta	480	Volts	Secondary Min.	1100	Volts
Secondary Max.	3811	Volts			

Schlumberger-Private

Company:	Landtech	**Project:**	ESP Design
Engineer:	Josh Geist	**Date:**	9/26/2018

Conditions at Operating Frequency

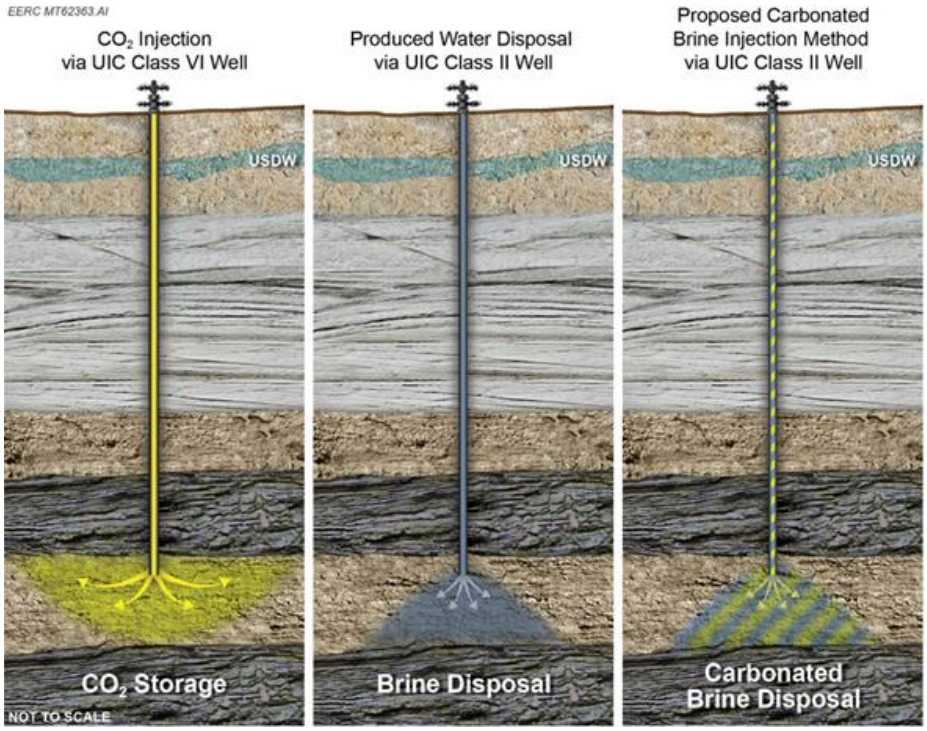
Operating Frequency	*47*	*Hz*	Volts @ Junction Box	*1546.3*	*Volts*
Motor Amp	*100.5*	*Amps*	KVA @ Junction Box	*268.79*	
Total Motor Load	*173.7*	*hp*	Motor Volts	*1361.5*	*Volts*

Schlumberger-Private

APPENDIX D

ASSESSMENT OF CARBONATED BRINE INJECTION AS LOW-RISK STRATEGY FOR GEOLOGIC CARBON STORAGE

NATIONAL ENERGY TECHNOLOGY LABORATORY



Assessment of Carbonated Brine Injection as Low-risk Strategy for Geologic Carbon Storage

20 October 2023

U.S. DEPARTMENT OF ENERGY | NATIONAL ENERGY TECHNOLOGY LABORATORY

Office of Fossil Energy and Carbon Management

DOE/NETL-2023/4328

Disclaimer

This project was funded by the United States Department of Energy, National Energy Technology Laboratory, in part, through a site support contract. Neither the United States Government nor any agency thereof, nor any of their employees, nor the support contractor, nor any of their employees, makes any warranty, express or implied, or assumes any legal liability or responsibility for the accuracy, completeness, or usefulness of any information, apparatus, product, or process disclosed, or represents that its use would not infringe privately owned rights. Reference herein to any specific commercial product, process, or service by trade name, trademark, manufacturer, or otherwise does not necessarily constitute or imply its endorsement, recommendation, or favoring by the United States Government or any agency thereof. The views and opinions of authors expressed herein do not necessarily state or reflect those of the United States Government or any agency thereof.

Cover Illustration: Graphical representation of proposed carbonated brine injection (CBI) method compared to traditional free-phase CO_2 injection via Class VI well and standard produced water disposal via Class II well. As shown in the center image, with the CBI method, the CO_2 remains dissolved into the brine, thereby eliminating the risk of free-phase CO_2 migration and negligible pressure changes when compared to standard Class II operations.

Suggested Citation: Xiong, W.; Belarbi, Z.; Thomas, R.; Crandall, D.; Tesfu, M.; Taunton, M.; Klapperich, R.; Kurz, M. *Assessment of Carbonated Brine Injection as Low-risk Strategy for Geologic Carbon Storage*; DOE.NETL-2023. 4328; NETL Technical Report Series; U.S. Department of Energy, National Energy Technology Laboratory: Pittsburgh, PA, 2023; p 56.
https://doi.org/10.2172/2204489

An electronic version of this report can be found at:

https://netl.doe.gov/energy-analysis/search

Assessment of Carbonated Brine Injection as Low-risk Strategy for Geologic Carbon Storage

Wei Xiong[1,2]; Zineb Belarbi[3,4]; Randal Thomas[3]; Dustin Crandall[5]; Merry Tesfu[6]; Meghan Taunton[6]; Ryan Klapperich[6]; Marc Kurz[6]

[1] National Energy Technology Laboratory, 626 Cochran Mill Road, Pittsburgh, PA 15236, USA

[2] NETL Support Contractor, 626 Cochran Mill Road, Pittsburgh, PA 15236, USA

[3] National Energy Technology Laboratory, 1450 SW Queen Avenue, Albany, OR 97321, USA

[4] NETL Support Contractor, 1450 SW Queen Avenue, Albany, OR 97321, USA

[5] National Energy Technology Laboratory, 3610 Collins Ferry Road, Morgantown, WV 26505, USA

[6] University of North Dakota, Energy & Environmental Research Center (EERC), 15 North 23rd Street, Stop 9018, Grand Forks, ND 58202, USA

DOE/NETL-2023/4328

20 October 2023

NETL Contacts:

Randal Thomas and Wei Xiong, Principal Investigators

Dustin Crandall, Technical Portfolio Lead

Bryan Morreale, Associate Laboratory Director for Research & Innovation, Research & Innovation Center

This page intentionally left blank.

Table of Contents

EXECUTIVE SUMMARY **1**
1. INTRODUCTION **3**
1.1 OVERVIEW OF SALTWATER DISPOSAL 4
1.2 OVERVIEW OF CARBON CAPTURE, UTILIZATION, AND STORAGE 6
1.3 THE CONNECTION BETWEEN SWD AND CCUS: THE CONCEPT OF CBI AND STORAGE 6
1.4 RESEARCH ON CBI AND STORAGE 8
2. METHODS **10**
2.1 RESERVOIR MODEL SETUP 10
2.2 PRODUCED WATER DATA 15
2.3 WELLBORE CORROSION MODEL 15
2.4 REACTIVE TRANSPORT MODEL 17
3. RESULTS **20**
3.1 RESERVOIR SIMULATION 20
3.2 WELLBORE CORROSION MODEL 24
3.3 REACTIVE TRANSPORT MODELING 27
4. DISCUSSIONS **37**
4.1 CO_2 CONCENTRATION FOR CBI 37
4.2 COMPATIBILITY OF EXISTING INFRASTRUCTURE 37
4.3 LONG-TERM STORAGE SAFETY 38
4.4 NANOBUBBLE TECHNOLOGY FOR CO_2 INJECTION 39
5. CONCLUSIONS **42**
6. REFERENCES **43**

This page intentionally left blank.

List of Figures

Figure 1: Graphical representation of a proposed CBI method compared to traditional free-phase CO_2 injection via a Class VI well and standard produced water disposal via a Class II well. As shown in the center, with the CBI method, the CO_2 remains dissolved into the brine, thereby eliminating the risk of free-phase CO_2 migration and negligible pressure changes when compared to standard Class II operations. 4
Figure 2: Distribution of active SWD wells in 2019 5
Figure 3: States with large wastewater injection volumes can sequester 53 Mtpa CO_2 using CBI. 7
Figure 4: Simulation results showing the amount of CO_2 dissolved in water and the CO_2 remaining in the gas phase at reservoir conditions for all scenarios. At a molality of approximately 0.80, the CO_2 is no longer fully saturated in the reservoir. 12
Figure 5: 2D Reactive transport model domain schematic. 17
Figure 6: BHP for Scenarios 1 to 12. BHP at the start of injection was approximately 2,300 psi. Stabilized BHP 2 years after injection was approximately 2,585 psi for Scenarios 1 to 8. In Scenarios 9 to 12 a rise in BHP was observed. 21
Figure 7: Illustration of the model results of Scenario 3, showing brine carrying dissolved CO_2 to the base of the reservoir. 22
Figure 8: Result of the side-by-side comparison of the 2,255 psi and 1,500 psi. 23
Figure 9: OLI simulation to predict scaling tendency of produced water with and without adding CO_2. Steam amount = 1L. (a). 0 mole/kg CO_2; (b). 0.2 mole/kg CO_2; (c). 0.6 mole/kg CO_2. 25
Figure 10: OLI simulation to predicted pH and corrosion rates of stainless-steel exposed to injected produced water with and without CO_2. 26
Figure 11: OLI simulation to predicted pH and corrosion rates of carbon steel UNS G10180 exposed to injected produced water with and without CO_2. 27
Figure 12: pH changes in the reservoir during injection period. 28
Figure 13: Dissolved solids changes in the reservoir during injection period. 28
Figure 14. Fluid density changes in the reservoir during injection period. 28
Figure 15: Mineral volume changes in the reservoir during injection period. 29
Figure 16: Porosity changes in the reservoir during injection period. 29
Figure 17: Dissolved carbon species changes in the reservoir during injection period. 30
Figure 18: Primary minerals saturation and volume during injection period. 31
Figure 19: Secondary precipitations at the end of the 20-year injection period. 32
Figure 20: pH, dissolved solids, and porosity during the shut-in period. 33
Figure 21: Dissolved carbon species during shut-in period. 34
Figure 22: Primary mineral volume percentage and saturation changes during the shut-in period. 35
Figure 23: Secondary mineral precipitates saturation during the shut-in period. 35
Figure 24: Dolomite volume percentage changes after 100 years of the shut-in period. 36
Figure 25: Storage security depends on a combination of physical and geochemical trapping. Over time, the physical process of residual CO_2 trapping and geochemical processes of solubility trapping and mineral trapping increase 39
Figure 26: Main mechanism of EOR and geological sequestration by CO_2 injection in the form of micro and nanobubbles 40
Figure 27: Schematic diagrams comparing CO_2 geological storage techniques 41

This page intentionally left blank.

List of Tables

Table 1: Reservoir Simulation Constant Parameters 11
Table 2: Results of Experimental Injection Simulation Scenarios 11
Table 3: Reservoir Performance Scenarios for Experimental Injection 13
Table 4: Results of Nine Predictive Injection Simulation Scenarios 13
Table 5: Simulation Initial Conditions for Additional Simulation Scenarios 14
Table 6: Reservoir Performance Scenarios at 1,500 psi and 2,255 psi 14
Table 7. Produced Water Chemistry for Modeling Input 15
Table 8: Chemical Composition of Produced Water - No Added CO_2; Steam Amount = 1L; Temperature 25 ℃, 1 atm 16
Table 9: Formation Rock-Fluid System and Injection Carbonated Brine Chemistry 18
Table 10: Formation Rock-Fluid System and Injection Carbonated Brine Chemistry 19
Table 11: Result of 12 Long-Term Predictive Injection Simulation Scenarios 20
Table 12: Result of 12 Long-Term Predictive Injection Simulation Scenarios with Low Initial Reservoir Pressure (1,500 psi) 23

This page intentionally left blank.

Acronyms, Abbreviations, and Symbols

Term	Description
BEST	Brine extraction and storage test
CBI	Carbonated brine injection
CCUS	Carbon capture, utilization, and storage
CMG	Computer Modeling Group
EERC	Energy & Environmental Research Center
EOR	Enhanced oil recovery
GWB	Geochemist's Workbench
IAP	Ion activity product
IRS	Internal Revenue Service
K_{sp}	Solubility Product Constant
PISC	Post-injection site closure
RTM	Reactive Transport Model
$scCO_2$	Supercritical carbon dioxide
SI	Scale Index
ST	Scaling Tendency
SWD	Saltwater disposal
TDS	Total dissolved solids
UIC	Underground injection control
USDW	Underground sources of drinking water
USGS	United States Geological Survey

Acknowledgments

This work was performed in support of the National Energy Technology Laboratory's (NETL) ongoing research under Carbon Storage Advanced R&D FWP by NETL's Research and Innovation Center. The authors wish to acknowledge Carbon Storage Advanced R&D FWP for programmatic guidance, direction, and support.

The authors also wish to acknowledge Ryan Hall from NGL Energy Partners for valuable discussions for site-related information. Thanks to James Gardiner for working on early lab and field work prior to this simulation project.

EXECUTIVE SUMMARY

Carbonated brine injection (CBI) has the potential for large-scale carbon sequestration throughout the oil and gas industry through its network of already existing Class II saltwater disposal (SWD) wells. Dedicated geological carbon storage typically results in the creation of a continuous phase of supercritical carbon dioxide ($scCO_2$) in the subsurface. Injection of fluid requires raising reservoir pressure above normal hydrostatic pressure for some distance away from the injection well. The existence of free-phase CO_2 at this elevated pressure incurs additional risk of leakage due to the combination of induced geomechanical stresses on the storage formation and the corrosive nature and higher mobility of CO_2. Long-term tracking of free-phase CO_2 is required to identify its migration in the subsurface.

For CBI, CO_2 is first dissolved into produced waters being injected into existing Class II SWD wells. Since the CO_2 is mixed with the produced water prior to subsurface injection, the benefits are predicted to include no migration of free-phase CO_2 and negligible pressure increase when compared to standard SWD injection. This technical report examined the risk profile of this alternative method with the hypothesis that there will be a lower risk profile from the absence of free-phase CO_2, resulting in a smaller area of potential impact compared to free-phase CO_2 injection methods and negligible pressure increase compared to standard SWD operations because of the aqueous-phase injection.

The main objective of this early-phase research was to evaluate the techno-economic feasibility and risk associated with combined brine and CO_2 storage in SWD wells using brine dissolution in the North Dakota portion of the Williston Basin. Three simulation studies were conducted to investigate: (1) CO_2 phases at different conditions, (2) wellbore compatibility, and (3) long-term storage fate in reservoir. (1) A simple reservoir model and injection simulations were created using data to represent the BEST (brine extraction and storage test) site, an operational SWD facility located near Watford City, North Dakota. The pressure evolution caused by CO_2 comingled in produced water injectate in a layer cake reservoir was then modeled while tracking aqueous CO_2 throughout the project. The salinity of the injection water, the salinity of the reservoir brine, and the amount of dissolved CO_2 comingled in the injection water were varied. (2) A wellbore corrosion model was performed using the CO_2 concentrations selected based on the reservoir modeling to examine the carbonated produced water impact on wellbore. (3) Reactive transport modeling was conducted with the optimal CO_2 concentration for this injection site to study the rock-fluid interactions and CO_2 fate in the reservoir.

Results suggest that CO_2 dissolved in produced water can be injected without appreciably increasing subsurface pressure or leakage risks. Pressure buildup was found to vary with salinity but not with CO_2 mass fraction. Simulation results show that lower CO_2 percent mass fraction leads to a higher amount of CO_2 that can be dissolved at a higher injection salinity. Furthermore, the long-term goal of dissolution trapping in a traditional carbon storage project is accomplished from the start, mitigating risks associated with potential migration of buoyant CO_2, so long as the reservoir pressure and temperature are used to determine the maximum mass fraction of the dissolved CO_2. Since pressure equilibrium following injection is not inhibited by two-phase flow, as seen in traditional carbon storage and sequestration, the CO_2 becomes a component of the brine and is stored in the aqueous phase, thereby reducing the CO_2 mobility in the storage reservoir, and results in the carbonated brine densities of the injected fluid similar to that of the native reservoir fluids, greatly reducing the risks associated with vertical and lateral mobility of

injected CO_2 and geomechanical stresses on the confining zones. The injection of carbonated produced water into existing SWD wells does not cause significant corrosion at optimal dissolved CO_2 amounts in the injected water.

Lastly, public data concerning produced water injection volumes were used to estimate that at 2% mass fraction, approximately 1 ton of CO_2 could be dissolved into every 198 barrels of brine. Since the volume of CO_2 that can be dissolved into produced water brine is dependent on brine salinity as well as reservoir temperature and pressure, 2% CO_2 mass fraction would likely be a very conservative estimate for basins outside of North Dakota, as the Williston Basin has among the highest produced water salinities in the country, with an average salinity of 300,000 ppm. Lower produced water salinity would result in the ability to dissolve more CO_2. However, using these conservative estimates, approximately 50 million tons of CO_2 could be dissolved into 10.5 billion barrels of produced water currently being injected into existing Class II injection wells in Texas, California, Oklahoma, Wyoming, Kansas, Louisiana, New Mexico, and North Dakota each year. With minimal capital investment and the current Internal Revenue Service 45Q tax credit of $0.425 per barrel of brine (at $85/ton), this represents a critical opportunity to use existing infrastructure and already permitted injection wells to sequester an appreciable amount of CO_2 in the subsurface at no increased risk to current Class II injection projects.

Regulatory considerations for CBI include the regulations surrounding aboveground storage of the produced water on-location and creating a path to approval under Class II injection wells. A pilot field demonstration would aid in answering some of the questions regulators might have surrounding CBI such as whether the wellbore tubing and casing would need to be retrofitted in any form.

1. INTRODUCTION

Dedicated geological carbon storage and sequestration typically result in the creation of a continuous phase of supercritical carbon dioxide ($scCO_2$) in the subsurface. Injection of fluid requires raising reservoir pressure above normal lithostatic pressure for some distance away from the injection well. The existence of free-phase CO_2 at this elevated pressure incurs additional risk of leakage due to the combination of induced geomechanical stresses on the storage formation and the corrosive nature and higher mobility of CO_2. Long-term tracking of free-phase CO_2 is required to identify its migration in the subsurface.

In this study, carbonated brine injection (CBI) was investigated as a low-risk CO_2 storage strategy, whereby CO_2 is first dissolved into produced waters being injected into existing Class II saltwater disposal (SWD) wells. Since the CO_2 is mixed with the produced water prior to subsurface injection, the benefits are predicted to include no migration of free-phase CO_2 and negligible pressure increase when compared to standard SWD injection (Figure 1). This project examined the risk profile of this alternative method with the hypothesis that (1) there will be a lower risk profile from the absence of free-phase CO_2, resulting in a smaller area of impact compared to free-phase CO_2 injection methods, and little to no pressure increase compared to standard SWD operations because of the aqueous-phase injection, and (2) CBI is compatible with existing Class II wells without causing significant corrosion issues.

The main objective of this early-phase research was to evaluate the techno-economic feasibility and risk associated with combined brine and CO_2 storage in SWD wells using brine dissolution in the North Dakota portion of the Williston Basin.

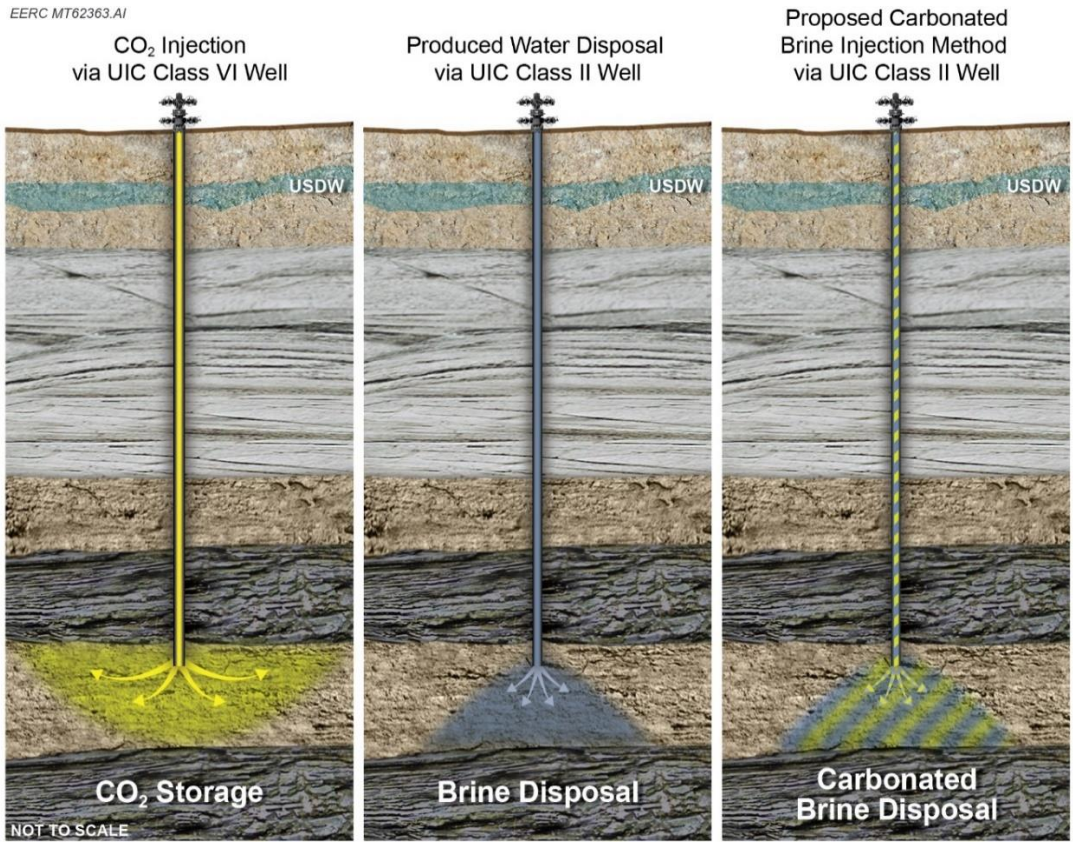


Figure 1: Graphical representation of a proposed CBI method compared to traditional free-phase CO_2 injection via a Class VI well and standard produced water disposal via a Class II well. As shown in the center, with the CBI method, the CO_2 remains dissolved into the brine, thereby eliminating the risk of free-phase CO_2 migration and negligible pressure changes when compared to standard Class II operations.

1.1 OVERVIEW OF SALTWATER DISPOSAL

Significant volumes of saltwater, commonly referred to as "produced water," are coproduced during oil and gas production from wells in unconventional plays such as the Bakken. Water production rate varies by location and geologic formation with Bakken and Three Forks production in the Williston Basin, generating an average of 1–1.5 barrels (bbl) of produced water per barrel of oil (Glazewski et al., 2020). Produced water management represents a significant technical and economic challenge for sustainable oil and gas production. Because of the high salinity and other compounds naturally occurring in the water, produced water needs to be managed in an environmentally safe manner. In North Dakota, for example, the primary means of management of produced water is disposal via subsurface injection, where 95% of produced water volumes are disposed of through injection into the Dakota Group (Figure 2). Since 1956, the Lower Cretaceous Dakota, which includes the Inyan Kara, Skull Creek, Newcastle, and Mowry Formations, has been the primary interval for SWD in North Dakota. Underground injection control (UIC) Class II injection is permitted for the entire Dakota Group; however, lowermost sands of the Inyan Kara Formation are typically the target injection zone for SWD (Bader, 2017). The Dakota Group is prevalent and laterally extensive throughout the Williston

Basin, with depths ranging from 1,800 to 6,220 ft and a thickness averaging 700 ft in areas coinciding with use for SWD (North Dakota Geological Survey, 2020). The Dakota Group contains the Mowry and Skull Creek shales and is capped by the shales of the Belle Fourche, Carlile, and ultimately Pierre Formations. The Dakota Group is also underlain by the shales of the Swift and Piper Formations. This package of laterally extensive reservoir and overlying and underlying cap rock makes the Dakota Group an ideal target for both SWD and CO_2 storage, although the Dakota is currently used almost exclusively for SWD. With produced water volumes intrinsically linked to oil and gas production volumes, increased oil and gas production in North Dakota over the past decade has resulted in more produced water needing disposal. In 2008, there were nearly 300 SWD wells distributed throughout the Williston Basin. By 2019, there were over 500 SWD wells, with most of the new wells located within the core of Bakken production (Figure 2).

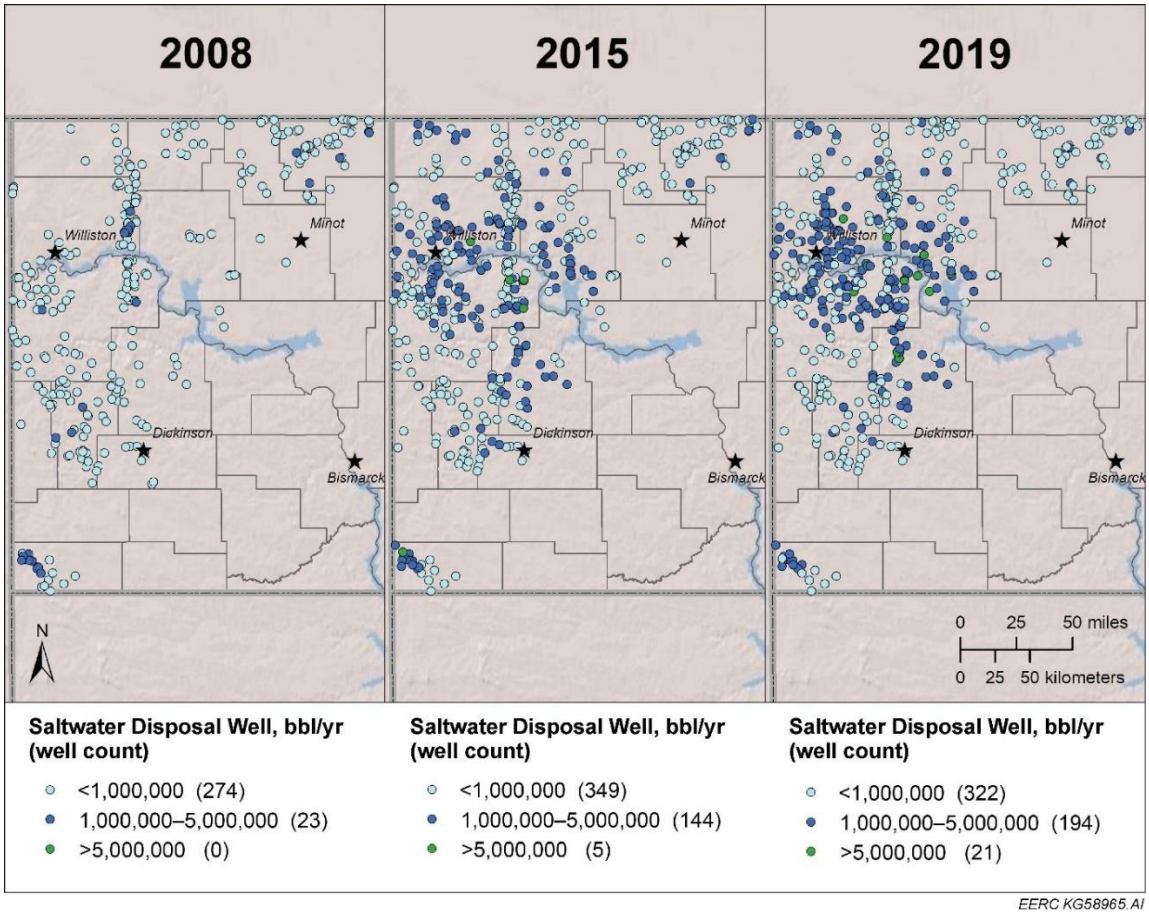


Figure 2: Distribution of active SWD wells in 2019 (data source: North Dakota Industrial Commission, 2020).

1.2 OVERVIEW OF CARBON CAPTURE, UTILIZATION, AND STORAGE

Capturing CO_2 emissions from large stationary sources before the CO_2 can be released to the atmosphere is one of the primary approaches to carbon management by which the use of fossil fuels can be maintained to meet increasing energy demands throughout the world. This approach, in conjunction with utilization and/or geologic storage, is termed carbon capture, utilization, and storage (CCUS) and includes a set of technologies that can greatly reduce CO_2 emissions from large point sources such as coal- and gas-fired power plants, natural gas-processing facilities, ethanol plants, and other industrial processes (Metz et al., 2005). CCUS involves the capture of CO_2 by separation from other gases, compression to a liquid or dense fluid state, and then, as with produced water disposal, transportation to an appropriate geological storage location for injection into deep geologic formations, ensuring safe and permanent storage (Metz et al., 2005).

Like produced water disposal, a suitable geologic formation would possess adequate volume, porosity, permeability, and wellbore integrity to safely accept and contain the expected amount of injected CO_2. Typically found in areas with thick accumulations of sedimentary rock known as basins, these formations include porous and permeable layers of rock (reservoirs) that may contain natural fluids, including very salty water (brine), oil, gas, and even CO_2. It is strongly recommended that the chosen formation is at a sufficient depth so that the temperature and pressure are high enough to ensure the injected CO_2 remains in a dense liquid or supercritical state. This greatly increases the storage capacity of the formation. Similar to produced water disposal, the formation must also possess a sealing unit (of sufficient thickness, mechanical integrity, and sufficiently low permeability) that will prevent upward migration of the injected CO_2 and negative impacts to underground sources of drinking water (USDW), defined by the U.S. Environmental Protection Agency UIC Program as water with salinity values of less than 10,000 mg/L.

Depleted hydrocarbon reservoirs are a focus for their storage potential because of their proven ability to store oil and gas for millions of years as well as the possible economic incentives offered through the utilization of the injected CO_2 in enhanced oil recovery (EOR). Deep saline formations, also commonly used for SWD, do not offer traditional economic incentives like those associated with EOR; however, they are more widespread and therefore more likely to be closer to large emission sources, reducing CO_2 transportation costs. Deep saline formations also possess the largest potential capacity because of their size and prevalence. The development of carbon credits such as the Enhancement of Carbon Dioxide Sequestration Credit (a.k.a. Section 45Q) tax program under the Internal Revenue Service (IRS) are also providing new economic incentives for storage in deep saline formations.

1.3 THE CONNECTION BETWEEN SWD AND CCUS: THE CONCEPT OF CBI AND STORAGE

As oil and gas production continues to increase in North Dakota, along with subsequent SWD and produced water management, and with the expansion of Section 45Q tax credits for CO_2 storage, oil and gas operators are looking at alternative ways to both manage SWD costs and reduce carbon footprint. One potential option is the mixing of CO_2 with the produced water prior to injection into Class II SWD wells.

With dissolved CBI, a stream of CO_2 is blended with the brine at the surface as it is injected into the storage formation, so dissolution is intrinsic to the injection process. The blending of CO_2

into the produced water stream results in the injection of a higher-density, CO_2-saturated brine that behaves like currently injected brines, sinking into and mixing with native formation fluids. Unlike traditional CO_2 injection methods, there is no mobile free-phase CO_2 plume. As a result, CBI removes differences in fluid compressibility between the brine phase and a sCO_2 phase. With a single, CO_2-saturated aqueous phase, post injection pressure equilibrium is not inhibited by two-phase flow, as this aqueous phase exhibits flow behavior similar to currently disposed brine in the disposal formation. In theory, this behavior would substantially reduce the area of impact and monitoring burden for this type of CO_2 storage compared to traditional CO_2 injection, since the injected CO_2 is already stabilized within the injected fluids. A limitation of this process is that a much smaller volume of CO_2 is likely to be able to be injected compared to typical free-phase CO_2 injection. However, if paired with thousands of existing SWD wells associated with oil and gas production in the U.S., CBI can make a significant contribution to CO_2 mitigation as an economical and low-risk means of CO_2 storage and should open CO_2 storage opportunities to many new participants.

Publicly available data on wastewater volumes in the U.S. show that 10.5 billion barrels of produced water are injected into Class II injection wells in the states of Texas, California, Oklahoma, Wyoming, Kansas, Louisiana, New Mexico, and North Dakota alone (Veil, 2015). Using CBI and assuming a conservative 2% mass fraction of CO_2 is added to each state's wastewater injection volumes, 53 million tons of CO_2 could be sequestered each year into pre-existing, permitted infrastructure. Figure 3 shows a heat map of volumes of CO_2 that could be sequestered using CBI, based on the publicly available data from Veil (2015).

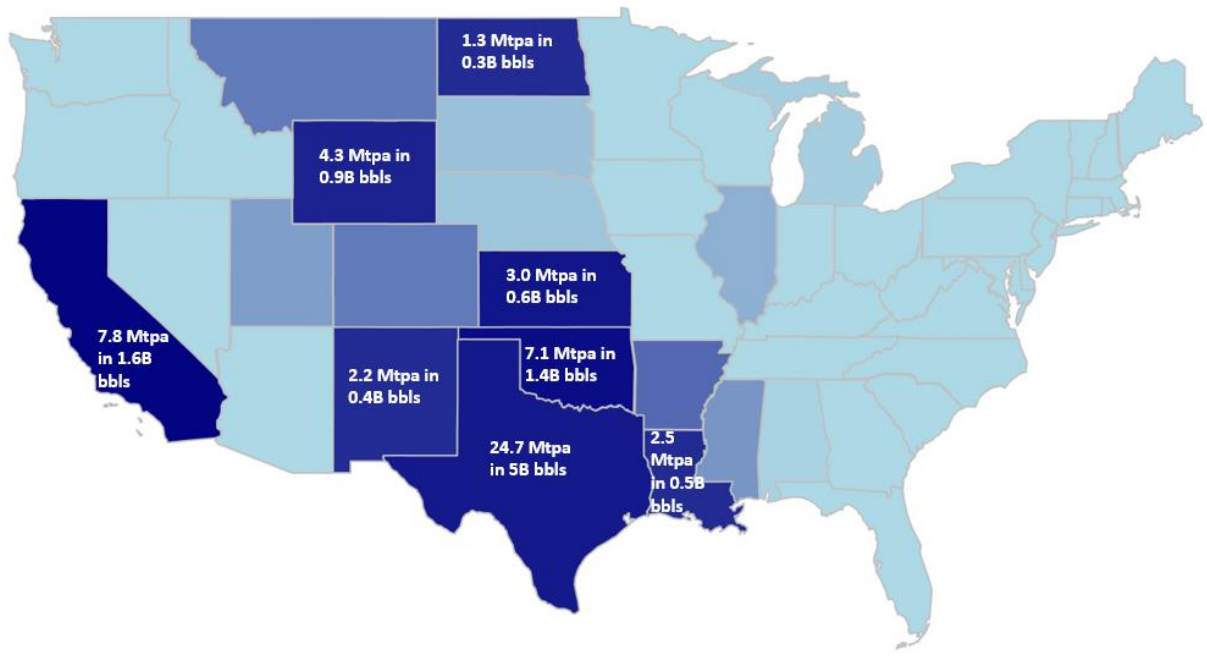


Figure 3: States with large wastewater injection volumes can sequester 53 Mtpa CO_2 using CBI.

The pace at which oil and gas operations have been increasing wastewater disposal volumes since 2015 suggests that the amounts shown on Figure 3 are conservative. In the state of North Dakota alone, only an estimated 253 million barrels of wastewater were being injected at that time. However, that volume is now past 800 million barrels of wastewater per year, suggesting over 4 Mtpa of CO_2 could be sequestered in North Dakota using CBI. Oil production in North Dakota increased to over 1.5 million barrels (MMbbl)/day in 2019. While production has decreased due to a downturn in oil prices, as of July 2020, production had recovered to over 1 MMbbl/day. A byproduct of oil and gas production is produced water which refers to the brine that is coproduced with oil. Volumes of produced water vary by location and geologic formation with Bakken production generating an average of 1–1.5 bbl of produced water per barrel of oil.

The existing Class II wellbore compatibility with CBI depends on the extent of chemical reactions and changes to the injection wells because of additional carbonic acid (H_2CO_3) in the produced water. The lowered pH supplies hydrogen as a reducible reactant to fuel the cathodic process, therefore, accelerating the corrosion process. This could lead to corrosion of the wellbore casing, tubing, packer, and surface equipment.

1.4 RESEARCH ON CBI AND STORAGE

While CBI as a method of carbon sequestration is a nascent technology, it was first proposed by Georgescu et al. (2006). CBI provides numerous benefits including immediate dissolution, negative buoyancy, and no free-phase CO_2. If the carbonated brine is denser than the reservoir brine, it will sink to the bottom of the reservoir, reducing the risk of upward CO_2 migration. Carbonated brine occupies only 5% greater volume than unsaturated brine, leading to a smaller displacement volume than bulk CO_2 injection when an equivalent volume of brine is produced (Burton and Bryant, 2009). Compared to CBI, $scCO_2$ injection initially has a smaller areal footprint per unit of CO_2 injected. However, because of high mobility and buoyancy, free CO_2 spreads out along the cap rock and ultimately occupies a larger area than carbonated brine, which sinks to the bottom of the reservoir (Ruprecht and Falta, 2012). Storage volumes are reduced by approximately 50% if CO_2 is dissolved into brine, as opposed to a separate supercritical fluid; additionally, CO_2-saturated brine is denser than undersaturated formation brines, causing CO_2 to migrate downward within a formation, as opposed to upward against the cap rock (Steele-MacInnis et al., 2013).

A few studies have examined CBI in specific regions around the world. Studies in the offshore region of the United Kingdom show that CBI enhances CO_2–brine stability and improves CO_2 sequestration by eliminating the buoyancy force and rapidly immobilizing the CO_2 (Eke et al., 2011). CBI was utilized at the CarbFix site in Iceland to demonstrate the efficacy of the method and to promote rapid mineralization (Sigfusson et al., 2015). Carbonated brine storage has been found to require less pore volume when reservoir brine is used as the dissolution agent (Wu et al., 2017). For example, in the Northeast German Basin, 4.7 billion tons of CO_2 could be stored in solution compared to 1.5 billion tons as free-phase CO_2 (Kühn et al., 2017).

Other studies have looked for methods to improve the process. For example, while surface mixing has been the most studied method of carbonating brine, mixing at depth reduces pressure mixing requirements (Pool et al., 2013). Downhole mixing reduces energy requirements, as the pressure of the formation is used to dissolve the CO_2 (Shariatipour et al., 2016). While mass fractions of dissolved CO_2 will ultimately be controlled by reservoir conditions and energy requirements, silica nanoparticles have been proposed to increase CO_2 concentration in water

(Fathollahi and Rostami, 2015). In laboratory studies, core floods with carbonated brine have also been shown to encourage CO_2 trapping via mineralization because of the additional availability of cations (Pearce et al., 2022; Rathnaweera et al., 2016). CBI may alter the wettability of reservoir rock (Motie and Assareh, 2020). Khan et al. (2021) previously proposed CBI through Class II injection wells, pointing out that the infrastructure for produced water disposal is already built and in place. Laboratory observations of CBI in wastewater from oil and gas operations may promote mineralization as another trapping mechanism (Pearce et al., 2021).

2. METHODS

This simulation-based research includes: 1) reservoir modeling to investigate CO_2 molality, phase change and pressure change at different salinity; 2) wellbore corrosion modeling to examine the wellbore compatibility with the injection of carbonated produced water; and 3) reactive transport modeling to check rock-fluid interactions in the reservoir during injection and long-term storage. The feasibility and safety of CBI as a low-rick geologic CO_2 sequestration strategy was assessed by analyzing the modeling results.

2.1 RESERVOIR MODEL SETUP

The Computer Modeling Group (CMG) simulation program was utilized in this project to create a reservoir model. Within the CMG launcher, several sub-programs were accessed to derive the desired simulation outcomes. Specifically, the Builder, GEM, and results graph components were employed to execute the simulations and procure the results. For this particular project, the Builder, GEM, and results graph functionalities were sufficient to conduct the simulations and achieve the desired outcomes.

The Builder component of CMG encompasses various aspects of data input, including grid creation, grid property definition, incorporation of production data, fluid properties, rock-fluid interactions, fluid models, and initial conditions. An assessment of CBI was conducted using representative data and properties from typical Williston Basin SWD wells that inject into the Inyan Kara Formation of the Dakota Group. The initial phase involved estimating the quantity of CO_2 that could be injected at specific brine volumes and injection pressures. These parameters were established based on existing SWD operations, adhering to Class II injection regulations.

Numerical simulations of CBI into the targeted formation were carried out across 16 scenarios. The objective was to ascertain the maximum amount of CO_2 that could be dissolved into the formation fluid, leaving no residual undissolved CO_2. A consistent injection rate of 8,000 barrels per day over 5 years was adopted for all scenarios, mirroring the operational practices at SWD sites within the Williston Basin.

To illustrate the process of CBI using a commercial simulator, a stream of injection with dissolved CO_2 molality was defined and utilized as the injection constraint. The reservoir was assumed to be fully saturated with brine (100% brine-saturated), featuring an initial formation salinity of 10,000 parts per million (ppm) and an injection salinity of 10,000 ppm. Molality (m), which expresses solution concentration, along with density and injection volume were the pivotal parameters in calculating the total amount of CO_2 dissolved in the reservoir conditions. To identify the maximal CO_2 dissolution into the injected fluid, scenarios were run with varying molality values ranging from 0.20 to 2.0, while maintaining all other parameters constant. Table 1 and Table 2 provide a breakdown of the simulation parameters and the scenarios that were evaluated. In Table 2, 0.75 mole represents the highest starting concentration at which essentially all of the CO_2 [99.999%] can be dissolved into the brine. At higher molality, not all CO_2 is dissolved.

Table 1: Reservoir Simulation Constant Parameters

Constant Parameters	Value
Injection Rate, bbl/day	8,000
Years of Injection	5
Reservoir Pressure, psi	2,255
Reservoir Temperature, °F	165
Injection Temperature, °F	60
Injection Fluid Salinity, ppm	10,000
Reservoir Fluid Salinity, ppm	10,000

Table 2: Results of Experimental Injection Simulation Scenarios

Sc.	Molality, mol/kg	Cumulative Injection of CO_2, gmol	CO_2 Dissolved in Water, gmol	CO_2 Dissolved in Water, tonne	CO_2 in Gas Phase, gmol	CO_2 Dissolved, %	Gas Phase, %	Total, %*
1	2.00	4,332,140,000	3,857,820,000	169,783	475,327,000	89.05	10.97	100.00
2	1.00	2,241,860,000	2,240,980,000	98,625	1,182,910	99.96	0.05	100.00
3	0.85	1,915,640,000	1,915,230,000	84,289	380,447	99.98	0.02	99.99
4	0.80	1,806,130,000	1,805,800,000	79,473	297,109	99.98	0.02	99.99
5	0.75	1,696,230,000	1,695,970,000	74,640	238,336	99.99	0.01	99.99
6	0.70	1,585,950,000	1,585,740,000	69,789	194,658	99.99	0.01	99.99
7	0.65	1,475,280,000	1,475,100,000	64,919	160,893	99.99	0.01	99.99
8	0.60	1,364,210,000	1,363,340,000	60,001	133,932	99.94	0.01	99.95
9	0.55	1,252,750,000	1,251,390,000	55,074	111,907	99.89	0.01	99.90
10	0.50	1,140,890,000	1,138,580,000	50,109	93,522	99.80	0.01	99.81
11	0.45	1,028,630,000	1,026,370,000	45,171	78,003	99.78	0.01	99.79
12	0.40	915,975,000	913,971,000	40,224	64,666	99.78	0.01	99.79
13	0.35	802,913,000	801,620,000	35,279	53,080	99.84	0.01	99.85
14	0.30	689,445,000	688,326,000	30,293	42,857	99.84	0.01	99.84
15	0.25	575,570,000	574,676,000	25,291	33,784	99.85	0.01	99.85
16	0.20	461,285,000	460,723,000	20,276	25,665	99.88	0.01	99.88

* May not equal 100% due to rounding.

The simulations encompassed a 1-year pre-injection phase (well shut-in, no injection), followed by 5 years of CBI, and concluded with a 1-year post-injection monitoring phase (well shut-in, no injection). This sequencing aimed to better understand the changes in reservoir conditions prior to and subsequent to the injection. Simulation findings revealed that within the molality range of 0.75 to 0.65, approximately 99.99% of CO_2 would be successfully dissolved into the reservoir fluid (as depicted in Figure 4).

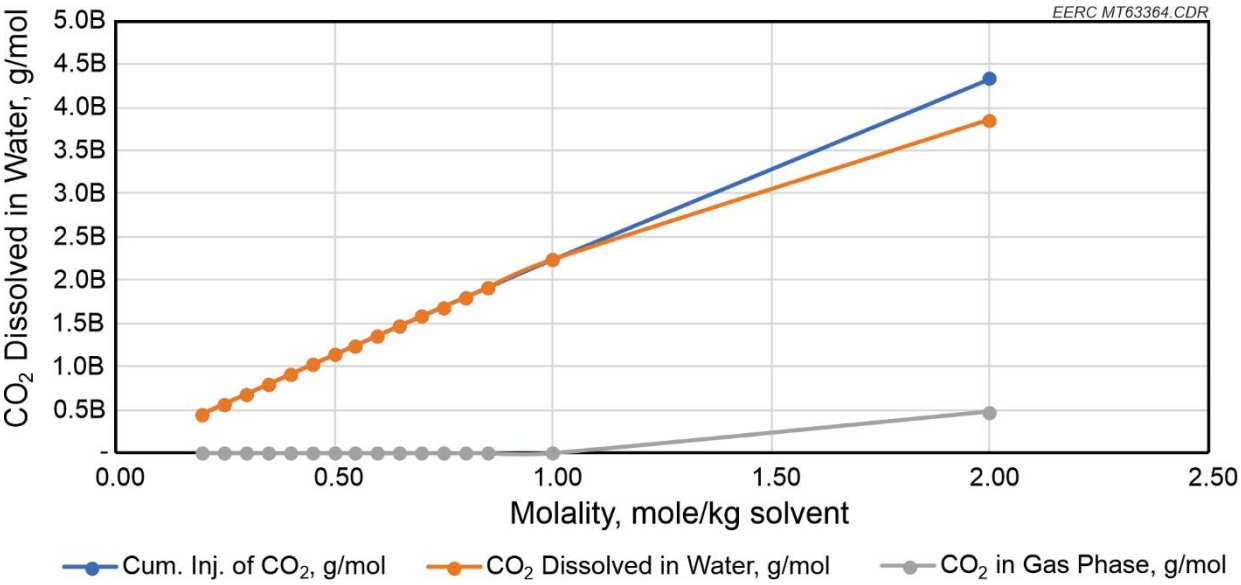


Figure 4: Simulation results showing the amount of CO_2 dissolved in water and the CO_2 remaining in the gas phase at reservoir conditions for all scenarios. At a molality of approximately 0.80, the CO_2 is no longer fully saturated in the reservoir.

Predictive simulations for carbonated brine storage were developed through the scaling up of the existing experimental simulation model to encompass an area around the injection well measuring 1,000 ft by 1,000 ft. A total of nine simulation models were constructed to systematically examine the intricate interplay among injection fluid salinity, reservoir fluid salinity, and CO_2 molality. The specifics of the simulation scenarios can be found in Table 3, while Table 4 provides a comprehensive breakdown of the results achieved for each individual scenario. In the scenarios involving the lowest injected and reservoir brine salinity (Scenarios 1–3), the entirety of the CO_2 volume dissolved into the injected fluid was retained in solution. As the injection brine salinity increased to levels more characteristic of standard SWD fluid salinities, the molality of the injected fluid emerged as a crucial factor. Within Scenarios 4–6, simulating 150,000 ppm TDS (total dissolved solids) injected fluid, the maximum CO_2 dissolution occurred at a concentration of 0.4 molality. In Scenarios 7–9, which represented 300,000 ppm TDS injected fluid, the optimal CO_2 dissolution occurred at a concentration of 0.6 molality.

Table 3: Reservoir Performance Scenarios for Experimental Injection

Scenario	Injection Fluid Salinity, ppm	Reservoir Fluid Salinity, ppm	Molality
1	10,000	10,000	0.2
2	10,000	10,000	0.4
3	10,000	10,000	0.6
4	150,000	20,000	0.2
5	150,000	20,000	0.4
6	150,000	20,000	0.6
7	300,000	20,000	0.2
8	300,000	20,000	0.4
9	300,000	20,000	0.6

Table 4: Results of Nine Predictive Injection Simulation Scenarios

Sc.	Molality, mole/kg solvent	Cumulative Injected CO_2, gmol	CO_2 Dissolved in Water, gmol	CO_2 in Gas Phase, gmol	CO_2 Dissolved, %	Gas Phase, %	Total, %*
1	0.2	500,413,000	499,979,000	58,266	99.91	0.012	99.93
2	0.4	544,937,000	544,870,000	54,529	99.99	0.010	99.99
3	0.6	633,511,000	633,433,000	79,993	99.99	0.013	100.00
4	0.2	500,413,000	485,680,000	187,048	97.10	0.037	97.10
5	0.4	544,937,000	544,936,000	347,791	99.99	0.064	100.00
6	0.6	633,511,000	625,504,000	7,795,840	98.74	1.231	99.97
7	0.2	500,413,000	486,711,000	13,389,000	97.26	2.676	99.94
8	0.4	544,937,000	522,326,000	22,048,200	95.85	4.046	99.90
9	0.6	184,272,000	184,261,000	45,575	99.99	0.0247	100.00

* May not equal 100% due to rounding.

While every evaluated scenario demonstrated CO_2 dissolution levels exceeding 95%, a molality of 0.2 might offer the optimal equilibrium between the injected CO_2 volume and the volume of CO_2 that remains in solution. This prompted an examination of the simulation cases to assess the long-term consequences of CO_2 within the reservoir.

Furthermore, supplementary simulations were undertaken to thoroughly assess the long-term consequences of CO_2 within the reservoir. A total of 12 distinct scenarios were examined, encompassing a 1-year pre-injection phase, followed by a 20-year period of CBI, and extending into a 100-year post-injection phase. This comprehensive timeframe was adopted to gain a profound understanding of the enduring effects of the CO_2 plume. The particulars of these additional simulation cases are detailed in Table 5, outlining the initial conditions.

Table 5: Simulation Initial Conditions for Additional Simulation Scenarios

Constant Parameters	Value
Injection Rate, bbl/day	8,000
Years of Injection • Pre-injection • Post-injection	20 1 100
Reservoir Pressure, psi	2,255
Reservoir Depth, ft	4,700
Reservoir Temperature, °F	165
Wellhead Temperature, °F	60

These simulation models investigated the dynamic interaction between injection fluid salinity, reservoir fluid salinity, and CO_2 molality. The specifics of the simulation scenarios for each case are presented in Table 6. Furthermore, to comprehend the storage capacity of the reservoir under varying conditions, different initial reservoir pressures were also considered. Specifically, these 12 simulation cases were re-executed utilizing initial reservoir pressures of 1,500 psi and 2,255 psi, enabling a comprehensive assessment of the impact of initial reservoir pressure on storage capacity.

Table 6: Reservoir Performance Scenarios at 1,500 psi and 2,255 psi

Scenario	Injection Fluid Salinity, ppm	Reservoir Fluid Salinity, ppm	Molality
1	100,000	10,000	0.2
2	200,000	10,000	0.2
3	300,000	10,000	0.2
4	400,000	10,000	0.2
5	100,000	20,000	0.4
6	200,000	20,000	0.4
7	300,000	20,000	0.4
8	400,000	20,000	0.4
9	100,000	30,000	0.6
10	200,000	30,000	0.6
11	300,000	30,000	0.6
12	400,000	30,000	0.6

2.2 PRODUCED WATER DATA

The produced water data from the region of interest were filtered from the United States Geological Survey (USGS) produced water database (Siefert et al., 2022). The filter was set in the sequence of North Dakota (State), Mckenzie (County), Bakken (Formation). The filtered Bakken produced water data were averaged after removing the data point with a charge imbalance above ±5%. Final data for geochemical related model input is listed in Table 7. Total carbon concentration is the sum of carbonate and bicarbonate concentration.

Table 7. Produced Water Chemistry for Modeling Input

Species	Name	Concentration	Unit
	Density	1.17	g/mL
	pH	5.94	
K+1	Potassium	4483.17	mg/L of K^+
Na+1	Sodium	75341.45	mg/L of Na^+
Ba+2	Barium	34.40	mg/L of Ba^{2+}
Ca+2	Calcium	16674.76	mg/L of Ca^{2+}
Fe+2	Iron II	124.71	mg/L of Fe2+
Mg+2	Magnesium	1091.15	mg/L of Mg^{2+}
Cr+3	Chromium III	0.69	mg/L of Cr^{3+}
Cl-1	Chloride	152006.21	mg/L of Cl^-
CO3-2	Carbonate	1631	mg/L of CO_3^{2-}
HCO3-1	Bicarbonate	341.79	mg/L of HCO_3^-
Total C	Carbon	32.78	mmol/L of total C
NO3-1	Nitrate	151.96	mg/L of NO_3^-
SO4-2	Sulfate	613.46	mg/L of SO_4^{2-}

2.3 WELLBORE CORROSION MODEL

An aqueous chemistry software called OLI Studio was used to model the data from the chosen power plants as streams. This program uses a stream analyzer to perform a variety of functions and water analysis. Stream Analyzer is a comprehensive thermodynamic tool that calculates speciation, scaling tendencies in the systems. The calculation of the aqueous solution speciation, concentrations, activities and transport properties of the reacting species in the brine was performed using the thermophysical module. The corrosion rates were calculated by quantifying the bulk chemistry, transport phenomena, and surface reactions through a thermophysical and electrochemical module using corrosion analyzer. The electrochemical module simulates the electrochemical reactions (oxidation and reduction) occurring on the steel surface were simulated using the electrochemical module.

Single-point calculations, determination of water quality properties, and corrosion analysis are some examples of the various useful functions that can be performed using the aqueous chemistry software. For this project, reconciliation and single-point calculations were the main operations used in analyzing the power plant streams. With the produced results from the software, comparisons and an analysis of software performance can be made.

Tubular materials, casing and long string made of carbon steel (API 5CT). API 5CT casing and tubing include grades L80-1, L80 9Cr (Cr 8%-10%), and L80 13Cr (Cr 12%-14%). For corrosion studies, 13Cr stainless-steel, super stainless-steel, and low carbon steel 1010 were considered. Increasing vertical depth of the reservoir means increasing the temperature and the partial pressure of CO_2 in wells. A parametric study was performed to simulate the changes in temperature inside the reservoir. USGS produced water data from North Dakota-McKenzie County-Bakken formation have been selected to perform this study. The chemical composition input for OLI is shown in Table 8. The effects of temperatures, pH, and CO_2 concentration, on corrosion are also investigated. The produced water without adding CO_2 contained 32.78 mmole/ L of HCO_3^- as C. CO_2 partial pressure of produced water with 0.2 mole/kg (8,800 mg/L) CO_2 correspond to 6.415 atm at 25 ºC, considering a 1 liter of produced water. However, CO_2 partial pressure for produced water with 0.6 mole/kg (26,400 mg/L) CO_2 correspond to 20 atm at 25 ºC, considering a 1 liter of produced water.

Table 8: Chemical Composition of Produced Water - No Added CO_2; Steam Amount = 1L; Temperature 25 ℃, 1 atm

Physical Parameters/Composition	Values
Density (g/L)	1.18
pH	5.94
K^+ (mg/L)	4483.17
Na^+ (mg/L)	75341.45
Ba^{2+} (mg/L)	34.4
Ca^{2+} (mg/L)	16674.76
Fe^{2+} (mg/L)	124.71
Mg^{2+} (mg/L)	1091.15
Cr^{3+} (mg/L)	0.69
Cl^- (mg/L)	152006.21
HCO_3^- as C (mmol/L)	32.78
NO_3^- (mg/L)	151.96
SO_4^{2-} (mg/L)	613.46

2.4 REACTIVE TRANSPORT MODEL

The 2D Reactive Transport Model (RTM) was performed using Geochemist's Workbench (GWB) 10.0 X2t module with the default thermo database. The reservoir setup was similar to the reservoir model. Domain dimension was set at 300 m × 300 m × 100 m. Well location was at x, y = 150 m, 150 m, center of the domain. The fluid discharge rate from the well was 1,280 m^3/day (8,000 bbl/day). In the default domain (Figure 5), the reservoir flow was from left to right. In this model, the reservoir flow rate was 0 and both left and right boundaries were set as open. The Longitudinal dispersivity was 100 cm and the transverse dispersivity was 10 cm. The diffusion coefficient was 10^{-6} cm^2/s. The nodes number was set 29 × 29. The temperature was set at 74 °C (160 °F) for reservoir reactions.

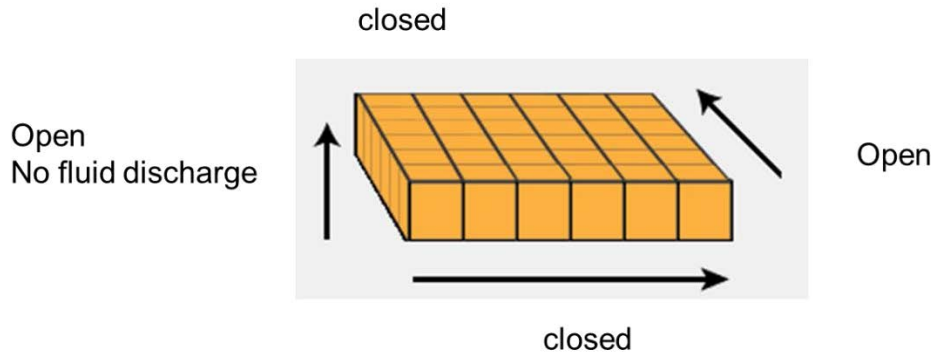


Figure 5: 2D Reactive transport model domain schematic.

From the core analysis conducted by Energy & Environmental Research Center (EERC), the Inyan Kara sandstone contains 70.5 vol% sandstone, 2.7 vol% clay, and 3.8 vol% siderite, resulting in 23% porosity. In the model, muscovite was chosen to represent the clay. The Inyan Kara formation water chemistry was obtained from previous report (Chu, 1991). The initial rock-fluid system data and the injection water data are listed in Table 9. The injection water is composed of the produced water chemistry, replacing the total carbon to the recommended dissolved CO_2 molality (0.2 molal) for carbonated brine.

Table 9: Formation Rock-Fluid System and Injection Carbonated Brine Chemistry

Formation	Concentration	Injection water	Concentration
Quartz	70.5 volume %	$SiO_2(aq)$	
Muscovite	2.7 volume %	Al^{+++}	
Siderite	3.8 volume %	Fe^{++}	124.71 mg/L
Mg^{++}	57 mg/L	Mg^{++}	1,091.15 mg/L
pH	6.1	pH	5.94
Ca^{++}	259 mg/L	Ca^{++}	16,674.76 mg/L
Na^{+}	7,114 mg/L	Na^{+}	75,341.45 mg/L
K^{+}	408 mg/L	K^{+}	4,483.17 mg/L
Cl^{-}	10,600 mg/L	Cl^{-}	152,006.21 mg/L
$SO4^{--}$	1,000 mg/L	SO_4^{--}	613.46 mg/L
$HCO3^{-}$	1,086 mg/L	HCO_3^{-} as C	0.2 molal
Ba^{++}		Ba^{++}	34.40 mg/L
NO_3^{-}		NO_3^{-}	151.96 mg/L

Mineral reactants are listed in Table 10. Quartz, muscovite, and siderite are primary minerals in the initial system. All the others are secondary minerals to precipitate. The kinetic rate (k, $mol/cm^2 \cdot s$) and activation energy (E, J/mol) were obtained from literature or set to similar minerals. Surface area of all minerals was assumed to be 1,000 cm^2/g for reservoir rock. Nucleus density was set at 1,000 cm^2/cm^3 for all secondary mineral precipitation. The injection period was set at 20 years with the injection fluid rate (1,280 m^3/day). After 20 years, the injection fluid rate was set at 0 for 100 years as the shut-in period.

Table 10: Formation Rock-Fluid System and Injection Carbonated Brine Chemistry

Minerals	k (mol/cm^2·s)	E (J/mol)	Reference
Quartz	1.00E-16	87,500	(Rimstidt and Barnes, 1980)
Muscovite	2.00E-16	64,000	(Nagy, 1995)
Siderite	2.00E-11	55,000	Set to dolomite
Barite	1.26E-12	30,800	(Palandri and Kharaka, 2004)
Calcite	1.58E-10	63,000	(Plummer et al., 1978)
Dolomite	2.00E-11	55,000	(Busenberg and Plummer, 1982)
Witherite	4.47E-12	41,900	Set to strontianite (Sonderegger et al., 1976)
Kaolinite	3.98E-16	64,000	(Sverdrup, 1990)
Dawsonite	1.00E-11	62,800	(Palandri and Kharaka, 2004)
Magnesite	4.57E-14	23,500	(Palandri and Kharaka, 2004)
Aragonite	1.58E-10	63,000	Set to calcite
Huntite	2.00E-11	55,000	Set to dolomite
Monohydrocalcite	1.58E-10	63,000	Set to calcite
Maximum Microcline	1.26E-15	58,000	Set to K-feldspar
K-feldspar	1.26E-15	58,000	(Helgeson et al., 1984)

3. RESULTS

3.1 RESERVOIR SIMULATION

3.1.1 High Reservoir Pressure

An experimental simulation was developed to measure the solubility of the injection fluid in the reservoir. A comprehensive experimental characterization was conducted to analyze the influence of molality and salinity on the solubility of CO_2 in brine. The results of the simulation highlight the pivotal role of molality and salinity in CBI. Table 4 presents a snapshot of the simulation outcomes, underscoring how molality and salinity govern the process. Additionally, a series of 12 simulation cases were executed to explore the enduring effects of CO_2 injection into the reservoir. The findings from these simulations are summarized in Table 11.

Table 11: Result of 12 Long-Term Predictive Injection Simulation Scenarios

Sc.	Injection Fluid Salinity (ppm)	Reservoir Fluid Salinity (ppm)	Molality (mole/kg)	CO_2 Dissolved, %	CO_2 Gas Phase, %
1	100,000	10,000	0.2	99.99%	0.01%
2	200,000	10,000	0.2	99.99%	0.01%
3	300,000	10,000	0.2	99.97%	0.02%
4	400,000	10,000	0.2	99.94%	0.04%
5	100,000	20,000	0.4	99.99%	0.01%
6	200,000	20,000	0.4	99.98%	0.02%
7	300,000	20,000	0.4	93.06%	6.93%
8	400,000	20,000	0.4	63.92%	36.07%
9	100,000	30,000	0.6	99.99%	0.01%
10	200,000	30,000	0.6	92.19%	7.80%
11	300,000	30,000	0.6	65.35%	34.64%
12	400,000	30,000	0.6	53.19%	46.79%

The outcomes show that in scenarios featuring lower reservoir brine salinity (Scenarios 1–3), the injected fluid retained the dissolved CO_2 in solution. Similarly, scenarios with lower injected fluid salinity (Scenarios 1, 5, and 9) exhibited successful retention of CO_2 in solution. However, higher salinity levels in both the injected fluid and reservoir brine led to the emergence of CO_2 in the gas phase within the reservoir. This underscores the substantial impact of injected and reservoir brine salinity on the phase behavior of CO_2. For instance, in Scenario 12, with an injected fluid salinity of 400,000 ppm TDS and a reservoir fluid salinity of 30,000 ppm TDS, representing the highest salinity concentration, approximately 35% of the CO_2 transitioned into the gas phase.

Molality also plays a crucial role in this context. When considering higher injection brine salinities, which are more representative of typical SWD fluid salinities, the molality of the injected fluid emerged as a key factor. Specifically, in Scenarios 1–4 with a molality of 0.2 mole/kg, the highest level of CO_2 dissolution occurred at lower salinities. This trend persisted in Scenarios 5–8 with a molality of 0.4 and Scenarios 9–12 with a molality of 0.6. Given typical reservoir and injection fluid salinities, a molality of 0.2 appears to strike the optimal balance between the injected CO_2 volume and the volume of CO_2 remaining in solution.

Figure 6 illustrates the model results of Scenario 1 to 12. Bottomhole pressure (BHP) built steadily throughout the simulation period while still remaining well below the maximum BHP for a typical SWD well in the Williston Basin (~3,000–3,300 psi). The the highest BHP observed in these tests came from Scenario 12 which reached 3,010 psi at the end of the injection phase. Scenario 12 represents the case with the highest tested salinity and dissolved CO_2 molality of 0.6.

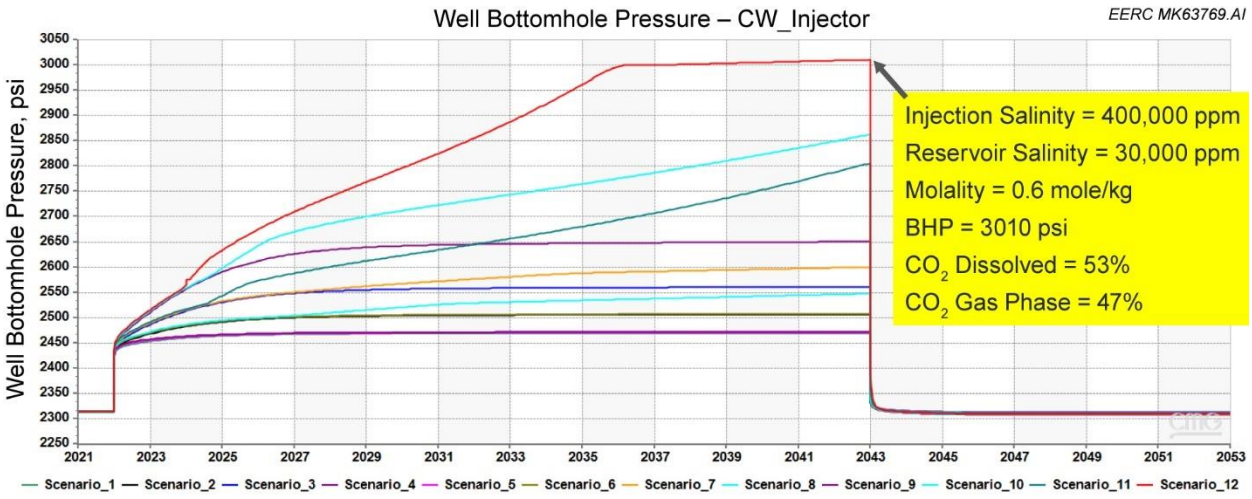


Figure 6: BHP for Scenarios 1 to 12. BHP at the start of injection was approximately 2,300 psi. Stabilized BHP 2 years after injection was approximately 2,585 psi for Scenarios 1 to 8. In Scenarios 9 to 12 a rise in BHP was observed.

In all the injection scenarios where the CO_2 remained fully dissolved, the dissolved CO_2 remains close to the injection well during and after injection as the injected brine with CO_2 tends to sink within the reservoir to below the injection well. As an example, Figure 7 illistrates the results from Scenario 3, 100 years after injection has ceased, showing the distribution of CO_2 molality stabilizing at the bottom of the reservoir. Some mixing diffusion is observed along the edges of the plume but this mixing zone does not extend far beyond the wellbore. This phenomenon suggests that CO_2 migration has a low likelyhood to occur with dissolved CO_2 injection.

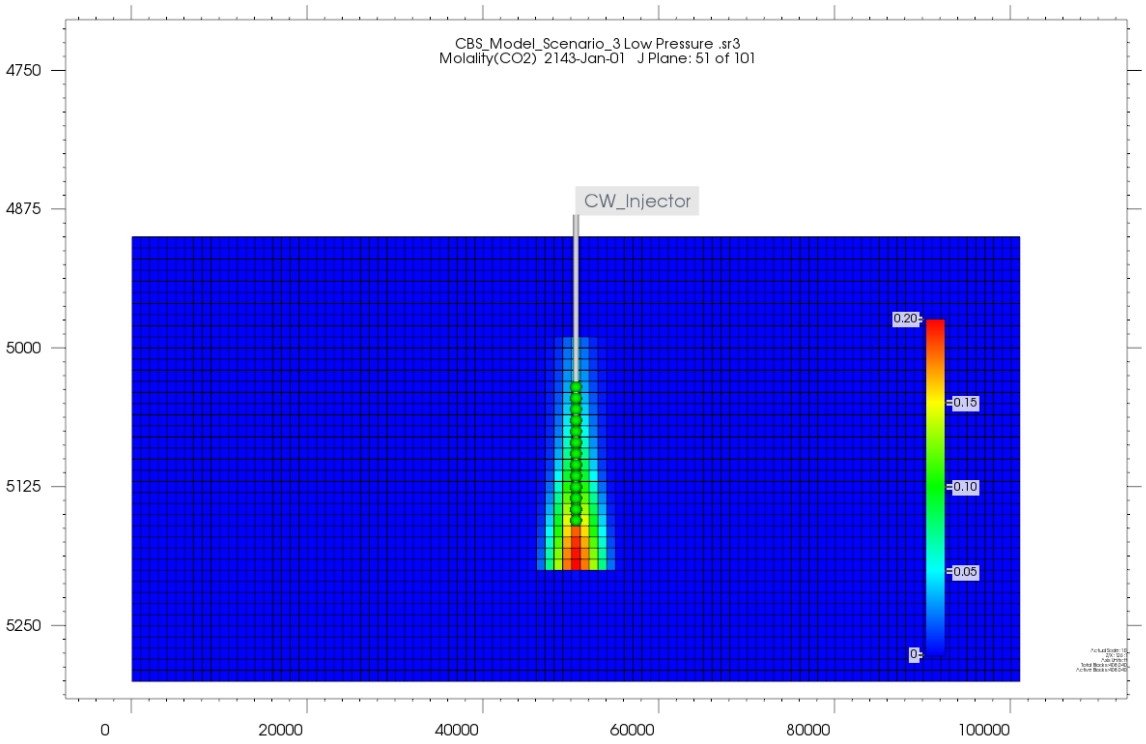


Figure 7: Illustration of the model results of Scenario 3, showing brine carrying dissolved CO_2 to the base of the reservoir.

3.1.2 Low Reservoir Pressure

Table 12 presents the outcomes of the 12 simulations conducted with an initial reservoir pressure of 1,500 psi. These simulations aimed to evaluate the effects of low initial reservoir pressure, although it is important to note that this initial pressure does not accurately represent actual reservoir conditions. The results indicate that CO_2 dissolution was slightly higher with lower initial reservoir pressure. However, the influence of lower initial reservoir pressure is not substantial when considering scenarios with lower reservoir and injection fluid salinities (Scenarios 1 to 6) and the resulting mass of CO_2 disolved was similar to that found with higher initial pressures (Table 11).

Table 12: Result of 12 Long-Term Predictive Injection Simulation Scenarios with Low Initial Reservoir Pressure (1,500 psi)

Scenario	Injection Fluid Salinity (ppm)	Reservoir Fluid Salinity (ppm)	Molality (mole/kg)	CO_2 Dissolved, %	CO_2 Gas Phase, %
1	100,000	10,000	0.2	99.99%	0.01%
2	200,000	10,000	0.2	99.99%	0.01%
3	300,000	10,000	0.2	99.98%	0.01%
4	400,000	10,000	0.2	99.96%	0.03%
5	100,000	20,000	0.4	99.99%	0.01%
6	200,000	20,000	0.4	99.99%	0.01%
7	300,000	20,000	0.4	87.04%	12.95%
8	400,000	20,000	0.4	70.31%	29.68%
9	100,000	30,000	0.6	99.99%	0.01%
10	200,000	30,000	0.6	94.72%	5.29%
11	300,000	30,000	0.6	76.15%	23.83%
12	400,000	30,000	0.6	59.85%	40.14%

Figure 8 illustrates side-by-side comparison of the result of the 2,255 psi and 1,500 psi test results. As shown in the Figure 8, the impact of lower initial reservoir pressure is less pronounced for lower injection fluid salinity, particularly for a molality of 0.2, which may represent the best case for maximizing the volume of CO_2 remaining in solution during injection.

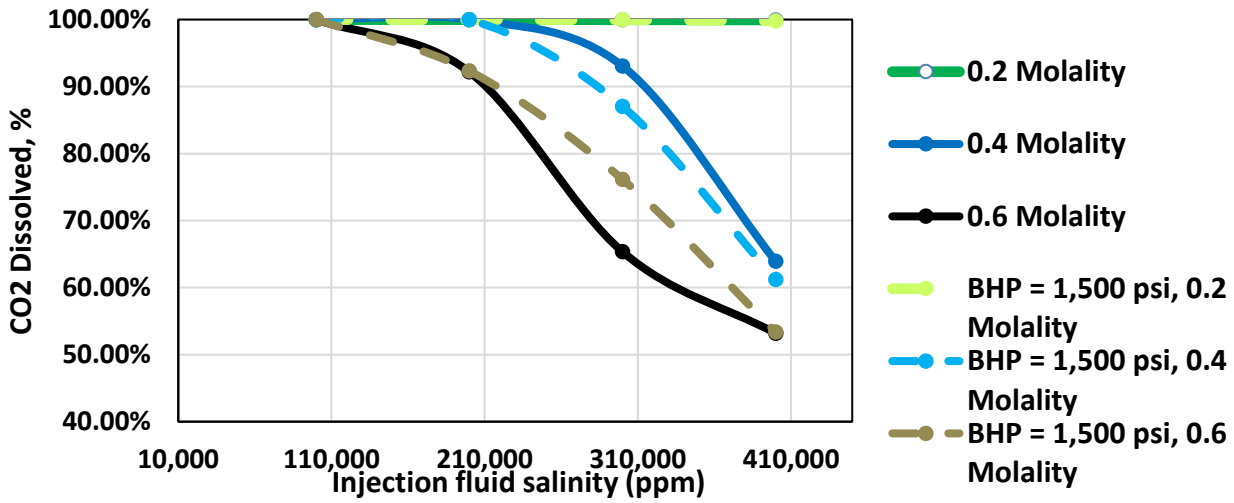


Figure 8: Result of the side-by-side comparison of the 2,255 psi, (solid line) and 1,500 psi, (dashed line).

3.2 WELLBORE CORROSION MODEL

3.2.1 Scaling Tendency Prediction of Carbonated Produced Water

Changes in temperature and CO_2 content injected into produced water may initiate pH changes, hence may begin the formation of scales. Scaling tendency (ST) or scale index (SI) can be used to evaluate the scale formation of produced water mixed with CO_2. The ST is the ratio of the ion activity product (IAP) to the solubility product constant (K_{sp}) (Equation 1). The SI is given by Equation 2.

$$Scaling\ tendency = \frac{C}{C_0} = \frac{IAP}{K_{sp}} \qquad \text{(Equation 1)}$$

Where, C: measured concentration, C_0: concentration at equilibrium, IAP: ion activity product and K_{sp}: thermodynamic solubility product constant.

$$SI = log_{10}\left(\frac{IAP}{K_{sp}}\right) = log_{10}\,(scaling\ Tendency) \qquad \text{(Equation 2)}$$

Thus,

- Scaling tendency < 1 or SI < 0: indicates sub-saturation, and the solid is not expected to form.
- Scaling tendency = 1 or SI = 0: indicates saturation, and the solid is in equilibrium with water.
- Scaling tendency > 1 or SI > 0: indicates supersaturation, and the solid is expected to form.

Based on reservoir scenarios discussed earlier, three different concentrations of CO_2 (0, 0.2, and 0.6 mole/kg) were selected for scale tendency evaluation using the OLI software. Figure 5 shows predicted scaling tendency produced water with and without adding CO_2. In the case of produced water without CO_2, the increase in temperature or amount of injected CO_2 did not affect the scaling tendency of barite ($BaSO_4$), Or- dolomite ($CaMg(CO_3)_2$), hematite (Fe_2O_3), and eskolaite (Cr_2O_3). At these conditions, the scaling tendency is equal to 1, which means that the solids are in equilibrium state with produced water, in exception for anhydrite ($CaSO_4$) where the scaling tendency at 25 ºC is below 1. In this case, no precipitation of $CaSO_4$ is expected. For water with 0.2 mole/kg CO_2, in addition to Cr_2O_3, Fe_2O_3, and $CaSO_4$, calcite ($CaCO_3$) and pyrrhotite (FeS) were in equilibrium state with carbonated produced water. For water with 0.6 mole/kg CO_2, the increase in temperature from 25 to 75 ºC did not affect the scaling tendency for Fe_2O_3, $CaSO_4$, calcite ($CaCO_3$), and $CaSO_4$. However, at temperatures below 45 ºC, Cr_2O_3 is not expected to precipitate (scaling tendency <1). Based on the results shown in Figure 9, the amount of CO_2 injected into produced water and temperature are the main factors affecting the chemical composition and the scaling tendency of the deposits.

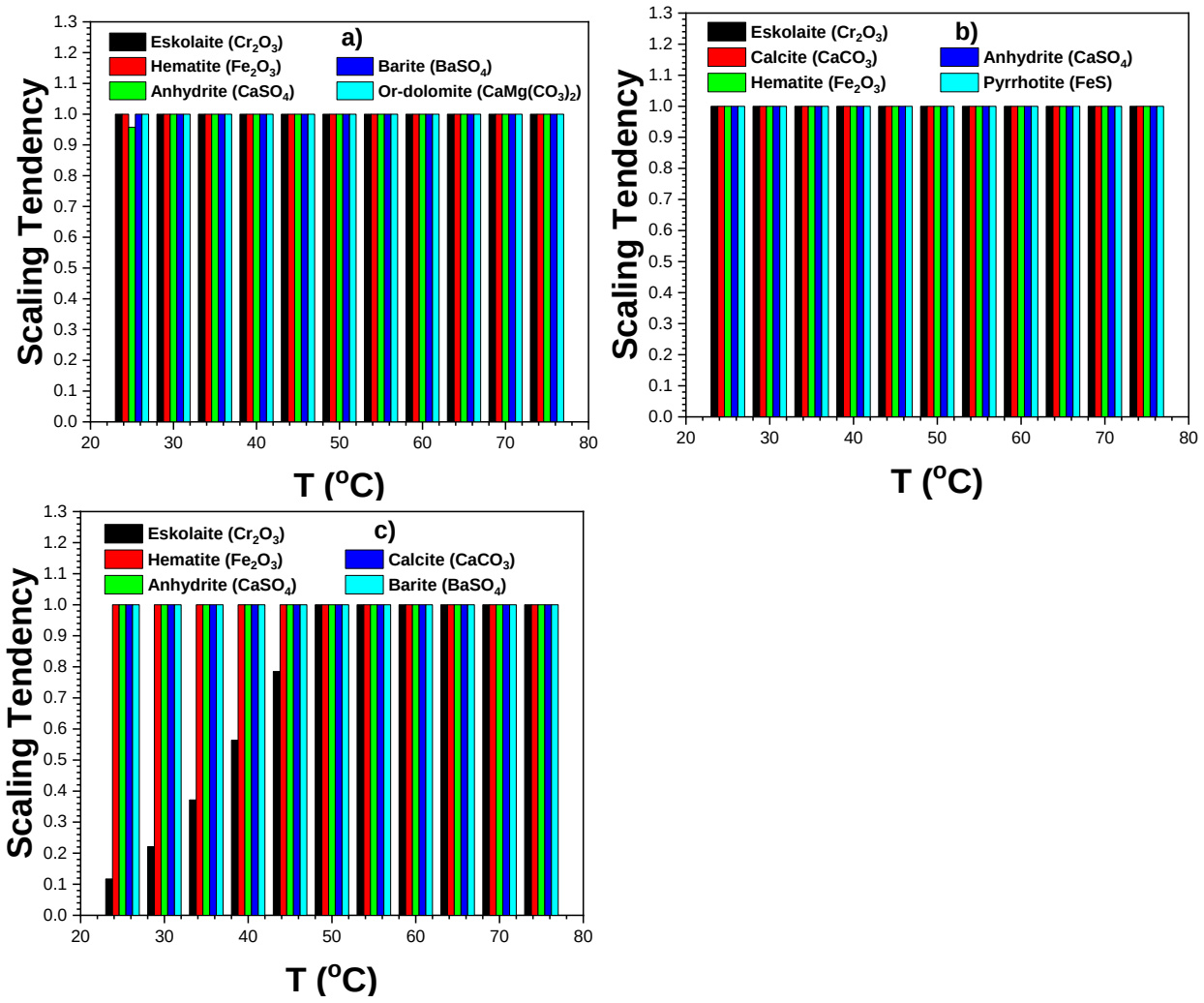


Figure 9: OLI simulation to predict scaling tendency of produced water with and without adding CO_2. Steam amount = 1L. (a). 0 mole/kg CO_2; (b). 0.2 mole/kg CO_2; (c). 0.6 mole/kg CO_2.

3.2.2 Corrosion Prediction of Steels in Carbonated Produced Water

The corrosion behavior of stainless-steel alloys was investigated in simulated CBI reservoir conditions. Corrosion rates and pH were predicted using OLI software. For comparison purposes, carbon steel (UNS G10180) was investigated under the same conditions as stainless-steel alloys. The effect of scaling was not considered during corrosion modeling. Figure 10 shows predicted corrosion rates and pH values calculated as a function of temperature and CO_2 content for the different tested stainless-steels. A higher corrosion rates for 13 Cr stainless-steel was predicted compared to super 13 Cr stainless-steel exposed to produced water with or without CO_2. In general, no significant differences are found between the corrosion rate values of stainless-steel exposed to produced water with or without CO_2. However, for both stainless-steel, corrosion rates increase with temperature, and corrosion rates are below 0.02 mm/y under tested conditions. The results show that stainless-steel alloys (13 Cr and super 13 Cr) have good

resistant to CO_2 corrosion due to the higher amount of Cr which can be beneficial for formation of protective scales or passive layer.

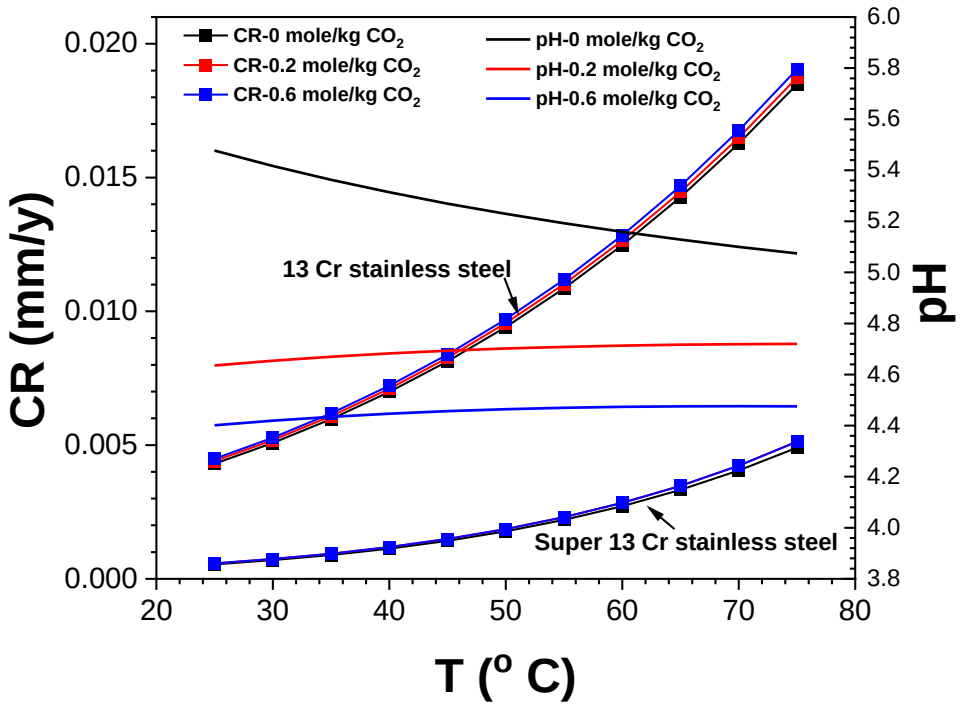


Figure 10: OLI simulation to predicted pH and corrosion rates of stainless-steel exposed to injected produced water with and without CO_2.

Figure 11 shows the corrosion rate of carbon steel as a function of temperature after exposure with produced water with and without CO_2. As shown in the results, the increase of CO_2 amount into produced water or increase in temperature led to a higher corrosion rate. A lower predicted corrosion rate was observed at lower temperatures and at 0 mole/kg CO_2. When dissolved CO_2 is present, the corrosion significantly increases with temperature, suggesting that dissolved CO_2 contributes to accelerating corrosion reaction.

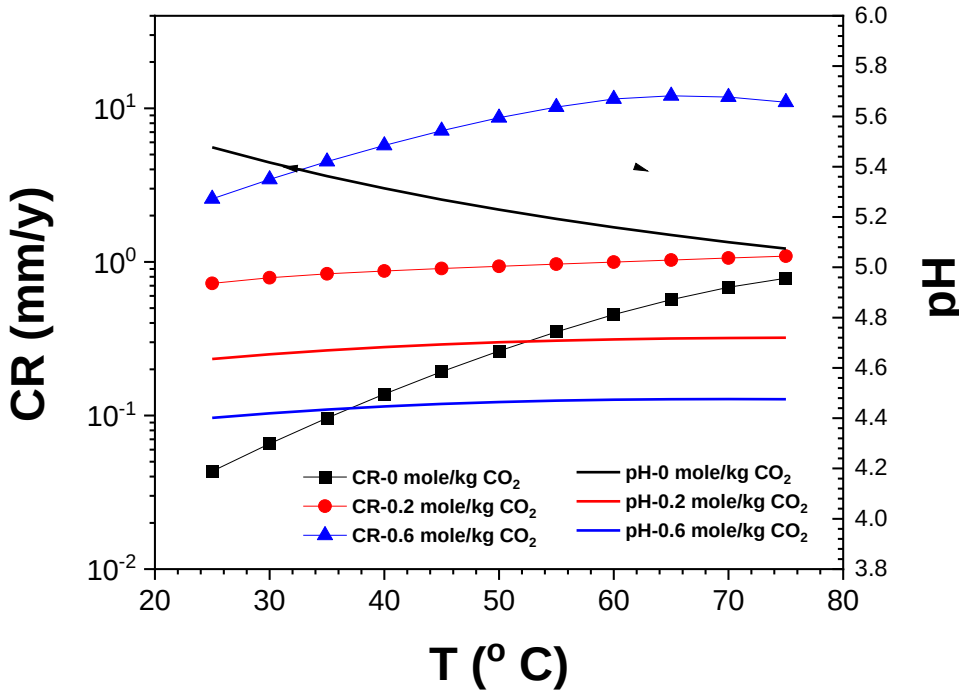


Figure 11: OLI simulation to predicted pH and corrosion rates of carbon steel UNS G10180 exposed to injected produced water with and without CO_2.

3.3 REACTIVE TRANSPORT MODELING

3.3.1 Injection Period (Year 0–20)

In the following figures, the results of the reactive transport modeling are shown as the top view to the reservoir, with the injection well in the center. During the CBI period, the pH change is shown in Figure 12 as a function of time. The initial reservoir pH is 6.1. The injected carbonated water decreases the pH. The central region pH is buffered with mineral dissolution. The dissolved solids (Figure 13) of the entire reservoir after 20 years of injection increases almost 10 times due to the high TDS of the produced water. Fluid density (Figure 14) increases accordingly.

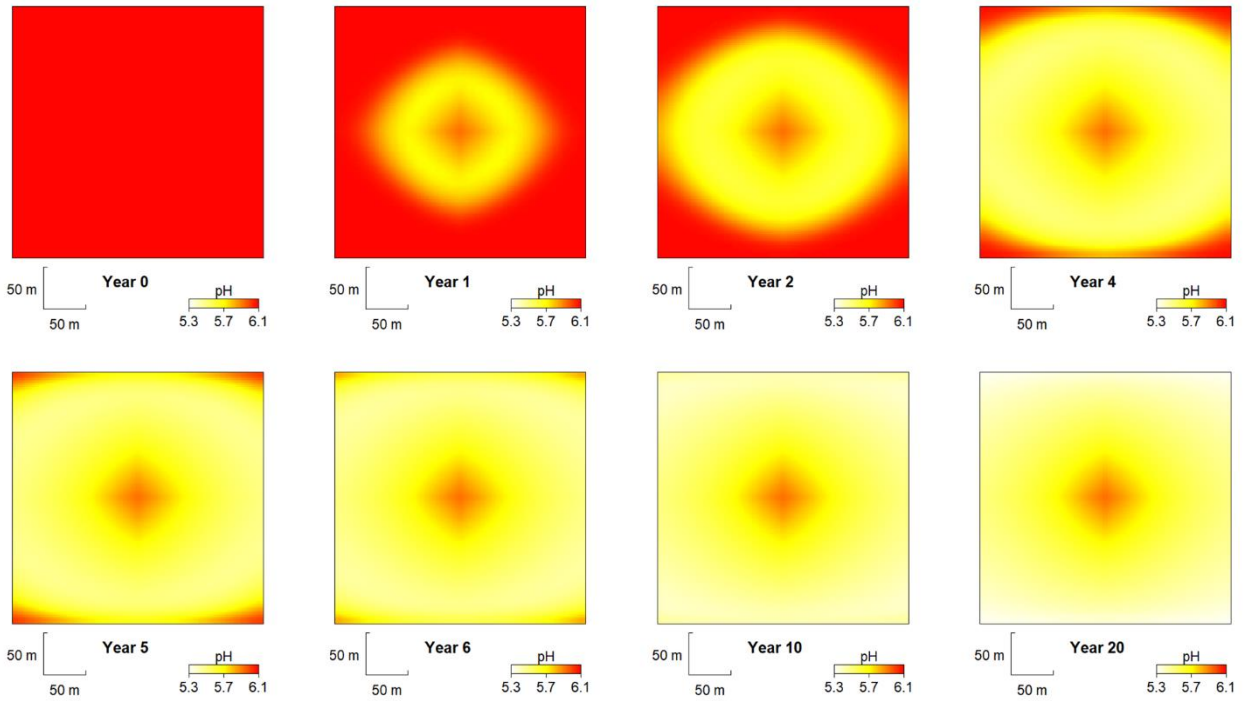


Figure 12: pH changes in the reservoir during injection period.

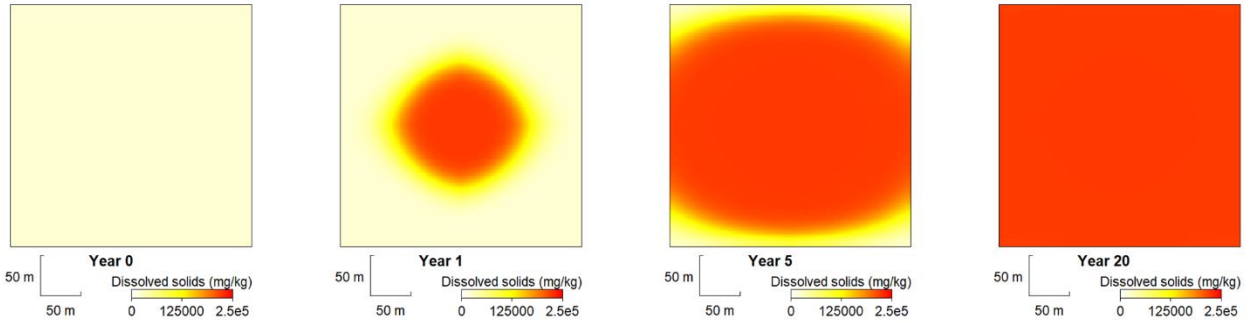


Figure 13: Dissolved solids changes in the reservoir during injection period.

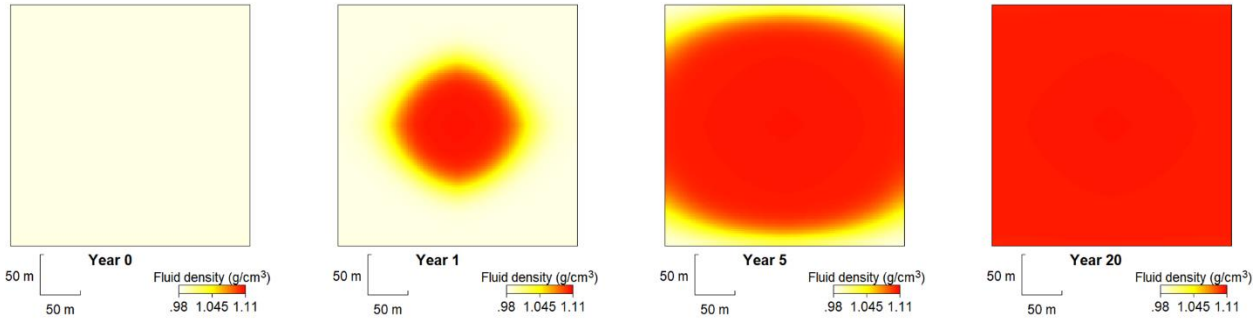


Figure 14. Fluid density changes in the reservoir during injection period.

This central region is where most rock-fluid interactions occur. Mineral volume (Figure 15) and porosity (Figure 16) are a result of mineral dissolution and precipitation. Overall, precipitation in the central region outweighs dissolution, resulting in an increased mineral volume, i.e., decreased porosity in this region. As the injected fluid spreads to further regions, the fluids became more geochemically equilibrated. Less mineral precipitation and dissolution are observed outside the central region.

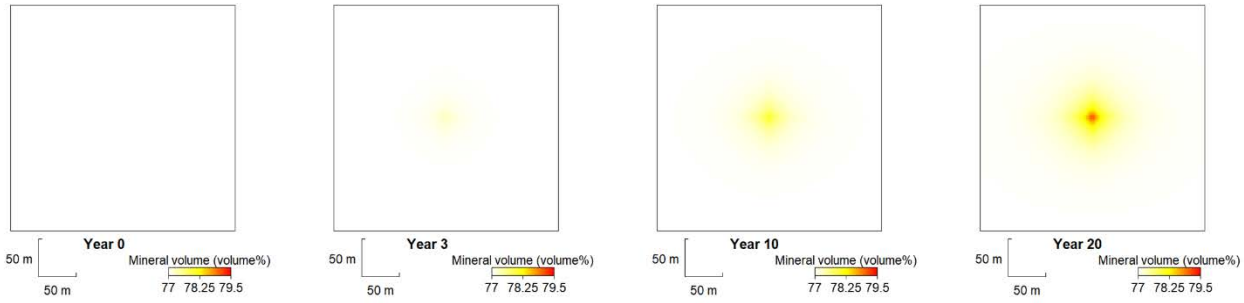


Figure 15: Mineral volume changes in the reservoir during injection period.

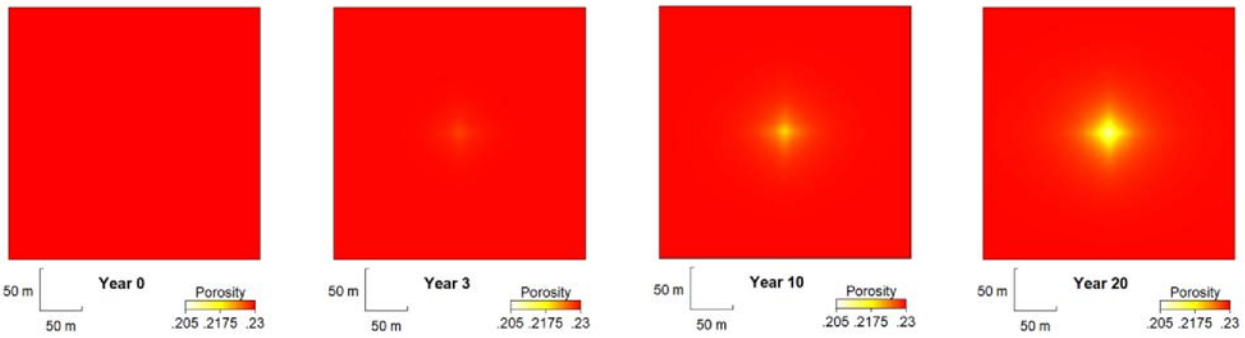


Figure 16: Porosity changes in the reservoir during injection period.

The total dissolved carbon amount increases and spreads to the entire reservoir (Figure 17). Among the dissolved carbon species, CO_2(aq) is the major component. In the central region where rock-fluid interactions are most intense, carbonate and bicarbonate species are present as a result of carbonate mineral dissolution and precipitation. The speciation of dissolved carbon is consistent with the pH changes and distribution (Figure 12).

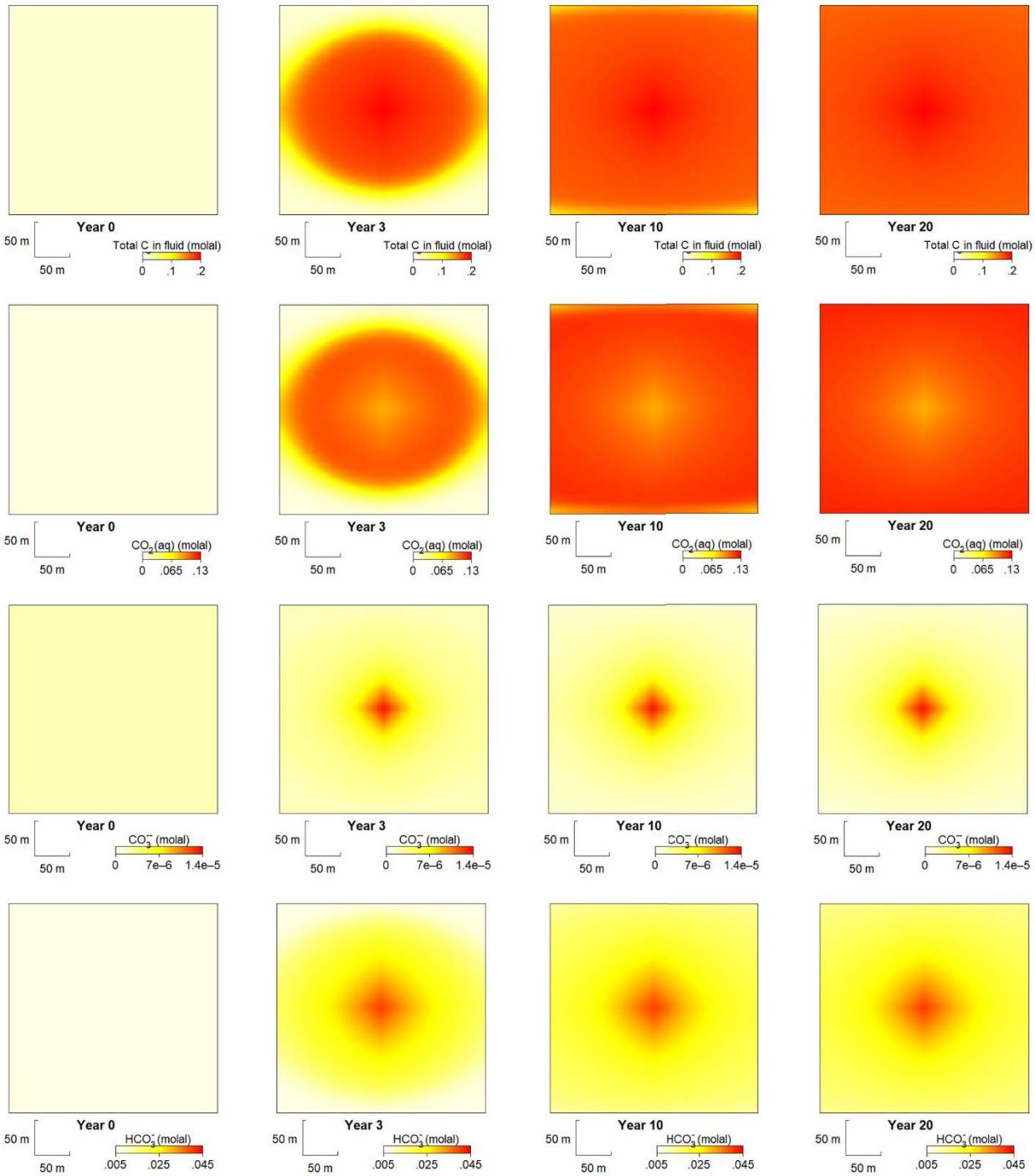


Figure 17: Dissolved carbon species changes in the reservoir during injection period.

For the primary minerals in the reservoir, quartz and muscovite undergo a dissolution-precipitation-redissolution process at the border of the injected fluid as the fluid goes outward from the injection point. This is reflected by the changes of the mineral saturation indices (Figure 18), as the mineral volume changes are not obvious with the large initial percentage. Siderite

continues to precipitate in the central region and slowly increases and spreads outwards due to the continuous supply of Fe^{2+} and CO_3^{2-} from the injected carbonated brine.

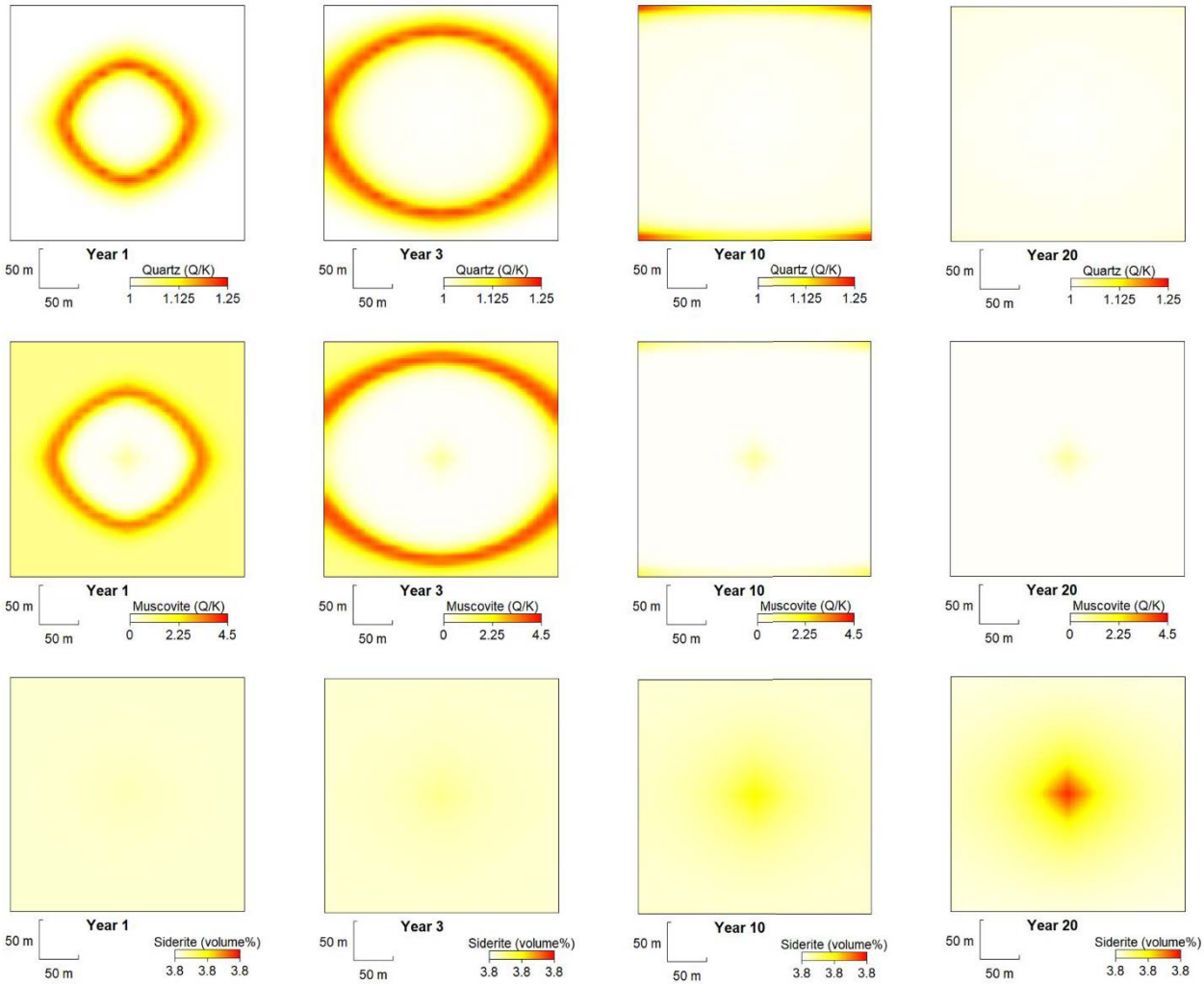


Figure 18: Primary minerals saturation and volume during injection period.

Most secondary precipitations are located in the central region where rock-fluid interactions occur. Figure 19 shows the secondary mineral volume percentage at the end of the 20-year injection period. Secondary precipitates are mostly composed of carbonate minerals (Ca, Mg, Ba carbonates) and some barite.

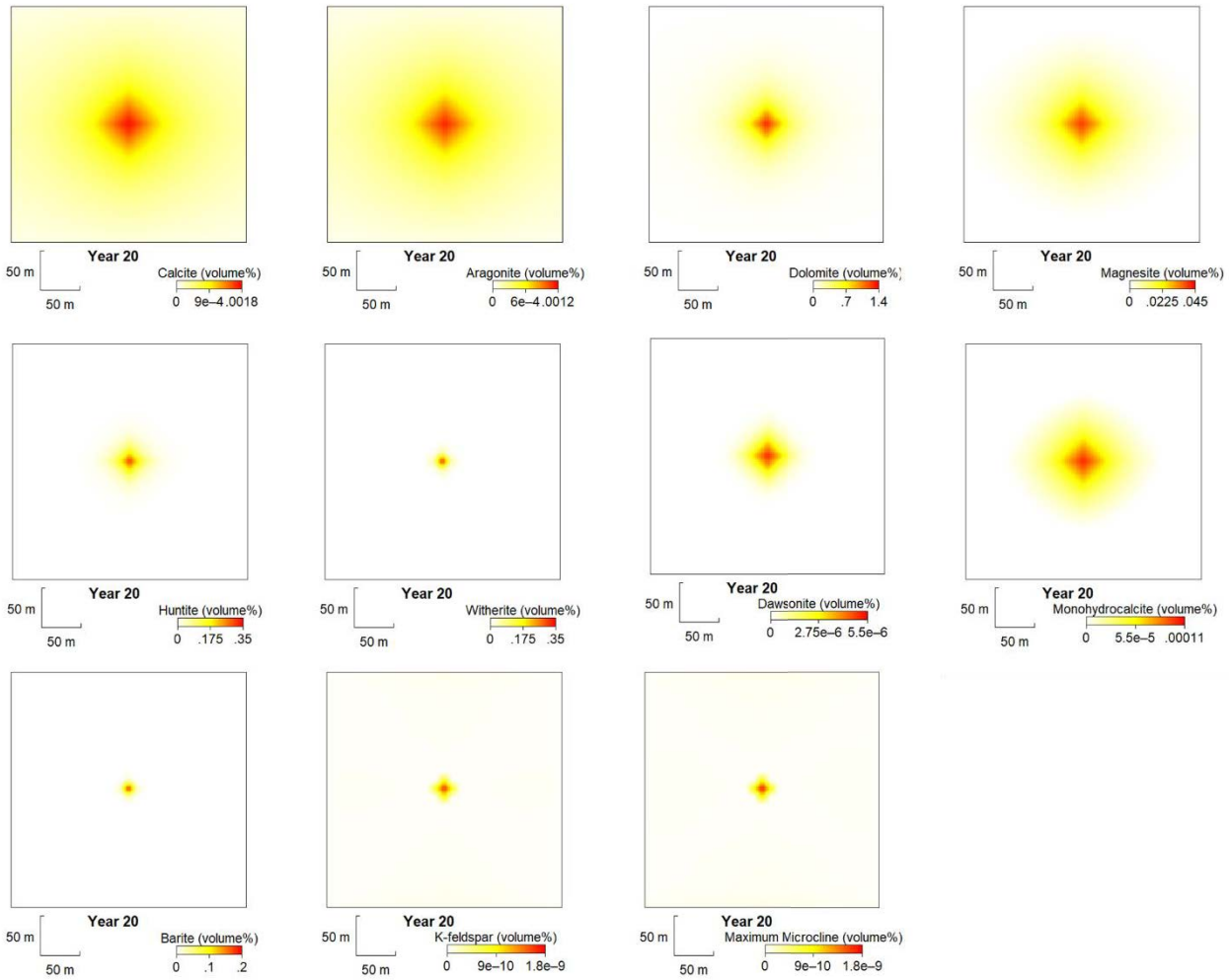


Figure 19: Secondary precipitations at the end of the 20-year injection period.

3.3.2 Shut-in Period (Year 20–120)

The pH continues decreasing slowly over 100 years of the shut-in period (Figure 20). There are no obvious changes for dissolved solids and porosity.

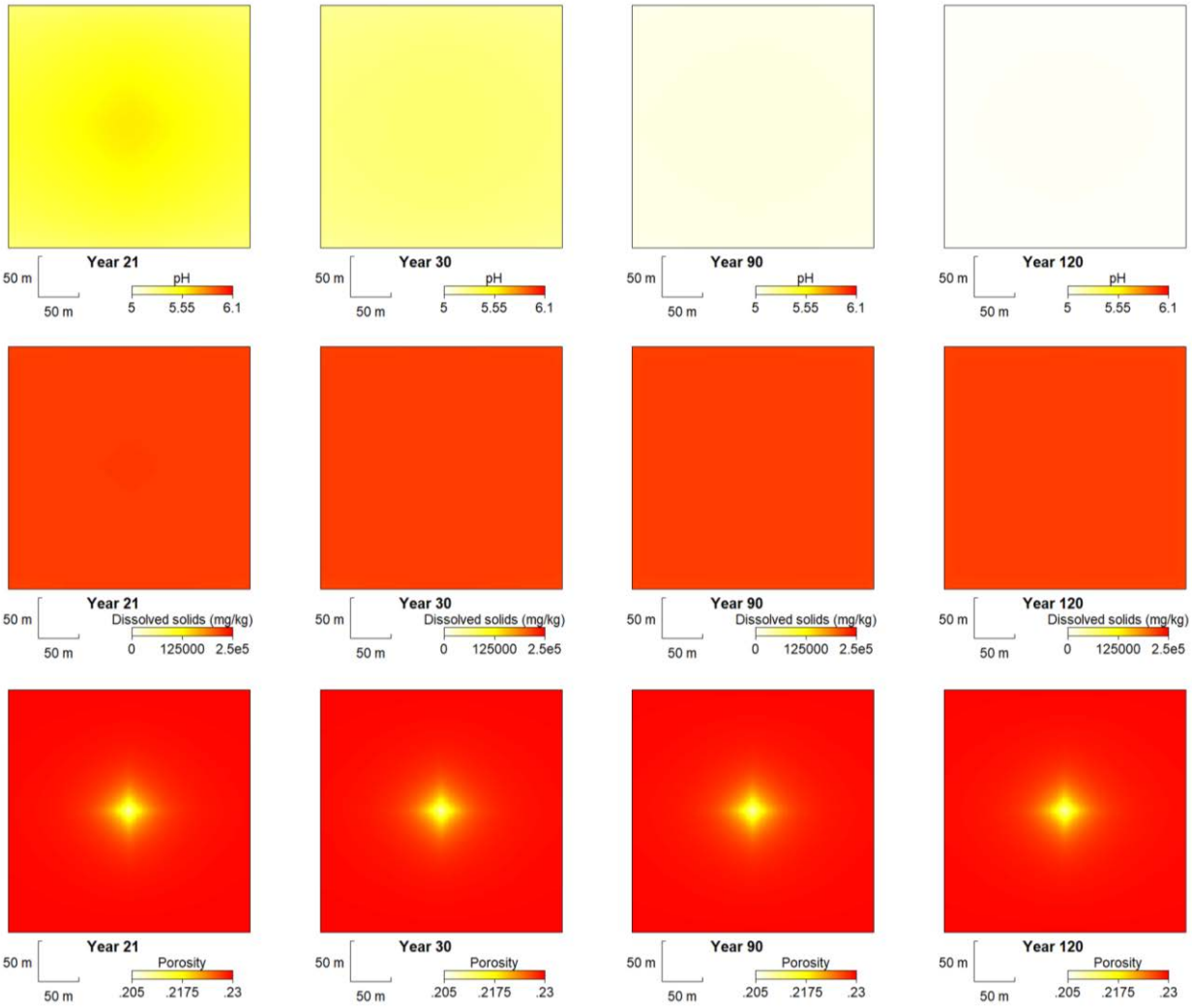


Figure 20: pH, dissolved solids, and porosity during the shut-in period.

The pH change is consistent with dissolved carbon speciation (Figure 21). As pH decreases from 5.5 to 5, CO_2(aq) concentration increases, and HCO_3^- concentration decreases. CO_3^{2-} is minimal in acidic solution, and keeps decreasing with decreased pH. The total dissolved carbon in the solution keeps decreasing slowly, indicating some carbon is sequestered through carbonate mineral precipitation over long-term storage.

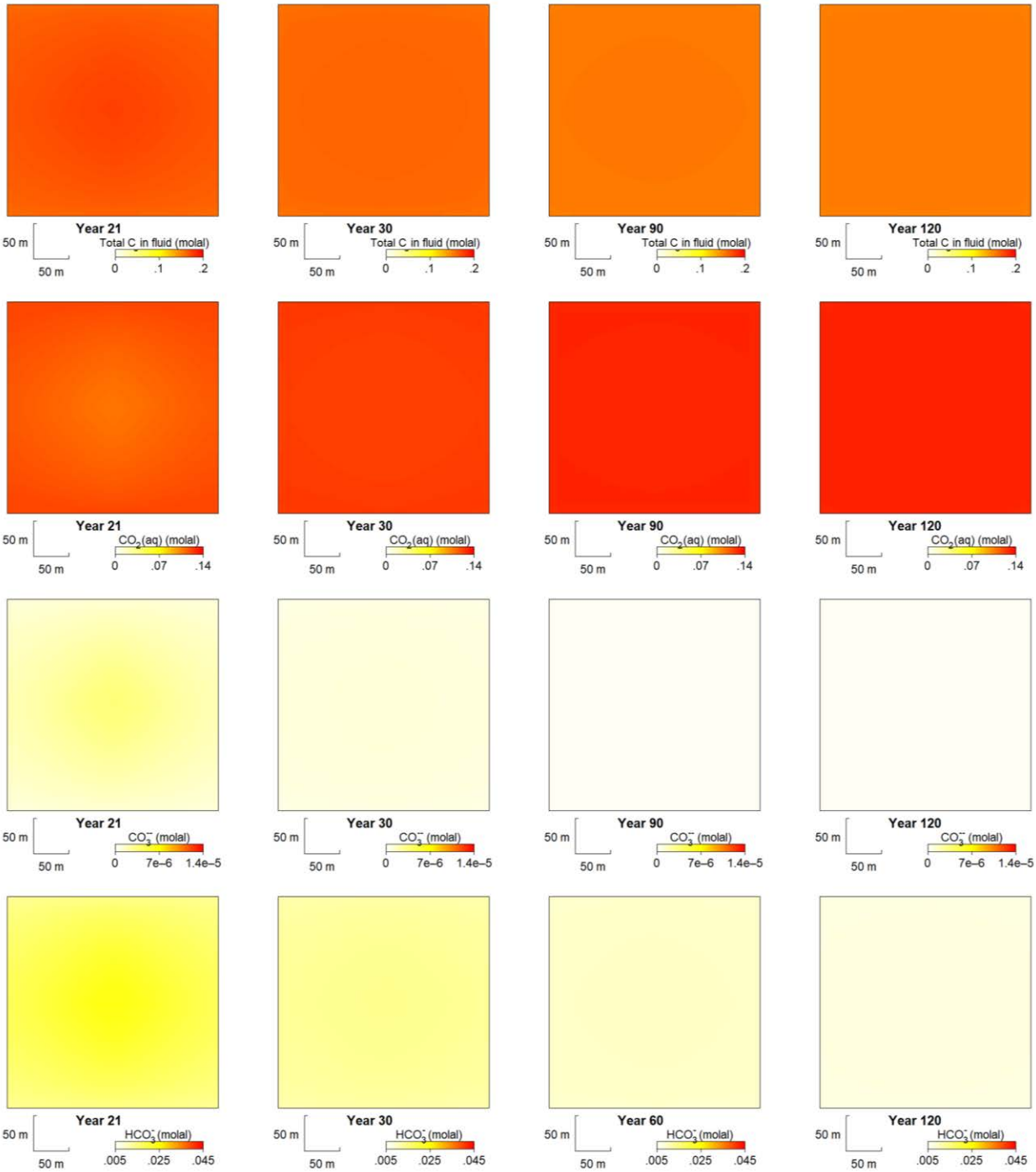


Figure 21: Dissolved carbon species during shut-in period.

For primary minerals in the sandstone, the increased siderite from the injection period keeps precipitating for a short time after injection stops (Figure 22). Then re-dissolves with decreasing pH. This is also reflected by the supersaturation status of siderite at Year 21, followed by undersaturation over the rest of the years. The change in all primary minerals is negligible comparing to their initial volume percentage.

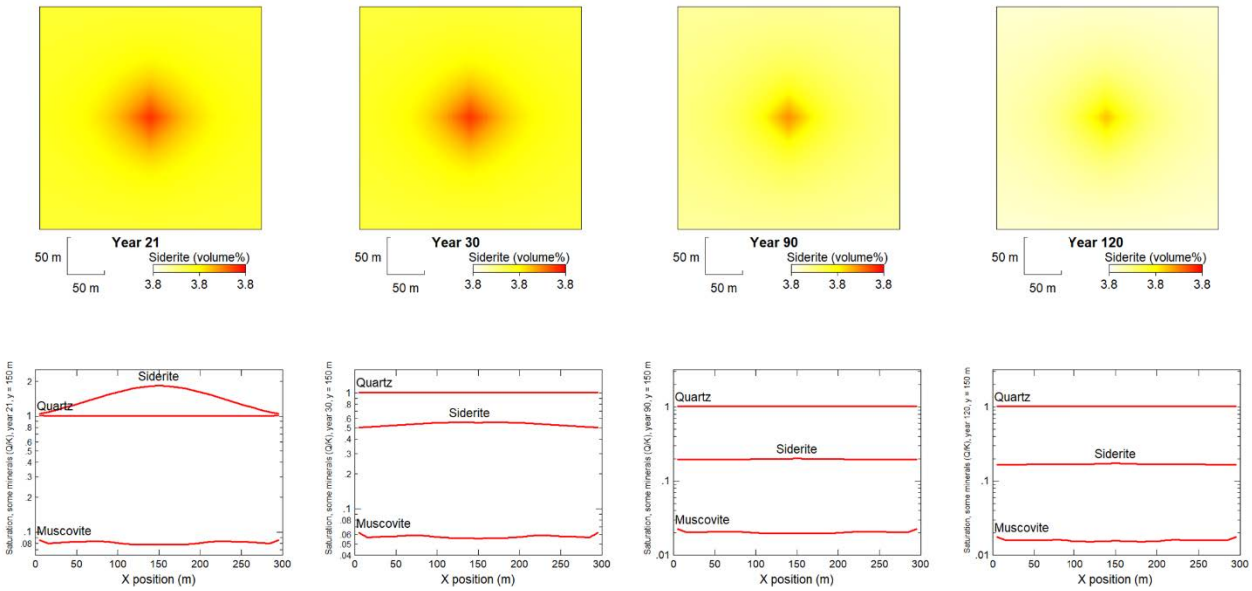


Figure 22: Primary mineral volume percentage and saturation changes during the shut-in period.

Many carbonate minerals are supersaturated when injection just stops. Over decades, only a few carbonate minerals (dolomite, calcite, and aragonite) are still supersaturated and tend to form continuously (Figure 23).

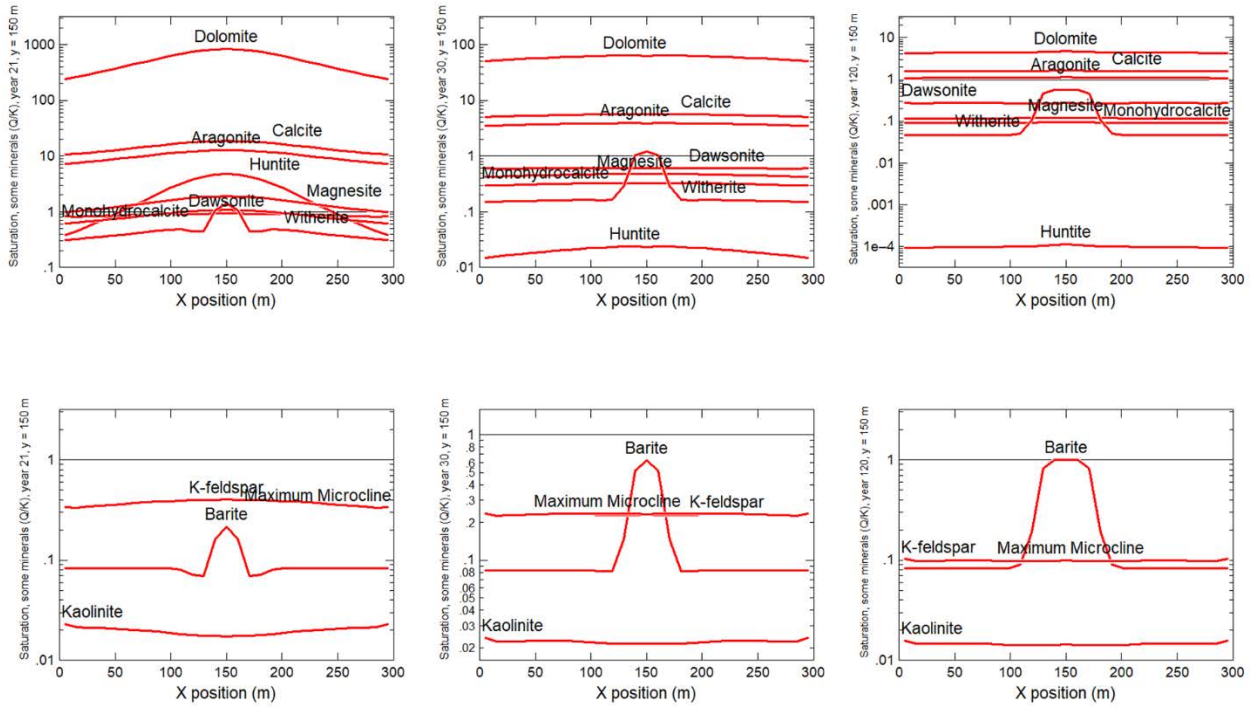


Figure 23: Secondary mineral precipitates saturation during the shut-in period.

Although some Ca- and Mg-containing carbonate minerals are supersaturated during the long-term storage, the overall mineral precipitation volume is small across the entire reservoir. Figure 24 shows an example of dolomite volume percentage change from Year 21 to Year 120.

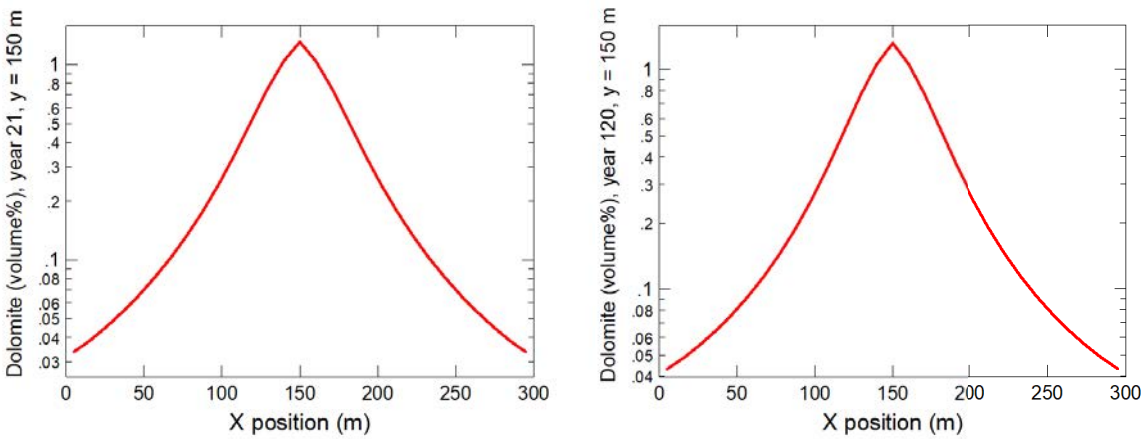


Figure 24: Dolomite volume percentage changes after 100 years of the shut-in period.

4. DISCUSSIONS

4.1 CO_2 CONCENTRATION FOR CBI

While the concept of CBI for CO_2 storage is still relatively new, carbonated waterflooding has been used for EOR and represents a critical proxy that produced water operators can borrow from to reduce the learning curve. As there are tens of thousands of disposal wells currently in operation across the U.S., there exists tremendous opportunity to take advantage of pre-existing infrastructure to accelerate deployment of CBI in the future. Pre-dissolving CO_2 into brine has the added benefit of accelerated CO_2 mineralization. As stated above, CarbFix demonstrated rapid mineralization by injecting carbonated water into porous basalts. Future efforts should highlight the mineralization potential of other reservoirs based on mineralogy, pressure, and temperature. Future projects should focus on field demonstration of CBI along with a breakdown of cost considerations.

An important parameter for CBI is CO_2 solubility, the amount of CO_2 that can be fully dissolved into the brine. CO_2 solubility in brine is found to be a function of three parameters: temperature, pressure, and salinity (Burton and Bryant, 2007). In general, CO_2 solubility in brine decreases with increasing temperature, increases with increasing pressure, and decreases with increasing salinity (Burton and Bryant, 2007; Frailey and Finley, 2009). Monovalent salts such as NaCl and KCl are found to inhibit dissolution more than divalent salts such as $CaCl_2$ or $MgCl_2$ (Burton and Bryant, 2007). Different brines have different compositions depending on location, but the dissolved salts in produced water typically consist primarily of sodium chloride (NaCl). Produced water salinity varies among basins, with the Williston Basin having some of the highest TDS concentrations, averaging 300,000 mg/L up to 350,000 mg/L (Glazewski et al., 2020). Previous studies have shown the solubility of CO_2 to be a function of temperature and depth, with depths beyond 2,000 feet showing the solubility of CO_2 in brine to remain nearly constant (Burton and Bryant, 2007). Rising temperature can also reduce fluid viscosity significantly, which can impact the injection capacity of a well (Bisweswar et al., 2020). Surface pump injection pressure and temperature also need to be taken into consideration, with the mixing temperature expected to be bounded by initial reservoir temperature and ambient temperature. The trend in surface dissolution of CO_2 into brine is that less brine is required when the mixing tank operates at higher pressures and lower temperatures (Burton and Bryant, 2009). Future efforts and field demonstration of CBI should include consideration of surface facilities and equipment.

4.2 COMPATIBILITY OF EXISTING INFRASTRUCTURE

The formation of carbonic acid (H_2CO_3) during CBI could lead to corrosion of the wellbore casing, tubing, packer, and surface equipment. When dissolved CO_2 is present, the corrosion is significantly increases with temperature, suggestion that dissolved CO_2 contribute to accelerating corrosion reaction. The rate of corrosion is highly dependent on the amount of CO_2 and temperature (Kahyarian and Nesic, 2020; Nesic, 2007). It was proven in literature that the increase in temperature accelerates electrochemical, chemical reactions, and mass transfer, diffusion of corrosive species to the surface, etc., involved in corrosion process (Kahyarian and Nesic, 2020; Nesic, 2007). Temperature has a strong influence on pH, which has a strong influence on the corrosion rate. The commonly accepted explanation is that with dissolved CO_2, the concentration of H_2CO_3 increases and accelerates the cathodic reaction. CO_2 corrosion might

be encountered in carbon steel or stainless-steel due to electrochemical reaction occurring on the steel surface. Dissolved CO_2 reacts with water to form carbonic species according to the following equations (Kahyarian and Nesic, 2020; Nesic, 2007):

$$CO_2 + H_2O \Leftrightarrow H_2CO_3 \qquad \text{(Equation 1)}$$

$$H_2CO_3 \Leftrightarrow HCO_3^- + H^+ \qquad \text{(Equation 2)}$$

$$HCO_3^- \Leftrightarrow CO_3^{2-} + H^+ \qquad \text{(Equation 3)}$$

When the steel surface is in contact with aqueous CO_2, electrochemical processes involving the anodic dissolution of iron (equation 4) and the cathodic evolution of hydrogen (equation 5) are taking place (Kahyarian and Nesic, 2020; Nesic, 2007).

$$Fe \Leftrightarrow Fe^{2+} + 2\,e^- \qquad \text{(Equation 4)}$$

$$2\,H^+ + 2\,e^- \Leftrightarrow H_2 \qquad \text{(Equation 5)}$$

Based on predicted corrosion results, carbon steel is more susceptible to CO_2 corrosion than 13 Cr stainless-steel and super 13 Cr-stainless-steel. Despite predicted corrosion rates, carbon steel can be preferred material because of its low cost. However, additional corrosion control measures, such as corrosion inhibitor injection, are required to control corrosion in wellbore materials. In addition, significant levels of dissolved oxygen can be expected in the BCI water, and while the downhole environment may be anoxic. Care should be taken to prevent the formation of differential aeration cells at the casing steel.

4.3 LONG-TERM STORAGE SAFETY

The success of geologic CO_2 storage depends on a combination of physical and geochemical trapping mechanisms (Figure 25) (Metz et al., 2005). Using CBI directly moves the trapping stage to solubility trapping. Dissolved CO_2 is no longer a separate phase, thereby eliminating the buoyant forces that drive it upwards.

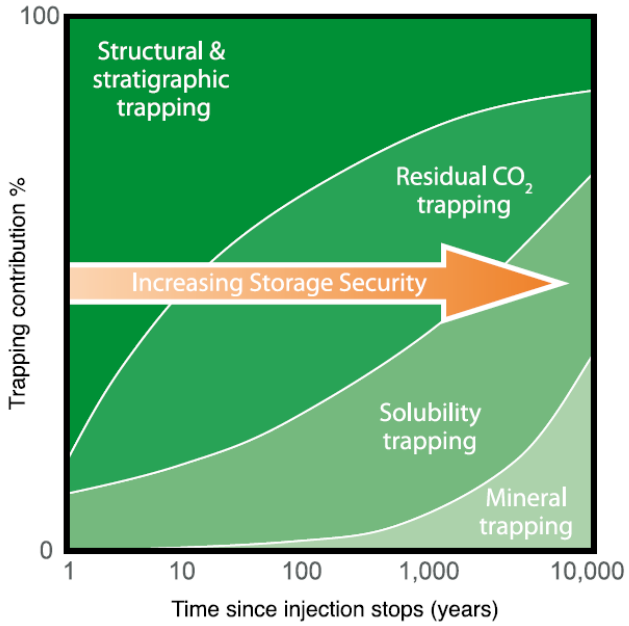


Figure 25: Storage security depends on a combination of physical and geochemical trapping. Over time, the physical process of residual CO_2 trapping and geochemical processes of solubility trapping and mineral trapping increase (Metz et al., 2005).

Using the method of CBI, CO_2 can be safely stored in sandstone reservoirs via solubility trapping. Though small amount of CO_2 converts to carbonate minerals, CO_2 remained in liquid phase in long-term storage. During the injection period, most rock-fluid geochemical interactions are limited in a certain region where the carbonated water is injected. The pH, dissolved carbon speciation, and amount are a result of mineral precipitation and dissolution. The porosity decrease due to mineral precipitation is small. Mineral precipitation due to rock-fluid interactions in the reservoir is unlikely to block flow pathways for injection. Geochemical changes during the long-term shut-in period are not obvious.

4.4 NANOBUBBLE TECHNOLOGY FOR CO_2 INJECTION

The nanobubble technology of dissolving CO_2 in the produced water is a promising application in CO_2 geological storage sites. This technology has been relatively mature. The features of micro and nanobubbles include excellent stability, high internal pressure, extremely large surface-to-volume ratio, and high gas dissolution rate (Figure 26) (Li et al., 2023).

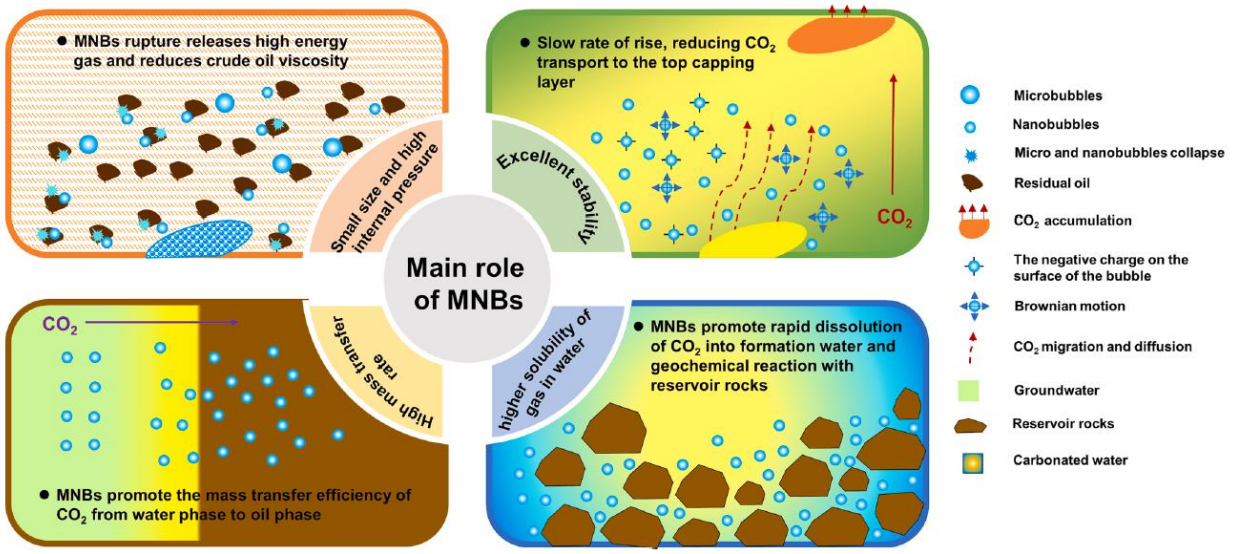


Figure 26: Main mechanism of EOR and geological sequestration by CO_2 injection in the form of micro and nanobubbles (Li et al., 2023).

Dissolving CO_2 nanobubbles in the produced water before or during injection could make it possible to allow all free-phase CO_2 to dissolve before reaching the reservoir (Figure 27) (Uemura et al., 2016). This technology makes CBI a low-risk CO_2 storage method compared to the traditional injection of supercritical CO_2 into the reservoir, where CO_2 needs a long time period to dissolve in groundwater.

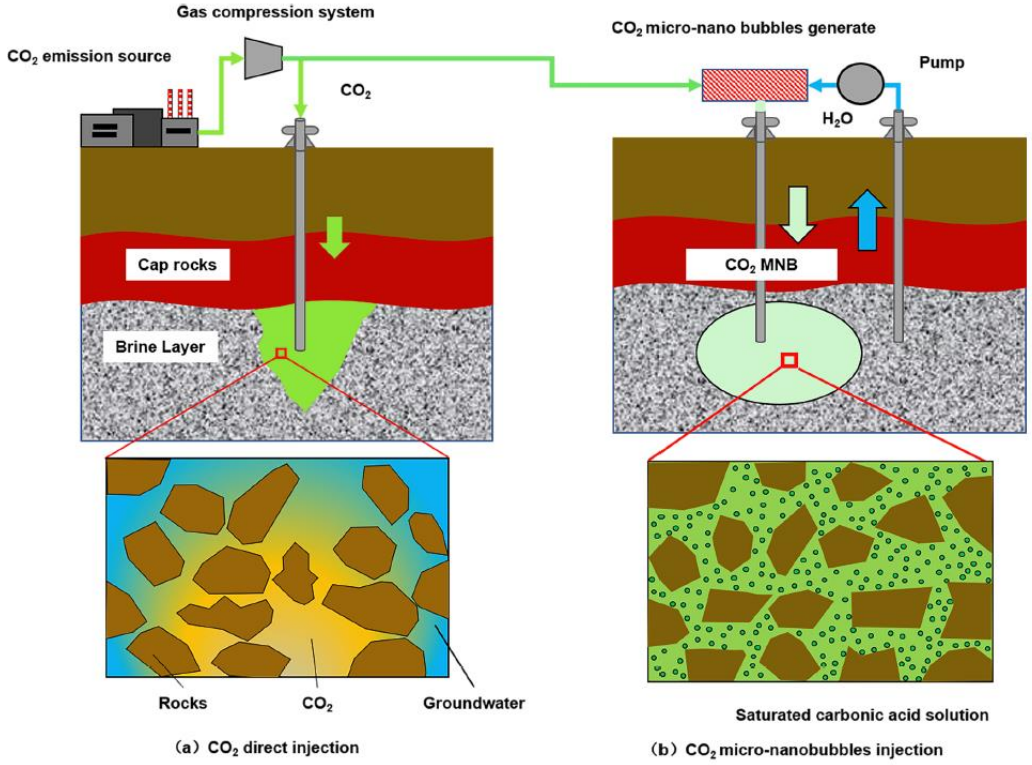


Figure 27: Schematic diagrams comparing CO_2 geological storage techniques (Uemura et al., 2016).

5. CONCLUSIONS

Carbonated brine storage is a low-risk geologic CO_2 sequestration strategy. Simulations of CBI at small CO_2 molality (0.2 mol/kg) were found to show no perceivable increases in reservoir pressure or impacts to brine viscosity or density due to the dissolved CO_2. When compared specifically to standard produced water disposal operations, pressure-driven risks such as leakage, induced seismicity, cap rock failure, and migration do not increase because of the inclusion of dissolved CO_2 in the brine injection stream. Since there are no anticipated increased risks, a delineated area of review for a Class II injection well is not anticipated to change with the integration of dissolved CO_2. Wellbore corrosion rates can be anticipated to be at an acceptable range to maintain CBI operations for years. Furthermore, since the pressure equilibrium is identical to the noncarbonated brine standard operations, the length of the post-injection site closure (PISC) period would not be impacted. Oftentimes, the carbonated brine will be denser than the reservoir brine, such that the CO_2-laden brine sinks to the bottom of the reservoir instead of migrating upward because of buoyancy. CO_2 is safely stored via dissolution sequestration in long term storage.

Dissolving CO_2 into produced water disposal streams creates a cash incentive through IRS Section 45Q tax credits. For permanent storage, the tax credit is currently \$85/ton of CO_2 sequestered (Bright, 2022). Given the current reservoir conditions of the Inyan Kara Formation with a reservoir pressure of 2,255 psi, formation temperature of 165 °F, and produced water salinity of 300,000 mg/L, at 2% CO_2 mass fraction, 1 ton of CO_2 could be dissolved into approximately every 200 bbl of Bakken produced water. This equates to approximately \$0.425/bbl of brine, a notable increase in cashflow for a produced water disposal operator. Since CO_2 solubility in brine is found to be a function of temperature, pressure, and salinity, a lower produced water salinity would result in a greater amount of CO_2 that could be dissolved and injected.

While a field demonstration to evaluate the economic impacts is necessary, it is anticipated that the incremental benefit of adding CO_2 to produced water disposal streams may outweigh the incremental costs of transport and pressure mixing under favorable conditions. Compared to new CCUS projects with bulk CO_2 injection, CBI enjoys the benefits of a pre-existing well and infrastructure that has already gone through the necessary permitting process. In the cases where injection rates do not warrant dedicated pipeline investment, trucking CO_2 to the well pad further reduces potential up-front costs. These considerations significantly reduce project capital expenditures and risk, particularly where several years of operating data exist to verify geologic models.

Regulatory considerations for CBI include the regulations surrounding aboveground storage of the produced water on location and creating a path to approval under Class II injection wells. A pilot field demonstration would aid in answering some of the questions regulators might have surrounding CBI such as whether the wellbore tubing and casing would need to be retrofitted in any form.

6. REFERENCES

Bader, J. W. Sequence Stratigraphy of the Inyan Kara Formation, Northwestern North Dakota: Extracting the Maximum from Minimal Core and Outcrop Data. AAPG Annual Convention and Exhibition, 2017.

Bisweswar, G.; Al-Hamairi, A.; Jin, S. Carbonated water injection: an efficient EOR approach. A review of fundamentals and prospects. *Journal of Petroleum Exploration and Production Technology* **2020,** *10*, 673–685.

Bright, M. The Inflation Reduction Act creates a whole new market for carbon capture. Clean Air Task Force: Boston, MA, 2022. https://www.catf.us/2022/08/the-inflationreduction-act-creates-a-whole-new-market-for-carbon-capture.

Burton, M.; Bryant, S. L. Eliminating buoyant migration of sequestered CO_2 through surface dissolution: implementation costs and technical challenges. *SPE Reservoir Evaluation & Engineering* **2007,** *12*, 399–407.

Burton, M.; Bryant, S. L. Surface dissolution: minimizing groundwater impact and leakage risk simultaneously. *Energy Procedia* **2009,** *1*, 3707–3714.

Busenberg, E.; Plummer, L. N. The kinetics of dissolution of dolomite in CO 2-H 2 O systems at 1.5 to 65 degrees C and O to 1 atm PCO 2. *American Journal of Science* **1982,** *282*, 45–78.

Chu, M. H. Study of the geothermal production potential in the Williston Basin, North Dakota; 1991.

Eke, P. E.; Naylor, M.; Haszeldine, S.; Curtis, A. CO_2/brine surface dissolution and injection: CO_2 storage enhancement. *SPE Projects, Facilities & Construction* **2011,** *6*, 41–53.

Fathollahi, A.; Rostami, B. Carbonated water injection: Effects of silica nanoparticles and operating pressure. *The Canadian Journal of Chemical Engineering* **2015,** *93*, 1949–1956.

Frailey, S. M.; Finley, R. J. Classification of CO_2 geologic storage: Resource and capacity. *Energy Procedia* **2009,** *1*, 2623–2630.

Georgescu, S.; Lindeberg, E.; Holt, T. Co-injection of CO_2 and water in non-sealed saline aquifers. International Conference on Greenhouse Gas Control Technologies, Trondheim, Norway, 2006.

Glazewski, K. A.; Taunton, M. A.; Wilson, W. I.; Kurz, B. A.; Kovacevich, J.; Azzolina, N. A.; Hamling, J. A.; Sorensen, J. A.; Steadman, E. N.; Harju, J. A.; Gorecki, C. D. Produced water management and recycling options in North Dakota, 2020.

Helgeson, H. C.; Murphy, W. M.; Aagaard, P. Thermodynamic and kinetic constraints on reaction rates among minerals and aqueous solutions. II. Rate constants, effective surface area, and the hydrolysis of feldspar. *Geochimica et Cosmochimica Acta* **1984,** *48*, 2405–2432.

Kahyarian, A.; Nesic, S. On the mechanism of carbon dioxide corrosion of mild steel: Experimental investigation and mathematical modeling at elevated pressures and non-ideal solutions. *Corrosion Science* **2020,** *173*, 108719.

Khan, C.; Pearce, J. K.; Golding, S. D.; Rudolph, V.; Underschultz, J. R. Carbon Storage Potential of North American Oil & Gas Produced Water Injection with Surface Dissolution. *Geosciences* **2021,** *11*, 123.

Kühn, M.; Kempka, T.; De Lucia, M.; Scheck-Wenderoth, M. Dissolved CO_2 storage in geological formations with low pressure, low risk and large capacities. *Energy Procedia* **2017,** *114*, 4722–4727.

Li, X.; Peng, B.; Liu, Q.; Liu, J.; Shang, L. Micro and nanobubbles technologies as a new horizon for CO2-EOR and CO_2 geological storage techniques: A review. *Fuel* **2023,** *341*, 127661.

Metz, B.; Davidson, O.; De Coninck, H.; Loos, M.; Meyer, L. *IPCC special report on carbon dioxide capture and storage*; Cambridge: Cambridge University Press, 2005.

Motie, M.; Assareh, M. CO_2 sequestration using carbonated water injection in depleted naturally fractured reservoirs: A simulation study. *International Journal of Greenhouse Gas Control* **2020,** *93*, 102893.

Nagy, K. Dissolution and precipitation kinetics of sheet silicates. *Reviews in Mineralogy and Geochemistry* **1995,** *31*, 173–233.

Nesic, S. Key issues related to modelling of internal corrosion of oil and gas pipelines–A review. *Corrosion Science* **2007,** *49*, 4308–4338.

North Dakota Geological Survey. 2020. https://www.dmr.nd.gov/ndgs/InyanKaraMaps/.

Palandri, J. L.; Kharaka, Y. K. *A Compilation of Rate Parameters of Water-Mineral Interaction Kinetics for Application to Geochemical Modeling*; Open File Report (OF 2004-1068); U.S. Geological Survey; 2004.

Pearce, J.; Khan, C.; Golding, S.; Rudolph, V.; Underschultz, J. Geological storage of CO_2 and acid gases dissolved at surface in production water. *Journal of Petroleum Science and Engineering* **2022,** *210*, 110052.

Pearce, J. K.; Dawson, G. K.; Sommacal, S.; Golding, S. D. Micro CT and experimental study of carbonate precipitation from CO_2 and produced water co-injection into sandstone. *Energies* **2021,** *14*, 6998.

Plummer, L.; Wigley, T.; Parkhurst, D. The kinetics of calcite dissolution in CO 2-water systems at 5 degrees to 60 degrees C and 0.0 to 1.0 atm CO 2. *American Journal of Science* **1978,** *278*, 179–216.

Pool, M.; Carrera, J.; Vilarrasa, V.; Silva, O.; Ayora, C. Dynamics and design of systems for geological storage of dissolved CO2. *Advances in Water Resources* **2013,** *62*, 533–542.

Rathnaweera, T.; Ranjith, P.; Perera, M.; Haque, A. Influence of CO_2–brine co-injection on CO_2 storage capacity enhancement in deep saline aquifers: an experimental study on Hawkesbury sandstone formation. *Energy & Fuels* **2016,** *30*, 4229–4243.

Rimstidt, J. D.; Barnes, H. The kinetics of silica-water reactions. *Geochimica et Cosmochimica Acta* **1980,** *44*, 1683–1699.

Ruprecht, C.; Falta, R. Comparison of supercritical and dissolved CO_2 injection schemes. Proceedings of TOUGH Symposium, Lawrence Berkeley National Laboratory, Berkeley, California, 2012.

Shariatipour, S. M.; Mackay, E. J.; Pickup, G. E. An engineering solution for CO_2 injection in saline aquifers. *International Journal of Greenhouse Gas Control* **2016,** *53*, 98−105.

Siefert, N.; Belarbi, Z.; Wenzlick, M. NEWTS USGS Produced Water Database, 2022. https://edx.netl.doe.gov/dataset/newts-usgs-produced-water-database. https://doi.org/10.18141/1890178

Sigfusson, B.; Gislason, S. R.; Matter, J. M.; Stute, M.; Gunnlaugsson, E.; Gunnarsson, I.; Aradottir, E. S.; Sigurdardottir, H.; Mesfin, K.; Alfredsson, H. A. Solving the carbon-dioxide buoyancy challenge: The design and field testing of a dissolved CO_2 injection system. *International Journal of Greenhouse Gas Control* **2015,** *37*, 213–219.

Sonderegger, J. L.; Brower, K.; Lefebre, V. A preliminary investigation of strontianite dissolution kinetics. *American Journal of Science* **1976,** *276*, 997−1022.

Steele-MacInnis, M.; Capobianco, R. M.; Dilmore, R.; Goodman, A.; Guthrie, G.; Rimstidt, J. D.; Bodnar, R. J. Volumetrics of CO_2 storage in deep saline formations. *Environmental Science & Technology* **2013,** *47*, 79−86.

Sverdrup, H. U. *The Kinetics of Base Cation Release due to Chemical Weathering*; University Press: Sweden, 1990.

Uemura, S.; Matsui, Y.; Kondo, F.; Tsushima, S.; Hirai, S. Injection of nanosized CO_2 droplets as a technique for stable geological sequestration. *International Journal of Greenhouse Gas Control* **2016,** *45*, 62−69.

Veil, J. US produced water volumes and management practices in 2012. Groundwater Protection Council, 2015.

Wu, B.; Li, X.; Teng, Y.; Lv, P.; Liu, Y.; Luo, T.; Zheng, J.; Wang, D.; Jiang, L. Characterizing the dissolution rate of CO_2-brine in porous media under gaseous and supercritical conditions. *Applied Sciences* **2017,** *8*, 4.





Sean Plasynski
Acting Director
National Energy Technology Laboratory
U.S. Department of Energy

John Wimer
Acting Chief Research Officer
Science & Technology Strategic Plans
& Programs
National Energy Technology Laboratory
U.S. Department of Energy

Bryan Morreale
Associate Laboratory Director for
Research & Innovation
Research & Innovation Center
National Energy Technology Laboratory
U.S. Department of Energy

NETL Technical Report Series

DocuSign Envelope ID: 2FA9A609-C360-4E53-8B28-BE8B77B6994A

BRINE TREATMENT TECHNOLOGY SUMMARY – BRINE EXTRACTION AND STORAGE TEST – PHASE II FINAL REPORT – VOLUME 2

Brine Extraction and Storage Test Phase II Final Report
Task 5.0 Deliverable 6 (D6)

Prepared for:

AAD Document Control

National Energy Technology Laboratory
U.S. Department of Energy
626 Cochrans Mill Road
PO Box 10940, MS 921-107
Pittsburgh, PA 15236-0940

Project Period: Phase I (BP1): September 1, 2015 – July 6, 2016
Phase II (BP2–BP4): July 7, 2016 – May 31, 2024
Cooperative Agreement No. DE-FE0026160
DUNS No. 102280781

Prepared by:

Marc D. Kurz
Nicholas S. Kalenze
Christopher L. Martin
John A. Hamling
Ryan J. Klapperich
Lonny L. Jacobson
Bradley G. Stevens

Energy & Environmental Research Center
University of North Dakota
15 North 23rd Street, Stop 9018
Grand Forks, ND 58202-9018
Phone (701) 777-5278
mkurz@undeerc.org

DocuSigned by:
Marc Kurz
4B86FEFFDB3941D...
Marc D. Kurz, Principal Investigator

2024-EERC-06-01

June 19, 2024

DocuSign Envelope ID: 2FA9A609-C360-4E53-8B28-BE8B77B6994A

EERC DISCLAIMER

LEGAL NOTICE This research report was prepared by the Energy & Environmental Research Center of the University of North Dakota (UND EERC) as an account of work sponsored by the U.S. Department of Energy (DOE) National Energy Technology Laboratory (SPONSOR). Because of the research nature of the work performed, neither UND EERC nor any of its employees makes any warranty, express or implied, or assumes any legal liability or responsibility for the accuracy, completeness, or usefulness of any information, apparatus, product, or process disclosed, or represents that its use would not infringe privately owned rights. Reference herein to any specific commercial product, process, or service by trade name, trademark, manufacturer, or otherwise does not necessarily constitute or imply its endorsement or recommendation by UND EERC. SPONSOR understands and accepts that this research report and any associated deliverables are intended for a specific project. Any modifications of the report or of any associated deliverables or use or reuse other than for the intended project is at the sole risk of the SPONSOR and without liability or legal exposure to UND EERC or to its directors, officers, or employees.

DOE DISCLAIMER

This report was prepared as an account of work sponsored by an agency of the United States Government. Neither the United States Government, nor any agency thereof, nor any of their employees, makes any warranty, express or implied, or assumes any legal liability or responsibility for the accuracy, completeness, or usefulness of any information, apparatus, product, or process disclosed, or represents that its use would not infringe privately owned rights. Reference herein to any specific commercial product, process, or service by trade name, trademark, manufacturer, or otherwise does not necessarily constitute or imply its endorsement, recommendation, or favoring by the United States Government or any agency thereof. The views and opinions of authors expressed herein do not necessarily state or reflect those of the United States Government or any agency thereof.

DocuSign Envelope ID: 2FA9A609-C360-4E53-8B28-BE8B77B6994A

TABLE OF CONTENTS

LIST OF FIGURES iii

LIST OF TABLES vii

EXECUTIVE SUMMARY viii

INTRODUCTION AND OBJECTIVES 1

STATUS OF AVAILABLE HIGH-TDS BRINE TREATMENT TECHNOLOGIES 2
- Focus and Need for High-TDS Brine Technologies 2
- Technology Assessment Classification 3
  - Pretreatment Technologies 3
  - High-TDS Treatment Technologies 4
  - Alternative Treatment Technologies 7

TEST BED TREATMENT FACILITY AND OPERATIONS 7
- Treatment Facility and Capabilities 7

TECHNOLOGY DEMONSTRATIONS 17
- Technology Solicitation and Selection Process 17

TECHNOLOGY PERFORMANCE EVALUATIONS 21
- MVR Technology 21
  - Introduction and Background 21
  - Description of Technology 21
  - Description of Testing 21
  - Results 24
  - Discussion and Conclusions 33
- AGMD Technology 34
  - Introduction and Background 34
  - Description of Technology 34
  - Description of Testing 35
  - Results 40
  - Techno-Economic Analysis 50
  - Discussion and Conclusions 51
- SCWD Technology 52
  - Introduction and Background 52
  - Description of Technology 52
  - Laboratory-Scale Testing 52
  - Results and Discussion 53
  - Field-Scale Testing 54
  - Results and Discussion 54
  - Lessons Learned 57
  - Techno-Economic Assessment 58

Continued . . .

DocuSign Envelope ID: 2FA9A609-C360-4E53-8B28-BE8B77B6994A

TABLE OF CONTENTS (continued)

ZMD Technology 58
Introduction and Background 58
Description of Technology 59
Description of Testing 60
Results 65
Discussion and Conclusions 69

SYNERGISTIC ACTIVITIES 70
Produced Water Management Through Geologic Homogenization, Conditioning, and Reuse 71
Produced Water Research Partnership – Produced Water Pilot-Scale Testing 73
Assessment of Carbonated Brine Injection Feasibility 75

DISCUSSION 76

CONCLUSIONS 78

HIGH-TDS TREATMENT PRESENTATION ..... Appendix A

PRESENTATION HIGHLIGHTING FACILITY AND CAPABILITIES ..... Appendix B

PROSPECTUS FOR TREATMENT FACILITY ..... Appendix C

EXTRACTED WATER TREATMENT TECHNOLOGY SELECTION PROCESS ..... Appendix D

DESALINATION TECHNOLOGY VENDOR QUESTIONNAIRE ..... Appendix E

TECHNOLOGY SELECTION SUMMARIES ..... Appendix F

UNIVERSITY OF PITTSBURGH FINAL REPORT – 2021 ..... Appendix G

OHIO UNIVERSITY FINAL REPORT – 2021 ..... Appendix H

UNIVERSITY OF KENTUCKY FINAL REPORT – 2023 ..... Appendix I

GHCR FINAL REPORT – 2022 ..... Appendix J

ASSESSMENT OF CARBONATED BRINE INJECTION REPORT – 2023 ..... Appendix K

DocuSign Envelope ID: 2FA9A609-C360-4E53-8B28-BE8B77B6994A

LIST OF FIGURES

1 Flow diagram of a generalized brine-dewatering process integrated with pretreatment and disposition of the brine 3

2 Brine treatment approaches and corresponding applicable inlet TDS concentrations and resulting brine waste concentration ranges 5

3 Classification of desalination technologies by main energy input 6

4 Map showing location of BEST project test location and facility site near Johnsons Corner, North Dakota 8

5 Front side of treatment facility showing large overhead doors to demonstration bay 9

6 Back side of treatment facility showing associated settling/storage tanks and piping infrastructure 9

7 View of incoming piping from produced water tanks and newly established ARM extraction well 10

8 Layout and electrical rating of test bed treatment facility 11

9 Gas detection sensor system located on wall inside demonstration bay 11

10 View of entire pretreatment system 12

11 View of demonstration bay, with office/lab/utility rooms in the background 13

12 Inside view of demonstration bay looking toward overhead door entry location 14

13 View of sump pump and brine supply piping to demonstrations 14

14 Skid power supply and step-down transformer 15

15 SCADA system control area with multiple computer displays 16

16 SCADA control schematic showing brine supply well components, settling tanks, and associated piping configuration 16

17 SCADA control schematic showing pretreatment system and technology demonstration brine supply and support components 17

18 MVR system operating at BEST facility 22

19 Sample of MVR system operator interface 23

20 Illustration of inlet brine and concentrate EC for Tests 1 and 2 26

21 Illustration of inlet brine and concentrate EC for Tests 3a and 3b 26

Continued . . .

DocuSign Envelope ID: 2FA9A609-C360-4E53-8B28-BE8B77B6994A

LIST OF FIGURES (continued)

22 Illustration of inlet brine and concentrate EC for Tests 4a and 4b 27

23 Illustration of inlet brine and concentrate EC for Tests 5a and 5b 27

24 Illustration of inlet brine and concentrate EC for Tests 6a and 6b 28

25 Energy consumption per cubic meter of distillate for each inlet salinity 29

26 Illustration of inlet brine and outlet concentrated brine conductivity 30

27 Illustration of inlet brine, outlet concentrated brine, and outlet distillate conductivity 30

28 Illustration of inlet brine salinity constituent trends 32

29 Illustration of concentrated brine salinity constituent trends 32

30 Illustration of outlet distillate salinity constituent trends 33

31 Schematic of the laboratory-scale DCMD system 36

32 Photographs of the laboratory DCMD system setup and module detail 36

33 AGMD module details: “unwound” view of the spiral-wound module layers and module fluid flow connections 37

34 Four-module AGMD pilot unit 38

35 Process flow diagram for overall AGMD pilot system 38

36 a) Photograph of the pilot system and b) integration schematic at the BEST facility 40

37 Permeate flux and conductivity for low-salinity brine testing with the DCMD module 41

38 Permeate flux and conductivity for high-salinity brine testing with DCMD module 42

39 Inside view of BEST testing facility during University of Pittsburgh technology demonstration 43

40 University of Pittsburgh personnel working on AGMD system 43

41 Permeate flux and conductivity for AGMD pilot testing with low-salinity brine 44

42 Brine feed and permeate flow rates during AGMD pilot testing with low-salinity brine... 45

43 Permeate flux and conductivity for AGMD pilot testing with high-salinity brine 47

44 Brine feed and permeate flow rates during AGMD pilot testing with high-salinity brine 48

Continued . . .

DocuSign Envelope ID: 2FA9A609-C360-4E53-8B28-BE8B77B6994A

LIST OF FIGURES (continued)

45 Estimated brine treatment costs for as-tested AGMD pilot system 50

46 Estimated brine treatment costs for a full-scale AGMD system as a function of a) brine heating temperature and b) permeate water recovery 51

47 Cross-sectional view of Ohio Joule-heated reactor 53

48 Photograph of testing at EERC BEST facility 55

49 Photograph of testing unit operation at EERC BEST facility 55

50 Schematic diagram of zeolite dewatering process and scanning electron microscope image of membrane cross-section morphology 59

51 Schematic diagram and photograph of the University of Kentucky's laboratory performance evaluation system for zeolite membranes 61

52 Bench-scale membrane module for University of Kentucky FAU zeolite membrane elements 62

53 Images of membrane and membrane modules 63

54 Process flow diagram for zeolite dewatering system (a) and photographs of system (b and c) 64

55 University of Kentucky zeolite dewatering system set up for field testing at the BEST facility 65

56 Laboratory-scale evaluation results for University of Kentucky membrane element: NaCl brine test results with varying brine concentrations at 115°C and 50 psig and EERC-blended water batch test at 108°C and 50 psig 66

57 Laboratory-scale evaluation results for HZM element: 20 wt% NaCl brine at 120°C and 100 psig and EERC-blended water at 120°C and 100 psig 66

58 Results of HZM module field test versus time: a) temperature of membrane module, b) conductivity-based rejection rate, c) module feed pressure, and d) permeate flux 68

59 Normal O&G operations in western North Dakota managing produced water via SWD wells extracted during oil production 71

60 Extracting fluids from a SWD target at a reasonable distance from active SWD injection wells for potential reuse in hydraulic fracturing 72

Continued . . .

DocuSign Envelope ID: 2FA9A609-C360-4E53-8B28-BE8B77B6994A

LIST OF FIGURES (continued)

61 Schematic showing pretreatment, TDS treatment, and sample collection locations..... 73

62 University of Pittsburgh membrane technology operations at BEST facility location and raw and treated effluent samples after treatment..... 74

63 Graphical representation of CBI compared to traditional free-phase CO_2 injection and standard produced water disposal..... 75

DocuSign Envelope ID: 2FA9A609-C360-4E53-8B28-BE8B77B6994A

LIST OF TABLES

1 Characteristics of Pretreatment Technologies: Mechanical Particulate Separation 4

2 Characteristics of Pilot-Ready Membrane Filtration Pretreatment Technologies 4

3 Summary of Commercial and Pilot-Ready Desalination Technologies 6

4 Technology Provider Communication List 18

5 Selected Technologies and Demonstration Timeline 20

6 List of Inlet Salinity Test Cases and Samples Collected for Laboratory Analysis 23

7 Summary of MVR Test Conditions/Results 25

8 MVR Water Chemistry Results, mg/L 31

9 Properties of the PTFE Membrane 37

10 Stream Analyses for the AGMD Pilot Testing with Low-Salinity Brine 46

11 Stream Analysis for the AGMD Pilot Testing with High-Salinity Brine 49

12 SCWD Laboratory Testing Results 54

13 Summary of SCWD Testing Parameters 54

14 Test 1 56

15 Test 2 56

16 Test 3 57

17 Test 4 57

18 Operational Parameters for Testing Conditions 58

19 Field Test Stream Analyses After Permeate Contamination 69

20 University of Kentucky Field Unit Energy Consumption for 69

21 Data for Each Individual Technology During High-TDS Field Testing 77

22 Energy Consumption for Treatment of ~170,000 mg/L TDS 78

DocuSign Envelope ID: 2FA9A609-C360-4E53-8B28-BE8B77B6994A

BRINE TREATMENT TECHNOLOGY SUMMARY – BRINE EXTRACTION AND STORAGE TEST – PHASE II FINAL REPORT – VOLUME 2

EXECUTIVE SUMMARY

The Energy & Environmental Research Center (EERC) conducted Phase II of the project entitled "Developing and Validating Pressure Management and Plume Control Strategies in the Williston Basin Through a Brine Extraction and Storage Test (BEST)."

Phase I was a 15-month study on potential methodologies for a field study of pressure management, culminating in site selection and experimental and site design. Phase II was an 8-year effort that involved constructing site facilities, conducting experiments, evaluating collected field data, and site decommissioning. The experimental portion was split into two collaborative components, one for the active reservoir management (ARM) experiment and a second component to develop a brine treatment technology test bed, i.e., the EERC BEST facility, and demonstrate potential water treatment technologies appropriate for high-saline brine at the project site. This report focuses on the high-saline brine treatment technology demonstrations. A separate companion report summarizes the results of the Phase II ARM experimental implementation and results.

The goal of the Phase II BEST brine treatment technology evaluations was to identify and further the development of promising brine treatment technologies through pilot-scale evaluation at the EERC BEST facility with the potential to successfully treat high-TDS (total dissolved solids) extracted water. For the purposes of technology evaluation, a brine salinity of approximately 180,000 mg/L TDS was selected as a metric, as this TDS level is representative of deep saline formation brines that are targeted for carbon dioxide (CO_2) injection and storage. The project included an assessment of treatment technologies for high-TDS brines, setup of the BEST test bed (a world-class facility for evaluating brine treatment technologies), and a series of technology demonstrations and synergistic research activities.

The brine treatment technology assessment was conducted to understand the status of high-salinity treatment technology development, identify potential research gaps, and determine the readiness level of potential demonstration candidates. The EERC communicated with over 30 different commercial and academic technology developers that offered various approaches to treating and/or managing high-TDS brines. Assessed treatment technologies were compared according to their treatment capabilities, performance, and energy requirements based on available data. Promising treatment technologies were selected for further screening and consideration for demonstration at the BEST test bed facility, with preference given to innovative technologies that had been previously supported through U.S. Department of Energy (DOE) Fossil Energy (FE) programs to develop innovative high-TDS brine treatment and desalination technologies. After review of all screening factors, e.g., applicability to high-TDS brine, previous DOE-sponsored development, and demonstration funding needs, the EERC recommended a total of four technologies to DOE for pilot-scale evaluation, and all four candidates were approved. The EERC worked with each respective entity to configure the test bed and schedule operations during a 4-year operating period from 2019 to 2023.

DocuSign Envelope ID: 2FA9A609-C360-4E53-8B28-BE8B77B6994A

Selected brine treatment technologies were evaluated at the EERC BEST test bed established at the field site for the Phase II ARM experiments in western North Dakota. The BEST test bed is colocated at an active saltwater disposal (SWD) site and is a world-class facility for quantitatively evaluating brine treatment technology performance; it has capabilities to blend multiple water sources and provide various levels of brine pretreatment according to the needs of the technology under evaluation. Automated data collection at the facility allows for mass and energy balance determination for systems under testing, and multiple sample collection points allow for stream analysis throughout the system.

The four technologies selected for pilot-scale evaluation consisted of thermal and membrane-assisted thermal approaches, which at the time of the assessment appeared to be the most applicable approaches for treating high-TDS brines. The test systems varied in their development status, from a fully engineered desalination system developed originally for seawater applications to early pilot-scale prototypes of laboratory-demonstrated concepts. As such, equipment reliability varied and the measured specific energy consumption per unit of recovered distillate was generally higher than the predicted performance for most of the systems. However, each technology demonstrated the ability to produce high-quality distillate from brine at the BEST facility under various parameters of brine salinity level and distillate recovery.

The majority of the technologies evaluated through this project were shown to be technically appropriate for the treatment and management of high-salinity brines, although some of the approaches may face scale-up challenges associated with energy consumption and/or membrane durability, factors that impact the economics of brine treatment. None of the tested technologies were operated long enough to experimentally establish materials lifetime and servicing intervals. However, as the engineering for these treatment technologies matures, the consistent brine-blending capabilities and the controlled environment of the BEST test bed can support longer-duration runs to establish reliable baselines for techno-economic analysis and even vendor performance specifications. Since the alternative to brine treatment is often injection well disposal, the economic feasibility of advanced brine treatment may depend on the regional availability and cost of SWD. To increase revenue potential going forward, it is likely that the most economical approach to the desalination and reduction of extracted brines will be to combine the desalination approach with waste heat utilization, by-product exploitation (i.e., HCl production), and/or critical mineral extraction (i.e., Li, Co, etc.). As a result, it is expected that future testing and development needs for brine treatment technology will need to support the evaluation of individual unit operations that perform specific functions like mineral extraction or acid production.

Additionally, water treatment technologies for use with ARM must be capable of addressing a range of formation water characteristics associated with the different locations and formation types targeted for CO_2 storage. While these initial technology demonstrations did not warrant extensive parametric study of input brine characteristics, the BEST test bed facility was designed with this need in mind. It is anticipated that as brine treatment technologies continue to mature and there is interest in evaluating differing water quality characteristics, the BEST facility will continue to be a useful platform for technology demonstration.

DocuSign Envelope ID: 2FA9A609-C360-4E53-8B28-BE8B77B6994A

BRINE TREATMENT TECHNOLOGY SUMMARY – BRINE EXTRACTION AND STORAGE TEST – PHASE II FINAL REPORT – VOLUME 2

INTRODUCTION AND OBJECTIVES

The Energy & Environmental Research Center (EERC) conducted Phase II of the project entitled "Developing and Validating Pressure Management and Plume Control Strategies in the Williston Basin Through a Brine Extraction and Storage Test (BEST)." The EERC was one of two entities from Phase I selected for continuation into Phase II, along with the Electric Power Research Institute (EPRI). During Phase I activities, an engineering design plan was developed that specified the protocols and procedures to be used in installing site infrastructure and designing and conducting a field implementation plan (FIP). The main objective was to utilize ongoing brine injection activities at an existing saltwater disposal facility (SDF), coupled with downgradient on-site formation water extraction, as a proxy study for understanding effects of applying such engineering controls on carbon dioxide (CO_2) injection and storage.

Phase II was conducted over 8 years and focused on the development and implementation of the FIP and validation of engineering strategies for managing formation pressure as well as predicting and monitoring differential pressure plume movement in the subsurface and validating differential pressure plume predictions through monitoring and simulation. The results of the overall project are expected to benefit future saline CO_2 storage projects through validation of techniques that reduce stress on sealing formations and consequently reduce risk of breaching sealing formations, reduce risk of brine and CO_2 intrusion into other formations, increase storage capacity, and reduce area of review.

Through the development and execution of the EERC's Phase II BEST program, a brine treatment technology test bed was also established for the purpose of providing a platform to assess promising and innovative technologies and approaches to brine treatment and reduction. The goal of this effort was to identify and further the development of promising brine treatment technologies through pilot-scale evaluation at the EERC BEST facility that have the potential to successfully treat high-TDS (total dissolved solids) extracted water. For the purposes of technology evaluation, a brine salinity of approximately 180,000 mg/L TDS was selected as a target as this TDS level is representative of deep saline formation (DSF) brines that are targeted for CO_2 injection and storage.

Specific objectives of the brine treatment test bed were to:

- Design and construct a technology development and test bed facility and platform for the evaluation of brine treatment technologies that have the potential of treating high-TDS extracted water for beneficial use as a means of managing and reducing extracted brine disposal volumes.

- Develop a brief overview and perform a status assessment of current and emerging technologies applicable to high-TDS brines appropriate for the treatment and ultimate generation of reusable water.

DocuSign Envelope ID: 2FA9A609-C360-4E53-8B28-BE8B77B6994A

- Solicit technology demonstrations from organizations offering innovative treatment approaches applicable to high-TDS brines previously supported through U.S. Department of Energy (DOE) National Energy Technology Laboratory (NETL) programs.

- Recommend selection of at least two technologies for pilot-scale demonstration and conduct technology performance evaluations at the EERC BEST facility. Evaluations were to include measurement and monitoring of all energy (e.g., electrical and propane) inputs as well as collection of samples of system influent and all effluent streams (e.g., treated water and concentrate) to determine energy, water, and material balances around the treatment system.

- Provide a final report on the status of emerging and applicable technologies and the results of the technical and economic assessments of each demonstrated technology.

- Leverage test bed capabilities and data collection by participating in DOE-approved synergistic activities relating to brine treatment and disposal.

This report focuses on the activities and associated information related to the development and operation of the test bed facility and testing platform and the identification, selection, and demonstration testing of high-TDS brine treatment technologies.

STATUS OF AVAILABLE HIGH-TDS BRINE TREATMENT TECHNOLOGIES

Focus and Need for High-TDS Brine Technologies

Extracted water treatment technologies compatible with active reservoir management (ARM) must be capable of addressing a range of water quality characteristics that depend largely on the location and type of formation targeted for CO_2 storage. Suitable formations are anticipated to range from DSFs to depleted oil and gas (O&G) reservoirs, each having potentially different formation water characteristics, particularly with respect to levels of suspended and dissolved solids, hardness, and organics content. Successful extracted water treatment likely requires multiple unit operations in the overall treatment system and will almost certainly require pretreatment to remove suspended solids and dissolved organics ahead of any desalination technology to prevent performance inhibition (Harto and Veil, 2011). As shown in Figure 1, a requisite first step for dewatering a brine is the pretreatment of the saline brine to mitigate conditions that will lead to rapid deterioration in the performance of downstream processes. Depending on the planned use of the treated brine, a final polishing step or process may be needed beyond the initial salinity treatment (U.S. Environmental Protection Agency, 2019).

DocuSign Envelope ID: 2FA9A609-C360-4E53-8B28-BE8B77B6994A

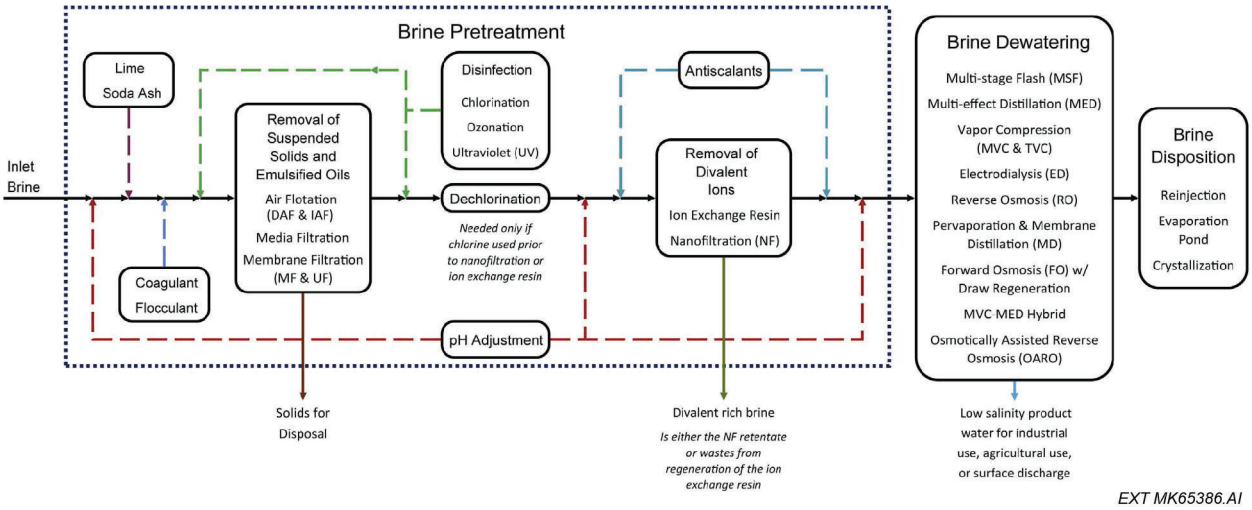


Figure 1. Flow diagram of a generalized brine-dewatering process integrated with pretreatment and disposition of the brine. Dashed lines represent possible chemical additions to the brine (Arena and others, 2017).

As part of this project, a technology assessment was conducted to better understand the status of high-salinity treatment technology development and potential research gaps and determine the readiness level of potential pilot-ready and commercial technologies with the potential to be utilized to pretreat and desalinate waters with salinities as high as 325,000 mg/L TDS. The assessment included a comparison of the treatment capabilities, performance, and energy requirements of applicable technologies where data were available.

Technology Assessment Classification

Pretreatment (Primary/Basic) Technologies

Pretreatment technologies provide for the removal of certain constituents that would otherwise inhibit or interfere with the operation of downstream unit operations. For extracted water, these constituents would likely include fine suspended solids or turbidity, dissolved organic matter, and scale-causing divalent ions or hardness. Pretreatment technology options are numerous and may include suspended solids separation, adsorption, softening, blending, hydrocyclone, air flotation, settling, coagulation/precipitation, media filtration, activated carbon absorption/ adsorption, electrocoagulation, and various other approaches. There are a range of mechanical particulate separation technologies that are currently commercially practiced. A summary of the technologies, along with strengths and weaknesses, is listed in Table 1.

DocuSign Envelope ID: 2FA9A609-C360-4E53-8B28-BE8B77B6994A

Table 1. Characteristics of Pretreatment Technologies: Mechanical Particulate Separation

Technology	Contaminants Treated	Strengths	Limitations
Gravity Settling[a]	Particulates	Equalizes flow, accommodates upsets, simple, low energy, minimal operation and maintenance.	Large footprint, long settling time required to remove small particles.
Microclarification[b]	Particulates, O&G	Small footprint versus conventional settling, removes 5–15-µm particles.	Potential for fouling, no flow equalization capacity, needs piloting.
Hydrocyclones[a]	Particulates, O&G	Minimal energy, removes 5–15-µm particles.	Potential for fouling, no flow equalization capacity, scale-up requires multiple parallel units.
Gas Flotation[a]	Particulates, O&G	Removes 25-µm particles (3–5 µm with coagulation pretreatment).	Higher pressures required for high-temperature feeds.
Media Filtration[a]	Particulates, O&G, TOC[c]	No TDS limitations, coagulation pretreatment improves removal.	Media replacement/ Regeneration.
Mechanically Assisted Filtration[d]	Particulates	Self-cleaning, low footprint, able to handle high solids.	Fouling tendency of mesh screens.

[a] Colorado School of Mines (2009).
[b] Silva and Dees (2015).
[c] Total organic compound.
[d] Examples: Tekkleen™ (Tekleen Automatic Filters, LLC, 2023); Spiral Water Technologies (2023); Tequatic™ (Amiad USA Inc., 2023).

Membrane filtration technologies commercially used for pretreatment are less numerous and include targeting various size ranges of particulates. Each of these filtration technologies and their associated strengths and weaknesses are listed in Table 2.

Table 2. Characteristics of Pilot-Ready Membrane Filtration Pretreatment Technologies

Technology	Contaminants Treated	Strengths	Limitations
Oil-Tolerant Microfiltration[a]	Particulates >1 µm	Low fouling in presence of excess flocculant, oily particulates.	Needs field pilot validation.
Oil-Rejecting Ultrafiltration[b]	Free oils, particulates >0.01 µm	Commercially proven product.	Each new application needs pilot validation.
Nanofiltration[c]	Divalent, multivalent ions; organics, microbials	Selectivity toward hardness species.	Requires pilot validation.

[a] Silva and Dees (2015).
[b] Sun (2014).
[c] Colorado School of Mines (2009).

High-TDS Treatment (Desalination) Technologies

There are several commercial and pilot-ready desalination technologies that can have application for water recovery from high-TDS extracted brine. These technologies, however, tend to be energy-intensive and have not been extensively documented in the treatment of high-TDS

DocuSign Envelope ID: 2FA9A609-C360-4E53-8B28-BE8B77B6994A

waters that are relevant to CO_2 storage scenarios. Figure 2 illustrates the average brine concentration ranges and limits of applicable treatment technology classes.

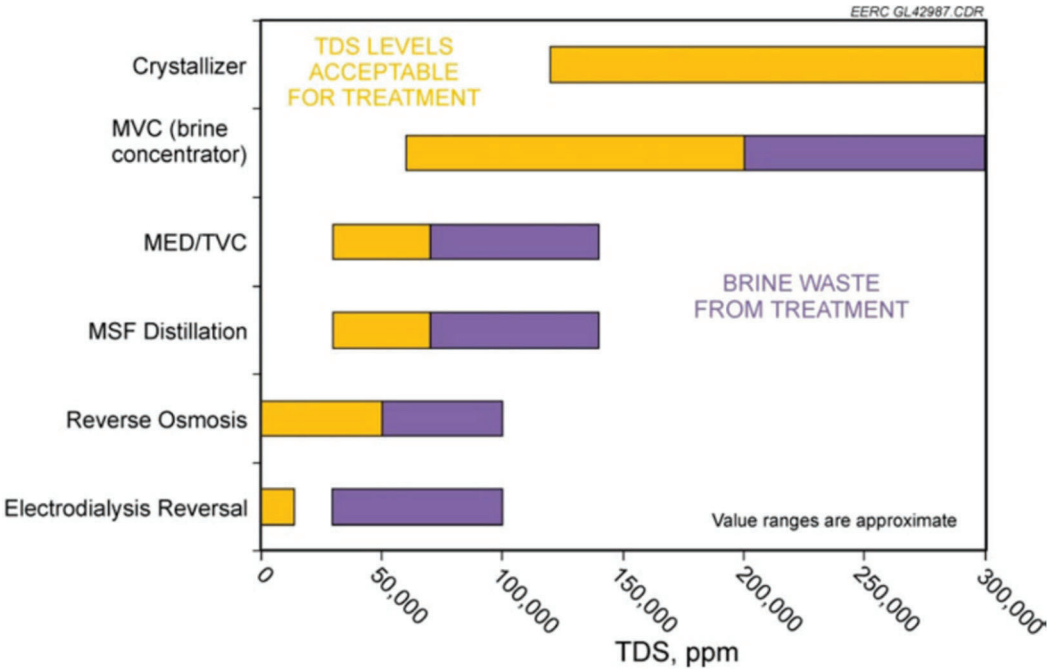


Figure 2. Brine treatment approaches and corresponding applicable inlet TDS concentrations and resulting brine waste concentration ranges (Stepan, 2017).

A classification of desalination technologies/approaches is shown in Figure 3. Each class of technology is organized by its primary energy input.

The most commonly used technologies for brine desalination for TDS concentrations exceeding ~70,000 mg/L include membrane filtration, thermal treatment approaches, and/or some combination of both technologies. Membrane filtration technologies include microfiltration, ultrafiltration, nanofiltration, forward osmosis (FO)/reverse osmosis (RO) and electrodialysis/ electrodialysis reversal. Thermal treatment technology approaches are more vast and include multistage flash distillation, membrane distillation (MD), multiple effect distillation, falling film evaporators, vapor compression/recompression, falling film–mechanical vapor recompression (MVR), humidification–dehumidification (HDH), freeze–thaw evaporation, low-temperature crystallization, and evaporation–crystallization (Stepan, 2017; Silva and Dees, 2015). Each of these approaches utilizes various forms of energy input, including electrical, natural, and waste energy/heat sources. Table 3 provides a summary of operating ranges and energy requirements for select desalination technology class, and each class of treatment technology is discussed in more detail in this section. Detailed information on each technology class and associated references can be found in the presentation in Appendix A.

DocuSign Envelope ID: 2FA9A609-C360-4E53-8B28-BE8B77B6994A

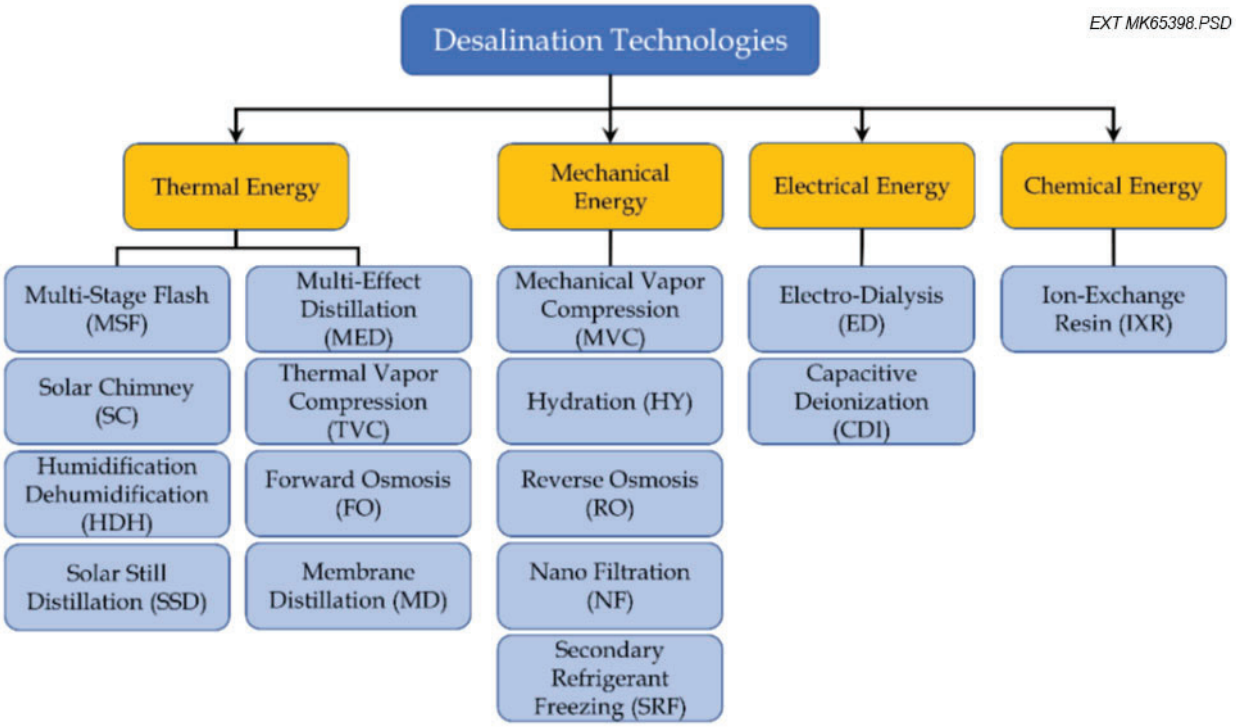


Figure 3. Classification of desalination technologies by main energy input (taken from Curto and others, 2021).

Table 3. Summary of Commercial and Pilot-Ready Desalination Technologies

Technology	Maximum Concentrate TDS, mg/L	Product Water TDS, mg/L	Typical Desalination Energy Requirements, kWh[a]/m^3 product water	Pretreatment Required (contaminants that must be removed)
Principal Energy Source: Electricity				
MVR[b]	295,000	<100	18.5	Soluble organics, O_2
Principal Energy Source: Heat or Refrigeration				
MD[c]	280,000 (24 wt%)	<10	14	Particulates, organics, surfactants
FO/RO[b]	200,000[d]	<350	275 (distillation column + brine stripper)	Soluble organics, particulates
HDH	295,000	<100	684 (without energy recovery)	Scaling salts, organics, particulates
Freeze–Thaw[b]	>40,000	1000	Passive (seasonal)	None
CoLD Crystallization[e]	>295,000	<100	187 kWhe + 3610 kWh steam[f]	NORM,[g] TCLP[h] metals

[a] kilowatt-hours.
[b] Colorado School of Mines (2009).
[c] Hardy and Shapiro (2014).
[d] McGinnis and others (2013).
[e] Crystallization of high-solubility salts at low temperature and deep vacuum.
[f] Shaw (2011).
[g] Naturally occurring radioactive material.
[h] Toxicity characteristic leaching procedure (Agency for Toxic Substances and Disease Registry, 2019).

DocuSign Envelope ID: 2FA9A609-C360-4E53-8B28-BE8B77B6994A

Alternative Treatment Technologies

Ion Exchange

In ion exchange (IX), removal of specific ions or compounds from a stream is facilitated by the exchange of a presaturated ion with the target ions on an IX resin. While IX is not typically used for the removal of monovalent chloride (Cl) salts, contaminant cationic solutes such as calcium (Ca), magnesium (Mg), barium (Ba), strontium (Sr), and radium (Ra) can be removed by cation exchange resins, and anionic solutes such as fluoride, nitrate, fulvates, humates, arsenate, selenate, chromate, and anionic complexes of uranium may be removed by anion exchange resins. IX resins are typically composed of synthetic resins or activated alumina. These resins are characterized as either strong or weak and may be acidic or basic in nature. Acidic IX resins are utilized to remove unwanted cations from solution, and IX systems are typically installed in fluidized, packed-bed configurations. IX is an established water treatment technology that is utilized for municipal drinking water treatment, wastewater treatment, and coal bed methane produced water treatment. The operational footprint for most IX processes includes packed resin beds and on-site regenerant and cleaning chemical storage. Typically, IX processes operate with minimal energy demand and may require only electricity for pumping fluids under low hydraulic pressure. This IX technology process can be used both to remove unwanted ions for water purification and for sequestering desired critical minerals for exploitation (Colorado School of Mines, 2009).

Although numerous technologies are potentially available for brine treatment, thermal treatment and thermally assisted membrane technologies appear most likely to be valid for desalination efforts with the high-salinity brines encountered in subsurface CO_2 storage settings. Energy intensity and membrane fouling appear to be the key limiting factors, economically and technically, in the application of these technologies at large scale. It is likely that the most economical approach to the desalination and reduction of extracted brines effort is to combine the desalination approach with waste heat utilization, by-product exploitation (i.e., HCl production), and/or critical mineral extraction (i.e., lithium [Li], cobalt [Co], etc.). The main goal of the treatment test bed developed through this project was to identify and evaluate innovative technologies that show promise of being a suitable approach to desalination efforts of the targeted high-TDS (~180,000 mg/L TDS) brines associated with carbon capture and storage targets.

TEST BED TREATMENT FACILITY AND OPERATIONS

Treatment Facility and Capabilities

As part of the BEST concept evaluation, a brine treatment technology development and test facility was designed, constructed, and operated to enable further development and evaluation of brine treatment technologies capable of addressing high-TDS brines associated with geologic CO_2 storage targets. Specific objectives of the treatment facility were to enable development, pilot testing, and advancement of commercially viable extracted and produced water treatment technologies that can meaningfully reduce brine disposal volumes and provide an alternate source of water and/or salable product(s) for beneficial use. The treatment facility was constructed at a

DocuSign Envelope ID: 2FA9A609-C360-4E53-8B28-BE8B77B6994A

commercially operated saltwater disposal (SWD) facility and is located near Johnsons Corner, approximately 13 miles east of Watford City, North Dakota, as shown in Figure 4, adjacent to State Highway 23.

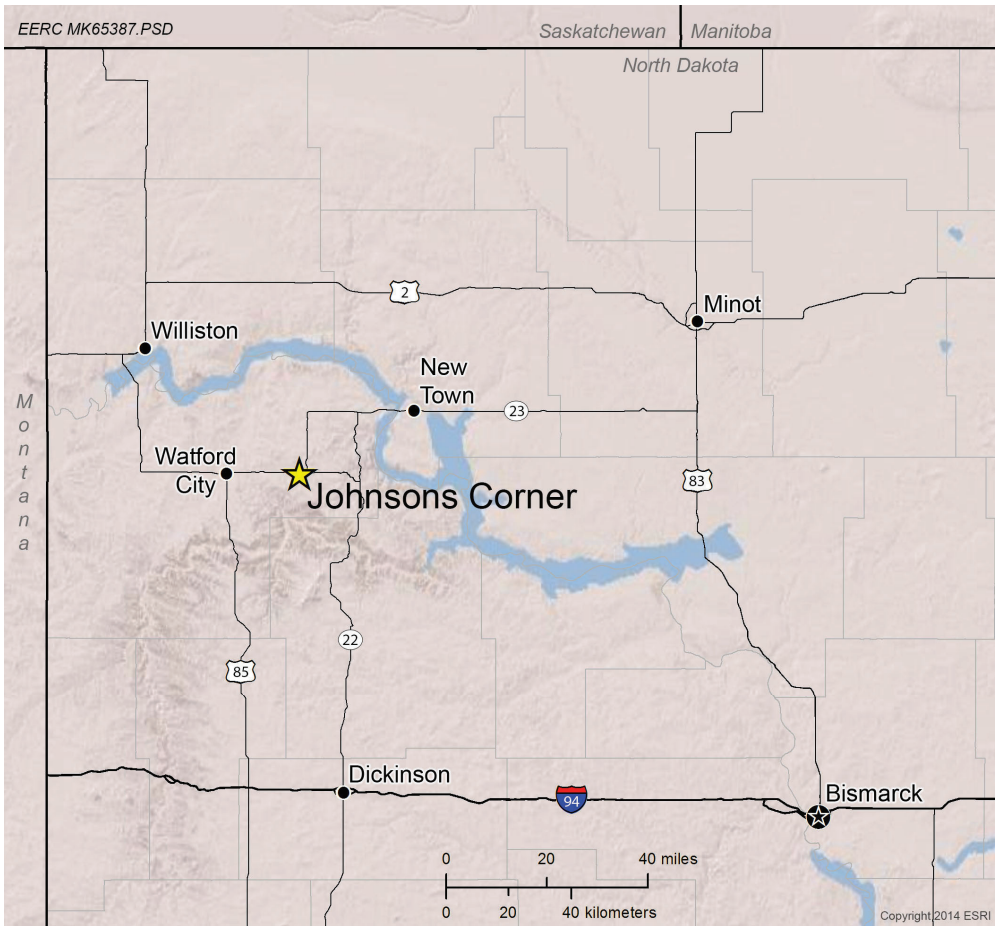


Figure 4. Map showing location of BEST project test location and facility site near Johnsons Corner, North Dakota.

The constructed brine treatment demonstration facility includes a permanent heated environmental enclosure measuring 60 by 80 feet, with 18-foot wall height, equipped with two large automatic overhead doors. The building is constructed on a sealed concrete pad with drainage containment and was designed with a large demonstration bay area able to accommodate up to semi (tractor–trailer)-sized technology skids. Figures 5 and 6 show the treatment facility building and associated tank and piping infrastructure.

DocuSign Envelope ID: 2FA9A609-C360-4E53-8B28-BE8B77B6994A



Figure 5. Front side of treatment facility showing large overhead doors to demonstration bay.



Figure 6. Back side of treatment facility showing associated settling/storage tanks and piping infrastructure.

DocuSign Envelope ID: 2FA9A609-C360-4E53-8B28-BE8B77B6994A

The test bed facility was integrated with ARM and SWD infrastructure and operations, shown in Figure 7, which allowed for access to produced water and extracted brines as well as concentrated brine reinjection capabilities. Flow capacities up to 25 gpm were possible, with the ability to blend brines and freshwater to achieve TDS concentrations ranging from 500 mg/L up to 330,000 mg/L with a variety of chemistries. A salinity concentration of approximately 180,000 mg/L TDS was targeted for purposes of this research; however, tailored blends were possible to suit capabilities and/or limitations of selected technologies.



Figure 7. View of incoming piping from produced water tanks (background) and newly established ARM extraction well.

The building was designed with a demonstration bay area having a Class 1, Division 2, electrical rating and a liquid collection sump pit and pump with a Class 1, Division 1, rating in the event of accidental release of flammable vapors or gases from technology testing. These spaces, along with an electrically unclassified adjacent office and control room area for project supervision and management activities, are schematically shown in Figure 8. The classified demonstration bay was equipped with a gas-monitoring system to warn against the formation of hazardous atmospheres during testing of treatment technologies, some of which may potentially not be Class 1, Division 1, electrically rated. The gas-monitoring system (Figure 9) comprised five separate alarm monitors designed to detect hydrogen sulfide (H_2S), nitrous oxide (NO_2), carbon monoxide (CO), methane (CH_4), and ethylene (C_2H_4), which consisted of the most likely hazardous components that could be encountered during anticipated operations. A power shunt fail-safe within the integrated supervisory control and data acquisition (SCADA) system was designed to immediately disconnect power to the building in the event a hazardous atmosphere was detected and triggered an alarm.

DocuSign Envelope ID: 2FA9A609-C360-4E53-8B28-BE8B77B6994A

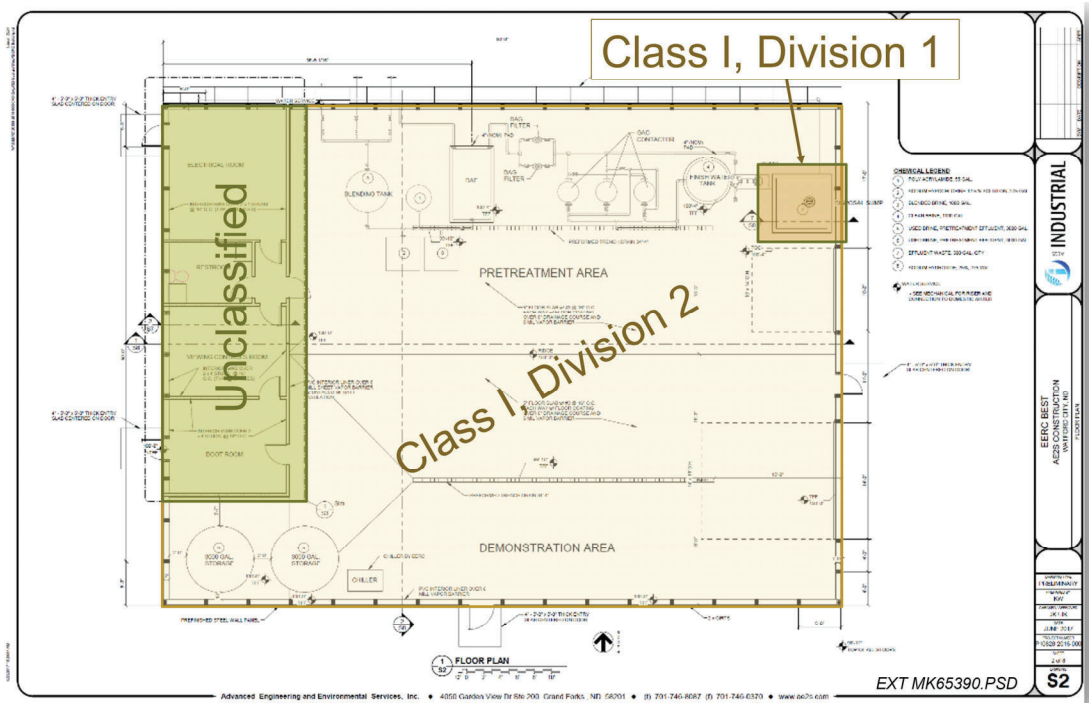


Figure 8. Layout and electrical rating of test bed treatment facility.



Figure 9. Gas detection sensor system located on wall inside demonstration bay.

DocuSign Envelope ID: 2FA9A609-C360-4E53-8B28-BE8B77B6994A

A brine pretreatment system was designed and implemented to ensure all technology evaluations used brine with similar and consistent compositions. The pretreatment system was designed to remove particulates, organics, and potential scale-forming constituents and consisted of chemical addition, dissolved air flotation (DAF), bag filters, granular activated carbon (GAC) filtration, and associated meters to ensure consistent and similar quality of the treated brine for all demonstrated technologies.

The pretreatment system (shown in Figure 10) consists of an automated blending configuration using pneumatic control valves on each supply line capable of combining extracted brines, Bakken produced water, and freshwater to achieve varying chemistries and salinity concentrations. Sodium hydroxide (30%) and bleach (sodium hypochlorite 12%) are metered into the brine mixture during the blending process to adjust the pH of the brine to approximately 10.5. After blending, and desired salinities are achieved, a coagulant and polymer solution are metered into the brine as it is introduced into a DAF system to where flocculated particulate and bottom sludges are skimmed off and pumped out of the process to an external poly sludge tank adjacent to the treatment building. The DAF process is designed to remove any potential scale-forming components of brine chemistry that may inhibit proper treatment in follow-on technologies. The DAF effluent flows through a set of sock filters (~10 µm) to remove remaining particulate and is then routed through a series of GAC beds to remove any dissolved organics, including dissolved hydrocarbons. The filtered brine is then considered “finished” and flows into a 1000-gallon storage tank from which it is fed to the technology skid being evaluated. Throughout



Figure 10. View of entire pretreatment system (blending tank through finished tank).

DocuSign Envelope ID: 2FA9A609-C360-4E53-8B28-BE8B77B6994A

the pretreatment process, conductivity meters are positioned in the flowlines to accurately understand the conductivity of the treated brine. Additionally, there are several sample ports throughout the system where samples can be collected to evaluate pH, particulate content, and dissolved organic constituents that may indicate the need to change out the GAC in the GAC vessels or make other adjustments to the pretreatment system.

After the "finish" water tank, there are a final flowmeter, conductivity meter, and turbidity meter to accurately assess the quantity and quality of the brine being fed into the technology skid. This information is also tracked and recorded in the SCADA system associated with the building and pretreatment system. Once the brine has been processed through a demonstration technology, samples can be routinely collected for analysis, and the resulting effluent streams are diverted into two separate tanks, one each for the concentrated brine and the clean treated water. For disposal of the test effluents, a series of flowlines and transfer pumps are able to recombine the fluids and transfer them out of the building and into the reinjection flow system. Figures 11 and 12 show the entire demonstration bay, with office area, pretreatment system, effluent storage tanks in the background, while Figure 13 shows the sump pump system and brine delivery piping components.



Figure 11. View of demonstration bay, with office/lab/utility rooms in the background.

DocuSign Envelope ID: 2FA9A609-C360-4E53-8B28-BE8B77B6994A



Figure 12. Inside view of demonstration bay looking toward overhead door entry location.



Figure 13. View of sump pump (lower right) and brine supply piping to demonstrations.

DocuSign Envelope ID: 2FA9A609-C360-4E53-8B28-BE8B77B6994A

Electrical requirements for each demonstration were supplied through a separate power transformer that was isolated from the rest of the building electrical supply. A separate junction box with sufficient 440-volt power supply and an associated step-down transformer (Figure 14) for lower voltage requirements (i.e., 220 and 110 volt) allowed for continual integrated monitoring and recording of power consumption variables (i.e., total watts, kWh, etc.) for each technology evaluation. Each demonstration technology was connected and disconnected to the power system by a contracted certified electrician, and data recording was controlled through software and the integrated SCADA system on-site.

Several components of the building operations, brine supply infrastructure, and pretreatment system were operated and monitored using an EERC-developed SCADA system. The SCADA system efficiently and accurately controlled operations, allowed for easy integration of new sensors and equipment, and enabled remote operation of some components. Figure 15 shows the SCADA system configuration on the monitors. The system had a modular design and ensured continuous data collection and storage. Components/parameters that were controlled, monitored, and/or data-recorded included system temperature and pressure, tank level, turbidity in flowlines, electrical conductivity (EC) (salinity inferred) of brine, flow status and rate, safety and alarm systems, and power consumption parameters for demonstration activities. Figures 16 and 17 show the specific SCADA control screens for the brine supply infrastructure and pretreatment system configuration. Overall site and treatment facility capabilities are illustrated and detailed in a presentation in Appendix B.



Figure 14. Skid power supply and step-down transformer.

DocuSign Envelope ID: 2FA9A609-C360-4E53-8B28-BE8B77B6994A



Figure 15. SCADA system control area with multiple computer displays.

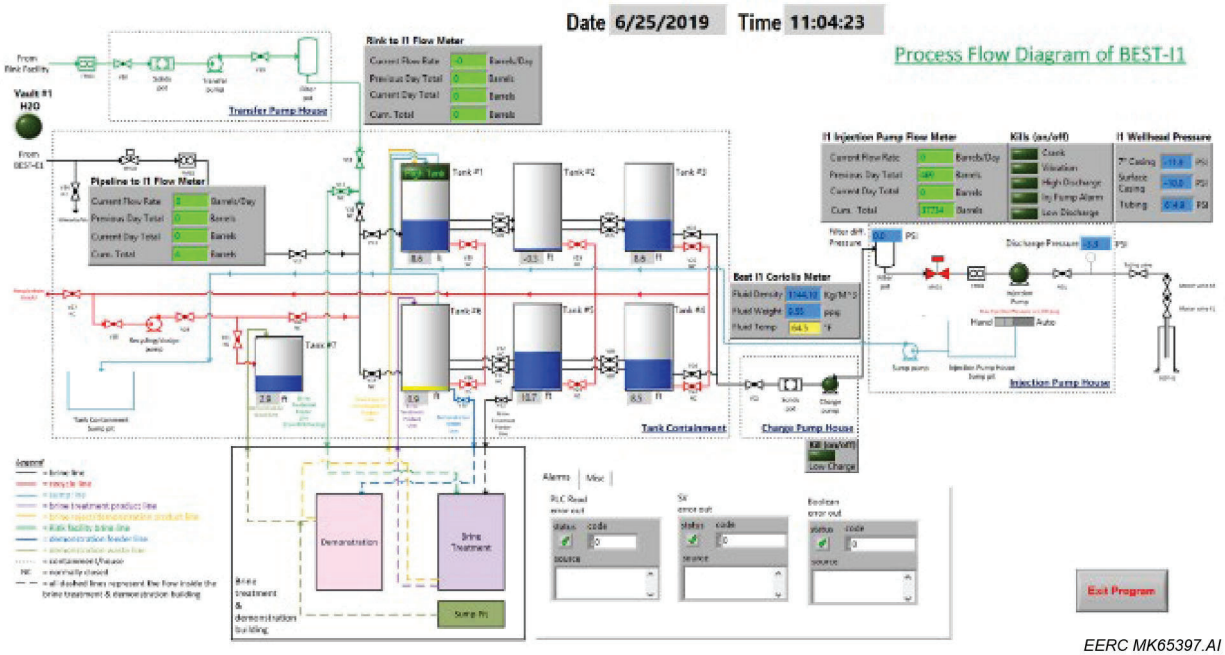


Figure 16. SCADA control schematic showing brine supply well components, settling tanks, and associated piping configuration.

DocuSign Envelope ID: 2FA9A609-C360-4E53-8B28-BE8B77B6994A

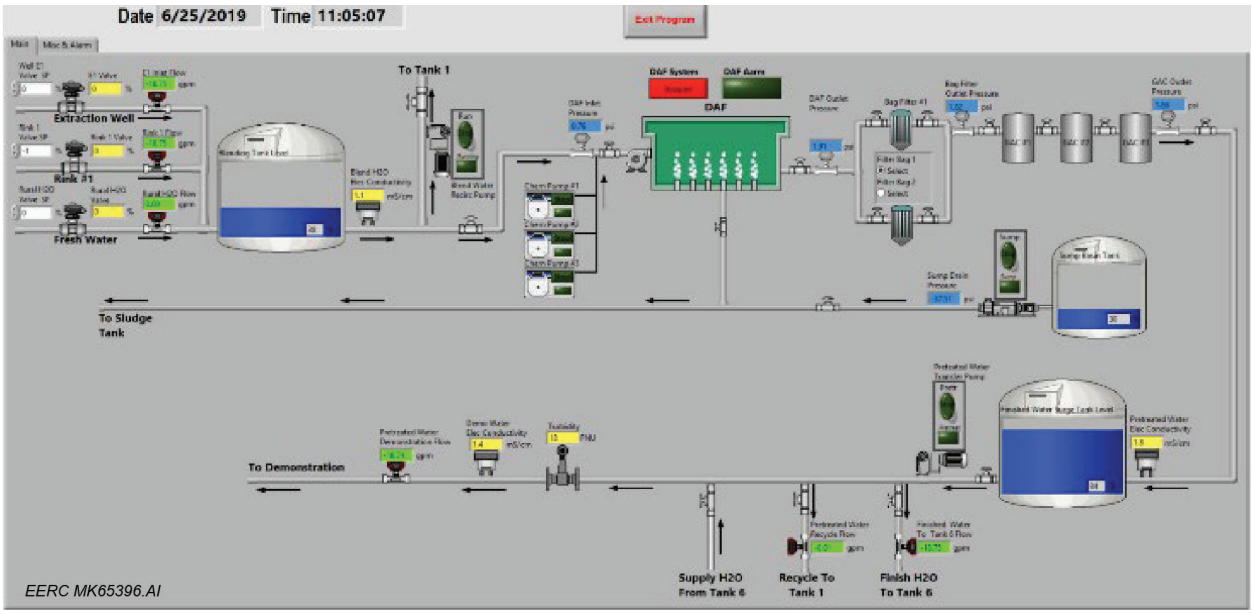


Figure 17. SCADA control schematic showing pretreatment system and technology demonstration brine supply and support components.

TECHNOLOGY DEMONSTRATIONS

As part of an outreach effort to disseminate information about the established test bed facility and encourage developers of innovative technologies to participate in potential demonstration activities, the EERC developed a presentation (Appendix B) and an informational prospectus (Appendix C) highlighting facility capabilities. EERC project management attended multiple brine treatment-related conferences/meetings and disseminated the information.

Technology Solicitation and Selection Process

The EERC collaborated with DOE and EPRI to identify, review, and select technologies with the potential to successfully treat high-TDS extracted water (180,000 mg/L on average). The selection process was conducted through a series of steps:

- Development of a pool of possible technology providers through survey, questionnaire, and discussion.
- Evaluation of technology providers using criteria agreed upon by a selection team made up of representatives of DOE, EPRI, and the EERC.
- Establishment of nondisclosure agreements with the selected developers to facilitate receiving detailed technology information (if required).
- Preparation of 2-page summaries by the EERC of the possible technologies for review by the selection team.

DocuSign Envelope ID: 2FA9A609-C360-4E53-8B28-BE8B77B6994A

- Review of the summaries, discussion among team members, and agreement by the selection team on possible water treatment technologies for field testing.

- Finalization of legal and engineering documentation with technology providers for testing of the selected technologies.

The selection process and preliminary screening criteria developed by the EERC and EPRI in collaboration with DOE were broad enough to apply to a large number of candidate technologies for demonstration. Further detail on this process and associated criteria can be found in Appendix D. The criteria were designed to discern among technology alternatives while trying to avoid duplication of demonstrations of the same basic technology type. The qualitative screening criteria were used to screen prospective technologies prior to quantitative screening and selection. As part of this screening process, the EERC communicated with over 30 different technology providers, shown in Table 4, that offer various approaches to treating and/or managing high-TDS brines.

Table 4. Technology Provider Communication List

ABR Process Development	Fairmont Brine Processing	Ohio University
Advanced Engineering and Environmental Services, Inc. (AE2S)	General Electric	Peoples Energy and Exploration, LLC
Agar Corporation, Inc	GreenBlu	Purestream
AGT Water Systems	Illinois State Geological Survey	RTI International
Caloris Thermal Process Technology	Los Alamos National Laboratory	RWL Water
Cavortex International Technologies	Mantra Energy Alternative	Slipstream ZLD
Cutting Edge Environmental, LLC	MGX Minerals	Southern Research Institute
De Nora Water Technologies	New Mexico Tech	Southwest Research Institute (SwRI)
Ecologic Solutions	Nick Siefert – NETL	University of Illinois
Encon Evaporators	Nuverra Environmental Solutions, Inc.	University of Kentucky Center for Applied Energy Research (CAER)
Enerstream Capital Partners	Oasys Water	University of Pittsburgh

As a continued part of the technology status assessment and screening process, the EERC evaluated several potentially applicable treatment technologies, and preference was given to innovative technologies that had been previously supported through DOE Fossil Energy (FE) programs (i.e., funding opportunity announcements (FOAs) 1095 and 1238) to develop innovative high-TDS brine treatment and desalination technologies. The EERC provided select technology providers with a copy of the technology-screening questionnaire, as shown in Appendix E, to further evaluate applicability of the technology and assess demonstration potential. Some entities were no longer pursuing brine treatment programs, had technologies that were not applicable for the appropriate salinity level, or were not able to demonstrate within the project timeline. Therefore, not all providers submitted, or were asked to submit, the technology-screening questionnaire as a continuation of the screening and selection process.

DocuSign Envelope ID: 2FA9A609-C360-4E53-8B28-BE8B77B6994A

Through review of the communications with select technology vendors and their responses to the questionnaire, the technologies were quantitatively scored by the EERC selection team on a scale of 1 to 10 in the areas of projected benefits, technology strengths, and organization strength. After thorough review of all components of the screening process, the EERC identified a total of four technologies, according to technology applicability, previous DOE-sponsored development, and demonstration funding requirements, and provided DOE project management with summaries of the suggested technologies for consideration of selection for demonstration activities. The technology recommendation summaries for each technology are included in Appendix F. DOE provided input and approval for the recommended technologies, and all four were selected for demonstration. Upon selection, letters of commitment from the selected technology providers were obtained, and any necessary confidentiality agreements were executed prior to demonstration phases of the project. The EERC then developed a schedule of operations for the selected technologies and conducted demonstrations over a period of 3 years within the established spring-to-fall operational periods. A listing of the selected technologies, with descriptions of the technology details, is provided in Table 5.

DocuSign Envelope ID: 2FA9A609-C360-4E53-8B28-BE8B77B6994A

Table 5. Selected Technologies and Demonstration Timeline

Technology	Class	Technology Developer	Technology Description	Demonstration(s) Completed
MVR	Thermal	NETL – Nick Siefert	MVR thermal treatment uses heat to distill high-salt-content water to steam, which is condensed into clean water. In an MVR evaporator, a compressor is used to add the energy required to boil the inlet water being treated. A portion of the concentrate is boiled to steam in the evaporator exchanger and separated from the liquid in the separator vessel. The steam is driven through the opposite side of the evaporator exchanger where it condenses to distilled water, releasing its latent heat to the boiling concentrate. Concentrate is continually pumped from the recirculation loop out of the unit to prevent the solution from reaching saturation. Thermal treatment processes have high-energy-input requirements; however, they do not have membranes that can be fouled and are technically suited for treating high-salinity waters.	August 2019, August 2021, and August 2022
Air Gap Membrane Distillation (AGMD)	Membrane/thermal	University of Pittsburgh	Membrane distillation is a unique technology that combines thermal and membrane separation processes utilizing hydrophobic microporous membranes. AGMD technology uses an air gap between the hot and cold sections in a membrane module to enable internal heat recovery and improve overall energy consumption in the process. AGMD can concentrate feed up to supersaturation, and the most significant advantages of the MD technology are low operating temperatures (40°–80°C) and pressures (near atmospheric), which make it suitable for integration with waste heat utilization.	October 2021 and September 2023
Supercritical Water Desalination (SCWD)	Thermal	Ohio University	The SCWD technology is an electrically powered distillation system with internal heat application and is expected to be a technical and economic improvement on thermal systems that are externally heated. SCWD employs internal heating through Joule heating, which is a result of power dissipation from current traveling through a nonideal conductor. The novel design allows for direct control of power applied to the brine using the EC of the brine when applying alternating current (AC), resulting in a lower-TDS-content vapor product and a concentrated brine liquid product.	November 2021
Zeolite Membrane Desalination (ZMD)	Membrane/thermal	University of Kentucky	The ZMB technology uses zeolite membranes with a pore size of 0.74 nm for desalination at transmembrane pressures below 200 psi. The pore size is smaller than the diameter of hydrated metal ions but larger than the diameter of water molecules. In addition to size exclusion separation, the zeolite membrane also employs super hydrophilicity and preferential dissolution of water within the matrix to move water across the membrane under mild temperatures (<120°C) and pressures (<200 psig).	November 2022

DocuSign Envelope ID: 2FA9A609-C360-4E53-8B28-BE8B77B6994A

TECHNOLOGY PERFORMANCE EVALUATIONS

MVR Technology

Introduction and Background

The EERC conducted the first pilot-scale technical evaluation on an MVR brine treatment technology system supplied by Dr. Nick Siefert of DOE NETL. The objective of the demonstration evaluation was to provide NETL with data pertaining to the applicability of the MVR technology for treating high-salinity waters and the resulting energy consumption data. The MVR technology was operated by treating brines with a range of elevated TDS at the EERC's BEST facility near Watford City, North Dakota. The goal of the technology demonstration was to provide NETL with necessary technical data on MVR operations on varying salinity concentrations and also provide a technology baseline for both technical feasibility and energy efficiency for comparison with future technology demonstrations at the BEST site. The data collected during the demonstration evaluation and subsequent calculations on the minimum theoretical work of separating water from these brines (conducted by NETL) was used to estimate efficiency of the MVR process at a range of values for inlet salinity and water recovery. The electrical consumption data were crucial for evaluating other technologies that may be tested at this scale at the BEST facility.

Description of Technology

The MVR system is a type of thermal treatment technology designed for the application of treating waters with elevated dissolved solids. Thermal treatment uses heat to distill high-salt-content water to steam, which is condensed into clean water. The process also produces an equal or lower-volume concentrate brine stream. In an MVR evaporator, a compressor is used to add the energy required to boil the inlet feedwater being treated. The feedwater passes through two heat exchangers where heat is absorbed from the distillate and concentrate products leaving the system. The feedwater then passes into a recirculation loop where concentrate circulates in an evaporator exchanger and a vapor–liquid separator. A portion of the concentrate is boiled to steam in the evaporator exchanger and separated from the liquid in the separator vessel. A compressor draws the steam off of the separator and boosts the pressure, which increases the temperature. The steam is driven through the opposite side of the evaporator exchanger where it condenses to distilled water, releasing its latent heat to the boiling concentrate. Concentrate is continually pumped from the recirculation loop out of the unit to prevent the solution from reaching saturation. The distillate and concentrate both pass through a heat exchanger on the way out of the system to transfer some of the remaining heat to the incoming feedwater. Thermal treatment processes have high-energy input requirements; however, they do not have membranes that can be fouled and are technically suited for treatment of high-salinity waters.

Description of Testing

The NETL-provided MVR pilot-scale technology skid was delivered to the EERC BEST facility near Watford City, North Dakota, on August 5, 2019. The skid was unloaded, placed within the BEST treatment facility, and connected to a metered power source by an on-site electrician. Figure 18 shows the MVR system set up and operating at the BEST facility. Two weeks of MVR

DocuSign Envelope ID: 2FA9A609-C360-4E53-8B28-BE8B77B6994A



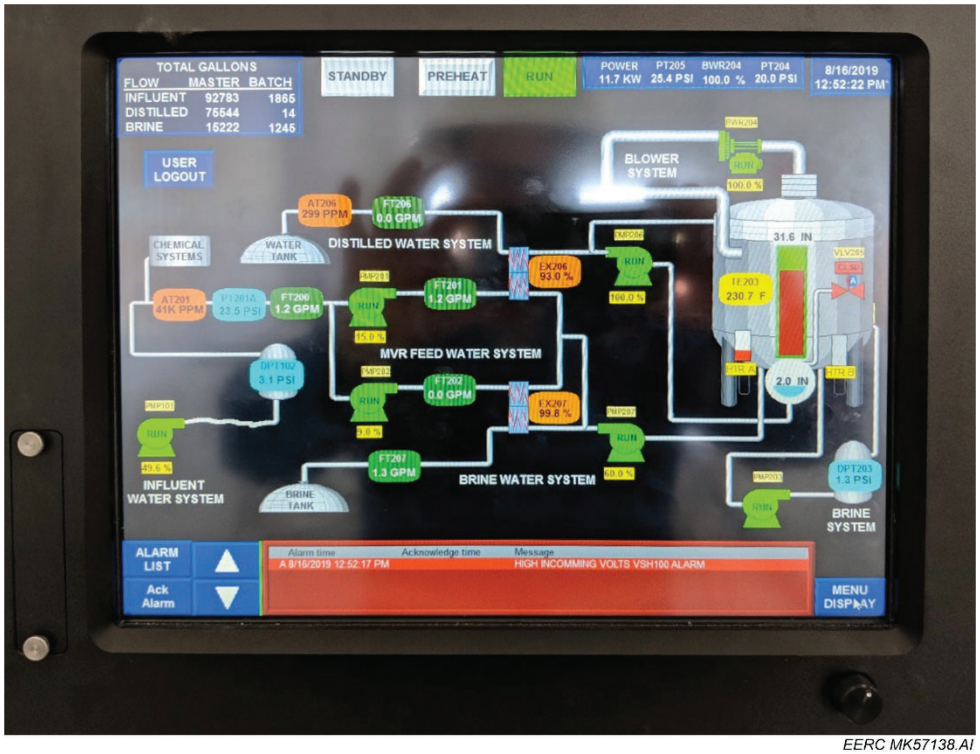
Figure 18. MVR system operating at BEST facility.

operation and testing were scheduled and conducted between August 12 and August 24, 2019. Dr. Seifert, NETL project manager, was on-site the first week with a NETL colleague to train EERC personnel on MVR operation and initiate testing. The second week of testing was conducted by EERC personnel only and entailed evaluation of progressively increasing inlet brine TDS concentrations.,. Testing was conducted on five inlet brine concentrations (listed in Table 6) ranging from approximately 22,000 to 169,000 mg/L TDS. Each test consisted of running the MVR system until steady-state conditions were achieved, followed by system operation between 40% and 60% distillate recovery while outlet brine concentrations increased and stabilized. Figure 19 shows an example of the MVR system interface during testing. Steady-state conditions were determined by obtaining relatively steady EC of inlet and outlet brines but also based on the process conditions of the MVR unit, including flow rates, temperatures, pressures, and tank volumes. Operational data collected for each test included power consumption, average flow rates and volumes into and out of the MVR unit, and salinity measurements (measured in real-time using EC). As part of constant data collection, varying distillate recoveries and energy consumption periods were examined for each salinity test case. Because EC was the only immediate, real-time brine analysis option available during testing, TDS concentrations (mg/L) were estimated and targeted to align with the proposed test cases identified in the original scope of work.

DocuSign Envelope ID: 2FA9A609-C360-4E53-8B28-BE8B77B6994A

Table 6. List of Inlet Salinity Test Cases and Samples Collected for Laboratory Analysis

Test No.	Approx. Inlet Salinity, mg/L TDS	Corresponding Inlet EC, mS/cm	Samples Collected			
			Inlet Brine, composite	Brine Concentrate, composite	Brine Concentrate, final	Fresh Distillate, composite
1	22,000	34,000	X	X	X	X
2	22,000	34,000			X	
3	50,000	70,000	X	X	X	X
4	73,000	93,000	X	X	X	X
5	105,000	123,000	X	X	X	X
6	169,000	181,000	X	X	X	X



EERC MK57138.AI

Figure 19. Sample of MVR system operator interface.

Data collection and sampling occurred throughout the entire operation of the MVR system for each test condition rather than only during steady-state operation in order to maximize the amount of data available should the unit fail before all tests were completed. The long-term viability of the MVR unit was unknown because of previous storage history. Coincidentally, the MVR test equipment (specifically the oil-cooling pump) began to leak at an increasing rate as TDS concentrations increased, and testing had to be terminated during testing of the maximum brine concentration (~169,000 mg/L TDS). Although testing was terminated on the highest TDS test, the anticipated number of operating days within the 2-week operation of the MVR was achieved.

DocuSign Envelope ID: 2FA9A609-C360-4E53-8B28-BE8B77B6994A

Throughout steady-state operation, samples of inlet brine, outlet brine concentrate, and outlet distillate were collected and analyzed for EC and pH every 30 minutes. Additional data, including inlet and outlet flow rates, volumes, and power consumption, were recorded and logged. For each salinity test case, samples of inlet brine, composite brine concentrate, and/or final brine concentrate and output distillate waters were collected and submitted to the EERC analytical laboratory for analysis of major anions and cations, including select metals.

Results

Operation of the MVR system resulted in an average increase of inlet brine salinity of 30% to 80%, as measured by the outlet brine concentrate. Table 7 summarizes the test conditions and average results for each of the tested salinity ranges in terms of inlet and outlet salinity and energy consumption. Tests at each salinity were evaluated in two phases, one being the period of operation prior to steady-state production of concentrated brine (pre-steady state) and the other being the period of operation where the brine concentrate EC was consistent (steady state). With the exception of Tests 1 (pre-steady state) and 2 (steady state), all graphical illustrations used an "a" and "b" designation to identify the pre-steady-state and steady-state test periods. The first test was broken into Tests 1 and 2 at the same salinity and did not use the "a" and "b" designation. This was done to ensure data filename designations were consistent for Dr. Siefert's data analysis. Figures 20–24 illustrate the inlet brine and concentrated brine EC throughout the duration of the pre-steady-state and steady-state periods of each test.

Tests 1 and 2 were both conducted with an average inlet salinity of 21,592 mg/L TDS, with an average pH of 5.2. The salinity of the final concentrate for each of Tests 1 and 2 was 25,163 and 28,593 mg/L, respectively, which is an increase of 17% and 32%, respectively. The pH of the final concentrated brines was 6.4 and 6.1, respectively. The distillate recovery achieved was 42% during the pre-steady-state testing period (Test 1) and increased to approximately 56% during assumed steady-state operations (Test 2). The distillate salinity was also measured as a composite for both tests and was 576 mg/L, with an average pH of 6.2. The average energy usage for Tests 1 and 2 was calculated to be 83 and 59 kWh/m^3 of produced distillate, respectively.

Test 3 was conducted with an average inlet salinity of 49,690 mg/L TDS and a pH of 3.7. The salinity of the final concentrate was measured at 77,168 mg/L, an increase of approximately 55%, with a pH of 7.31. The distillate recovery achieved during testing was 50% for the pre-steady-state period (3a) and 43% for the steady-state period (3b). The distillate salinity was measured at 531 mg/L, with a pH of 10.2. The average energy usage for Tests 3a and 3b was calculated to be 65 and 84 kWh/m^3 of produced distillate, respectively. Test 4 was conducted with an average inlet salinity of 72,742 mg/L TDS and pH of 4.9. The salinity of the final concentrate was measured at 129,609 mg/L, an increase of approximately 78%, with an average pH of 6.3. The distillate recovery achieved during testing was 46% for the pre-steady-state period (4a) and 45% for the steady-state period (4b). The distillate salinity was measured at 783 mg/L, with a pH of 9.7. The average energy usage for Tests 4a and 4b was calculated to be 68 and 74 kWh/m^3 of produced distillate, respectively.

DocuSign Envelope ID: 2FA9A609-C360-4E53-8B28-BE8B77B6994A

Table 7. Summary of MVR Test Conditions/Results

Test No.	MVR Inlet, TDS, mg/L	MVR Concentrate, composite, TDS, mg/L	MVR Concentrate, final		MVR Distillate, composite		Average Energy Usage per Unit of Distillate, kWh/m^3
			TDS, mg/L	% Recovery	TDS, mg/L	% Recovery	
1[1]	21,592	NA[3]	25,163	58	576	42	83
2[2]			28,593	44		56	79
3a[1]	49,690	NA	77,168	50	531	50	65
3b[2]				57		43	84
4a[1]	72,742	122,474	129,609	54	783	46	68
4b[2]				55		45	74
5a[1]	105,568	164,052	169,966	60	807	40	74
5b[2]				58		42	71
6a[1]	168,698	241,310	253,655	57	1046	43	122
6b[2]				56		44	100

[1] Denotes pre-steady-state operation phase.
[2] Denotes steady-state operation phase.
[3] Not analyzed.
Note: Steady-state operation was assumed when MVR concentrate EC stabilized.

DocuSign Envelope ID: 2FA9A609-C360-4E53-8B28-BE8B77B6994A

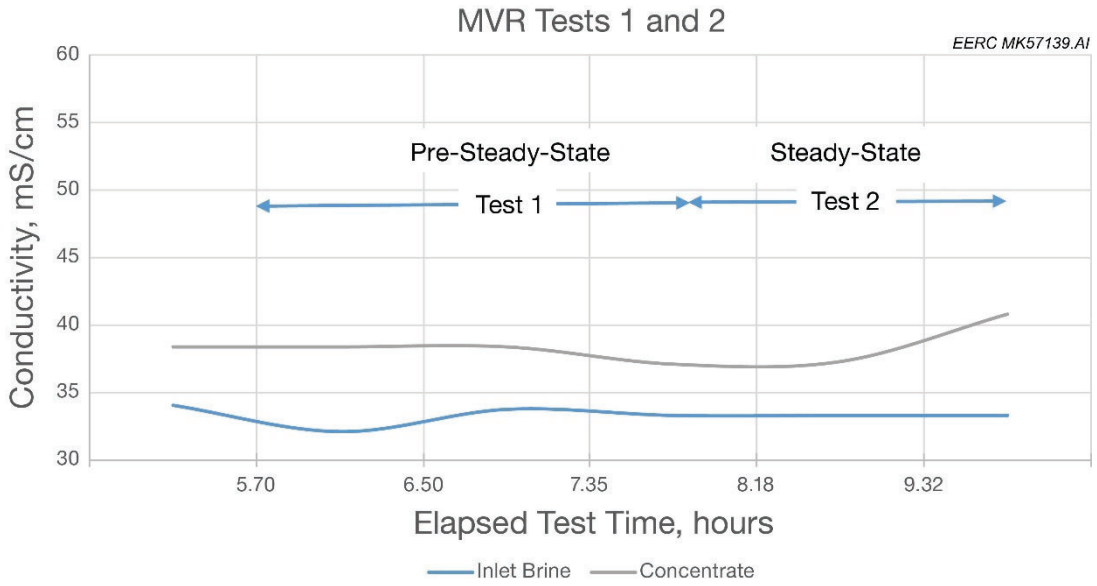


Figure 20. Illustration of inlet brine and concentrate EC for Tests 1 and 2.

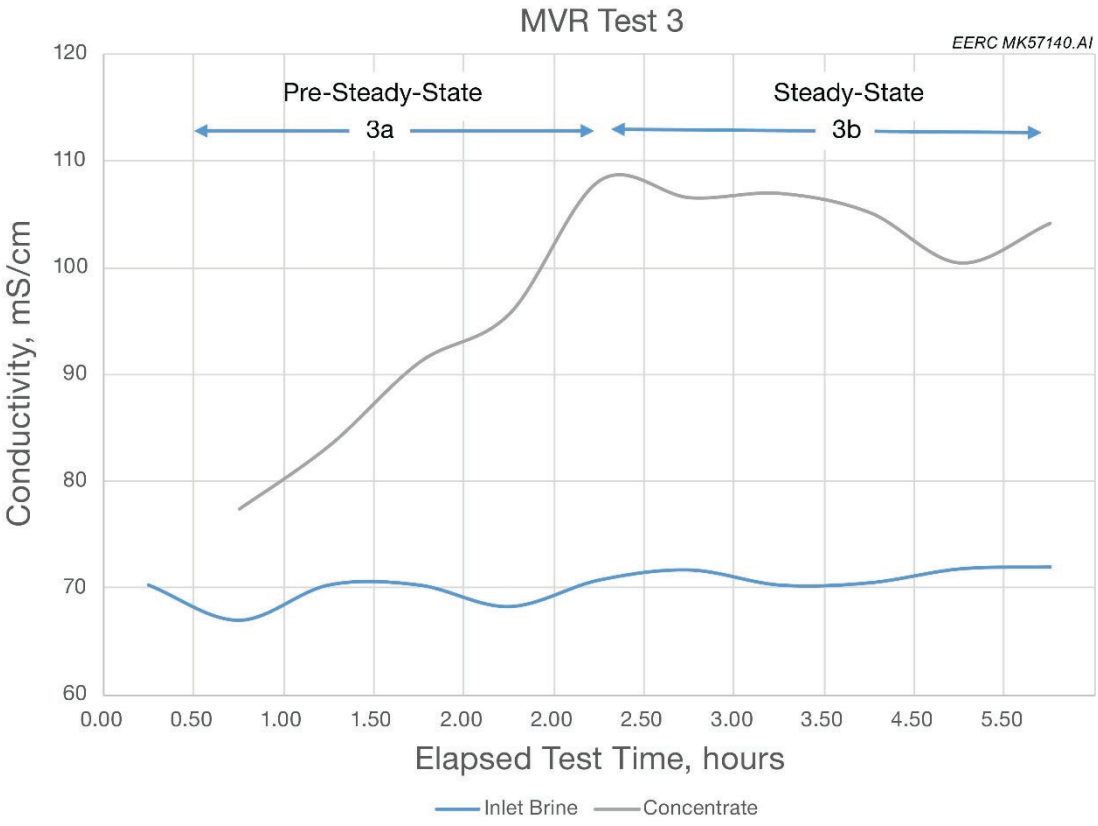


Figure 21. Illustration of inlet brine and concentrate EC for Tests 3a and 3b.

DocuSign Envelope ID: 2FA9A609-C360-4E53-8B28-BE8B77B6994A

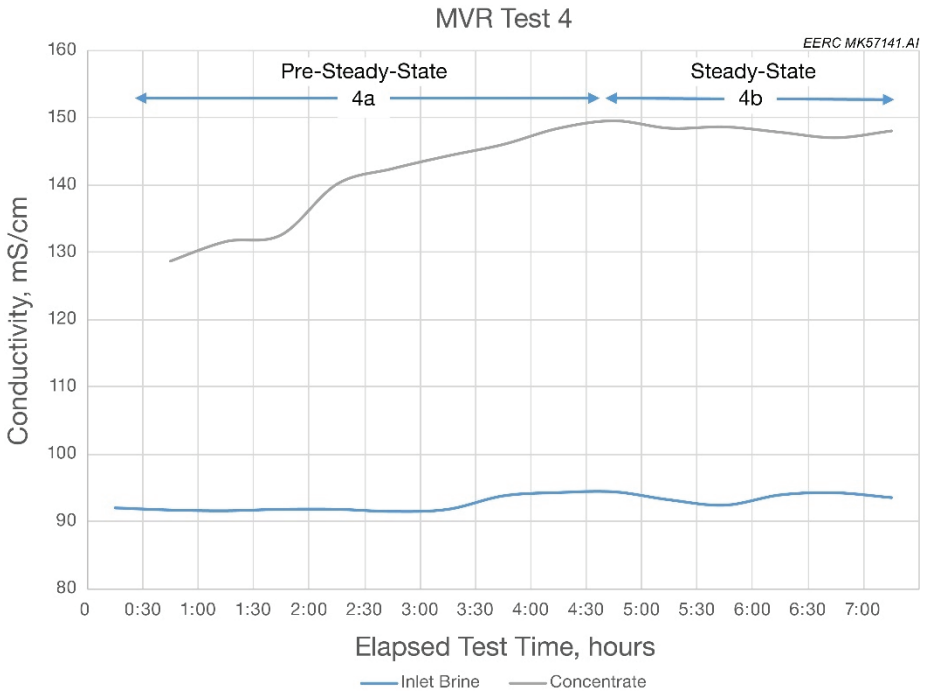


Figure 22. Illustration of inlet brine and concentrate EC for Tests 4a and 4b.

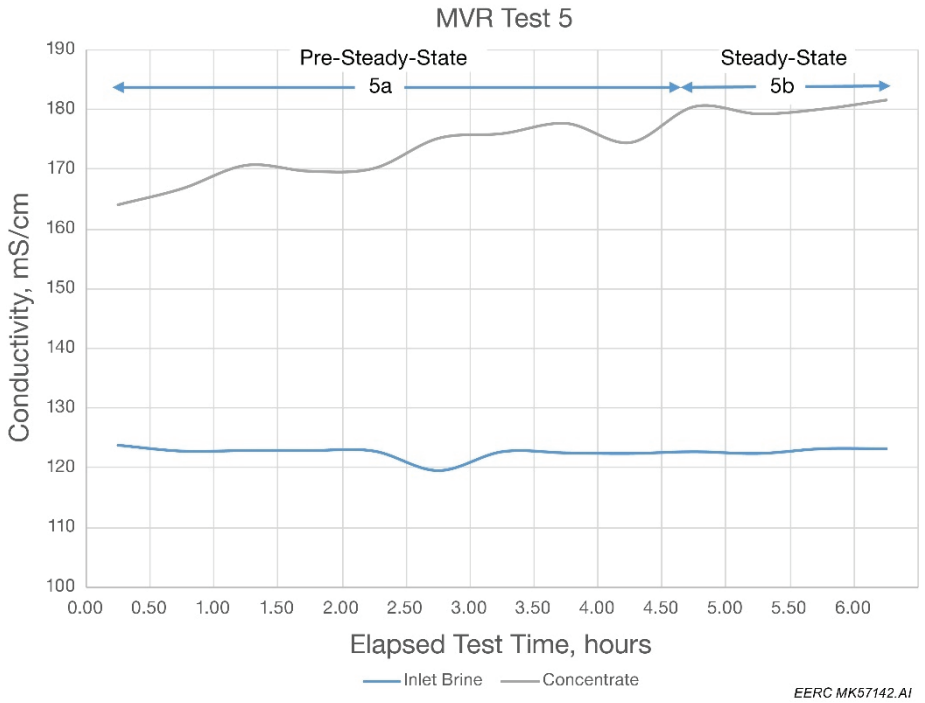


Figure 23. Illustration of inlet brine and concentrate EC for Tests 5a and 5b.

DocuSign Envelope ID: 2FA9A609-C360-4E53-8B28-BE8B77B6994A

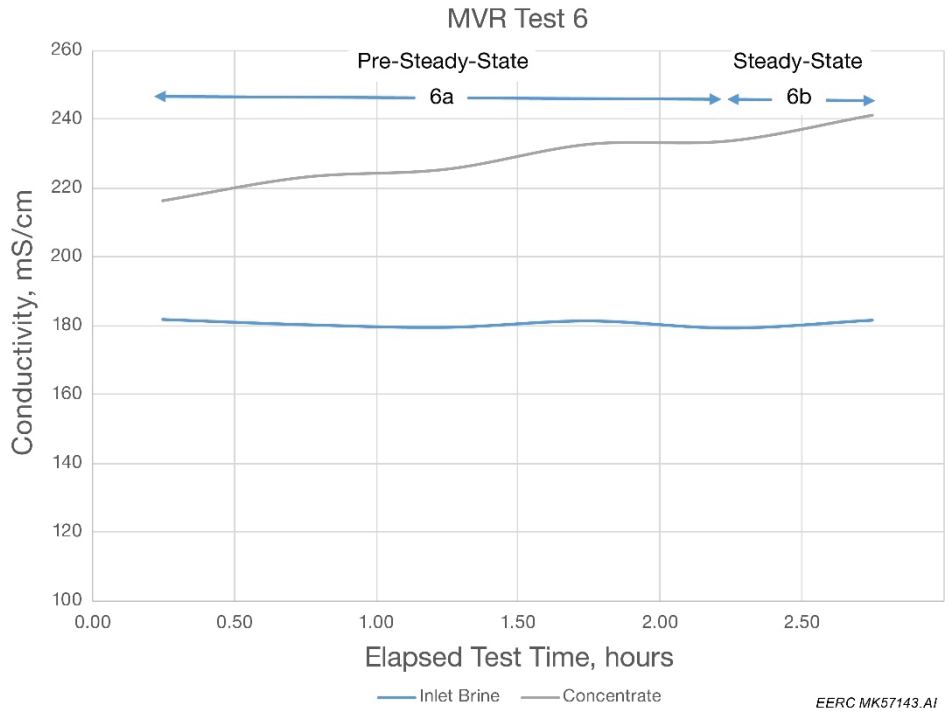


Figure 24. Illustration of inlet brine and concentrate EC for Tests 6a and 6b.

Test 5 was conducted with an average inlet salinity of 105,568 mg/L TDS and a pH of 4.8. The salinity of the final concentrate was measured at 169,966 mg/L, an increase of approximately 61%, with a pH of 5.6. The distillate recovery achieved during testing was 40% for the pre-steady-state period (5a) and 42% for the steady-state period (5b). The distillate salinity was measured at 807 mg/L, with an average pH of 9. The average energy usage for Tests 5a and 5b was calculated to be 74 and 71 kWh/m^3 of produced distillate, respectively.

Test 6 was conducted with an average inlet salinity of 168,698 mg/L TDS and a pH of 4.6. The salinity of the final concentrate was measured at 253,655 mg/L, an increase of approximately 50%, with a pH of 5.2. The distillate recovery achieved during testing was 43% for the pre-steady-state period (6a) and 44% for the steady-state period (6b). The distillate salinity was measured at 1046 mg/L, with a pH of 9.11. The average energy usage for Tests 6a and 6b was calculated to be 122 and 100 kWh/m^3 of produced distillate, respectively.

Figure 25 illustrates the average energy usage, kWh/m^3 of distillate production, as the inlet salinity increases. The values were relatively similar for the first four inlet salinities and increased by about 45% at the highest tested inlet salinity. However, this increase in energy consumption coincides with an onset of mechanical failures on the MVR unit (i.e., leaking oil pump on blower system). For this reason, it is unclear which action, increasing inlet salinity or mechanical issues, is causal to the increase in energy usage.

DocuSign Envelope ID: 2FA9A609-C360-4E53-8B28-BE8B77B6994A

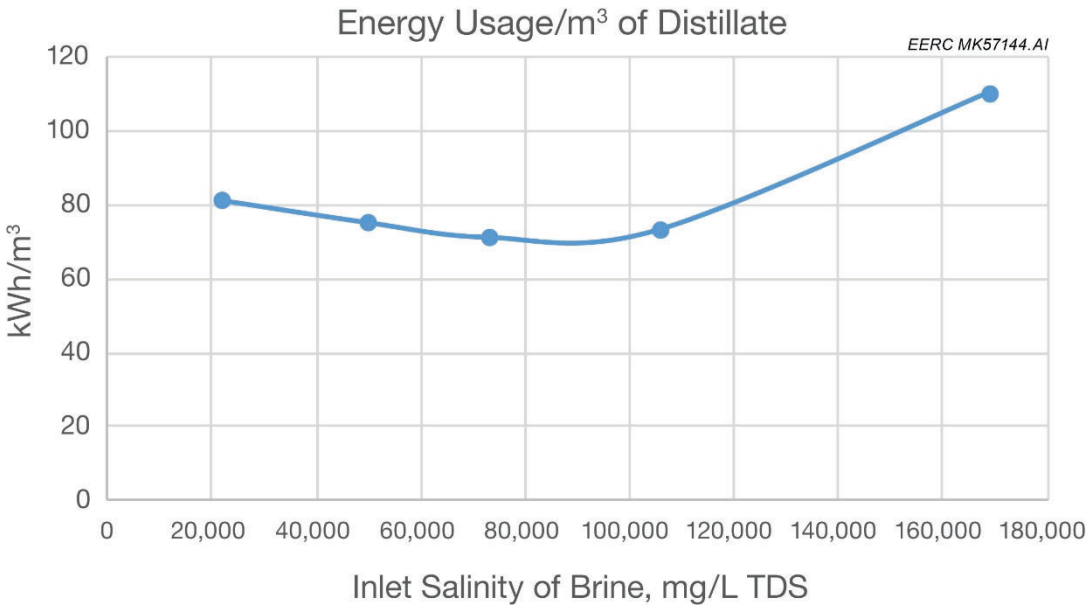


Figure 25. Energy consumption per cubic meter of distillate for each inlet salinity.

Figure 26 summarizes the EC trends for the inlet brine and outlet brine concentrate for each of the six tests. The concentrated brine salinity increases as the inlet brine salinity of each test condition increases, as was seen with the overall TDS results. EC is not directly proportional to TDS; however, a known correlation was used to estimate TDS during testing and to identify steady-state operation. Figure 27 illustrates the same inlet and outlet brine EC trends but also includes the outlet distillate EC values. The values in this figure are plotted on a logarithmic scale to better show the low EC values of the distillate. Although the EC of the outlet brine shows significant increases with increasing inlet brine salinity, the ECs of the distillate are continually low and increase only slightly as the inlet brine salinity increases.

As part of each test, samples of the composite inlet brine, composite outlet concentrated brine, final outlet concentrated brine, and final outlet distillate were collected and submitted for analysis at the EERC's in-house analytical laboratory. The composite outlet concentrated brine samples were only obtained for Tests 4, 5, and 6. Selected analytical results are shown in Table 8.

As expected, most constituent concentrations increased in the composite and final brine samples. While the distillate water is relatively absent of ions, it exhibited a slight increase in constituents as the salinity of the inlet brine increased. As shown in Figure 28, selected ions of the inlet brine increase proportionally to the overall total TDS concentration. Similarly, the concentration of the selected ions increase proportionally to total TDS in the concentrated brine, as illustrated in Figure 29, and do not show any species selectivity. The selected ions of the distillate waters, as shown in Figure 30, show a similar increasing trend with increasing inlet brine salinity.

DocuSign Envelope ID: 2FA9A609-C360-4E53-8B28-BE8B77B6994A

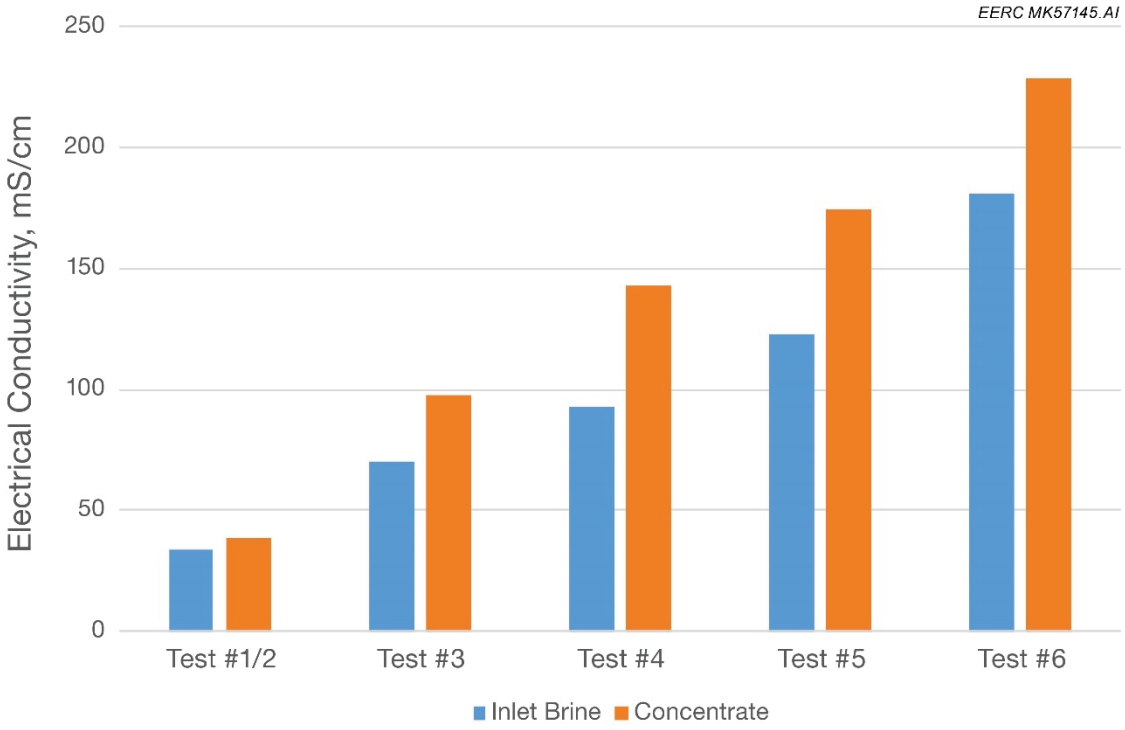


Figure 26. Illustration of inlet brine and outlet concentrated brine conductivity.

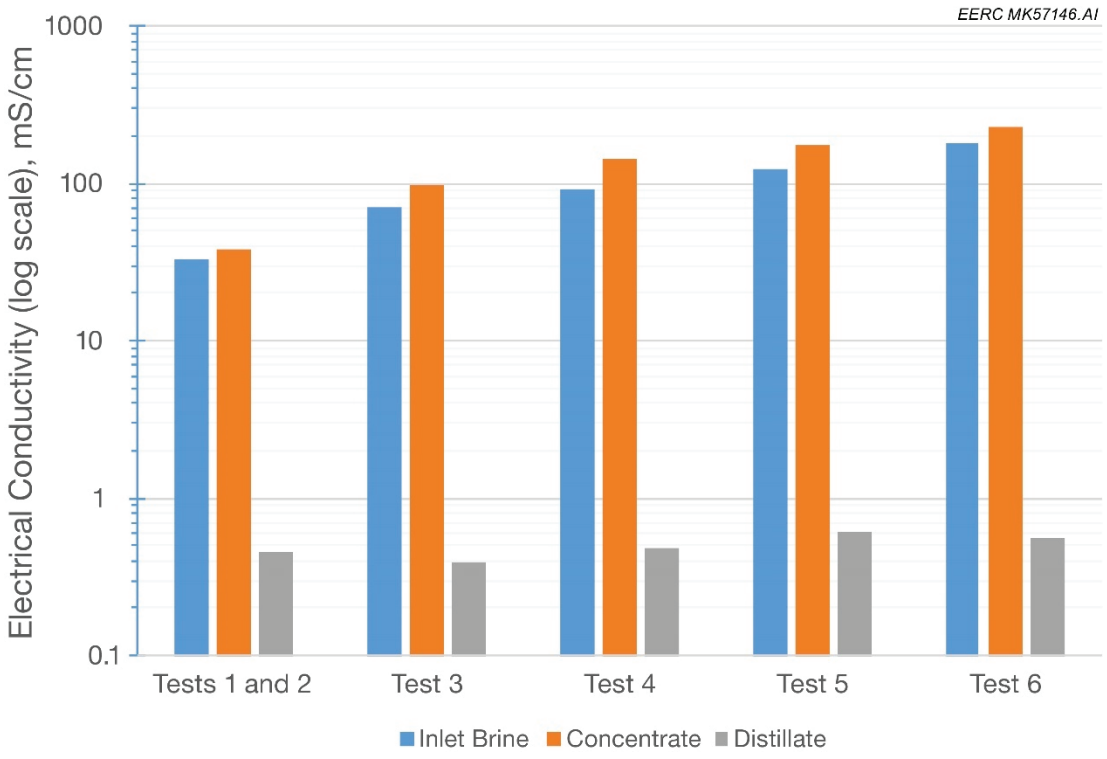


Figure 27. Illustration of inlet brine, outlet concentrated brine, and outlet distillate conductivity (log scale).

DocuSign Envelope ID: 2FA9A609-C360-4E53-8B28-BE8B77B6994A

Table 8. MVR Water Chemistry Results, mg/L

	TDS	Na	K	Ca	Mg	Sr	NH_4	P	Si	SO_4	NO_3	Br	Cl
TEST 1													
Inlet	21,952	6520	598	1250	92	101	146	<20	<20	480	<10	60	12,700
Concentrate Final	25,163	7480	692	1430	159	114	111	<20	<20	587	<10	70	14,500
Distillate Final	576	2.47	<1	11.0	1.1	0.879	360	<0.1	<0.1	<1	<1	<1	4.78
TEST 2													
Concentrate Final	28,593	8290	768	1580	175	128	110	<20	<20	660	<10	70	16,800
TEST 3													
Inlet	49,690	13,800	1230	3200	191	253	383	<20	<20	654	29.2	150	29,800
Concentrate Final	77,168	21,400	1890	4940	484	384	326	<20	<20	1040	49.5	220	46,400
Distillate Final	531	47.0	4.24	11.0	1.1	0.879	360	<0.1	<0.1	2.1	<1	<1	105
TEST 4													
Inlet	72,742	21,600	1820	4790	280	387	589	<20	<20	548	20	206	42,500
Concentrate Composite	122,474	35,000	3050	8020	590	651	780	<20	<20	1030	70	356	72,900
Concentrate Final	129,609	36,300	3200	8450	606	677	880	<20	<20	1020	73	380	78,000
Distillate Final	783	70.6	6.8	16.4	1.4	1.4	202	<0.1	<0.1	2.3	<1	<1	187
TEST 5													
Inlet	105,568	30,000	2580	6600	384	544	816	<20	<20	584	50	310	63,700
Concentrate Composite	164,052	45,400	4010	10,400	688	846	1190	<20	<20	920	66	496	99,900
Concentrate Final	169,966	47,400	4270	10,800	711	898	1260	<20	<20	960	140	514	103,000
Distillate Final	807	111	11.0	24.5	1.90	2.15	152	<0.1	<0.1	3.1	<1	<1	278
TEST 6													
Inlet	168,698	47,100	4,270	10,900	647	897	1400	<20	<20	810	120	554	102,000
Concentrate Composite	241,310	68,400	6280	16,100	1010	1330	2220	<20	<20	1100	108	752	144,000
Concentrate Final	253,655	71,700	6640	16,700	1050	1400	2210	<20	<20	990	130	832	152,000
Distillate Final	1046	225	21.0	52.8	3.60	4.62	109	<0.1	<0.1	3.9	<1	<1	500

DocuSign Envelope ID: 2FA9A609-C360-4E53-8B28-BE8B77B6994A

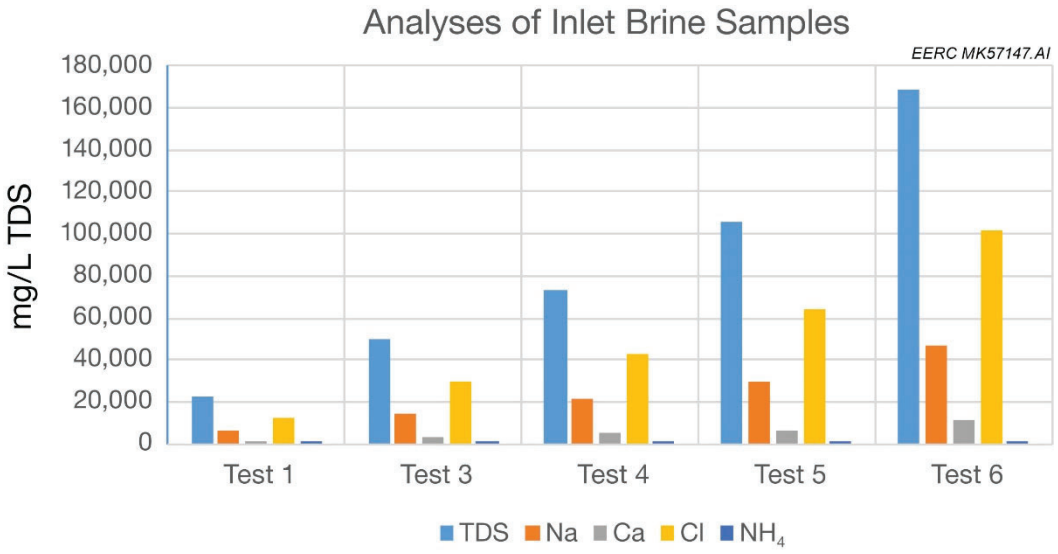


Figure 28. Illustration of inlet brine salinity constituent trends.

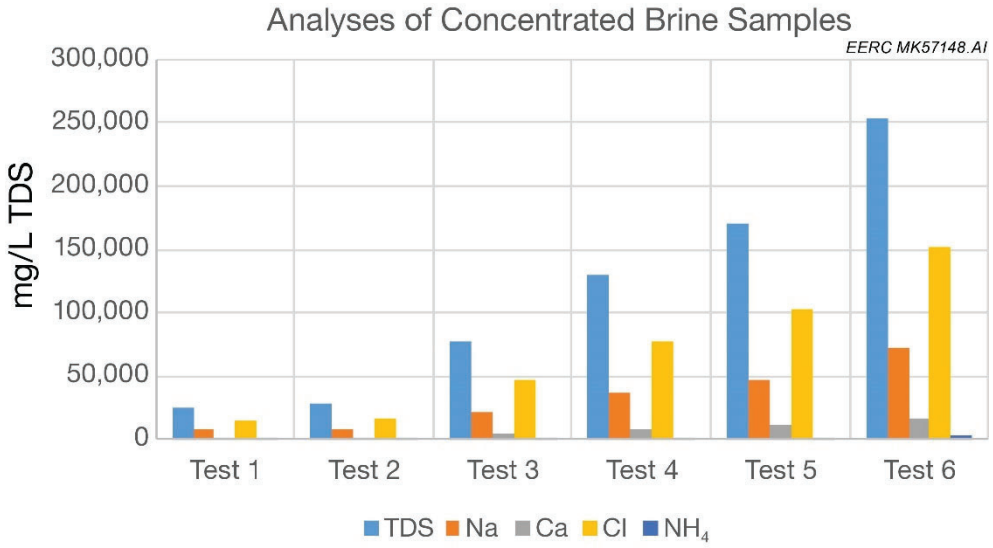


Figure 29. Illustration of concentrated brine salinity constituent trends.

The one exception to this trend was ammonium. The ammonium ion concentration of the outlet distillate demonstrated a decreasing trend as the salinity of the inlet brine increased. This observation is explained further in the Discussion and Conclusions section. The pH of the inlet brine ranged from 3.7 to 5.2, with an average of 4.6. The resulting brine concentrate samples increased in pH and ranged from 5.2 to 7.3, with an average of 6.2. The distillate waters increased in pH, ranging from 9.1 to 10.2, with an average of 9.6.

DocuSign Envelope ID: 2FA9A609-C360-4E53-8B28-BE8B77B6994A

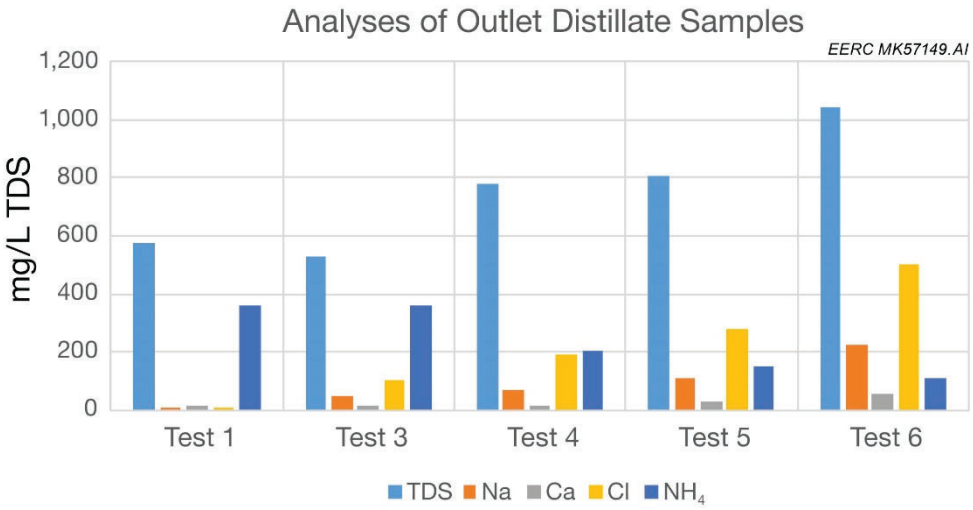


Figure 30. Illustration of outlet distillate salinity constituent trends.

Discussion and Conclusions

The MVR unit was tested at a wide variety of input brine concentrations, thereby meeting the goal of the NETL program and satisfying the BEST project demonstration objectives. Additionally, the MVR unit was able to successfully treat all of the input brine streams that were tested. Extensive water chemistry analytical and system electrical usage data were provided to the NETL project manager. The outlet concentrated brine exhibited a 30% to 80% increase in salinity when compared to the inlet brine, and the outlet distillate salinity ranged from approximately 550 mg/L TDS in the lowest-salinity test to 1050 mg/L TDS in the highest-salinity test. These distillate salinity values are quite low and, in all cases, just barely exceed the U.S. Environmental Protection Agency secondary contaminant drinking water standard of 500 mg/L TDS (U.S. Environmental Protection Agency, 2019). It is anticipated that optimization of system operations could yield TDS concentrations that would meet the drinking water standard.

The inlet brines tested were Na–Cl-dominant waters, and the MVR unit was very effective at removing (concentrating) these Na–Cl constituents. The various cations and anions of the inlet brines were also proportionally concentrated with increasing concentration of TDS. Moderate concentrations of ammonium ions (NH_4) were also present in the inlet brines, resulting in elevated levels of NH_4 in the outlet concentrated brines. However, the outlet distillate waters exhibited a decreasing trend of ammonium ion concentrations. The average pH of the outlet distillate water was relatively high at approximately 10.0; therefore, the ammonium ions may have been liberated (dissociated) and off-gassed (as ammonia [NH_3]) from the distillate outlet waters during testing, resulting in the decreasing trend. This is supported by the presence of hydroxide (OH) ions (from ammonium dissociation) in the distillate waters and the absence of most other cations or anions. Solubility of ammonia in water increases with decreasing pH, and the volatility of ammonia increases with increasing pH (Agency for Toxic Substances and Disease Registry, 2019). Therefore, it is likely that the higher pH of the distillate waters allowed the ammonium ions to dissociate and allowed the free ammonia to volatilize. However, the outlet concentrated brine pH was relatively neutral (approximately 6.2 on average) which kept the ammonium ions stable in the

DocuSign Envelope ID: 2FA9A609-C360-4E53-8B28-BE8B77B6994A

brine without off-gassing. This theory is anecdotally supported by the presence of an ammonia smell from the outlet distillate waters, and not the outlet concentrated brine, during test operations.

Energy consumption was relatively stable throughout most of the tests, ranging between 59 and 84 kWh/m^3 of outlet distillate, but increased to 122 kWh/m^3 of outlet distillate for the final test at 169,000 mg/L TDS. However, this increase in energy consumption coincides with an onset of mechanical failures on the MVR unit (i.e., leaking oil pump on blower system). For this reason, it is unclear whether increasing inlet salinity or mechanical issues caused the increase in energy usage.

This particular MVR unit was also designed and constructed to desalinate ocean water for U.S. military personnel in remote locations and automated to ensure easy operation. Therefore, it was not designed to be energy-efficient, as many of the energy requirements for the system are to support the automated controls and operation. The tests conducted did, however, give a good technological baseline for the energy requirements necessary for treatment of a variety of brine concentrations.

AGMD Technology

Introduction and Background

The EERC facilitated testing of a membrane distillation unit developed by the University of Pittsburgh for the treatment of brines with high-TDS levels that are typical of produced water from deep geologic sources. Testing was conducted at the EERC's BEST facility near Watford City, North Dakota, with the overall goal of demonstrating the technical feasibility and commercial potential AGMD technology to recover high-quality water from brines for beneficial reuse. The test unit evaluated at the BEST site was developed based on prior laboratory-scale research conducted at the University of Pittsburgh with a direct contact membrane distillation (DCMD) unit. Key results from this earlier development testing are also included in this summary to highlight the advantages offered by the AGMD configuration that was selected for BEST site testing. Information for this summary, including data and figures, was primarily drawn from the final technical report provided by the University of Pittsburgh to the EERC, which is included in its entirety in Appendix G.

Description of Technology

The dewatering system developed by the University of Pittsburgh uses membrane distillation as an alternative to other desalination technologies like RO, MVR, multistage flash distillation (MSFD), or multieffect distillation (MED). In membrane distillation, the membrane element separates the feed brine and the permeate streams. Since the membrane is hydrophobic, it blocks the transmission of liquid-phase contaminants while allowing water vapor to pass and condense on the other side to form the permeate stream. Membrane distillation offers near 100% rejection of nonvolatile compounds in contrast to RO, requires less compressor power than MVR, and can use lower-temperature thermal energy than MSFD or MED. Membrane distillation also operates with a much lower pressure differential than RO, which places less stringent requirements on membrane mechanical properties.

DocuSign Envelope ID: 2FA9A609-C360-4E53-8B28-BE8B77B6994A

Several configurations of membrane distillation have been proposed that can be categorized according to the configuration of the permeate side of the membrane, e.g., whether permeate liquid is in direct contact with the membrane (i.e., DCMD) or whether the membrane is in contact with vapor and, if so, how the composition of the vapor space is controlled. Laboratory development at the University of Pittsburgh was based on a DCMD configuration, but AGMD was selected for the pilot-scale BEST testing because of advantages with respect to improving thermal efficiency and limiting the transfer of volatile contaminants. In AGMD, the permeate side of the membrane and the liquid permeate itself are separated by an air gap, which insulates the membrane matrix by minimizing conduction heat-transfer losses to the cooler permeate. The air gap imposes a mass transfer resistance that the permeate vapor (and any volatile contaminants) must pass through, but this resistance is outweighed by other advantages including thermal isolation and possible recovery of latent heat, relatively high permeate flux, reduced transfer of volatile contaminants, and a lower tendency to experience membrane fouling or pore wetting.

Description of Testing

Test results are presented for both laboratory-scale testing of a DCMD configuration and BEST facility testing of a pilot-scale AGMD system. In both instances membrane performance was characterized by the water recovery (%) and the normalized permeate flux (in $L/m^2/hr$, or LMH) as defined in Equations 1 and 2, respectively. In Equation 2, A is the nominal membrane area and ρ_w is the density of the high-quality water permeate.

$$\% \text{ Recovery} = \frac{\text{Total mass of permeate collected at time t (g)}}{\text{Initial mass of the feed solution (g)}} \text{ X } 100 \qquad \text{[Eq. 1]}$$

$$\text{Flux (LMH)} = \frac{\text{Mass of permeate collected during the time period } \Delta t \text{ (g)}}{\text{A } (\text{cm}^2) * \Delta t \text{ (min)} * \rho_w \text{ (g/mL)}} \text{ X } 600 \qquad \text{[Eq. 2]}$$

Laboratory DCMD Testing

All laboratory-scale experiments at the University of Pittsburgh used a DCMD module with a 40 cm^2 (20 cm × 2 cm) flat sheet membrane in the experimental system that was operated in batch (concentrating) mode. The laboratory system is shown in Figures 31 and 32.

Commercially available hydrophobic microporous polytetrafluoroethylene (PTFE) membranes with polypropylene supports were obtained from Aquastill, Netherlands. The manufacturer's membrane specifications are provided in Table 9. Spacers (1 mm thick) were stacked on top of the membrane from both sides to ensure even distribution of the feed and permeate flows. Feed solution was heated to operating temperature (60°C) using a hot plate and was circulated using a centrifugal pump. Cool deionized (DI) water was circulated on the permeate side using a centrifugal pump, and its temperature was maintained at 20°C using a laboratory chiller. As permeate accumulated in the collection tank, the overflow was weighed and its conductivity measured continuously with a conductivity meter.

DocuSign Envelope ID: 2FA9A609-C360-4E53-8B28-BE8B77B6994A

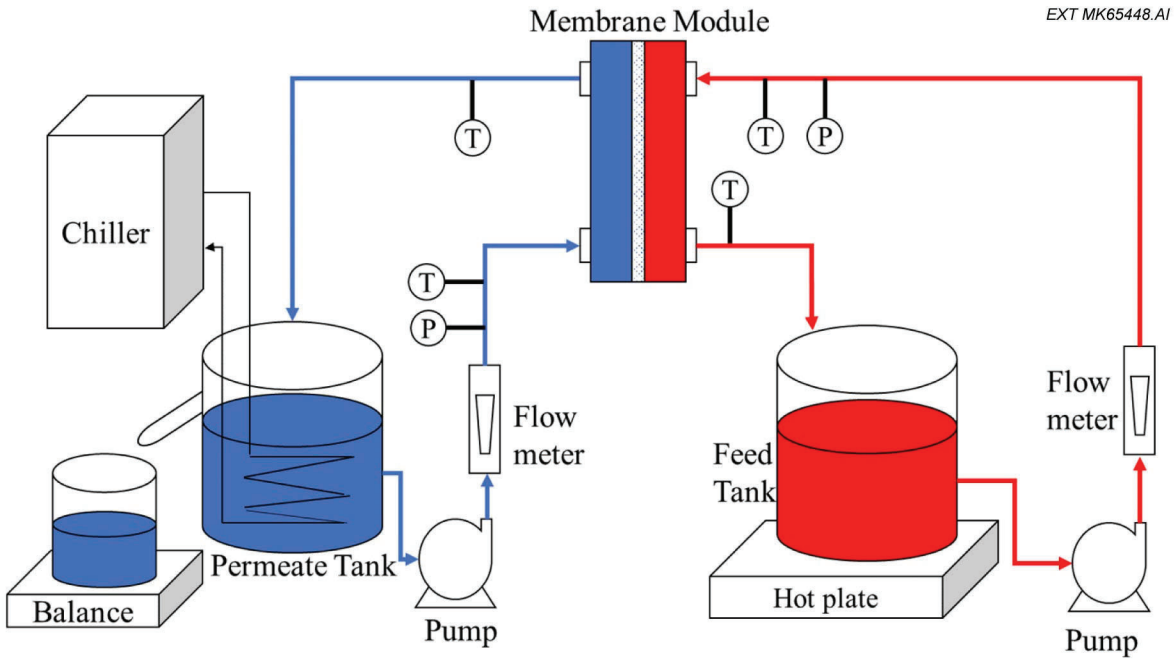


Figure 31. Schematic of the laboratory-scale DCMD system.

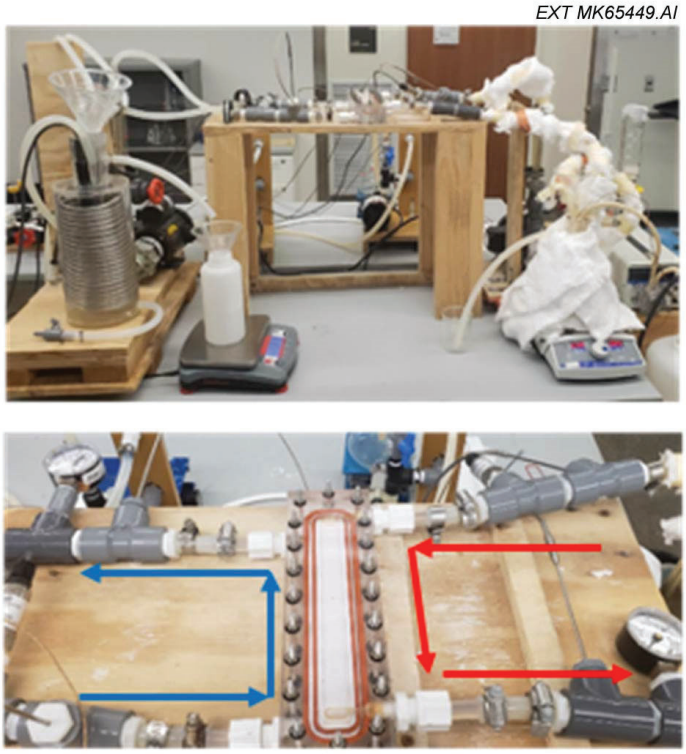


Figure 32. Photographs of the laboratory DCMD system setup (top) and module detail (bottom).

DocuSign Envelope ID: 2FA9A609-C360-4E53-8B28-BE8B77B6994A

Table 9. Properties of the PTFE Membrane

Membrane	Mean Pore Size, μm	Thickness, mm	Contact Angle	Liquid Entry Pressure, bar	Porosity, %
PTFE	0.45	0.13–0.23	139.6°	2.5	85

Pilot System for BEST Facility Testing

The pilot AGMD system produced water permeate and brine concentrate from the high-TDS feed brine that was blended at the BEST facility. The pilot system consisted of four AGMD membrane modules with polypropylene supports; two modules were used during operation and two were held in standby. The membrane modules were spiral-wound AGMD modules with approximately 26 m^2 of surface area per module. Figure 33 shows the construction of and flows through a single module, where the hot brine channel and air gap are separated by the membrane, the air gap is in contact with the cold brine channel through the condenser, and the feed brine is circulated through both hot and cold brine channels. Permeate is obtained in the air gap channel.

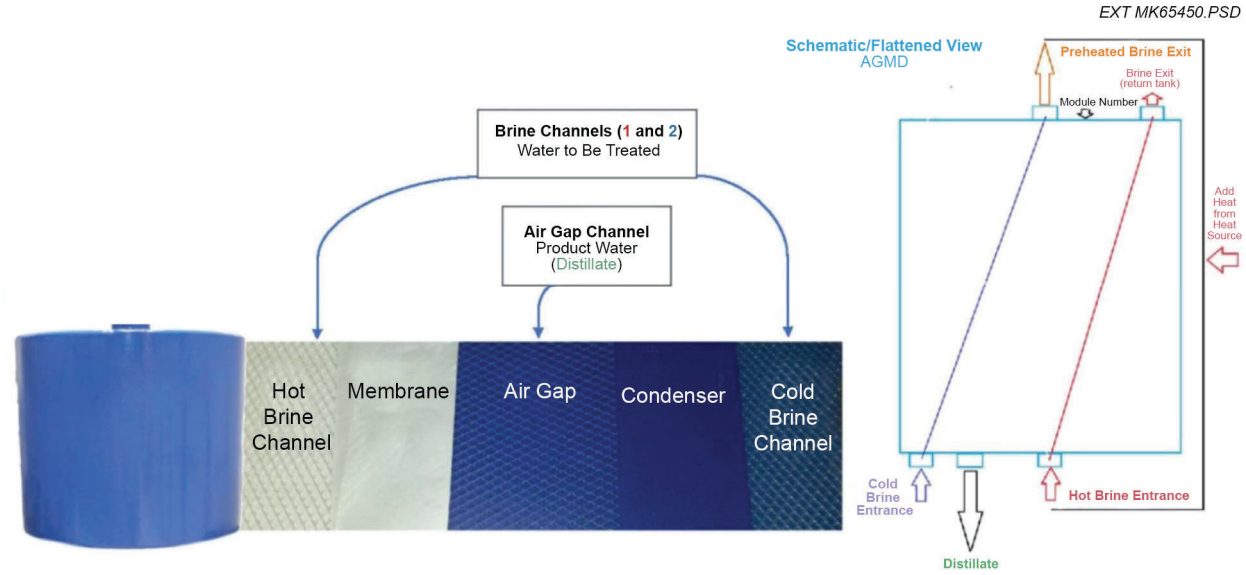


Figure 33. AGMD module details: "unwound" view of the spiral-wound module layers (left) and module fluid flow connections (right).

Design and manufacturing of the pilot AGMD unit was performed by Aquastill (Figure 34). The unit was designed to generate 0.5 gpm of permeate from 1 gpm of brine feed with a TDS of approximately 100,000 mg/L (i.e., 50% water recovery). Integration of the two active AGMD modules into the overall pilot system is shown in Figure 35. The system comprised five tanks: feed tank (T-7), heating tank (T-3), hot brine tank (T-2), cold brine tank (T-1), and permeate tank (T-8). Pretreated brine was fed to the pilot plant (Tank T-8) using gravity through a water meter for measuring the feed flow rate. Feed from T-7 was transferred to T-2 and T-1 using a pump

DocuSign Envelope ID: 2FA9A609-C360-4E53-8B28-BE8B77B6994A



Figure 34. Four-module AGMD pilot unit.

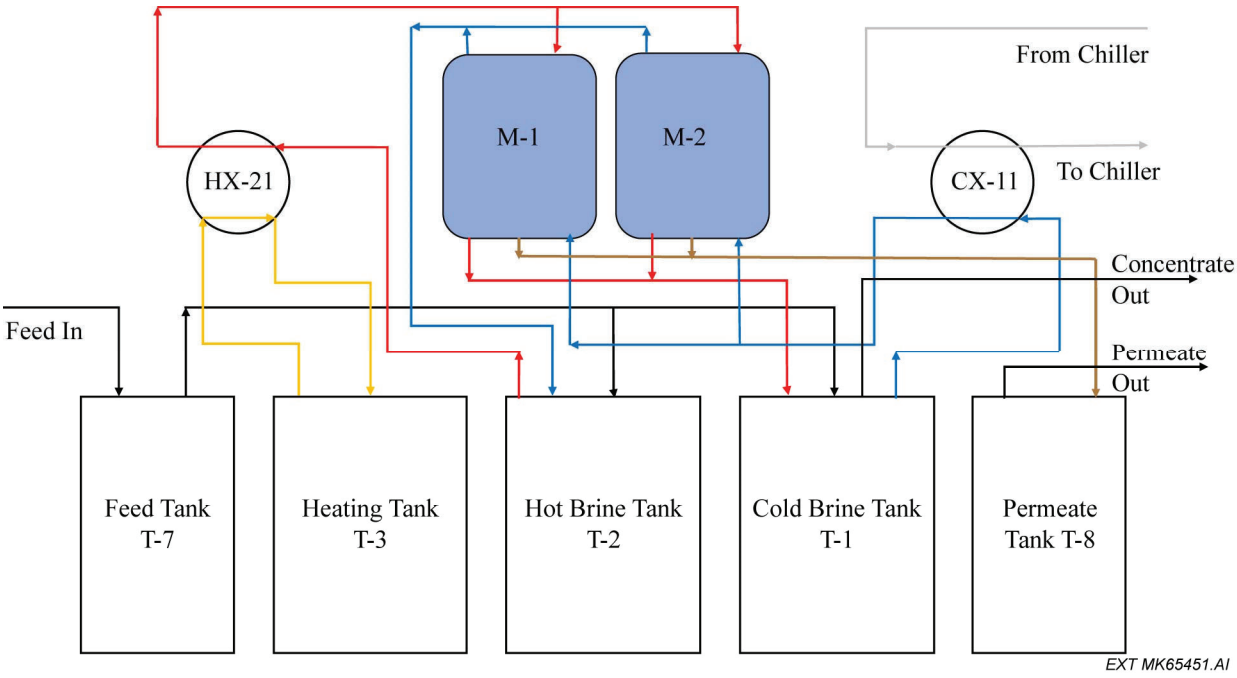


Figure 35. Process flow diagram for overall AGMD pilot system.

DocuSign Envelope ID: 2FA9A609-C360-4E53-8B28-BE8B77B6994A

(pumps not shown). During autofill operation, the levels of T-2 and T-1 were maintained at desired values. The heating tank was equipped with four 9-kW$_e$ heating elements to maintain temperature. Water from the heating tank was pumped through the hot side heat exchanger (HX-21), and brine from T-2 was pumped to the other side of HX-21. Heated feed from T-2 went through the hot side of the modules and was returned to T-1. At the same time, brine from T-1 was pumped through the cold-side heat exchanger (CX-11). Cooling fluid (35% propylene glycol solution) from the chiller was circulated through the other side of CX-11. Cooled brine from T-1 was circulated in the cold brine channel of the membrane module before returning to T-2.

Vapor transfer occurred across the membranes because of the temperature difference between the hot and cold brine channels, and these vapors were condensed in the air gap channel. Condensed permeate was withdrawn from the modules using a vacuum generated in T-8 using a submersible pump and a venturi valve. Permeate product was pumped from T-8 while the concentrate was removed from T-1. The number and volume of these discharges was recorded and used to evaluate system performance. Other collected data include temperatures in the heating tank, permeate tank, and at the inlet and outlet of both the channels in the module and pressure at the inlet and outlet of both the channels in the module and the vacuum line. In addition, the conductivity of brine inlet from T-1 and permeate from the modules was recorded.

The pilot plant was operated in one of two modes, “balance mode” or “feed-and-bleed mode.” In balance mode, brine from T-1 was transferred to T-2 through the cold channel in the module while the brine from T-2 was transferred to T-1 through the hot channel in the module. As distillate was produced, fresh brine was fed to these tanks to maintain desired levels. Balance mode was used to increase TDS of the concentrate which increased water recovery; it was used primarily to transition between test conditions.

In the feed-and-bleed mode, the system was operated to maintain the brine conductivity at the desired level by removing the concentrate from T-1 while replacing the volume with fresh brine from T-7. Concentrate discharge and fresh feed addition occurred simultaneously to maintain concentrate conductivity at the desired value, which kept water recovery constant during steady-state test conditions.

Figure 36 shows a photograph and schematic of the setup used during testing at the BEST site. Pretreated, blended brine was stored in a 3000-gallon pretreated feed storage tank and was filtered through a 5-µm oil absorption baghouse filter followed by filtration through a 0.45-µm polypropylene cartridge filter using a 1-hp, five-stage feed pump. The baghouse and cartridge filters were used to remove any suspended solids that might be present in the pretreated brine. The filtered brine was stored in a 1000-gallon horizontal feed tank. After AGMD treatment, concentrate and permeate from the system were pumped to a 1000-gallon conical bottom discharge tank. Brine from the discharge tank was pumped to an on-site waste tank using a ¾-hp pump. A 10-ton chiller was used for the cooling needs of the pilot system.

DocuSign Envelope ID: 2FA9A609-C360-4E53-8B28-BE8B77B6994A

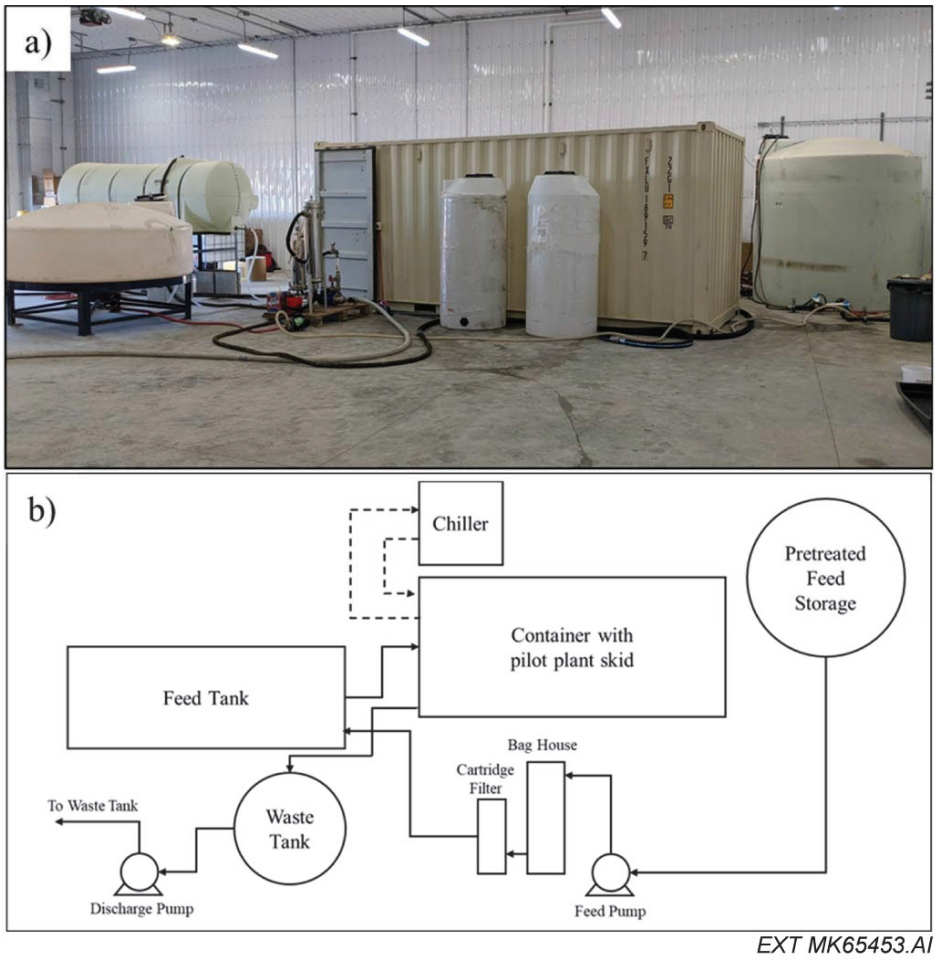


Figure 36. a) Photograph of the pilot system and b) integration schematic at the BEST facility.

Results

Laboratory-Scale DCMD Module

Laboratory testing was conducted at the University of Pittsburgh using brine blended at the BEST site with a nominal TDS of 90,000 mg/L. The as-received brine constituted a low-salinity test condition for which the recorded permeate flux and conductivity are shown in Figure 37. During the initial 8 hours of this test, the brine was concentrated to achieve 50% water recovery (i.e., a concentrated brine TDS ~180,000 mg/L). The decrease in permeate flux observed during this period was primarily due to the increase in feed salinity, leading to a decrease in the feed solution vapor pressure. After this initial period, concentrate salinity was maintained at 180,000 mg/L by continuously adding a makeup stream of raw brine and withdrawing the overflow (purge) stream from the feed tank. Permeate flux remained constant during the subsequent 48 hours of operation at a constant concentration. However, the permeate conductivity increased steadily during this period and was linked to an increase in permeate ammonium ion concentration from the passage of volatile ammonia through the membrane.

DocuSign Envelope ID: 2FA9A609-C360-4E53-8B28-BE8B77B6994A

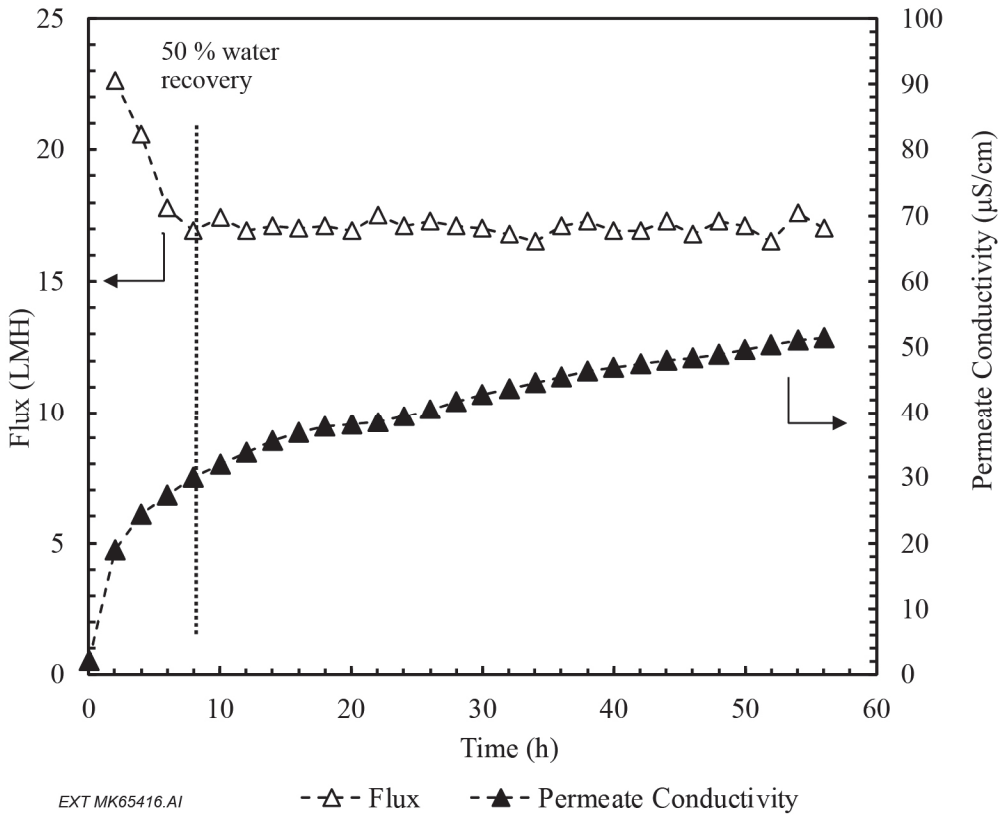


Figure 37. Permeate flux and conductivity for low-salinity brine testing with the DCMD module.

A second high-salinity DCMD test condition was created by treating the concentrate produced during the low-salinity testing. The concentrate had a nominal TDS of 180,000 mg/L, and Figure 38 shows the permeate flux and conductivity from this test. During the initial 8 hours of operation, the feed was concentrated to achieve 30% water recovery (i.e., a concentrate TDS of approximately 257,000 mg/L) and was then switched to feed-and-bleed mode by continuously supplying the freshwater and taking the purge out of the feed tank to maintain steady state. Similar to the low-salinity DCMD testing, the decrease in permeate flux during the initial 8 hours of high-salinity testing was due to reduction in vapor pressure, whereas the flux remained constant throughout the next 16 hours of steady-state operation. Likewise, the increase in permeate conductivity was likely due to passage of ammonia present in the feed brine solution.

DocuSign Envelope ID: 2FA9A609-C360-4E53-8B28-BE8B77B6994A

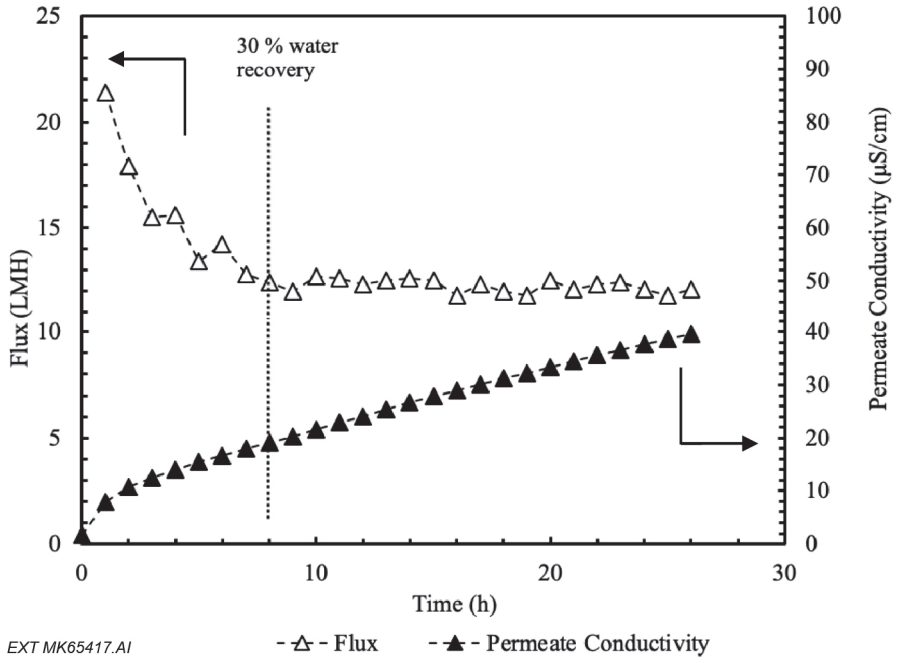


Figure 38. Permeate flux and conductivity for high-salinity brine testing with DCMD module.

Pilot-Scale AGMD System

The pilot system trial was conducted at the BEST site with pretreated brine October 5–14, 2021. After setup of the system at the BEST site, validation testing was conducted with NaCl solution. Treatment evaluation trials were then conducted in two stages with low (~90,000 mg/L)- and high (~180,000 mg/L)-salinity brines to evaluate different water recoveries. Figures 39 and 40 show the University of Pittsburgh technology system setup at the BEST site in October 2021.

DocuSign Envelope ID: 2FA9A609-C360-4E53-8B28-BE8B77B6994A



Figure 39. Inside view of BEST testing facility during University of Pittsburgh technology demonstration.



Figure 40. University of Pittsburgh personnel working on AGMD system.

DocuSign Envelope ID: 2FA9A609-C360-4E53-8B28-BE8B77B6994A

Figure 41 presents the permeate flux and conductivity data for the AGMD pilot system while treating low-salinity brine. The initial 14 hours of testing represents the transition from the validation test solution to the low-salinity brine blend while operating in balance mode. The figure shows a decrease in permeate flux with an increase in feed-side concentration due to vapor pressure decrease caused by increasing TDS. Feed concentration was continued until the TDS on the feed side reached about 174,000 mg/L (conductivity of 178 mS/cm), which represented 52.9% water recovery. After achieving 52.9% water recovery, the pilot system was shifted to steady-state operation for 22 hours. Permeate flux (~1.66 LMH) was virtually constant during this period of operation, along with permeate conductivity (in contrast to the DCMB test trend), indicating constant rejection of salts throughout the operation time. Brine feed and permeate flow rates corresponding to Figure 41 are shown in Figure 42.

After operating the pilot system at 52.9% water recovery for 22 hours, the salt concentration was reduced to 162,000 mg/L (conductivity = 170 mS/cm) to reach a test condition of 50.3% water recovery. The constant flux (~2.0 LMH) and permeate conductivity indicate no deterioration in AGMD module performance with 50% water recovery.

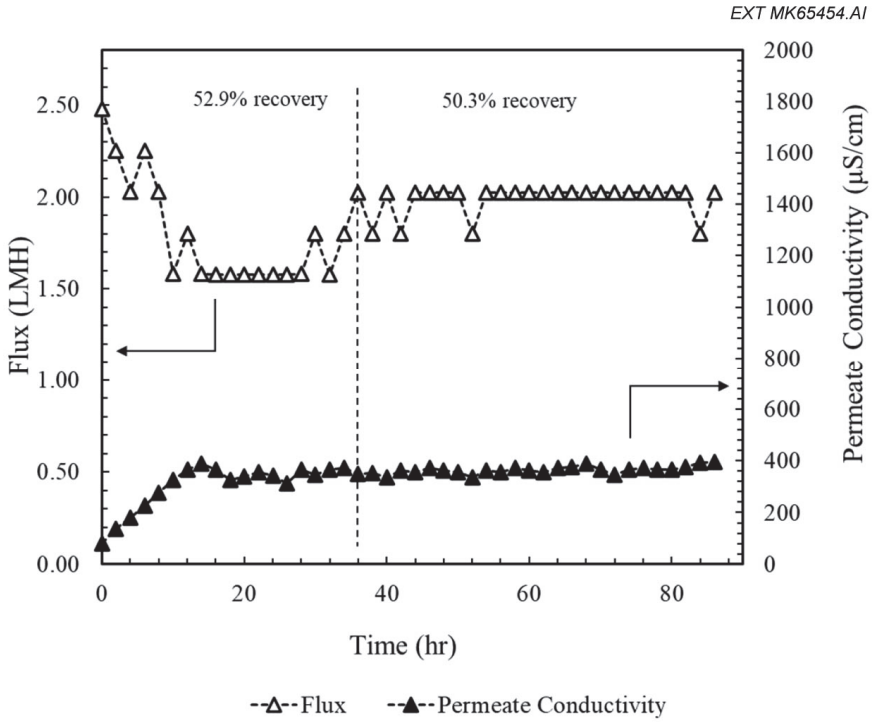


Figure 41. Permeate flux and conductivity for AGMD pilot testing with low-salinity brine.

DocuSign Envelope ID: 2FA9A609-C360-4E53-8B28-BE8B77B6994A

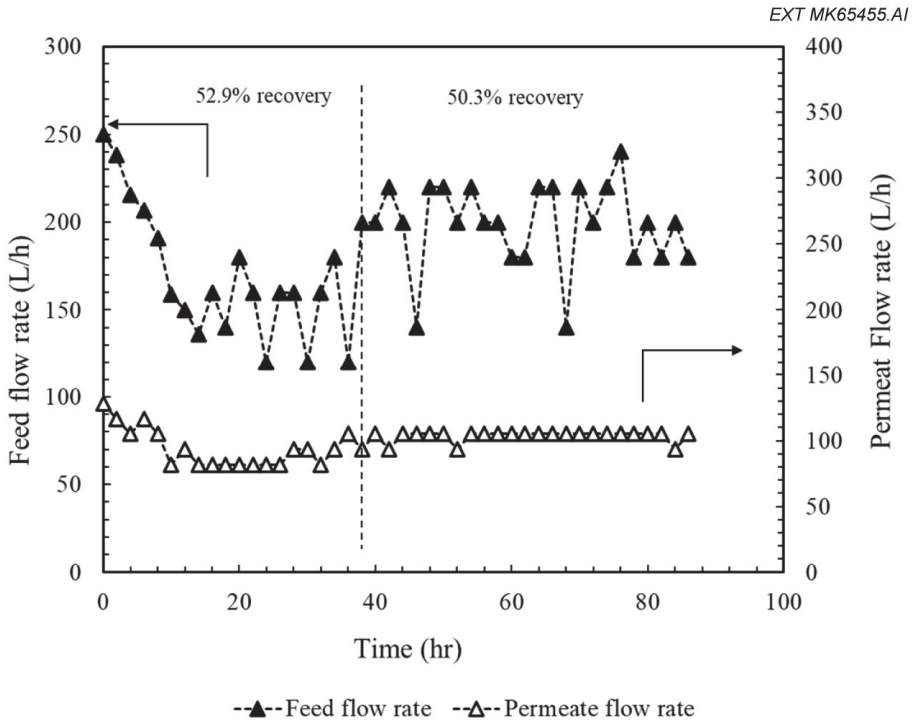


Figure 42. Brine feed and permeate flow rates during AGMD pilot testing with low-salinity brine.

Table 10 shows water quality analysis of samples collected during the low-salinity brine testing. The results show that for the initial period of 22 hours, the pretreated brine had TDS of 82,600 mg/L, while the concentrate TDS was 174,000 mg/L, thereby indicating 52.9% water recovery. In the later 50 hours, the TDS of pretreated brine was about 80,400 mg/L and the concentrate TDS was about 162,000 mg/L, indicating 50.3% water recovery. The permeate TDS of 390 and 380 mg/L, respectively, indicates 99.8% rejection of salts by the pilot system. Permeate analysis shows the presence of alkalinity, ammonia, and TOC. The passage of NH_3 vapor, alkalinity in the form of CO_2 gas, and TOC in the form of volatile organics with the water vapor led to their presence in the permeate.

DocuSign Envelope ID: 2FA9A609-C360-4E53-8B28-BE8B77B6994A

Table 10. Stream Analyses for the AGMD Pilot Testing with Low-Salinity Brine

		52.9% Water Recovery			50.3% Water Recovery		
Parameter	**Units**	**Feed**	**Concentrate**	**Permeate**	**Feed**	**Concentrate**	**Permeate**
Alkalinity as HCO_3^-	mg/L	575	778	0.0	574	731	0.0
Alkalinity as CO_3^{2-}	mg/L	0.0	0.0	60.5	0.0	0.0	51.3
Alkalinity as OH^-	mg/L	0.0	0.0	59.7	0.0	0.0	65.4
Alkalinity as $CaCO_3$	mg/L	471	638	277.0	471	599	278.0
Ammonia	mg/L	588	1160	72.1	439	997	69.5
Ba	mg/L	4	9	0.1	4	8	0.1
Boron (B)	mg/L	170	380	3.2	127	344	2.0
Bromide (Br)	mg/L	271	582	1.0	268	533	1.0
Ca	mg/L	5550	11,800	7.9	5410	10,500	7.7
Cl	mg/L	48,000	103,000	91.3	47,400	97,700	84.9
Co	mg/L	1.0	1.0	0.1	1.0	1.0	0.1
Conductivity	µS/cm	117,000	198,000	357.0	116,000	97,700	351.0
Density	g/cm^3	1.1	1.1	1.0	1.1	1.0	0.0
Iron	mg/L	<1.0	<1.0	0.1	<1.0	<1.0	1.0
Li	mg/L	23	49	0.2	23	44	0.2
Mg	mg/L	348	736	0.6	339	668	0.6
Manganese (Mn)	mg/L	0.3	0.3	0.1	0.1	0.1	0.1
pH	–	8.2	7.5	10.0	8.1	7.6	10.0
Potassium (K)	mg/L	2240	4590	4.2	2150	4130	4.0
Silicon	mg/L	<20	<20	0.5	<20	<20	0.5
Sodium (Na)	mg/L	24,400	50,400	44.8	23,200	45,500	41.9
Sr	mg/L	466	975	0.7	451	881	0.7
Sulfate (SO_4)	mg/L	278	501	1.0	281	492	1.0
TDS	mg/L	82,600	174,000	390.0	80,400	162,000	380.0
TOC	mg/L	370	360	340.0	385	356	390.0
Total Suspended Solids (TSS)	mg/L	181	414	10.0	248	382	10.0
Zinc	mg/L	0.5	0.5	0.5	0.5	0.6	0.5

DocuSign Envelope ID: 2FA9A609-C360-4E53-8B28-BE8B77B6994A

After the completion of low-salinity feed testing, high-salinity brine was introduced for additional tests. Blended brine of 173,000 mg/L TDS was first concentrated to reach TDS in the concentrate of 228,000 mg/L, representing a 24.1% water recovery. As seen in Figure 43, the permeate flux remained constant at ~1.71 LMH with permeate conductivity of ~450 µS/cm for 20 hours of operation at this recovery. The pilot plant was then operated using the same inlet brine to reach a concentrate TDS of 246,000 mg/L, which corresponds to 29.2% water recovery. The concentrate conductivity was approximately 210 mS/cm, whereas the permeate conductivity was maintained at ~590 µS/cm, and the permeate flux remained constant at ~1.63 LMH for 30 hours of operation. After these 30 hours, pilot system operation was adjusted to achieve a concentrate TDS of 240,000 mg/L, which corresponds to 30.8% water recovery when using a feed brine with TDS of 166,000 mg/L. Permeate flux remained constant at ~1.49 LMH with conductivity of ~680 µS/cm for an additional 42 hours of operation. Brine feed and permeate flow rates corresponding to Figure 43 are shown in Figure 44.

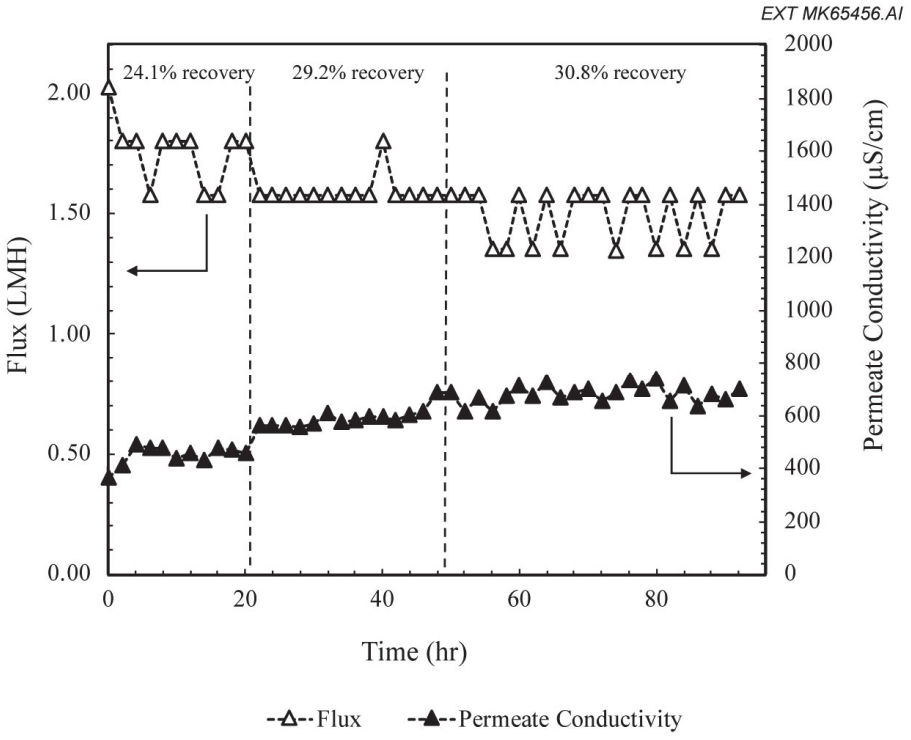


Figure 43. Permeate flux and conductivity for AGMD pilot testing with high-salinity brine.

DocuSign Envelope ID: 2FA9A609-C360-4E53-8B28-BE8B77B6994A

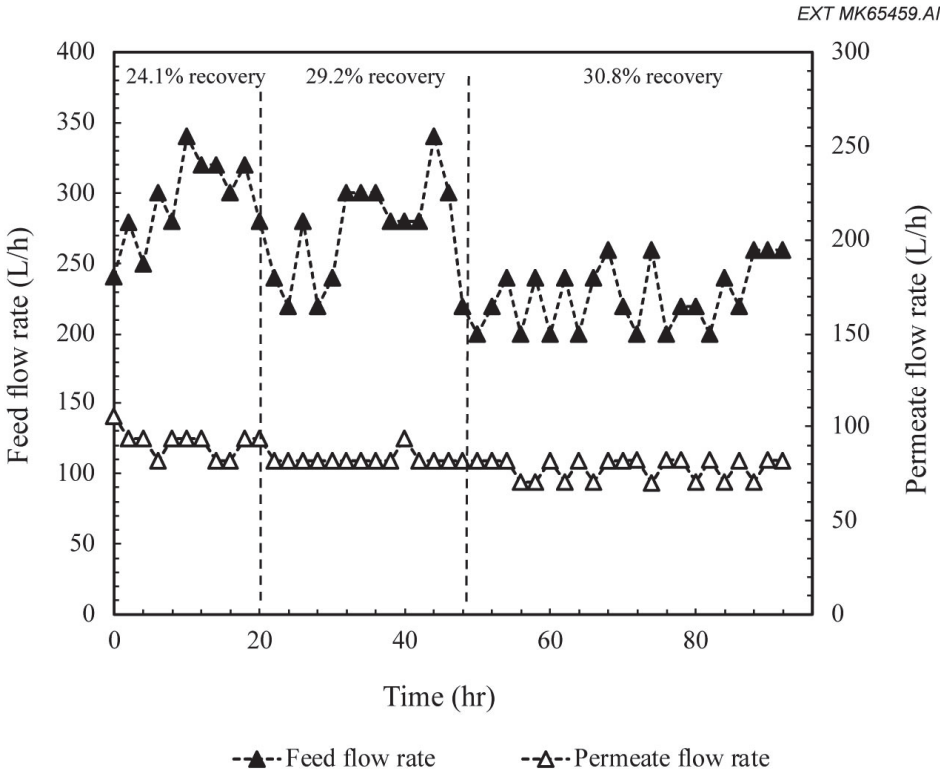


Figure 44. Brine feed and permeate flow rates during AGMD pilot testing with high-salinity brine.

Table 11 shows the analysis results of water samples collected during the high-salinity brine tests. During the first 20 hours, the feed TDS was 173,000 mg/L and permeate TDS was 410 mg/L, indicating 99.8% salt rejection. During the next 30 and 42 hours, permeate TDS was 460 and 510 mg/L, respectively, indicating 99.7% salt rejection. Similar to the first trial with low-salinity brine, passage of CO_2, NH_3, and volatile organics led to their respective concentrations in the permeate samples.

DocuSign Envelope ID: 2FA9A609-C360-4E53-8B28-BE8B77B6994A

Table 11. Stream Analysis for the AGMD Pilot Testing with High-Salinity Brine

		24.1% Water Recovery			29.2% Water Recovery			30.8% Water Recovery		
Parameter	**Units**	**Feed**	**Concentrate**	**Permeate**	**Feed**	**Concentrate**	**Permeate**	**Feed**	**Concentrate**	**Permeate**
Alkalinity as HCO_3^-	mg/L	710	776	0.0	601	731	0.0	612	724	0.0
Alkalinity as CO_3^{2-}	mg/L	582	0	51.3	0	0	64.6	0	0	54.4
Alkalinity as OH^-	mg/L	1570	0	38.5	0	0	29.9	0	0	27.5
Alkalinity as $CaCO_3$	mg/L	582	628	199.0	493	599	196.0	502	593	171.0
Ammonia	mg/L	1570	1980	71.0	1430	1900	64.6	1340	1880	108.0
Ba	mg/L	9	13	0.1	9	14	0.1	8	13	0.1
B	mg/L	370	438	3.7	350	459	4.0	340	454	4.8
Br	mg/L	619	783	1.0	611	835	1.0	561	834	1.0
Ca	mg/L	11,600	15,300	10.8	11,400	17,100	14.8	11,500	163	16.3
Cl	mg/L	103,000	135,000	130.0	104,000	144,000	165.0	97,600	143,000	181.0
Co	mg/L	<1.0	<1.0	0.1	<1.0	<1.0	0.1	<1.0	<1.0	0.1
Conductivity	µS/cm	196,000	221,000	544.0	196,000	226,000	655.0	195,000	227,000	715.0
Density	g/cm^3	1.1	1.2	1.0	1.1	1.2	1.0	1.1	1.2	1.0
Iron	mg/L	1.0	2.8	0.1	<1.0	<1.0	0.1	<1.0	<1.0	0.1
Li	mg/L	53	68	0.2	52	73	0.2	51	72	0.2
Mg	mg/L	731	972	0.9	730	1080	1.2	717	1030	1.3
Mn	mg/L	5.5	8.3	0.1	6.9	10.5	0.1	7.3	11.1	0.1
pH	–	7.4	7.1	9.6	7.4	7.0	9.7	7.4	6.9	9.6
K	mg/L	4660	6060	6.2	4620	6680	7.7	4520	6470	8.5
Silicon	mg/L	<20	<20	0.5	<20	<20	0.5	<20	<20	0.5
Na	mg/L	49,300	64,800	64.5	48,600	71,400	80.7	47,800	68,100	88.8
Sr	mg/L	941	1,310	0.9	973	1430	1.2	977	1350	1.4
SO_4	mg/L	315	392	1.0	334	418	1.0	301	413	1.0
TDS	mg/L	173,000	228,000	410.0	174,000	246,000	460.0	166,000	240,000	510.0
TOC	mg/L	840	692	1,240.0	900	758	1,220.0	800	686	1,050.0
TSS	mg/L	482	828	10.0	615	945	10.0	533	609	10.0
Zinc	mg/L	0.5	0.7	0.5	0.5	1.0	0.5	0.5	0.8	0.5

DocuSign Envelope ID: 2FA9A609-C360-4E53-8B28-BE8B77B6994A

Techno-Economic Analysis

Results from pilot-scale testing were used to estimate brine treatment costs using AGMD for the as-tested system and to justify the treatment cost potential for an optimized full-scale plant that can be compared to existing alternatives like MVR, MSFD, and/or MED. Analysis of pilot data resulted in process thermal efficiencies from 47% up to 59% for the various test conditions of brine salinity and water recovery. These values fell short of the design thermal efficiency of 76%, and in general, efficiency was sensitive to the amount of water recovery, with efficiency decreasing as recovery was increased. This trend is visible for the as-tested AGMD treatment costs presented in Figure 45, i.e., treatment costs increase with water recovery due, in part, to lower thermal efficiency. The pilot-scale treatment costs were based on the capital expense for the pilot system and the measured energy consumption at the BEST facility. Electricity was the operational energy source for the pilot system, and energy cost calculations assumed a rate of $0.069/kWh.

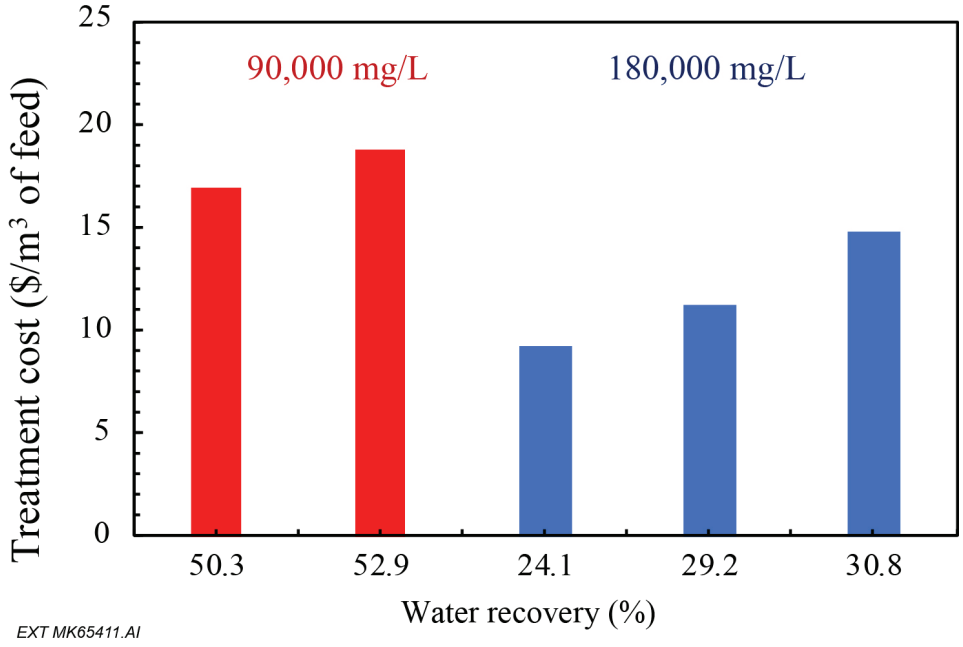


Figure 45. Estimated brine treatment costs for as-tested AGMD pilot system.

Treatment cost estimates were also prepared for an optimized, full-scale plant based on AGMD that was designed to treat 500 gpm of high-salinity (i.e., TDS ~180,000 mg/L) brine feed with 35% permeate water recovery. Performance of the full-scale plant was estimated using process models developed by the University of Pittsburgh. Treatment cost estimates were found to be sensitive to various operating parameters like hot channel inlet temperature and water recovery percentage as well as energy cost i.e., for steam and electricity, and equipment parameters, e.g., membrane cost, membrane permeability coefficient, and membrane gap size.

DocuSign Envelope ID: 2FA9A609-C360-4E53-8B28-BE8B77B6994A

Full-scale treatment costs are presented in Figure 46 for the parameters of hot channel inlet temperature and water recovery. As shown in the figure, costs for full-scale AGMD treatment were estimated to be significantly lower than those calculated for the as-tested pilot system. Key reasons for the cost reduction are attributed to the following: 1) the pilot system used an oversized chiller and heater, 2) the pilot system used electricity as the heating source as opposed to steam, and 3) the full-scale system design was highly optimized compared to the pilot-scale system.

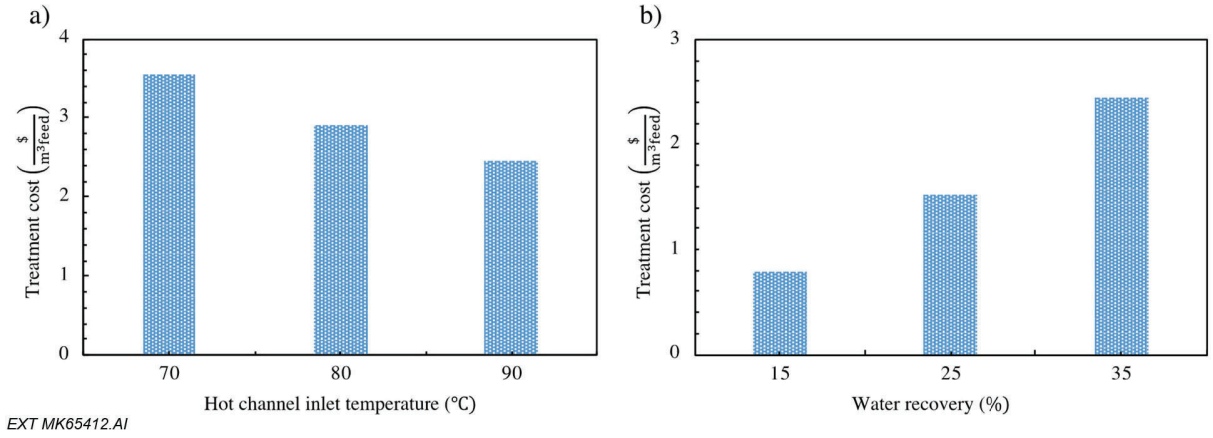


Figure 46. Estimated brine treatment costs for a full-scale AGMD system as a function of a) brine heating temperature and b) permeate water recovery.

Discussion and Conclusions

The membrane distillation process developed by the University of Pittsburgh was able to successfully extract reusable water from high-TDS brines typical of geologic sources, both in the laboratory and at the BEST field site. Laboratory-scale studies showed that DCMD can be used to recover 50% and 30% of high-quality permeate from the low- and high-salinity brines, respectively. At pilot scale, steady-state AGMD treatment of low-salinity brine was conducted for 72 hours while recovering 52.9% and 50.3% of high-quality permeate suitable for industrial or agricultural use. Further, high-salinity brine with ~170,000 mg/L TDS was concentrated with AGMD to recover 24.1%, 29.2%, and 30.8% of permeate water over a total period of 92 hours.

For each brine salinity level that was tested at pilot scale, permeate flux decreased with each increase in water recovery; however, permeate flux remained constant during each test period to suggest that no significant membrane degradation occurred during the test period. Ion rejection in the permeate generally exceeded 99.7% for all AGMD testing, but membrane distillation allowed the passage of volatile species, including alkalinity, ammonia, and TOC. The presence of these impurities in the permeate stream may be acceptable or may necessitate polishing water treatment, depending on the downstream application.

DocuSign Envelope ID: 2FA9A609-C360-4E53-8B28-BE8B77B6994A

While the pilot-scale testing showed promising trends with respect to membrane life, these components can experience wear and tear due to continuous use as well as scaling and fouling when treating high-salinity brines. Thus membrane modules might require cleaning at regular intervals and replacement in case of leakage or physical damage. Therefore, future evaluation of brine treatment with membrane distillation should involve larger-capacity and longer-duration pilot studies to refine these operational cost estimates. Additionally, scaled-up pilot equipment should incorporate more of the design optimizations identified by the research team to validate assumptions about their techno-economic impact.

SCWD Technology

Introduction and Background

The EERC facilitated a demonstration test with Ohio University to evaluate a pilot-scale version of its developed technology. The objective of this work was to field-test Ohio University's novel SCWD reactor on highly saline water containing TDS levels 90,000 mg/L and greater. Field testing was intended to accomplish two goals: 1) determine desalination performance capabilities and 2) establish energy input requirements per unit of "clean" water product for comparison with other technologies tested.

Description of Technology

SCWD systems, like the other technologies tested, receive a high-TDS brine and produce a highly concentrated condensate and a low-TDS permeate. Ohio University has developed a novel SCWD reactor based on a Joule heating design. Most reactors of this design rely on external heating whereas the Ohio University reactor utilizes internal heating by applying AC directly to the conductive brine itself, resulting in a lower-TDS vapor product (sometimes referred to as permeate) and a concentrated TDS liquid product (sometimes referred to as concentrate). Figure 47 provides a reactor cross section to aid in understanding how internal Joule heating is accomplished. A more detailed description of the reactor can be found on pages 2 and 3 of the final technical report provided by Ohio University in Appendix H.

Laboratory-Scale Testing

Ohio University performed several tests of the SCWD system at its laboratory in Athens, Ohio. These tests are summarized in this report, and a detailed narrative can be found in the final technical report provided by Ohio University included in Appendix H.

The purpose of these experiments was to evaluate the ability to employ direct electrical heating of highly saline waters and develop information regarding thermodynamic properties associated with multicomponent dissolved solids brines.

Initial testing consisted of treating two synthetic multicomponent brines of different TDS concentrations (50,000 and 180,000 mg/L) at three pressures (230, 250, and 280 bar) for a minimum of 90 minutes for each test. Each test was operated at a constant inlet flow rate of 100 mL/minute.

DocuSign Envelope ID: 2FA9A609-C360-4E53-8B28-BE8B77B6994A

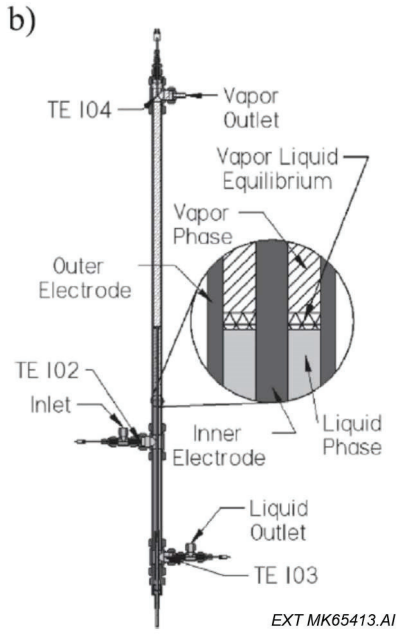


Figure 47. Cross-sectional view of Ohio Joule-heated reactor.

The natural produced waters targeted for this research are NaCl-dominant. To maintain consistency and component ratios, Na was introduced using Na carbonate, $NaSO_4$, and NaCl, while Cl was introduced using CaCl, BaCl, SrCl, and NaCl.

In addition, testing modeling was also completed on synthetic brines consisting of only Na and Cl at TDS concentrations of 50,000 and 180,000 mg/L and 250 bar pressure. These results were used for comparison with previous research of others.

In a second series of tests, the desalination system was tested on produced water from the Utica–Point Pleasant shale formation (UPP). To allow comparison with previous testing, the UPP produced water, with an initial TDS concentration of 255,000 mg/L, was diluted with DI water to a TDS concentration of 180,000 mg/L and the system was operated at pressures of 230 and 250 bar.

Results and Discussion

The Ohio University desalination system produces two outlet streams; a low-TDS vapor stream is recovered from the top of the reactor and a concentrated liquid stream exits the bottom. The Ohio University desalination system showed good results related to the removal of TDS from the inlet brine. Removal efficiencies for the various brines and operational parameters ranged from 95% to 99%, resulting in a water vapor product with TDS concentrations between 600 and 2800 mg/L and water vapor recovery rates ranging from 20% to 40% by volume. Results of laboratory trials, specifically TDS concentration results, are shown in Table 12.

DocuSign Envelope ID: 2FA9A609-C360-4E53-8B28-BE8B77B6994A

Table 12. SCWD Laboratory Testing Results

	Inlet TDS, mg/L	Outlet Vapor TDS, mg/L	TDS Removal Efficiency, %
NaCl, 250 bar	60,693	2011	96.6
Multicomponent, 230 bar	41,639	655	98.4
Multicomponent, 250 bar	44,262	1240	97.2
Multicomponent, 280 bar	59,130	2836	95.2
UPP, 230 bar	178,014	609	99.7
UPP, 250 bar	179,910	1175	99.4

Field-Scale Testing

Ohio University delivered and set up its SCWD system at the EERC's BEST facility with the intent to perform a series of tests on two brines (≈90,000 mg/L TDS and ≈180,000 mg/L TDS) at various recovery rates. System operation was performed the same as previous laboratory testing, and a summary of the testing parameters is shown in Table 13.

Table 13. Summary of SCWD Testing Parameters

Test Number	Inlet Brine Concentration, mg/L	Inlet Flow Rate, cm^3/min	Permeate Recovery Rate, %
1	82,500	100	50
	82,300	100	50
	81,500	100	50
2	173,000	100	34
	173,000	100	34
3	172,000	70	40
4	173,000	70	50

After 1 day of setup and shakedown activities and approximately 4 hours of warm-up, a series of steady-state tests was performed. Test 1 operated for approximately 18 hours at an inlet flow rate of 100 cubic centimeters per minute (cm^3/min) and a permeate recovery rate of 50%. Test 2 was a 17.5-hour test at the same parameters as Test 1 except the higher inlet brine concentration. Test 3 was another high-TDS test lasting for approximately 18 hours and at inlet flow rate of 70 cm^3/min and a recovery rate of 40%. Test 4 was the same as Test 3 with an attempt at a 50% permeate recovery rate, and it lasted for only 2 hours. Photographs of the field-based testing are shown in Figures 48 and 49.

Results and Discussion

A summary of the field testing results is provided here, and a more detailed description can be found in the December 20, 2021, final technical report provided by Ohio University included in Appendix H. Generally speaking, the Ohio desalination system performance in the field was consistent with the laboratory performance.

DocuSign Envelope ID: 2FA9A609-C360-4E53-8B28-BE8B77B6994A



Figure 48. Photograph of testing at EERC BEST facility.



Figure 49. Photograph of testing unit operation at EERC BEST facility.

System performance during field operations with Williston Basin brines was similar to system performance in the laboratory with various natural and synthetic brines. Water recovery rates ranged from 30% to 50% and had an average TDS concentration of 1430 mg/L, which is a 99.2% ion rejection. A complete listing of the system chemistry for each test is provided in Tables 14–17.

DocuSign Envelope ID: 2FA9A609-C360-4E53-8B28-BE8B77B6994A

Table 14. Test 1 (Samples 1, 2, and 3)

Parameter	Unit	Inlet Brine	Outlet Concentrate	Outlet Permeate
TDS	mg/L	82,100	138,667	1213
Conductivity at 25°C	µS/cm	122,333	180,667	2390
pH		6.46	6.92	8.77
Na	mg/L	23,500	38,833	58.2
Ca	mg/L	5573	9217	16.3
Mg	mg/L	342	569	2.1
Sr	mg/L	458	761	0.89
K	mg/L	2157	3573	3.8
Mn	mg/L	<0.5	569	<0.1
B	mg/L	382	1830	57.7
Ba	mg/L	4.3	7.0	<0.05
Li	mg/L	21.1	37.6	<0.2
Cl	mg/L	48,300	82,367	366
Br	mg/L	247	418	1.1
SO_4	mg/L	299	177	<1.0

Table 15. Test 2 (Sample 4 and 5)

Parameter	Unit	Inlet Brine	Outlet Concentrate	Outlet Permeate
TDS	mg/L	173,000	261,000	1370
Conductivity at 25°C	µS/cm	200,000	249,000	3900
pH		4.17	5.84	7.39
Na	mg/L	48,000	71,850	75.4
Ca	mg/L	11,800	17,550	8.7
Mg	mg/L	723	1090	1.8
Sr	mg/L	983	1460	0.78
K	mg/L	4480	6780	5.4
Mn	mg/L	6.7	10.6	<0.1
B	mg/L	500	1495	96.6
Ba	mg/L	9.7	14.1	<0.05
Li	mg/L	50.5	64.7	<0.2
Cl	mg/L	104,000	166,000	711
Br	mg/L	539	877	1.2
SO_4	mg/L	314	301	<1.0

An increase in outlet concentration was observed in all tests except for Test 3 (Sample 6) where the constituents had a decrease from inlet brine to outlet concentration. This decrease in outlet concentration was because of sample collection occurring just after system maintenance where freshwater flushing was used to correct filter plugging. Subsequent sample collection and resulting analysis indicated a return to the normal increase in outlet concentration trend in relation to the inlet brine.

DocuSign Envelope ID: 2FA9A609-C360-4E53-8B28-BE8B77B6994A

Table 16. Test 3 (Sample 6)

Parameter	Unit	Inlet Brine	Outlet Concentrate	Outlet Permeate
TDS	mg/L	172,000	76,500	1480
Conductivity at 25°C	µS/cm	205,000	112,000	4040
pH		4.14	7.20	7.90
Na	mg/L	48,700	21,600	48.6
Ca	mg/L	11,800	5320	11.1
Mg	mg/L	741	346	4.5
Sr	mg/L	993	436	1.3
K	mg/L	4580	2050	4.6
Mn	mg/L	6.8	3.3	<0.1
B	mg/L	486	1080	106
Ba	mg/L	9.7	4.2	<0.05
Li	mg/L	49.5	19.5	<0.2
Cl	mg/L	103,000	43,300	676
Br	mg/L	529	231	5.9
SO_4	mg/L	314	642	<1.0

Table 17. Test 4 (Sample 7)

Parameter	Unit	Inlet Brine	Outlet Concentrate	Outlet Permeate
TDS	mg/L	173,000	277,000	1660
Conductivity at 25°C	µS/cm	206,000	252,000	4600
pH		4.15	5.63	7.65
Na	mg/L	47,400	77,300	78.8
Ca	mg/L	11,700	19,000	11.2
Mg	mg/L	721	1170	2.0
Sr	mg/L	986	1550	0.95
K	mg/L	4560	7350	5.6
Mn	mg/L	6.7	11.5	0.12
B	mg/L	469	1240	119
Ba	mg/L	9.6	15.1	<0.05
Li	mg/L	49.2	68.4	<0.2
Cl	mg/L	105,000	166,000	912
Br	mg/L	535	884	1.8
SO_4	mg/L	324	309	<1.0

Lessons Learned

In their report, Ohio University staff noted a few areas where lessons were learned from operating the desalination system in the field:

- Desalination shipping: Since the desalination system was built for operation in a laboratory, it lacked the supports to adequately secure piping during transport. Although the lack of supports did not result in any breakage, it did result in the loosening of connections and subsequent leaks during start-up.

DocuSign Envelope ID: 2FA9A609-C360-4E53-8B28-BE8B77B6994A

- Supply chain: Because COVID-19 components made of specialized material were either unavailable or significantly delayed, resulting in the use of components made of less than desirable material.

- Operation of the desalination system in the field took place as expected with the exception of unexpected clogging of inlet and outlet filters. Adjustments to the inlet brine chemistry were made to mitigate the issue.

Techno-Economic Assessment

Beyond performance verification, the goal of the field testing was to determine energy intensity of the current system and utilize those data to calculate the energy intensity associated with a 100-gallon-per-minute-scale system. Ohio University used a combination of previous system operation in the laboratory, modeling with Aspen Plus software, and field observations at the BEST facility in North Dakota.

Three components are responsible for system electrical demand: pump, preheater, and desalinator. The pump demand was minimal, representing only 1%–2%. The preheater demand ranged from 49% to 79%, while the desalinator was responsible for between 24% and 44%. Based on the data collected from the various tests performed at the BEST facility, summarized in Table 18, the energy intensity ranged from 50 to 91 kWh per barrel (bbl). For the purposes of this report, energy intensity is defined as the quantity of energy used to produce a unit of treated water vapor.

Table 18. Operational Parameters for Testing Conditions

Inlet Concentration, mg/L	Operating Pressure, bar	Pump Power, kW	Preheater Power, kW	Desalinator, kW	Total Power, kW
90	190	136	4303	2797–4397	7236–8836
180	190	136	6732	1694–2723	8564–9593
180	250	182	6692	2118–3404	8992–10,278
180	280	205	9240	2206–3546	11,650–12,990

ZMD Technology

Introduction and Background

The EERC facilitated testing of a zeolite membrane-based dewatering system developed by the University of Kentucky for treating high-TDS brines that are typical of produced water from deep geologic sources. Testing was conducted at the EERC's BEST facility near Watford City, North Dakota. The goal of the technology demonstration was to conduct an evaluation of the University of Kentucky's bench-scale membrane system, which was scaled up from laboratory-scale validation testing that was previously conducted by the University of Kentucky. Relevant results from the laboratory evaluation are included in this field-testing summary since they are useful for understanding the performance observed at the BEST facility. Information for this

DocuSign Envelope ID: 2FA9A609-C360-4E53-8B28-BE8B77B6994A

summary, including the data and figures, was primarily drawn from the final technical report provided by the University of Kentucky to the EERC, which is included in its entirety in Appendix I.

Description of Technology

The dewatering system developed by the University of Kentucky uses zeolite membranes supported on a porous alumina substrate to separate water from high-concentration and hypersaline feed streams. Because of their high salt and TDS content, these streams have high osmotic pressure that exceeds the separation capacity of existing polymeric membranes used for conventional RO treatment of lower-salinity water sources like seawater. RO membranes are also susceptible to fouling and can pass low-molecular-weight organic compounds that might be found in some produced water sources. Zeolite membranes, in comparison, resist fouling and have pore sizes defined by their crystal lattice structure to result in high selectivity regarding which molecules are allowed to pass. The University of Kentucky's system is based on faujasite (FAU) zeolite membranes with a 0.74-nm pore size, which is larger than the size of a water molecule at 0.27 nm but approximately the same size or smaller than a range of hydrated ions having sizes of 0.66 to 0.82 nm.

The zeolite dewatering concept is diagrammed in Figure 50, which shows a crossflow of feed brine on the zeolite face of the membrane with water adsorption and transport through the zeolite and porous support layers that form a water permeate stream leaving the membrane's inner surface. The zeolite membranes were operated at transmembrane pressures less than 200 psig and temperatures less than 120°C. The University of Kentucky claims that the preferential solubility of water at the elevated temperature and pressure in the membrane matrix facilitates water transport across the membrane and flux is a function of the applied pressure and temperature. The brine feed

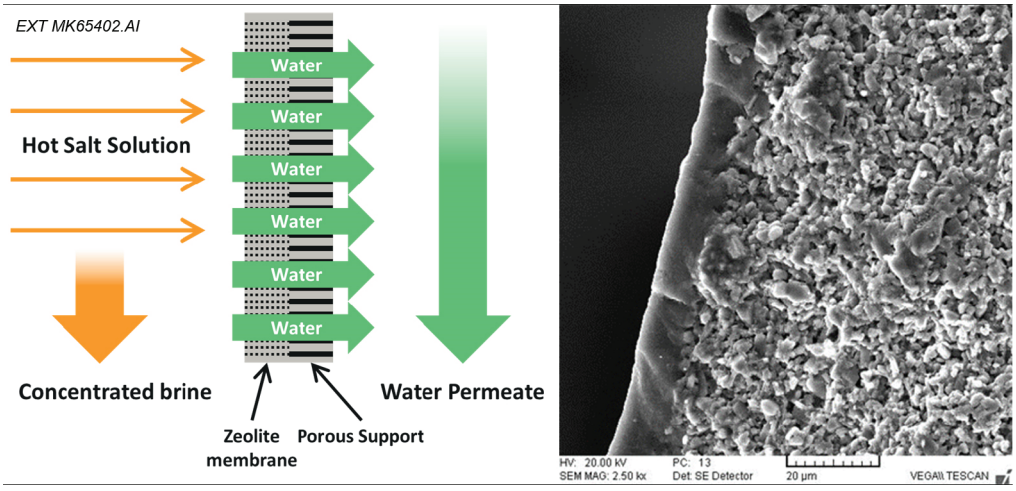


Figure 50. Schematic diagram of zeolite dewatering process (left) and scanning electron microscope (SEM) image of membrane cross-section morphology (right). In the SEM image, the zeolite is the dense layer on the left, outer surface and is layered on the more porous alumina support.

DocuSign Envelope ID: 2FA9A609-C360-4E53-8B28-BE8B77B6994A

is pressurized to produce the transmembrane pressure needed to prevent brine vaporization. Permeate pressure is not specified, but a temperature drop across the membrane allows permeate recovery in the liquid phase but suggests permeate temperature beyond the boiling point may yet result in the vaporization of the permeate stream.

The University of Kentucky zeolite dewatering system appears conceptually similar to the process of pervaporation, where a semipermeable membrane is used to separate a volatile product from a potentially volatile solvent on the feed side and where the transport gradient for moving product across the membrane is created by evaporating product from the permeate side of the membrane. Pervaporation is used for separating mixtures that form an azeotrope that limits the maximum product purity achievable in a single-stage distillation column. According to the University of Kentucky, the process avoids the need for vacuum pumping and employs preferential water dissolution under pressurized moderate-temperature operation to prevent permeate contamination with other volatile species, particularly organic compounds, that might be present in the brine feed.

The specific energy consumption for zeolite dewatering provided by the University of Kentucky was less than 10 kWh/m^3 of recovered water. Presumably, this was a combined thermal and mechanical energy demand (i.e., brine sensible heating and pumping to operating pressure) since the stated assumptions included a 5°C sensible heating load and approximately 60% water recovery. The University of Kentucky acknowledges that sufficient water recovery, good thermal energy management, and heat recovery are required to achieve this metric. In pervaporation, permeate product evaporation is commonly assisted by drawing a vacuum on the permeate membrane side to lower the vaporization temperature of the product, but that feature was not needed as part of the University of Kentucky's test systems.

Description of Testing

Testing details are provided for each of the three sets of test results that are summarized: 1) laboratory-scale test setup for individual membrane elements, 2) a bench-scale test stand for testing multielement modules, and 3) a field skid for testing multielement membrane modules at the BEST facility.

Membrane-dewatering performance was assessed using the parameters of membrane flux, J (in kg/m^2/hr), rejection rate, R (%), and water recovery, WR (%), as defined in Equations 3, 4, and 5, respectively.

$$J = m_p / At \qquad \text{[Eq. 3]}$$

$$R = (C_f - C_p) / C_f \qquad \text{[Eq. 4]}$$

$$WR = V_p / V_f \qquad \text{[Eq. 5]}$$

In the equations, m_p represents the weight of permeate solution through the membrane (kg), A is the effective membrane area (m^2), and t refers to the operation time (hr). C_f and C_p represent the conductivity of the feed and permeate solutions, respectively. Rejection rate was also computed

DocuSign Envelope ID: 2FA9A609-C360-4E53-8B28-BE8B77B6994A

based on the measured concentration of target compounds, e.g., TDS. V_f and V_p represent the volume of the feed and permeate solutions, respectively. Units used to calculate rejection rate and water recovery need only to be consistent since those results were only presented as a ratio.

Laboratory Membrane Element Testing

The laboratory-scale membrane test system at the University of Kentucky comprised a solution reservoir, pump, heating element, single-cell membrane cell, and permeate sample collector (Figure 51). During system operation, the feed solution, e.g., synthetic brine solution or an EERC-provided water blend, was fed into the system via the pump. The water was heated to operating temperature using a resistive thermal element and passed through the membrane module where treated water permeated the membrane while the dissolved ions and other solids exited the feed compartment as retentate. The permeate stream was cooled and collected separately; samples were periodically taken and analyzed to compute rejection rate, membrane flux, and water recovery. The retentate was cooled down and circulated back to the solution reservoir. The feed solution could be replaced with DI water for cleaning and maintenance. The laboratory setup allowed testing a range of water recovery conditions, including low recovery during a single-pass treatment to higher recoveries that increase retentate concentration effects like concentration polarization.

Laboratory dewatering was conducted at temperatures ranging from 80° to 120°C, while the pressure of the feed side was adjusted with a back-pressure regulator to 50–100 psig, such that the feed brine and retentate remained in the liquid phase in the membrane module. For example, at a pressure of 40 psia, the boiling point of water is elevated to 131°C. Furthermore, colligative properties of the concentrated brines further elevate the boiling point above that of pure water.

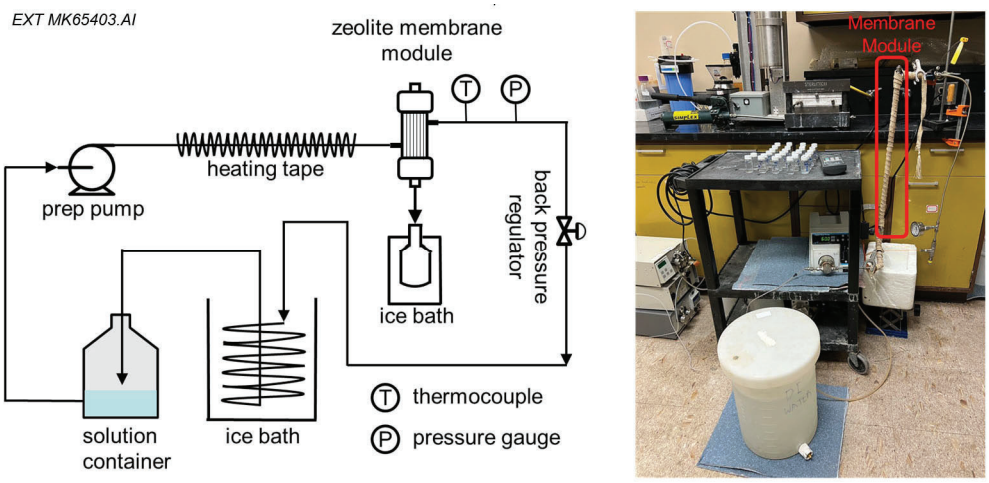


Figure 51. Schematic diagram and photograph of the University of Kentucky's laboratory performance evaluation system for zeolite membranes.

DocuSign Envelope ID: 2FA9A609-C360-4E53-8B28-BE8B77B6994A

Bench-Scale Test Stand for Multielement Modules

Laboratory evaluation results for two zeolite membrane materials were provided by the University of Kentucky: FAU zeolite membranes developed by the University of Kentucky and commercially available zeolite membranes from Hitachi Zosen Corporation (HZM membranes). The University of Kentucky membranes were previously developed and evaluated for dewatering carbon-rich amine solvents and flue gas desulfurization wastewater. The commercial HZM membranes conform to the manufacturer's specifications and have a proven track record in industrial applications.

The bench-scale test stand developed by the University of Kentucky was used to test multielement membrane modules that form the basis for scaling up the technology to higher water throughputs. Modules for both membranes (University of Kentucky and HZM) were composed of individual tubular membrane elements sealed together in a manifold at one end and individually capped at the other. Membrane elements for the University of Kentucky FAU membranes had an inner diameter of 2.9 mm, an outer diameter of 5.7 mm, and were 75 cm long. The University of Kentucky membrane module, Figure 52, comprised 19 individual elements with an approximate total membrane area of 0.26 m^2 and a packing density of 250 m^2/m^3. The manifold end of these elements was sealed together in a "puck" manifold made from garolite. The commercial alternative HZM membranes had an inner diameter of 11.2 mm, an outer diameter of 16.3 mm, and were 113 cm long. The HZM membrane module, Figure 53, comprised six HZM elements for an approximate total membrane surface of 0.31 m^2. In contrast to the University of Kentucky membranes, the HZM membranes possessed a solid tube surface at the manifold end that was suitable for sealing with compression-style tube fittings. As a result of this difference, the manifold for the HZM membrane elements was sealed using individual compression fittings instead of the monolithic puck approach used for the University of Kentucky FAU membrane module.

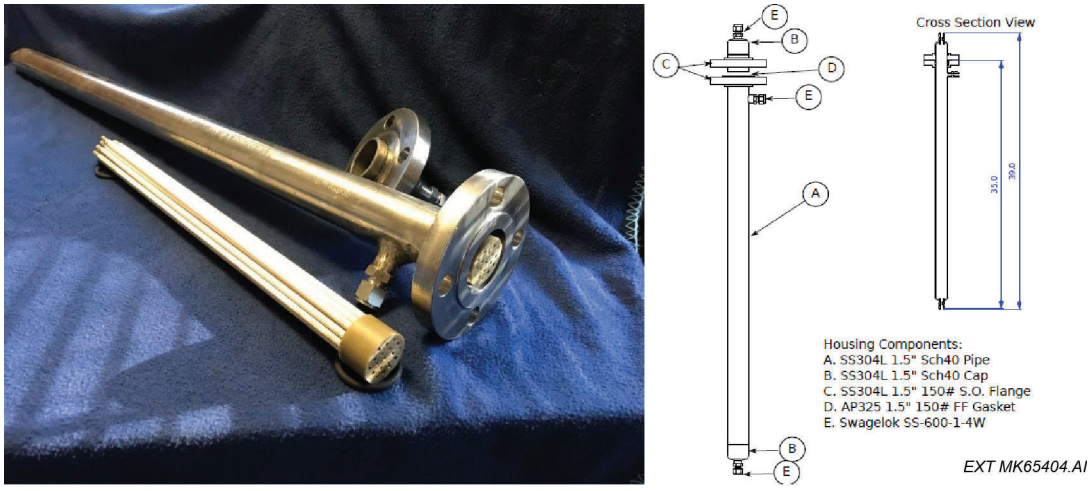


Figure 52. Bench-scale membrane module for University of Kentucky FAU zeolite membrane elements.

DocuSign Envelope ID: 2FA9A609-C360-4E53-8B28-BE8B77B6994A

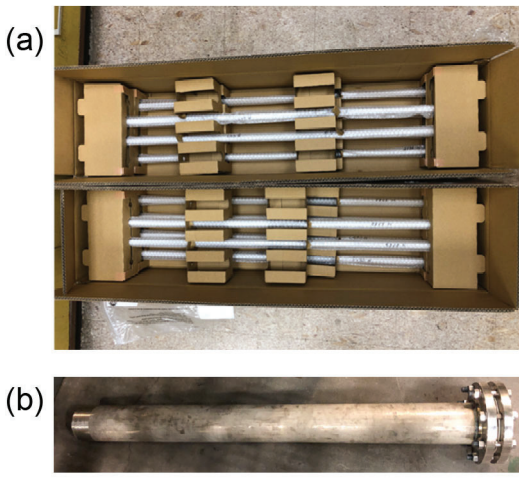


Figure 53. Images of membrane and membrane modules.

The bench-scale test stand is detailed in Figure 54; it could test the University of Kentucky zeolite or HZM membrane modules. During operation, the feedwater was circulated at a constant flow rate up to a maximum of 1.4 gal/min. Feed brine heating took place in a pressurized, 10-gallon heating vessel using immersion heating elements. The heating pressure vessel was designed to withstand temperatures up to 232°C and pressures up to 200 psig. Membrane module retentate pressure was controlled via a back-pressure control regulator, and heating control used a feedback temperature controller. Permeate was collected in sample containers and analyzed for dissolved solids content and composition to quantify membrane performance.

DocuSign Envelope ID: 2FA9A609-C360-4E53-8B28-BE8B77B6994A

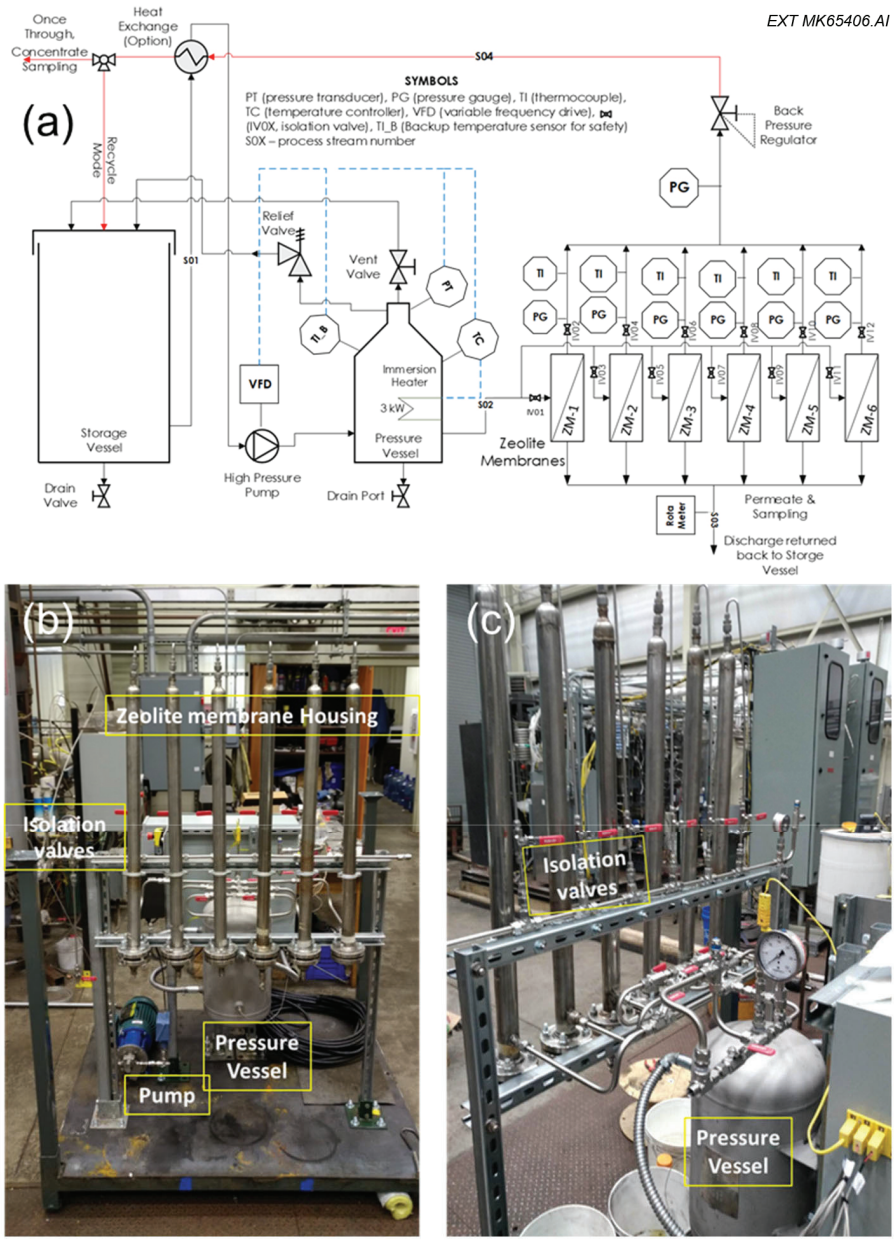


Figure 54. Process flow diagram for zeolite dewatering system (a) and photographs of system (b and c). It should be noted that insulation normally surrounding the membranes is not shown in the photos.

Field Skid for BEST Facility Testing

The University of Kentucky created a transportable test system for evaluation at the BEST facility (Figure 55). Its design and operation mimicked that of the bench-scale system described above. The unit was transported to the EERC's BEST facility near Watford City, North Dakota, in 2022. After a period of equipment setup, the University of Kentucky field skid was tested on November 7, 2022.

DocuSign Envelope ID: 2FA9A609-C360-4E53-8B28-BE8B77B6994A



Figure 55. University of Kentucky zeolite dewatering system set up for field testing at the BEST facility.

Results

The University of Kentucky provided laboratory-scale validation data for both its FAU zeolite membrane and HZM. Test solutions included NaCl brine at various concentrations (as a synthetic produced water) and blended water provided by the EERC that had approximately 170,000 ppm TDS. Key laboratory evaluation results are summarized in Figures 56 and 57.

While the laboratory-scale test conditions in Figures 56 and 57 are not directly comparable across the two membranes, key takeaways from these tests include the following:

- There was a noticeable reduction in permeate flux between the NaCl brine and the EERC-blended water sample for both membranes. A definitive cause cannot be assigned since more than one key test parameter was changed between the simulant and EERC blend tests, e.g., TDS level and its chemical composition. However, results with the HZM element suggest that the more complex chemical composition of the EERC-blended water sample was the critical parameter instead of the absolute TDS level.

DocuSign Envelope ID: 2FA9A609-C360-4E53-8B28-BE8B77B6994A

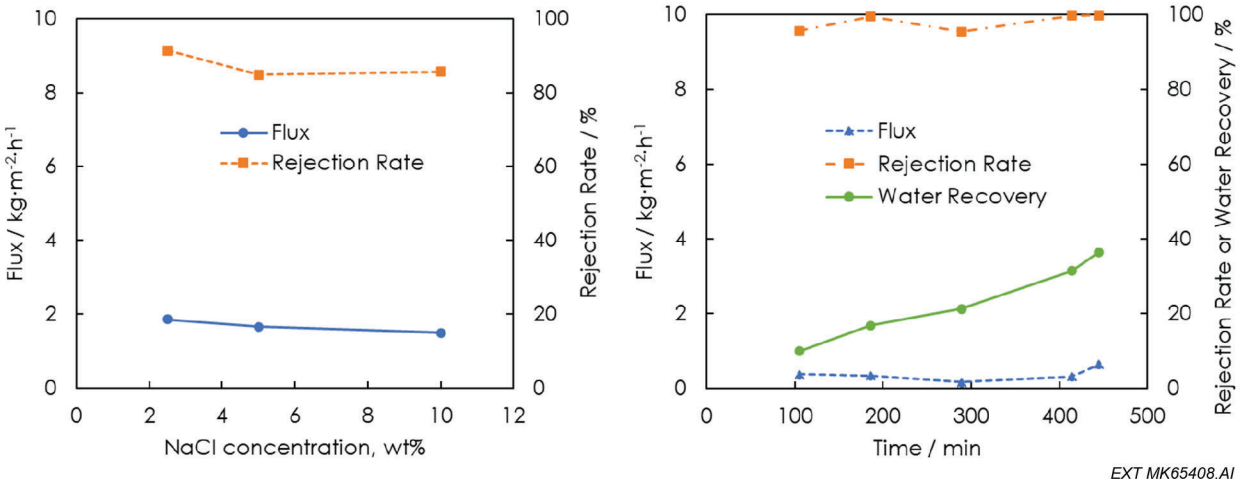


Figure 56. Laboratory-scale evaluation results for University of Kentucky membrane element: NaCl brine test results with varying brine concentrations at 115°C and 50 psig (left) and EERC-blended water batch test at 108°C and 50 psig (right).

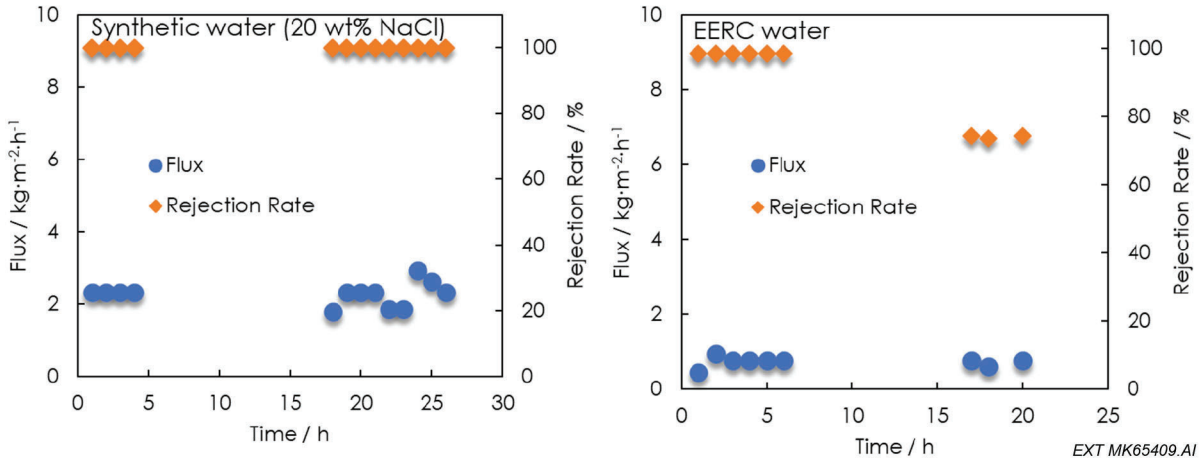


Figure 57. Laboratory-scale evaluation results for HZM element: 20 wt% NaCl brine at 120°C and 100 psig (left) and EERC-blended water at 120°C and 100 psig (right).

- Permeate flux levels were of the same order of magnitude for both membranes, and both were relatively stable during the course of testing. The University of Kentucky membrane produced about 0.4 kg/m^2/hr of permeate from the blended water sample, compared to 0.74 kg/m^2/hr for the HZM element when processing the same EERC-blended water. It should be noted that this is also a case where other parameters were not held constant, and the higher temperature of the HZM test (120° vs. 108°C) and/or higher pressure (100 vs. 50 psig) may have also impacted permeate flux.

DocuSign Envelope ID: 2FA9A609-C360-4E53-8B28-BE8B77B6994A

- Permeate quality for both membranes was good and generally exceeded a 90% conductivity-based rejection rate on average. Further, rejection of TOC in the blended water sample (706 mg/L inlet TOC concentration) was determined to be more than 96% for the University of Kentucky membrane.

During the development and testing of the membrane modules, the University of Kentucky experienced challenges with respect to the fragility of the membrane elements and the mechanical design of one of the membrane modules. Elements made of both membranes, the University of Kentucky's FAU and HZM, were fragile and some were broken, requiring repairs and/or plugging broken membrane tubes to proceed. Accessing elements that were centrally located in the tube bundle was difficult for the University of Kentucky module since the membrane elements could not be individually separated from the molded puck manifold. Sealing around the circumference of the puck also presented challenges that resulted in contamination of the permeate from feed brine leaking around the outer edge of the puck. Given these issues with the University of Kentucky module's operation, the University of Kentucky proceeded on with field testing using the HZM module since its design used tube compression fittings for sealing and it allowed individual membrane element replacement. The resulting HZM module underwent bench-scale validation testing, and results were similar to those reported for the individual element tests.

Field testing of the HZM module took place on November 7, 2022, at the BEST facility using a flow of blended produced water with a TDS concentration of approximately 150,000 mg/L. Feedwater flow rate was approximately 0.1 L/min for this test, and feed pressure was 50 psig. Feed temperature was ramped to an approximate operating range of 90° to 100°C, as shown in Figure 58(a). Permeate flow began after reaching operating temperature, and the measured permeate flux during this period, Figure 58(d), agreed well with those observed by the University of Kentucky during laboratory- and bench-scale evaluations. Similarly, the rejection rate for this period was good and the rejection rate based on ongoing conductivity monitoring exceeded 95%, Figure 58(b).

DocuSign Envelope ID: 2FA9A609-C360-4E53-8B28-BE8B77B6994A

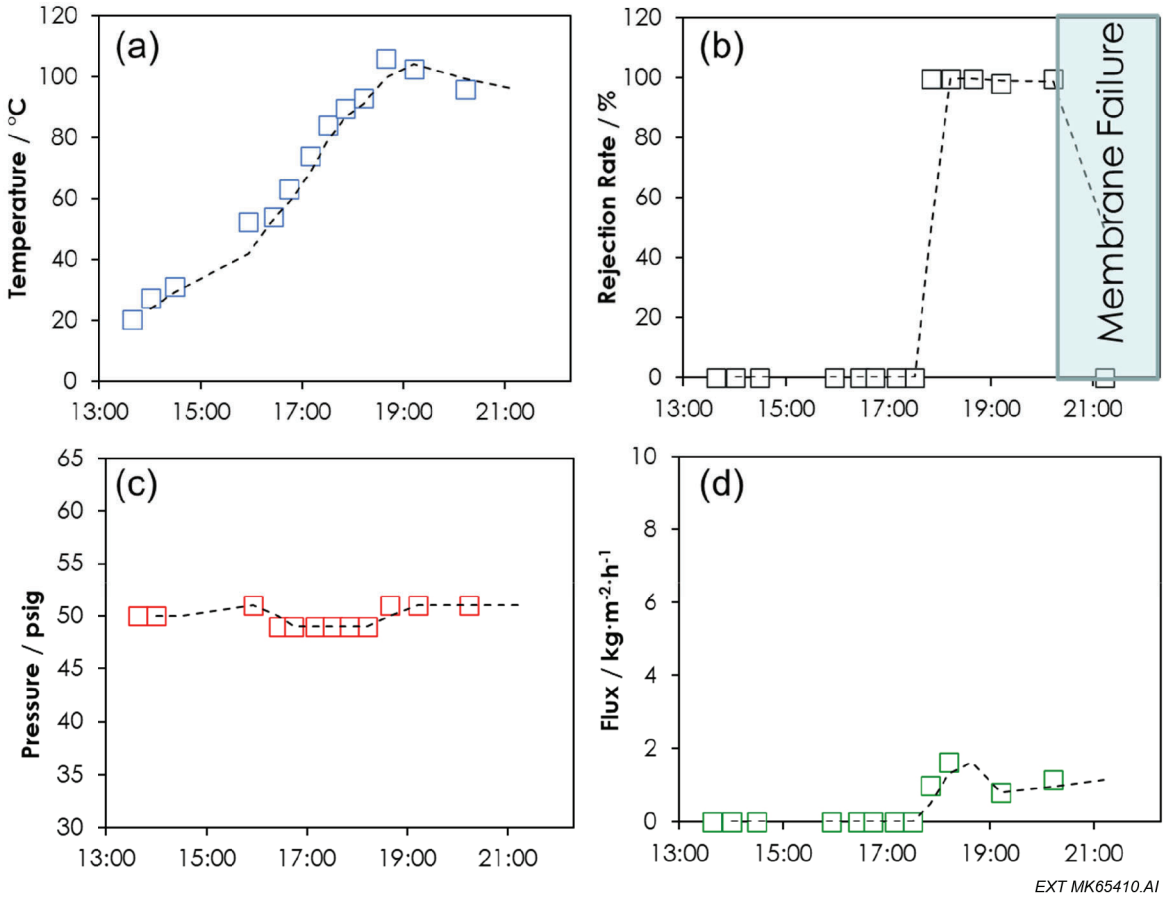


Figure 58. Results of HZM module field test versus time: a) temperature of membrane module, b) conductivity-based rejection rate, c) module feed pressure, and d) permeate flux.

After approximately 2 hours of operation at temperature, a previous membrane tube repair began leaking that allowed untreated brine to contaminate the permeate and significantly reduce the apparent rejection rate, Figure 9(b). Unfortunately, this problem was not recognized until after samples were collected for quantitative chemical analysis, and the module was not yet at optimal water recovery conditions. These analyses for the feed, concentrate (retentate), and permeate streams are provided in Table 19. Because of the leak and permeate contamination, these results indicate a poor rejection rate of 20% to 30% based on TDS and TOC concentration values.

Energy consumption of the field unit was recorded by the BEST facility data acquisition system, and the results are provided in Table 20. During the 2-hour test period between 19:00 and 21:00 hours, a total of 3.06 kWh was consumed and approximately 592 mL of permeate was recovered. These data result in a specific energy consumption of 5170 kWh/m^3 during the field test.

DocuSign Envelope ID: 2FA9A609-C360-4E53-8B28-BE8B77B6994A

Table 19. Field Test Stream Analyses After Permeate Contamination

Property	Feed	Concentrate	Permeate	Unit	Rejection, %	Concentration Factor, #
Alkalinity, as Bicarbonate (HCO_3^-)	385	384	278	mg/L	27.79	1.00
Alkalinity, as Carbonate (CO_3=)	0	0	0	mg/L		
Alkalinity, as OH^-	0	0	0	mg/L		
Alkalinity, Total as $CaCO_3$	316	314	228	mg/L	27.85	0.99
Ba	8.5	9.2	6.8	mg/L	20.00	1.08
B	248	268	202	mg/L	18.55	1.08
Br	467	523	381	mg/L	18.42	1.12
Ca	9960	11,200	7840	mg/L	21.29	1.12
Cl	89,500	100,000	72,500	mg/L	18.99	1.12
Co	1	1	1	mg/L	0.00	1.00
Conductivity at 25°C	184,000	193,000	154,000	uS/cm	16.30	1.05
Density	1.1	1.11	1.08	g/mL	1.82	1.01
Iron	1	1	1	mg/L	0.00	1.00
Li	31.1	34.4	24.4	mg/L	21.54	1.11
Mg	616	683	491	mg/L	20.29	1.11
Mn	5.3	5.9	4.3	mg/L	18.87	1.11
pH	7.36	7.2	7.45	pH	–1.22	0.98
K	3830	4230	3020	mg/L	21.15	1.10
Silicon	10	10	10	mg/L	0.00	1.00
Na	41,400	44,900	32,300	mg/L	21.98	1.08
Sr	833	917	656	mg/L	21.25	1.10
SO_4	219	205	174	mg/L	20.55	0.94
TDS	148,000	164,000	118,000	mg/L	20.27	1.11
TOC	674	841	470	mg/L	30.27	1.25
Zinc	0.55	1.1	0.75	mg/L	–36.36	2.00

Table 20. University of Kentucky Field Unit Energy Consumption for November 7, 2022

Test Duration, minutes	120
Total Energy Consumed, kWh	3.06
Total Permeate Volume, mL (m^3)	592 (0.00059)
Average Permeate Flow, mL/min (m^3/hr)	4.93 (0.00030)
Treatment Specific Energy Consumption, kWh/m^3	5170

Discussion and Conclusions

The zeolite membrane dewatering system developed by the University of Kentucky was shown to be effective for treating high-TDS blended water from the EERC's BEST facility. A salt rejection of over 95% was demonstrated by comparing the EC of the permeate to that of the feed brine. However, the brief extent of field testing was not sufficient to produce refined operational data that could be used to update techno-economic projections for the technology. Ultimately,

DocuSign Envelope ID: 2FA9A609-C360-4E53-8B28-BE8B77B6994A

testing ended because of mechanical failures associated with the fragile zeolite membrane elements.

The field unit tested at the BEST facility was more than 20 times the scale of the laboratory membrane testing reported by the University of Kentucky. Handling the larger zeolite membranes needed for this scale-up proved to be difficult and, so far, appears to be the key shortcoming of the approach. The University of Kentucky's initial attempt to modularize its in-house FAU zeolite membrane elements was unsuccessful because of the mechanical design of the puck-style manifold, which limited the ability to repair or service individual elements. The commercial HZM elements allowed the use of compression fittings in the University of Kentucky membrane housing, which resulted in a more serviceable manifold design; however, these elements were also very fragile and some were broken during shipment which necessitated repairs that led to a critical failure during the field test.

The University of Kentucky plans to continue developing the technology by improving the manifold design for the University of Kentucky membrane elements and seek a replacement commercial membrane supplier because Hitachi has since discontinued the HZM elements used for these tests. As part of the design improvements, it seems that addressing the fragility of the membrane elements should be a top priority, and the lessons learned from this project will facilitate a solution. The application of produced water treatment will likely involve transport to remote locations where rough handling should be expected. Given that operational environment, equipment reliability will be a key evaluation criterion for potential end users and any shortcomings will impact technology adoption.

The abbreviated field test at low-water-recovery conditions was also insufficient to validate claims of the specific energy consumption for the zeolite membrane dewatering system. The University of Kentucky projected a specific energy consumption of less than 10 kWh/m^3 for a system similar to the field test unit that operates at approximately 60% water recovery and a 5°C sensible heating demand. The team acknowledges the importance of sufficient water recovery, efficient thermal management, and heat recovery to reach this heating load. On the other hand, the limited experimental data suggest a specific energy consumption of 5170 kWh/m^3, compared to expectations. The measured specific energy consumption was likely impacted by the small scale and/or nonoptimum/inefficient operation of the field unit, and it should not be taken as indicative of the concept's future potential. However, the University of Kentucky's projected energy consumption of less than 10 kWh/m^3 energy consumption should be validated during future development testing.

SYNERGISTIC ACTIVITIES

Multiple synergistic efforts related to brine treatment approaches, CO_2 sequestration, pressure mitigation, and produced water management were conducted as separate and independent projects and were enhanced through the leveraged access to the testing facility and/or sample and data access existing as part of the BEST facility and project activities. Summaries of these efforts are provided below.

DocuSign Envelope ID: 2FA9A609-C360-4E53-8B28-BE8B77B6994A

Produced Water Management Through Geologic Homogenization, Conditioning, and Reuse

The EERC conducted a study on the recycling of water used in O&G operations from regions of North Dakota. The project investigated a novel produced water management strategy, referred to as geologic homogenization, conditioning, and reuse (GHCR), which aims to use a subsurface geologic formation as a natural medium for managing produced water recycling and reuse. Normal O&G operations in western North Dakota manage produced water via SWD wells extracted during oil production, as shown in Figure 59. The general concept of GHCR is to extract fluids from a SWD target at a reasonable distance from active SWD injection wells for potential reuse in hydraulic fracturing or for other purposes, as shown in Figure 60. The extracted water is expected to be of improved quality as the geologic formation has essentially filtered the SWD water, and the extraction of fluids also helps relieve pressures in the formation, which would extend the life of the nearby SWD well(s). The goal of the project was to assess the techno-economic viability of the GHCR concept using the Inyan Kara Formation as the geologic target formation.

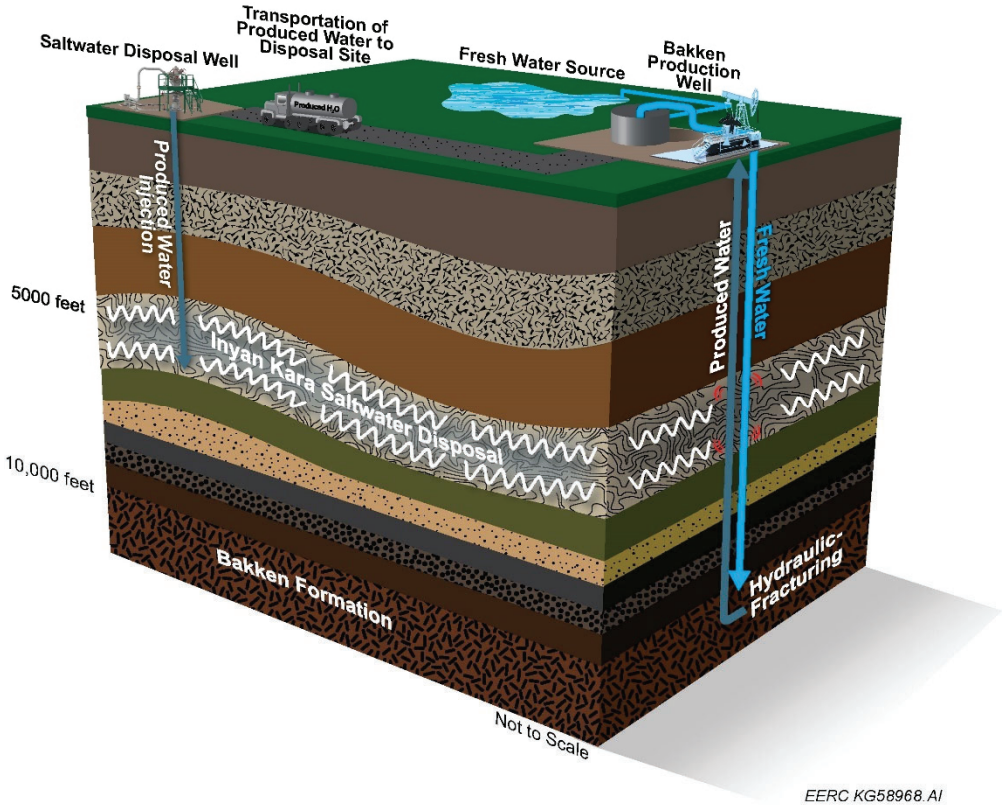


Figure 59. Normal O&G operations in western North Dakota managing produced water via SWD wells extracted during oil production.

DocuSign Envelope ID: 2FA9A609-C360-4E53-8B28-BE8B77B6994A

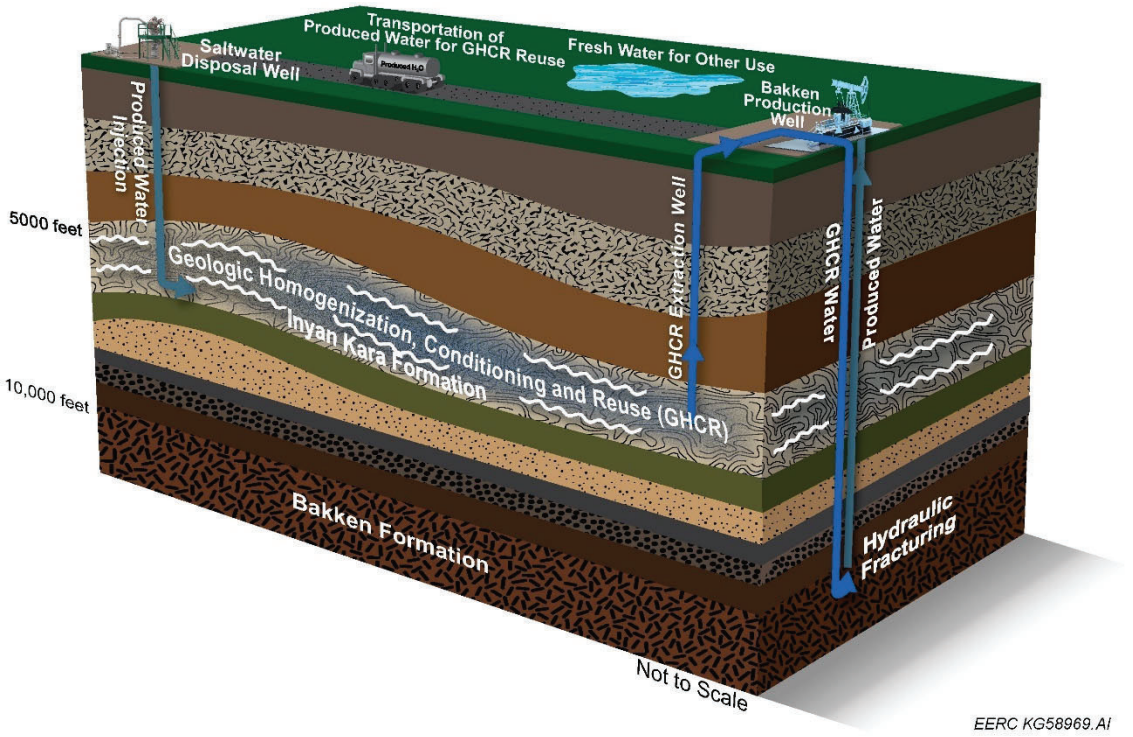


Figure 60. Extracting fluids from a SWD target at a reasonable distance from active SWD injection wells for potential reuse in hydraulic fracturing.

The BEST location provided a unique opportunity to evaluate the GHCR concept at a commercial SWD field site. The two existing SWD wells provided commercial SWD operations, while the BEST E-1 well, which was drilled to the west of the two SWD wells, allowed for the extraction of water that could be sampled to evaluate water quality. The BEST site was extremely valuable for the project as samples were collected from not only commercial SWD operations, allowing for additional analysis of Bakken produced water, but the extracted water allowed for water chemistry analysis of an operating site that essentially replicates the GHCR concept in a field application. These data points and SWD operations allowed for geologic and geochemical modeling and simulations that helped evaluate the long-term performance and commercial viability of the GHCR concept. Further, the BEST site provided the basis for setting up laboratory experiments that replicated the Inyan Kara Formation and SWD injection.

This study revealed that pursuing GHCR could be an option to manage produced water in North Dakota under certain techno-economic conditions. Laboratory testing, field sample collection, and numeric simulations of the BEST site all indicated that the GHCR concept is technically feasible and can provide consistent-quality water for O&G industry use while potentially reducing formation pressure in the Inyan Kara Formation. Economic analysis indicates that there are site-specific scenarios where GHCR implementation can be competitive with conventional water management. The GHCR concept addresses some of the challenges that hinder more traditional approaches to recycling in the industry in the state, such as surface storage of

DocuSign Envelope ID: 2FA9A609-C360-4E53-8B28-BE8B77B6994A

high-saline fluids. The full report discussing the specific activities, results, and discussion of the GHCR concept can be found in Appendix J.

Produced Water Research Partnership – Produced Water Pilot-Scale Testing

The EERC participated in a joint research effort with NETL project manager Nick Siefert, the University of Pittsburgh, and Colorado School of Mines (CSM) to conduct pilot-scale treatment testing on multiple brines at the BEST treatment facility in September 2023. The brines tested included O&G produced waters from the Permian and Eagle Ford Basins of Texas and the Denver–Julesburg (DJ) Basin of Colorado. A preconcentrating step, using RO at CSM, was performed on two of the brines prior to shipping to the BEST site location for additional treatment using the University of Pittsburgh's AGMD technology. Each brine was analyzed and characterized after each stage of conditioning (pretreatment) and TDS concentration/treatment technology applied (i.e., RO or AGMD). Figure 61 shows a basic diagram of brine pretreatment, brine-concentrating technology, and sample collection locations throughout the evaluation.

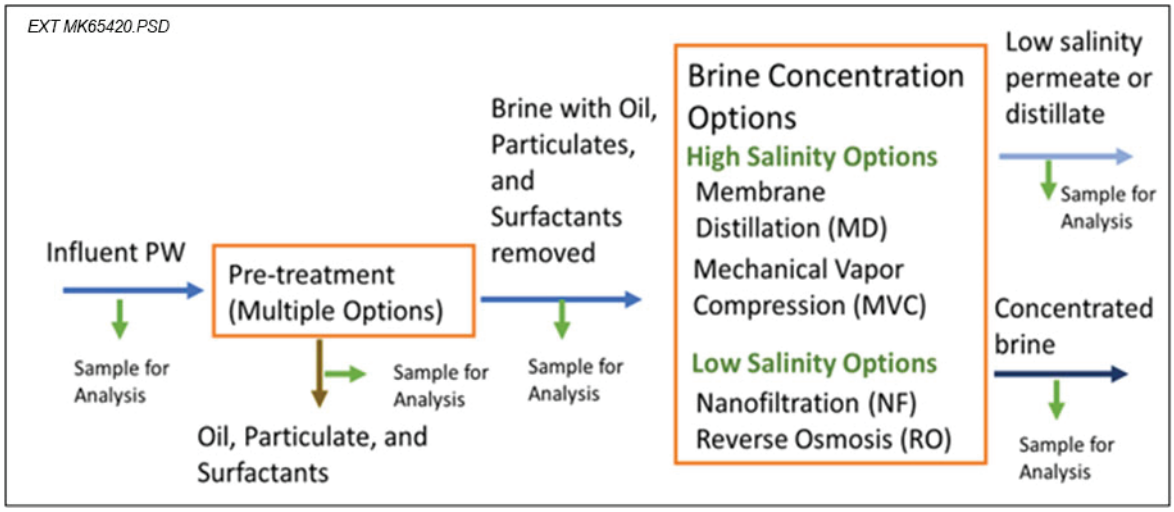


Figure 61. Schematic showing pretreatment, TDS treatment, and sample collection locations.

The overall objective of the research conducted was to fully characterize the aqueous chemistry at every stage of the treatment train. Clean water recovery rates ranged from 20% to 50% depending on the quality of each input brine, and the final AGMD treatment approach yielded greater than 99% salt rejection. Figure 62 shows the University of Pittsburgh testing equipment at the BEST facility and samples of the raw and treated waters from one of the basins evaluated.

DocuSign Envelope ID: 2FA9A609-C360-4E53-8B28-BE8B77B6994A



Figure 62. University of Pittsburgh membrane technology operations at BEST facility location (top) and raw and treated effluent samples after treatment (bottom).

DocuSign Envelope ID: 2FA9A609-C360-4E53-8B28-BE8B77B6994A

This collaborative research project, leveraging use of the BEST treatment facility, demonstrated the effectiveness of using dynamic pretreatment and desalination technologies to recover high-quality water suitable for possible reuse. The project also provided the opportunity to determine and evaluate brine chemistry data from multiple O&G producing basins at various points throughout the production, conditioning, and desalination treatment processes.

Assessment of Carbonated Brine Injection Feasibility

The EERC participated in a Leidos-sponsored research effort, directed by NETL, to conduct a modeling and simulation feasibility assessment of the injection of carbonated brine into the subsurface. In this study, carbonated brine injection (CBI) was investigated as a low-risk CO_2 storage strategy, whereby CO_2 is first dissolved into oilfield produced waters being injected into existing Class II SWD wells. Since the CO_2 is mixed with the produced water prior to subsurface injection, the benefits were predicted to include no migration of free-phase CO_2 and negligible pressure increase when compared to standard SWD injection. A visualization of the different injection approaches is shown in Figure 63. This study used the reservoir conditions and characteristics present in the Class II brine disposal wells found in the North Dakota Bakken play, which predominantly injects into a regionally extensive brine formation, the Inyan Kara Formation.

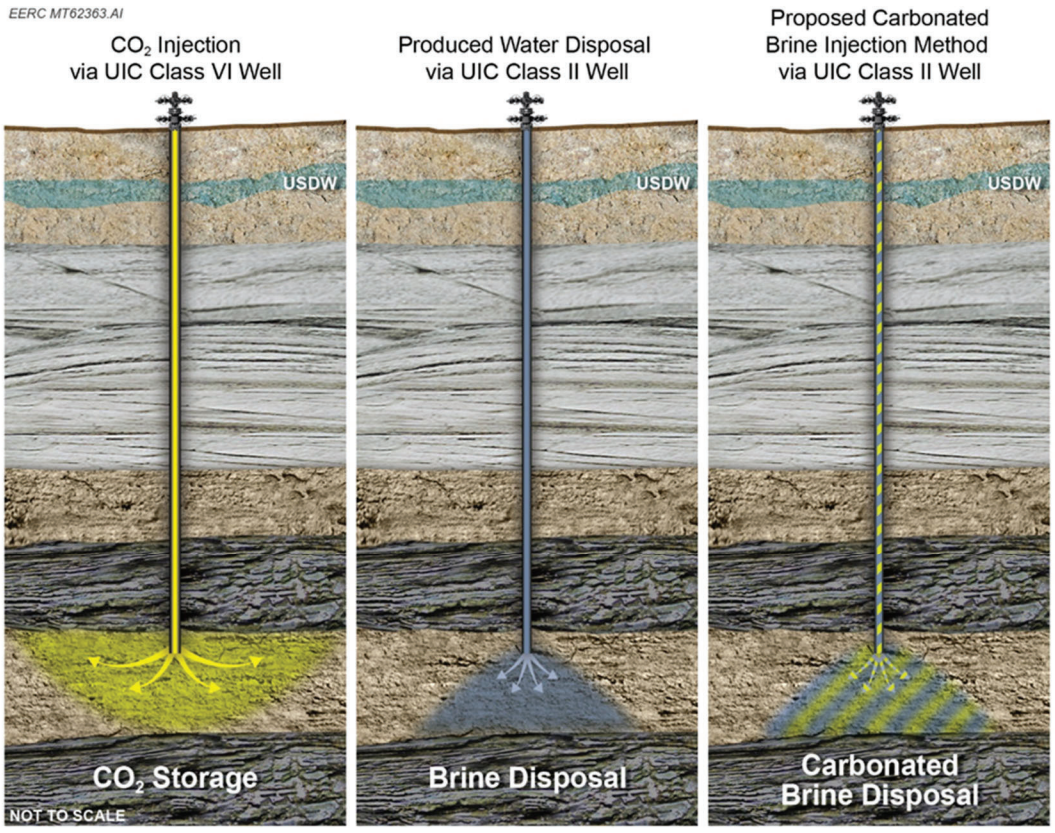


Figure 63. Graphical representation of CBI compared to traditional free-phase CO_2 injection and standard produced water (brine) disposal.

DocuSign Envelope ID: 2FA9A609-C360-4E53-8B28-BE8B77B6994A

Data obtained as part of the BEST ARM task, including stratigraphy, formation pressures, hydraulic gradients, permeability, porosity, etc., were used to populate specific components of the geologic and simulation models used for the CBI evaluation. Three simulation studies were conducted to investigate: 1) CO_2 phases at different conditions, 2) wellbore compatibility, and 3) long-term storage fate in the reservoir. Simple reservoir model and injection simulations were created using data to represent the BEST site, an operational SWD facility located near Watford City, North Dakota.

Simulations of CBI at small CO_2 molality (0.2 mol/kg) were found to show no perceivable increases in reservoir pressure or impacts to brine viscosity or density due to the dissolved CO_2. When compared specifically to standard produced water disposal operations, pressure-driven risks such as leakage, induced seismicity, cap rock failure, and migration do not increase with the inclusion of dissolved CO_2 in the brine injection stream. Evaluation of wellbore corrosion rates showed minimal change with the inclusion of dissolved CO_2 in the brine injection, enabling CBI operations for years. Finally, the carbonated brine was found to be denser than the reservoir brine, such that the CO_2-laden brine sinks to the bottom of the reservoir instead of migrating upward due to buoyancy forces, which typically happens during injection of dense-phase CO_2 for geologic storage.

Overall, CBI and storage in North Dakota's Inyan Kara Formation appear to be a low-risk geologic sequestration strategy. There does not appear to be any increased risks with CBI when compared to standard produced water disposal operations, and it is benefitted by the ability to use existing well infrastructure in comparison to new carbon capture, utilization, and storage (CCUS) projects. The full report on the CBI assessment can be found in Appendix K.

DISCUSSION

Multiple technologies were evaluated throughout the operational period of the test bed facility (2019–2023). Thermal and membrane-assisted thermal technologies were likely to be the most applicable for the targeted high-salinity brines (~180,000 mg/L TDS) and were the focus of the technology selection and resulting evaluations. Overall, each technology demonstrated, with varying degrees of success, the ability to recover relatively fresh distillate water and produce a concentrated brine effluent with varying inlet salinity ranges and at multiple recovery rates. In addition to the on-site pilot-scale testing, each technology underwent both laboratory and pilot system testing at each respective facility before being mobilized to North Dakota for demonstration. It should be noted that each technology varied in scale, making comparable analysis challenging.

The MVR system yielded results for a wide range of inlet salinities and provided a good database of water recovery rates, brine concentration, low-salinity distillate, and overall energy consumption for comparison with subsequent technologies. This specific MVR system, however, was developed for the military and designed to desalinate ocean water. Therefore, it was not designed to be energy-efficient, as many of the energy requirements for the system are to support the automated controls and operation. The tests conducted did, however, give a good technological

DocuSign Envelope ID: 2FA9A609-C360-4E53-8B28-BE8B77B6994A

baseline for the treatment of a variety of brine concentrations. Table 21 shows the major parameter data collected for all technologies while testing on the high-TDS brines. Because of the failure of the zeolite membrane housing seals, as well as failure of the membranes themselves, the data provided are from the laboratory assessment of the technology.

Table 21. Data for Each Individual Technology During High-TDS Field Testing

Technology	Inlet Feed Salinity, mg/L TDS	Inlet Feed Rate, gpm	Ion Rejection, %	Permeate Recovery %	Permeate/ Distillate Quality, mg/L TDS	Brine Concentrate, mg/L TDS
MVR	170,000	2.00	99.6	44	1046	253,000
AGMD	174,000	0.50	99.7	30	460	246,000
SCWD	173,000	0.03	99.2	34	1370	261,000
ZMD (lab)[1]	170,000	0.03	90.0	10	NM	NM[2]

[1] Laboratory data on the zeolite technology were substituted for field data because of premature membrane housing failure resulting in contaminated permeate product.
[2] Not measured.

The Ohio University SCWD technology demonstrated consistent system performance between both the laboratory- and field-based testing in North Dakota. The permeate water recovery rate was approximately 34%, with permeate quality measured around 1370 mg/L of TDS, resulting in greater than 99% ion rejection. Similarly, the University of Pittsburgh AGMD technology achieved high ion rejection, approximately 30% overall permeate recovery, and below-drinking-water-standard permeate quality. Additionally, the AGMD technology was the most advanced-scale technology, comparable to the MVR system, and maintained consistent steady-state operation throughout testing.

The ZWD technology was relatively successful during testing at University of Kentucky laboratories; however, multiple challenges arose when attempting to transport and test the system in North Dakota, resulting in limited field demonstration data. Overall, permeate quality for the membranes tested was good with over 90% ion rejection, based on laboratory findings, however, water recovery rates were modestly low, approximately 10%, and associated distillate and brine concentrate composition was not measured and is unknown.

Electrical power consumption was monitored for each technology during their respective demonstrations, and a total energy usage calculation in kWh per unit of permeate/distillate was determined for each steady-state condition on the high-salinity brine target of approximately 170,000 mg/L TDS. Table 22 illustrates the average energy usage for each technology and the associated estimated cost per bbl of produced water. The energy usage for both the AGMD and SCWD technologies was significantly higher than the MVR usage; however, power consumption results may not be indicative of full-scale application because of scale-up issues and overall small size of the technologies. The energy consumption for the ZMD technology was likely impacted by the small scale and/or nonoptimum/inefficient operation of the field unit, and it should not be taken as indicative of the concept's true potential. However, the University of Kentucky's projected energy consumption of less than 10 kWh/m^3 energy, as described in its own techno-economic assessment, is likely unrealistic and should be validated through further testing.

DocuSign Envelope ID: 2FA9A609-C360-4E53-8B28-BE8B77B6994A

Table 22. Energy Consumption for Treatment of ~170,000 mg/L TDS

Technology	Average Permeate Recovery, %	Average Energy Usage per Unit of Distillate, kWh/m^3	Estimated Treatment Cost[1], $/bbl
MVR	40	100–122	15–19
AGMD	30	690	109
SCWD	34	300–546	47–87
ZMD	10	5170[2]	820[2]

[1] Based on an electrical cost of $0.069 per kWh.
[2] This extraordinarily high result is because of membrane failure resulting in nonrepresentative calculations.

Similar to energy usage, the estimated treatment costs for each technology in Table 22 should also be considered preliminary values that may not be entirely indicative of more developed, commercialized systems. While the EERC BEST test bed is a world-class facility for quantifying the mass and energy balance for brine treatment technologies, the technology delivered for testing is the responsibility of the developer. As discussed in each technology test summary, these pilot-scale systems were sometimes early-stage, nonoptimized prototypes, and unexpected failures impacted some evaluation results. However, aside from technology readiness concerns, the BEST facility is well-suited for establishing the techno-economic performance of advanced brine treatment. One techno-economic sensitivity study for treating O&G produced water based on MVR (Wenzlick and Siefert, 2020) suggests that combined MVR cost (operating and capital) had the largest negative impact on the cost of treatment, and for the baseline cases in that study, MVR cost averaged 67% of the total cost of treatment. It is reasonable to expect that treatment cost for other approaches (especially those that are fundamentally driven by thermal energy) would be similarly dominated by the energy-intensive step and that BEST facility testing is capable of capturing the most significant drivers of treatment cost.

CONCLUSIONS

Extracted water treatment technologies compatible with ARM must be capable of addressing a range of water quality characteristics that depend largely on the location and type of formation targeted for CO_2 storage. Suitable formations are anticipated to range from DSFs to depleted O&G reservoirs, each having potentially different formation water characteristics, particularly with respect to levels of suspended and dissolved solids, hardness, and organics content. While these initial technology demonstrations did not warrant extensive parametric study of input brine characteristics, the BEST test bed facility was designed with this need in mind. It is anticipated that as brine treatment technologies continue to mature and there is interest in evaluating differing water quality characteristics, the BEST facility could continue to be a useful platform for technology demonstration.

Overall, a majority of the technologies evaluated through this project are theoretically appropriate, on a technical basis, for the treatment and management of high-salinity brines, however, technical challenges involving scale-up and overall economics are limiting. Energy intensity and membrane durability appear to be the key limiting factors, economically and technically, in the application of these technologies at large scale. None of the tested technologies

DocuSign Envelope ID: 2FA9A609-C360-4E53-8B28-BE8B77B6994A

were operated long enough to experimentally establish baseline performance with respect to materials lifetime and servicing intervals. As the engineering for these treatment technologies matures, the consistent brine-blending capabilities and the controlled environment of the BEST test bed can support longer-duration endurance runs to establish such baselines for techno-economic analysis and even vendor performance specifications.

Since the alternative to brine treatment is often injection well disposal, the economic feasibility of advanced brine treatment may depend on the regional availability and cost of SWD. To increase revenue potential going forward, it is likely that the most economical approach to the desalination and reduction of extracted brines will be to combine the desalination approach with waste heat utilization, by-product exploitation (i.e., HCl production), and/or critical mineral extraction (i.e., Li, Co, etc.). As a result, it is expected that future testing and development needs for brine treatment technology will need to support the evaluation of individual unit operations that perform specific functions like mineral extraction or acid production. To support technology testing of this kind, the pretreatment infrastructure at the BEST test bed will need to be evaluated with respect to the needs of each technology and possibly augmented if necessary.

REFERENCES

Agency for Toxic Substances and Disease Registry, 2019, Toxicological profiles—ammonia chemical and physical information: www.atsdr.cdc.gov/toxprofiles/tp126-c4.pdf (accessed December 2019).

Amiad USA Inc., 2023, Amiad water systems: https://tequatic.amiad.com/ (accessed September 2023).

Arena, J.T., Jain, J.C., Lopano, C.L., Hakala, J.A., Bartholomew, T.V., Mauter, M.S., and Siefert, N.S., 2017, Management and dewatering of brines extracted from geologic carbon storage sites: International Journal of Greenhouse Gas Control, v. 63, p. 194–214.

Colorado School of Mines, 2009, An integrated framework for treatment and management of produced water, technical assessment of produced water treatment technologies: RPSEA Project 07122-12.

Curto, D., Franzitta, V., and Guercio, A., 2021, A review of the water desalination technologies: Applied Sciences, v. 11, p. 670. https://doi.org/10.3390/app11020670.

Hardy, A., and Shapiro, A., 2014, NORM mitigation and clean water recovery, Part II—mechanical vapor compressor-driven membrane distillation for produced water: Niskayuna, New York, GE Global Research.

Harto, C.B., and Veil, J.A., 2011, Management of water extracted from carbon sequestration projects: Environmental Science Division, Argonne National Laboratory.

DocuSign Envelope ID: 2FA9A609-C360-4E53-8B28-BE8B77B6994A

McGinnis, R.L., Hancock, N.T., Nowosielski-Slepowron, M.S., and McGurgan, G.D., 2013, Pilot demonstration of the NH_3/CO_2 forward osmosis desalination process on high salinity brines: Desalination, v. 312, p. 67–74.

Shaw, W., 2011, The real cost of ZLD for shale gas frac water in the Marcellus Shale play, *in* 72nd International Water Conference, Orlando, Florida, November 13–17: Proceedings, p. 17–18, https://eswp.com/wp-content/uploads/2015/04/IWC2011OnSiteGuide.pdf (accessed May 2023).

Silva, J., and Dees, E., 2015, Extracted water treatment technology assessment: GE Global Research, December 2015.

Spiral Water Technologies, Inc., 2023, https://www.spiralwater.com/ (accessed September 2023).

Stepan, D.J., 2017, High-TDS water treatment technology review: Energy & Environmental Research Center, December 2017.

Sun, J., 2014, Four Membrane Cleaning Profiles with Micro-90® Alkaline Cleaning Solution, Micro® Green Clean Biodegradable Cleaner and Micro® A07 Citric Acid Cleaner; International Products Corporation, September 2014; www.ipcol.com/wp-content/uploads/FourMembraneCleaningProfiles.pdf (accessed September 2023).

Tekleen Automatic Filters, LLC; https://www.tekleen.com/ (accessed September 2023).

U.S. Environmental Protection Agency, 2019, Secondary drinking water standards—guidance for nuisance chemicals: www.epa.gov/dwstandardsregulations/secondary-drinking-water-standards-guidance-nuisance-chemicals#table (accessed December 2019).

Wenzlick, M., and Siefert, N., 2020, Techno-economic analysis of converting oil and gas produced water into valuable resources: Desalination, v. 481.

DocuSign Envelope ID: 2FA9A609-C360-4E53-8B28-BE8B77B6994A

APPENDIX A

HIGH-TDS TREATMENT PRESENTATION

DocuSign Envelope ID: 2FA9A609-C360-4E53-8B28-BE8B77B6994A



DocuSign Envelope ID: 2FA9A609-C360-4E53-8B28-BE8B77B6994A



DocuSign Envelope ID: 2FA9A609-C360-4E53-8B28-BE8B77B6994A

Disclaimer

This presentation was prepared as an account of work sponsored by an agency of the United States Government. Neither the United States Government, nor any agency thereof, nor any of their employees, makes any warranty, express or implied, or assumes any legal liability or responsibility for the accuracy, completeness, or usefulness of any information, apparatus, product, or process disclosed or represents that its use would not infringe privately owned rights. Reference herein to any specific commercial product, process, or service by trade name, trademark, manufacturer, or otherwise does not necessarily constitute or imply its endorsement, recommendation, or favoring by the United States Government or any agency thereof. The views and opinions of authors expressed herein do not necessarily state or reflect those of the United States Government or any agency thereof.

DocuSign Envelope ID: 2FA9A609-C360-4E53-8B28-BE8B77B6994A

High-TDS Waters

- **Brackish**
  - 500 to 35,000 mg/L TDS
- **Saline**
  - 35,000 to 50,000 mg/L TDS
- **Brines**
  - > 50,000 mg/L TDS

- Bakken Flowback
  - 200,000+ mg/L TDS
- Bakken Produced Water
  - 300,000+ mg/L TDS
- Deep Saline Formation Water
  - 10,000 to 300,000 mg//L

DocuSign Envelope ID: 2FA9A609-C360-4E53-8B28-BE8B77B6994A

Produced Water Characteristics

- Dispersed and dissolved oils and organics
  - Mix of oil components: BTEX, PAHs, phenols…
- Dissolved minerals and salts
  - Cl^-, SO_4^{2-}, CO_3^{2-}, HCO_3^-, Na^+, K^+, Ca^{2+}, Ba^{2+}, Mg^{2+}, Fe^{2+} and Sr^{2+}
- Production chemicals
  - Scale and corrosion inhibitors, friction reducers, biocides…
- Dissolved gases
  - CH_4, CO_2, H_2S,
- Naturally Occurring Radioactive Materials?

DocuSign Envelope ID: 2FA9A609-C360-4E53-8B28-BE8B77B6994A

Deep Saline Formation (DSF) Water

- Subsurface waters that are extracted from formations to accommodate the geologic storage of carbon dioxide.
- TDS is highly variable depending on subsurface reservoir conditions.
- DSF water may contain hydrocarbons in reservoirs that were not previously considered as having economically recoverable resources – Residual Oil Zones that are potential candidate for CO_2 storage.

DocuSign Envelope ID: 2FA9A609-C360-4E53-8B28-BE8B77B6994A

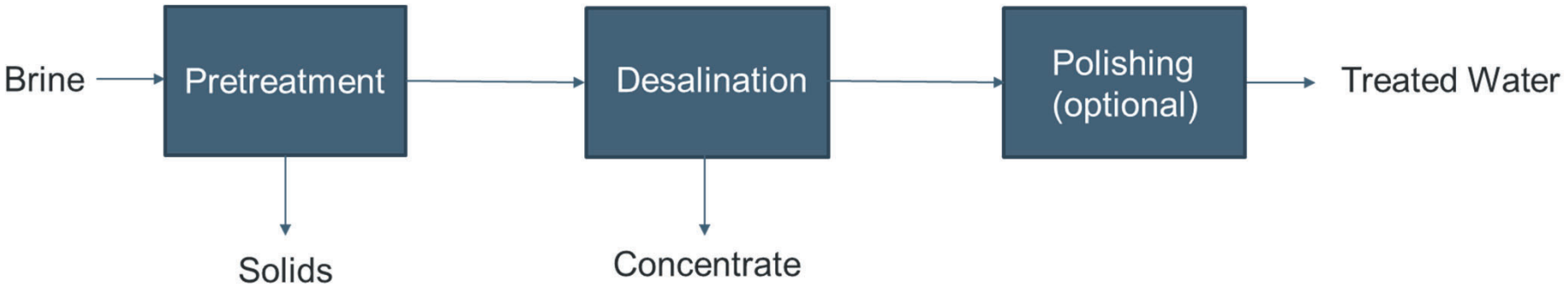
Treatment of High-TDS Waters

- Treatment and handling of high-TDS waters is dependent on water quality and the potential for beneficial reuse.
  - Disposal via deep well injection is typically the most cost-effective method.
    - Minimal treatment required – flotation and gravity settling prior to injection.
  - Relatively lower-TDS waters may be economically treated
    - Minimal treatment requirements
    - Regions of high water demand (drought-prone areas)
    - Nearby demand for treated water (transportation can be expensive).
  - High-TDS waters are less likely to be economically treated using existing technology
    - Current area of research and technology development.
    - Requires pretreatment to remove problematic constituents

DocuSign Envelope ID: 2FA9A609-C360-4E53-8B28-BE8B77B6994A

High-TDS Water Treatment Technologies

- Successful treatment of high-TDS waters will involve a systematic combination of individual technologies integrated into an overall treatment process.
  - Pretreatment (primary treatment)
  - High-TDS water treatment (desalination)
  - Effluent polishing (tertiary treatment)
  - Concentrate/residuals treatment



DocuSign Envelope ID: 2FA9A609-C360-4E53-8B28-BE8B77B6994A

High-TDS Water Pretreatment

- Pretreatment Objectives
  - Organics removal
    - Free and dissolved oil, emulsions, and natural gas condensates
  - Suspended solids removal
    - Formation solids
  - Hardness removal
    - Scale-causing constituents – calcium, magnesium, iron, barium…

DocuSign Envelope ID: 2FA9A609-C360-4E53-8B28-BE8B77B6994A

Pretreatment

- ***Technologies***
  - Blending
  - Flotation
  - Settling
  - Coagulation/precipitation
  - Media Filtration
  - Activated carbon adsorption
  - Electrocoagulation

- ***Considerations***
  - Chemical additions
    - Safety requirements
    - Added costs
  - Sludge generation
    - Waste disposal costs
  - Hazardous waste production
    - Hazardous waste disposal costs

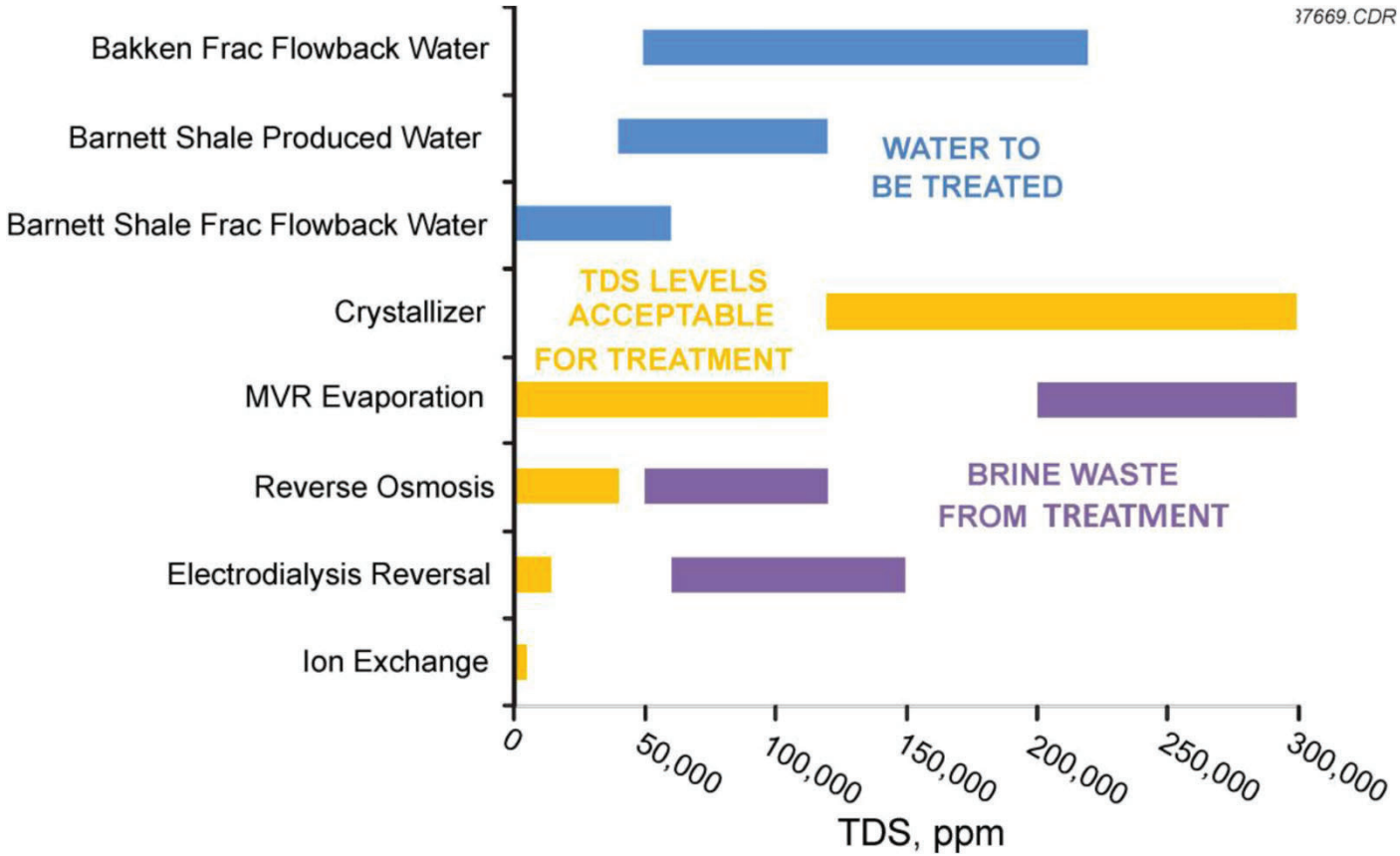
DocuSign Envelope ID: 2FA9A609-C360-4E53-8B28-BE8B77B6994A

High-TDS Water Treatment Technologies

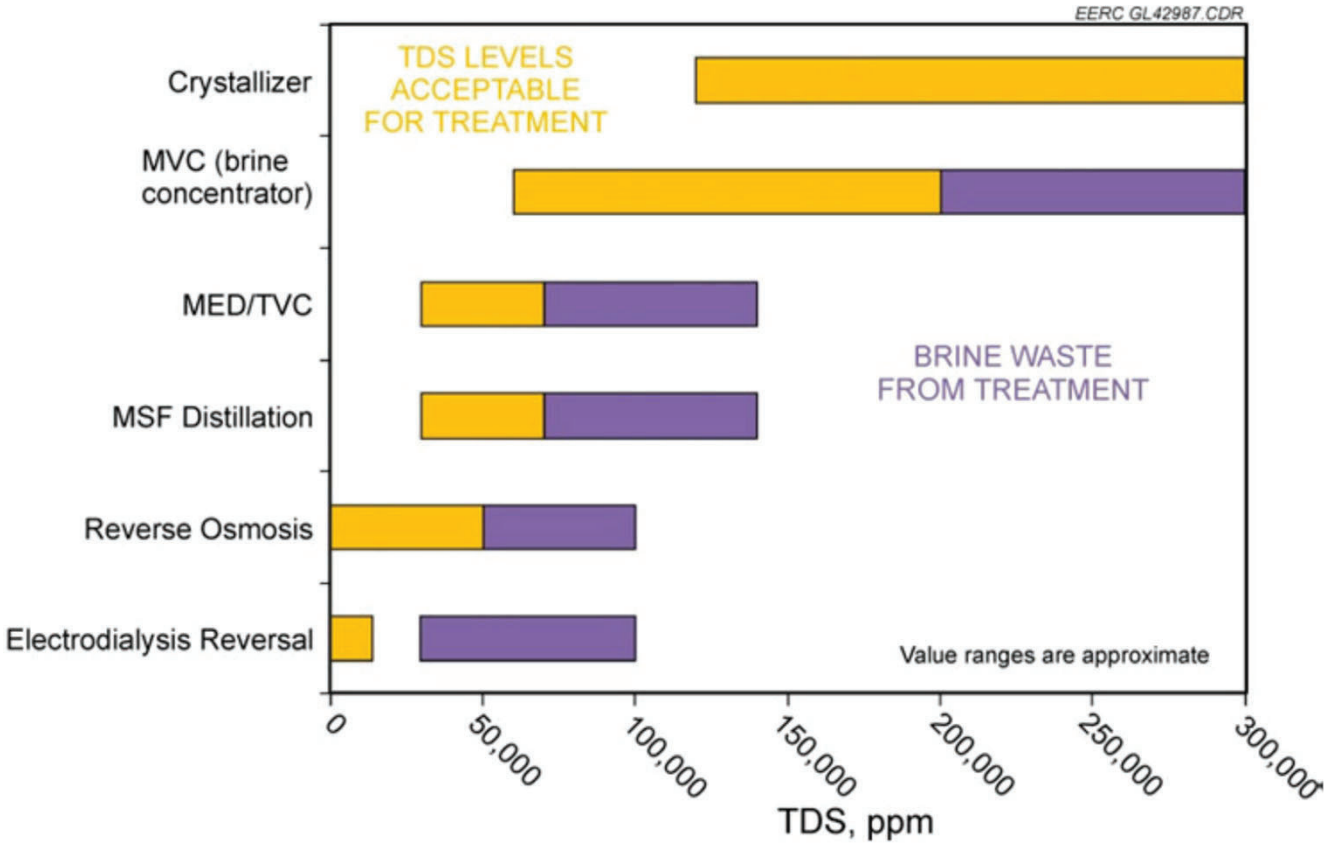
- ***Membrane Filtration***
  - Microfiltration
  - Ultrafiltration
  - Nanofiltration
  - Reverse Osmosis
  - Forward Osmosis
  - Electrodialysis
  - Membrane Distillation
- ***Thermal Treatment***
  - Multistage flash distillation
  - Multiple-effect evaporation
  - Vapor compression
  - Mechanical vapor recompression
  - Falling Film
  - Humidification–Dehumidification
  - Freeze-thaw evaporation

DocuSign Envelope ID: 2FA9A609-C360-4E53-8B28-BE8B77B6994A

Applicability of Technologies



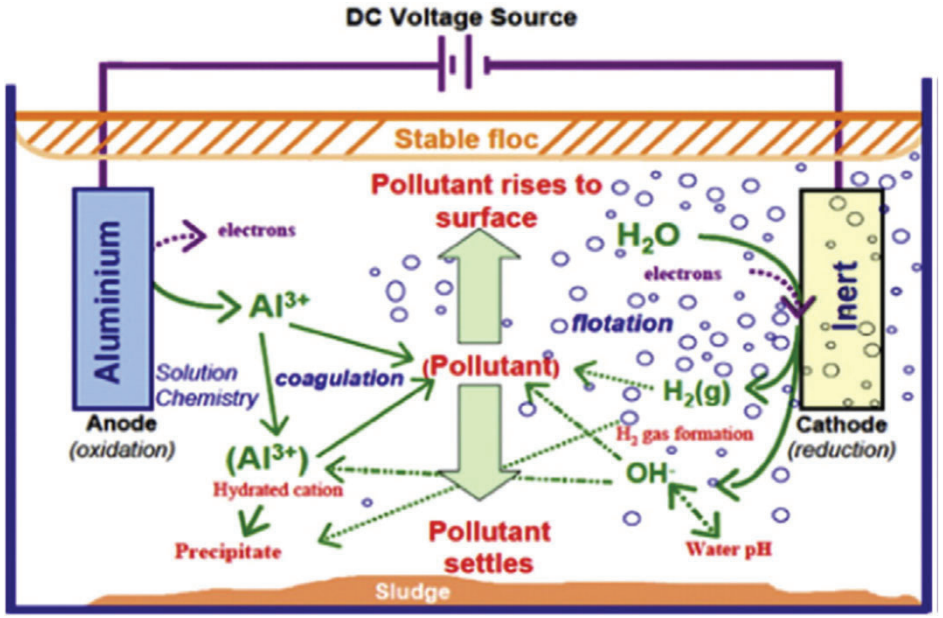
DocuSign Envelope ID: 2FA9A609-C360-4E53-8B28-BE8B77B6994A



DocuSign Envelope ID: 2FA9A609-C360-4E53-8B28-BE8B77B6994A

Electrocoagulation

- Technology combines multiple mechanisms for the removal of oils, bacteria, suspended solids and multivalent ions.
  - Application of an electric current to provide electrodissolution of a sacrificial anode (Fe or Al) to promote coagulation.
- Pros:
  - Simple, easy to operate
  - Removal of colloids
  - Stand-alone or pretreatment to enable other desalination technologies, depending on effluent quality requirements
  - Reduced or eliminated chemical use
- Cons:
  - Need to replace sacrificial electrodes
  - Lack of large-scale, high-TDS water demonstrations
  - Limited data on high-TDS waters



Source: Hakizimana and others, 2017

DocuSign Envelope ID: 2FA9A609-C360-4E53-8B28-BE8B77B6994A

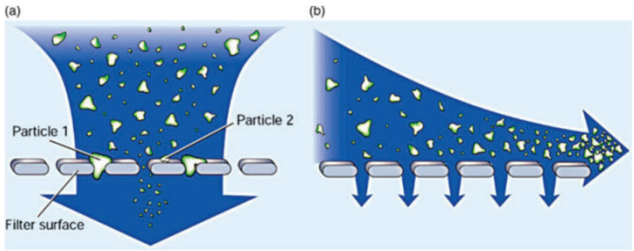


Membrane-based Technologies

DocuSign Envelope ID: 2FA9A609-C360-4E53-8B28-BE8B77B6994A

Membrane Filtration

- Microporous films with specific pore size ratings
  - Polymeric membranes
  - Ceramic membranes
- Crossflow configurations to enhance flux and allow longer filter runs
- Pressure is the driving force



Comparison of dead-end a crossflow filtration (Igunnu and Chen, 2012)

Technologies

- Microfiltration (suspended solids)
  - 0.1 – 5 µm
- Ultrafiltration (suspended solids)
  - 0.01 – 0.1 µm
- Nanofiltration (rejects multivalent ions)
  - 0.001 – 0.01 µm
- Reverse Osmosis (rejects monovalent ions)
  - 0.0001 – 0.001 µm

DocuSign Envelope ID: 2FA9A609-C360-4E53-8B28-BE8B77B6994A

Reverse Osmosis

Utilizes a pressure gradient to drive water molecules through semipermeable membranes while concentrating dissolved ions and bacteria in a reject stream

- ***Operational Issues***
  - High concentration gradient near membrane surface can result in scale formation and membrane fouling leading to low permeate flux (flow/unit membrane surface area).
  - Organic fouling of membranes can result in reduced water flux and compromised permeate quality

- ***Pros:***
  - Proven technology
  - Enhanced performance with adequate pretreatment
  - Hybrid applications

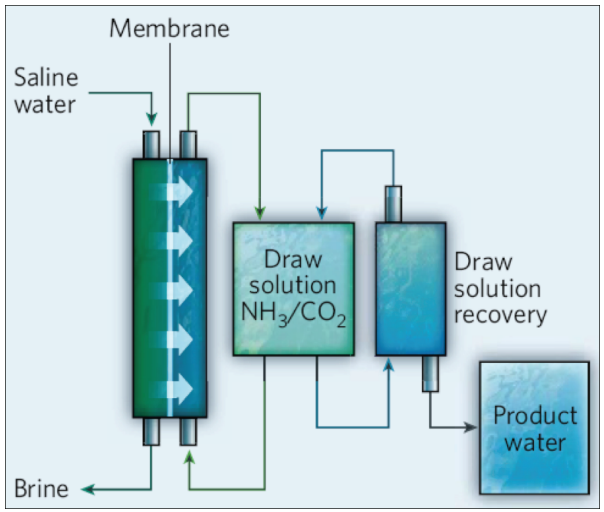
- ***Cons***
  - Limited application to water with TDS levels less than around 50,000 mg/L.
  - Generation of a concentrate stream

DocuSign Envelope ID: 2FA9A609-C360-4E53-8B28-BE8B77B6994A

Forward Osmosis

Utilizes an osmotic pressure gradient as the driving force to induce net water flow through a membrane into a “draw” solution

- Water diffuses through a membrane from low osmotic pressure to high osmotic pressure solutions



- ***Pros:***
  - Capable of treating higher TDS waters*
  - Less energy intensive*
  - Membrane fouling potential is low and reversible
  - Hybrid applications: FO-MSF, FO-MED reduces scale issues associated with thermal processes

- ***Cons:***
  - Relatively low rates*
  - Requires water recovery from draw solution
  - Needs demonstration on high-TDS water

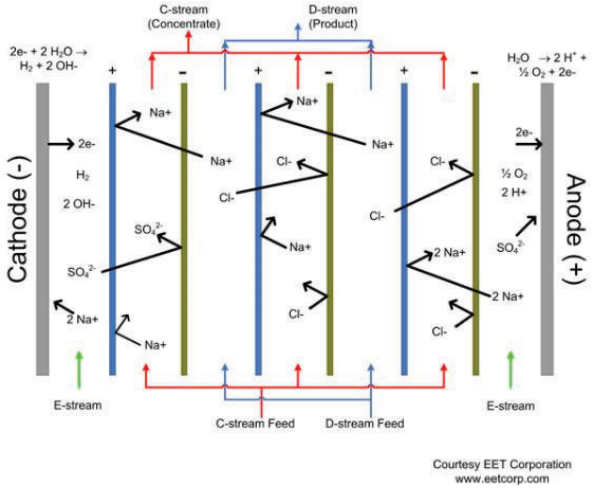
* Compared to reverse osmosis

DocuSign Envelope ID: 2FA9A609-C360-4E53-8B28-BE8B77B6994A

Electrodialysis (ED)/Electrodialysis Reversal (EDR)

Membrane processed, during which ions are transported through semi permeable membranes under the influence of an electric field.

- A series of stacked membranes are cation and anion selective. Applying a current creates the electrical field where cations migrate toward the cathode, pass through the cation-exchange membrane and are rejected by the anion-exchange membrane, and vice versa for negatively charged anions that migrate to the anode.
- EDR use periodic reversal of polarity to reduce scaling and fouling and promote higher water recovery.



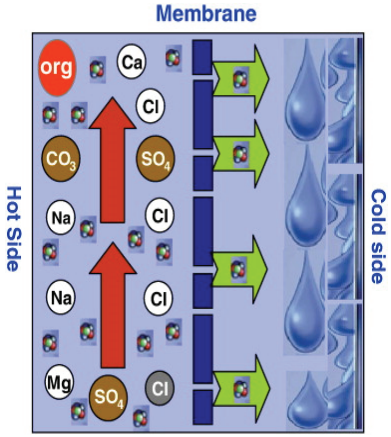
- Cost effective up to 8000 mg/L TDS
- Lab-scale tests on produced waters
- Potential for acid/base production

DocuSign Envelope ID: 2FA9A609-C360-4E53-8B28-BE8B77B6994A

Membrane Distillation (MD)

A thermally-driven phase change process where water vapor passes through a hydrophobic membrane that provides a barrier to liquid flow.

- MD is driven be vapor pressure differences across the membrane surface
- Different membrane configurations
  - Direct contact MD
  - Air gap MD
  - Sweeping gas MD
  - Vacuum MD



- Pros:
  - Low operating temperature
  - Low operating pressure
  - Plastic components alleviate potential corrosion issues
  - Larger membrane pore size – less fouling
- Cons:
  - Low permeate flux (compared to RO)
  - Mass transfer resistance due to trapped air in the membrane
  - Conductive heat losses can be quite large

DocuSign Envelope ID: 2FA9A609-C360-4E53-8B28-BE8B77B6994A

Thermal Technologies

DocuSign Envelope ID: 2FA9A609-C360-4E53-8B28-BE8B77B6994A

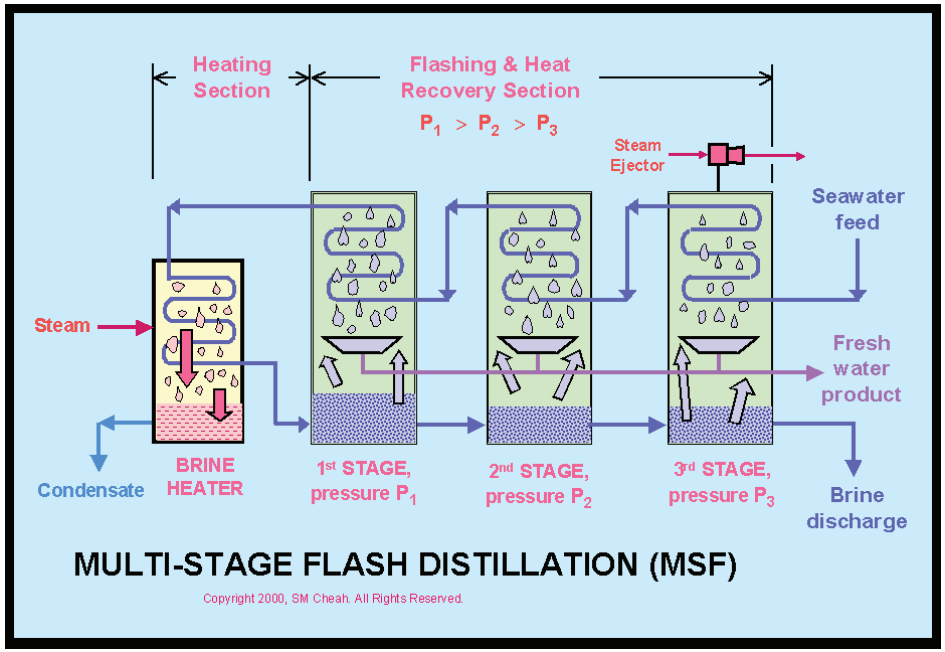
Thermal Treatment Technologies

- Multistage flash distillation
- Multiple-effect evaporation
- Vapor compression
- Mechanical vapor recompression
- Falling Film Evaporators
- Humidification–Dehumidification
- Freeze-thaw evaporation

DocuSign Envelope ID: 2FA9A609-C360-4E53-8B28-BE8B77B6994A

Multistage Flash (MSF) Distillation

- MSF distillation is based on evaporating water through multiple stages of pressure reduction as opposed to boiling. Pre-heated water flows through different stages of reduced pressure where it flashes to steam.
  - Developed for desalination of sea water
  - Water recovery is 15 – 20%
  - Energy requirement is 3.35 to 4.70 kWh/bbl
  - Decreased market share because of competition with membrane technologies

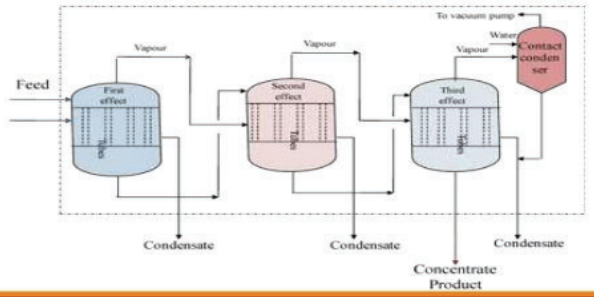


DocuSign Envelope ID: 2FA9A609-C360-4E53-8B28-BE8B77B6994A

Multiple Effect Evaporation

- Sequential flow through multiple evaporators where vapor from a preceding effect heats the subsequent effect operating at lower pressure to produce additional vapor that is ultimately recovered as product water

Multiple effect evaporator

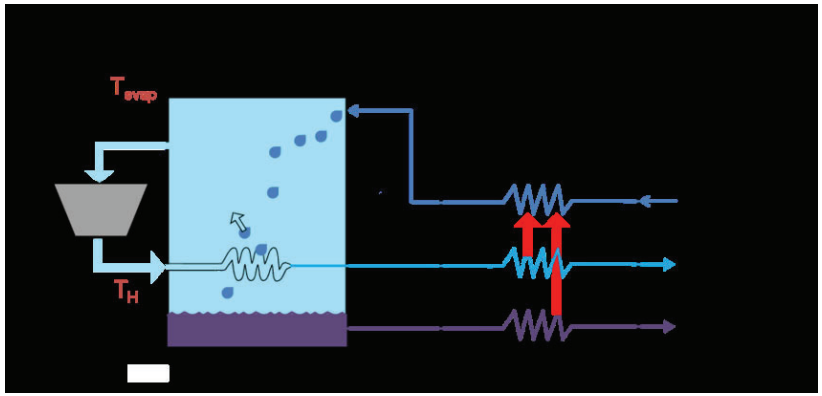


- Efficiency gained through the combination of several evaporators.
- Condensed steam recovered as pure water
- Falling film evaporators developed to improve heat transfer and overcome scaling issues
- 1.3 to 1.9 kWh/bbl

DocuSign Envelope ID: 2FA9A609-C360-4E53-8B28-BE8B77B6994A

Vapor Compression/Recompression

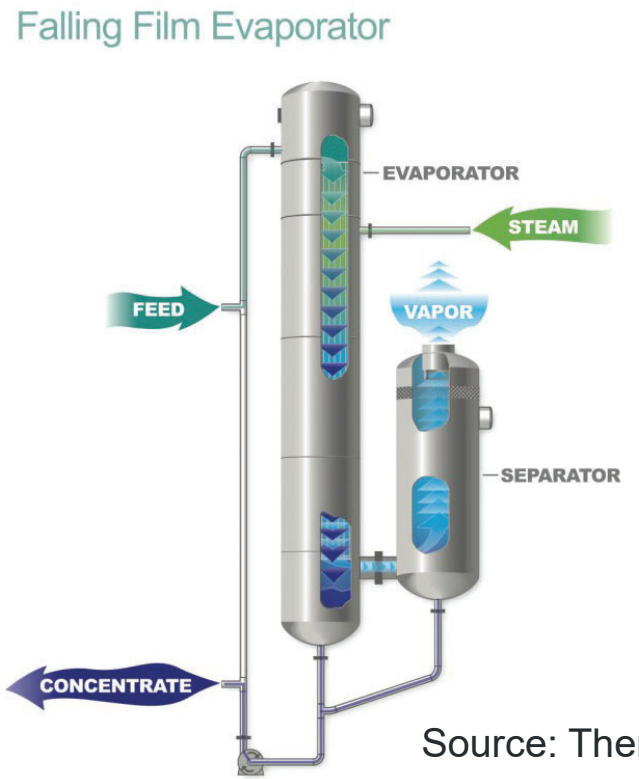
- System where vapor produced in evaporation is compressed thermally or mechanically (MVR) to raise the temperature and pressure of the vapor. Latent heat rejected during condensation is used to generate additional vapor.
- Can operate at lower temperatures (70°C) which reduces scale formation problems
- Lower energy consumption compared to reverse osmosis



DocuSign Envelope ID: 2FA9A609-C360-4E53-8B28-BE8B77B6994A

Falling Film Evaporators

- Combined with other evaporator configurations to improve heat transfer and reduce scale formation rates.
- High-TDS water flows downward as a film, typically inside a heating tube.
- Steam is typically the heating medium on the outside of the tube.
- Produces distilled water and a concentrated brine.

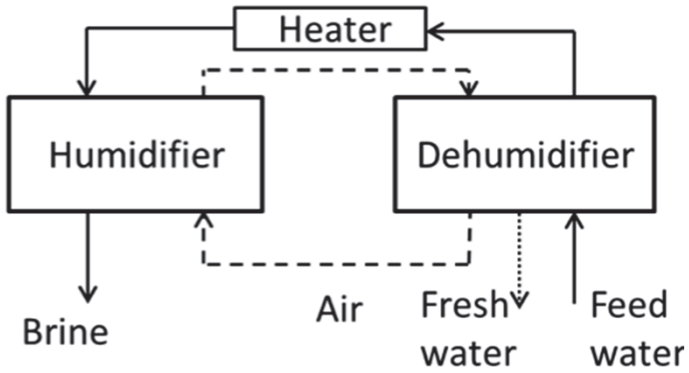


Source: Thermal Kinetics

DocuSign Envelope ID: 2FA9A609-C360-4E53-8B28-BE8B77B6994A

Humidification-Dehumidification (HDH)

- Thermal desalination technology
  - Air is humidified through direct contact with brine.
  - Indirect vapor contact with cold brine in the dehumidifier causes vapor to condense and produce fresh water.
- Pros:
  - Simple process can utilize waste heat
  - Moderate installation and operating costs.



DocuSign Envelope ID: 2FA9A609-C360-4E53-8B28-BE8B77B6994A

Freeze-Thaw Evaporation (FTE®)

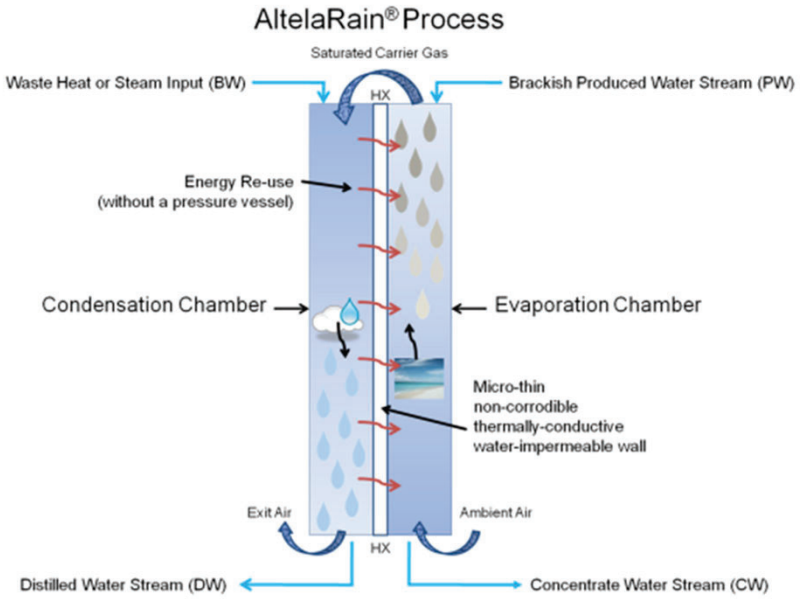
- Process developed by EERC and BC Technologies.
- Employs natural freezing, thawing, and evaporation ponds for produced water management.
- Freezing produces relatively pure-water ice crystals and a concentrated liquid brine that is drained from the ice pile and pumped to brine storage/evaporation ponds.
- Melted ice produces low-TDS water for beneficial use.
- Requires locations with freezing climates for a substantial period.
- Significant land area requirements.



DocuSign Envelope ID: 2FA9A609-C360-4E53-8B28-BE8B77B6994A

AltelaRain®

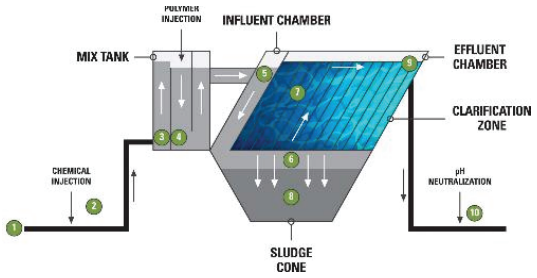
- Low temperature, low pressure, evaporation–condensation process
- Claimed benefits include:
  - Low capital requirements
  - Low operating costs
  - Leverages precedent-setting regulatory frameworks
  - Precise control of economics
  - Low maintenance
  - Highly scalable
  - Reduced facility requirements
  - Extremely high quality of treated water
- 2600 bpd treatment rate
- TDS as high as 180,000 mg/L field operations

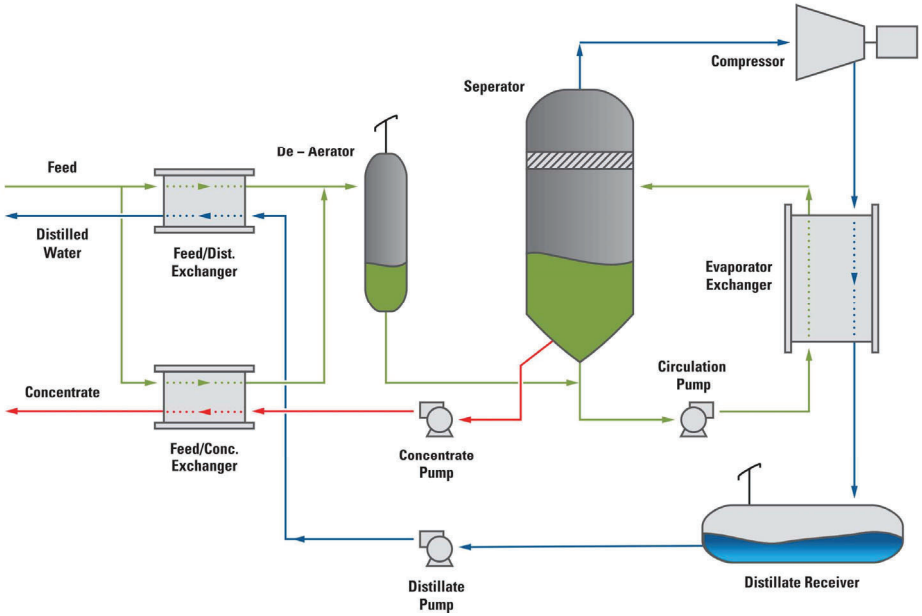


DocuSign Envelope ID: 2FA9A609-C360-4E53-8B28-BE8B77B6994A

NOMAD™ – Fountain Quail Water Management

- Mechanical Vapor Recompression
- NOMAD™ consists of an evaporation unit, a power generation unit and an auxiliary support and control unit
- System capable of generating 2,000 BPD of distilled water
- Can be combined with ROVER™ pretreatment for suspended solids and hardness reduction



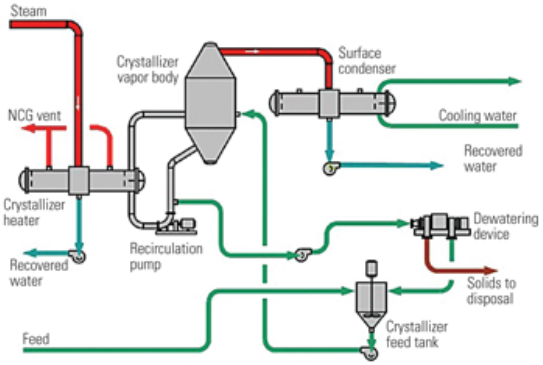


NOMAD™ MVR Process

DocuSign Envelope ID: 2FA9A609-C360-4E53-8B28-BE8B77B6994A

Zero Liquid Discharge (ZLD) Evaporation-Crystallization

- High-TDS brine is evaporated in a crystallizer to yield a solid salt product and a small crystallizer purge stream.
- Crystallization installations are capital intensive.
- Relatively high costs are due to both the energy cost and the capital cost for the crystallizer and associated heat exchange equipment, which requires titanium on most fluid-wetted surfaces.
- Requires extensive brine pretreatment and chemical addition which increase costs.
- Disposal of salts may be an issue, particularly if hazardous materials are present.





DocuSign Envelope ID: 2FA9A609-C360-4E53-8B28-BE8B77B6994A

Summary

- Treatment of high-TDS waters for beneficial use presents significant technological and economic challenges.
- Treatment requirements will depend on the desired use of the treated water.
- Treatment of high-TDS produced waters for reuse in oilfield applications (hydraulic fracturing, waterflooding, drilling fluids, etc.) may be economic where water availability is an issue.
- Production of potable water from high-TDS produced water is likely not economically feasible.
- Production of chemicals from produced water can offset treatment costs and provide a valuable commodity (acids, bases, rare earth elements, etc.)
-

DocuSign Envelope ID: 2FA9A609-C360-4E53-8B28-BE8B77B6994A

- **Fundamentals of Zero Liquid Discharge System Design**
- 10/01/2011 | William A. Shaw, POWER Magazine
- http://www.powermag.com/fundamentals-of-zero-liquid-discharge-system-design/?pagenum=2

DocuSign Envelope ID: 2FA9A609-C360-4E53-8B28-BE8B77B6994A

APPENDIX B

PRESENTATION HIGHLIGHTING FACILITY AND CAPABILITIES

DocuSign Envelope ID: 2FA9A609-C360-4E53-8B28-BE8B77B6994A

Energy & Environmental Research Center (EERC)

BRINE EXTRACTION AND STORAGE TEST (BEST) DEMONSTRATION TEST SITE

DE-FE0026160

U.S. Department of Energy National Energy Technology Laboratory
Water Technologies Project Review Meeting
September 17, 2020 – 1:30 p.m. ET

John Hamling
Assistant Director, Integrated Projects

© 2020 University of North Dakota Energy & Environmental Research Center.

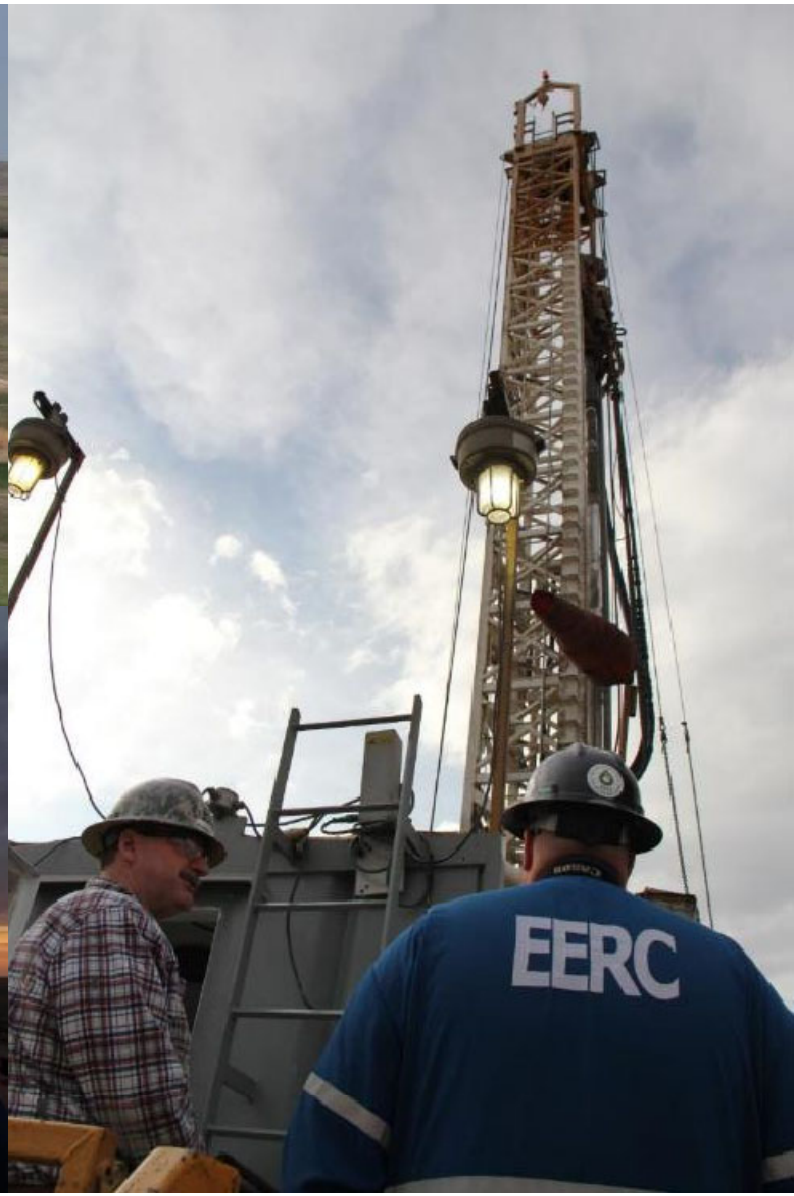
DocuSign Envelope ID: 2FA9A609-C360-4E53-8B28-BE8B77B6994A

NORTH DAKOTA

BRINE TREATMENT USER FACILITY







EERC

UND UNIVERSITY OF NORTH DAKOTA

DocuSign Envelope ID: 2FA9A609-C360-4E53-8B28-BE8B77B6994A

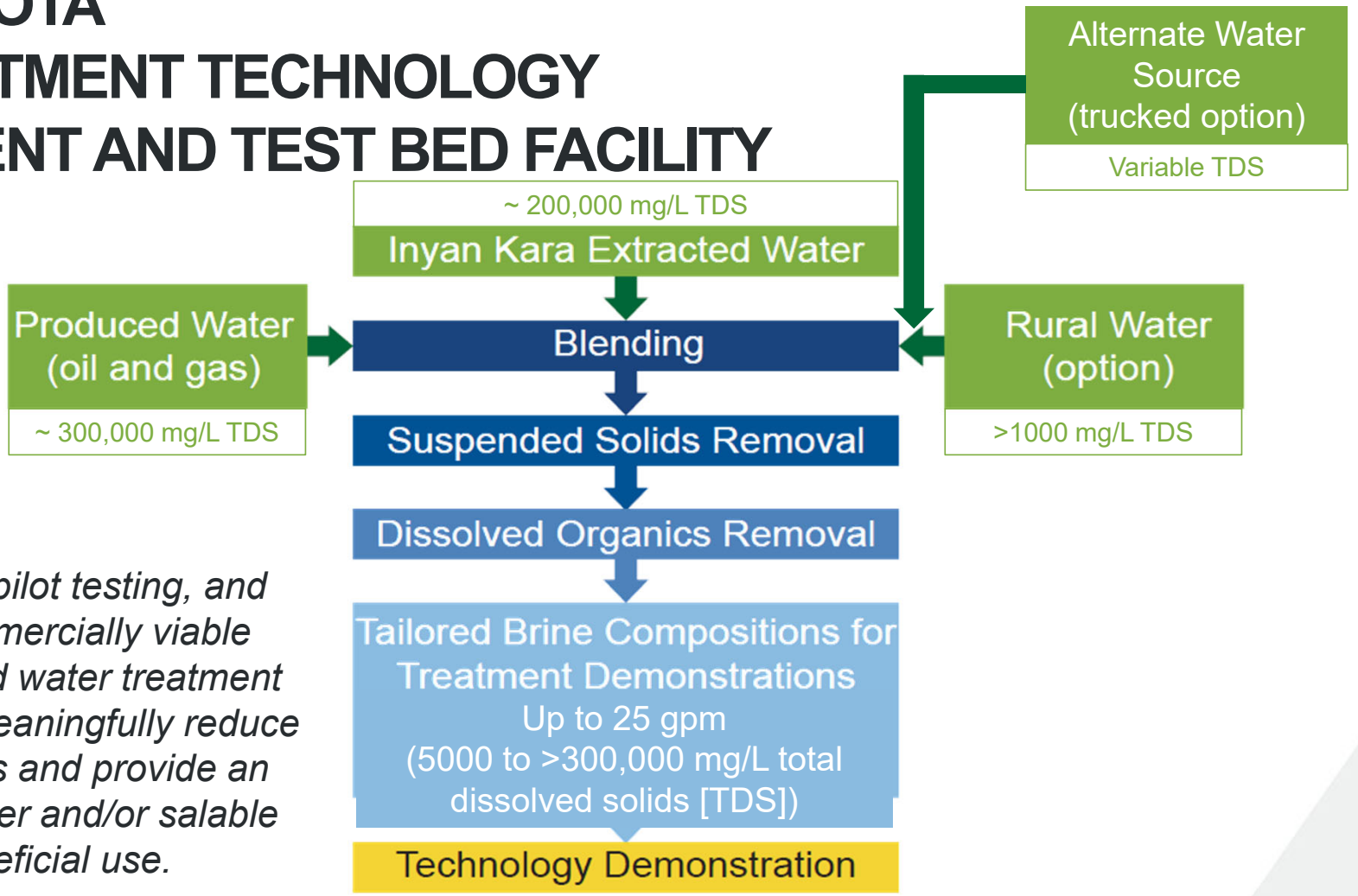
NORTH DAKOTA BRINE TREATMENT TECHNOLOGY DEVELOPMENT AND TEST BED FACILITY



Implement and operate a brine treatment technology development and test facility to enable development of brine treatment technologies capable of treating high-total dissolved solids (TDS) brines associated with geologic CO_2 storage targets.

DocuSign Envelope ID: 2FA9A609-C360-4E53-8B28-BE8B77B6994A

NORTH DAKOTA BRINE TREATMENT TECHNOLOGY DEVELOPMENT AND TEST BED FACILITY

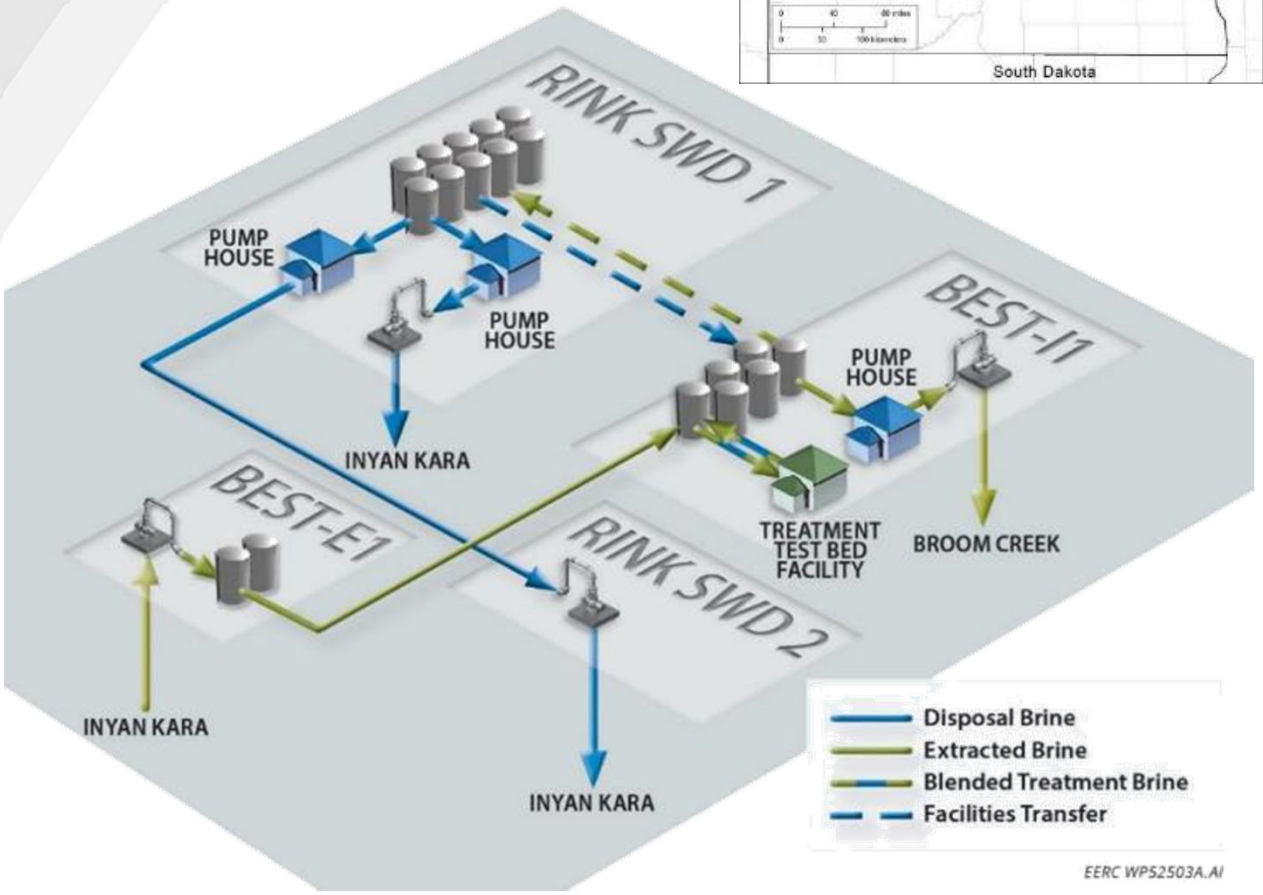


Enable development, pilot testing, and advancement of commercially viable extracted and produced water treatment technologies that can meaningfully reduce brine disposal volumes and provide an alternate source of water and/or salable products for beneficial use.

DocuSign Envelope ID: 2FA9A609-C360-4E53-8B28-BE8B77B6994A

THE SITE





EERC WPS2503A.AI



DocuSign Envelope ID: 2FA9A609-C360-4E53-8B28-BE8B77B6994A



North Dakota water treatment test bed facility available for demonstration of produced water treatment technologies.

EERC
UND NORTH DAKOTA





Enable development, pilot testing, and advancement of commercially viable extracted and produced water treatment technologies that can meaningfully reduce brine disposal volumes and provide an alternate source of water and/or salable products for beneficial use.

TEST BED FACILITY CAN REPLICATE EXTRACTED WATERS THAT ARE REPRESENTATIVE OF LOCATIONS/ SOURCES THROUGHOUT THE UNITED STATES





SITE SPECS

- 60' x 80' building (16 ft walls)
- 60' demonstration bay (accommodates semi-tractor-trailer)
- 200 kW electric power
- Two overhead doors
- Demonstration bay, water pretreatment area, and control room
- Heated and insulated
- Air handling/exchange
- Hazardous environment detection/evacuation alarm
- Temporary semi-storage tanks for demonstrations apply
- Waste handling and disposal on site
- Pilot treatment rates ranging up to 20 gpm
- 90–60 day continuous operations
- Capable of RO/NSS operations



FACILITY CAN BE READILY ADAPTED FOR USE WITH ALTERNATE FLUID COMPOSITIONS OR TREATMENT PROCESSES

- Alternate water sources trucked and offloaded at site
- Pretreatment and conditioning can be modified to replicate broader influent specifications
- Blending of alternate fluid chemistries for characterization of water or chemical treatment processes
- Test beds for enabling technologies (e.g., power/thermal supply, environmental conditioning, ...)
- On-site SWD/hydrocarbon disposal/reuse waste handling
- Can accommodate propane ($2,000-gal tank) and/or nonpotable cooling water (90 gpm)



CONTROL ROOM

- Instrumentation and control (DCS) for valves and compressors
- Data collection
- Energy and thermal monitors
- H&S (environment, health, and safety) and operability systems (e.g., pretreatment systems, hazardous environment monitoring, etc.)
- Remote, real-time, secure access



ACKNOWLEDGMENT

This is a collaborative effort with Nuverra Environmental Solutions and the U.S. Department of Energy (DOE) National Energy Technology Laboratory (NETL).

Developing and Validating Pressure Management and Plume Control Strategies in the Williston Basin Through a Brine Extraction and Storage Test

John Harding, Marc Kurz, Ryan Klapperich, Lonny Jacobson, and Robert Jensen

undeerc.org

EERC Nuverra ENERGY CMG Schlumberger

DocuSign Envelope ID: 2FA9A609-C360-4E53-8B28-BE8B77B6994A

WATFORD CITY, NORTH DAKOTA

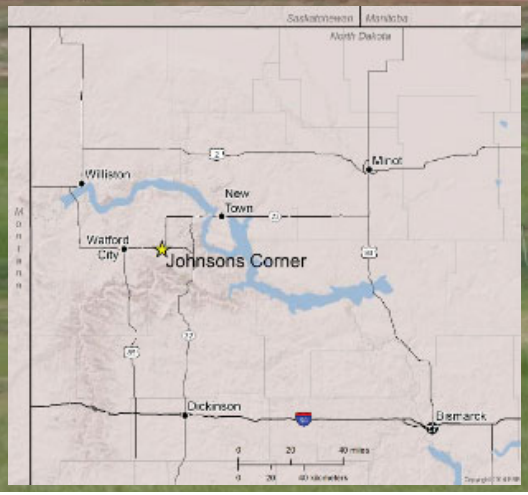
Oil & Gas Industrial Hub

- Population: ~15,000
- Lodging and restaurants
- 24-hour services



15 MILES EAST OF WATFORD CITY

ON HIGHWAY 23



DocuSign Envelope ID: 2FA9A609-C360-4E53-8B28-BE8B77B6994A

WATER TREATMENT DEMONSTRATION FACILITY



- Permanent environmental enclosure (24/7/365 ready)
  - 60’ x 80’ (18’ wall height)
  - Air-handling and exchange
  - Class I Division 2-rated
- 53’ demonstration bay with concrete floor
- Two overhead doors
- Integrated with active reservoir management (ARM) and saltwater disposal (SWD) infrastructure
- Treatment rates up to 25 gpm (bench to pilot)
- Blending and pretreatment



- Sized to accommodate up to a semi-tractor–trailer-sized demonstration
- 300 kW electric power
- Waste management
- Propane (5000-gal tank)*
- Noncontact cooling water (30 gpm)*

* Can be accommodated.

DocuSign Envelope ID: 2FA9A609-C360-4E53-8B28-BE8B77B6994A

BLENDING AND PRETREATMENT

Blending of water to a target TDS level of 180,000 mg/L

… or tailored blends
<5000 mg/L TDS
to
>300,000 mg/L TDS

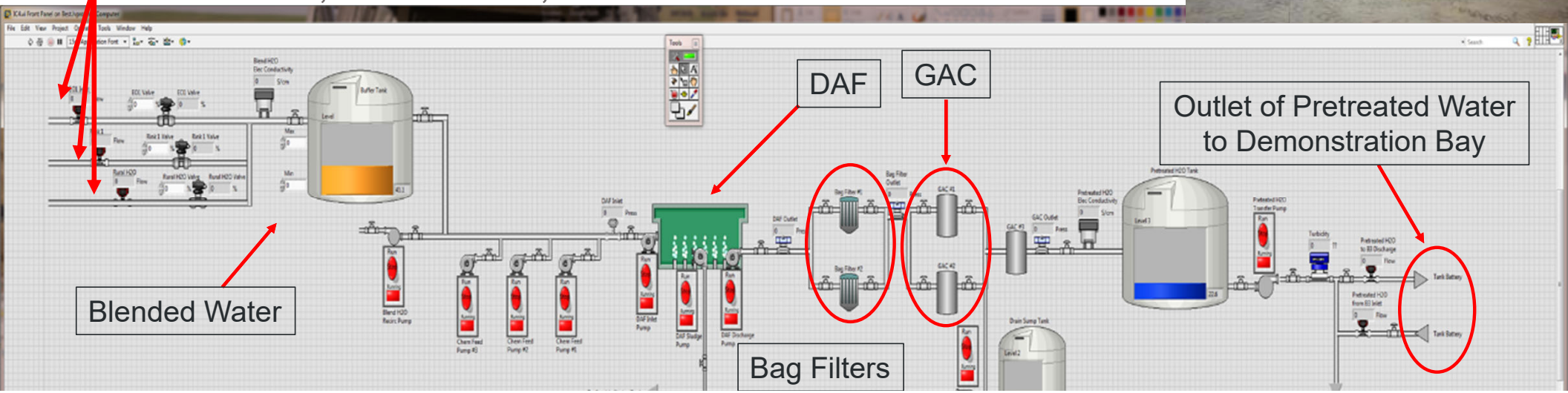
to suit capabilities and/or limitations of selected technologies.

- Suspended solids removal (dissolved air flotation [DAF]).
- Filter bags.
- Dissolved organics removal (granular activated carbon [GAC]).
- Facility can be adapted for use with alternate fluid compositions and treatment/pretreatment processes.



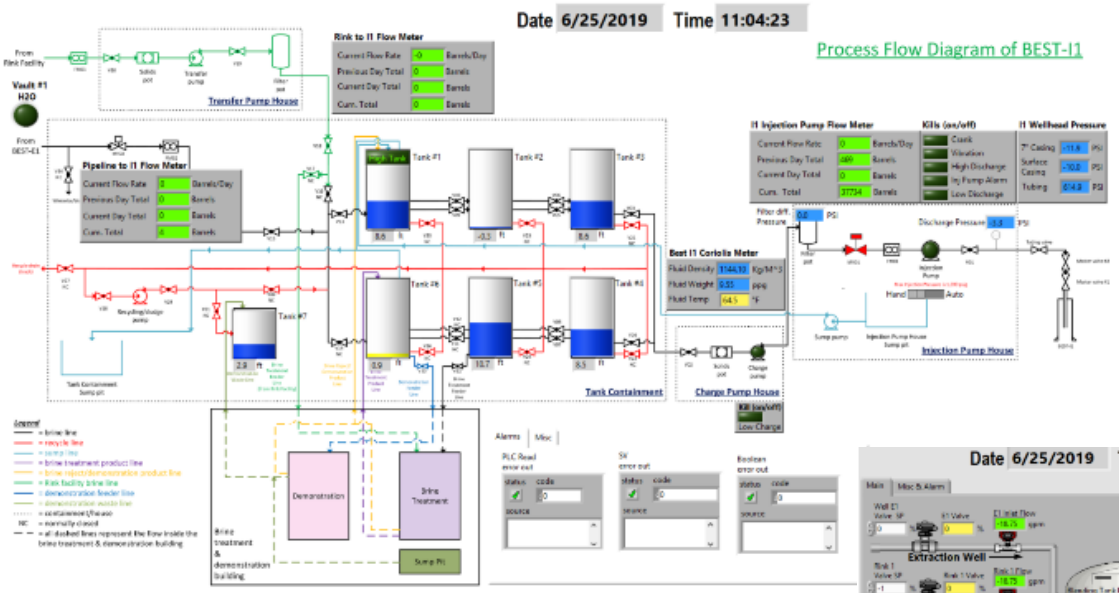


EXTRACTED, PRODUCED, AND FRESHWATER SOURCE



DocuSign Envelope ID: 2FA9A609-C360-4E53-8B28-BE8B77B6994A

SCADA, REMOTE MONITORING AND CONTROLS



FACILITIES

- Influent and effluent flow rates and composition
- Chemical usage
- Energy and thermal use/load
- HSE and operability systems (e.g., pretreatment systems, hazardous environmental monitoring…)
- Remote, real-time, secure access

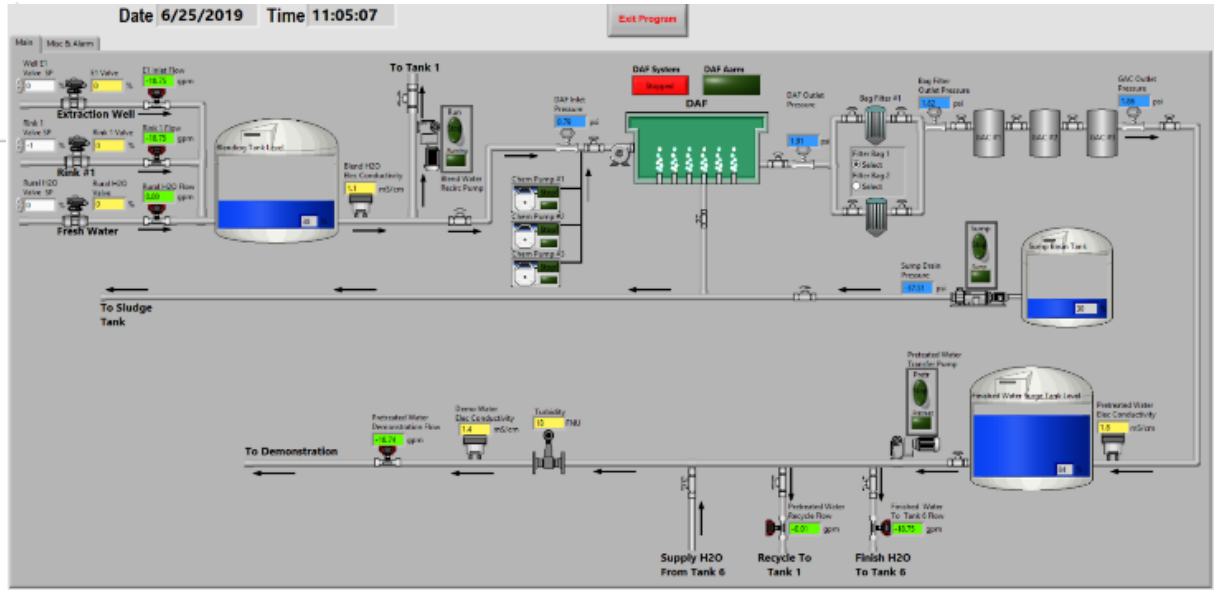


Water Blending and Pretreatment

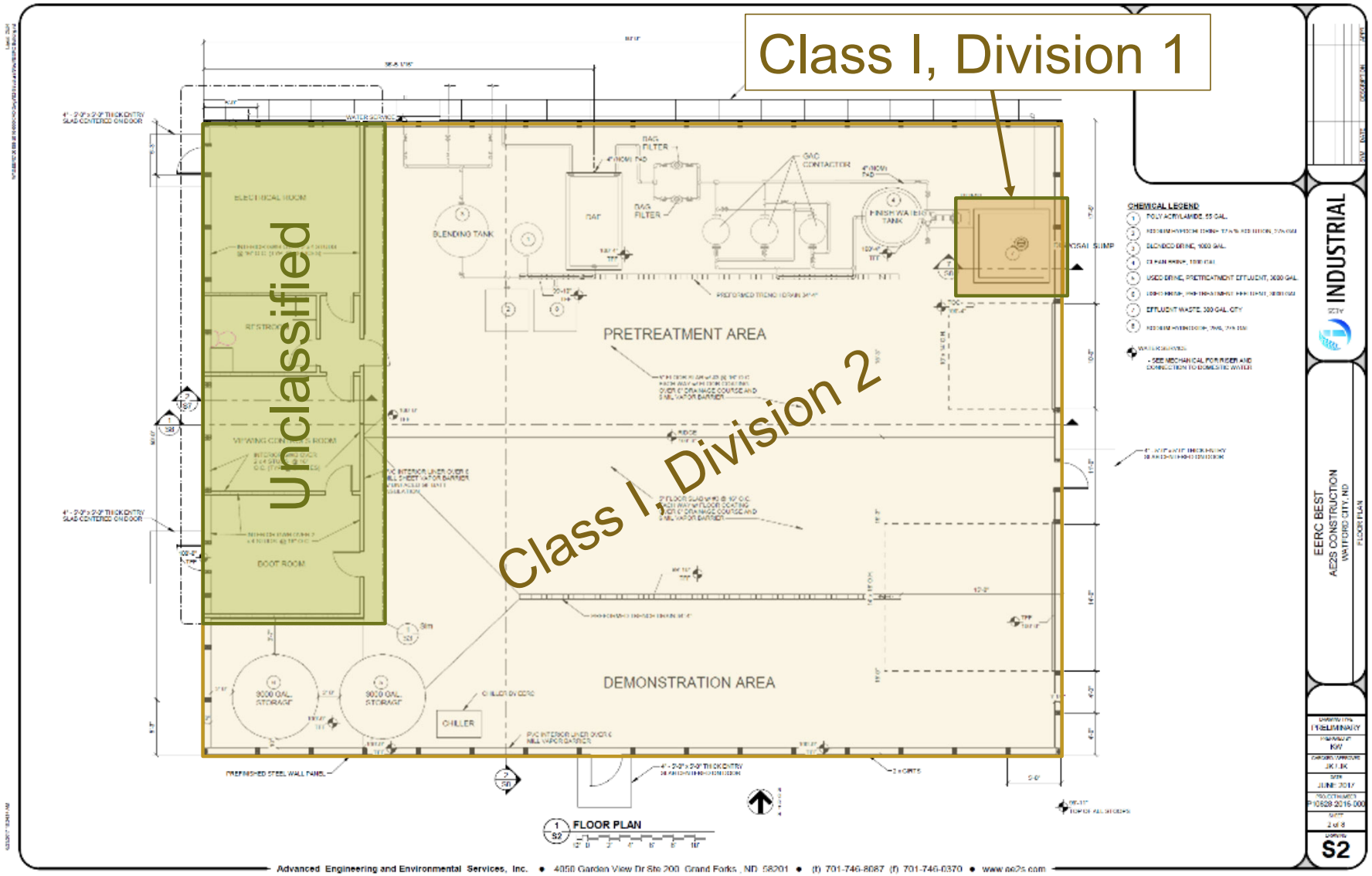


Finished Water Supply for Demonstrations

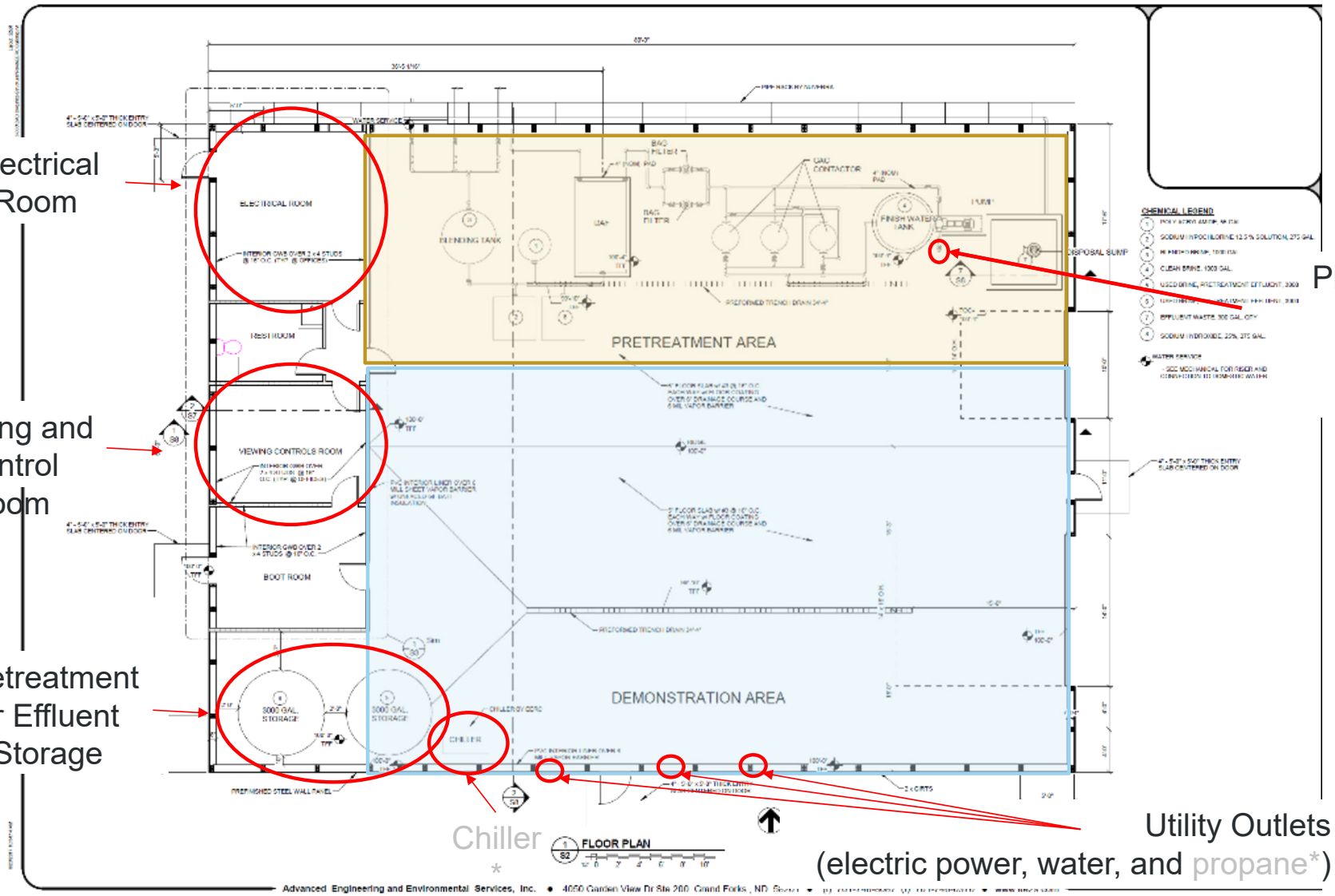
BLENDING AND PRETREATMENT



DocuSign Envelope ID: 2FA9A609-C360-4E53-8B28-BE8B77B6994A



DocuSign Envelope ID: 2FA9A609-C360-4E53-8B28-BE8B77B6994A



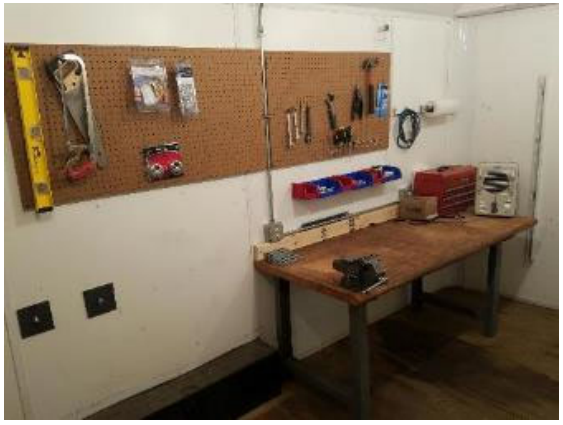
DocuSign Envelope ID: 2FA9A609-C360-4E53-8B28-BE8B77B6994A

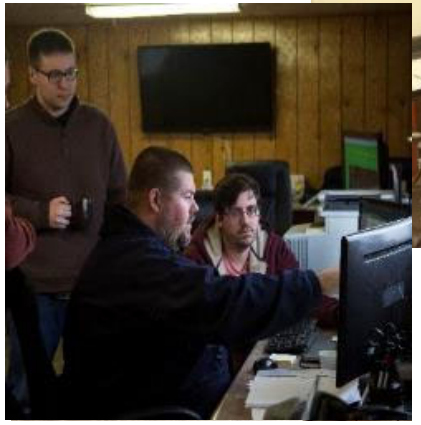
MOBILE WORKSHOP AND COMMAND CENTER

MULTIUSE OFFICE, MEETING AND WORKSPACE







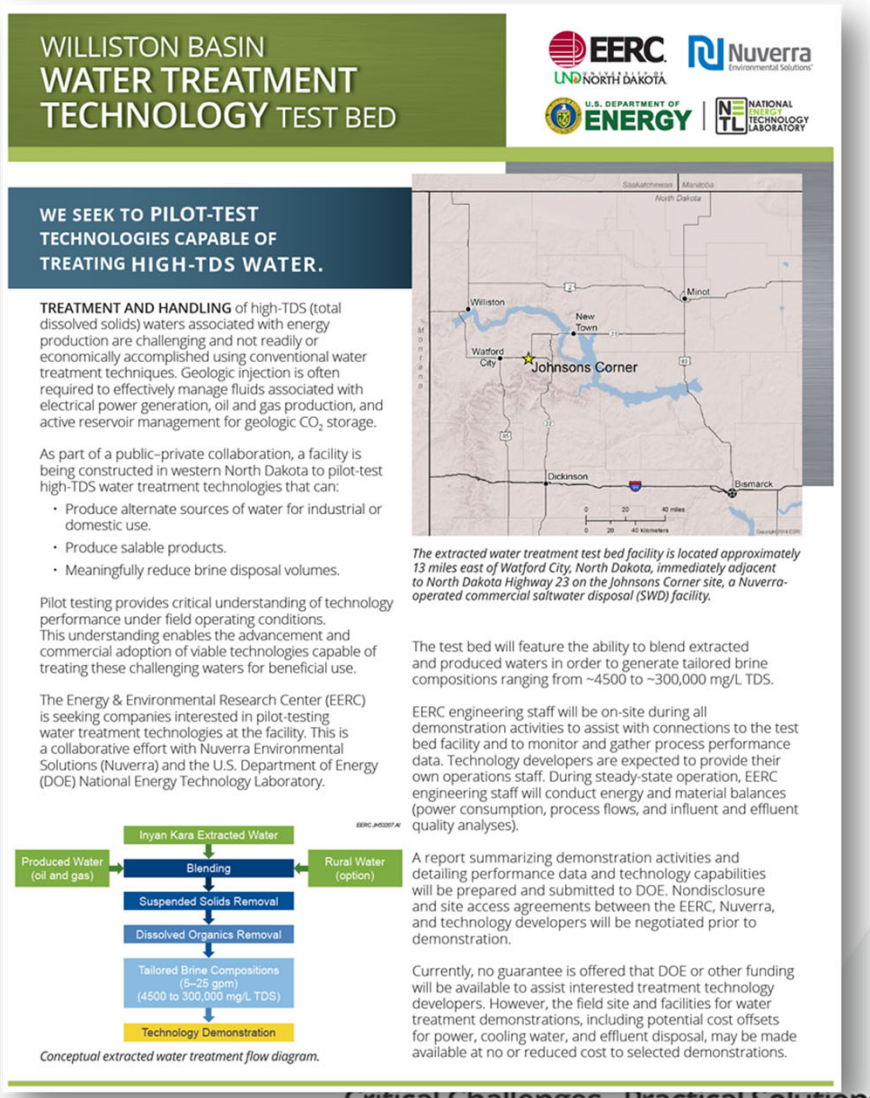




DocuSign Envelope ID: 2FA9A609-C360-4E53-8B28-BE8B77B6994A



- Seeking to develop and test two or more brine treatment technologies at the North Dakota brine treatment technology development and test bed facility.
- Enable development of brine treatment technologies capable of treating high-TDS brines associated with geologic CO_2 storage targets. (**~180,000** mg/L TDS).
  - Alternate source of water
  - Reduced disposal volumes
  - Salable products for beneficial use
- Cost offsets may be made available for highly qualified technologies.



WILLISTON BASIN
WATER TREATMENT TECHNOLOGY TEST BED

EERC | Nuverra Environmental Solutions | U.S. Department of Energy | National Energy Technology Laboratory

WE SEEK TO PILOT-TEST TECHNOLOGIES CAPABLE OF TREATING HIGH-TDS WATER.

TREATMENT AND HANDLING of high-TDS (total dissolved solids) waters associated with energy production are challenging and not readily or economically accomplished using conventional water treatment techniques. Geologic injection is often required to effectively manage fluids associated with electrical power generation, oil and gas production, and active reservoir management for geologic CO_2 storage.

As part of a public–private collaboration, a facility is being constructed in western North Dakota to pilot-test high-TDS water treatment technologies that can:

- Produce alternate sources of water for industrial or domestic use.
- Produce salable products.
- Meaningfully reduce brine disposal volumes.

Pilot testing provides critical understanding of technology performance under field operating conditions. This understanding enables the advancement and commercial adoption of viable technologies capable of treating these challenging waters for beneficial use.

The Energy & Environmental Research Center (EERC) is seeking companies interested in pilot-testing water treatment technologies at the facility. This is a collaborative effort with Nuverra Environmental Solutions (Nuverra) and the U.S. Department of Energy (DOE) National Energy Technology Laboratory.

The extracted water treatment test bed facility is located approximately 13 miles east of Watford City, North Dakota, immediately adjacent to North Dakota Highway 23 on the Johnsons Corner site, a Nuverra-operated commercial saltwater disposal (SWD) facility.

The test bed will feature the ability to blend extracted and produced waters in order to generate tailored brine compositions ranging from ~4500 to ~300,000 mg/L TDS.

EERC engineering staff will be on-site during all demonstration activities to assist with connections to the test bed facility and to monitor and gather process performance data. Technology developers are expected to provide their own operations staff. During steady-state operation, EERC engineering staff will conduct energy and material balances (power consumption, process flows, and influent and effluent quality analyses).

A report summarizing demonstration activities and detailing performance data and technology capabilities will be prepared and submitted to DOE. Nondisclosure and site access agreements between the EERC, Nuverra, and technology developers will be negotiated prior to demonstration.

Currently, no guarantee is offered that DOE or other funding will be available to assist interested treatment technology developers. However, the field site and facilities for water treatment demonstrations, including potential cost offsets for power, cooling water, and effluent disposal, may be made available at no or reduced cost to selected demonstrations.

Conceptual extracted water treatment flow diagram.

Critical Challenges. Practical Solutions.

EERC | UND University of North Dakota | U.S. Department of Energy | NETL National Energy Technology Laboratory

DocuSign Envelope ID: 2FA9A609-C360-4E53-8B28-BE8B77B6994A

TECHNOLOGY TESTING

BRINE TREATMENT DEVELOPMENT FACLITY







EERC | UND UNIVERSITY OF NORTH DAKOTA | U.S. DEPARTMENT OF ENERGY | NETL NATIONAL ENERGY TECHNOLOGY LABORATORY

Critical Challenges. Practical Solutions.

DocuSign Envelope ID: 2FA9A609-C360-4E53-8B28-BE8B77B6994A

NORTH DAKOTA BRINE TREATMENT FACILITY

POTENTIAL ADAPTATION FOR EXPANDED APPLICATIONS

Facility can be readily adapted for use with alternate fluid compositions or treatment processes.

- Alternate water sources trucked and offloaded at site.
- Pretreatment and conditioning can be modified to replicate broader influent specifications.
- Blending of additives to replicate target fluid chemistries.
- Application of cascade technologies (e.g., power/thermal supply, pretreatment/conditioning…).
- On-site SWD and waste handling.



DocuSign Envelope ID: 2FA9A609-C360-4E53-8B28-BE8B77B6994A

NORTH DAKOTA BRINE TREATMENT FACILITY

POTENTIAL ADAPTATION FOR EXPANDED APPLICATIONS

- Oil and gas fluid conditioning (e.g., emulsion breaking, corrosion, scale inhibitors, fluid compatibility testing, etc.)
- Produced water treatment
- Electric power generation wastewater treatment
- Industrial and municipal waste and water treatment
- Mineral resource recovery
- Agricultural water treatment
- Geologic conditioning and homogenization as a means of water pretreatment
- Benchmarking the economic and technical limits of water treatment technologies (e.g., MVR)
- Collaboration with other federal, state, or industry groups



DocuSign Envelope ID: 2FA9A609-C360-4E53-8B28-BE8B77B6994A

John Hamling
Assistant Director, Integrated Projects
jhamling@undeerc.org
701.777.5472 (phone)

Energy & Environmental Research Center
University of North Dakota
15 North 23rd Street, Stop 9018
Grand Forks, ND 58202-9018

www.undeerc.org
701.777.5000 (phone)
701.777.5181 (fax)



DocuSign Envelope ID: 2FA9A609-C360-4E53-8B28-BE8B77B6994A

APPENDIX C

PROSPECTUS FOR TREATMENT FACILITY

DocuSign Envelope ID: 2FA9A609-C360-4E53-8B28-BE8B77B6994A

WILLISTON BASIN WATER TREATMENT TECHNOLOGY TEST BED

WE SEEK TO PILOT-TEST TECHNOLOGIES CAPABLE OF TREATING HIGH-TDS WATER.

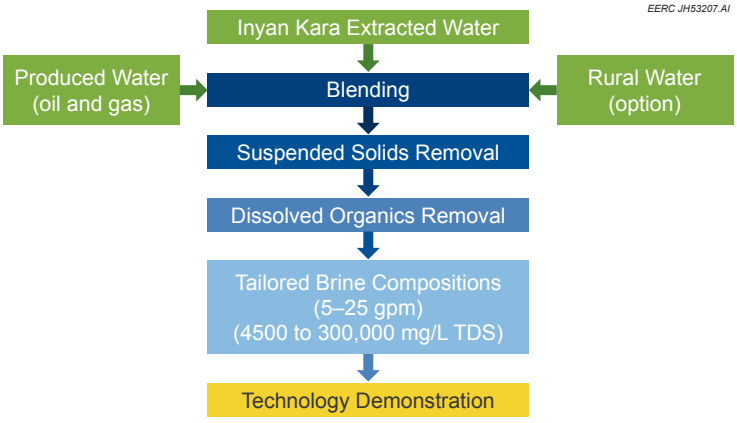
TREATMENT AND HANDLING of high-TDS (total dissolved solids) waters associated with energy production are challenging and not readily or economically accomplished using conventional water treatment techniques. Geologic injection is often required to effectively manage fluids associated with electrical power generation, oil and gas production, and active reservoir management for geologic CO_2 storage.

As part of a public–private collaboration, a facility is being constructed in western North Dakota to pilot-test high-TDS water treatment technologies that can:

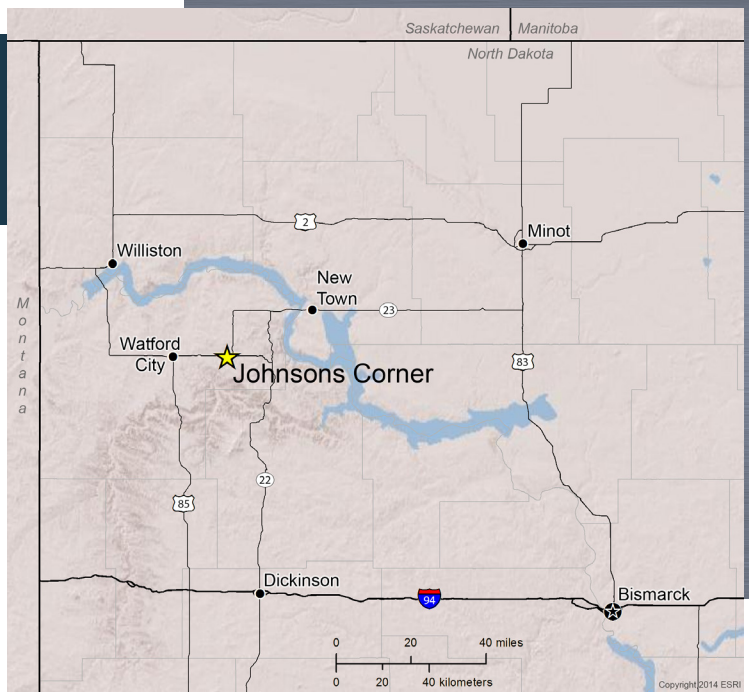
- Produce alternate sources of water for industrial or domestic use.
- Produce salable products.
- Meaningfully reduce brine disposal volumes.

Pilot testing provides critical understanding of technology performance under field operating conditions. This understanding enables the advancement and commercial adoption of viable technologies capable of treating these challenging waters for beneficial use.

The Energy & Environmental Research Center (EERC) is seeking companies interested in pilot-testing water treatment technologies at the facility. This is a collaborative effort with Nuverra Environmental Solutions (Nuverra) and the U.S. Department of Energy (DOE) National Energy Technology Laboratory.



Conceptual extracted water treatment flow diagram.



The extracted water treatment test bed facility is located approximately 13 miles east of Watford City, North Dakota, immediately adjacent to North Dakota Highway 23 on the Johnsons Corner site, a Nuverra-operated commercial saltwater disposal (SWD) facility.

The test bed will feature the ability to blend extracted and produced waters in order to generate tailored brine compositions ranging from ~4500 to ~300,000 mg/L TDS.

EERC engineering staff will be on-site during all demonstration activities to assist with connections to the test bed facility and to monitor and gather process performance data. Technology developers are expected to provide their own operations staff. During steady-state operation, EERC engineering staff will conduct energy and material balances (power consumption, process flows, and influent and effluent quality analyses).

A report summarizing demonstration activities and detailing performance data and technology capabilities will be prepared and submitted to DOE. Nondisclosure and site access agreements between the EERC, Nuverra, and technology developers will be negotiated prior to demonstration.

Currently, no guarantee is offered that DOE or other funding will be available to assist interested treatment technology developers. However, the field site and facilities for water treatment demonstrations, including potential cost offsets for power, cooling water, and effluent disposal, may be made available at no or reduced cost to selected demonstrations.

DocuSign Envelope ID: 2FA9A609-C360-4E53-8B28-BE8B77B6994A

BLENDED AND PRETREATED WATER CHARACTERISTICS

The table below shows the typical composition of a blended water that could be treated at the site.

Parameter	Value, mg/L
B	303
Li	46
Na	49,900
K	5010
Mg	680
Ca	13,800
Sr	1140
Ba	24
Fe	46
Mn	12
P	<15
Si	<20
Fluoride	<7
Sulfate	167
NO_2 and NO_3 (as nitrogen)	<4
Chloride	108,700
TSS[1]	–
TOC[2]	–
TDS	180,000
Total Hardness as $CaCO_3$	38,700

[1]TSS (total suspended solids).
[2]TOC (total organic carbon).

TEST BED FEATURES

The site will include a heated building with a concrete floor that is integrated with the on-site formation water extraction and disposal infrastructure. The building will accommodate a standard semi tractor–trailer (53 ft long).

UTILITIES

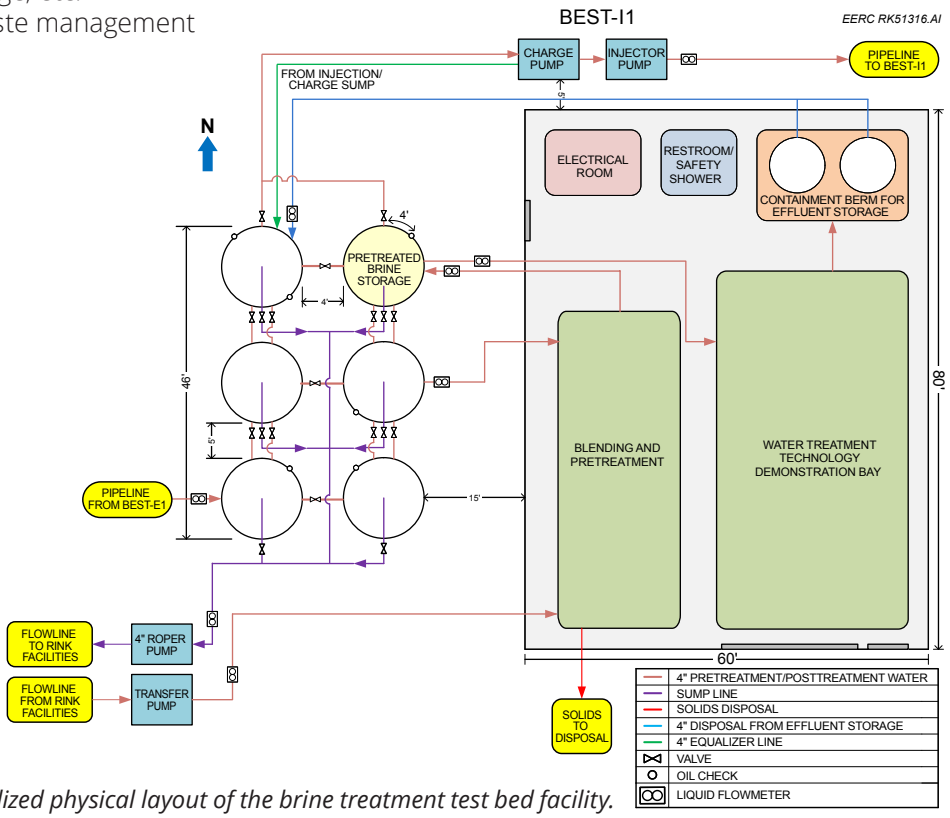
- Up to 300 kW of electric power
- Propane (5000-gal tank)
- Noncontact cooling water (30 gpm)

DEMONSTRATION TEST TRIALS

- Pilot treatment rates ranging from 1 to 25 gpm
- 30–60+-day extended-duration tests (desired minimum of two maintenance cycles)
- Monitoring of energy, flow, chemical usage, etc.
- Waste management

EXTRACTED WATER PRETREATMENT

- Blending of formation waters (Bakken and Inyan Kara Formations) to target a TDS level of 180,000 mg/L or tailored blends to suit capabilities and/or limitations of specific technologies
- Suspended solids removal
- Dissolved organics removal
- Ability to provide Bakken produced and/or flowback water for suitable demonstrations



Conceptualized physical layout of the brine treatment test bed facility.

If you are interested in demonstrating a brine treatment technology at this site or for more information, please contact:

Marc Kurz
Senior Geologist and Process Chemistry and Development Team Lead
(701) 777-5278, mkurz@undeerc.org

John Hurley
Principal Materials Scientist
(701) 777-5159, jhurley@undeerc.org

John Hamling
Assistant Director for Integrated Projects
(701) 777-5472, jhamling@undeerc.org

Energy & Environmental Research Center
15 North 23rd Street, Stop 9018
Grand Forks, ND 58202-9018
www.undeerc.org

EERC | U.S. DEPARTMENT OF ENERGY | NETL NATIONAL ENERGY TECHNOLOGY LABORATORY | Nuverra Environmental Solutions

© 2019 University of North Dakota Energy & Environmental Research Center.

DocuSign Envelope ID: 2FA9A609-C360-4E53-8B28-BE8B77B6994A

APPENDIX D

EXTRACTED WATER TREATMENT TECHNOLOGY SELECTION PROCESS

DocuSign Envelope ID: 2FA9A609-C360-4E53-8B28-BE8B77B6994A

EXTRACTED WATER TREATMENT TECHNOLOGY SELECTION PROCESS

The Energy & Environmental Research Center (EERC) and Electric Power Research Institute (EPRI) will work with the U.S. Department of Energy (DOE) to identify and field-test technologies that have the potential to successfully treat high-TDS (total dissolved solids) extracted water (180,000 mg/L on average). The selection process will follow a series of steps:

- Development of a pool of possible technology providers through survey, questionnaire, and discussion.
- Evaluation of technology providers using criteria agreed upon by a selection team made up of members from DOE, the EERC, and EPRI.
- Establishment of nondisclosure agreements with the selected developers in order to receive detailed information.
- Preparation of 2-page summaries by the EERC and EPRI of the possible technologies for review by the DOE, EERC, and EPRI selection team.
- Review of the summaries, discussion among team members, and agreement by the selection team on possible water treatment technologies for field testing.
- Finalization of legal and engineering documentation with technology providers for testing of the selected technologies.

At a minimum, each technology provider must comply with the host site's health, safety, and environment requirements and terms and conditions of the site access agreement, which will be reviewed by DOE, the EERC, EPRI, and the respective site hosts. The EERC and EPRI will solicit information on possible technologies and their vendors from networks of industry contacts, technical papers, and information searches. The EERC and EPRI will confirm interest from possible technology providers in supplying critical technology information and in participating in a potential site demonstration. Information from interested technology providers will be obtained, and a 2-page summary of their technologies, readiness, and economic benefits will be prepared by the EERC and EPRI for consideration by the selection team.

Preliminary screening criteria have been developed by the EERC and EPRI that are broad enough to apply to a large number of candidate technologies for demonstration. The criteria will discriminate among technology alternatives while making an effort to avoid duplication of demonstrations of the same basic technology type. The criteria are qualitative as related to DOE objectives and budget considerations and quantitative as listed below.

Qualitative screening criteria include the following:

- Project funding availability
- Cost of testing
- Cost of further development
- Site compatibility and ease of accommodation

Qualitative screening criteria will be used to screen prospective technologies prior to quantitative screening and selection. The process will give priority to those technologies associated

DocuSign Envelope ID: 2FA9A609-C360-4E53-8B28-BE8B77B6994A

with DOE-funded projects awarded for the development of innovative high-TDS brine pretreatment and desalination technologies (DOE FOA0001095 and DOE FOA0001238) that successfully satisfy technology-screening criteria. If a given technology satisfies the screening criteria and is among those selected for demonstration, additional consideration may be given to those technology providers that have the ability to provide cost share that reduces the cost of demonstration.

The technologies will be quantitatively scored by the selection team on a scale of 1 to 10 in the areas of projected benefits, technology strengths, and organization strength. The ranking of technologies will be accomplished through the following weighting factors:

1. Projected benefits – 50%
   a. Reduction in brine disposal/injection costs
   b. Production of salable products
   c. Valuation of treated water for reuse
   d. Enablement of other treatment technologies (i.e., novel pretreatments)
   e. Previously funded by DOE

2. Technology strengths – 40%
   a. Scientific soundness
   b. Readiness level
   c. Safety considerations
   d. Waste generation (environmental impact)
   e. Scalability
   f. Maximum brine concentration that can be treated

3. Organization strength – 10%
   a. Intellectual property or license ownership
   b. Capability for further development
   c. Technical and management team

After selection, letters of commitment from the selected technology providers will be obtained, and any necessary confidentiality agreements will be executed prior to demonstration phases of the project. The EERC and EPRI will then develop a schedule of operations for the selected technologies. Technology demonstration activities will be coordinated to coincide with formation water extraction during active reservoir management testing. The EERC test bed facility is scheduled to be operational from summer 2017 through spring 2020. The EPRI test bed facility is scheduled to be operational from summer 2018 through winter 2020.

DocuSign Envelope ID: 2FA9A609-C360-4E53-8B28-BE8B77B6994A

APPENDIX E

DESALINATION TECHNOLOGY VENDOR QUESTIONNAIRE

DocuSign Envelope ID: 2FA9A609-C360-4E53-8B28-BE8B77B6994A

DESALINATION TECHNOLOGY VENDOR QUESTIONNAIRE

The Energy & Environmental Research Center (EERC) and Electric Power Research Institute (EPRI) are working with the U.S. Department of Energy (DOE) to identify and field-test technologies that have the potential to successfully treat high-TDS (total dissolved solids) extracted water (180,000 mg/L on average). This work is being performed under the DOE-funded Brine Extraction and Storage Test (BEST) Phase II Program. While there is no guarantee that DOE or other funding will be made available to assist interested brine treatment technology providers, the field site and facilities may be made available to interested technology providers for technology demonstrations. Additionally, providers that undergo and screen through an evaluation process and rank highly may receive some cost offsets for power, cooling water, and effluent disposal and could potentially include development, mobilization, and operation costs if funding is made available.

Two BEST program technology demonstration test bed sites are being established. The EERC site is located at a saltwater disposal facility, approximately 12 miles east of Watford City, North Dakota. The demonstration test bed will be an enclosed building capable of housing standard semi (tractor–trailer)-sized technology skids. Propane, electric power (300 kVA), and cooling water (30 gpm) will be available at the test bed. Influent will be a blend of a saline extracted groundwater and produced water from oil and gas operations. The waters will be blended to achieve the target level of 180,000 mg/L TDS and pretreated to remove suspended solids and dissolved organics. Projected characteristics of the blended water are presented in Appendix A.

EERC engineering staff will be on-site during all demonstration activities to assist with connections to the test bed facility and to monitor and gather process performance data. Technology providers are expected to provide their own operations staff, with assistance provided by the EERC where appropriate. During steady-state operation, EERC engineering staff will conduct energy and material balances (power consumption, process flows, and influent and effluent quality analyses). Effluent from individual technologies will be collected, temporarily stored, and reinjected into the extracted water disposal well in accordance with all applicable rules and regulations. Any solids and/or sludges generated during the demonstrations will be analyzed to determine hazardousness (metals, naturally occurring radioactive materials [NORM]) prior to disposal.

The EPRI site is located at Plant Smith near Panama City, Florida, where wastewater from the ash pond, blowdown water from the cooling towers, and reclaimed water is being collected and injected under an existing underground injection control (UIC) permit. Up to four test beds, consisting of 60-ft-long open-air bays (compacted gravel pads) will be provided along with on-site utilities (natural gas or propane, electrical, cooling water, and process water) and temporary office facilities. The project will produce ~166,000 mg/L TDS brine from the Tuscaloosa Formation, and it can be blended with the plant waters, producing intermediate waters of any composition ranging from ~1000 to 166,000 mg/L TDS (Appendix E2). The maximum flow rate available for testing will be 25 gallons a minute. Anticipated pretreatment will consist of removal of suspended solids and water softening (upon request).

DocuSign Envelope ID: 2FA9A609-C360-4E53-8B28-BE8B77B6994A

EPRI and contract staff will be on-site during pilot testing activities to assist with utility connections and daylight facility operations and to provide third-party process validation. Similar to the EERC project, technology vendors will be responsible for mobilizing/demobilizing, operating, and maintaining their equipment and collecting test data. EPRI and contract staff will conduct energy and material balances (power consumption, process flows, influent and effluent quality analyses). Effluent from individual technologies including treated, reject, and process waters will be collected, temporarily stored, and reinjected into the extracted water disposal well in accordance with all applicable rules and regulations. Any solids and/or sludges generated during the demonstrations will be collected and analyzed to determine hazardousness (metals, NORM) prior to off-site disposal. Any individual technologies that generate nonhazardous and hazardous waste as part of their treatment process will be required to handle, store, and dispose of said waste under manifest in accordance with applicable state and federal regulations.

The following questionnaire seeks information from interested technology developers that can be used to assess technology readiness level and vendor willingness to participate in the demonstration program. Please indicate areas where information is available but not provided because of proprietary or confidential nature.

1. Technology
   - Maximum concentration of brine that can be desalinated.
   - Technology description including pretreatment requirements.
   - Technical barriers to commercialization.
   - Is a pilot-scale system available or under development that could be used to demonstrate the technology in the 1–5 gal/min range in the summers of 2017 to 2019?
     - Preferred timeframe
   - If a pilot system is not available, how long would it take to build one that could treat a brine flow rate of 1 to 5 gallons/min?
   - List any pretreatment requirements that, based on the characteristic information provided in Appendix E1, would be required to successfully demonstrate your technology.

2. Economics Based on Treating 90,000 and 180,000 mg/L TDS Brine
   - Cost to perform a field demonstration of a 1- to 5-gal/min system lasting at least 30 days and at least two cleaning cycles (if applicable).
   - What is your preferred duration and cost of field testing should it exceed the 30-day minimum trial period specified above?
   - Is a commercial product produced, and what is its typical use and value?

3. Business
   - Intellectual property or license ownership.
   - Development plan to bring technology to a commercial scale.
   - Sources of current and previous funding (just who, not $ amount).
   - Ability to fund or partially fund a pilot field demonstration.
   - Willingness to enter into a site access agreement that limits access and host liability.
   - All technology providers must comply with health, safety, and environmental requirements of the site host.

DocuSign Envelope ID: 2FA9A609-C360-4E53-8B28-BE8B77B6994A

4. Field Testing
   - Do you have any field testing data? If so, please provide the following where available:
     - Input fluid composition
     - Test duration and treatment rate
     - Effluent/product recovery efficiency
     - Effluent/product quality or composition
     - Relative amount of waste streams and their composition and disposal methods
     - Time between cleaning/maintenance cycles.
     - Residual waste disposal costs.
     - Estimated pretreatment capital expenditure (CAPEX) and operating expenses (OPEX) for a 500-gal/min system.
     - Estimated primary treatment CAPEX and OPEX for a 500-gal/min system.
     - Estimated relative energy costs with comparison to simple evaporation for a 500-gal/min system.

   The reviewers request that you please limit your input to a maximum of 20 pages.

DocuSign Envelope ID: 2FA9A609-C360-4E53-8B28-BE8B77B6994A

APPENDIX E1

EERC BEST BLENDED AND PRETREATED WATER CHARACTERISTICS

DocuSign Envelope ID: 2FA9A609-C360-4E53-8B28-BE8B77B6994A

Energy & Environmental Research Center (EERC)
Brine Extraction and Storage Test (BEST) Blended and Pretreated Water Characteristics

Parameter	Value, mg/L
Boron	303
Lithium	46
Sodium	49,900
Potassium	5010
Magnesium	680
Calcium	13,800
Strontium	1140
Barium	24
Iron	46
Manganese	12
Phosphorus	<15
Silicon	<20
Fluoride	<7
Sulfate	167
NO_2 and NO_3 (as nitrogen)	<4
Chloride	108,700
Total Suspended Solids	–
Total Organic Carbon	–
Total Dissolved Solids	180,000
Total Hardness (as $CaCO_3$)	38,700

DocuSign Envelope ID: 2FA9A609-C360-4E53-8B28-BE8B77B6994A

APPENDIX E2

EPRI BEST END MEMBER WATER QUALITY ANALYSIS

DocuSign Envelope ID: 2FA9A609-C360-4E53-8B28-BE8B77B6994A

Electric Power Research Institute (EPRI) Brine Extraction and Storage Test (BEST) End Member Water Quality Analysis

Parameter	Ash Pond[1]	Tuscaloosa TIW-1
Major Elements, mg/L		
Alkalinity, Total	87	48
Calcium	82	18,000
Chloride	540	106,000
Potassium	19	
Magnesium	32	1,800
Sodium	320	40,000
Sulfate	210	426
Trace Constituents, mg/L		
Aluminum	0.06	1.9 [2]
Ammonia	NA[3]	23
Barium	0.14	0.0076
Boron	2.6	41
Cadmium	0.00095	<0.048
Copper	0.0011	0.065
Fluoride	0.18	<0.050
Iron	<0.05	17
Manganese	0.011	32
Lead	0.0002	<0.013
Phosphorus, total	0.087	1.1
Silicon	1.6	21[4]
Zinc	1.4	1.4
Environmental Conditions		
pH, field	NA	5.98
Temp. °C, field		33
Specific Conductance (Field), uS/cm	NA	174,100
Other, mg/L		
Total Dissolved Solids	1300	238,000
Hardness (as $CaCO_3$)	NA	52,000
Organics, ug/L		
Benzene	NA	0.049
Chloroform	NA	0.78[2]
Total Organic Carbon	4.3	7.6

[1] Additional constituents were detected that are not report in the table and are available on request.
[2] The reported value is between the laboratory detection limit and the laboratory practical quantitation limit; analyte is present but concentration is estimated.
[3] Not available.
[4] The analyte was detected in both the sample and the associated laboratory method blank.

DocuSign Envelope ID: 2FA9A609-C360-4E53-8B28-BE8B77B6994A

APPENDIX F

TECHNOLOGY SELECTION SUMMARIES

DocuSign Envelope ID: 2FA9A609-C360-4E53-8B28-BE8B77B6994A

WATER TREATMENT TECHNOLOGY SELECTION FOR TESTING AT BEST BRINE TREATMENT TEST BED FACLITIES

Technology Provider: U.S. Department of Energy National Energy Technology Laboratory (NETL) Research and Innovation Center (RIC)

Point of Contact: Dr. Nicholas Siefert

Technology to Be Tested: Pilot-scale MVR (mechanical vapor recompression) unit

Technology Category: Thermal

Requested Site and Time Frame: North Dakota, Quarter 3 2019

Goal: Parametric testing of the pilot MVR system will be conducted for water salinities ranging from 35,000- to 180,000-mg/L TDS (total dissolved solids). The results will provide benchmark performance data for comparison with membrane and other competing technologies. The proposed testing aligns with the goals and objectives of the BEST program.

SCREENING CRITERIA (qualitative)

Estimated Cost of Testing: $100,752
Funding: Testing including operation and transportation funded by technology provider.
Cost of Further Deployment: No additional cost anticipated; the MVR unit is currently operational, has been operationally tested at NETL's facilities, and is appropriately scaled for the proposed tests.
Site Compatibility and Ease of Accommodation: The MVR unit is compatible with the North Dakota brine treatment facility. The facility is capable of accommodating the operational range of the MVR pilot unit and the proposed test program without modification. The unit is electrically powered. A hazard assessment determined that the unit is not anticipated to produce emissions or unacceptable HSE risks that are beyond designed capabilities of the EERC BEST facility.

Quantitative

Projected Benefits (out of 50)
(benefits to consider: a) reduction in brine disposal/injection costs, b) production of salable products, c) valuation of treated water for reuse, d) enablement of other treatment technologies, and e) previously funded by DOE)

NETL/RIC is conducting research to demonstrate advanced membrane-based technologies that can concentrate effluent streams to high concentrations while reducing both the energy and capital cost of the brine concentration step by 50%. To make a fair comparison between membrane-based technologies and other competing technologies, tests will be conducted on a pilot-scale MVR unit that NETL procured and repaired from the U.S. Army. The proposed MVR unit represents a benchmark for competing brine treatment technologies. The unit is capable of concentrating brine to over 204,000-mg/L TDS, reducing the volume of brine that would require subsequent disposal. The net volume reduction in water is proportional to the salinity reduction of the input water. The output is fresh water that can displace other freshwater sources for industrial or domestic use and, as such, would have a commensurate value. No value-add products are anticipated. This work is funded by DOE.

The data collected at the EERC will be used with calculations by NETL on the minimum theoretical work of separating water from these brines to estimate the efficiency of the MVR process at a range of values for inlet salinity and water recovery. These values of electricity consumption and efficiency will provide a crucial benchmark for other technologies being developed and tested at this scale, including other technologies that may be tested at the BEST site. Results of the testing could inform efficiency or operational advancements that could improve the cost effectiveness of this or competing technologies.

Score: 45

DocuSign Envelope ID: 2FA9A609-C360-4E53-8B28-BE8B77B6994A

Technology Strengths (out of 40)
(strengths to consider: a) scientific soundness, b) readiness level, c) safety considerations, d) waste generation, e) scalability, and f) maximum brine concentration that can be treated)

The NETL RIC's pilot unit is designed to treat high-salinity brines to produce a high-purity treated water output. MVR systems represent an established technology adapted to treating higher-salinity and lower-quality waters produced or extracted from geologic systems. The unit has been repaired/modified and successfully tested at NETL's facilities and is ready for testing at the BEST site. The MVR unit has an operational range of 35,000–200,000+-ppm TDS, which is a candidate for testing at the EERC BEST site. Throughputs are estimated at 2.5 gallons/min or less (varying with input brine salinity), and waste streams comprise concentrated brine which will be blended and reinjected at the BEST facilities. These operational parameters are within the operational design of the EERC BEST site, which can accommodate throughputs up to 25 gal/min and salinities up to 300,000-mg/L TDS.

As the first demonstration at the North Dakota brine treatment test bed facility, the benchmark testing of the MVR pilot unit will provide evaluation of the various control systems and monitoring equipment designed for managing and tracking system performance under operational conditions. Conducting the first test with the MVR unit in place will have the synergistic benefit of enabling the EERC to demonstrate the capabilities of the test bed facility to other technology vendors without the risk of impacts from a fully novel water treatment technology. The performance of the facility during this initial test will provide confidence to technology providers interested in testing at the first-of-its-kind test facility associated with the North Dakota BEST project.

Score: 35

Organization Strengths (out of 10)
(strengths to consider: a) intellectual property or license ownership, b) capability of further development, and c) technical and management team)

NETL RIC has a well-defined research program and is prepared to fund the test program. The MVR unit has been tested at NETL facilities by a well-qualified technical team who will be on-site for testing at the North Dakota brine treatment test bed facility. NETL and the EERC have a long-standing business relationship and corporate familiarity. Data generated through the proposed testing will be publically available and not restricted by IP or other licenses.

Score: 10

Total Score: 90 out of 100

RECOMMENDATION: Selection and Testing at the North Dakota Facility in Quarter 3 of 2019.

Select NETL RIC's MVR pilot unit for testing at the EERC BEST site in Q3 of 2019. The MVR technology has favorable performance characteristics and aligns with BEST program goals and objectives. The testing will be funded by the technology provider, resulting in nominal impact to future testing at the site. NETL RIC's MVR pilot system is the only operational and tested system that has indicated that it is ready and available for testing at the North Dakota test bed facility in Q3 of 2019.

DocuSign Envelope ID: 2FA9A609-C360-4E53-8B28-BE8B77B6994A

WATER TREATMENT TECHNOLOGY SELECTION FOR TESTING AT BEST BRINE TREATMENT TEST BED FACLITIES

Technology Provider: Ohio University

Point of Contact: Dr. Jason Trembly

Technology to Be Tested: Supercritical Water Desalination (SCW)

Scale of Technology: 8 gallon per hour - GPH (0.13 gallon per minute - GPM)

Technology Category: Thermal (Internally Heated Distillation)

Requested Site and Time Frame: North Dakota, Quarter 2 and/or 3 2021.

Goal: The main objective of this demonstration is to evaluate pilot-scale operation of Ohio University's Supercritical Water (SCW) Desalination system at the University of North Dakota's (UND) Brine Extraction Storage Test (BEST). The main goal is to evaluate technical feasibility and commercial potential of SCW technology to treat high-TDS brines (~180,000 mg/L) and recover high quality water for beneficial reuse.

SCREENING CRITERIA (qualitative)

Estimated Cost of Testing: ~$280,111 ($224,089 requested in EERC funding).

Funding: The Energy and Environmental Research Center (EERC) will utilize program funding provided by NETL to support the development, mobilization, and demonstration activities conducted by Ohio University. Ohio University is also providing $56,022 in cost share to support the demonstration effort.

Cost of Further Deployment: Ohio University will utilize provided funding to refurbish the SCWD modular unit and mobilize and conduct the required field-based demonstration.

Site Compatibility and Ease of Accommodation: A modular unit of the SCWD technology was previously fabricated and is ready for deployment and is compatible with the North Dakota brine treatment facility. The facility can accommodate the operational needs (i.e., electrical utilities and brine pretreatment) of the pilot unit and the proposed test program without modification. The unit is electrically powered. A hazard assessment will be conducted to ensure the system is not anticipated to produce emissions or unacceptable HSE risks that are beyond designed capabilities of the EERC BEST facility.

Quantitative

Projected Benefits (out of 50)
(benefits to consider: a) reduction in brine disposal/injection costs, b) production of salable products, c) valuation of treated water for reuse, d) enablement of other treatment technologies, and e) previously funded by DOE)

Ohio University has developed a supercritical water desalination (SCWD) treatment process applicable to high-salinity brines and has been previously funded and supported through the fossil energy program (DE-FE0026315). The technology is currently at a small pilot-scale level with a transportable, modular unit having been constructed that is capable of processing and treating brines at approximately 0.13 gpm (8gph).

Pilot scale testing at the EERC BEST testbed facility through this effort will aid in demonstrating the feasibility of moving the SCWD technology beyond the small-scale and towards industrial-scale application. Pilot-scale demonstration of the SCWD technology under realistic operating conditions will offer insights into how the technology compares to baseline testing results of a similar thermal treatment system (mechanical vapor recompression – MVR) previously tested at the EERC facility. Results will be analyzed to determine desalination energy requirements as a function of operating pressure and brine TDS content. Although the current scale of the

DocuSign Envelope ID: 2FA9A609-C360-4E53-8B28-BE8B77B6994A

technology is smaller than desired for pilot testing, it will provide a direct comparison to the baseline mechanical vapor recompression (MVR) technology that was previously evaluated with the assistance of Nick Siefert at NETL.

Score: 45

Technology Strengths (out of 40)
(strengths to consider: a) scientific soundness, b) readiness level, c) safety considerations, d) waste generation, e) scalability, and f) maximum brine concentration that can be treated)

Ohio University has developed a supercritical water desalination (SCWD) treatment process applicable to high-salinity brines. The SCWD technology is an electrically powered distillation system with internal heat application and is expected to be a technical and economic improvement on thermal systems that are externally heated. Externally heated systems possess high thermal lag, promoting scale development, and have high manufacturing costs when scaled up for commercial application. The SCWD employs internal heating through joule-heating, which is a result of power dissipation from current traveling through a non-ideal conductor. The novel design allows for direct control of power applied to the brine using the electrical conductivity of the brine when applying AC current, resulting in a lower TDS content vapor product and a concentrated brine liquid product. The anticipated operational range of the technology is 50,000 to 180,000 mg/L TDS at a throughput rate of approximately 8 gallon per hour (0.13 gpm). This operational range is within the operational design of the EERC BEST facility, which can accommodate throughputs of up to 25 gpm and salinities of up to 300,000 mg/L TDS.

Score: 30

Organization Strengths (out of 10)
(strengths to consider: a) intellectual property or license ownership, b) capability of further development, and c) technical and management team)

Ohio University's Institute for Sustainable Energy and the Environment has a well-defined research program with a history of conducting research projects competitively awarded on a national level. The University was previously supported by DOE's fossil energy program to complete an initial phase of technology development related to high-TDS brine treatment. The proposed pilot-scale testing at the EERC BEST facility will provide a third-party evaluation of the technology and data generated through the effort will assist with further advancement of this promising technology.

Score: 10

Total Score: 85 out of 100

RECOMMENDATION: Selection and Testing at the North Dakota BEST Facility in Quarter 2 or 3 of 2021.

Select Ohio University's SCWD pilot unit for testing at the EERC BEST site in Q2/Q3 of 2021. The SCWD technology has favorable performance characteristics and aligns with BEST program goals and objectives. The testing will be funded by the EERC with program funding provided by NETL, with limited cost share provided by Ohio University.

DocuSign Envelope ID: 2FA9A609-C360-4E53-8B28-BE8B77B6994A

WATER TREATMENT TECHNOLOGY SELECTION FOR TESTING AT BEST BRINE TREATMENT TEST BED FACLITIES

Technology Provider: University of Pittsburgh (U of Pitt), Department of Civil and Environmental Engineering

Point of Contact: Dr.Vidic Radisav

Technology to Be Tested: Air Gap Membrane Distillation Technology

Scale of Technology: Approximately 1 gallon per minute (GPM)

Technology Category: Membrane/Thermal (Membrane-Assisted Thermal Distillation)

Requested Site and Time Frame: North Dakota, Quarter 2 and/or 3 2021.

Goal: The main objective of this demonstration is to evaluate technical feasibility and commercial potential of air gap membrane distillation (AGMD) technology to treat high-TDS brines (~180,000 mg/L) and recover high quality water for beneficial reuse. The results from laboratory and pilot-scale testing will be used to develop a final techno-economic analysis to enable potential wide-scale deployment of membrane distillation technology for treatment of high-salinity brines.

SCREENING CRITERIA (qualitative)

Estimated Cost of Testing: ~$203,232

Funding: The Energy and Environmental Research Center (EERC) will utilize program funding provided by NETL to support the development, mobilization, and demonstration activities conducted by the University of Pittsburgh.

Cost of Further Deployment: The University of Pittsburgh (U of Pitt) will utilize provided funding to conduct laboratory scale testing with provided brine to define pretreatment requirements for optimal operation of the AGMD system, and to mobilize and conduct the required pilot-scale, field-based demonstration.

Site Compatibility and Ease of Accommodation: An electrically powered modular unit of the AGMD technology was previously fabricated and is ready for deployment and is compatible with the North Dakota brine treatment facility. The facility can accommodate the operational needs of the pilot unit (i.e., electrical utilities and brine pretreatment) and the proposed test program without modification. A hazard assessment will be conducted to ensure the system is not anticipated to produce emissions or unacceptable HSE risks that are beyond designed capabilities of the EERC BEST facility.

Quantitative

Projected Benefits (out of 50)
(benefits to consider: a) reduction in brine disposal/injection costs, b) production of salable products, c) valuation of treated water for reuse, d) enablement of other treatment technologies, and e) previously funded by DOE)

The U of Pitt air gap membrane distillation (AGMD) technology research has been previously funded and supported through the fossil energy program (DE-FE0024061) and has developed and constructed a modular unit capable of processing and treating brines at approximately 1 gpm. This project will enable a coordinated effort focused on developing largely unexplored AGMD technology for application in the energy sector (e.g., active reservoir management for CO2 sequestration) with a specific focus on water recovery from high salinity brines. Pilot scale testing will aid in demonstrating the feasibility of moving the AGMD technology beyond lab scale and towards industrial-scale application. It will enable water recovery from the high salinity brine to provide high quality permeate suitable for several beneficial uses like agriculture, livestock, and industrial applications. In addition, the volume of the original brine that requires disposal will be reduced, which will reduce the overall water and environmental footprint of the energy industry. Pilot-scale demonstration of AGMD technology under realistic operating conditions will offer insights into how AGMD will overcome the shortcomings, limitations, and

DocuSign Envelope ID: 2FA9A609-C360-4E53-8B28-BE8B77B6994A

challenges of other technologies for the treatment of high salinity brines and will reveal the key technical risks/issues of this promising technology. Perceived technology gaps and R&D needed for commercialization of AGMD technology as well as development pathway for applying AGMD in the energy sector can be addressed based on the results of this study.

Score: 45

Technology Strengths (out of 40)
(strengths to consider: a) scientific soundness, b) readiness level, c) safety considerations, d) waste generation, e) scalability, and f) maximum brine concentration that can be treated)

Amongst advanced treatment approaches, MD is a unique technology that combines thermal and membrane separation processes. Initial studies focused on the application of MD for treatment of reject streams from reverse osmosis (RO) desalination plants and more recently there has been renewed interest in MD for treatment of high salinity produced water from the oil and gas industry. MD is a non-isothermal vapor pressure driven separation process that utilizes hydrophobic microporous membranes with high liquid entry pressure (LEP) to prevent water from passing through the membrane at pressures below the LEP. Hot liquid feed flows on one side of the membrane and pure vapors that traverse across the membrane are collected on the cool permeate side. The configuration of MD depends on the manner in which the vapors are collected and condensed. Air Gap MD (AGMD) technology uses an air gap between the hot and cold sections in a membrane module to enable internal heat recovery and improve the overall energy consumption in this process. AGMD can concentrate the feed up to supersaturation (e.g., TDS of 300,000 mg/L) to achieve very high-water recovery. The most significant advantages of the MD technology are the low operating temperature (e.g., 40-80 ^{o}C) and near atmospheric pressures, which makes it particularly suitable for integration with waste heat. Operating an MD plant using waste heat can dramatically reduce the operating cost for treatment of produced water to rival the typical cost of the sea water desalination by RO.

Score: 35

Organization Strengths (out of 10)
(strengths to consider: a) intellectual property or license ownership, b) capability of further development, and c) technical and management team)

The U of Pitt Department of Civil and Environmental Engineering is a well-known research entity with a history of conducting research programs competitively awarded on a national level. For several years, the U of Pitt team has been developing the membrane distillation (MD) technology for treatment of high salinity wastewater generated by the unconventional oil and gas industry. Their work has resulted in a significant body of scientific knowledge and publications focused on lab scale investigations, detailed process modeling, systems-level analysis, including techno-economic models, integration of MD with waste heat, and optimization studies at regional scale for water management using emerging MD technology. The current body of knowledge meets the criteria for Technology Readiness level (TRL) 4-5 and the next logical step for the advancement of this technology towards commercial applications is the proposed pilot-scale demonstration under realistic field conditions.

Score: 10

Total Score: 90 out of 100

RECOMMENDATION: Selection and Testing at the North Dakota Facility in Quarter 2 or 3 of 2021.

Select U of Pitt's AGMD pilot unit for testing at the EERC BEST site in Q2Q3 of 2021. The AGMD technology has favorable performance characteristics and aligns with BEST program goals and objectives. The testing will be funded by the EERC with program funding provided by NETL.

DocuSign Envelope ID: 2FA9A609-C360-4E53-8B28-BE8B77B6994A

WATER TREATMENT TECHNOLOGY SELECTION FOR TESTING AT BEST BRINE TREATMENT TEST BED FACLITIES

Technology Provider: University of Kentucky (UK) Center for Applied Energy Research (CAER)

Point of Contact: Dr. Ayokunle Omosebi

Technology to Be Tested: Zeolite Membrane Dewatering Technology

Scale of Technology: Approximately 0.1 gallon per minute (GPM)

Technology Category: Membrane (Zeolite-derived)

Requested Site and Time Frame: North Dakota, Quarter 4 2021.

Goal: The main objective of this demonstration is to evaluate small pilot-scale operation and technical feasibility of a zeolite-membrane dewatering technology to treat high-total dissolved solids (TDS) brines (~180,000 mg/L) and recover high quality water for beneficial reuse. The results from both laboratory membrane testing and pilot-scale demonstration testing will help determine applicability for treatment of high-salinity brines.

SCREENING CRITERIA (qualitative)

Estimated Cost of Testing: $133,054

Funding: The Energy and Environmental Research Center (EERC) will utilize program funding provided by NETL to support the development, mobilization, and demonstration activities conducted by the University of Kentucky (UK) Center for Applied Energy Research (CAER).

Cost of Further Deployment: The UK CAER will utilize provided funding to conduct laboratory scale testing with provided brine to define pretreatment requirements for optimal operation of the zeolite-membrane system, and to mobilize and conduct the required pilot-scale, field-based demonstration.

Site Compatibility and Ease of Accommodation: An electrically powered modular unit of the zeolite-membrane technology will be fabricated and prepared for deployment and is anticipated to be compatible with the North Dakota brine treatment facility. The facility can accommodate the operational needs of the pilot unit (i.e., electrical utilities and brine pretreatment) and the proposed test program without modification. A hazard assessment will be conducted to ensure the system is not anticipated to produce emissions or unacceptable HSE risks that are beyond designed capabilities of the EERC BEST facility.

Quantitative

Projected Benefits (out of 50)
(benefits to consider: a) reduction in brine disposal/injection costs, b) production of salable products, c) valuation of treated water for reuse, d) enablement of other treatment technologies, and e) previously funded by DOE)

The UK CAER's innovative zeolite-membrane dewatering technology has been previously funded and supported through the US-China Clean Energy program within DOE and has developed a small bench-scale unit capable of processing and treating brines at approximately 0.02 gpm. Initial results have shown applicability to high-salinity brines of at least 100,000 mg/L TDS. Additional research and scale-up activities supported as part of the EERC BEST facility demonstration, will assess applicability to higher-TDS brines, and provide needed data and information to overcome technical barriers to commercialization by facilitating improved permeate flux with thinner membrane layers and active packed surface area using micro-scale tubes. Pilot scale testing (at approximately 0.1 gpm) will aid in demonstrating the feasibility of moving the zeolite membrane technology beyond lab scale and towards pilot-scale and possible industrial-scale application. It will enable water recovery from the high salinity brine to provide high quality permeate suitable for several beneficial uses like agriculture, livestock, and industrial applications. Perceived technology gaps, including capital cost of zeolite membranes and life expectancy limitations

DocuSign Envelope ID: 2FA9A609-C360-4E53-8B28-BE8B77B6994A

due to scaling components, can be overcome through advanced R&D efforts focused on improved permeate flux using thinner membranes and identification of problematic chemistry.

Score: 40

Technology Strengths (out of 40)
(strengths to consider: a) scientific soundness, b) readiness level, c) safety considerations, d) waste generation, e) scalability, and f) maximum brine concentration that can be treated)

The UK CAER technology uses zeolite membranes for desalination at transmembrane pressures below 200 psi. The pore size of a zeolite membrane (0.74 nm) is smaller than the kinetic diameter of hydrated metal ions but larger than the diameter of the water molecules (0.27 nm). In addition to size exclusion, the zeolite membrane also employs super hydrophilicity and preferential dissolution of water within the matrix to shuttle water across the membrane under mild temperatures (<120 C) and pressures (<100 psig). The influent to the membrane requires pretreatment for turbidity, TOC, and scaling by processes like those used for nanofiltration and reverse osmosis. Small bench-scale testing has been successfully completed on brines of approximately 100,000 mg/L TDS, however, initial proof-of-concept testing on ~180,000 mg/L TDS brines supplied by the EERC BEST facility using their membranes has indicated applicability to higher TDS brines. The scaled-up modular system will be fabricated and placed on a transportable skid using state-of-the-art equipment and supplies and incorporate all required safety considerations. Although the technology is currently at a smaller than desired scale, data and information helpful to the further scale-up and technology advancement will be achieved through the planned demonstration.

Score: 30

Organization Strengths (out of 10)
(strengths to consider: a) intellectual property or license ownership, b) capability of further development, and c) technical and management team)

The UK CAER is a well-known research entity with a history of conducting research programs competitively awarded on a national level. Funding awards of support have been secured from multiple agencies including, ARPA-E, DOE-NETL, Kentucky DEDI, and a consortium of industry. Since 2009, the UK CAER team has been developing zeolite dewatering membranes for various organic and inorganic solutions and has expressed willingness to offset development and demonstration costs by conducting some of the scale-up efforts using cost-share derived within their state and/or organization. UK CAER has conducted initial scale-up of these membranes and examined their stability in amine solvents in a conventional CO_2 capture process with flue gas produced from coal-fired feed and 100,000 mg/L sodium chloride brine. If successful performance is again demonstrated at the higher scale at the EERC BEST demonstration facility, UK CAER is also anticipating commercializing the technology with one of its current business partners.

Score: 10

Total Score: 80 out of 100

RECOMMENDATION: Selection and Testing at the North Dakota Facility in Quarter 4 of 2021.

Select UK CAER's zeolite membrane pilot unit for testing at the EERC BEST site in Q4 of 2021. The membrane technology has favorable performance characteristics and aligns with BEST program goals and objectives. The testing will be funded by the EERC with program funding provided by NETL.

DocuSign Envelope ID: 2FA9A609-C360-4E53-8B28-BE8B77B6994A

APPENDIX G

UNIVERSITY OF PITTSBURGH
FINAL REPORT – 2021

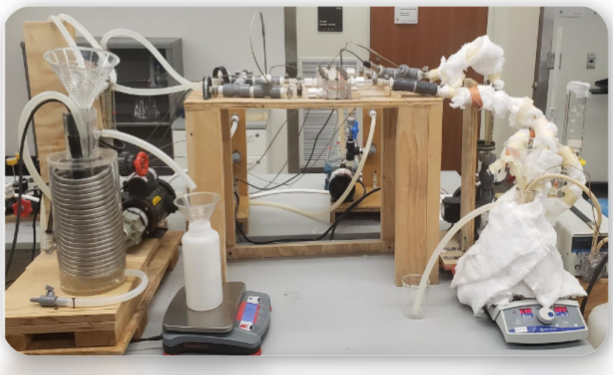
DocuSign Envelope ID: 2FA9A609-C360-4E53-8B28-BE8B77B6994A

Field Demonstration of Air Gap Membrane Distillation Technology with High-TDS Brine

Final Technical Report

Subcontract No:

June 1, 2021 - December 31, 2021





Principal Author:
Radisav D. Vidic

Contributing Authors:
Ritesh Pawar
Zhewei Zhang

Submitted to:
UND EERC

Submitted by:
University of Pittsburgh
Department of Civil and Environmental Engineering
Pittsburgh, PA 15261

DocuSign Envelope ID: 2FA9A609-C360-4E53-8B28-BE8B77B6994A

EXECUTIVE SUMMARY

This study evaluated technical feasibility of using membrane distillation for treatment of high-TDS brine from a deep saline formation in the Williston Basin of North Dakota with an objective to recover high-quality water for agricultural/industrial use and reduce the volume of high salinity brine that needs to be sent to disposal facilities.

Prior to field demonstration, extensive lab-scale experiments using a direct contact membrane distillation (DCMD) system were performed with actual low and high salinity brine from EERC BEST site. The lab-scale system operated with low salinity brine (~ 90,000 mg/L) at feed and permeate temperatures of 60° and 20°C, respectively achieved permeate flux of 17 Liters/m^2/hr (LMH) at 50% water recovery. No membrane fouling was observed at these operating conditions. Constant permeate flux of 12.5 LMH at 30% water recovery was obtained wen treating high salinity brine (~180,000 mg/L). Minimal membrane scaling was observed when treating the high salinity brine. Conductivity monitoring of the permeate revealed a slow but steady increase in permeate TDS, which was attributed to ammonia transfer from the raw brine to the permeate side. Ammonia transfer to the permeate side also led to an increase in permeate pH.

A field trial was conducted with a pilot-scale air gap membrane distillation (AGMD) system equipped with two membrane modules with 26 m^2 of PTFE membrane each. This pilot system was designed to treat 1 gpm of high salinity brine (i.e., TDS of 100,000 mg/L) with and achieve 50% water recovery. The field demonstration was conducted in October 2021 with 3 days of continuous operation using low salinity brine and 4 days of operation with high salinity brine. The pilot-scale system was operated at 50.8 and 52.9% water recovery when treating low salinity brine and achieved >99.7% salt rejection. The pilot-scale system was operated at 24.1, 29.2 and 30.8% water recovery with high salinity brine and achieved >99.8% salt rejection. Detail process model was used for techno-economic analysis of AGMD

DocuSign Envelope ID: 2FA9A609-C360-4E53-8B28-BE8B77B6994A

technology to estimate the treatment cost for an optimized 0.5 MGD AGMD plant and was compared with the treatment cost estimated from electricity consumption recorded during the pilot-scale operation. The cost of treatment of high salinity brine with 35% water recovery based on this process model was in the range of 2-3 $/m^3 of brine, whereas the cost based on the electricity consumption during the pilot plant trials was 7-15 $/m^3 of brine. The higher cost in the case of pilot plant trials was due to the oversized heater and chiller, less than optimal pilot plant design and operating conditions and use of commercial steam for heating in an optimized 0.5 MGD plant.

This study demonstrated technical feasibility of using MD for treatment of high-TDS brine to recover high-quality water suitable for industrial/agricultural use. MD treatment represents a viable technical solution in the arsenal of high-TDS brines management strategies that would dramatically reduce the water footprint of unconventional oil and gas industry.

DocuSign Envelope ID: 2FA9A609-C360-4E53-8B28-BE8B77B6994A

TABLE OF CONTENTS

1. INTRODUCTION 5

1.1. MEMBRANE DISTILLATION 5

1.2. AIR GAP MEMBRANE DISTILLATION (AGMD) 6

1.3. STUDY OBJECTIVES 7

2. LABORATORY-SCALE STUDIES 8

2.1. MATERIAL AND METHODS 8

2.2. RESULTS AND DISCUSSION 11

3. PILOT-SCALE DEMONSTRATION 15

3.1. MATERIALS AND METHODS 15

3.2. RESULTS AND DISCUSSION 21

3.3. TECHNO-ECONOMIC ASSESSMENT 31

4. CONCLUSIONS 37

5. REFERENCES 39

6. APPENDIX 48

DocuSign Envelope ID: 2FA9A609-C360-4E53-8B28-BE8B77B6994A

1. INTRODUCTION

1.1. Membrane Distillation

Desalination has emerged as a promising technology to address the problems related to water security [1]. Membrane-based processes like Reverse Osmosis (RO) and Multistage Flash (MSF) are some of the leading examples of desalination technologies used on a commercial scale [2]. However, RO is limited to about 70,000 mg/L of TDS as it reaches the operational limit for the feed osmotic pressure [3]. Membrane Distillation (MD) is an emerging technology for desalination of produced water [4] that offers 100% rejection of non-volatile compounds, lower operating temperature than conventional distillation processes, the ability to utilize low-grade thermal energy, less stringent requirements for membrane mechanical properties, and lower operating pressure than conventional pressure-driven membrane processes [5–7].

Over the past two decades, there have been considerable improvements in the membranes for MD applications as well as improvements in the performance and energy cost of MD systems [8]. MD can achieve up to 99.9 and 99.5% rejection of salts [9,10] and organic compounds [11,12], respectively and has been shown to be effective in removing heavy metals from wastewater [13] and concentrated radioactive waste [14]. MD has been evaluated for brackish water [15] and seawater desalination [16,17], food industry applications [18] and acid recovery [19,20]. Like any other membrane-based separation process, MD faces a major challenge from fouling due to the accumulation of inorganic and organic contaminants on the membrane surface [21–23]. Additionally, membrane wetting is a unique feature in MD systems that might be more critical than fouling as it leads to a decrease in performance and permeate quality [24–26]. In short, both membrane fouling and wetting have adverse impacts on MD and need to be mitigated to maintain stable performance and requisite water recovery [27,28].

DocuSign Envelope ID: 2FA9A609-C360-4E53-8B28-BE8B77B6994A

Over the past decade, numerous bench-scale studies have been conducted to evaluate different treatment options for hypersaline brines [29,30] and produced waters [31–34]. Different types of pretreatment methods like oxidation, filtration, flocculation, coagulation, and adsorption for the removal of selected contaminants [35–38] and surface-modified membranes [39–41] have been widely studied for the treatment of produced water using MD technologies. However, membrane distillation is not yet used for wastewater treatment on a commercial scale [42,43]. Several MD pilot-scale studies were primarily focused on seawater and brackish water desalination [44,45], as well as low salinity wastewaters from pharmaceutical residues and flue gas condensates [46]. Recently, there has been an increase in drive to further these studies with coal seam produced water [47], hypersaline solutions [48], and even with just high salinity sodium chloride solutions [49,50]. The largest commercial application of MD so far is a 10 m^3/day plant for seawater desalination utilizing waste heat from a local power generation station [51]. However, there are no long-term pilot-scale studies with actual produced waters.

1.2. Air Gap Membrane Distillation (AGMD)

MD configurations commonly discussed in the literature include Direct contact (DCMD), air gap (AGMD), permeate gap (PGMD), conductive gap (CGMD), sweeping gas (SGMD), and vacuum (VMD) membrane distillation [52]. Air Gap Membrane Distillation (AGMD) system was chosen for the pilot scale tests due to a gap is present between the membrane and the coolant compartment, which is filled with air [53]. The gap present between the two compartments provides thermal insulation which reduces the thermal losses through membrane matrix. On the other hand, the air gap provide mass transfer resistance since the water vapors need to diffuse through the gap before condensing. There are several advantages of AGMD configuration comparing with other MD configurations, such as no contact of

DocuSign Envelope ID: 2FA9A609-C360-4E53-8B28-BE8B77B6994A

permeate with membrane, relatively high flux, low thermal losses and less tendency to undergo fouling [54]. The most important benefit of AGMD as compared to the other configurations is to reduce the conduction loss [55]. Also, since coolant stream is separated from the hot water vapor by the condenser, internal recovery of latent heat recovery is possible for AGMD [56]. Other major advantage of AGMD is lower risk of membrane pore wetting [57]. Due to all the mentioned advantages and readiness of AGMD technology for desalination purposes, the pilot plant studies were conducted with AGMD modules obtained from Aquastill, NL.

1.3. Study objectives

The main objective of this study is to demonstrate technical feasibility and commercial potential of air gap membrane distillation (AGMD) technology to treat high-TDS (total dissolved solids) extracted water (~90,000 and ~180,000 mg/L) and recover high-quality water for beneficial reuse. Laboratory scale studies with real wastewater and mathematical modeling were employed to assess capabilities and limitations of AGMD and define key design and operating parameters for a pilot-scale demonstration of this technology at EERC BEST site in North Dakota. The demonstration was conducted using the pretreated brine (pretreatment done by BEST site team) with low (~90,000 mg/L) and high (~180,000 mg/L) salinity to achieve different water recoveries. The results from pilot-scale demonstration were used for techno-economic analysis to enable penetration and wide-scale deployment of membrane distillation technology for treatment of high salinity brines.

DocuSign Envelope ID: 2FA9A609-C360-4E53-8B28-BE8B77B6994A

2. LABORATORY-SCALE STUDIES

2.1. Material and Methods

The composition of pretreated brine obtained from EERC BEST site in North Dakota is shown in Table 1.

Table 1. Composition of the pretreated brine sample

Parameter	Value	Units
Alkalinity as CaCO3	446	mg/L
Barium	4.2	mg/L
Boron	0	mg/L
Bromide	276	mg/L
Calcium	5,440	mg/L
Chloride	47,000	mg/L
Iron	0.5	mg/L
Lithium	20.6	mg/L
Magnesium	383	mg/L
Manganese	0.5	mg/L
Potassium	2,080	mg/L
Sodium	21,400	mg/L
Strontium	432	mg/L
Sulfate	216	mg/L
TDS	86,000	mg/L
TOC1270	316	mg/L
Conductivity	116,000	µS/cm
pH	8.1	-

Commercially available hydrophobic microporous polytetrafluoroethylene (PTFE) with polypropylene support membranes were obtained from Aquastill, Netherlands. The properties of the membrane as provided by the manufacturer are shown in Table 2.

DocuSign Envelope ID: 2FA9A609-C360-4E53-8B28-BE8B77B6994A

Table 2. Properties of PTFE membrane used in this study

Membrane	Mean Pore size (μm)	Thickness (mm)	Contact angle (°)	Liquid Entry Pressure (bar)	% porosity of the membrane
PTFE	0.45	0.13-0.23	139.6	2.5	85

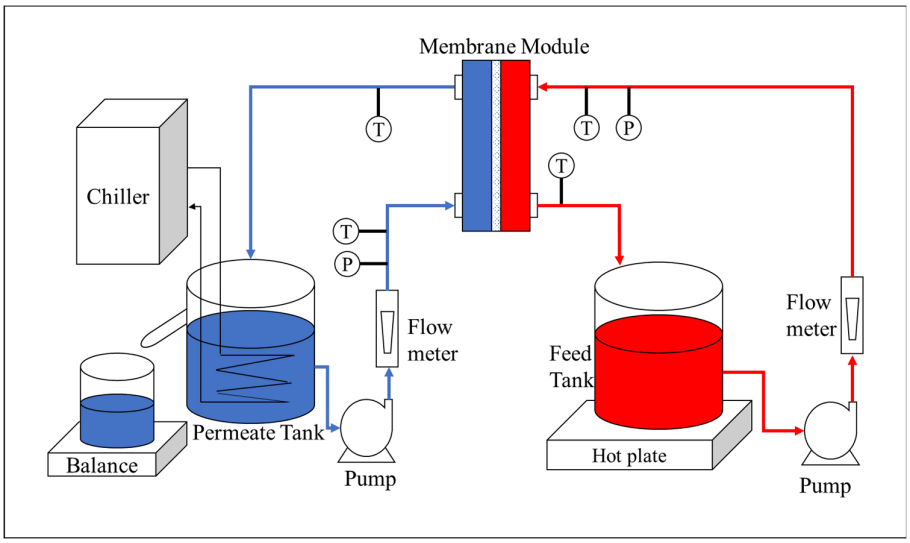


Figure 1. Schematic of laboratory-scale DCMD system

All laboratory-scale experiments in this study were carried out using a Direct Contact Membrane Distillation (DCMD) module with a 40 cm^2 (20 cm x 2 cm) flat sheet membrane in the experimental system operated in batch (concentrating) mode shown in Figure 1. The 1-mm thick spacers with a porosity of 0.77 (Delstar Technologies, PA) were stacked on top of the membrane from both sides to ensure even distribution of the feed and permeate flow. The feed solution was heated to a desired temperature (60 ºC) using a hot plate and was circulated using a centrifugal pump (Baldor Reliance, Fort Smith, AZ). DI water was circulated on the permeate side using a centrifugal pump and its temperature was maintained at 20 ºC using a chiller (M75, Thermo Fisher Scientific Inc., Pittsburgh, PA). The overflow from permeate tank was collected in a beaker and its weight was monitored with a balance (Ohaus Corp., Parsippany, NJ) while

DocuSign Envelope ID: 2FA9A609-C360-4E53-8B28-BE8B77B6994A

its conductivity was continuously monitored using a conductivity meter (Orion VersaStar Pro, Thermo Fisher Scientific Inc., Pittsburgh, PA). The laboratory-scale experimental DCMD setup is shown in Figure 2. Water recovery was calculated using the following equation:

$$\%\ \text{Recovery} = \frac{\text{Total mass of permeate collected at time t (g)}}{\text{Initial mass of the feed solution (g)}}\ \text{X}\ 100$$

The permeate flux was calculated using the following equation:

$$\text{Flux (LMH)} = \frac{\text{Mass of permeate collected during the time period } \Delta t\ \text{(g)}}{\text{A (cm}^2\text{)} * \Delta t\ \text{(min)} * \rho_w\ \text{(g/mL)}}\ \text{X}\ 600$$

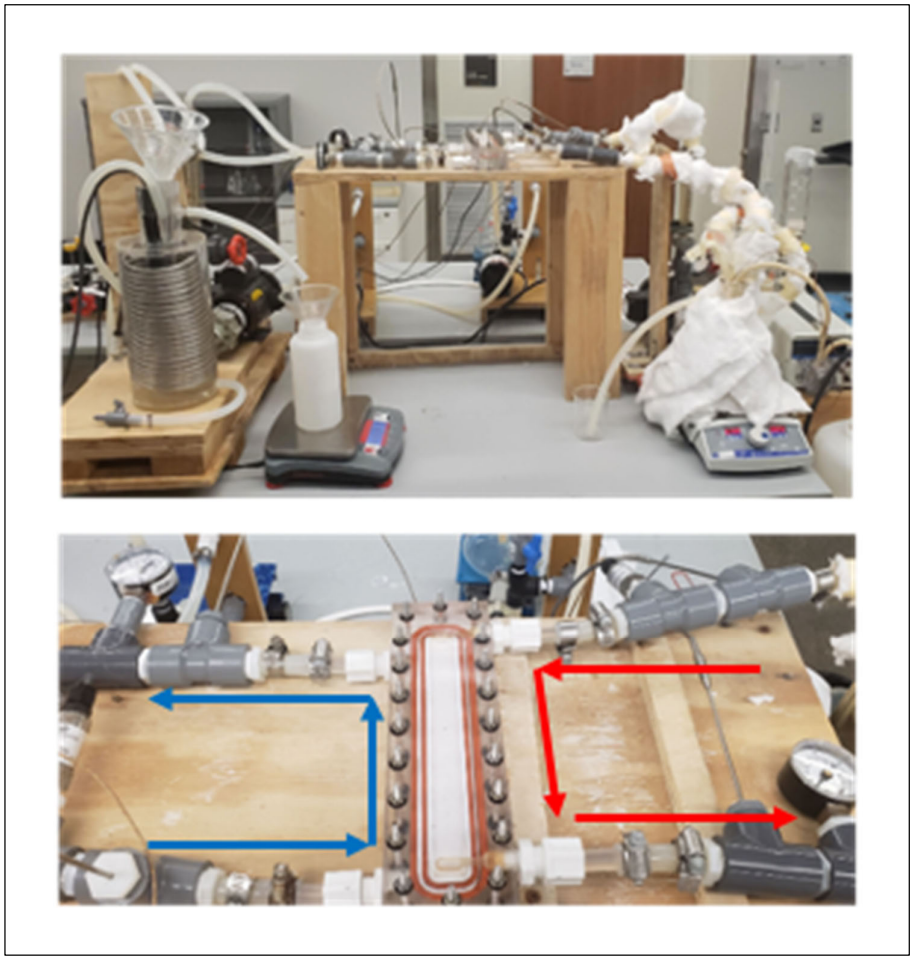


Figure 2. Picture of laboratory-scale DCMD experimental setup (top) and module (bottom)

DocuSign Envelope ID: 2FA9A609-C360-4E53-8B28-BE8B77B6994A

2.2. Results and Discussion

2.2.1. PhreeQC Simulations

Initial water recovery was assessed using chemical equilibrium modeling (i.e., PhreeQC with Pitzer activity corrections that are valid for high salinity solutions). Preliminary analysis using the average water quality provided by EERC (TableA1) suggests that calcite will be the main precipitant that will form on the feed side (Figure 3) that could potentially foul the membrane. Our previous studies on calcite fouling in MD system have shown that a small amount of calcite may attach to the membrane surface but will not affect the permeate flux since the calcite scales are typically highly porous and do not affect vapor transport from the feed side to the permeate side.

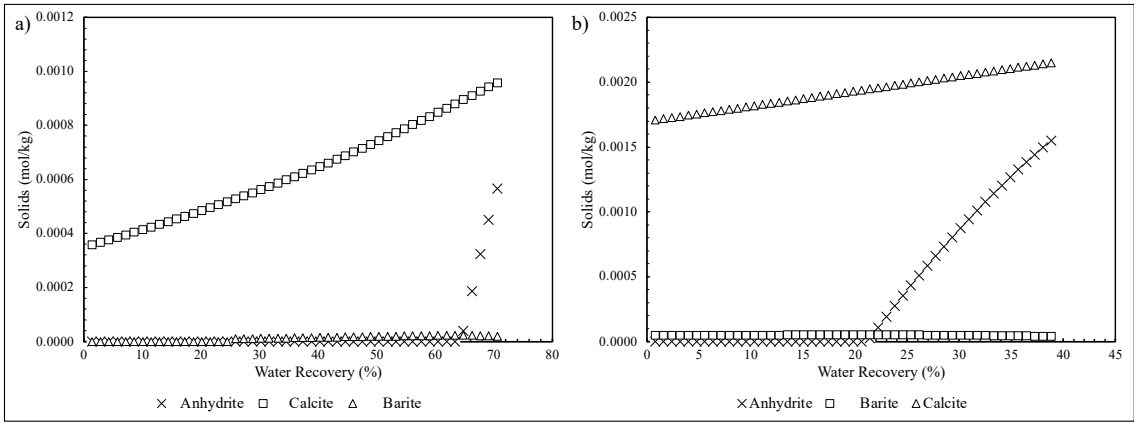


Figure 3. Solids formation as a function of water recovery for EERC Brine with TDS of (a) low and (b) high salinity

However, it is not possible to predict the exact behavior of the calcite scale in this brine and it will be necessary to conduct studies with a laboratory-scale MD system using the actual brine provided by EERC and the same membrane that will be employed in the pilot-scale system to determine the amount of calcite scale that can be tolerated in the field demonstration without any impact on technology performance.

DocuSign Envelope ID: 2FA9A609-C360-4E53-8B28-BE8B77B6994A

2.2.2. Laboratory-scale DCMD with low salinity brine

Brine obtained from EERC BEST site (detailed analysis in Section 2.1) was used as feed solution in the laboratory-scale system described in Section 2.1. Figure 4 shows the permeate flux and conductivity achieved by the PTFE membrane in this test. During the initial 8 hours, the brine was concentrated to achieve 50% water recovery (concentrated brine TDS ~ 180,000 mg/L). The decrease in permeate flux observed during this period was primarily due to the increase in feed salinity leading to a decrease in the feed solution vapor pressure. After this initial period, the feed salinity was maintained at 180,000 mg/L by continuously adding a makeup stream of raw brine and withdrawing the overflow (purge) stream from the feed tank. The flux remained constant during the 48 hours of operation at a constant concentration. However, the permeate conductivity kept increasing steadily even at the constant feed concentration.

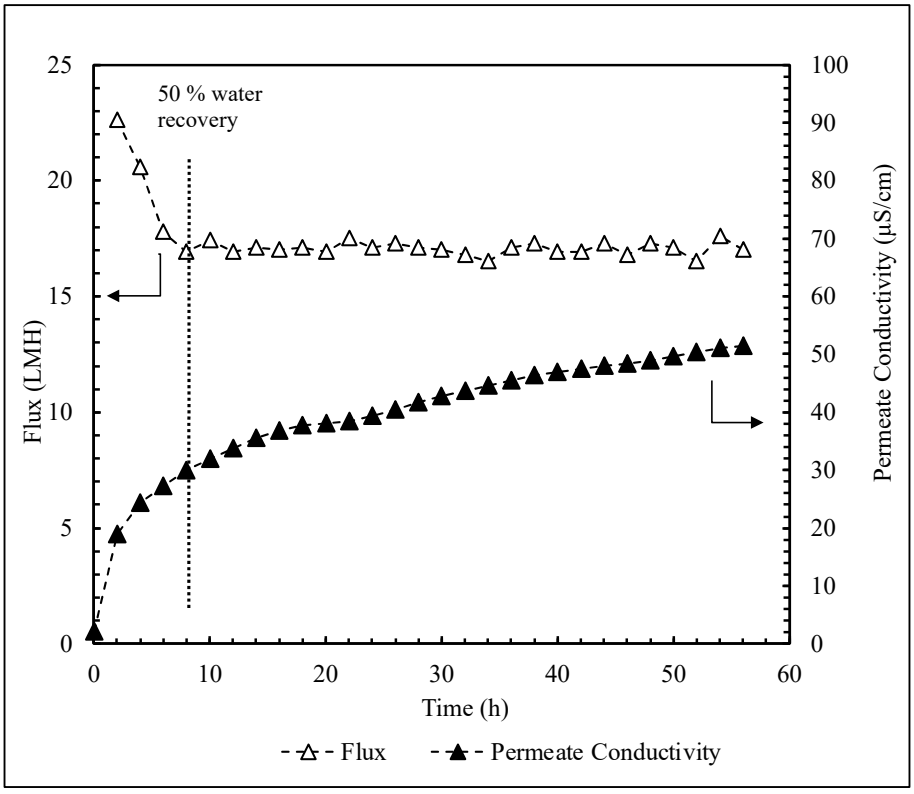


Figure 4. Permeate flux and conductivity in a long-term laboratory-scale test with low salinity brine

DocuSign Envelope ID: 2FA9A609-C360-4E53-8B28-BE8B77B6994A

A constant permeate flux during the long-term operation without an exponential increase in the permeate conductivity suggests that the permeate conductivity rise was not due to membrane wetting caused by scaling or fouling of the membrane [58,59]. To further confirm this hypothesis, SEM/EDX analysis (Figure A1, Appendix) of the used membrane revealed no scale formation on the membrane surface. It was observed that the permeate pH increased continuously during the steady-state operation accompanied by the increase in ammonium ion concentration in the permeate. The observed conductivity increase is due to the passage of ammonia from the feed side to the permeate side followed by protonation to form ammonium ion [60,61]. These long-term laboratory-scale results confirmed the ability of membrane distillation to obtain high-quality permeate from highly saline brines while achieving 50% water recovery.

2.2.3. Laboratory-scale DCMD with high salinity brine

The concentrate (TDS = 180,000 mg/L) obtained from the laboratory-scale experiment in Section 2.2.2. was used as a feed in this experiment. Figure 5 shows the permeate flux and conductivity achieved by the PTFE membrane in this test. During the initial 8 hours of operation, the feed was concentrated to achieve 30% water recovery (concentrate TDS = 257,000 mg/L) and then the switched to constant concentration mode by continuously supplying the fresh water and taking the purge out of the feed tank. The decrease in permeate flux during the initial 8 hours is due to reduction in the vapor pressure, whereas the flux remained constant throughout the next 16 hours indicating steady behavior. The increase in the permeate conductivity was most probably due to passage of ammonia present in the feed brine solution. However, SEM/EDS analysis of the used membrane (Figure A2, Appendix) showed minor precipitation of salts (primarily Fe and Ca) on the membrane surface. The precipitation of salts had no effect on the MD performance for 16 hours of operation, but the effect on long-

DocuSign Envelope ID: 2FA9A609-C360-4E53-8B28-BE8B77B6994A

term operation need to be investigated in a long-term field study. Hence, it was decided that the pilot plant operation would be conducted by slowly increasing the water recovery up to 30% by carefully monitoring the operating parameters to avoid potential scaling of the membranes.

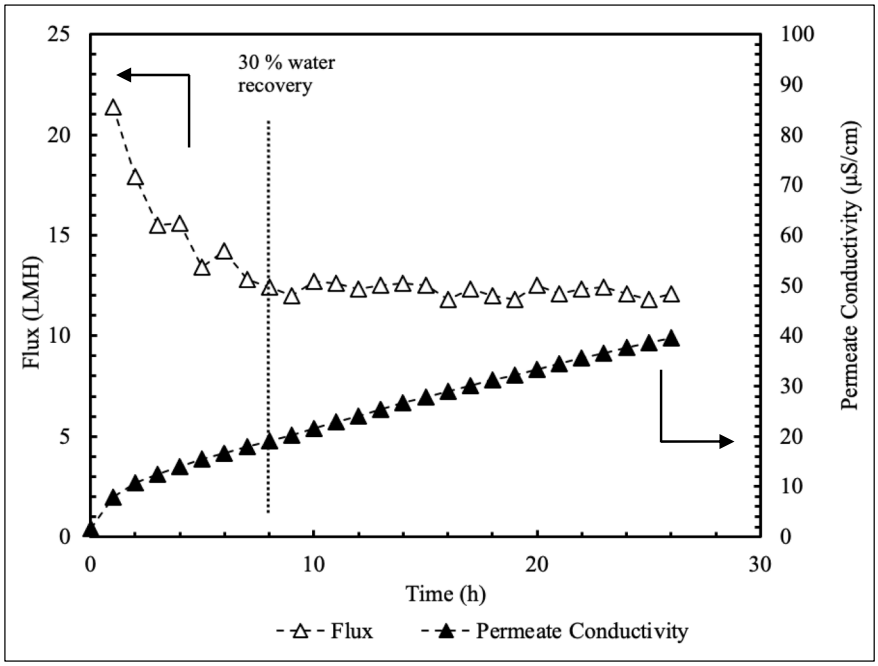


Figure 5. Permeate flux and conductivity in a long-term laboratory-scale test with 180,000 mg/L brine

DocuSign Envelope ID: 2FA9A609-C360-4E53-8B28-BE8B77B6994A

3. PILOT-SCALE DEMONSTRATION

3.1. Materials and Methods

3.1.1. Pilot plant design

The design and manufacturing of the pilot plant was done by Aquastill, NL. The pilot plant was specifically designed for this project to generate 0.5 gpm permeate from 1 gpm brine with TDS of approximately 100,000 mg/L (50% water recovery). The design and operating parameters are summarized in Table 3, while system specifications are listed in Table 4.

Table 3. Pilot plant design parameters

Parameters	Value	Units
Process Conditions		
Circulation/module	1.6	m^3/h
T membrane, in	80	°C
T condenser, out	71	°C
T condenser, in	35	°C
T membrane, out	40.6	°C
Salinity at start	98	gr/kg
Recovery req.	50	%
Airgap pressure	550	mbar
T feed	30	°C
Module Parameters		
Area of module modeled	25.9	m^2
Envelope length	2.7	m
Flux, calculated	2.4	LMH
Gain output ratio	2.7	--
Spec. Energy consumption	855.7	kJ/kg
Electrical consumption	0.4	kWh/m^3
Produced Distillate per module	63.2	L/h
Hydraulic Pressure losses module	175.1	mbar
T distillate estimated	50	°C

Table 4. System specifications

DocuSign Envelope ID: 2FA9A609-C360-4E53-8B28-BE8B77B6994A

Parameters	Value	Units
Distillate required	113	L/h
Feed	226	L/h
Brine	113	L/h
Feed Salinity	196	gr/kg
Number of modules	2	pcs
Total circulation flow	3.2	m^3/h
Heating HX	27	kW, thermal
Cooling CX	18	kW, thermal

The mass and energy balance at steady-state operation is shown in Figure 6.

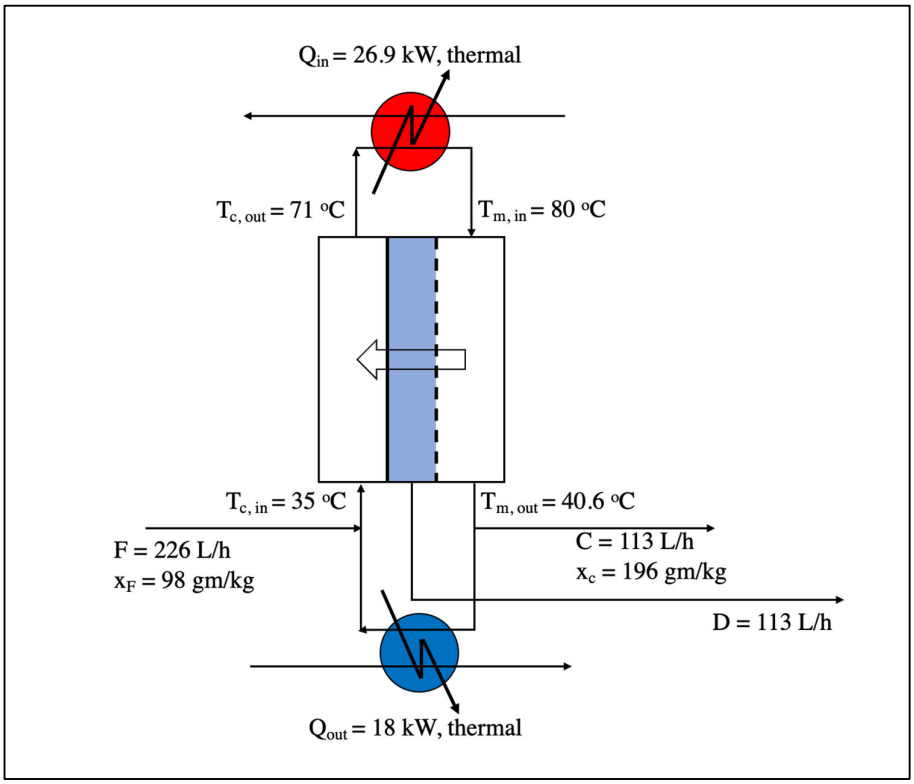


Figure 6. Steady-state heat and mass balance design conditions

3.1.2. Pilot plant setup and operation

The pilot plant system is used to produce distillate and concentrated brine from the inlet brine. The pilot plant consists of four modules with PTFE membrane with PP support, with two modules in operation and 2 as stand by. The membrane modules are spiral wound Air Gap

DocuSign Envelope ID: 2FA9A609-C360-4E53-8B28-BE8B77B6994A

Membrane Distillation (AGMD) modules with approximately 26 m^2 membrane area per module. Figure 7 shows the details of the channels inside the module. The hot brine channel and air gap are separated by the membrane. The air gap is in contact with the cold brine channel through the condenser. The brine to be treated is circulated in hot and cold brine channels and permeate is obtained in the air gap channel.

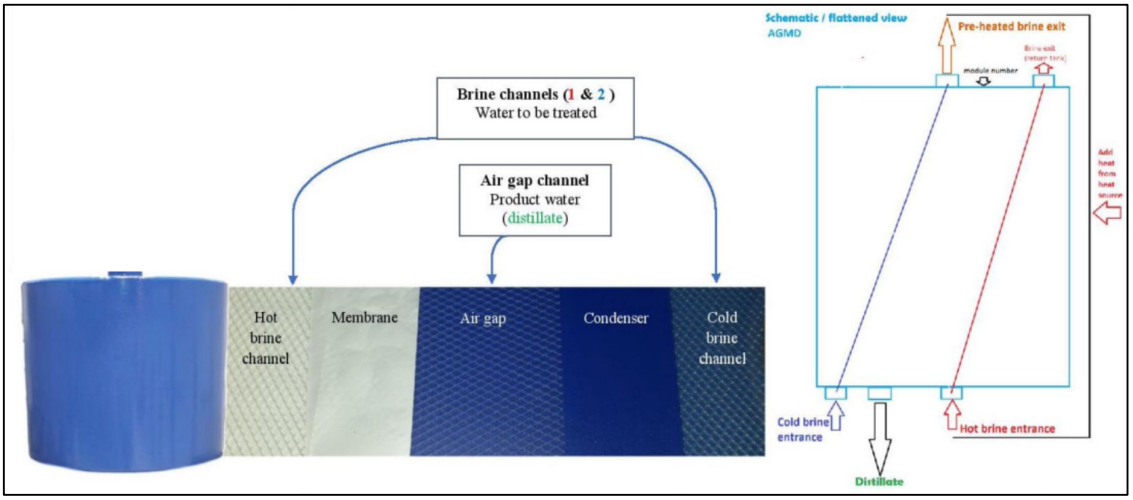


Figure 7. Schematic of membrane module showing channels for hot and cold brine as well for the permeate

Figure 8 shows the process flow diagram of the pilot plant system. The pilot plant consists of five tanks; Feed Tank (T-7), Heating Tank (T-3), Hot Brine Tank (T-2), Cold Brine Tank (T-1), and Permeate Tank (T-8). Pretreated brine is fed to the pilot plant (Tank T-8) using gravity through a water meter for measuring the feed flow rate. Feed from tank T-7 is transferred to tanks T-2 and T-1 using pump P-7 (pumps not shown). Autofill mode operation maintains the levels of tanks T-2 and T-1 at desired values. The heating tank is equipped with four 9 kW heating elements to maintain the temperature of the heating tank. The water from the heating tank is circulated through the hot side heat exchanger (HX-21) using pump P-3. The brine from tank T-2 is pumped to the other side of HX-21 using pump P-2. The heated

DocuSign Envelope ID: 2FA9A609-C360-4E53-8B28-BE8B77B6994A

feed from tank T-2 goes through the hot side of the modules and is returned to the tank T-1. At the same time, brine from tank T-1 is pumped through the cold side heat exchanger (CX-11) using pump P-1. The other side of CX-11 circulates cooling fluid (35% Propylene Glycol Solution) from the chiller. The cooled brine from Tank T-1 is circulated in the cold brine channel of the membrane module and returned to Tank T-2.

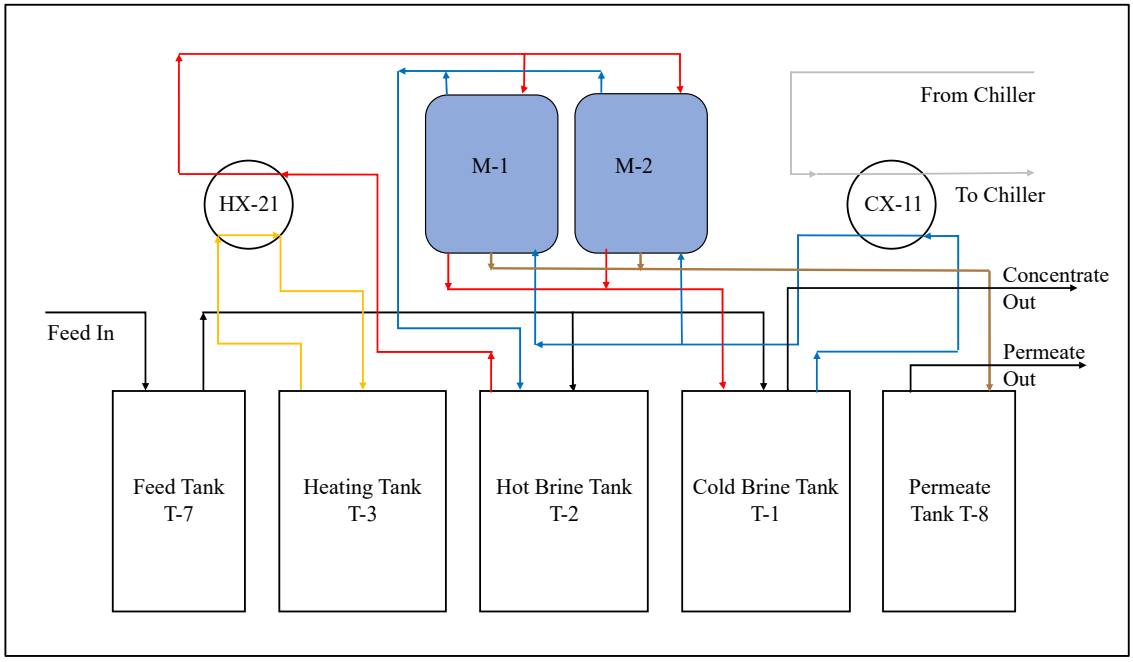


Figure 8. Process flow diagram of the pilot plant system

Due to the temperature difference between the hot and cold brine channels, vapor transfer occurs across the membrane and these vapors are condensed in the air gap channel. The condensed distillate is withdrawn from the modules using a vacuum which is generated in the tank T-8 using a submersible pump (P-10) and venturi valve. The permeate from tank T-8 and concentrate from tank T-1 are pumped from the pilot plant system using pumps P-8 and P-9, respectively. The number and volume of these discharges are recorded to evaluate the pilot plant performance. The temperatures in the heating tank, permeate tank, and inlet and outlet of both the channels in the module are continuously monitored. Also, the pressure at the inlet and

DocuSign Envelope ID: 2FA9A609-C360-4E53-8B28-BE8B77B6994A

outlet of both the channels in the module and the vacuum line is monitored. In addition, the conductivity of brine inlet from Tank T-1 and permeate from the modules is recorded. The detailed piping and instrumentation diagram is shown in Appendix (Figure A3). Figure 9 shows the picture of the pilot plant system.



Figure 9. Picture of pilot plant system with four modules

The pilot plant can be operated in ‘balance mode’ or ‘feed and bleed mode’. In balance mode, the brine from T-1 is transferred to T-2 through the cold channel in the module while the brine from T-2 is transferred to T-1 through the hot channel in the module. As membrane distillation happens, distillate is produced, and fresh brine is fed to these tanks using autofill mode to maintain the desired levels in all tanks. In the “feed and bleed” mode, the system operates to maintain the brine conductivity at the desired level by removing the concentrate from Tank T-1. To maintain the desired range of concentrate, pump P-9 will pump out the concentrate, and pump P-7 will feed in fresh brine from Tank T-7. The concentrate brine

DocuSign Envelope ID: 2FA9A609-C360-4E53-8B28-BE8B77B6994A

discharge, fresh feed addition and stabilizing occur in series to maintain the brine conductivity between the desired conductivity values.

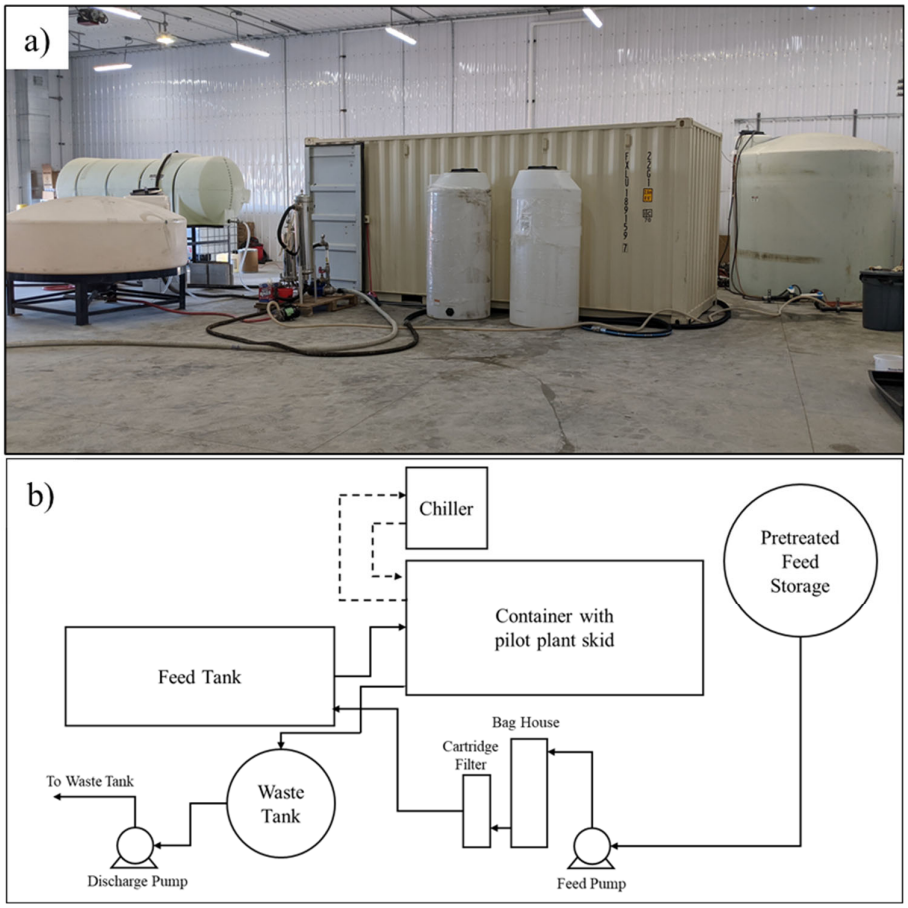


Figure 10. a) Picture and b) Schematic of the pilot plant setup

Figure 10 shows the picture and schematic of the setup used during the pilot plant trial at EERC BEST site. The pretreated brine was stored in the 3,000-gallon Pretreated Feed Storage Tank. Pretreated brine was filtered through a 5-micron oil absorption baghouse filter (OAS-5-M02E, Filtra-systems, Farmington Hills, MI) followed by the filtration through 0.45-micron polypropylene cartridge filter (FS-PR-0.45-20-226-B, Filtra-systems, Farmington Hills, MI) using a 1 HP 5-stage feed pump (3HM05N07T6PBQE, Xylem Inc., Auburn, NY). The baghouse and cartridge filters were used to remove any suspended solids that might be

DocuSign Envelope ID: 2FA9A609-C360-4E53-8B28-BE8B77B6994A

present in the pretreated brine. The filtered brine was stored in 1000-gallon horizontal feed tank (N-44241, Plastic-Mart.com). After MD, concentrate and permeate from the pilot plant are pumped to the 1000-gallon conical bottom discharge tank. The brine from the discharge tank was pumped to the on-site waste tank using a 3/4 HP pump (368A-98, AMT, Royersford, PA). A 10-ton chiller (OPC10-A7, Haskris, Elk Grove Village, IL) was used to meet the cooling needs of the pilot system while a 35% propylene glycol solution was used as a working fluid.

3.2. Results and Discussion

The pilot plant trial was conducted at the EERC BEST site with the pretreated brine from October 05 – 14, 2021. The trials were conducted in two stages with low (~90,000 mg/L) and high (~180,000 mg/L) salinity brines to achieve different recoveries.

3.2.1. Pilot plant test with low salinity brine

During the first part of this trial, the pilot plant was operated in recirculation mode by mixing the concentrate and distillate back in the feed tank. During start-up 2,000 mg/L NaCl solution (conductivity = 3.8 mS/cm) was used on the feed side of the modules. During this test, the permeate conductivity remained low (<10 μS/cm), indicating proper operation of membrane modules with salt rejection greater than 99.7%. The hot side module inlet temperature was 75 ºC and the cold side module inlet temperature was 20 ºC.

After validating plant operation with NaCl solution, pretreated brine was continuously added to the system while permeate was discharged (feed and bleed mode) to achieve a target feed salinity of about 174,000 mg/L, which took about 14 hours. Figure 11 shows the decrease in permeate flux with an increase in feed side concentration due to vapor pressure lowering by TDS increase and continuous permeate conductivity increase due to the passage of the

DocuSign Envelope ID: 2FA9A609-C360-4E53-8B28-BE8B77B6994A

ammonia from the feed side to the permeate side. The concentration of the feed was continued until the TDS on the feed side reached about 174,000 mg/L (conductivity of 178 mS/cm), which represents 52.9 % water recovery.

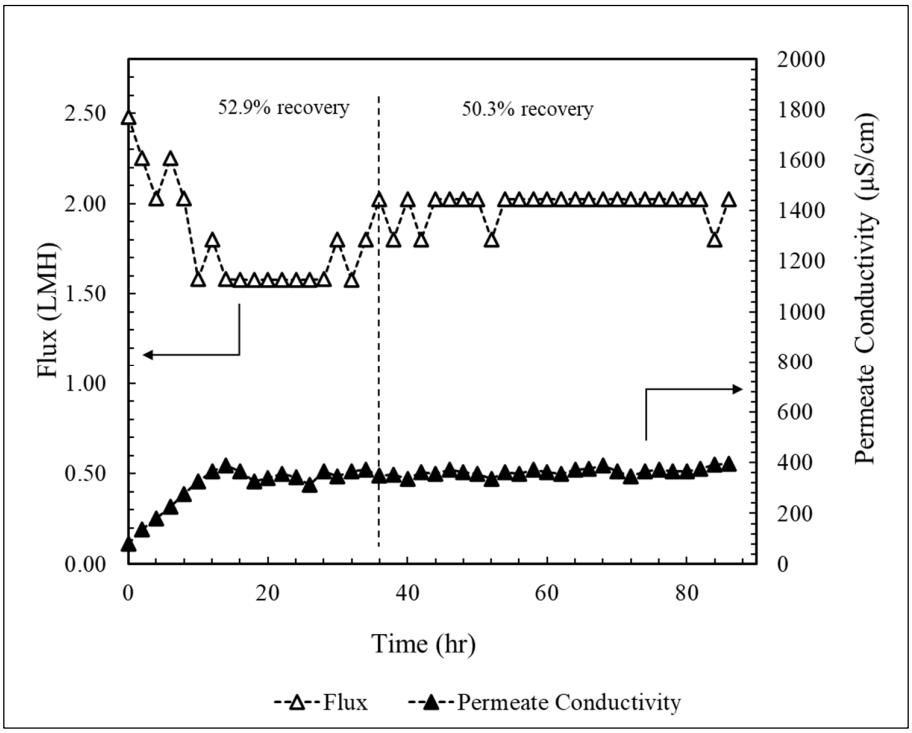


Figure 11. Permeate flux and conductivity using low salinity brine with achieving 52.9% and 50.3% water recovery

After concentrating the brine to the desired value to achieve 52.9% water recovery, the pilot plant was operated in a steady-state mode to maintain these conditions. Figure 11 shows the permeate flux and conductivity for 22 hours of steady-state operation. Permeate flux (~1.66 LMH) was virtually constant during this period of operation while the permeate conductivity remained constant indicating constant rejection of salts throughout the operation time. The steady flux and permeate conductivity of ~400 µS/cm indicate successful long-term operation of MD system in the field to recover high quality permeate that can be reused in industry/agriculture and reduce the volume of brine that needs to be disposed of. Figure 12 and

DocuSign Envelope ID: 2FA9A609-C360-4E53-8B28-BE8B77B6994A

Figure 13 depict the concentrate and permeate conductivity during the operations and feed and permeate flow rates, respectively.

After maintaining the steady state conditions for 22 hours, the salt concentration was reduced to 162,000 mg/L (conductivity = 170 mS/cm) to achieve 50% water recovery and the pilot plant was operated in steady state mode to continuously achieve this water recovery. Figure 11 shows the permeate flux and conductivity for next 50 hours of steady-state operation. The constant flux (~2.0 LMH) and permeate conductivity indicate no deterioration in the MD performance with achieving 50% water recovery.

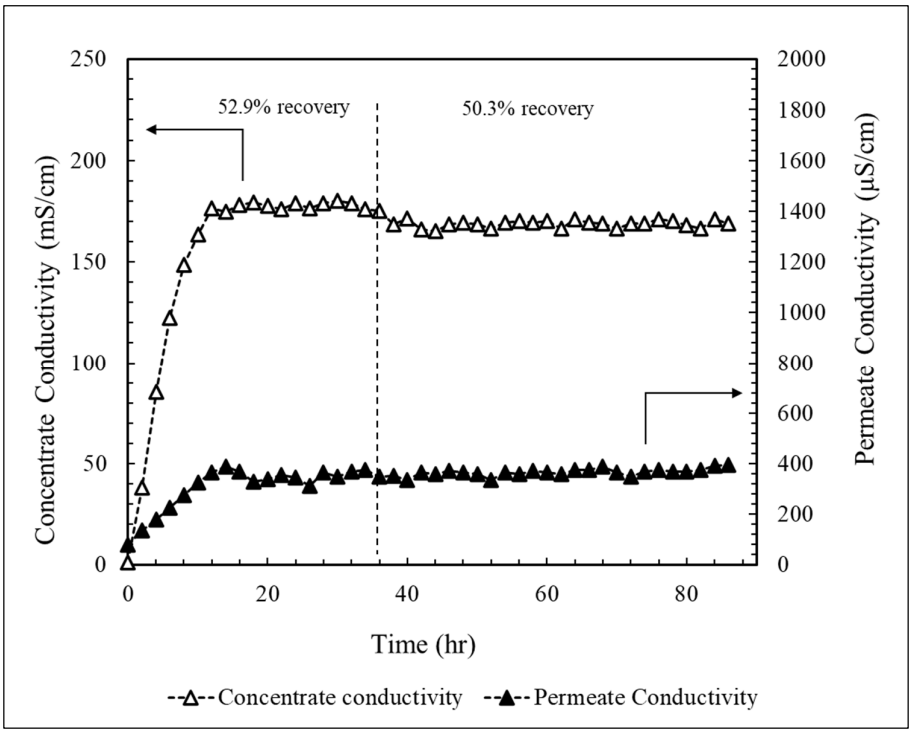


Figure 12. Concentrate and permeate conductivity with low salinity brine achieving 52.9% and 50.3% water recovery

Table 5 shows water quality analysis of samples collected during the operation with two different water recoveries. The results show that for the initial period of 22 hours pretreated brine had TDS of 82,600 mg/L while the concentrate TDS was 174,000 mg/L, thereby

DocuSign Envelope ID: 2FA9A609-C360-4E53-8B28-BE8B77B6994A

indicating 52.9% water recovery. In the later 50 hours, the TDS of pretreated brine was about 80,400 mg/L and the concentrate TDS was about 162,000 mg/L indicating 50.3% water recovery. The permeate TDS of 390 mg/L and 380 mg/L, respectively indicate 99.8% rejection of salts by using the commercially available PTFE membrane used in the pilot system. Additionally, analysis of permeate show the presence of significant concentrations of alkalinity, ammonia and TOC. The passage of NH_3, alkalinity in the form of CO_2, and TOC in the form of volatile organics with the water vapors led to the increase in their concentrations in the permeate. The concentrations of divalent cations in the feed and the concentrate indicated water recoveries determined from TDS analysis.

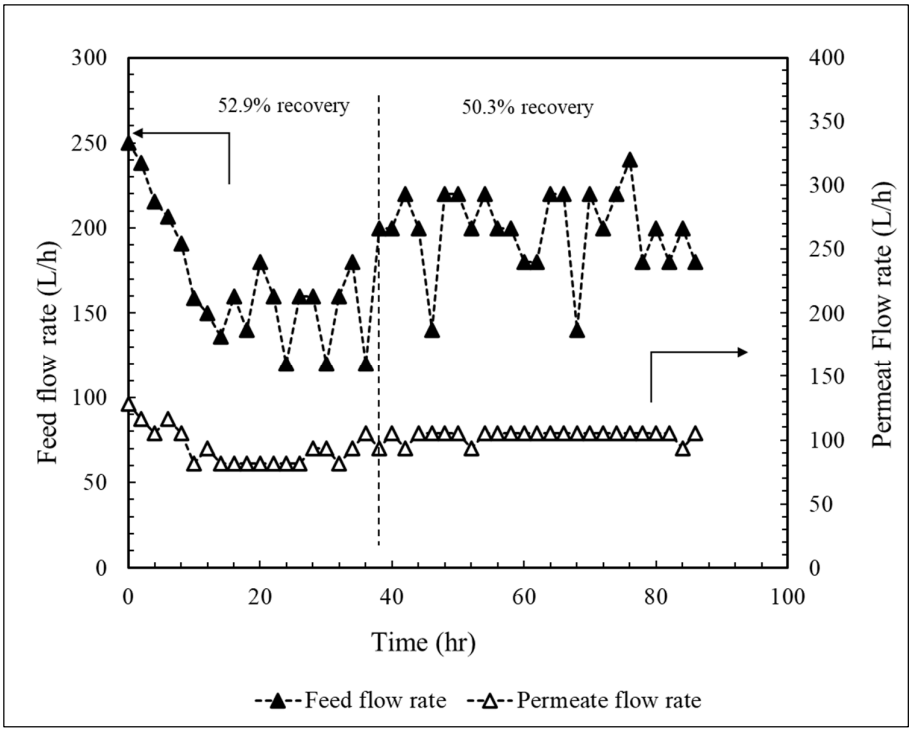


Figure 13. Feed and permeate flow rates with low salinity brine achieving 52.9% and 50.3% water recovery

DocuSign Envelope ID: 2FA9A609-C360-4E53-8B28-BE8B77B6994A

Table 5. Analysis results of samples collected from trial with low salinity brine

(all units are in mg/L unless specified otherwise)

	52.9 % water recovery			**50.3 % water recovery**		
	Feed	**Concentrate**	**Permeate**	**Feed**	**Concentrate**	**Permeate**
Alkalinity as HCO_3^-	575	778	0.0	574	731	0.0
Alkalinity as CO_3^{2-}	0.0	0.0	60.5	0.0	0.0	51.3
Alkalinity as OH^-	0.0	0.0	59.7	0.0	0.0	65.4
Alkalinity as $CaCO_3$	471	638	277.0	471	599	278.0
Ammonia	588	1,160	72.1	439	997	69.5
Barium	4	9	0.1	4	8	0.1
Boron	170	380	3.2	127	344	2.0
Bromide	271	582	1.0	268	533	1.0
Calcium	5,550	11,800	7.9	5,410	10,500	7.7
Chloride	48,000	103,000	91.3	47,400	97,700	84.9
Cobalt	1.0	1.0	0.1	1.0	1.0	0.1
Conductivity (µS/cm)	117,000	198,000	357.0	116,000	97,700	351.0
Density (g/cm^3)	1.1	1.1	1.0	1.1	1.0	0.0
Iron	<1.0	<1.0	0.1	<1.0	<1.0	1.0
Lithium	23	49	0.2	23	44	0.2
Magnesium	348	736	0.6	339	668	0.6
Manganese	0.3	0.3	0.1	0.1	0.1	0.1
pH (no units)	8.2	7.5	10.0	8.1	7.6	10.0
Potassium	2,240	4,590	4.2	2,150	4,130	4.0
Silicon	<20	<20	0.5	<20	<20	0.5
Sodium	24,400	50,400	44.8	23,200	45,500	41.9
Strontium	466	975	0.7	451	881	0.7
Sulfate	278	501	1.0	281	492	1.0
TDS	82,600	174,000	390.0	80,400	162,000	380.0
TOC1270	370	360	340.0	385	356	390.0
TSS	181	414	10.0	248	382	10.0
Zinc	0.5	0.5	0.5	0.5	0.6	0.5

DocuSign Envelope ID: 2FA9A609-C360-4E53-8B28-BE8B77B6994A

3.2.2. Pilot plant test with high salinity brine

After the completion of the first trial with low salinity feed, the high salinity brine was introduced for the subsequent trials. Treated brine of 173,000 mg/L TDS was first concentrated to reach TDS in the concentrate of 228,000 mg/L to achieve 24.1% water recovery. As seen in Figure 14, the permeate flux remained constant at ~1.71 LMH with permeate conductivity of ~450 μS/cm for 20 hours of operation. Figure 15 and Figure 16 depict the concentrate and permeate conductivity during the operations and feed and permeate flow rates, respectively.

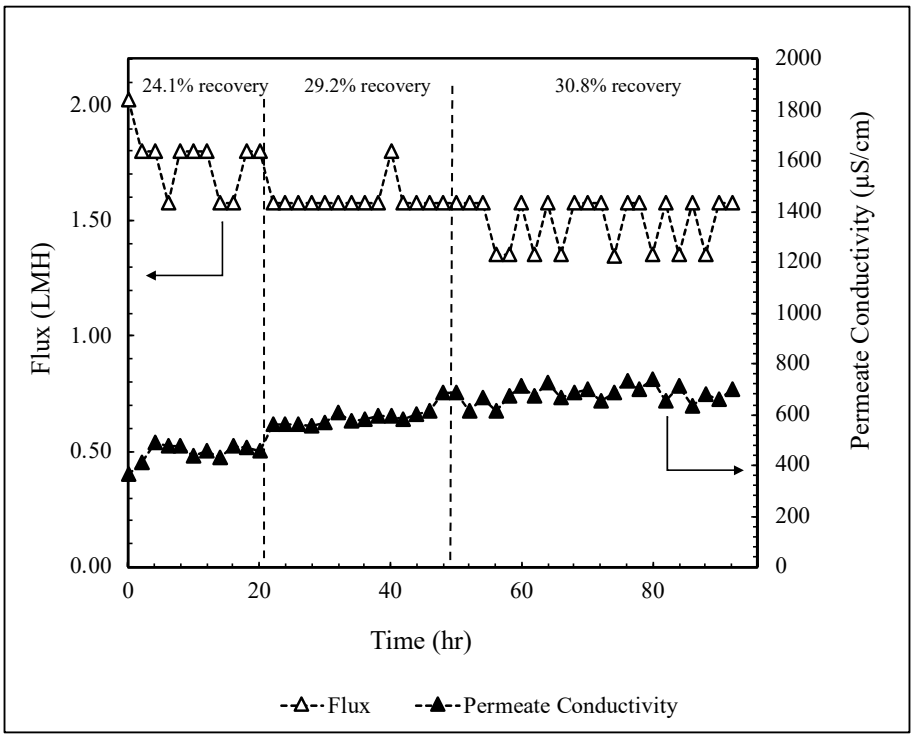


Figure 14. Permeate flux and conductivity with high salinity brine achieving 24.1%, 29.2% and 30.8% water recovery

The pilot plant was then operated using the same inlet brine to achieve TDS of the concentrate of 246,000 mg/L, which corresponds to 29.2% water recovery. The concentrate conductivity was approximately 210 mS/cm, whereas the permeate conductivity was maintained at ~ 590 μS/cm.

DocuSign Envelope ID: 2FA9A609-C360-4E53-8B28-BE8B77B6994A

As seen in Figure 14, the permeate flux remained constant at ~1.63 LMH for 30 hours of operation. After 30 hours, the plant operation was adjusted to achieve TDS in the concentrate of 240,000 mg/L, which corresponds to 30.8 % water recovery when using the feed brine with TDS of 166,000 mg/L. The flux remained constant at ~1.49 LMH with permeate conductivity of ~ 680 µS/cm for 42 hours of operation.

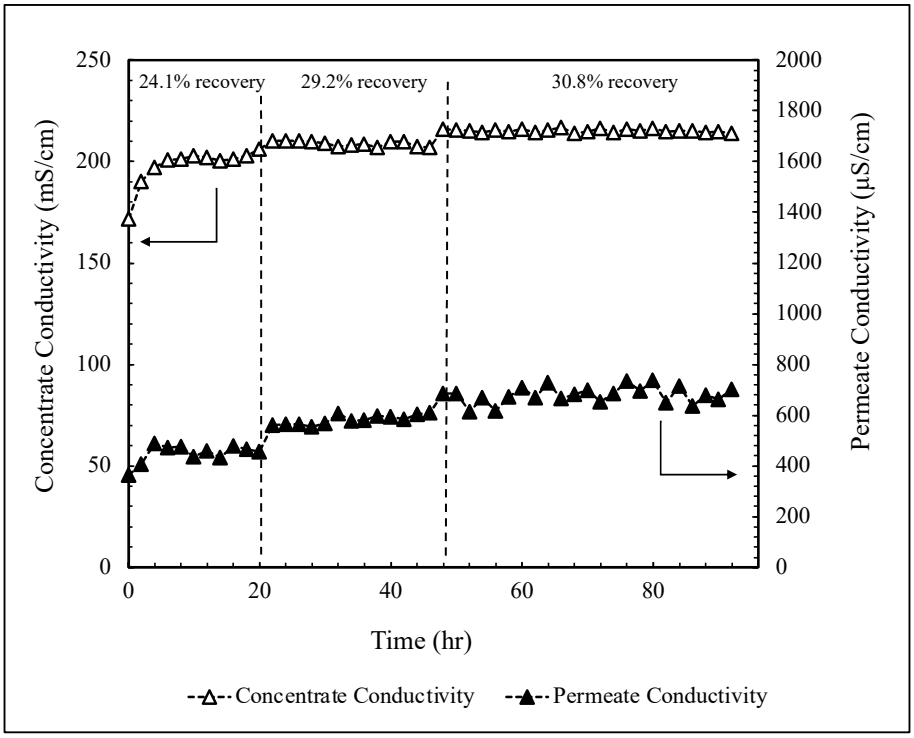


Figure 15. Feed and permeate conductivity with high salinity brine achieving 24.1%, 29.2% and 30.8% water recovery

Table 6 shows the analysis results of water samples collected during the trials. During the first 20 hours, the feed TDS was 173,000 mg/L and permeate TDS was 410 mg/L indicating 99.8% salt rejection. During the next 30 and 42 hours, permeate TDS was 460 mg/L and 510 mg/L, respectively, indicating 99.7 % salt rejection. Similar to first trial with low salinity brine, passage of CO_2, NH_3 and volatile organics led to increase in their respective concentrations in the permeate samples. The lower rejection of volatile compounds can lead to contamination of

DocuSign Envelope ID: 2FA9A609-C360-4E53-8B28-BE8B77B6994A

permeate leading to increase in permeate conductivity and Total Organic Carbon (TOC) content.

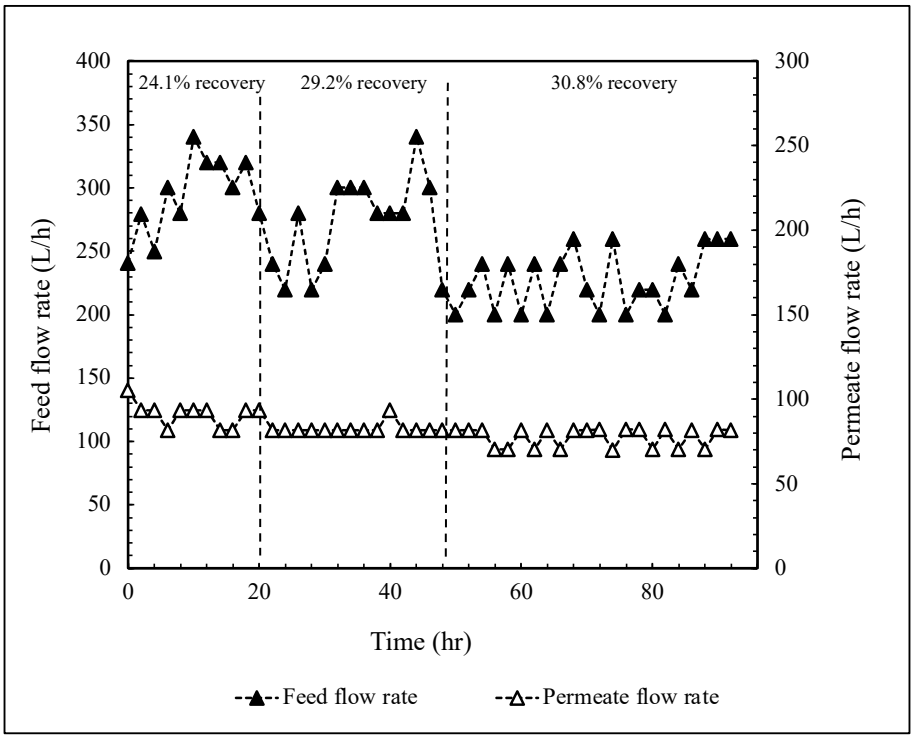


Figure 16. Feed and permeate flow rates with high salinity brine achieving 24.1%, 29.2% and 30.8% water recovery

DocuSign Envelope ID: 2FA9A609-C360-4E53-8B28-BE8B77B6994A

Table 6. Analysis results of samples collected from trial with high salinity brine

(all units are in mg/L unless specified otherwise)

	24.1% water recovery			**29.2% water recovery**		
	Feed	**Concentrate**	**Permeate**	**Feed**	**Concentrate**	**Permeate**
Alkalinity as HCO_3^-	710	776	0.0	601	731	0.0
Alkalinity as CO_3^{2-}	582	0	51.3	0	0	64.6
Alkalinity as OH^-	1,570	0	38.5	0	0	29.9
Alkalinity as $CaCO_3$	582	628	199.0	493	599	196.0
Ammonia	1,570	1,980	71.0	1,430	1,900	64.6
Barium	9	13	0.1	9	14	0.1
Boron	370	438	3.7	350	459	4.0
Bromide	619	783	1.0	611	835	1.0
Calcium	11,600	15,300	10.8	11,400	17,100	14.8
Chloride	103,000	135,000	130.0	104,000	144,000	165.0
Cobalt	<1.0	<1.0	0.1	<1.0	<1.0	0.1
Conductivity (µS/cm)	196,000	221,000	544.0	196,000	226,000	655.0
Density (g/cm^3)	1.1	1.2	1.0	1.1	1.2	1.0
Iron	1.0	2.8	0.1	<1.0	<1.0	0.1
Lithium	53	68	0.2	52	73	0.2
Magnesium	731	972	0.9	730	1,080	1.2
Manganese	5.5	8.3	0.1	6.9	10.5	0.1
pH (no units)	7.4	7.1	9.6	7.4	7.0	9.7
Potassium	4,660	6,060	6.2	4,620	6,680	7.7
Silicon	<20	<20	0.5	<20	<20	0.5
Sodium	49,300	64,800	64.5	48,600	71,400	80.7
Strontium	941	1,310	0.9	973	1,430	1.2
Sulfate	315	392	1.0	334	418	1.0
TDS	173,000	228,000	410.0	174,000	246,000	460.0
TOC1270	840	692	1,240.0	900	758	1,220.0
TSS	482	828	10.0	615	945	10.0
Zinc	0.5	0.7	0.5	0.5	1.0	0.5

DocuSign Envelope ID: 2FA9A609-C360-4E53-8B28-BE8B77B6994A

	30.8% water recovery		
	Feed	**Concentrate**	**Permeate**
Alkalinity as HCO_3^-	612	724	0.0
Alkalinity as CO_3^{2-}	0	0	54.4
Alkalinity as OH^-	0	0	27.5
Alkalinity as $CaCO_3$	502	593	171.0
Ammonia	1,340	1,880	108.0
Barium	8	13	0.1
Boron	340	454	4.8
Bromide	561	834	1.0
Calcium	11,500	163	16.3
Chloride	97,600	143,000	181.0
Cobalt	<1.0	<1.0	0.1
Conductivity (µS/cm)	195,000	227,000	715.0
Density (g/cm^3)	1.1	1.2	1.0
Iron	<1.0	<1.0	0.1
Lithium	51	72	0.2
Magnesium	717	1,030	1.3
Manganese	7.3	11.1	0.1
pH (no units)	7.4	6.9	9.6
Potassium	4,520	6,470	8.5
Silicon	<20	<20	0.5
Sodium	47,800	68,100	88.8
Strontium	977	1,350	1.4
Sulfate	301	413	1.0
TDS	166,000	240,000	510.0
TOC1270	800	686	1,050.0
TSS	533	609	10.0
Zinc	0.5	0.8	0.5

Table 7 shows the summary of results related to TDS characteristics and flow rates of feed, concentrate and permeate streams obtained during the pilot plant trails. The permeate flux, water recoveries, and salt rejection are also included. For low salinity brine, with increase

DocuSign Envelope ID: 2FA9A609-C360-4E53-8B28-BE8B77B6994A

in water recovery, the flux decreased from 2 LMH to 1.66 LMH for 50.3 % and 52.9% water recovery respectively. Similarly, for high salinity brine the flux decreased from 1.71 LMH to 1.63 LMH and then to 1.49 LMH with increase in recovery from 24.1% to 29.2% and 30.8%. In all cases, >99.7% salt rejection was obtained throughout the trial.

Table 7. Summary of results obtained during the pilot plant trials

Parameter	**Design**	**Pilot Plant Trial**				
Inlet Brine TDS (mg/L)	100,000	80,400	82,600	173,000	174,000	166,000
Outlet Brine TDS (mg/L)	200,000	162,000	174,000	228,000	246,000	240,000
Permeate TDS (mg/L)	0	380	390	410	460	510
Water recovery (%)	50	50.3	52.9	24.1	29.2	30.8
Feed flow rate (gpm)	1.0	0.88	0.67	1.41	1.18	0.92
Permeate flow rate (gpm)	0.5	0.46	0.38	0.39	0.37	0.34
Permeate flux (LMH)	2.4	2.00	1.66	1.71	1.63	1.49
Rejection (%)	100%	99.8%	99.8%	99.8%	99.7%	99.7%

3.3. Techno-economic assessment

Table 8 shows the summary of performance parameters obtained during the pilot plant trials. The criteria used for assessing the performance of the pilot-plant are described below.

The thermal efficiency of an MD system is defined as the ratio of the total enthalpy of the permeated vapor to the total heat transferred across the membrane.

$$\text{Thermal Efficiency (\%)} = \frac{A_{mem} * J * \rho_p * \Delta H_v}{\dot{m}_f * C_p * \rho_f * (T_{cold,out} - T_{cold,in})}$$

where, A_{mem} = membrane area, J = permeate flux, ρ_f = feed density, ρ_p = permeate density, ΔH_v = Heat enthalpy, m_f = feed mass flow rate, C_p = Specific heat capacity of feed solution, $T_{cold,out}$ = Temperature at the cold side membrane outlet, $T_{cold,\,in}$ = Temperature at the cold side membrane inlet.

DocuSign Envelope ID: 2FA9A609-C360-4E53-8B28-BE8B77B6994A

Specific Thermal Energy Consumption (STEC) is the measure of the heat required per unit of distillate produced.

$$\text{Specific Thermal Energy Consumption (STEC)} = \frac{\dot{m}_f * C_p * \rho_f * (T_{hot,in} - T_{cold,out})}{A_{mem} * J * \rho_p}$$

Where, $T_{hot,in}$ = Temperature at the hot side membrane inlet.

The gain output ratio (GOR) is a measure of how efficient MD system is in terms of heat recovery. It is defined as the ratio of useful heat to the total heat input of the system.

$$\text{Gain Output Ratio (GOR)} = \frac{\Delta H_v * A_{mem} * J * \rho_p}{\dot{m}_f * C_p * \rho_f * (T_{hot,in} - T_{cold,out})}$$

Table 8. Summary of performance parameters obtained during the pilot plant trials

Parameter	Design	Pilot Plant Trial				
Water recovery (%)	50	50.3	52.9	24.1	29.2	30.8
Feed flow rate (L/h)	226	199.8	152.5	320.5	269.0	208.7
Permeate flow rate (L/h)	113	104.2	86.6	89.0	84.7	77.7
Permeate flux (LMH)	2.4	2.00	1.66	1.71	1.63	1.49
T membrane, in (°C)	80.0	73.5	73.1	73.5	73.7	73.7
T condenser, out (°C)	71.0	64.8	64.7	63.2	62.9	62.3
T condenser, in (°C)	35.0	20.2	20.3	20.1	20.3	20.8
T membrane, out (°C)	40.6	30.8	30.3	30.9	31.5	32.0
Thermal Efficiency (%)	76.0%	58.5%	48.8%	51.6%	49.8%	46.9%
Gain Output Ratio (GOR)	2.9	2.9	2.5	2.1	1.9	1.6
Specific Energy Consumption (kJ/kg)	779.8	789.7	920.5	1095.4	1207.1	1388.8
Time (hr)		50.0	22.0	20.0	30.0	42.0
Total electrical consumption (kWh)		2421.21	1241.53	1086.36	1285.69	2405.56
Specific electrical consumption (kWh/m^3 of feed)	0.2	242.37	370.08	169.48	159.31	274.41
Specific electrical consumption (kWh/m^3 of permeate)	0.4	464.62	651.34	610.51	506.26	737.44

DocuSign Envelope ID: 2FA9A609-C360-4E53-8B28-BE8B77B6994A

Based on the results from pilot plant trials, the thermal efficiency and Gain Output Ratio (GOR) trends are shown in Figure 17. With increase in water recovery, the thermal efficiency as well as GOR decreases.

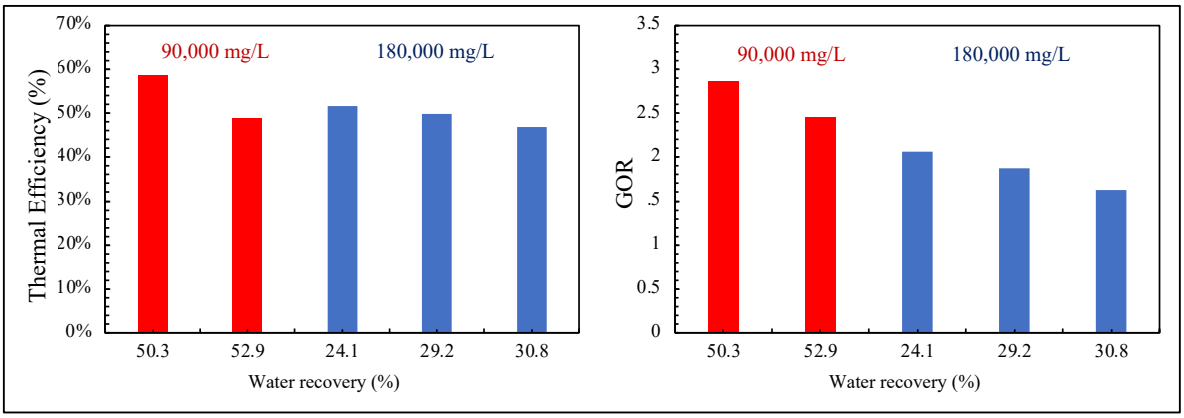


Figure 17. Thermal efficiency and Gain Output Ratio (GOR) with different water recoveries

Assuming the electricity cost of 0.069 $/KWh, the cost of treatment of high salinity brine by the pilot plant per m^3 of feed is summarized in Figure 18.

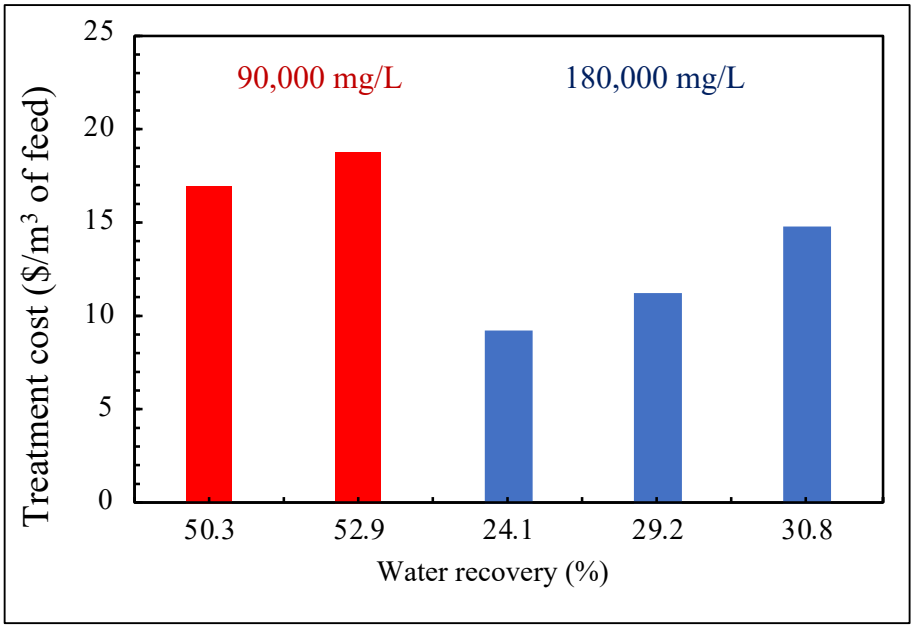


Figure 18. Treatment cost of high salinity brines in $/$m^3$ based on electrical consumption from pilot plant trial

DocuSign Envelope ID: 2FA9A609-C360-4E53-8B28-BE8B77B6994A

Figure 19 shows a process flow diagram (PFD) for an optimized 500 gal/min (31.6 kg/sec) AGMD system designed to achieve 35% water recovery when treating high salinity brine (i.e., TDS ~ 180,000 mg/L). This PFD is used for preliminary process analysis, TEA, and energy analysis based on the process models developed by our research group.

Table 9 provides a summary of CapEx and OpEx costs for a PFD shown in Figure 19. All units are in $/m^3 of feed to allow for direct comparison of AGMD system with and without external chiller. The option without a chiller is only feasible if the volume of the feed tank is sufficiently large to absorb excess heat from HX-1. If that is not the case, it would be necessary to install a chiller to enable proper operation to the plant. The treatment costs calculated can vary depending on the various operating parameters like hot channel inlet temperatures, water recovery percentage, as well as on the fixed parameters like variation in steam and electricity cost, membrane cost, membrane permeability coefficient and membrane gap size.

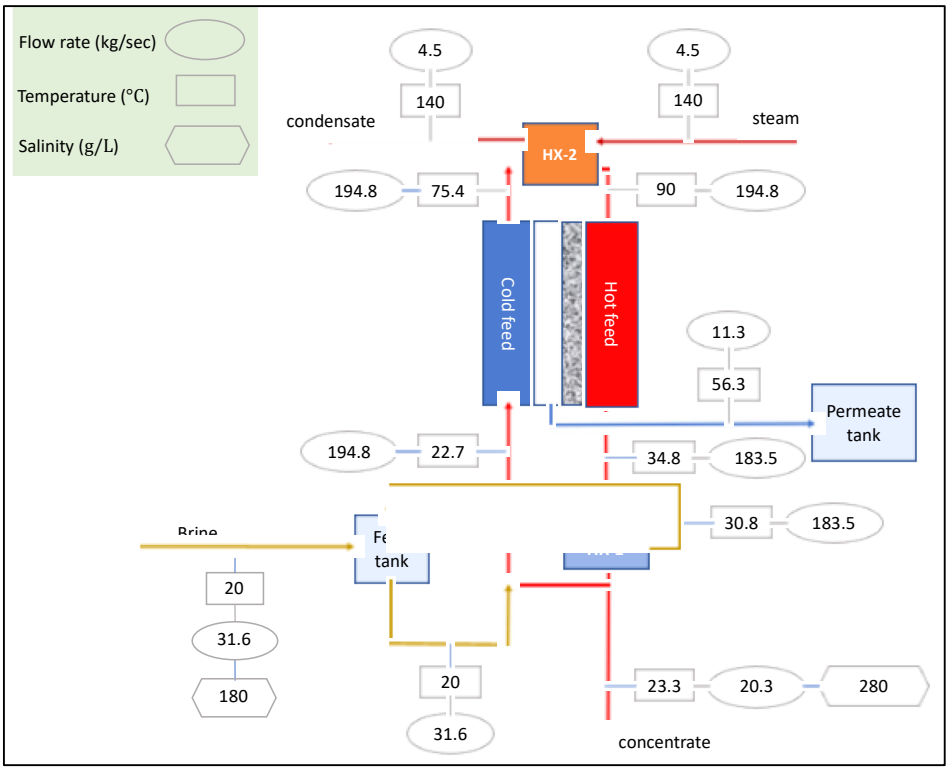


Figure 19. PFD for the AGMD system to treat 500 gal/min of EERC brine with TDS of 180,000 mg/L with 35% water recovery

DocuSign Envelope ID: 2FA9A609-C360-4E53-8B28-BE8B77B6994A

Table 9. CapEx and OpEx for and optimized AGMD system treating brine with TDS of 180,000 mg/L with 35% water recovery

	With Chiller	Without Chiller
Chiller	0.016	0
Heat exchanger	0.003	0.004
Membrane and module	0.202	0.16
Installation (pumps and pipes)	0.074	0.07
Storage tank	0.187	0.187
Total capital cost	**0.489**	**0.427**
Chilling	0.542	0
Heating	0.909	1.019
Membrane replacement	0.453	0.359
Pump	0.046	0.031
Total operating cost	**1.952**	**1.409**
Total cost	**2.441**	**1.836**

The effect of inlet temperature and water recovery percentage on the treatment cost for a system that includes a chiller is shown in Figure 20.

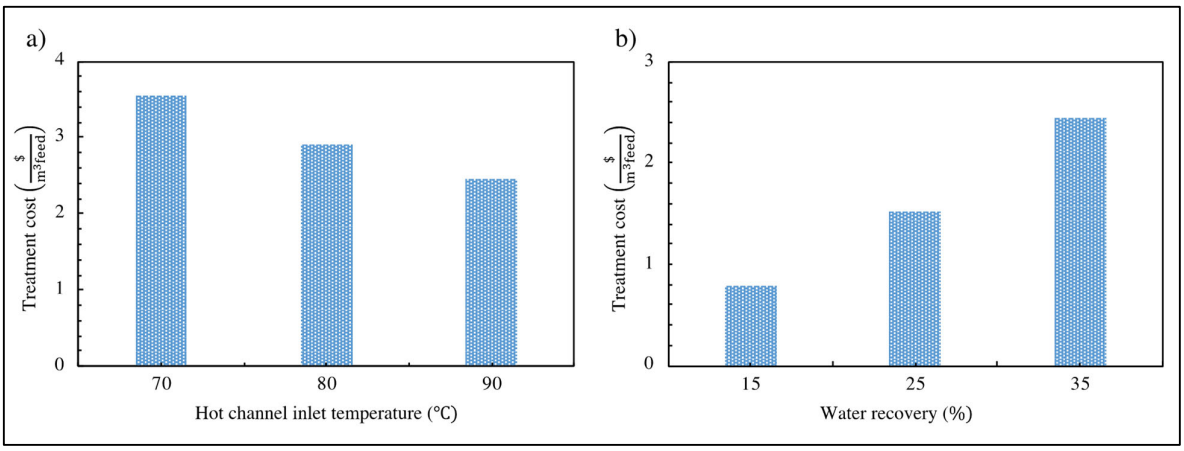


Figure 20. Effect of a) Hot channel inlet temperature, and b) Water recovery (%) on treatment cost in $/m^3 of feed

The cost estimates for a full scale plant are significantly lower than those obtained from the pilot plant tests for two reasons: a) the pilot plant used oversized chiller and heater and the heating was done using electrical energy as opposed to steam and b) the full scale system was highly optimized compared to the pilot-scale system. In addition:

DocuSign Envelope ID: 2FA9A609-C360-4E53-8B28-BE8B77B6994A

- Stream salinity and flowrates and temperatures, module dimensions, membrane specific area, stream Reynolds number, recycle ratios, heat exchanger and chiller and pump sizes are the variables in the design of the full scale system that are tuned to their optimal value in order to achieve the lowest possible cost. Any deviation from the determined optimum values could result in significant cost increase.
- All calculations for the full scale system are performed under the premise that no flooding occurs in AGMD gap under ideal conditions. However, in the real world, water bridging, or flooding may occur, thereby reducing AGMD performance to that of Permeate Gap MD (PGMD). Flooding is dependent on the gap size and the ratio of condensation to water removal, which depends on the surface of the cooling wall and spacer material.
- Although the steam cost used in the design of a full scale system is based on commonly accepted assumptions from the literature, it is not an accurate estimate of the steam production cycle (i.e., boiler, etc.).

Nevertheless, the cost estimate for an optimized full scale treatment plant can be used when comparing AGMD technology to other treatment alternatives like Mechanical Vapor Compression (MVR), multi-stage flash distillation (MSFD) or multi-effect distillation (MED).

DocuSign Envelope ID: 2FA9A609-C360-4E53-8B28-BE8B77B6994A

4. CONCLUSIONS

This study evaluated technical feasibility of using membrane distillation for desalination of high-TDS brines. Laboratory scale studies showed that membrane distillation can be used to recover 50% and 30% of high-quality permeate from the low and high salinity brines, respectively. An increase in permeate conductivity observed in the laboratory-scale DCMD module was due to the passage of ammonia from the feed side to the permeate side followed by protonation to ammonium ion. The permeate flux remained constant indicating no scaling/fouling of the membrane during the long-term laboratory tests.

Based on a successful laboratory-scale experiments, a pilot-scale system to achieve 50% water recovery when treating 1 gpm of brine was deployed to the EERC BEST site in Watford city, ND. The pilot plant was first operated using pretreated high and low salinity brine provided by the BEST site team. Low salinity brine treatment with V-AGMD resulted in successful steady-state operation of the pilot system for 3 days where the brine was concentrated with recovering 52.9% and 50.3% high quality permeate suitable for industrial/agricultural use. This study demonstrated the operation a of commercial PTFE membrane with a steady flux with 99.7% ion rejection from the feed. Further, high salinity brine with ~170,000 mg/L was concentrated to recover 24.1%, 29.2%, and 30.8% water over the period of 92 hours. The flux dropped with increase in water recoveries whereas >99.8% ion rejection was observed throughout the trial. The passage of alkalinity, ammonia and TOC in the permeate can led to requirement of polishing the water depending on the downstream application. The economic assessment for treatment cost per m^3 of the feed was calculated based on the electricity consumptions during the trial and modelling results are reported. Successful demonstration of MD technology under realistic fed conditions offers additional management strategies for brine generated by the unconventional oil and gas industry to reduce its water footprint.

DocuSign Envelope ID: 2FA9A609-C360-4E53-8B28-BE8B77B6994A

Like most membrane processes, MD can be easily scaled-up to full-scale applications to treat high salinity wastewaters from oil and gas industry. However, membrane modules used for longer time can experience wear and tear due to continuous use as well as scaling and fouling when treating high salinity brines. Thus, membrane modules might require cleaning at regular intervals and replacement in case of leakage or physical damage. Further application of MD technology for high salinity treatment would also require pilot-scale studies that are conducted for a longer period of time (i.e., months). These tests would provide a better idea of the membrane cleaning requirements and will be used to validate the initial operating cost estimates. Also, these long-term tests would provide insights into continuously operating MD system with high salinity brines of variable quality and quantity. This enhanced pilot-scale testing should be done using a large number of membrane modules (e.g., several tens) operating in parallel to demonstrate system performance at a larger scale (e.g., feed flowrate of 25 gpm). In addition, it would be necessary to optimize pretreatment process for continuous and reliable operation for each high-TDS brine quality that may be encountered in the field to enable further penetration of MD technology into oil and gas industry.

DocuSign Envelope ID: 2FA9A609-C360-4E53-8B28-BE8B77B6994A

5. REFERENCES

[1] U.K. Kesieme, N. Milne, H. Aral, C.Y. Cheng, M. Duke, Economic analysis of desalination technologies in the context of carbon pricing, and opportunities for membrane distillation, Desalination. 323 (2013) 66–74. https://doi.org/10.1016/j.desal.2013.03.033.

[2] T. Mezher, H. Fath, Z. Abbas, A. Khaled, Techno-economic assessment and environmental impacts of desalination technologies, Desalination. 266 (2011) 263–273. https://doi.org/10.1016/j.desal.2010.08.035.

[3] G.P. Thiel, E.W. Tow, L.D. Banchik, H.W. Chung, J.H. Lienhard V, Energy consumption in desalinating produced water from shale oil and gas extraction, Desalination. 366 (2015) 94–112. https://doi.org/10.1016/j.desal.2014.12.038.

[4] A. Subramani, J.G. Jacangelo, Emerging desalination technologies for water treatment: A critical review, Water Research. 75 (2015) 164–187. https://doi.org/10.1016/j.watres.2015.02.032.

[5] K.W. Lawson, D.R. Lloyd, Membrane distillation, 124 (1997) 1–25.

[6] L.M. Camacho, L. Dumée, J. Zhang, J. de Li, M. Duke, J. Gomez, S. Gray, Advances in membrane distillation for water desalination and purification applications, Water (Switzerland). 5 (2013) 94–196. https://doi.org/10.3390/w5010094.

[7] A. Alkhudhiri, N. Darwish, N. Hilal, Produced water treatment: Application of Air Gap Membrane Distillation, Desalination. 309 (2013) 46–51. https://doi.org/10.1016/j.desal.2012.09.017.

[8] B. Li, K.K. Sirkar, Novel membrane and device for direct contact membrane distillation-based desalination process, Industrial and Engineering Chemistry Research. 43 (2004) 5300–5309. https://doi.org/10.1021/ie030871s.

DocuSign Envelope ID: 2FA9A609-C360-4E53-8B28-BE8B77B6994A

[9] T.Y. Cath, V.D. Adams, A.E. Childress, Experimental study of desalination using direct contact membrane distillation: A new approach to flux enhancement, Journal of Membrane Science. 228 (2004) 5–16. https://doi.org/10.1016/j.memsci.2003.09.006.

[10] A.M.M. Shirazi, Desalination of Saline Water Using Direct Contact Membrane Distillation, 17 (2011) 28–36.

[11] M. Xie, L.D. Nghiem, W.E. Price, M. Elimelech, A forward osmosis-membrane distillation hybrid process for direct sewer mining: System performance and limitations, Environmental Science and Technology. 47 (2013) 13486–13493. https://doi.org/10.1021/es404056e.

[12] M. Gryta, K. Karakulski, A.W. Morawski, Purification of oily wastewater by hybrid UF/MD, Water Research. 35 (2001) 3665–3669. https://doi.org/10.1016/S0043-1354(01)00083-5.

[13] V.V.U.I.B.V. and V.N.N. P.P. Zolotarev, Karpov Physico-Chemical Research Institute, ul. Obukha 10. Moscow 103064. Russia, Journal of Hazardous Materials. 37 (1994) 77–82.

[14] M. Khayet, Treatment of radioactive wastewater solutions by direct contact membrane distillation using surface modified membranes, Desalination. 321 (2013) 60–66. https://doi.org/10.1016/j.desal.2013.02.023.

[15] Z. Zhang, O.R. Lokoare, A. V Gusa, R.D. Vidic, Pretreatment of brackish water reverse osmosis (BWRO) concentrate to enhance water recovery in inland desalination plants by direct contact membrane distillation (DCMD), Desalination. 508 (2021) 115050. https://doi.org/10.1016/j.desal.2021.115050.

[16] S.T. Hsu, K.T. Cheng, J.S. Chiou, Seawater desalination by direct contact membrane distillation, Desalination. 143 (2002) 279–287. https://doi.org/10.1016/S0011-9164(02)00266-7.

DocuSign Envelope ID: 2FA9A609-C360-4E53-8B28-BE8B77B6994A

[17] X. Ji, E. Curcio, S. Al Obaidani, G. Di Profio, E. Fontananova, E. Drioli, Membrane distillation-crystallization of seawater reverse osmosis brines, Separation and Purification Technology. 71 (2010) 76–82. https://doi.org/10.1016/j.seppur.2009.11.004.

[18] J. Kujawa, E. Guillen-Burrieza, H.A. Arafat, M. Kurzawa, A. Wolan, W. Kujawski, Raw Juice Concentration by Osmotic Membrane Distillation Process with Hydrophobic Polymeric Membranes, Food and Bioprocess Technology. 8 (2015) 2146–2158. https://doi.org/10.1007/s11947-015-1570-4.

[19] U.K. Kesieme, N. Milne, C.Y. Cheng, H. Aral, M. Duke, Recovery of water and acid from leach solutions using direct contact membrane distillation, Water Science and Technology. 69 (2014) 868–875. https://doi.org/10.2166/wst.2013.788.

[20] A.A. Hassan, H. Adel Jabbar, Direct Contact Membrane Distillation for Separation of Hcl From A Mixture of Acids, Journal of Engineering. 24 (2018) 41. https://doi.org/10.31026/j.eng.2018.06.04.

[21] O.R. Lokare, S. Tavakkoli, S. Wadekar, V. Khanna, R.D. Vidic, Fouling in direct contact membrane distillation of produced water from unconventional gas extraction, Journal of Membrane Science. 524 (2017) 493–501. https://doi.org/10.1016/j.memsci.2016.11.072.

[22] H. Julian, Y. Ye, H. Li, V. Chen, Scaling mitigation in submerged vacuum membrane distillation and crystallization (VMDC) with periodic air-backwash, Journal of Membrane Science. 547 (2018) 19–33. https://doi.org/10.1016/j.memsci.2017.10.035.

[23] X. Du, Z. Zhang, K.H. Carlson, J. Lee, T. Tong, Membrane fouling and reusability in membrane distillation of shale oil and gas produced water: Effects of membrane surface wettability, Journal of Membrane Science. 567 (2018) 199–208. https://doi.org/10.1016/j.memsci.2018.09.036.

DocuSign Envelope ID: 2FA9A609-C360-4E53-8B28-BE8B77B6994A

[24] X. Wen, F. Li, B. Jiang, X. Zhang, X. Zhao, Effect of surfactants on the treatment of radioactive laundry wastewater by direct contact membrane distillation, Journal of Chemical Technology and Biotechnology. 93 (2018) 2252–2261. https://doi.org/10.1002/jctb.5568.

[25] H. Chang, B. Liu, Z. Zhang, R. Pawar, Z. Yan, J.C. Crittenden, R.D. Vidic, A Critical Review of Membrane Wettability in Membrane Distillation from the Perspective of Interfacial Interactions, Environmental Science and Technology. (2021). https://doi.org/10.1021/acs.est.0c05454.

[26] M. Gryta, Long-term performance of membrane distillation process, Journal of Membrane Science. 265 (2005) 153–159. https://doi.org/10.1016/j.memsci.2005.04.049.

[27] S. Goh, J. Zhang, Y. Liu, A.G. Fane, Fouling and wetting in membrane distillation (MD) and MD-bioreactor (MDBR) for wastewater reclamation, Desalination. 323 (2013) 39–47. https://doi.org/10.1016/j.desal.2012.12.001.

[28] Z. Wang, S. Lin, Membrane fouling and wetting in membrane distillation and their mitigation by novel membranes with special wettability, Water Research. 112 (2017) 38–47. https://doi.org/10.1016/j.watres.2017.01.022.

[29] N.A. Mohammad Ameen, S.S. Ibrahim, Q.F. Alsalhy, A. Figoli, Highly salinewater desalination using direct contact membrane distillation (DCMD): Experimental and simulation study, Water (Switzerland). 12 (2020). https://doi.org/10.3390/W12061575.

[30] J.A. Bush, J. Vanneste, T.Y. Cath, Membrane distillation for concentration of hypersaline brines from the Great Salt Lake: Effects of scaling and fouling on performance, efficiency, and salt rejection, Separation and Purification Technology. 170 (2016) 78–91. https://doi.org/10.1016/j.seppur.2016.06.028.

DocuSign Envelope ID: 2FA9A609-C360-4E53-8B28-BE8B77B6994A

[31] M. Malmali, P. Fyfe, D. Lincicome, K. Sardari, S.R. Wickramasinghe, Selecting membranes for treating hydraulic fracturing produced waters by membrane distillation, Separation Science and Technology (Philadelphia). 52 (2017) 266–275. https://doi.org/10.1080/01496395.2016.1244550.

[32] M. Al-Salmi, M. Laqbaqbi, S. Al-Obaidani, R.S. Al-Maamari, M. Khayet, M. Al-Abri, Application of membrane distillation for the treatment of oil field produced water, Desalination. 494 (2020). https://doi.org/10.1016/j.desal.2020.114678.

[33] A. Deshmukh, C. Boo, V. Karanikola, S. Lin, A.P. Straub, T. Tong, D.M. Warsinger, M. Elimelech, Membrane distillation at the water-energy nexus: Limits, opportunities, and challenges, Energy and Environmental Science. 11 (2018) 1177–1196. https://doi.org/10.1039/c8ee00291f.

[34] O.R. Lokare, S. Tavakkoli, S. Wadekar, V. Khanna, R.D. Vidic, Fouling in direct contact membrane distillation of produced water from unconventional gas extraction, Journal of Membrane Science. 524 (2017) 493–501. https://doi.org/10.1016/j.memsci.2016.11.072.

[35] Z. Zhang, X. Du, K.H. Carlson, C.A. Robbins, T. Tong, Effective treatment of shale oil and gas produced water by membrane distillation coupled with precipitative softening and walnut shell filtration, Desalination. 454 (2019) 82–90. https://doi.org/10.1016/j.desal.2018.12.011.

[36] T. Tong, K.H. Carlson, C.A. Robbins, Z. Zhang, X. Du, Membrane-based treatment of shale oil and gas wastewater: The current state of knowledge, Frontiers of Environmental Science and Engineering. 13 (2019). https://doi.org/10.1007/s11783-019-1147-y.

DocuSign Envelope ID: 2FA9A609-C360-4E53-8B28-BE8B77B6994A

[37] G.P. Thiel, J.H. Lienhard V, Treating produced water from hydraulic fracturing: Composition effects on scale formation and desalination system selection, Desalination. 346 (2014) 54–69. https://doi.org/10.1016/j.desal.2014.05.001.

[38] H. Cho, Y. Choi, S. Lee, Effect of pretreatment and operating conditions on the performance of membrane distillation for the treatment of shale gas wastewater, Desalination. 437 (2018) 195–209. https://doi.org/10.1016/j.desal.2018.03.009.

[39] C.A. Robbins, Y. Yin, A.J. Hanson, J. Blotevogel, T. Borch, T. Tong, Mitigating membrane wetting in the treatment of unconventional oil and gas wastewater by membrane distillation: A comparison of pretreatment with omniphobic membrane, Journal of Membrane Science. 645 (2022) 120198. https://doi.org/10.1016/j.memsci.2021.120198.

[40] Z. Anari, A. Sengupta, K. Sardari, S.R. Wickramasinghe, Surface modification of PVDF membranes for treating produced waters by direct contact membrane distillation, Separation and Purification Technology. 224 (2019) 388–396. https://doi.org/10.1016/j.seppur.2019.05.032.

[41] X. Du, Z. Zhang, K.H. Carlson, J. Lee, T. Tong, Membrane fouling and reusability in membrane distillation of shale oil and gas produced water: Effects of membrane surface wettability, Journal of Membrane Science. 567 (2018) 199–208. https://doi.org/10.1016/j.memsci.2018.09.036.

[42] L.M. Camacho, L. Dumée, J. Zhang, J. de Li, M. Duke, J. Gomez, S. Gray, Advances in membrane distillation for water desalination and purification applications, Water (Switzerland). 5 (2013) 94–196. https://doi.org/10.3390/w5010094.

[43] H. Chang, T. Li, B. Liu, R.D. Vidic, M. Elimelech, J.C. Crittenden, Potential and implemented membrane-based technologies for the treatment and reuse of flowback and

DocuSign Envelope ID: 2FA9A609-C360-4E53-8B28-BE8B77B6994A

produced water from shale gas and oil plays: A review, Desalination. 455 (2019) 34–57. https://doi.org/10.1016/j.desal.2019.01.001.

[44] R.G. Raluy, R. Schwantes, V.J. Subiela, B. Peñate, G. Melián, J.R. Betancort, Operational experience of a solar membrane distillation demonstration plant in Pozo Izquierdo-Gran Canaria Island (Spain), Desalination. 290 (2012) 1–13. https://doi.org/10.1016/j.desal.2012.01.003.

[45] J. Koschikowski, M. Wieghaus, M. Rommel, V.S. Ortin, B.P. Suarez, J.R. Betancort Rodríguez, Experimental investigations on solar driven stand-alone membrane distillation systems for remote areas, Desalination. 248 (2009) 125–131. https://doi.org/10.1016/j.desal.2008.05.047.

[46] U. Fortkamp, H. Royen, M. Klingspor, Ö. Ekengren, A. Martin, D.M. Woldemariam, Membrane Distillation pilot tests for different wastewaters Separation of pharmaceutical residues and treatment of flue gas condensate with Xzero Membrane Distillation in Pilot Scale at Hammarby Sjöstadsverk, 2236. www.ivl.se.

[47] H.C. Duong, A.R. Chivas, B. Nelemans, M. Duke, S. Gray, T.Y. Cath, L.D. Nghiem, Treatment of RO brine from CSG produced water by spiral-wound air gap membrane distillation - A pilot study, Desalination. 366 (2015) 121–129. https://doi.org/10.1016/j.desal.2014.10.026.

[48] J. Minier-Matar, A. Hussain, A. Janson, S. Adham, IPTC 17481 Treatment of Produced Water from Unconventional Resources by Membrane Distillation, 2014. http://onepetro.org/IPTCONF/proceedings-pdf/13IPTC/All-13IPTC/IPTC-17481-MS/1490426/iptc-17481-ms.pdf/1.

[49] J. Minier-Matar, A. Hussain, A. Janson, F. Benyahia, S. Adham, Field evaluation of membrane distillation technologies for desalination of highly saline brines, Desalination. 351 (2014) 101–108. https://doi.org/10.1016/j.desal.2014.07.027.

DocuSign Envelope ID: 2FA9A609-C360-4E53-8B28-BE8B77B6994A

[50] R. Schwantes, L. Bauer, K. Chavan, D. Dücker, C. Felsmann, J. Pfafferott, Air gap membrane distillation for hypersaline brine concentration: Operational analysis of a full-scale module–New strategies for wetting mitigation, Desalination. 444 (2018) 13–25. https://doi.org/10.1016/j.desal.2018.06.012.

[51] N. Thomas, M.O. Mavukkandy, S. Loutatidou, H.A. Arafat, Membrane distillation research & implementation: Lessons from the past five decades, Separation and Purification Technology. 189 (2017) 108–127. https://doi.org/10.1016/j.seppur.2017.07.069.

[52] T. Horseman, Y. Yin, K.S. Christie, Z. Wang, T. Tong, S. Lin, Wetting, Scaling, and Fouling in Membrane Distillation: State-of-the-Art Insights on Fundamental Mechanisms and Mitigation Strategies, ACS ES&T Engineering. 1 (2021) 117–140. https://doi.org/10.1021/acsestengg.0c00025.

[53] H. Attia, M.S. Osman, D.J. Johnson, C. Wright, N. Hilal, Modelling of air gap membrane distillation and its application in heavy metals removal, Desalination. 424 (2017) 27–36. https://doi.org/10.1016/j.desal.2017.09.027.

[54] A. Kujawska, J.K. Kujawski, M. Bryjak, M. Cichosz, W. Kujawski, Removal of volatile organic compounds from aqueous solutions applying thermally driven membrane processes. 2. Air gap membrane distillation, Journal of Membrane Science. 499 (2016) 245–256. https://doi.org/10.1016/j.memsci.2015.10.047.

[55] H. Attia, S. Alexander, C.J. Wright, N. Hilal, Superhydrophobic electrospun membrane for heavy metals removal by air gap membrane distillation (AGMD), Desalination. 420 (2017) 318–329. https://doi.org/10.1016/j.desal.2017.07.022.

[56] H.C. Duong, A.R. Chivas, B. Nelemans, M. Duke, S. Gray, T.Y. Cath, L.D. Nghiem, Treatment of RO brine from CSG produced water by spiral-wound air gap membrane

DocuSign Envelope ID: 2FA9A609-C360-4E53-8B28-BE8B77B6994A

distillation - A pilot study, Desalination. 366 (2015) 121–129. https://doi.org/10.1016/j.desal.2014.10.026.

[57] L. García-Fernández, B. Wang, M.C. García-Payo, K. Li, M. Khayet, Morphological design of alumina hollow fiber membranes for desalination by air gap membrane distillation, Desalination. 420 (2017) 226–240. https://doi.org/10.1016/j.desal.2017.07.021.

[58] M. Rezaei, D.M. Warsinger, J.H. Lienhard V, M.C. Duke, T. Matsuura, W.M. Samhaber, Wetting phenomena in membrane distillation: Mechanisms, reversal, and prevention, Water Research. 139 (2018) 329–352. https://doi.org/10.1016/j.watres.2018.03.058.

[59] M. Gryta, Separation of saline oily wastewater by membrane distillation, Chemical Papers. 74 (2020) 2277–2286. https://doi.org/10.1007/s11696-020-01071-y.

[60] N. Dow, J. Villalobos García, L. Niadoo, N. Milne, J. Zhang, S. Gray, M. Duke, Demonstration of membrane distillation on textile waste water assessment of long term performance, membrane cleaning and waste heat integration, Environmental Science: Water Research and Technology. 3 (2017) 433–449. https://doi.org/10.1039/c6ew00290k.

[61] A. Zoungrana, İ.H. Zengin, O.K. Türk, M. Çakmakcı, Ammoniacal nitrogen reclamation by membrane distillation from high ammonia polluted solutions, Chemical Papers. 74 (2020) 1903–1915. https://doi.org/10.1007/s11696-019-01034-y.

DocuSign Envelope ID: 2FA9A609-C360-4E53-8B28-BE8B77B6994A

6. APPENDIX

Table A1. Produced water analysis provided by EERC

Parameter	Value		Units
Alkalinity as CaCO3	101.1	202.3	mg/L
Barium	3.8	7.5	mg/L
Boron	171.4	342.9	mg/L
Bromide	162.9	325.7	mg/L
Calcium	5,914.3	11,828.6	mg/L
Chloride	54,000.0	108,000.0	mg/L
Iron	39.6	79.2	mg/L
Lithium	24.7	49.4	mg/L
Magnesium	360.0	720.0	mg/L
Manganese	6.3	12.5	mg/L
Phosphorus	9.0	18.0	mg/L
Potassium	1,885.7	3,771.4	mg/L
Silicon	9.0	18.0	mg/L
Sodium	26,742.9	53,485.7	mg/L
Strontium	531.4	1,062.9	mg/L
Sulfate	102.9	205.7	mg/L
TDS	90,000.0	180,000.0	mg/L
TOC1270	544.3	1,088.6	mg/L
TSS	65.1	130.3	mg/L
pH	6.0	5.7	

DocuSign Envelope ID: 2FA9A609-C360-4E53-8B28-BE8B77B6994A

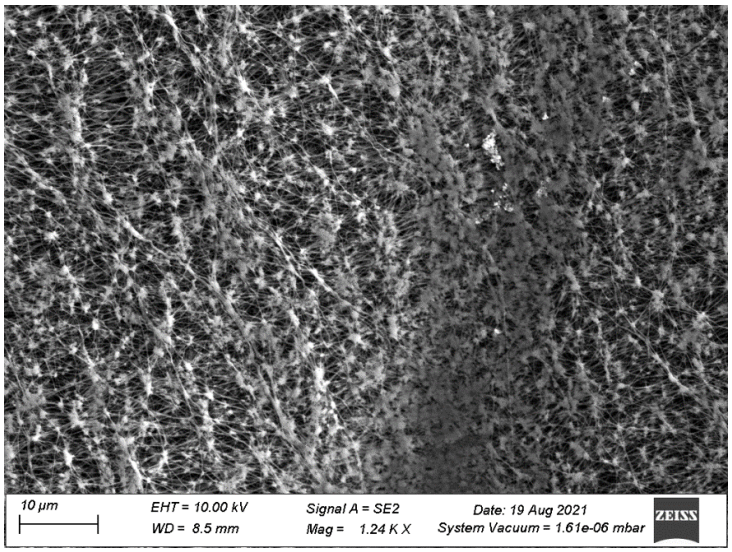


Figure A1. SEM image of the membrane used in DCMD module with low salinity brine(~90,000 mg/L)concentrated 50% water recovery

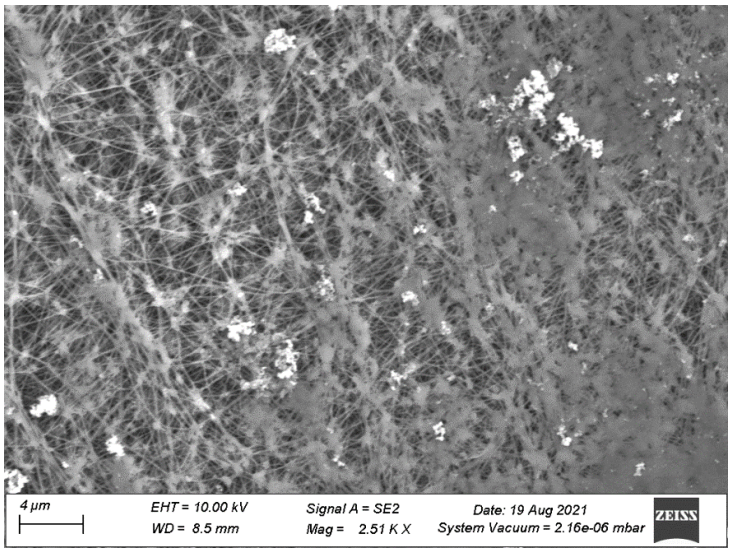


Figure A2. SEM image of the membrane used in DCMD module with high salinity brine (~180,000 mg/L) concentrated 30% water recovery

DocuSign Envelope ID: 2FA9A609-C360-4E53-8B28-BE8B77B6994A

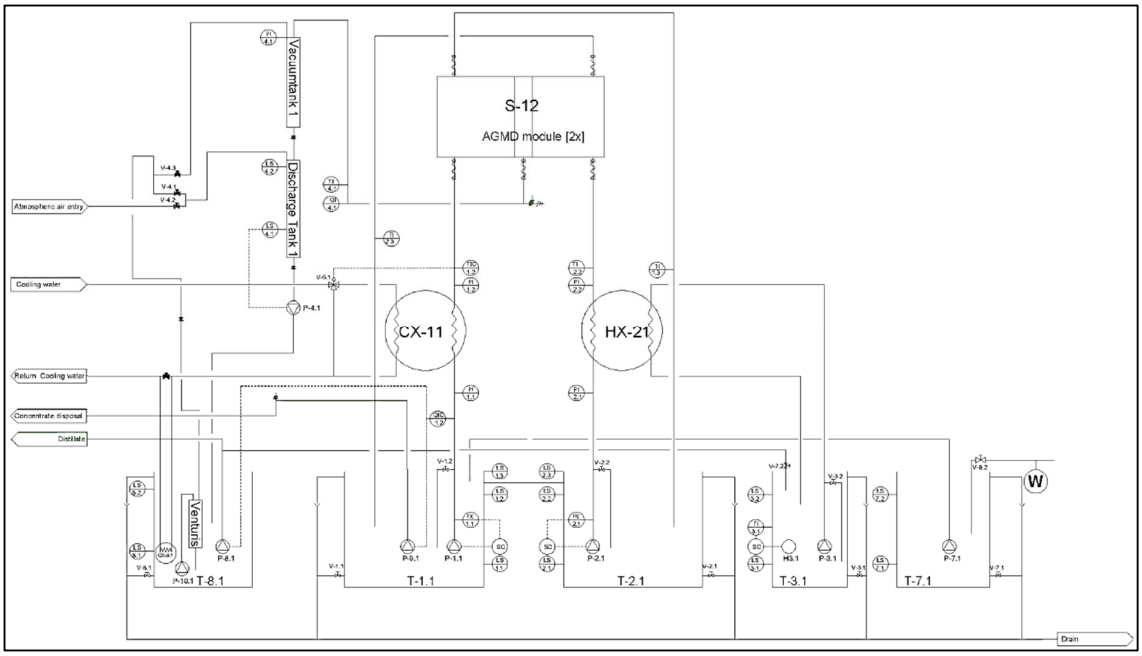


Figure A3. PID Diagram of the pilot-scale system

DocuSign Envelope ID: 2FA9A609-C360-4E53-8B28-BE8B77B6994A

APPENDIX H

OHIO UNIVERSITY FINAL REPORT – 2021

DocuSign Envelope ID: 2FA9A609-C360-4E53-8B28-BE8B77B6994A

Supercritical Water Desalination Technology Demonstration
At the University of North Dakota EERC BEST Site

Prepared For: University of North Dakota

Authors: Logan Veley, Joshua Jordan, Issam Khoury, and Jason Trembly

December 20th, 2021

DocuSign Envelope ID: 2FA9A609-C360-4E53-8B28-BE8B77B6994A

1 Introduction

1.1 U.S. Produced Water Generation and Management

Oil and natural gas generated from unconventional reservoirs have played a significant role in meeting U.S. energy demand over the past decade. Produced water is an aqueous byproduct generated along with hydrocarbons, with estimates of over 24 billion bbl of the waste generated by the U.S. in 2017 [1]. Produced water may contain high salinities (measured as "total dissolved solids", or TDS), dissolved organic components, and naturally occurring radioactive material (NORM), complicating treatment. Low TDS-containing produced waters are readily reused in well development opportunities. As produced water TDS increases, the ability to directly reuse the waste product decreases as dissolved components may interfere with reservoir chemistry, resulting in decreased production and injection well disposal as the predominant management method.

High salinity-produced waters are generated from conventional and unconventional resources [2]. In particular, produced water generated by unconventional reservoirs with the Appalachian Basin and Bakken reservoirs can contain high TDS, organic material, and in some instances, naturally occurring radioactive material (NORM). Produced water desalination techniques that have been considered for high salinity produced water include membranes (reverse (RO) and forward (FO) osmosis), multi-stage stage flash and multi-effect distillation, and mechanical vapor compression (MVC). However, operational data for such technologies have typically been limited to produced water containing below 75,000 $mg \cdot L^{-1}$ TDS.

1.2 Supercritical Water Desalination Technology

Among the techniques being developed for high salinity-produced waters, supercritical water desalination (SCWD) is capable of producing a clean water product in conjunction with a concentrated brine [3], [4] or solid salt product [3], [5], [6]. Most supercritical water reactors utilize externally heated designs, which have high thermal lag, internal scaling issues, and manufacturing costs. Due to these issues, such systems are unable to be cost-effectively scaled. Ohio University (OHIO) has developed an alternative design utilizing Joule-heating to accomplish SCWD of produced water to address this issue. This novel design allows for direct control of power applied to the brine using the electrical conductivity of the brine when applying an alternating current (AC), resulting in a lower TDS content vapor product and a concentrated TDS liquid product. To date, OHIO has conducted laboratory tests with the Joule-heated technology with simulated and field-derived produced waters containing up to 180,000 $mg \cdot L^{-1}$ TDS [3], [4]. The purpose of this project is to conduct field testing to estimate energy requirements for treating Williston Basin derived brine containing up to 180,000 $mg \cdot L^{-1}$ using OHIO's SCWD technology.

1.3 Project Objectives

The purpose of this project is to evaluate the ability of OHIO's SCWD technology to continuously remediate field-derived brine containing up to 180,000 $mg \cdot L^{-1}$ TDS at the University of North Dakota's (UND) Energy & Environment Research Center (EERC) BEST Facility. Specific objectives included the following:

- Prepare OHIO's Joule-heated SCWD technology for a field demonstration trial at UND's BEST facility located in Watford City, ND,
- Experimentally determine process energetics associated in recovering 25-50% clean water from brine containing 90,000 and 180,000 $mg \cdot L^{-1}$, and
- Project process energetics associated with a commercial-scale SCWD brine remediation process treating 100 gal/min of waste.

The following document sections report the methodologies, experimental results, and process simulations fulfilling these project objectives.

DocuSign Envelope ID: 2FA9A609-C360-4E53-8B28-BE8B77B6994A

2 Methodologies

2.1 SCWD Technology Operation

A supercritical water test system using Joule-heating to treat brines was developed to investigate the proposed water management process. A process and instrumentation diagram of the prototype test system and a cross-section view of the desalinator are shown in Figure 1. The system utilizes a high-pressure liquid chromatography pump (P-100) to supply a flow rate up to 300 mL per minute. The brine was pumped through a high-pressure tube in tube heat exchanger (HX-100) to recover heat from the processed fluid, followed by a preheater (HX-101) to control the desalinator inlet temperature. The desalinator has a radial electrode configuration with an inner electrode diameter of 0.25 in. and is constructed from Hastelloy C-276. The 1 in. Hastelloy C-276 tubular body of the desalinator is used as the outer electrode with an inner diameter of 0.76 in., resulting in a 0.255 in. gap between the electrodes. The inner electrode has 24 inched of exposed surface along the length of the desalinator, however, the inner electrode is not entirely immersed in the highly concentrated brine during steady-state operation. The potential for electrochemical reactions in the desalinator was analyzed through experimental recording of the current as the electrode voltage was slowly ramped, the effective power from electrochemical reactions was estimated and used in the final results calculations.

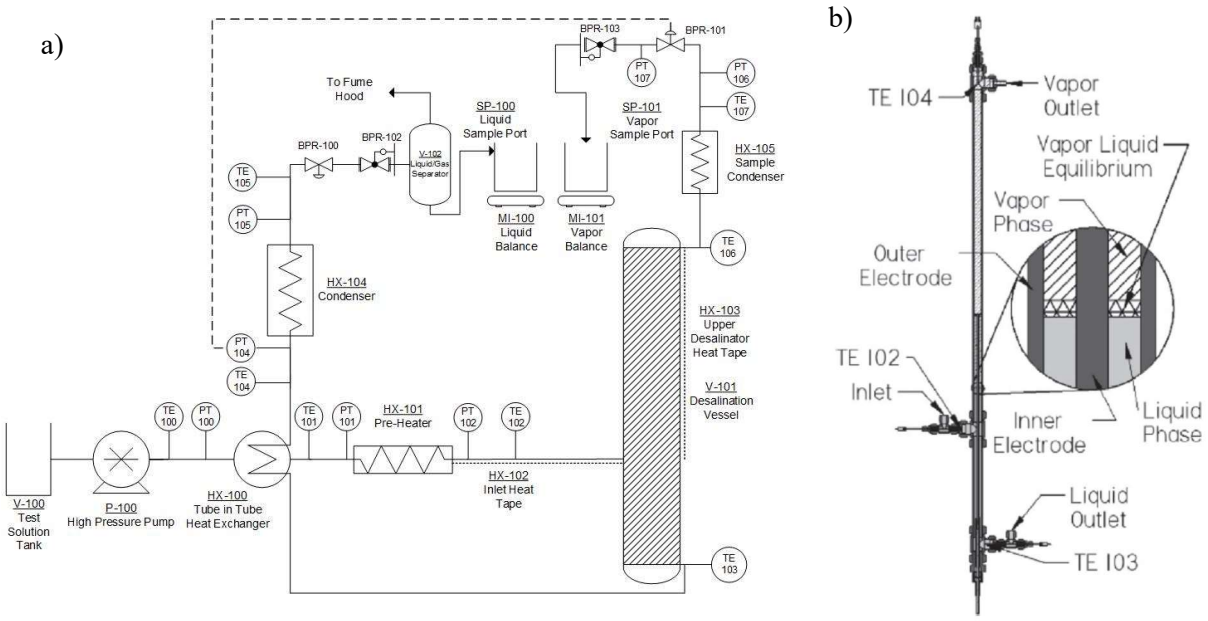


Figure 1. (a) Process and instrumentation diagram for the Joule-heated desalination system. (b) Cross section view of the Joule-heated desalinator. A close-up view of the vapor liquid equilibrium is shown.

The system is controlled by a National Instruments CRio controller running embedded LabVIEW software. Temperature is measured and recorded at essential points in the process using Type K thermocouples which directly contact the process fluid. Temperature measurements for thermodynamic analysis are located at the inlet to the desalinator (TE 102), as well as the vapor outlet (TE 104) and the liquid outlet (TE 103). System pressure is monitored at the inlet and outlets of the desalinator. See Figure 1 for all essential pressure and temperature measurement locations. Data was logged at an interval of 5 s for the duration of the experimental trials. Desalinator voltage was controlled using a variable transformer with a step down voltage transformer, both rated at 10 kVA. The transformer combination allows for operation up to 833 A at 12 VAC or 416 A at 24 VAC. All trials were conducted at a frequency of 60 Hz, allowing for direct usage of utility power without the need for frequency modification. The voltage and

DocuSign Envelope ID: 2FA9A609-C360-4E53-8B28-BE8B77B6994A

amperage waveforms were measured in real time, allowing for calculation of the true power, phase angle, and desalinator resistance.

To achieve steady-state operation, it was necessary to control the pressure and flowrate of both the vapor and liquid effluents from the system. The liquid effluent was used to control the system pressure on a feedback control loop using a pressure transducer mounted downstream of the desalinator (PT-105). Liquid level in the desalinator was determined by measuring the resistance of the desalinator. Once a steady state concentration was achieved in the desalinator, the resistance could be used to control the desalinator level via a process control valve (BPR-101). This setup allowed for a dynamic control of the desalinator liquid level. If power is increased, the vapor fraction in the desalinator is increased, dropping the desalinator liquid level and in turn lowering the liquid effluent flowrate. The liquid and condensed vapor product flow rates were measured using Mettler Toledo ICS435 and Mettler Toledo PG6002-S balances.

CPOES determined TDS content of the vapor effluent for the major cation and anion constituents. Water recovery rates were tested in the range of 20 to 80% for previously tested brines containing 50,000 – 180,000 mg·L^{-1} [3], [4]. Experimental testing of the UND brine was performed at water recoveries ranging from 30 to 50 %. The water recovery percentage was limited to avoid supersaturation within the desalinator, preventing salt precipitation within the vessel. Water recovery was calculated using Eq. (1):

$$\text{Water Recovery (\%)} = \frac{\dot{m}_v}{\dot{m}_i} \tag{1}$$

where $\dot{m}_i$ (g·min^{-1}) is the inlet mass flowrate and $\dot{m}_v$ (g·min^{-1}) is the vapor stream mass flowrate.

2.2 Process Simulation

The SCWD process was simulated with Aspen Plus v.10 software using the electrolyte non-random two liquid (ELECNRTL) model to estimate fluid thermodynamic properties. The Aspen simulation (Figure 2**Figure** 2.) was used to estimate material and energy balances for the process, except for the desalinator. The ELECNRTL model has significant error when used to simulate brines past water's critical point; thus, it was necessary to supplement this portion of the simulation with operational data made available by this project and a previous study [4]. Desalinator power requirements were simulated based upon prior experimental results using FORTRAN code in a user-defined operation block. The specific water recovery was a user-defined input which defined the ratio of vapor to liquid mass flow rate driven by desalinator power consumption. In addition, simulation stream temperatures exiting the desalinator (estimated by ELECNRTL) were corrected based on experimental data [3], [4].

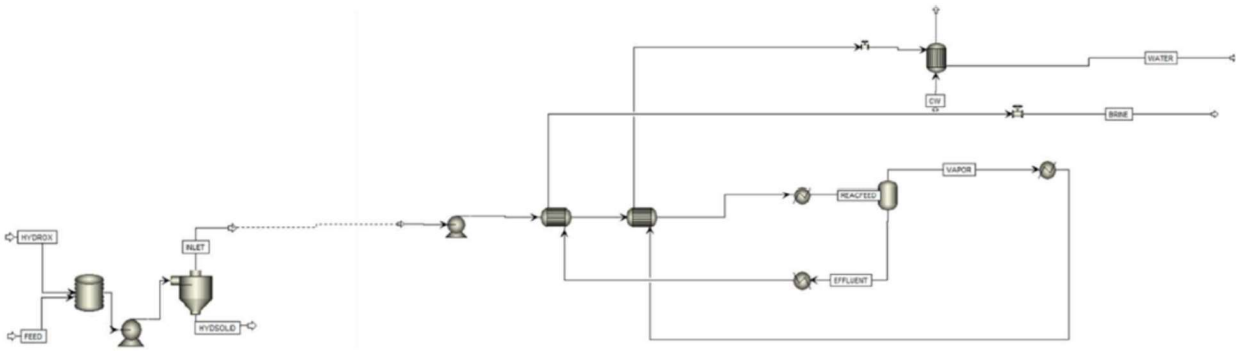


Figure 2. Aspen Plus Simulation for SCWD Brine Concentration Process.

DocuSign Envelope ID: 2FA9A609-C360-4E53-8B28-BE8B77B6994A

The inlet brine salinities of 90,000 and 180,000 mg·L^{-1} were selected for treatment based upon analyses of brines tested at the BEST Site and provided by the University of North Dakota. Details of the brine composition are provided in Table 1. The preheater and flash vessel blocks are used in tandem to estimate energy requirements for the desalinator electrode; the flash vessel is used to estimate recovery ratios, while the aforementioned FORTRAN code is used to account for brine heat of vaporization. The liquid effluent is charged to an additional heat exchanger to recover thermal energy in the brine concentration case.

Table 1. Evaluated Brine Compositions at UND BEST Facility.

Major Constituents	**90 g·L^{-1} UND Brine**	**180 g·L^{-1} UND Brine**
	(mg·L^{-1})	(mg·L^{-1})
Na^{+}	23,500 ± 82	47,700 ± 300
Ca^{2+}	5,540 ± 36	11,750 ± 50
Mg^{2+}	342 ± 3	722 ± 1
Sr^{2+}	458 ± 4	985 ± 2
K^{+}	2,157 ± 26	4,520 ± 40
Mn^{2+}	< 0.5	6.7
B^{3+}	382 ± 57	485 ± 16
Ba^{2+}	4.3 ± 0.1	9.7 ± 0.1
Li^{+}	21.1 ± 0.5	49.9 ± 0.7
Cl^{-}	48,300 ± 82	104,500 ± 500
Br^{-}	247 ± 2	537 ± 2
SO_4^{2-}	299 ± 2	319 ± 5
TDS	82,100 ± 432	173,000 ± 0

DocuSign Envelope ID: 2FA9A609-C360-4E53-8B28-BE8B77B6994A

3 Field Testing Results

3.1 Water Recovery and Energetics

Field demonstration trials conducted at the EERC BEST facility sought out to investigate the capabilities of the Joule-heating SCWD system to produce clean water from 90 and 180 g·L^{-1} TDS multicomponent brines produced from oil and gas wells in the Williston basin. Figure 3 shows approximately 30 minutes of representative operating data from a single experimental trial of 180 g·L^{-1} UND brine processed at 23 MPa and 100 mL·min^{-1}. The steady state operation of the prototype system is indicated by the stable operation of the vapor and liquid product flowrates (Figure 3a), the steady average desalinator power (Figure 3b), and the inlet and product temperatures (Figure 3b). The average desalinator reactor power (Figure 3b) was approximately 998.9 ± 25.7 W throughout the duration of the trial. The vapor product concentration TDS (Figure 3c) averages to 2,225 mg·L^{-1} over the period of the run. As the operation continued, the vapor TDS decreases to a steady state concentration as the system purges the brine in the vapor product system that was present prior to the fluid transitioning into the pseudocritical state. The steady state parameters of the 90 and 180 g·L^{-1} UND trials at an inlet flowrate of 100 mL·min^{-1} are provided in Table 2.

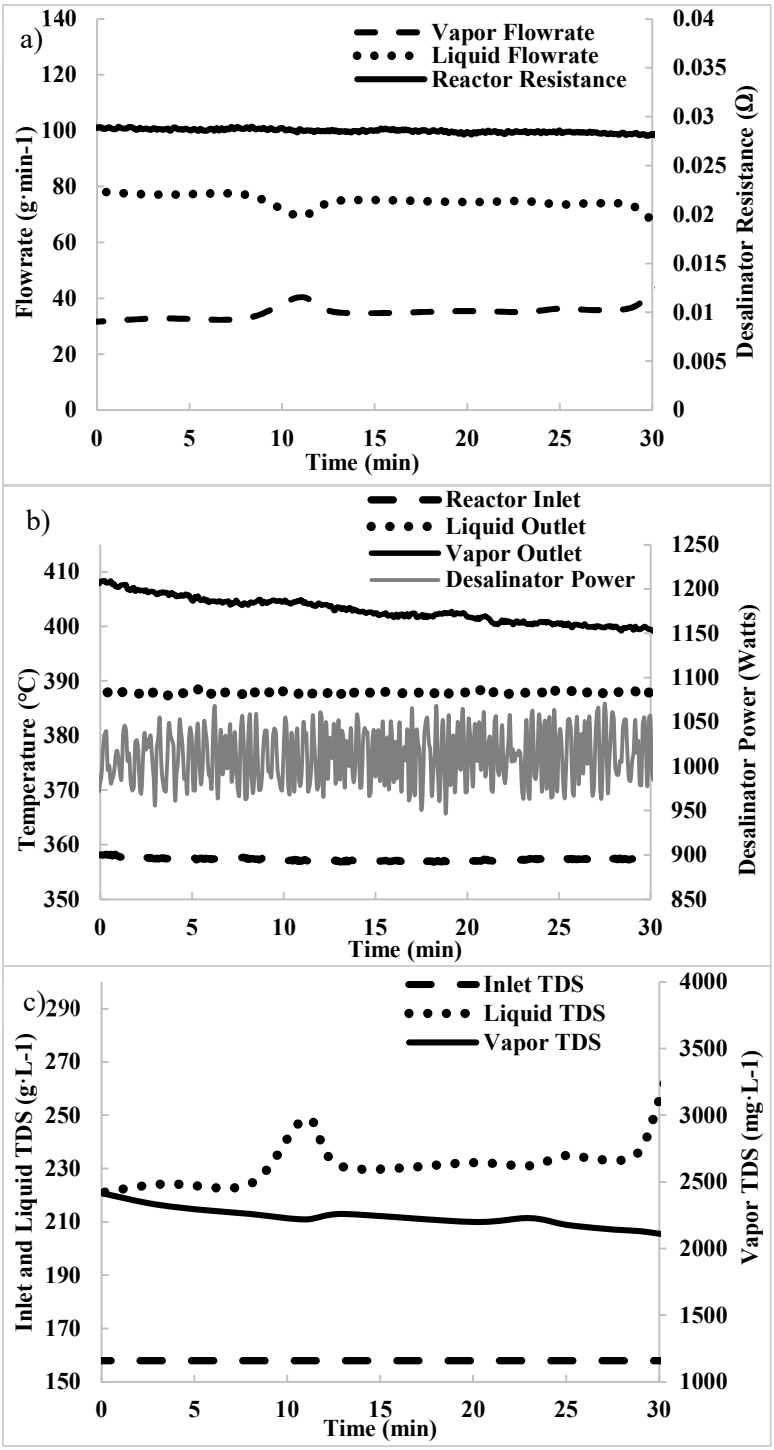


Figure 3: Representative operating data of a 180 g·L^{-1} trial. a) desalinator reactor resistance and product flowrates, b) reactor inlet and outlet temperatures and desalinator power, c) inlet and outlet concentrations.

DocuSign Envelope ID: 2FA9A609-C360-4E53-8B28-BE8B77B6994A

Table 2: The operating parameters of the 100 mL·min^{-1} experimental trials for the 90 and 180 g·L^{-1} UND brines.

90 g·L^{-1} UND		
	Operating Pressure (bar)	
	189.95 ± 0.16	
Pseudocritical (°C)	361.6	
Inlet (°C)	323.68 ± 1.34	
Vapor Outlet (°C)	375.18 ± 0.83	
Liquid Outlet (°C)	367.37 ± 0.85	
T_{VLE} (°C)	369.40	
$\dot{m}_{inlet}$ (g·min^{-1})	104.27	
Inlet TDS (ppm)	82,100 ± 432	
Vapor TDS (ppm)	1,213 ± 152	
180 g·L^{-1} UND		
	Operating Pressure (bar)	
	190.03 ± 0.26	230.02 ± 0.78
Pseudocritical (°C)	361.6	377.5
Inlet (°C)	336.1 ± 4.00	356.34 ± 2.88
Vapor Outlet (°C)	378.44 ± 4.71	401.43 ± 7.86
Liquid Outlet (°C)	374.65 ± 1.13	387.40 ±1.73
T_{VLE} (°C)	360.72	387.33
$\dot{m}_{inlet}$ (g·min^{-1})	109.99	109.99
Inlet TDS (ppm)	173,000 ± 0	158,000
Vapor TDS (ppm)	1,473 ± 132	2,225 ± 108

The Joule-heating in the desalinator reactor converts the electrical power directly into thermal energy in the liquid brine. Figure 4 shows how the water recovery from the vapor product is dependent on the power supplied to the desalinator electrode. The UND brine trials indicated by the grey markers are shown overlain with previous SCWD experimental results from simulated and UPP field derived brines [3], [4]. The water recovery analysis can be viewed in two regions. The simulated 50 and 180 g·L^{-1} multicomponent brines indicated by the black markers show a sharper increase in water recovery per desalinator power compared to the experimental trials of the field derived 180 g·L^{-1} UPP brine and the field derived 90 and 180 g·L^{-1} UND brines.

DocuSign Envelope ID: 2FA9A609-C360-4E53-8B28-BE8B77B6994A

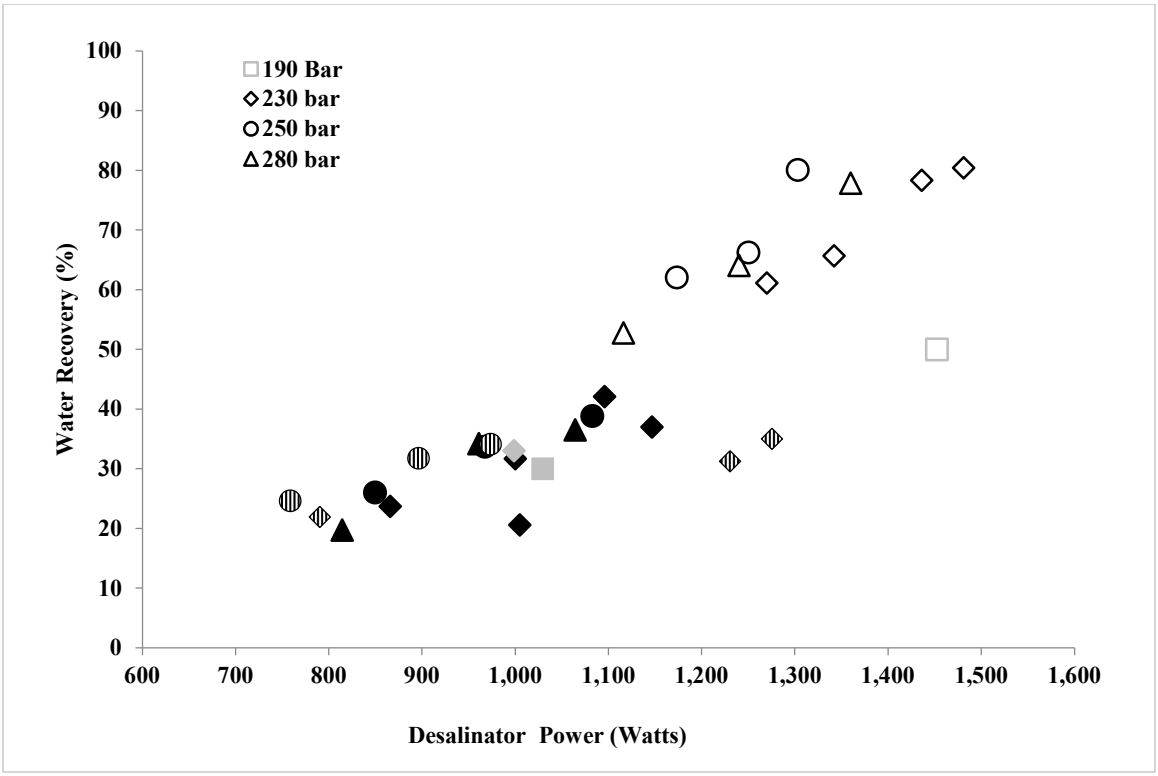


Figure 4: Water recovery per desalinator reactor power. All trials were conducted at an inlet flowrate of 100 mL·min^{-1}. Hollow gray markers represent the 90 g·L^{-1} UND brine data. Solid gray markers represent the 180 g·L^{-1} UND brine data. Hollow black markers represent the 50 g·L^{-1} simualted brine data. Solid black markers represent the 180 g·L^{-1} simulated brine data. Striped black markers represent the 180 g·L^{-1} UPP brine data [3], [4].

To further model and understand the energetics of the brine desalination via Joule-heating, the energy required to produce clean water must be understood. The energy needed to produce a low concentration vapor from the brine in the reactor is represented by Δh_{vap} [4]. The enthalpy of vaporization is calculated using an energy balance around the top and bottom of the desalinator reactor [4]. Figure 5 presents the enthalpy of vaporization values derived from the UND experimental trials overlain with values derived from previous SCWD trials [3], [4]. Enthalpy of vaporization values are reported on a kJ·kg^{-1} of vapor product basis. The energy required to generate low-concentration vapor from the 90 g·L^{-1} UND brine was determined to be 1,272 ± 98 kJ·kg^{-1} at 190 bar, and the energy for the 180 g·L^{-1} UND brine was found to be 1,112 ± 181 kJ·kg^{-1} and 1,137 kJ·kg^{-1} at 190 and 230 bar respectively. Similar to the trend distinguished in Figure 4 above, Figure 5 shows that the field derived brines, UPP and UND, appear to have significantly higher energy requirements compared to the simulated brine tests.

DocuSign Envelope ID: 2FA9A609-C360-4E53-8B28-BE8B77B6994A

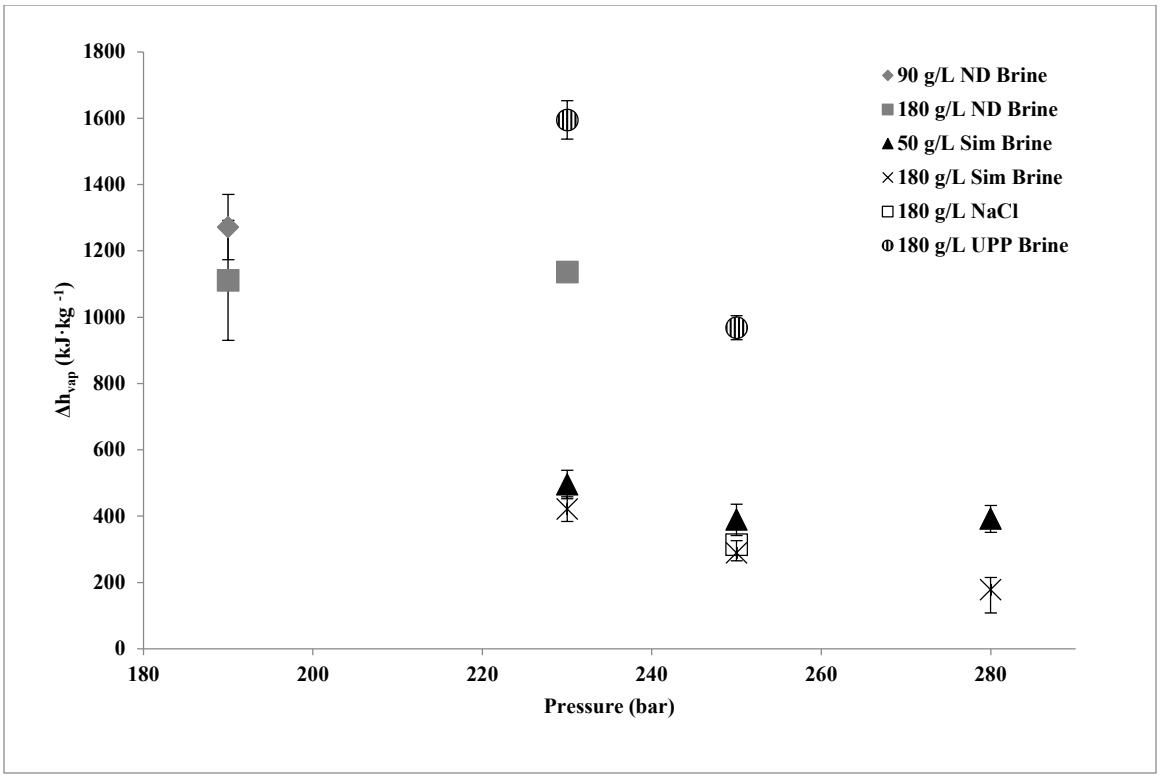


Figure 5: The enthalpy of vaporization of experimentally tested brines based on operating pressure [3], [4].

3.2 Water Product Quality

The water recovered from the vapor product produced during operation was analyzed. When treated at 190 bar the vapor product had TDS concentrations of 1,213 ± 152 and 1,473 ± 132 mg·L^{-1} for the 90 and 180 g·L^{-1} UND brines respectively. Ogden et al. found that vapor product concentration increased as operating pressure increased due to increase in supercritical water vapor density [3], [4].

Table 3 shows the vapor product concentrations for the 90 and 180 g·L^{-1} UND brine trials at 190 bar [7]. The vapor product concentrations for the previously completed simulated and UPP brine trials are provided in Table 4 for comparison [3], [4].

DocuSign Envelope ID: 2FA9A609-C360-4E53-8B28-BE8B77B6994A

Table 3: The vapor product concentrations of the experimental UND brine trials [7].

Solution	90 g·L^{-1} UND	180 g·L^{-1} UND
Pressure (bar)	190	190
Constituents	(mg·L^{-1})	(mg·L^{-1})
Na^{+}	58.2 ± 7.8	76.5 ± 3.7
Ca^{2+}	16.3 ± 10.8	9.5 ± 1.2
Mg^{2+}	2.1 ± 0.9	1.9 ± 1.0
Sr^{2+}	0.9 ± 0.4	0.8 ± 0.1
K^{+}	3.8 ± 0.6	5.4 ± 0.3
Mn^{2+}	0.1	0.1
B^{3+}	57.7 ± 7.8	104.0 ± 12.7
Ba^{2+}	< 0.05	< 0.05
Li^{+}	< 0.2	< 0.2
Cl^{-}	366 ± 119	778 ± 95
Br^{-}	1.1 ± 0.1	1.4 ± 03
SO_4^{2-}	< 1	< 1
TDS	1,213 ± 152	1,473 ± 132

DocuSign Envelope ID: 2FA9A609-C360-4E53-8B28-BE8B77B6994A

Table 4: The vapor concentration results for the experimental simulated and UPP brine trials [3], [4].

Solution	50 and 180 g·L^{-1} Simulated	50 and 180 g·L^{-1} Simulated	50 and 180 g·L^{-1} Simulated	180 g·L^{-1} UPP	180 g·L^{-1} UPP
Pressure (bar)	230	250	280	230	250
Constituents	(mg·L^{-1})	(mg·L^{-1})	(mg·L^{-1})	(mg·L^{-1})	(mg·L^{-1})
Na^{+}	232.08 ± 29.82	440.37 ± 66.78	1,038.59 ± 77.76	183.49 ± 12.43	375.60 ± 34.59
Ca^{2+}	15.03 ± 18.81	13.60 ± 11.53	24.46 ± 8.19	37.78 ± 6.63	58.88 ± 15.60
K^{+}	7.71 ± 11.26	4.97 ± 0.75	10.09 ± 2.49	1.56 ± 0.21	3.56 ± 0.47
Ba^{2+}	0.30 ± 0.57	0.11 ± 0.23	1.73 ± 2.37	–	–
Mg^{2+}	–	–	–	7.74 ± 2.02	10.94 ± 4.10
Sr^{2+}	0.49 ± 0.55	0.62 ± 0.39	0.81 ± 0.34	2.21 ± 0.46	3.60 ± 0.10
Cl^{-}	–	–	–	525.66 ± 19.16	876.36 ± 46.59
TDS	655.1 ± 158.5	1,240.0 ± 237.7	2836.1 ± 97.5	622.3 ± 163.7	1,167.7 ± 249.3

3.3 Lessons Learned

Machine Operation:

Since OHIO's SCWD system uses an in-house built system, a combination of National Instruments hardware and LabVIEW allows for the successful operation of OHIO's SCWD machine following easy preset steps listed in the operation manual. Certain aspects of the machine's operation require knowledge of the water chemistry being treated. This creates a challenge when working with new water formulations. The team that demonstrated at the EERC BEST site did not face any issues operating the equipment as they were experienced in the operations of the SCWD system.

Supply-Chain Challenges:

Due to supply-chain challenges during the SARS COVID-19 pandemic and the short duration of the project, the team was faced with issues of acquiring required materials in a timely manner. The SCWD system uses C-276 Hastelloy tubing and fittings to be able to cope with the corrosive water and the high heat and pressure used in the system. One fitting could not be replaced with a Hastelloy equivalent. In substitute, a 316 stainless steel fitting was used. The material resulted in a reduced life for the fitting and the need to replace it on a more frequent basis. As shown in Figure 6, the stainless-steel fitting did fail during operation at the EERC BEST site.

DocuSign Envelope ID: 2FA9A609-C360-4E53-8B28-BE8B77B6994A



Figure 6: The stainless-steel fitting failed from corrosion during the field demonstration testing.

Equipment Shipping:

Shipping this equipment was streamlined because the OHIO's SCWD unit was already installed on a steel pallet. The main issue was to ensure that auxiliary tubing and parts located outside the periphery of the pallet could be removed and re-installed at the EERC BEST site. In addition, the remaining process tubing and fittings needed to be structurally supported to not come loose during the shipping process. Some tubing and fittings had to be replaced at the EERC BEST site because they were damaged from vibrations during the shipping process.

Field Operations:

Field installation of the OHIO SCWD system is rudimentary since the machine only requires a cooling water source, a 120V single phase power source, and a 208V single phase power source. The OHIO SCWD unit was equipped with fittings to accept a garden hose for the cooling water and sufficient length of electric cable to reach the electric supply at the EERC BEST site. The challenge at the BEST site was to find a suitable power source, since the only readily available power source was a 480V 3 phase connection. Power was pulled from the mechanical room instead of the monitored feed for operation of the machine, and power consumption was monitored using the machine's integrated National Instrument's system.

In addition, the chemistry of the water to be treated was not fully known. Increases in the vapor product PH caused some precipitate from the solution to clog the inlet and outlet filters. During the field demonstration, adjustments were made to the water PH by the addition of hydrochloric acid to the inlet brine. Had the water chemistry been fully known prior to experimental trials, arrangements would have been made to mitigate the presence of precipitate prior to operations.

DocuSign Envelope ID: 2FA9A609-C360-4E53-8B28-BE8B77B6994A

4 Commercial-Scale Process Energetic Simulations

The energetics for a commercial-scale Joule-heated brine treatment process capable of treating 100 gal·min^{-1} of brine was estimated using a previously reported Aspen Plus process simulation [3]. An operational case where the waste was concentrated to generate ten-pound brine and clean water products was evaluated. Brine TDS concentration scenarios of 90 and 180 g·L^{-1} were considered. Three operating pressures were evaluated (190, 250, and 280 bar) utilizing desalinator data determined as part of this (Figure 5) and previous studies [3], [4].

Process power usage is associated with three key units including the pump, preheater, and desalinator. The pump pressurizes the brine fluid, the pre-heater provides sensible heat to increase fluid temperature to near its saturation temperature, and desalinator power is primarily associated with generating clean water product (i.e. vapor generation). Desalinator heating efficiency was evaluated from 56 – 90%, based upon inefficiencies determined in previous studies. Electrical power is supplied to the pump and desalinator, while electrical or thermal power could be utilized at the pre-heater.

Table 5 presents process power requirements for the analyzed scenarios. The pump requirement was minimal, accounting for less than 2% of total power requirements in all cases. The pre-heater required 48% or greater of the total power requirements across all cases. Increasing brine TDS content results in marginally higher overall power requirements. Although desalinator power required to treat brine at its saturation temperature reduced with salinity, sensible heat increased by a greater proportion (36%), resulting in an overall greater process power requirement (9-32%). As expected, the 90 g·L^{-1} brine generated a greater volume of clean water (67.5 vs. 49.7 gpm) and less ten-pound brine (32.5 vs. 50.3 gpm) than the 180 g·L^{-1} brine. Increasing system pressure increased pre-heater sensible heat addition, caused by the associated increase in saturation temperature, while desalinator power was nearly constant. Process energetics for generating ten-pound brine from wastewater containing 90 to 180 g·L^{-1} are 50.6 – 90.9 kWh$_e$/bbl.

Table 5. Summary of Process Energetics Associated with Joule-Heated Supercritical Process for Treating 100 gal/min brine.

Concentration (g·L^{-1})	Pressure (bar)	Pump (kW)	Pre-heater (kW)	Desalinator (kW)	Total (kW)	Clean Water (gpm)	10 lb Brine (gpm)
90	190	136	4,303	2,797 - 4,397	7,236 - 8,836	67.5	32.5
180	190	136	6,732	1,694 - 2,723	8,564 - 9,593	49.7	50.3
180	250	182	6,692	2,118 - 3,404	8,992 - 10,278	49.7	50.3
180	280	205	9,240	2,206 - 3,546	11,650 - 12,990	49.7	50.3

DocuSign Envelope ID: 2FA9A609-C360-4E53-8B28-BE8B77B6994A

5 Summary

The results reported above demonstrate the OHIO's Joule-heated SCWD system's capability to treat the 90 and 180 $g \cdot L^{-1}$ hypersaline brines derived from the Williston basin during the field demonstration trials at the EERC BEST site. The system achieved steady operation across water recoveries ranging from 30 – 50%, and the clean water produced at 190 bar had an average TDS of 1,343 ± 211 $mg \cdot L^{-1}$. Water recovery and enthalpy of vaporization of the UND brines were found and compared to previous experimental trials of the simulated and field derived UPP brines. Comparisons to previous brine trials showed differing relationships between the field derived brines (UND and UPP) and the simulated brines when looking at water recovery versus desalinator power and enthalpy of vaporization versus operating pressure.

Using the data from the UND brine experimental trials, the Aspen Plus simulation was used to model the energetics of a commercial scale process operating at 100 $gal \cdot min^{-1}$. Energy consumption for the pump, the preheater, and the Joule-heating desalinator were predicted for simulated conditions of the treatment of the 90 and 180 $g \cdot L^{-1}$ brines at different pressures. Process energetics for generating ten-pound brine from the waste brines was estimated to be 50.6 – 90.9 kWh_e/bbl.

6 Acknowledgments

The authors would like to thank Mr. Marc Kurz, Mr. Bradley Stevens, and the EERC staff members for their assistance with planning and organizing the field demonstration at the EERC BEST site. The authors would like to thank Mr. Sean Smith for his assistance with experimental work and system preparation for the field demonstration.

DocuSign Envelope ID: 2FA9A609-C360-4E53-8B28-BE8B77B6994A

7 References

[1] J. Veil, "U.S. Produced Water Volumes and Management Practices in 2017," Feb. 2020.
[2] M. S. Blondes *et al.*, "U.S. Geological Survey National Produced Waters Geochemical Database v2.3 (PROVISIONAL)," p. 41.
[3] C. M. Able, D. D. Ogden, and J. P. Trembly, "Sustainable management of hypersaline brine waste: Zero liquid discharge via Joule-heating at supercritical condition," *Desalination*, vol. 444, pp. 84–93, Oct. 2018, doi: 10.1016/j.desal.2018.07.014.
[4] D. D. Ogden and J. P. Trembly, "Desalination of hypersaline brines via Joule-heating: Experimental investigations and comparison of results to existing models," *Desalination*, vol. 424, pp. 149–158, Dec. 2017, doi: 10.1016/j.desal.2017.10.006.
[5] S. van Wyk, S. O. Odu, A. G. J. van der Ham, and S. R. A. Kersten, "Design and results of a first generation pilot plant for supercritical water desalination (SCWD)," *Desalination*, vol. 439, pp. 80–92, Aug. 2018, doi: 10.1016/j.desal.2018.03.028.
[6] R. Kaplan, D. Mamrosh, H. H. Salih, and S. A. Dastgheib, "Assessment of desalination technologies for treatment of a highly saline brine from a potential CO2 storage site," *Desalination*, vol. 404, pp. 87–101, Feb. 2017, doi: 10.1016/j.desal.2016.11.018.
[7] M. Kurz, "BEST-Ohio Demonstration at BEST Site (11/9/21 - 11/11/21)," Energy & Environment Research Center, EERC Analytical Research Lab 54980, Dec. 2021.

DocuSign Envelope ID: 2FA9A609-C360-4E53-8B28-BE8B77B6994A

APPENDIX I

UNIVERSITY OF KENTUCKY
FINAL REPORT – 2023

DocuSign Envelope ID: 2FA9A609-C360-4E53-8B28-BE8B77B6994A

Demonstration of Zeolite Dewatering System for EERC Produced/Blended Water Treatment

Final Technical Summary Report

Performance Period
7/1/2021 – 12/31/2023

Principal Authors:
Feng Zhu and Ayokunle Omosebi

University of Kentucky, Lexington, KY

Report Issued
10/20/23

SUBMITTED BY
University of Kentucky Research Foundation
109 Kinkead Hall, Lexington, KY 40506-0057

Ayokunle Omosebi, PI, ayokunle.omosebi@uky.edu

Xin Gao, Co-I, xin.gao@uky.edu

Kunlei Liu, Co-I, kunlei.liu@uky.edu

SUBMITTED TO
Energy and Environmental Research Center

Marc Kurz, Project Manager, mkurz@undeerc.org

DocuSign Envelope ID: 2FA9A609-C360-4E53-8B28-BE8B77B6994A

ACKNOWLEDGEMENT: The University of Kentucky (UKy) is grateful to the Energy & Environmental Research Center (EERC) for the support of this project. The project team is also grateful to the UKy research personnel for their assistance, notably Steve Suumers, John Adams, Emmanuel Ohiomoba, Prakhar Sharma, Neng Huang, and Jesse Okorafor, for various contributions to the project.

DocuSign Envelope ID: 2FA9A609-C360-4E53-8B28-BE8B77B6994A

ABSTRACT

This report summarizes the work done to develop and demonstrate a zeolite dewatering system for treating EERC-produced/blended water (150,000 - 180,000 ppm TDS) at up to 0.1 gal/min scale. The UKy technology uses zeolite membranes for water extraction at transmembrane pressures below 100 psig. In addition to size exclusion, the zeolite membrane employs preferential dissolution of water to shuttle water across the membrane under mild temperatures (<120 °C) and pressures (<100 psig). The project's objectives included the construction of the bench-scale membrane dewatering unit, evaluating and operating the unit using synthetic and EERC-produced water, and shipment and testing of the membrane unit at the EERC site in Watford City, ND. The project results verified UKy's approach to treating hypersaline streams using zeolite dewatering technology, including removing organic and inorganic solids in a single unit operation at modest operating temperatures and pressures.

DocuSign Envelope ID: 2FA9A609-C360-4E53-8B28-BE8B77B6994A

Table of Contents

1 PROJECT SUMMARY 5
1.1 Overview 5
1.2 Key Results 5
2 BACKGROUND AND TECHNOLOGY DESCRIPTION 6
2.1 Project Background and Objectives 6
2.2 Overview of Technology 7
2.3 Process Description 8
2.3.1. Laboratory zeolite membrane dewatering operations 8
2.3.2. Construction of membrane module 9
2.3.3. Bench-scale zeolite membrane dewatering operation 10
2.3.4. Field skid for zeolite membrane dewatering operation 13
3 PROJECT TECHNICAL RESULTS 14
3.1 Lab-scale Membrane Performance Evaluation 14
3.1.1 UKy Zeolite Membrane 14
3.1.2 HZM Membrane from Hitachi Zosen 16
3.2 Bench-scale Membrane Performance Evaluation 17
3.3 Field Test of Zeolite Dewatering System 19
4 FUTURE WORK/OTHER AREA OF INTEREST 22
5 CONCLUSION AND LESSONS LEARNED 23
6 LIST OF EXHIBITS 25
7 REFERENCES 26
8 LIST OF ACRONYMS AND ABBREVIATIONS 27

DocuSign Envelope ID: 2FA9A609-C360-4E53-8B28-BE8B77B6994A

1 PROJECT SUMMARY

1.1 Overview

This report details the demonstration of a zeolite dewatering system developed by UKy for treating high-salinity EERC-produced/blended water. The system utilizes ceramic zeolite membranes supported on porous alumina and enclosed in a housing for water extraction under mild temperatures and pressures. The core of this technology is the zeolite membrane, designed to separate water from high concentration and hypersaline feed streams, where high osmotic pressure and material and mechanical stability requirements for polymeric membranes are typically prohibitive. The performance of the dewatering system was evaluated at both lab and bench scales, using both UKy-developed and Hitachi Zosen zeolite membranes. The results showed promising rejection rates and flux values, although challenges such as o-ring seal failures and membrane fragility were encountered. In field tests at the EERC facility in North Dakota, the system demonstrated effective water treatment capabilities. However, there were lessons learned, including overheating compromising the integrity of the tested membranes. The project's results verified that zeolite membranes present a promising solution for high-salinity water treatment and removing organic content from the feed water.

1.2 Key Results

The major accomplishments of this project are highlighted below:

- *Scaled up the zeolite dewatering process by >20X from a 0.014 m^2 membrane unit to a 0.3 m^2 bench-scale test unit to treat EERC water.*
- *Achieved ~2X up-concentration, ~40% water recovery, and >95% inorganic salt and organic content rejection of EERC water during lab-scale zeolite dewatering tests at ~108℃ and 50 psig, including flux stability at the test conditions.*
- *Demonstrated stabilized >90% salt rejection during the initial field-testing phase prior to complications from overheating compromising the integrity of repaired membranes. Post-testing analysis data shows rejection of organic and inorganic content.*
- *Learned lessons in zeolite scale-up and development.*

DocuSign Envelope ID: 2FA9A609-C360-4E53-8B28-BE8B77B6994A

2 BACKGROUND AND TECHNOLOGY DESCRIPTION

2.1 Project Background and Objectives

In recent years, water security has remained a key concern as freshwater resources are consumed without/with limited replacement for energy security. Water is an important ingredient in oil and gas extraction in North Dakota, leading to the need for field-test technologies for treating high Total Dissolved Solids (TDS) oil-field brines/extracted water [1]. Oil-field brines, characterized by their high salinity and TDS (180,000 mg/L on average), represent a challenging opportunity whereby treating these brines can yield an alternative water source for industrial applications, thereby reducing the need for freshwater resources and/or significantly reducing brine disposal volumes at sufficient water recoveries [2, 3]. Furthermore, the potential recovery of economically valuable materials from these brines offers an added incentive for their treatment.

Reverse Osmosis (RO) membrane is an established technology with a proven track record in various desalination applications. The RO process forces water under pressure through a semi-permeable membrane, allowing water molecules to pass through while rejecting most dissolved salts and impurities. However, while RO membranes offer a robust solution for water desalination, they come with their own set of challenges. Firstly, the process requires significant energy input, primarily because of the high pressure to push water through the membrane, especially when treating large volumes of high TDS water [4]. Secondly, RO membranes are susceptible to fouling. Over time, impurities, especially organic compounds, can accumulate on the membrane surface, reducing its efficiency and increasing the frequency of maintenance and replacement [5]. This fouling not only affects the performance of the RO system but also escalates operational costs. Furthermore, the efficiency of RO membranes in rejecting certain ions and compounds can vary. While they are generally effective in removing common salts, usually at TDS below 35,000 mg/L, some low molecular weight organics might pass through, necessitating additional treatment steps or post-treatment polishing. This variability in rejection rates means that while RO is a powerful tool in the water treatment arsenal, it might not always be the most efficient or cost-effective solution for every TDS water source. Chemical and thermal processes are also options for water treatment but come with their requirements on energy consumption when waste heat is unavailable and chemical waste disposal.

Zeolite membranes have emerged as a promising solution for water treatment, particularly in applications requiring the desalination of high-salinity brines. One of the significant advantages of zeolite membranes is their higher selectivity for specific ions due to their tunable size. According to the size discrepancies of water (2.76 Å) and hydrated ions (6.62-8.24 Å) [6], the small-sized windows of their lattice can achieve a molecular sieving effect of allowing water molecules to pass through the membrane pores while impeding hydrated salt ions, reaching high ion rejection degrees. Another standout feature of zeolite membranes is their unique molecular structure, which inherently resists the adhesion of organic compounds [7]. This resistance ensures consistent water flow rates and reduces the frequency and intensity of maintenance operations, leading to longer membrane lifetimes and reduced operational costs. In this application, the water flux of the zeolite membrane dewatering process is facilitated by preferential water solubility in the zeolite membranes. Because of the excellent hydrophilicity of the zeolite membrane applied in the dewatering process, water molecules are preferentially absorbed in the membrane pores, which facilitates selective water transport [8, 9]. Additionally, zeolite membranes are energy efficient as

DocuSign Envelope ID: 2FA9A609-C360-4E53-8B28-BE8B77B6994A

they operate at low pressures. Their natural porosity and selective ion transport mechanisms allow for efficient water flow without high energy inputs, making them a viable option for water treatment. A review of zeolite membranes, their properties and applications can be found in Ref [10].

A recent study indicated that Faujasite (FAU) zeolite membranes can overcome the water flux and ion selectivity tradeoff by enhancing water molecule sorption and diffusion through their relatively large pore size (0.74 nm) and relative hydrophobicity [11]. Previously, UKy developed FAU zeolite membrane modules with the desired packing densities and stable flux to dewater carbon-rich amine solvents on a 0.1 MWth bench unit and has also employed FAU zeolite membranes to pursue near zero liquid discharge in FGD water treatment and achieved >50% water recovery and >99% salt rejection [12]. In this project, UKy developed and demonstrated a zeolite dewatering system for treating EERC-produced/blended water (~170,000 ppm TDS) at up to 0.1 gal/min scale. The UKy technology uses zeolite membranes for water extraction at transmembrane pressures below 200 psig. In addition to size exclusion, the zeolite membrane employs preferential dissolution of water within the matrix to shuttle water across the membrane under mild temperatures (<120 °C) and pressures (<100 psig). The project objectives are shown in **Exhibit 2.1**.

Exhibit 2.1. Project Objectives.

Objectives

- Construction of a bench-scale zeolite membrane dewatering unit.
- Evaluation and operation of membrane dewatering unit at bench-scale with synthetic and EERC-supplied water.
- Shipment and demonstration of the membrane module at the EERC site.

2.2 Overview of Technology

UKy developed FAU-type zeolite membranes supported on alumina to treat high-salinity EERC water. In detail, the zeolite membranes were sealed and mounted in a stainless-steel cell with an effective membrane area from 0.014 m^2 (lab-scale) to 0.3 m^2 (bench-scale). The EERC-produced/blended water (~170,000 ppm TDS) was heated and continuously delivered to the membrane module at a steady flow rate. Dewatering was conducted at temperatures up to 120 °C, and the pressure of the feed side was adjusted with a back pressure regulator up to 100 psig. Because of the excellent hydrophilicity of the zeolite membrane, water molecules are preferentially absorbed in the membrane pore matrix compared to salt molecules, which results in selective water transport. In addition, the uniform pore size of the FAU zeolite membrane (0.74 nm) falls between the sizes of the water molecule (0.27 nm) and hydrated ions (0.66-0.82 nm). The water molecules can easily pass through the membrane pores, while salt ions are more hindered (**Exhibit 2.2**). Furthermore, Donnan exclusion can shrink their effective pore size. During dewatering testing, the feed and permeate flow rates and their concentration/conductivity are measured to determine membrane flux, salt rejection, water recovery, and concentration factor, where calibration curves can be used for conductivity-concentration conversions for simple synthetic solutions. Additionally, ex-situ sampling analysis, including ion chromatography (IC) and inductively coupled plasma (ICP), can provide speciation data. This project focused on the design and scale-up of zeolite membrane dewatering, including its application for treating EERC-produced/blended water.

DocuSign Envelope ID: 2FA9A609-C360-4E53-8B28-BE8B77B6994A

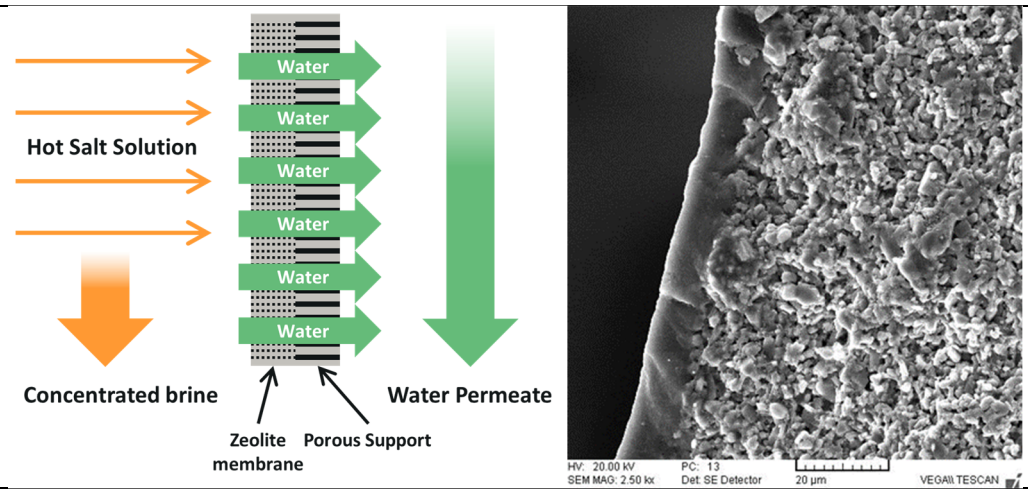


Exhibit 2.2. Schematic diagram for the zeolite dewatering process and scanning electron microscope (SEM) picture of the membrane cross-section morphology. In the SEM picture, zeolite (left, dense structure) is layered on alumina support (right, more porous structure).

2.3 Process Description

2.3.1. Laboratory zeolite membrane dewatering operations

The lab-scale membrane system comprises a solution reservoir, pump, heating element, single-cell membrane cell, and permeate sample collector (**Exhibit 2.3**). During system operation, the feed solution, e.g., synthetic water or EERC-produced/blended water with high salinity and TDS content, is fed into the system via the pump. The water is heated using a resistive thermal element and undergoes selective ion/solids removal in the membrane module, resulting in desalination as the treated water passes through, leaving the dissolved ions/solids in the feed compartment to exit as retentate. After cooling the permeate sample, it is periodically removed from the system and analyzed for rejection rate, flux, and water recovery. The retentate is cooled down and circulated back to the solution reservoir. The feed solution could be replaced with deionized water for cleaning and maintenance. A large reservoir volume relative to the permeate rate can facilitate single-pass conditions as water recovery is maintained at less than 10%, where higher water recoveries can be used to evaluate the effect of concentration factors, including concentration polarization. Dewatering was conducted at temperatures ranging from 80 °C to 120 °C, while the pressure of the feed side was adjusted with a back pressure regulator to 50-100 psig, such that the process water remained in the liquid phase in the membrane module during testing. For example, at a pressure of 40 psia, the boiling point is 131°C. Furthermore, colligative properties further elevate the boiling points. The membrane dewatering performances were assessed using the parameters of membrane flux (J, kg·m^{-2}·h^{-1}), rejection rate (R, %), and water recovery (WR, %) in the following Equations (1)-(3):

$$J = m_p/At \quad (1)$$

$$R = (C_f - C_p)/C_f \times 100\% \quad (2)$$

$$WR = V_p/V_f \quad (3)$$

Where m_p represents the weight of permeate solution through the membrane (kg), A is the effective membrane area (m^2), t refers to the operation time (h). C_f and C_p represent the

DocuSign Envelope ID: 2FA9A609-C360-4E53-8B28-BE8B77B6994A

conductivity of the feed and permeate solutions, respectively. V_f and V_p represent the volume of the feed and permeate solutions.

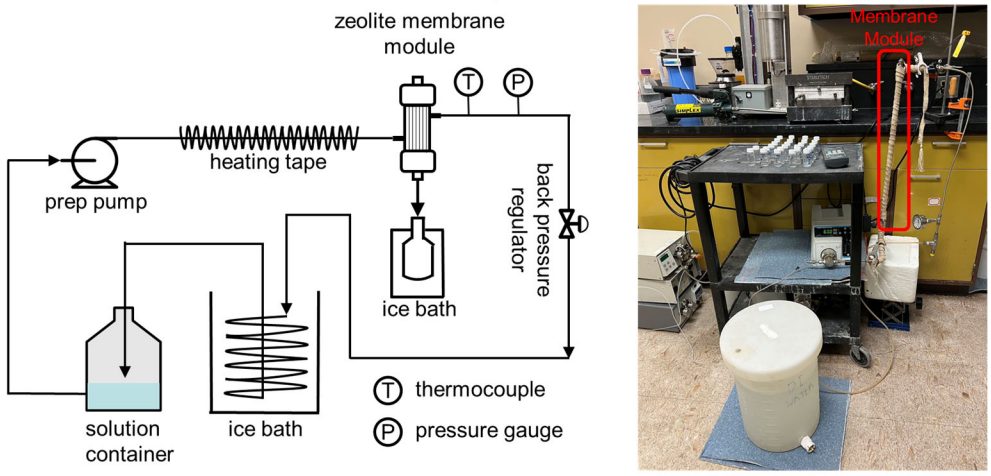


Exhibit 2.3. Schematic diagram and picture of lab-scale performance evaluation system for zeolite membranes.

2.3.2. Construction of membrane module

During the execution of the project, UKy developed two membrane modules, including bundles of in-house fabricated zeolite membranes and commercial Hitachi Zosen membranes in custom-designed UKy housing.

UKy zeolite membrane module:

The FAU zeolite membranes developed by UKy are assembled into a membrane module to ensure optimal performance and durability. Each individual membrane boasts dimensions with an inner diameter (ID) of 2.9 mm and an outer diameter (OD) of 5.7 mm, extending to a length of 75 cm. In the assembly process, a total of 19 such membranes are combined to form a cohesive membrane bundle. One end of all the membranes is sealed together in a unified structure, referred to as a puck. Conversely, the opposite ends of the membranes are individually sealed, ensuring precision and integrity in the sealing process. Once assembled, this membrane bundle is carefully installed within a customized stainless-steel housing. This housing is specifically tailored to accommodate the bundle, ensuring a snug and secure fit. To provide a leak-proof system and maintain the integrity of the membranes, the housing employs a flange and gasket sealing mechanism. The resultant module offers a total membrane area of ~0.26 m^2, with a packing density of approximately 250 m^2/m^3. This design ensures efficient water treatment while maximizing the use of space, making the zeolite membrane module a compact solution for dewatering applications.

DocuSign Envelope ID: 2FA9A609-C360-4E53-8B28-BE8B77B6994A

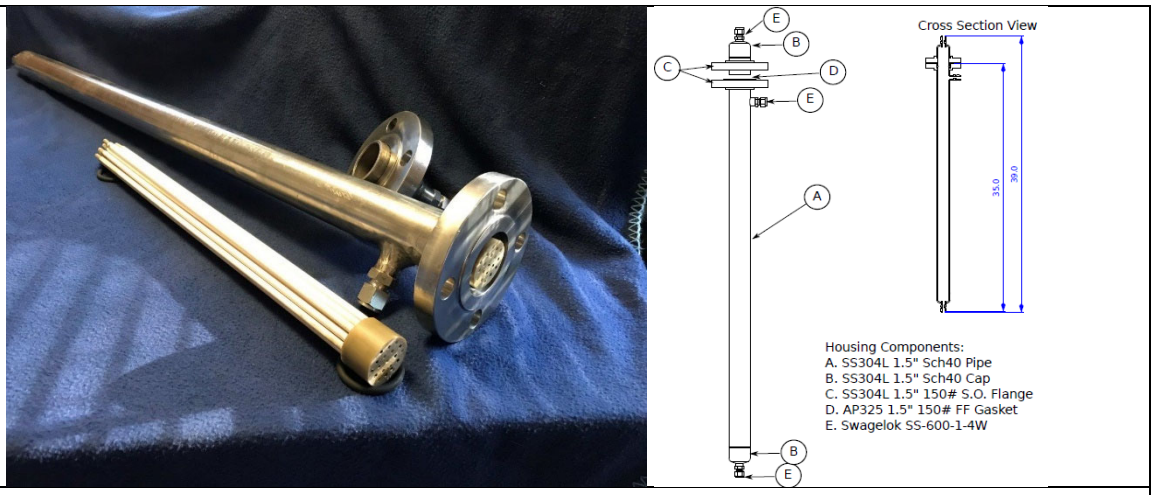


Exhibit 2.4. Bench-scale membrane module for the UKy zeolite membrane.

UKy HZM membrane module:

Commercial zeolite membranes from Hitachi Zosen Corporation (HZM membranes) were used as an alternative to develop the zeolite dewatering system. Each membrane has an inner diameter of 11.2 mm, an outer diameter of 16.3 mm, and spans a length of 113 cm. In creating the membrane bundle, six of these membranes are combined. For the system's reliability and effectiveness, every membrane is individually sealed. One end is sealed with a ceramic tip, ensuring a strong and tight connection, while the other end is secured with a solid, non-porous tube that can accommodate Swawgelok/compression fittings. After assembly, the membrane bundle is placed inside a custom-designed stainless-steel housing that fits the zeolite membranes, and to ensure that the system remains sealed and pressurized, a flange and gasket method is used. The total surface area of this membrane module is ~0.31 m^2, giving enough room for the water treatment by zeolite membranes.

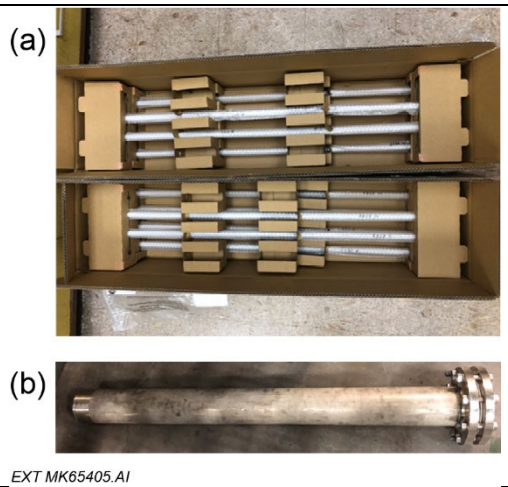


Exhibit 2.5. (a) Diagram of Hitachi Zosen membrane; (b) Picture of received Hitachi membranes; (c) UKy constructed membrane module.

2.3.3. Bench-scale zeolite membrane dewatering operation

The bench-scale zeolite dewatering system was designed to demonstrate the membrane module for treating EERC water (high salinity, primarily composed of sodium chloride) or synthetic NaCl

DocuSign Envelope ID: 2FA9A609-C360-4E53-8B28-BE8B77B6994A

solutions at nominal operating conditions, including 80-120 °C and 50-100 psig. The dewatering system is shown in **Exhibit 2.6**. The UKy zeolite or Hitachi membrane modules can be configured in the system. During normal operation, the feed water is circulated at a constant flow rate, up to a maximum of 1.4 gal/min. Before accessing the zeolite membranes, the process water is fed to a 10-gallon heating vessel, where it is heated using immersion heaters to ensure that the water is at the optimal temperature for the dewatering process. The heating pressure vessel was designed to withstand temperatures up to 232 °C and pressures up to 200 psig. After deaerating, priming, and ensuring all lines are liquid-filled, the pressure of the membrane module is regulated via backpressure control and temperature is maintained with a controller. During the membrane separation process, its unique microporous structure allows for selective ion removal at the applied pressure and temperature, thereby efficiently treating the high-salinity EERC water. In the pressure control train, the pressure switches, transmitters, and gauges, all made of stainless steel, continuously monitor the pressure during dewatering, ensuring it remains within the desired range. A Proportional–integral–derivative (PID) temperature monitor and control unit oversees the system's thermal control. This controller is designed to cut off power to the heaters and shut down the pump if temperatures exceed 150 °C, ensuring the system's safety. After passing through the zeolite membranes, the treated water is collected in glass bottles. The control system and electrical layout are shown in **Exhibit 2.6**. The equipment and instrumentation used in the bench-scale unit are shown in **Exhibit 2.7**.

At the start of testing, the conductivity/TDS of the starting solution is sampled. The pressure, temperature, permeate rate, and TDS are then continuously monitored and logged during operation. The feed and permeate flow rates and their concentration/conductivity are measured to determine membrane flux, salt rejection, water recovery, and concentration factor. This zeolite dewatering system incorporated advanced materials and instrumentation, ensuring efficient and safe treatment of high-salinity EERC water. The system is safely depressurized at the end of testing, and the treated water is collected and stored.

DocuSign Envelope ID: 2FA9A609-C360-4E53-8B28-BE8B77B6994A

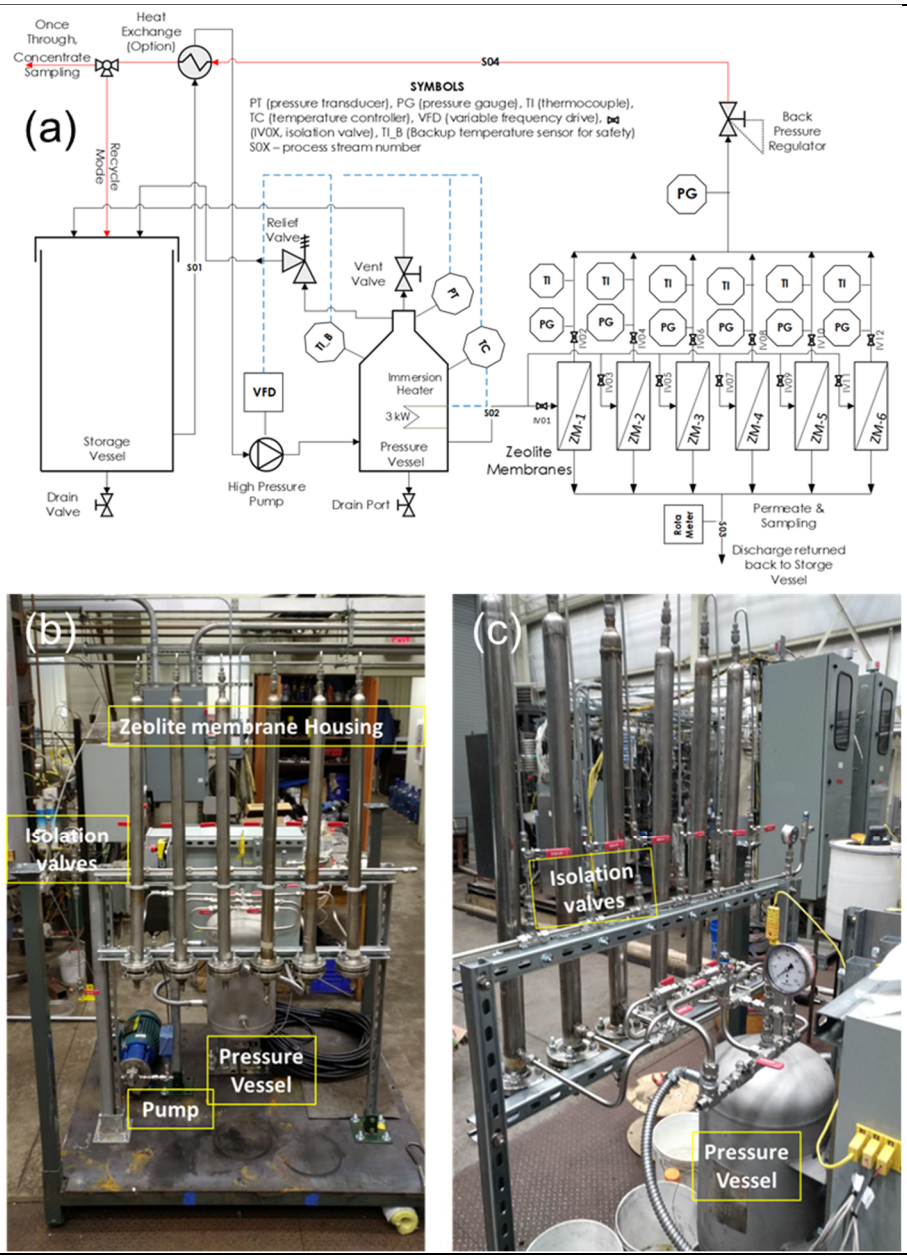


Exhibit 2.6. (a) Process flow diagram for zeolite dewatering system; (b-c) Pictures of the zeolite dewatering system. Note that insulation on the membranes is not shown.

Exhibit 2.7. Equipment and instrumentation list.

Item	**Information**
EERC water	Primarily sodium chloride
Synthetic water as an option	Primarily sodium chloride
Variable frequency drive	KB Electronics Inc KBDA-45 (GRY)
Pump	H-Series Mag-Drive Rotary Gear Positive Displacement Pump, Max Temp 260 °C, Max discharge pressure 300 psi, Max flow 1.4 GPM

DocuSign Envelope ID: 2FA9A609-C360-4E53-8B28-BE8B77B6994A

Heater	Compact Screw-Plug Immersion Heaters for Chemical Solutions, 120 VAC, 1000 W (x3), Incoloy
Pressure vessel	316 SS, 10 gallons, max temp 232 ℃, max pressure 200 psi, ASME stamped and not modified
Zeolite membrane modules	Ceramic, Nominal operation with feed side @ 80 -120 ℃, 60 - 100 psi; Membranes are insulated Module housing is stainless steel
Backpressure regulator	Hylock RV Series, Maximum pressure 300 psi @ -23 to 204 ℃, SS316 Body, SS631 spring
Pressure relief valve	Hylok RV Series, Cracking pressure 10-250 psig, Maximum pressure 300 psi @ -23 to 204 ℃, SS316 Body, SS631 spring
Pressure switch	15-300 psi, 1500 psi max, SS 316
Pressure transmitter	0-300 psi, 600 psi max, 4-20 mA, SS 304
Pressure gauge	316 SS, corrosion-resistant, 0-300 psi
Temperature monitor and control	PID controller; It cuts off power to the heater and is wired to shut off the pump if the temperature exceeds 150 ℃; Does not have a high temp alarm with a relay output
Storage tanks	EERC storage vessel and HDPE vessel
Tubing	1/4” x .049 wall 316 SS; 1/2” x .035 wall 316 SS; The tubing after the pump and before the membrane are insulated

2.3.4. Field skid for zeolite membrane dewatering operation

The zeolite membrane dewatering field skid (**Exhibit 2.8**) is a comprehensive setup designed to evaluate the efficiency of the dewatering process for EERC water at the Watford City, ND, EERC testing facility. A commissioning was conducted using a water sample with a concentration of 180,000 mg/L. The primary metric for assessing TDS removal was conductivity, with the feed conductivity recorded at approximately 175 mS/cm. The feed water was continuously circulated within the system, and its flow rate was measured using an in-line flow meter and/or graduated volumetric flasks and stopwatch. Before heating, the system was pressurized to a range of 40-70 psi. Notably, at room temperature, there should be little to no permeate produced. The feed water’s temperature was then elevated to around 100 °C to initiate the dewatering process. As the operation progressed, permeate was collected from the permeate tube at the bottom of the module. The conductivity and permeate volume were recorded before returning to the reservoir. By monitoring the permeate volume against the time taken, the system provided valuable data on the permeate rate and the overall water recovery efficiency. The EERC’s power monitoring system tracked energy consumption.

DocuSign Envelope ID: 2FA9A609-C360-4E53-8B28-BE8B77B6994A



Exhibit 2.8. Pictures of the zeolite dewatering system for the field test at the EERC testing facility in Watford City, ND.

3 PROJECT TECHNICAL RESULTS

In order to support field demonstration at the EERC testing facility in Watford City, ND, initial assessments were done at a lab scale that provided insights into key performance metrics for the UKy and Hitachi membranes and the extent of scaling up required for field demonstration. Building on this foundational knowledge, membrane modules were constructed and transitioned to bench-scale tests, practical conditions were more closely simulated, and the testing methodologies were refined. Finally, the test skid was shipped to the EERC facility for field testing. The results presented in this section cover the performance period and offer a pointed view of the zeolite membrane's potential and efficacy.

3.1 Lab-scale Membrane Performance Evaluation

3.1.1 UKy Zeolite Membrane

UKy developed FAU-type zeolite membranes as an alternative to treat hypersaline streams where high pressure and membrane stability at those pressures encumber their applications. For example, a 10 wt% sodium chloride stream would require an estimated osmotic pressure of ~1538 psi, far exceeding the mechanical stability requirement for RO, typically ~ 1000 psi. Unlike the polymeric membrane's pressure-driven performance, zeolite dewatering employs the preferential solution and transport of water within the membrane matrix under modest temperatures (e.g.,115 °C) and pressures (e.g., 80 psig) to facilitate water treatment. UKy FAU zeolite membrane was investigated for its potential for hypersaline applications. A synthetic water comprising a 10 wt% NaCl solution was used as the feed solution. The evaluation was conducted under controlled conditions of 115 °C and 30 psig. As shown in **Exhibit 3.1,** the findings from the synthetic water test were promising,

DocuSign Envelope ID: 2FA9A609-C360-4E53-8B28-BE8B77B6994A

revealing a permeate conductivity below 80 μ S·cm^{-1} (>99% salt rejection) and membrane flux of 4.8 kg·m^{-2}·h^{-1} sustained over a 40-hour operational period.

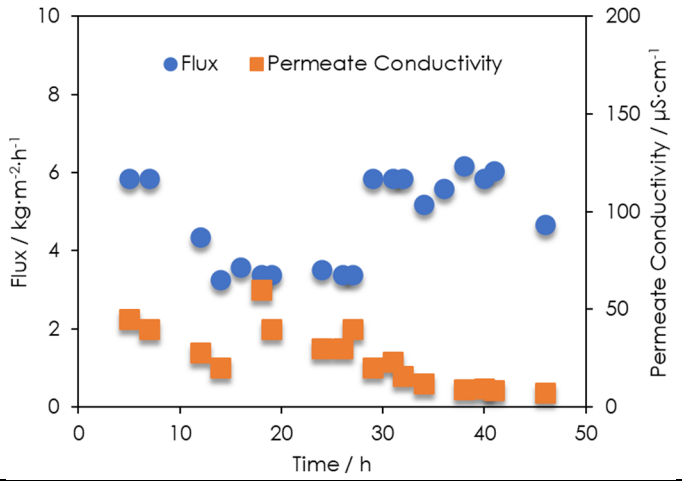


Exhibit 3.1. Performance test of UKy zeolite membrane.

Exhibit 3.2 illustrates the influence of feed salt concentrations on the desalination efficacy of the UKy zeolite membrane under conditions of 115 °C and 50 psig. The water flux decreases with increasing the feed concentration. Specifically, the water flux decreases from 1.86 kg·m^{-2}·h^{-1} to 1.50 kg·m^{-2}·h^{-1} as the feed concentration increases from 2.5 to 10 wt%, while the ion rejection decreased but remained high (around 90%) even for desalination of 10 wt% NaCl solution. Compared to the 8 mm membrane (**Exhibit 3.1**), the flux decline may be attributed to reduced water dissolution at the lower operating pressure. The decrease in rejection rate is attributed to salt flux through intercrystalline pores due to an increasing driving force with concentration, which may lead to precipitation on the permeate side [13]. With increasing the feed concentration, more ionic clusters are formed, and the electrostatic interaction between the ions and the polarized water becomes stronger. Therefore, the driving forces available (effective pressure to overcome the osmotic pressure) for water permeation decreases, leading to the reduction of water flux [14]. Compared to **Exhibit 3.1**, a slightly thicker zeolite layer adopted during membrane development for testing in **Exhibit 3.2** explains the reduced flux.

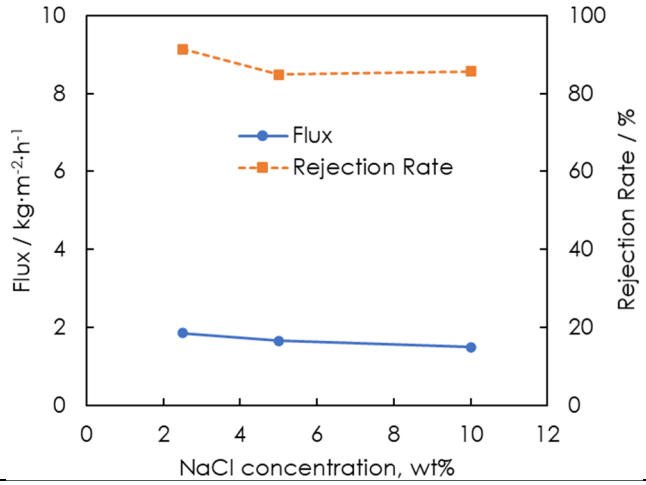


Exhibit 3.2. Membrane performance as a function of feed NaCl concentration.

DocuSign Envelope ID: 2FA9A609-C360-4E53-8B28-BE8B77B6994A

Water recovery is a critical parameter in evaluating desalination processes, and improving water recovery typically means a lower volume of waste disposal. UKy FAU zeolite membranes were investigated for treating ~170,000 ppm EERC water. As shown in **Exhibit 3.3**, the water recovery was monitored by measuring the amount of collected permeate water, ensuring the feed solution remained at a steady 120 mL. A consistent temperature of 108 °C and pressure at 50 psig was maintained during the operation. Compared to previous testing with 10 wt% NaCl, the reduced flux of ~0.4 kg/[m^2-hr] for ~17 wt% EERC water is consistent with the effect of concentration in **Exhibit 3.2**. A water recovery of 40% was achieved within 7.5 hours while maintaining the rejection rate above 95%. In addition to employing conductivity data for TDS, the total organic carbon (TOC) measurements were also carried out on the water samples to determine the membrane's ability to remove organic compounds. TOC was measured with samples collected via the Hach methods 10128 and 10129, involving the initial removal of inorganic carbon under acidic conditions, persulfate digestion at 104 °C, and colorimetric detection in the presence of a chemical indicator. The results show that TOC rejection reached >96% for a feed solution containing >706 mg/L TOC. The results from TOC measurements showed that the membrane achieved a TOC reduction of >96% at an applied temperature of 107 °C and pressure of 50 psig, which agrees with the salt rejection rate result, as shown in **Exhibit 3.3**.

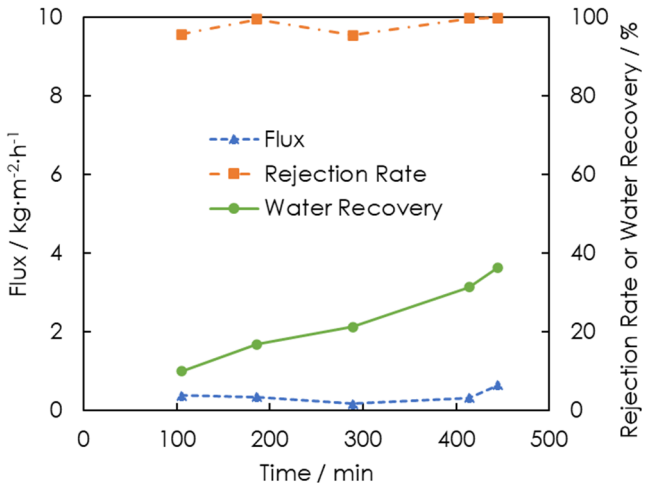


Exhibit 3.3. Results of membrane performance (flux, rejection rate, water recovery) as a function of operation time.

3.1.2 HZM Membrane from Hitachi Zosen

In addition to the UKy FAU membranes, commercial zeolite membranes from Hitachi Zosen Corporation were also explored for developing a UKy module. As discussed earlier, the module was called the UKy HZM membrane module. These commercially available membranes (HZM membranes) have undergone rigorous quality control and have a proven track record in the industry. To ensure their suitability for EERC water treatment, two distinct feed solutions were employed for the validation test: a synthetic water composed of a 20 wt% NaCl solution and the EERC water. The tests were conducted at an elevated temperature of 120 °C and a pressure of 100 psig, spanning an overnight duration. As shown in **Exhibit 3.4**, when subjected to the synthetic water, the membrane exhibited a rejection rate exceeding 99.5% consistently over a 24-hour operational period. Concurrently, the membrane flux was maintained at a commendable 2.28 kg·m^{-2}·h^{-1}. On transitioning to the EERC water, the performance of the HZM membrane remained

DocuSign Envelope ID: 2FA9A609-C360-4E53-8B28-BE8B77B6994A

robust, achieving a rejection rate of over 99.5% for an initial 6-hour span and an average rejection of 90% over the 20-hour evaluation period. The flux remained relatively stable at 0.74 $kg \cdot m^{-2} \cdot h^{-1}$ over a 20-hour operation, suggesting that the membrane integrity was largely preserved. These results show that the HZM membrane is a promising candidate for the UKy module for EERC water treatment applications.

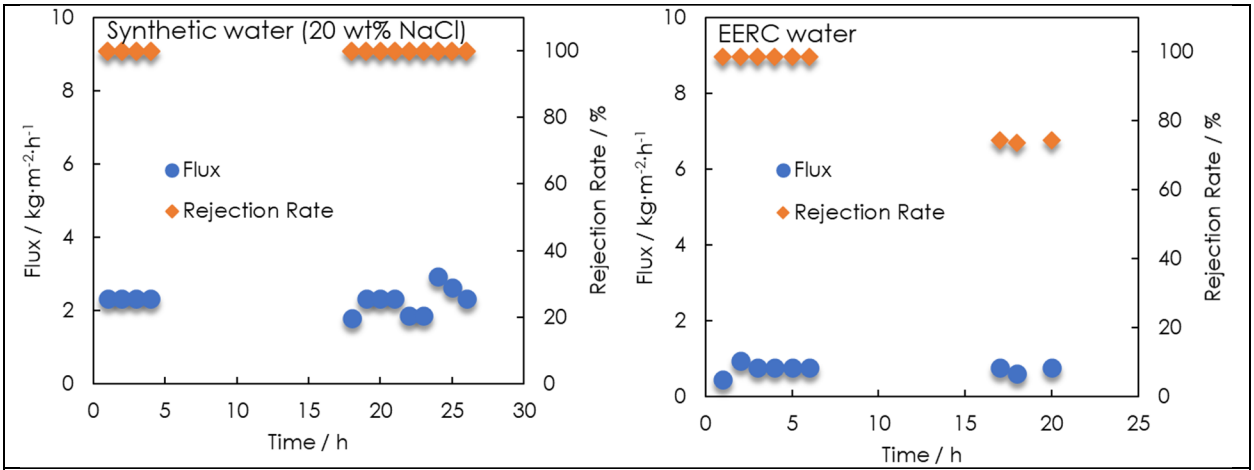


Exhibit 3.4. Stability test of HZM membranes. The operation continued overnight, but no additional data was collected until the subsequent day.

3.2 Bench-scale Membrane Performance Evaluation

As detailed in sections 2.3.2 and 2.3.3, bench-scale skids were developed, including the UKy zeolite and HZM. For developing the UKy zeolite membrane skid, there were a couple of challenges, mainly mechanical in nature: Firstly, the failure of ethylene propylene diene monomer (EPDM) o-rings led to an unintended bypass of the process feed directly to the permeate side of the housing. This issue can be attributed to the O-ring's deformation or potential degradation, a consequence of its cyclical expansion and contraction during the operational phases of heating and cooling. **Exhibit 3.5b** shows a compromised O-ring after module disassembly. Secondly, the difficulty of repairing non-periphery membranes on the puck became evident. The puck's design, combined with the inherent fragility of the zeolite membranes, made repairs a delicate endeavor. Any inappropriate mechanical pressure exerted during the repair process posed a risk of further membrane damage, which can be seen in **Exhibit 3.5c**.

DocuSign Envelope ID: 2FA9A609-C360-4E53-8B28-BE8B77B6994A

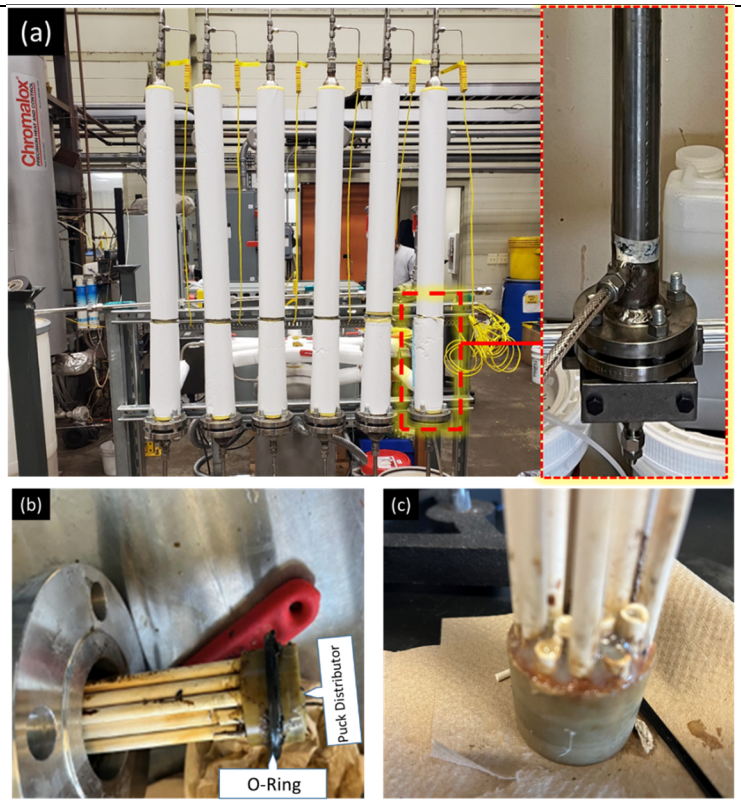


Exhibit 3.5. Picture of (a) bench-scale membrane performance evaluation system and an isolated single membrane housing with the flanged section exposed, (b) membrane puck distributor and o-ring seal after disassembly with compromised o-ring obvious, and (c) a membrane repaired by using epoxy to seal leak spots, with more broken membranes due to fragility.

Considering these challenges, particularly the O-ring seal issues, the development continued with the UKy HZM membrane module, which employed a compression fitting sealing mechanism. The membrane module setup is indicated in **Exhibit 3.6**. Each of the tubular membrane was sealed by compression fitting separately. However, due to the fragility of the membrane, some membranes were broken during shipment. They were repaired by using epoxy coupling to affix broken sections. Commissioning of the HZM membrane module was conducted in the bench-scale unit using EERC water as feed brine. **Exhibit 3.7a** shows the experimentally observed rejection rate for the HZM membrane module during the dewatering test as a function of temperature. The pressure on the feed side was maintained at about 60 psig for all experiments. The rejection rate increased to above 90% when the temperature reached 100-105 °C. At these conditions, the solution remained in the liquid phase on the membrane face, and a higher temperature increased preferential water dissolution, which enhanced its driving force for permeation through the membrane; additionally, the self-diffusion coefficient of water was also accelerated at higher temperatures [15]. As shown in **Exhibit 3.7b**, it takes about 3 hours to heat up all the solution in the membrane module to this targeted temperature range and initiate the dewatering process, generating a flux of 0.45 $kg \cdot m^{-2} \cdot h^{-1}$ and a rejection rate over 90%. The observed flux and rejection are similar to those observed during the membrane evaluation (**Exhibit 3.4**).

DocuSign Envelope ID: 2FA9A609-C360-4E53-8B28-BE8B77B6994A



Exhibit 3.6. Example of HZM membrane assembly with compression fitting and picture of installed membrane module.

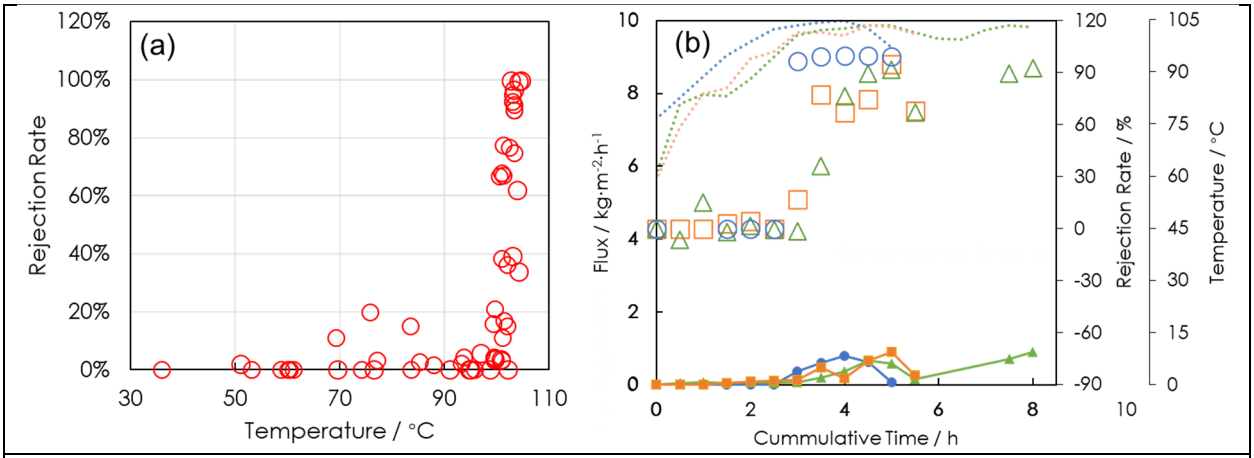


Exhibit 3.7. (a) Rejection rate as a function of temperature; (b) Membrane performance evaluation results (Flux: solid line+filled symbol; Rejection rate: open symbol; Temperature: dash line) of HZM membrane module using EERC water as feed brine.

3.3 Field Test of Zeolite Dewatering System

The field test was conducted at the EERC testing facility in Watford City, North Dakota, using the UKy HZM membrane module dewatering skid (**Exhibit 2.8**). The testing was conducted using the EERC water sample with a concentration of 150,000 mg/L TDS. The feed water flow rate for the system was > 0.1 L/min. Before heating, the system was pressurized to 50 psig. As the operation progressed, permeate was collected, and the conductivity and volume were recorded to calculate the rejection rate and flux. During testing on November 7, 2022, as shown in **Exhibits 3.8a** and **3.8d**, the temperature reached above 90 °C from 18:00 and started to generate permeate. After stabilizing the rejection rate, sample collection started at 20:30 for ICP analysis (**Exhibit 3.9**). The results indicate 20-30% TDS and TOC rejection, whereby a diminished rejection resulted from the membrane module failure after 6.5 hours of operation due to overheating the membrane module. During operation, direct heating using resistive heating tape wound along the membrane housing was employed due to problems with the immersion heater in the pressure heating vessel. Poor temperature control compromised the coupling previously used to fix broken HZM membranes,

DocuSign Envelope ID: 2FA9A609-C360-4E53-8B28-BE8B77B6994A

causing internal leakage and reducing the TDS and TOC rejection. However, the sample collection included periods before and after failure; therefore, separation performance was still observed but diminished. From conductivity measurement, >95% TDS rejection was maintained before failure. **Exhibit 3.10** illustrates the energy consumption resulting from 19:00 hours to 21:00 hours of the field test. During the test period, a total of 3.0 kWh was consumed, and approximately 592 mL of treated water recovered as permeate, resulting in an energy consumption of 5161 kWh/m^3. The significant energy cost resulted from the small unit size, water recovery, and poor thermal management. For a similar unit sized to operate at ~60% water recovery and assuming sensible heating of 5 °C temperature difference (assuming good thermal management and recovery), it is estimated that less than 10 kWh/m^3 will be required.

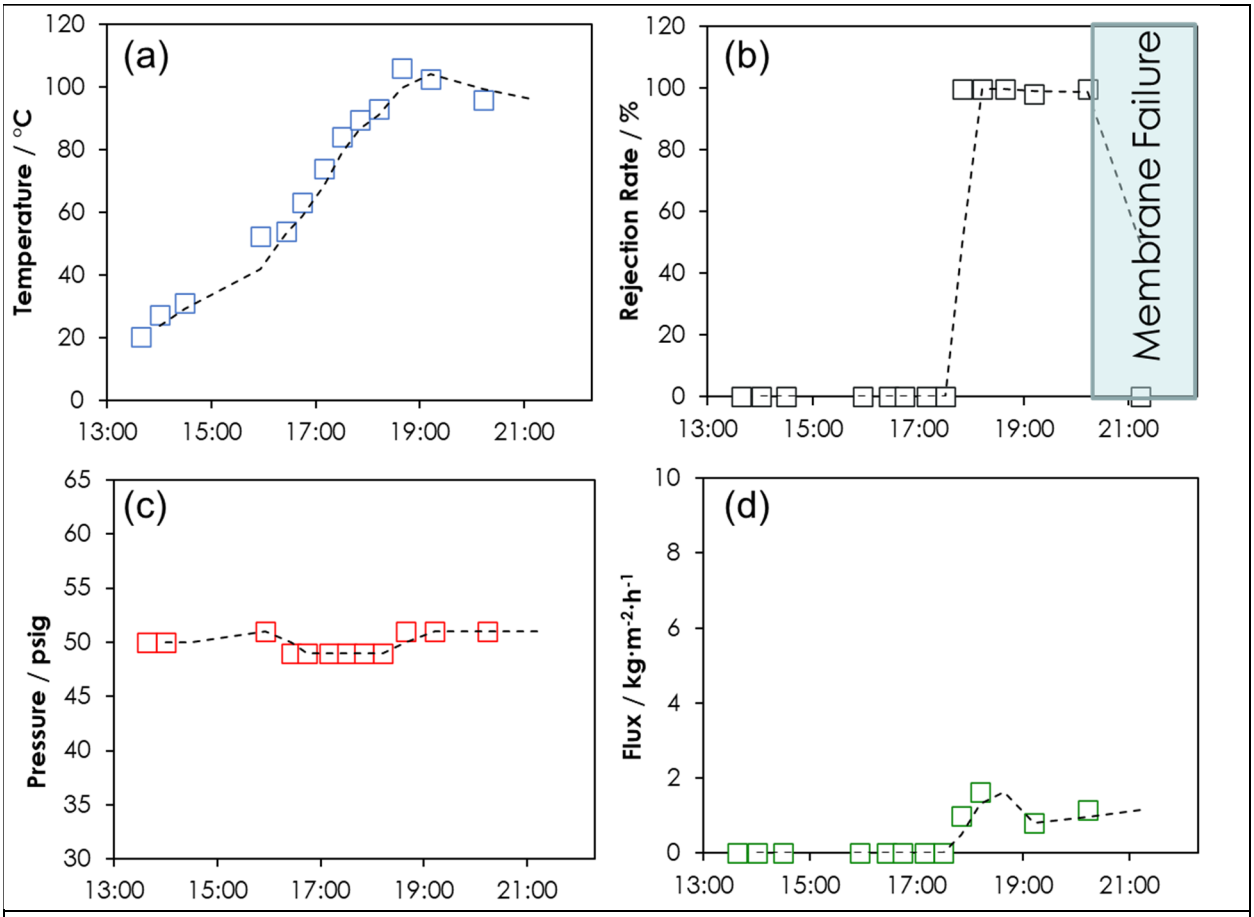


Exhibit 3.8. Results of membrane field test as a function of time: (a) temperature of membrane module, (b) salt rejection rate, (c) pressure of membrane module, (d) membrane total flux.

DocuSign Envelope ID: 2FA9A609-C360-4E53-8B28-BE8B77B6994A

Exhibit 3.9. Summary of ICP analysis for the permeate sample from the EERC field test.						
					Rejection	**Concentration Factor**
Property	**Feed**	**Concentrate**	**Permeate**	**Unit**	**%**	**#**
Alkalinity, as Bicarbonate (HCO_3^-)	385	384	278	mg/L	27.79	1.00
Alkalinity, as Carbonate (CO_3=)	0	0	0	mg/L		
Alkalinity, as Hydroxide (OH^-)	0	0	0	mg/L		
Alkalinity, Total as $CaCO_3$	316	314	228	mg/L	27.85	0.99
Barium	8.5	9.2	6.8	mg/L	20.00	1.08
Boron	248	268	202	mg/L	18.55	1.08
Bromide	467	523	381	mg/L	18.42	1.12
Calcium	9960	11200	7840	mg/L	21.29	1.12
Chloride	89500	100000	72500	mg/L	18.99	1.12
Cobalt	1	1	1	mg/L	0.00	1.00
Conductivity at 25 °C	184000	193000	154000	uS/cm	16.30	1.05
Density	1.1	1.11	1.08	g/mL	1.82	1.01
Iron	1	1	1	mg/L	0.00	1.00
Lithium	31.1	34.4	24.4	mg/L	21.54	1.11
Magnesium	616	683	491	mg/L	20.29	1.11
Manganese	5.3	5.9	4.3	mg/L	18.87	1.11
pH	7.36	7.2	7.45	pH	-1.22	0.98
Potassium	3830	4230	3020	mg/L	21.15	1.10
Silicon	10	10	10	mg/L	0.00	1.00
Sodium	41400	44900	32300	mg/L	21.98	1.08
Strontium	833	917	656	mg/L	21.25	1.10
Sulfate	219	205	174	mg/L	20.55	0.94
Total Dissolved Solids	148000	164000	118000	mg/L	20.27	1.11

DocuSign Envelope ID: 2FA9A609-C360-4E53-8B28-BE8B77B6994A

Total Organic Carbon	674	841	470	mg/L	30.27	1.25
Zinc	0.55	1.1	0.75	mg/L	-36.36	2.00

Exhibit 3.10. Energy consumption results from the field test at the EERC facility.	
Time Duration, minute	120
Total Energy Consumed, kWh	3.06
Average Permeate Rate, cm^3/min	4.9
Average Permeate Rate, m^3/h	0.0003
Total Volume treated, m^3	0.0006
Energy Consumption, kWh/m^3	5161.7

4 FUTURE WORK/OTHER AREA OF INTEREST

As an alternative to the puck-style configuration, the Hitachi Zosen zeolite membranes (HZM) were purchased, used to form the UKy HZM module, and evaluated for conducting field tests where they showed promising results. However, in January 2022, Hitachi reported that these membranes were discontinued and no longer available for purchase. In our pursuit of an alternative, we sourced a 4-channel hollow fiber zeolite membrane from Jiangsu Xuyi Hitech Co. based in Nanjing, China (**Exhibit 4.1**). The company has scaled up the production of its 4-channel membrane, offering membrane modules with expansive surface areas of 4 m^2 and 8 m^2 (**Exhibit 4.2**) tailored for different industrial applications. Preliminary tests on this membrane have been promising, yielding a flux of 3.9 $kg \cdot m^{-2} \cdot h^{-1}$ and a rejection rate surpassing 99.5%. However, a point of concern remains the potential damage to the thin membrane fibers during international shipping, given the inherent fragility of zeolite membranes. As we look forward to future work of interest, in addition to exploring options for manifolding the UKy membranes, the Nanjing membrane unit can be a candidate for treating EERC water and other hypersaline waters, warranting further exploration and optimization.

DocuSign Envelope ID: 2FA9A609-C360-4E53-8B28-BE8B77B6994A

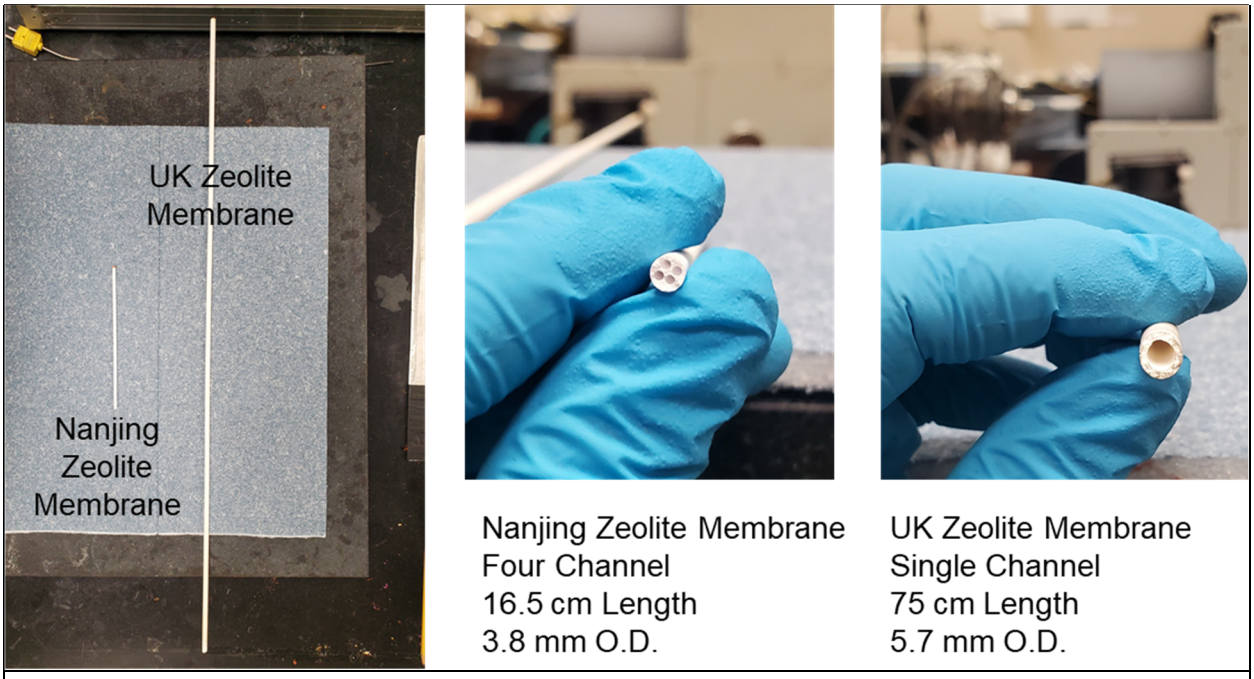


Exhibit 4.1. Comparison of UKy zeolite membrane and 4-channel Nanjing zeolite membrane.

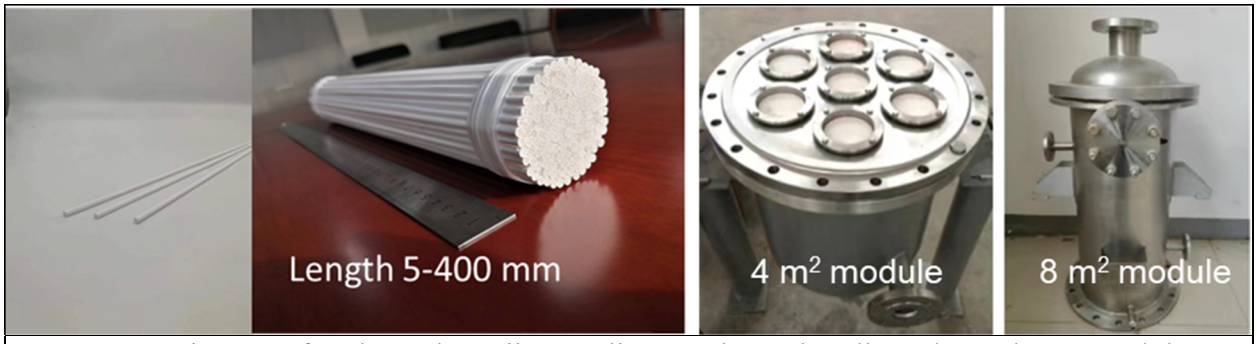


Exhibit 4.2. Pictures of 4-channel Nanjing zeolite membrane bundle and membrane modules.

5 CONCLUSION AND LESSONS LEARNED

This report summarizes the work done to develop and demonstrate a zeolite dewatering system for treating EERC-produced/blended water. The UKy technology employs zeolite membranes for water extraction at transmembrane pressures below 200 psig. The project results verified UKy's approach to treating hypersaline streams using zeolite dewatering technology, including removing organic and inorganic solids in a single unit operation at modest temperatures and pressure. During lab scale evaluation at ~108℃ and 50 psig with EERC water, ~2X up-concentration was achieved, including ~40% water recovery and >95% salt and organic content rejection. The flux was stable at the test conditions. The dewatering process was scaled up by >20X from a 0.014 m^2 membrane unit to a 0.3 m^2 bench-scale test unit to treat EERC water at the Watford City test center.

UKy learned much during the execution of this project, especially on handling larger zeolite membranes due to their fragility. The initial attempt to modularize the process was unsuccessful due to O-ring stability and complications with the puck design, especially the lack of easy access

DocuSign Envelope ID: 2FA9A609-C360-4E53-8B28-BE8B77B6994A

to membranes when repairs need to be made. The now-discontinued Hitachi membranes were favored alternatives since they were sealed using swage-type fittings. However, during shipment, some of the membranes were broken due to fragility but were recoupled. The membranes continued to deliver good results but were damaged due to overheating during field testing. Membrane security during shipment needs further exploration; otherwise, they must be made on-site.

During the field evaluation, the zeolite dewatering process demonstrated stabilized >90% salt rejection during the initial field-testing phase prior to complications from overheating that damaged the membrane repair couplings. Post-analysis of the samples also confirms the rejection of organic and inorganic content, thereby demonstrating the capability of the UKy approach.

DocuSign Envelope ID: 2FA9A609-C360-4E53-8B28-BE8B77B6994A

6 LIST OF EXHIBITS

Exhibit 2.1. Project Objectives.
Exhibit 2.2. Schematic diagram for the zeolite dewatering process and scanning electron microscope (SEM) picture of the membrane cross-section morphology.
Exhibit 2.3. Schematic diagram and picture of lab-scale performance evaluation system for zeolite membranes.
Exhibit 2.4. Bench-scale membrane module for the UKy zeolite membrane.
Exhibit 2.5. (a) Diagram of Hitachi Zosen membrane; (b) Picture of received Hitachi membranes; (c) UKy constructed membrane module.
Exhibit 2.6. (a) Process flow diagram for zeolite dewatering system; (b-c) Pictures of the zeolite dewatering system. Note that insulation on the membranes is not shown.
Exhibit 2.7. Equipment and instrumentation list.
Exhibit 2.8. Pictures of the zeolite dewatering system for the field test at the EERC testing facility in Watford City, ND.
Exhibit 3.1. Stability test of UKy zeolite membrane (UKy prior testing result).
Exhibit 3.2. Results of membrane performance as a function of feed NaCl concentration.
Exhibit 3.3. Results of membrane performance (flux, rejection rate, water recovery) as a function of operation time.
Exhibit 3.4. Stability test of HZM membranes.
Exhibit 3.5. Picture of (a) bench-scale membrane performance evaluation system and an isolated single membrane housing with the flanged section exposed, (b) membrane puck distributor and o-ring seal after disassembly with compromised o-ring obvious, and (c) a membrane repaired by using epoxy to seal leak spots, with more broken membranes due to fragility.
Exhibit 3.6. Example of HZM membrane assembly with compression fitting and picture of installed membrane module.
Exhibit 3.7. (a) Rejection rate as a function of temperature; (b) Membrane performance evaluation results (Flux: solid line+filled symbol; Rejection rate: dash line+open symbol; Temperature: dash line) of HZM membrane module using EERC water as feed brine.
Exhibit 3.8. Results of membrane field test as a function of time: (a) temperature of membrane module, (b) salt rejection rate, (c) pressure of membrane module, (d) membrane total flux.
Exhibit 3.9. Summary of ICP analysis for the permeate sample from the EERC field test.
Exhibit 3.10. Energy consumption results from the field test at the EERC facility.
Exhibit 4.1. Comparison of UKy zeolite membrane and 4-channel Nanjing zeolite membrane.
Exhibit 4.2. Pictures of 4-channel Nanjing zeolite membrane bundle and membrane modules.

DocuSign Envelope ID: 2FA9A609-C360-4E53-8B28-BE8B77B6994A

7 REFERENCES

[1] Hamling, J., *NORTH DAKOTA BRINE EXTRACTION AND STORAGE TEST.* 2019.

[2] Lee, R. and L. Li, *Treating Coalbed Natural Gas Produced Water for Beneficial Use by MFI Zeolite Membranes*. 2008, New Mexico Institute of Mining and Technology, Socorro, NM (United States).

[3] Newmark, R.L., S.J. Friedmann, and S.A. Carroll, *Water challenges for geologic carbon capture and sequestration.* Environmental management, 2010. **45**: p. 651-661.

[4] Al-Karaghouli, A. and L.L. Kazmerski, *Energy consumption and water production cost of conventional and renewable-energy-powered desalination processes.* Renewable and Sustainable Energy Reviews, 2013. **24**: p. 343-356.

[5] Lee, S., W.S. Ang, and M. Elimelech, *Fouling of reverse osmosis membranes by hydrophilic organic matter: implications for water reuse.* Desalination, 2006. **187**(1-3): p. 313-321.

[6] Yan, Y., et al., *A graphene-like membrane with an ultrahigh water flux for desalination.* Nanoscale, 2017. **9**(47): p. 18951-18958.

[7] Lim, Y.-G., et al., *Development of integrated volatile organic compound purification system using tubular NaA zeolite membrane: Experimental and theoretical insights into vapor permeation and pervaporation process.* Separation and Purification Technology, 2023. **325**: p. 124692.

[8] Shah, D., et al., *Pervaporation of alcohol–water and dimethylformamide–water mixtures using hydrophilic zeolite NaA membranes: mechanisms and experimental results.* Journal of Membrane Science, 2000. **179**(1-2): p. 185-205.

[9] Kita, H., et al., *Synthesis of a zeolite NaA membrane for pervaporation of water/organic liquid mixtures.* Journal of Materials Science Letters, 1995. **14**(3): p. 206-208.

[10] Bowen, T.C., R.D. Noble, and J.L. Falconer, *Fundamentals and applications of pervaporation through zeolite membranes.* Journal of Membrane Science, 2004. **245**(1-2): p. 1-33.

[11] Li, S., et al., *Pervaporation of water/THF mixtures using zeolite membranes.* Industrial & engineering chemistry research, 2001. **40**(21): p. 4577-4585.

[12] Omosebi, A., et al., *Intensified Flue Gas Desulfurization Water Treatment for Reuse, Solidification, and Discharge*. 2020, Univ. of Kentucky, Lexington, KY (United States).

[13] Duke, M.C., et al., *Seawater desalination performance of MFI type membranes made by secondary growth.* Separation and purification technology, 2009. **68**(3): p. 343-350.

[14] Yang, J., et al., *Influences of inorganic salts on the pervaporation properties of zeolite NaA membranes on macroporous supports.* Microporous and mesoporous materials, 2014. **192**: p. 60-68.

[15] Guo, S., et al., *Simulation of adsorption, diffusion, and permeability of water and ethanol in NaA zeolite membranes.* Journal of Membrane Science, 2011. **376**(1-2): p. 40-49.

DocuSign Envelope ID: 2FA9A609-C360-4E53-8B28-BE8B77B6994A

8 LIST OF ACRONYMS AND ABBREVIATIONS

EERC	Energy and Environmental Research Center
WR	Water recovery
SR	Salt rejection
UKy	University of Kentucky
TDS	Total Dissolved Solids
RO	Reverse Osmosis
FAU	Faujasite
IC	Ion Chromatography
ICP	Inductively Coupled Plasma
SEM	Scanning Electron Microscope
ID	Inner Diameter
OD	Outer Diameter
PID	Proportional–Integral–Derivative
ND	North Dakota
EPDM	Ethylene Propylene Diene Monomer
TOC	Total Organic Carbon

DocuSign Envelope ID: 2FA9A609-C360-4E53-8B28-BE8B77B6994A

APPENDIX J

GHCR FINAL REPORT – 2022

DocuSign Envelope ID: 2FA9A609-C360-4E53-8B28-BE8B77B6994A

SUBTASK 3.2 – PRODUCED WATER MANAGEMENT THROUGH GEOLOGIC HOMOGENIZATION, CONDITIONING, AND REUSE

Final Topical Report

(for the period of February 1, 2020, through January 31, 2022)

Prepared for:

AAD Document Control

National Energy Technology Laboratory
U.S. Department of Energy
626 Cochrans Mill Road
PO Box 10940, MS 921-107
Pittsburgh, PA 15236-0940

Cooperative Agreement No.: DE-FE0024233
DOE Technical Monitor: Joseph Renk

Prepared by:
Kyle A. Glazewski
Christopher L. Martin
Arelys Salazar
Christopher J. Beddoe
Carolyn M. Nyberg
Meghan A. Taunton
Joshua G. Regorrah
Marc D. Kurz
Kevin C. Connors
James L. Vritis
Loreal V. Heebink
Darren D. Schmidt
John A. Hamling
Bethany A. Kurz
James A. Sorensen
Xuefei Zhang
Chantsalmaa Dalkhaa

Energy & Environmental Research Center
University of North Dakota
15 North 23rd Street, Stop 9018
Grand Forks, ND 58202-9018

2022-EERC-01-10

January 2022

DocuSign Envelope ID: 2FA9A609-C360-4E53-8B28-BE8B77B6994A

EERC DISCLAIMER

LEGAL NOTICE This research report was prepared by the Energy & Environmental Research Center (EERC), an agency of the University of North Dakota, as an account of work sponsored by the U.S. Department of Energy (DOE) National Energy Technology Laboratory (NETL). Because of the research nature of the work performed, neither the EERC nor any of its employees makes any warranty, express or implied, or assumes any legal liability or responsibility for the accuracy, completeness, or usefulness of any information, apparatus, product, or process disclosed or represents that its use would not infringe privately owned rights. Reference herein to any specific commercial product, process, or service by trade name, trademark, manufacturer, or otherwise does not necessarily constitute or imply its endorsement or recommendation by the EERC.

ACKNOWLEDGMENT

This material is based upon work supported by DOE NETL under Award No. DE-FE-0024233.

DOE DISCLAIMER

This report was prepared as an account of work sponsored by an agency of the United States Government. Neither the United States Government, nor any agency thereof, nor any of their employees, makes any warranty, express or implied, or assumes any legal liability or responsibility for the accuracy, completeness, or usefulness of any information, apparatus, product, or process disclosed, or represents that its use would not infringe privately owned rights. Reference herein to any specific commercial product, process, or service by trade name, trademark, manufacturer, or otherwise does not necessarily constitute or imply its endorsement, recommendation, or favoring by the United States Government or any agency thereof. The views and opinions of authors expressed herein do not necessarily state or reflect those of the United States Government or any agency thereof.

DocuSign Envelope ID: 2FA9A609-C360-4E53-8B28-BE8B77B6994A

TABLE OF CONTENTS

LIST OF FIGURES iii

LIST OF TABLES vii

DEFINITIONS viii

EXECUTIVE SUMMARY x

1.0 INTRODUCTION 1

2.0 BAKKEN WATER MANAGEMENT 3
- 2.1 Freshwater Trends 3
- 2.2 Bakken Produced Water Trends 6
- 2.3 Bakken Produced Water Chemistry 7
- 2.4 SWD Trends 10
- 2.5 Produced Water Recycling and Reuse Discussion 12
- 2.6 Produced Water Recycling Approach—GHCR Concept 14

3.0 LABORATORY AND FIELD EVALUATION OF GHCR CONCEPT 16
- 3.1 Laboratory Column Testing 16
  - 3.1.1 Sand Column Test 16
  - 3.1.2 Inyan Kara Outcrop Column 23
  - 3.1.3 Inyan Kara Core Column 31
  - 3.1.4 Key Observations for the Three Laboratory Column Tests 37
- 3.2 Field Evaluation 38
  - 3.2.1 Field Sampling Results 39
  - 3.2.2 Key Observations from the Field Sampling and Evaluation 42

4.0 GEOLOGIC MODELING AND NUMERICAL SIMULATION EVALUATION OF GHCR CONCEPT 43
- 4.1 Field Numerical Models 43
- 4.2 Field Simulation Work Descriptions 45
- 4.3 Field Numerical Modeling and Simulation Results 46
  - 4.3.1 Sensitivity Analysis – Number of Wells and Distance Between Wells 47
- 4.4 Key Observations from Numerical Simulation 54

5.0 TECHNO-ECONOMIC ANALYSIS OF GHCR CONCEPT 55
- 5.1 TEA Technical Inputs 56
  - 5.1.1 Inyan Kara Pressure Management 56
  - 5.1.2 GHCR Produced Fluid Characteristics 58
- 5.2 Regulatory Considerations 59
  - 5.2.1 Review of Regulatory Environment 59
  - 5.2.2 Review of Various States' Regulation of Produced Water 62

Continued . . .

DocuSign Envelope ID: 2FA9A609-C360-4E53-8B28-BE8B77B6994A

TABLE OF CONTENTS (continued)

5.2.3 Regulatory Discussion 64
5.3 GHCR Cost Modeling 65
5.3.1 Cost Assumptions 66
5.3.2 Oil and Gas Production Profiles 68
5.3.3 Water Demand and Disposal Profiles 68
5.4 TEA Results 70
5.4.1 Centralized GHCR 74
5.5 Key Observations from the TEA 76
5.5.1 Technical Evaluation 76
5.5.2 Regulatory Considerations 77
5.5.3 Economic Analysis 78

6.0 CONCLUSIONS 78

7.0 MILESTONES 79

8.0 REFERENCES 80

DocuSign Envelope ID: 2FA9A609-C360-4E53-8B28-BE8B77B6994A

LIST OF FIGURES

1-1 North Dakota stratigraphic column 2

2-1 Plot showing industrial water use in MMbbl from permitted sites for oil-related activities from 2008 through 2020 as compared to the average fracture fluid volume per well and the wells completed in each year 5

2-2 Freshwater use 2008–2020 by water use 6

2-3 Approximate locations of Bakken produced water samples collected during this project 8

2-4 Applicability of various desalination technologies 9

2-5 Volumes of all water injected into North Dakota SWD wells since 1956 10

2-6 Annual SWD injection volume by geologic group from 2008 to 2020 11

2-7 Illustrative diagram for a well using an intermediate casing string, or "Dakota string," and a typical well diagram without the addition of a Dakota string 12

2-8 Traditional approach to water management 14

2-9 GHCR concept involving the addition of an extraction well and utilizing that water as hydraulic fracturing makeup water for Bakken wells 15

3-1 Conductivity measurements of laboratory sand column test outlet fluid samples 19

3-2 TSS measurements of laboratory sand column test outlet fluid samples 20

3-3 Sulfate measurements of laboratory sand column test samples 20

3-4 TDS measurements of laboratory sand column test samples 21

3-5 TOC measurements of laboratory sand column test samples 21

3-6 Conductivity measurements of laboratory outcrop column test outlet fluid samples 25

3-7 TDS measurements of laboratory outcrop column test samples 26

3-8 Sulfate measurements of laboratory outcrop column test samples 27

3-9 Magnesium measurements of laboratory outcrop column test samples 28

3-10 TSS measurements of laboratory outcrop column test outlet fluid samples 29

3-11 TOC measurements of laboratory outcrop column test samples 29

Continued . . .

DocuSign Envelope ID: 2FA9A609-C360-4E53-8B28-BE8B77B6994A

LIST OF FIGURES (continued)

3-12 Conductivity measurements of laboratory core column test outlet fluid samples..... 35

3-13 TDS measurements of laboratory core column test samples..... 35

3-14 Sulfate measurements of laboratory core column test samples..... 36

3-15 TOC measurements of laboratory core column test samples..... 37

3-16 BEST project site..... 39

3-17 TDS measurements collected from the BEST E1 well..... 41

3-18 Sulfate measurements collected from the BEST E1 well..... 41

3-19 TOC measurements collected from the BEST E1 well..... 42

4-1 Field numerical model for Inyan Kara Formation..... 44

4-2 Field numerical model showing the distance in miles from the E1 producer well to Rink SWD 1 and SWD 2 – Scenario 1..... 46

4-3 Three production wells with a distance between Rink SWD 1 and SWD 2 of 0.3 miles – Scenario 4..... 47

4-4 Scenario 1 TDS values for BEST E1 producer well during the simulated prediction of 2022 to 2042..... 49

4-5 Scenario 1 formation pressure with only water production from BEST E1 well..... 49

4-6 Scenario 1 total water produced and water rate for BEST E1 well..... 50

4-7 Scenario 4 changes in the water salinity for each of the four production wells..... 51

4-8 Scenario 4 formation pressure with water production from BEST E1 well plus three production wells..... 51

4-9 Scenario 4 formation pressure with water production from BEST E1 well plus three production wells..... 52

4-10 Average salinity values calculated from all the producer wells in accordance with each of the scenarios..... 53

5-1 Typical Bakken LOE breakdowns..... 55

5-2 Connors and others model results replotted according to pressure-affected distance..... 57

Continued . . .

DocuSign Envelope ID: 2FA9A609-C360-4E53-8B28-BE8B77B6994A

LIST OF FIGURES (continued)

5-3 Active water supply wells in North Dakota 60
5-4 Oil and gas decline curves assumed in the TEA 68
5-5 Time profiles for water demand assumed in the TEA..... 69
5-6 SWD profiles assumed in the TEA 70
5-7 NPV cost breakdowns for the nominal-value TEA cases 72
5-8 NPV sensitivity to off-site SWD cost..... 73
5-9 NPV sensitivity to freshwater cost 74
5-10 NPV sensitivity to the ratio of oil wells to GHCR wells..... 75

DocuSign Envelope ID: 2FA9A609-C360-4E53-8B28-BE8B77B6994A

LIST OF TABLES

2-1 Trend in Produced Water Generation in the Bakken Since 2008 7

3-1 Sand Column Test – Pure Quartz Sand Size Distribution 17

3-2 Sand Column Test – Starting Conditions 17

3-3 Sand Column Test – Inyan Kara Synthetic Brine and Bakken Produced Water Analysis 18

3-4 Sand Column Test – XRF Results for Pretest and Posttest Samples from the Inlet and Outlet of the Column 22

3-5 Sand Column Test – XRD Results for Posttest Samples from the Inlet and Outlet of the Column 22

3-6 Outcrop Column Test – Inyan Kara Outcrop Sand Size Distribution 23

3-7 Outcrop Column Test – Starting Conditions 23

3-8 Outcrop Column Test – Inyan Kara Synthetic Brine and Bakken Produced Water Analysis 24

3-9 Outcrop Column Test – XRF Results for Pretest and Posttest Samples from the Inlet and Outlet of the Column 30

3-10 Outcrop Column Test – XRD Results for Pretest and Posttest Samples from the Inlet and Outlet of the Column 30

3-11 Outcrop Column Test – Data for Core Plugs Used in Core Flood Test 32

3-12 Outcrop Column Test – Starting Conditions 32

3-13 Core Column Test – Inyan Kara Synthetic Brine and Bakken Produced Water Analysis 34

4-1 Field Numerical Simulation Scenarios 45

4-2 Summary of the Simulation Results for the Number of Wells and Distance Between Wells 54

4-3 Summary of the Simulation Results When the Water Injection Rate Was Reduced for the Number of Wells and Distance Between Wells 54

5-1 Summary of North Dakota Regulations Relevant for GHCR Produced Water Regulatory Jurisdictions and References 61

Continued . . .

DocuSign Envelope ID: 2FA9A609-C360-4E53-8B28-BE8B77B6994A

LIST OF TABLES (continued)

5-2 Produced Water Ownership and Liability Findings in Six States 63
5-3 TEA Case Details 65
5-4 TEA Considered Costs 66
5-5 Nominal TEA Costs 67
5-6 Economic Evaluation Metrics for the Nominal TEA Case Assumptions 71
5-7 Qualitative Comparison of Cost Drivers Between Local and Central GHCR 76
7-1 Milestones 80

DocuSign Envelope ID: 2FA9A609-C360-4E53-8B28-BE8B77B6994A

DEFINITIONS

Acre-foot – 1 acre-foot equals 325,851 gallons, enough water to cover an acre of land 1 foot deep.

Bakken petroleum system production – Includes both Bakken and Three Forks production.

Barrel (bbl) – One barrel equals 42 gallons.

cm^3 – Cubic centimeter.

Flowback water – Hydraulic fracturing fluid that is produced back out of the wellbore upon completion of the hydraulic fracturing stimulation. Depending on the formation being hydraulically fractured, a percentage of the hydraulic fracturing fluid remains in the formation.

FracFocus – A publicly accessible website where oil and gas production operators can disclose information about ingredients used in hydraulic fracturing fluids at individual wells (fracfocus.org).

Hydraulic fracturing – An oil and gas well stimulation process that typically involves injecting water, sand, and chemicals under high pressure into a formation via the well. This process is intended to create new fractures in the rock as well as increase the size, extent, and connectivity of existing fractures. Hydraulic fracturing is a well stimulation technique used commonly in low-permeability rocks like tight sandstone, shale, and some coal beds to increase oil and/or gas flow to a well from petroleum-bearing rock formations. Application of hydraulic fracturing is one of the cornerstone techniques that results in commercial oil production from the Bakken. Nearly all Bakken petroleum system wells are hydraulically fractured.

Lay-flat hose/pipe – Lay-flat hose is made from polyvinyl chloride (PVC). As the name suggests, one of its key properties is the ability to be laid flat for storage purposes; it is used for the delivery of water in roles such as construction or irrigation when it is not easy to transport water.

Makeup water – Water used for hydraulic fracturing.

Maintenance water – Freshwater injected into a producing well to reduce salt and scale precipitation within the well tubing that can reduce production. Maintenance water is a common practice to prevent the high salt content of Bakken production water from precipitating in wells and inhibiting production.

Mbbl – Thousand barrels.

MMbbl – Million barrels.

Produced water – Includes a combination of flowback water and native formation brine that is coproduced with oil during production. Produced water volumes in this document include flowback and native formation brine.

DocuSign Envelope ID: 2FA9A609-C360-4E53-8B28-BE8B77B6994A

Saltwater disposal (SWD) – A produced water management method of reinjecting produced water back into the subsurface for the purposes of disposal.

Slickwater fracturing – A method of hydrofracturing that involves adding chemicals to water to increase fluid flow. Slickwater fracturing typically uses higher volumes of water compared to gel-based fracturing.

Total dissolved solids (TDS) – A measure of the dissolved combined content of all inorganic and organic substances present in a liquid. TDS concentrations are often reported in part per million (ppm) or milligram per liter (mg/L).

Water cut – The ratio of produced water to the volume of total liquids produced (produced water volume/total liquids volume).

DocuSign Envelope ID: 2FA9A609-C360-4E53-8B28-BE8B77B6994A

SUBTASK 3.2 – PRODUCED WATER MANAGEMENT THROUGH GEOLOGIC HOMOGENIZATION, CONDITIONING, AND REUSE

EXECUTIVE SUMMARY

The Energy & Environmental Research Center (EERC) was awarded a contract by the North Dakota Industrial Commission (NDIC) Oil and Gas Research Program (NDIC No. G-051-101) to conduct a study on the recycling of water used in oil and gas operations, also known as produced water, from oil- and gas-producing regions of North Dakota as directed by Section 19 of North Dakota House Bill 1014. This final report provides a compilation of results of the study, which include regulatory, scientific, technological, and feasibility methods and considerations associated with North Dakota produced water management. The report provides a synopsis of this project's previously submitted produced water assessment report entitled "Produced Water Management and Recycling Options in North Dakota" (Energy & Environmental Research Center, 2020), with updated values provided as appropriate. The report provides the results from the investigation of a novel produced water management strategy, referred to as geologic homogenization, conditioning, and reuse (GHCR), which aims to use a subsurface geologic formation as a natural medium for managing produced water recycling and reuse.

Water management is a significant technical and economic challenge for sustainable oil and gas production, and water volumes are intrinsically linked to oil production volumes. North Dakota oil production rose to over 1.5 million barrels (MMbbl)/day in 2019, and despite a downturn in oil price in early 2020, North Dakota oil production has recovered to 1.1 MMbbl/day as of August 2021. Bakken petroleum system development between 2008 and 2020 has resulted in a nearly fourfold increase in produced water volumes to 642 MMbbl/yr in 2020 after peaking at 740 MMbbl/yr in 2019 and a fivefold increase in saltwater disposal (SWD) volumes to 565 MMbbl/yr in 2020 after a peak of 682 MMbbl/yr in 2019. Produced water and SWD volumes are forecasted to double by 2030.

SWD is the primary method of produced water management used in North Dakota, with approximately 95% of the SWD volume occurring through subsurface injection into sandstones of the Dakota Group (Dakota). Localized pressurization of the Dakota resulting from SWD and projected increases in produced water volumes could impact the economics of North Dakota oil production. As a result, there is an emerging need to pursue alternative produced water management approaches, including recycling and reuse. While produced water recycling is not yet widespread, commercial operators are making strides in overcoming the technical challenges of using high salinity produced water in completion operations (Marathon Oil, 2020). As water management continues to be a key focal point in companies' environmental, social, and governance (ESG) initiatives, focus on water management, including recycling, will likely continue to increase.

Laboratory column testing, field sample collection, geologic modeling and numerical simulation, and techno-economic analysis all indicate that GHCR could feasibly be implemented as a potential water management option. Laboratory column testing and field sample collection indicate that the Inyan Kara sandstone and native formation fluid are capable of homogenizing with the Bakken produced water to a point where the fluid composition appears to stabilize. Extracting that stabilized fluid could be considered homogeneous and capable of providing

DocuSign Envelope ID: 2FA9A609-C360-4E53-8B28-BE8B77B6994A

individual batches of hydraulic fracturing fluid. Numerical simulation results indicate that extraction of fluids from the Inyan Kara in a GHCR implementation scenario is capable of reducing formation pressure, which would help ease localized pressurization of the Inyan Kara and extend the available capacity for nearby existing SWD wells. Economic analysis indicates that there are scenarios where GHCR implementation can be a competitive or even lower-cost option than a conventional water management approach. Site-specific conditions will dictate the economic potential of GHCR, but potentially attractive sites for GHCR implementation will be those that are located above a pressurized zone of the Inyan Kara, need six or more Bakken infill wells, and face high costs for conventional SWD and/or freshwater. Based on the regulatory review, drilling into the Inyan Kara for SWD and to harness as a source water for industrial use have precedent in North Dakota, and a workable regulatory solution for GHCR seems likely. However, restrictions in the state regarding surface storage and transport of produced fluids may limit some activities, which will affect how GHCR could ultimately be implemented.

In summary, this study reveals pursuing GHCR can be a viable approach to water management in North Dakota. The GHCR concept addresses some of the challenges that hinder the more traditional approaches to recycling in the industry. Furthermore, an assessment of the current landscape of water management within the state reveals the ongoing trend of increasing volumes of produced water and SWD. Projections reveal that the volumes of produced water that need to be managed are expected to double over the next decade (Energy & Environmental Research Center, 2020). With the continued development of the Bakken and continuing driving factors related to ESG initiatives, implementing a practice such as GHCR is a feasible approach to adding recycling of produced water to industry within the state.

This subtask was cofunded through the EERC–U.S. Department of Energy Joint Program on Research and Development for Fossil Energy-Related Resources Cooperative Agreement No. DE-FE0024233. Nonfederal funding was provided by the North Dakota Industrial Commission Oil and Gas Research Program.

References

Energy & Environmental Research Center, 2020, Produced water management and recycling options in North Dakota: Final Report for North Dakota Legislative Management Energy Development and Transmission Committee and North Dakota Industrial Commission.

Marathon Oil, 2020, Sustainability report: https://cdn.sanity.io/files/ghcnw9z2/website/91744eb6ef8fbe59505a911c6b8d2e8dd9a537fa.pdf?dl (accessed November 2021).

DocuSign Envelope ID: 2FA9A609-C360-4E53-8B28-BE8B77B6994A

SUBTASK 3.2 – PRODUCED WATER MANAGEMENT THROUGH GEOLOGIC HOMOGENIZATION, CONDITIONING, AND REUSE

1.0 INTRODUCTION

The Energy & Environmental Research Center (EERC) was awarded a contract by the North Dakota Industrial Commission (NDIC) Oil and Gas Research Program (OGRP) (NDIC No. G-051-101) to conduct a study on the recycling of water used in oil and gas operations, also known as produced water, from oil- and gas-producing regions of North Dakota as directed by Section 19 of North Dakota House Bill 1014. This final report provides a compilation of results of the study, including regulatory, scientific, technological, and feasibility methods and considerations associated with North Dakota produced water management. The report provides a synopsis of this project's previously submitted produced water assessment report entitled "Produced Water Management and Recycling Options in North Dakota" (Energy & Environmental Research Center, 2020), with updated values provided as appropriate. The report will provide the results from the investigation into a novel produced water management strategy, referred to as geologic homogenization, conditioning, and reuse (GHCR), which aims to use a subsurface geologic formation as a natural medium for managing produced water recycling and reuse.

Throughout this report, reference will be made to data collected from "Bakken" wells. This is intended to indicate wells within the North Dakota portion of the Bakken petroleum system (Bakken), which includes wells produced from the Three Forks Formation and the Bakken Formation (Figure 1-1). Data shown throughout Section 2.0 will largely focus on the 2008 to 2020 (last complete year of record) time period, with other dates noted when appropriate. In the first half of 2020, the spread of the COVID-19 pandemic led to shutdowns and implementation of restrictions across the world. States enacted a variety of temporary restrictions to limit the gathering of people, which greatly impacted airline and ground travel. Refiners of gasoline and jet fuel are the first and fourth consumers of crude oil in the United States, and the reduction in demand impacted oil prices and crude oil stocks. The market conditions forced operators to reduce production rates to avoid exceeding storage capacity. The unique conditions are reflected in the data sets within Section 2.0, which generally show peak values in 2019 and a reduction in 2020, reflecting the downturns in production. However, looking into 2021, oil prices and production levels have returned to a more "normal" level, so one would expect the water management data sets to bounce back.

Water management represents a significant technical and economic challenge for sustainable oil and gas production, and water volumes are intrinsically linked to oil production. With sustained levels of production in North Dakota, there will be significant demand for freshwater use and produced water management (i.e., formation water and flowback water) and associated disposal. North Dakota surpassed 1.5 million barrels (MMbbl) per day of oil production in November 2019 (North Dakota Department of Mineral Resources, 2020), and despite a downturn in oil price in early 2020, production in the state has recovered to 1.1 MMbbl/day in August 2021 (North Dakota Department of Mineral Resources, 2021). Oil prices appear to have recovered, as oil prices increased from ~$8/bbl (North Dakota light sweet crude) in May 2020 to over $70/bbl in October

DocuSign Envelope ID: 2FA9A609-C360-4E53-8B28-BE8B77B6994A

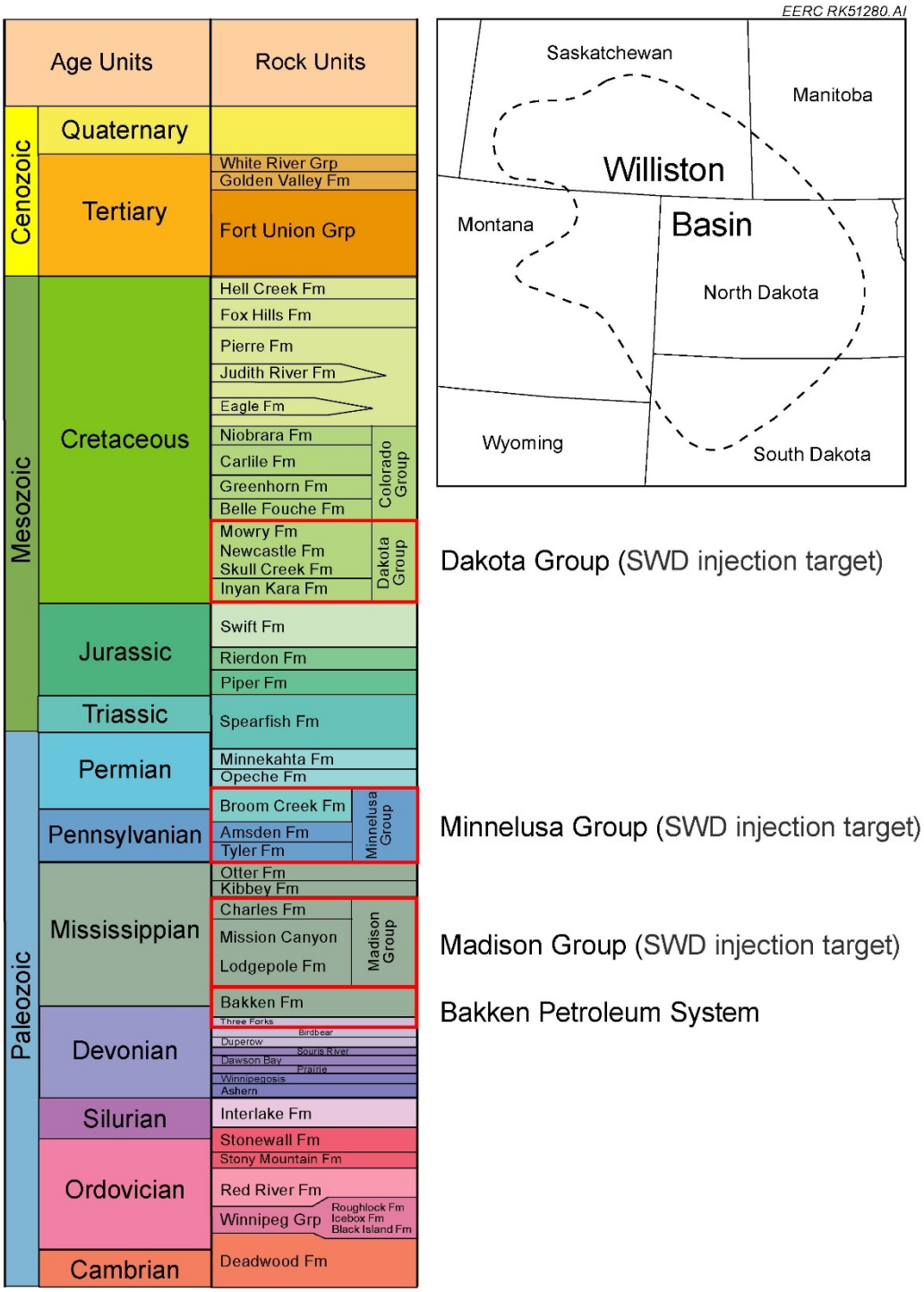


Figure 1-1. North Dakota stratigraphic column (SWD is saltwater disposal).

DocuSign Envelope ID: 2FA9A609-C360-4E53-8B28-BE8B77B6994A

2021. Even accounting for the slowdown, produced water volumes exceeded 600 MMbbl for 2020, which exceeds 2018 volumes. Furthermore, using conservative projections, produced water volumes are forecasted to more than double by 2030 (Energy & Environmental Research Center, 2020).

The EERC has been investigating the GHCR concept, which uses a subsurface geologic formation as a natural medium for produced water management. This concept takes advantage of the hypothesized natural processes occurring in the subsurface (e.g., filtering, mixing, diluting, etc.) and extracts the water at some distance from a disposal well. GHCR uses existing oil and gas industry practices by using an extraction well to produce a mixture of native formation water that is mixed with produced water from SWD operations. If viable, the GHCR concept could address recycling challenges by producing a better, more consistent quality fluid while also providing subsurface storage that eliminates some of the environmental risks behind water handling required for traditional recycling methods. The investigation into the GHCR concept and accompanying results are described in this report.

2.0 BAKKEN WATER MANAGEMENT

Water management within the oil and gas industry in North Dakota can be broken into three general components: freshwater use, produced water, and SWD. These three components are all closely related, and they all generally follow the same trends as oil production, in this case production primarily from the Bakken. As oil production increases, freshwater consumption trends increase, as more freshwater is used for drilling, completion, and well maintenance activities. Likewise, increased oil production brings increased volumes of produced water, which includes flowback (water from stimulation activity) and formation water (primarily from the Bakken). Finally, as produced water volumes increase, that water needs to be disposed of, which, in North Dakota, primarily means increased volumes of SWD.

Bakken water management was discussed in greater detail in the EERC's report entitled "Produced Water Management and Recycling Options in North Dakota" (Energy & Environmental Research Center, 2020), and Section 2.0 will provide a short review, taken from the EERC report, of Bakken water management, with some relevant updates to the data provided (i.e., values updated to include 2020, where appropriate).

2.1 Freshwater Trends

Freshwater is used in the oil and gas industry in a variety of applications. Water is a primary component of drilling mud, which lubricates and cools the drill bit and removes drill cuttings from the wellbore. In unconventional well stimulations, freshwater mixed with chemicals is used to hydraulically fracture and stimulate a well. Freshwater is used to maintain well operation. This "maintenance water" typically transports chemicals down the annulus of a well to treat downhole components for scaling, corrosion, and other undesirable operational conditions. The nearly saturated properties of Bakken produced water can require dilution from maintenance water to prevent precipitation of salts in production tubing and surface equipment. While not used on every producing well, this technique, known as well maintenance, brine dilution, desalting, or well

DocuSign Envelope ID: 2FA9A609-C360-4E53-8B28-BE8B77B6994A

flushing, typically uses 15–50 bbl/well/day, with the volumes per well depending on the local conditions (e.g., total dissolved solids [TDS] of formation fluids, temperature drop in the wellbore) of the individual well.

The vast expansion of water supply and associated handling infrastructure in the Bakken region has helped industry meet water demand for oil and gas development. Information on changes that have occurred in water use as a result of oil and gas development in North Dakota is derived from reported industrial water use from the North Dakota State Water Commission (NDSWC) and reported water use for hydraulic activities from Enverus (Drilling Info) and FracFocus. Since 2008, annual oil and gas-related water use in North Dakota has increased from just over 13.5 MMbbl (~1740 acre-feet) in 2008 to more than 290 MMbbl (~37,380 acre-feet) in 2019 before dropping down to 140 MMbbl (~18,000 acre-feet) in 2020 (Figure 2-1).

Improved stimulation techniques, increase in lateral lengths, and the number of fracture treatment stages have led to an increase in the volumes of fluid (freshwater mixed with fracturing chemicals) injected per well during a stimulation from about 15,000 bbl per well (~1.9 acre-feet per well) in 2008 to about 215,000 bbl per well (~25.8 acre-feet per well) in 2020 (Figure 2-1), as derived from data available from over 14,600 wells completed over that time period. Over the last 5 years (2016–2020), freshwater use for hydraulic fracturing is about 80% of the oil and gas industry's total freshwater use volumes, based on NDSWC-reported use and FracFocus- and Enverus-reported clean water use. Contributing to water demand are the success and emerging prevalence of slickwater stimulations that require pumping 3 to 4 times the volume of water at a higher injection rate than previous gel-based stimulations.

Freshwater use on a per-well basis has grown substantially over the last decade. Trends indicate that while water use has begun to stabilize, freshwater use will continue to remain high. Total water use during the next several years will be driven by number of producing wells completed and increasing water use per well. Sustained freshwater use directly contributes to and is proportional to flowback, which is one of several contributors to produced water volumes. Increased water volumes impact the economics of oil production through water supply and water disposal costs.

While freshwater use volumes for the oil and gas industry have grown over the recent decade, the industry's share of total freshwater use when compared to all water users is relatively small. From 2016 to 2020, oil-related industrial water use is 1.18 billion bbl (~151,000 acre-feet), representing 9% of North Dakota's total freshwater use of 13.8 billion bbl (~1.78 million acre-feet). As shown in Figure 2-2, oil industry water use trails volumes used for irrigation, municipal, and power generation uses.

DocuSign Envelope ID: 2FA9A609-C360-4E53-8B28-BE8B77B6994A

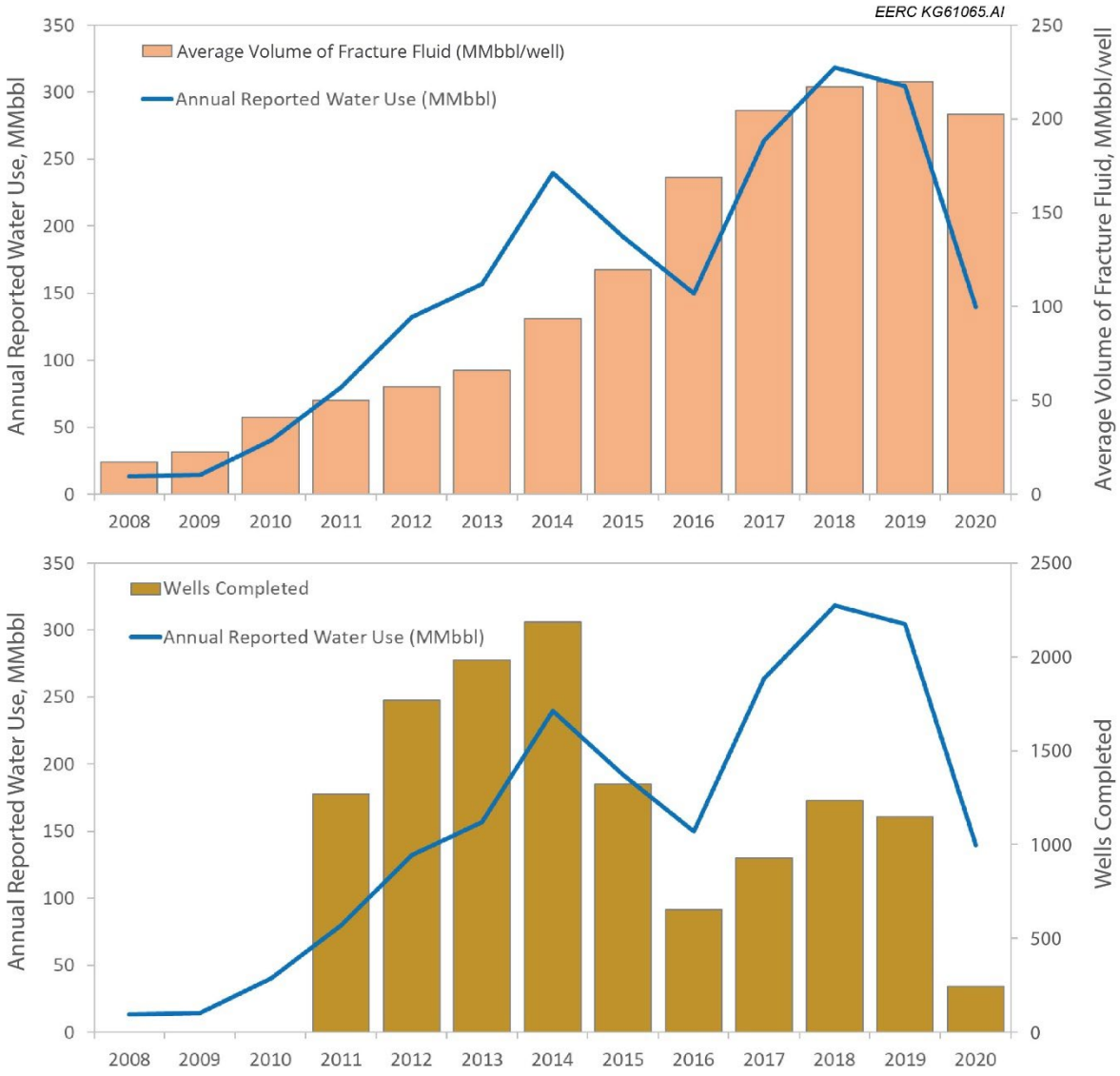


Figure 2-1. Plot showing industrial water use in MMbbl from permitted sites for oil-related activities (left *y*-axis) from 2008 through 2020 as compared to the average fracture fluid volume per well (top panel, MMbbl, right *y*-axis) and the wells completed in each year (bottom panel, right *y*-axis) (data source: NDSWC and Enverus).

DocuSign Envelope ID: 2FA9A609-C360-4E53-8B28-BE8B77B6994A

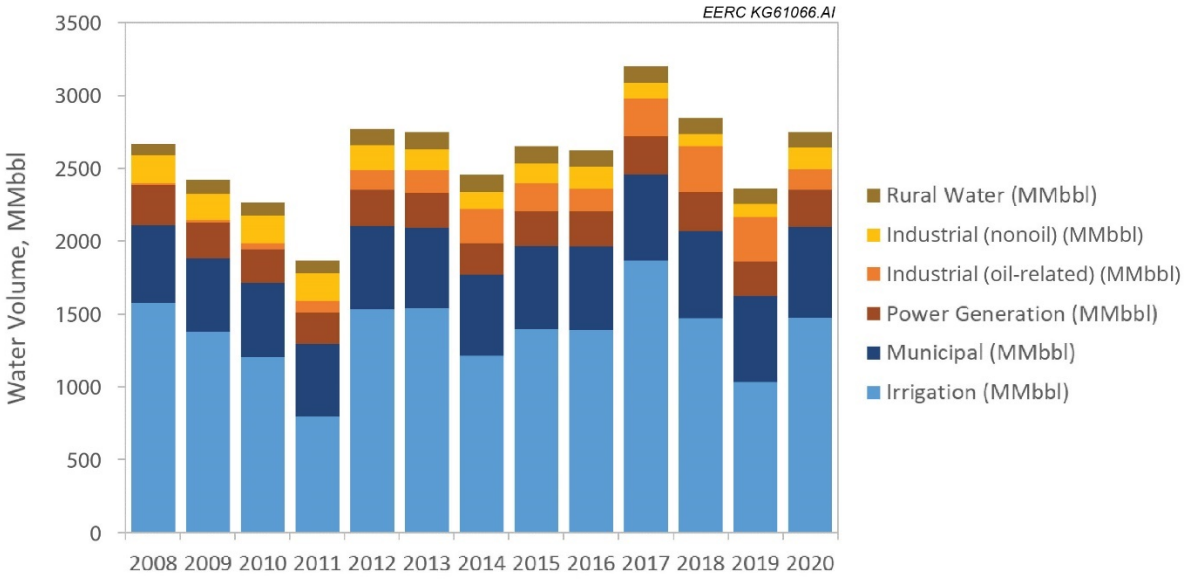


Figure 2-2. Freshwater use 2008–2020 by water use (data source: NDSWC).

2.2 Bakken Produced Water Trends

Produced water refers to brine that is coproduced with oil. Produced water volumes presented in this document include both water that was injected during well stimulation (i.e., hydraulic fracturing) and flows back during production, also referred to as flowback water, and native formation brine that is coproduced with oil. The volumes of produced water vary by geologic formation and location, and terms such as water cut describe the ratio of water produced compared to the volume of fluids produced (i.e., water and oil). Bakken production is typically associated with 1–1.5 bbl of produced water per bbl of oil (water cut of ~50%). Bakken produced water is highly saline, with TDS ranging up to 350,000 mg/L. As a point of comparison, seawater is approximately 35,000 mg/L TDS, or 10 times less salty than typical Bakken brine.

Produced water volumes for the state of North Dakota have increased from 150 MMbbl/yr in 2008 to 642 MMbbl/yr in 2020 after peaking at 740 MMbbl/yr in 2019. The volumes of water produced from the Bakken increased from 6.4 MMbbl/yr in 2008 to 519.7 MMbbl/yr in 2020 (Table 2-1). While the increase is partially attributable to a greater number of producing wells, the average volume of water produced per well is also increasing.

As annual oil production increases, trends suggest that annual water production will increase as well, and in some areas at an even greater rate with higher water cuts on a per-well basis. Increased water production volumes will be associated with increased water management costs, impacting the economics of oil production.

DocuSign Envelope ID: 2FA9A609-C360-4E53-8B28-BE8B77B6994A

Table 2-1. Trend in Produced Water Generation in the Bakken Since 2008*

Year	Total Producing Bakken Wells	Total Produced Water, MMbbl	Average Annual Produced Water per Well, bbl
2008	887	6.4	7169
2009	1356	12.2	8971
2010	2136	32.6	15,282
2011	3387	64.1	18,934
2012	5184	135.3	26,092
2013	7151	194.1	27,138
2014	9326	283.9	30,438
2015	10,777	337.3	31,297
2016	11,425	313.8	27,464
2017	12,368	370.0	29,914
2018	13,575	493.1	36,325
2019	14,762	599.4	40,606
2020	15,073	519.7	34,481

* North Dakota Industrial Commission (2021).

2.3 Bakken Produced Water Chemistry

An essential component in the advancement of water recycling and reuse opportunities in North Dakota is the understanding of produced water chemistry. Publicly available data indicate that the water chemistry varies considerably throughout the Williston Basin, making water treatment options challenging and may require varying treatment approaches. Bakken produced water is regarded as highly saline, with TDS concentrations generally on the order of 300,000 mg/L and levels approaching 350,000 mg/L not uncommon. According to a study by the U.S. Bureau of Reclamation and Colorado School of Mines comparing produced water from basins across the western United States, the Williston Basin exhibits the most geographical variance by state of any of the basins studied (Benko, 2008).

To gain a better understanding of Bakken water quality and variability, produced water samples were taken, during this project, from various SWD sites throughout the Williston Basin. TDS levels ranged from 242,000 to 340,000 mg/L (Figure 2-3). For comparison, the average salinity of ocean water is 35,000 mg/L. The majority of the TDS content in Bakken produced water is from high sodium and chloride concentrations; however, other constituents are also present in significant quantities, such as calcium, sulfate, and magnesium. Calcium content has been reported at ranges between 7540 and 13,500 mg/L, with magnesium, potassium, strontium, and sulfate all reported in concentrations of 1000 ppm or greater (Stepan and others, 2010). This was confirmed with samples taken during this project that show calcium content ranges from 13,200 to 22,600 mg/L. Magnesium samples ranged from about 1000 to 1500 mg/L, while potassium ranged from 4500 to 9700 mg/L. While not impossible to treat, the high-TDS waters produced from the Bakken are challenging to handle when developing economical water treatment and reuse options. Figure 2-4 presents the applicability of desalination technologies over a range of TDS

DocuSign Envelope ID: 2FA9A609-C360-4E53-8B28-BE8B77B6994A

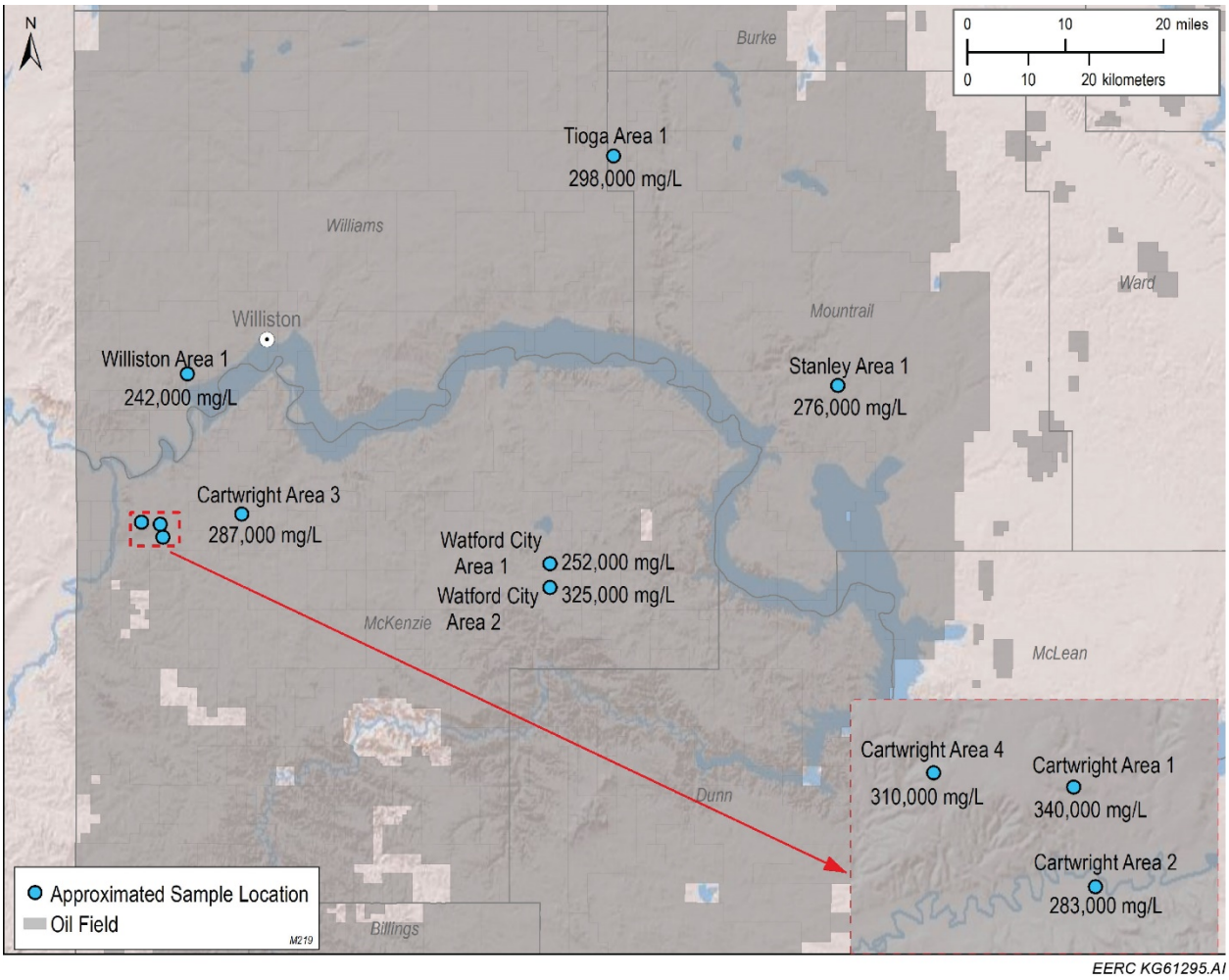


Figure 2-3. Approximate locations of Bakken produced water samples collected during this project.

concentrations. Traditional desalination technologies such as reverse osmosis (RO) typically are capable of treating waters with TDS levels up to 40,000 mg/L. Thermal treatment technologies such as mechanical vapor recompression (MVR) are more applicable to treating high-TDS waters, such as those found in certain Bakken flowback situations, particularly if MVR is coupled with pretreatment to reduce the concentration of divalent ions typically associated with scaling. Even with pretreatment, the very high sodium chloride in Bakken produced water requires special consideration for treatment components to prevent wellbore corrosion. Expensive alloys or metals such as titanium that are resistant to corrosion and chloride stress cracking will be required for high-temperature thermal recovery processes treating chloride-rich Bakken flowback water (Stepan and others, 2010).

DocuSign Envelope ID: 2FA9A609-C360-4E53-8B28-BE8B77B6994A

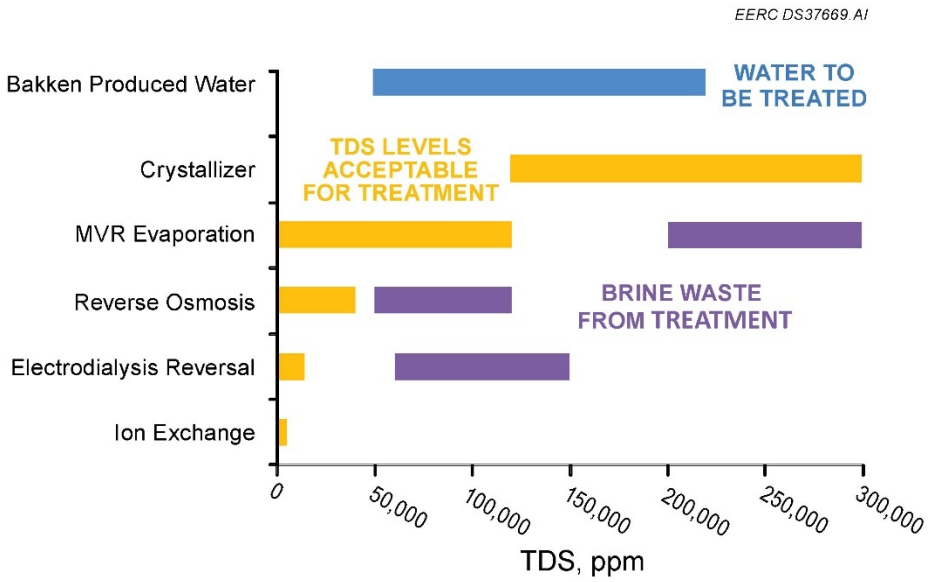


Figure 2-4. Applicability of various desalination technologies.

In addition to high salt content, Bakken water typically contains various metals and other elements (e.g., barium, iron, lithium, etc.) (Stepan and others, 2010) that could be of particular interest for critical mineral recovery and extraction. To the EERC's knowledge, no comprehensive studies have been conducted to systematically identify high-value materials (HVMs) within Williston Basin brines produced from North Dakota, although a limited number of brine analyses performed by the EERC as well as brine characterization data collected by the U.S. Geological Survey (USGS) provide enough compelling data to suggest that a more targeted evaluation of HVMs in the North Dakota portion of the Williston Basin may be warranted. Analysis of lithium in Bakken produced water samples collected and analyzed shows that there are some locations where lithium concentrations are near or above 100 mg/L (what is considered by some to be an economically recoverable concentration). Samples tested had a range of 57–113 mg/L (see Appendix A for full analyses), with most of the higher concentrations found toward the western side of the Williston Basin near the Montana border. Elevated concentrations of iron and barium were also observed in this area. Thus, while HVM concentrations may not be elevated across the entire basin, there are locations that may warrant further investigation.

Recycling and reuse applications tolerant of high-TDS levels such as hydraulic fracture makeup water are the most practical applications for Bakken produced water. Treatment options that target low-TDS levels such as domestic or agricultural use are logistically challenged at industrial scales for high-TDS fluids that contain >30% high-salinity solids that would need to be subsequently disposed of. Further treatment and use for agricultural, domestic, or municipal uses are not recommended or likely to be tolerated until the health effects of all chemical constraints are understood. Therefore, in-industry recycling and reuse applications or mineral recovery applications are likely the most practical and viable options in the near term.

DocuSign Envelope ID: 2FA9A609-C360-4E53-8B28-BE8B77B6994A

2.4 SWD Trends

Just as freshwater supply locations have increased as a result of North Dakota's expanding oil and gas industry, so has the number of disposal wells, commonly referred to as SWD wells. While SWD wells are used to dispose of maintenance and production water for conventional oil and gas production, the majority of the SWD wells in North Dakota are a result of Bakken production. While most produced water is disposed of through SWD wells, some produced water is recycled and used in secondary recovery (e.g., waterflood) or during drilling and completion operations. Available data do not provide for specific use volumes; however, there will be a difference in total SWD volumes and produced water volumes reflected in the data. Figure 2-5 shows the total volume of fluid injected into North Dakota SWD wells by year since 1956, illustrating the dramatic and exponential increase in SWD volumes as a result of Bakken development. The primary injection zones for SWD are formations of the Dakota Group, the Minnelusa Group, and the Madison Group (Figures 1-1 and 2-6). SWD volumes for the Madison and Minnelusa have remained relatively steady, as shown in Figure 2-6. Over 95% of SWD in North Dakota is going into the Dakota, primarily into the Inyan Kara Formation, the Dakota's lowermost sandstone interval. The Inyan Kara is an ideal target for SWD, with proper confining zones and a long history of successful operation. Since 1956, nearly 7.0 billion bbl of produced water has been injected into North Dakota SWD wells (North Dakota Industrial Commission, 2021). Forecasts indicate that by 2030, 1.96 to 2.69 billion bbl of produced water will need to be managed annually (Energy & Environmental Research Center, 2020).

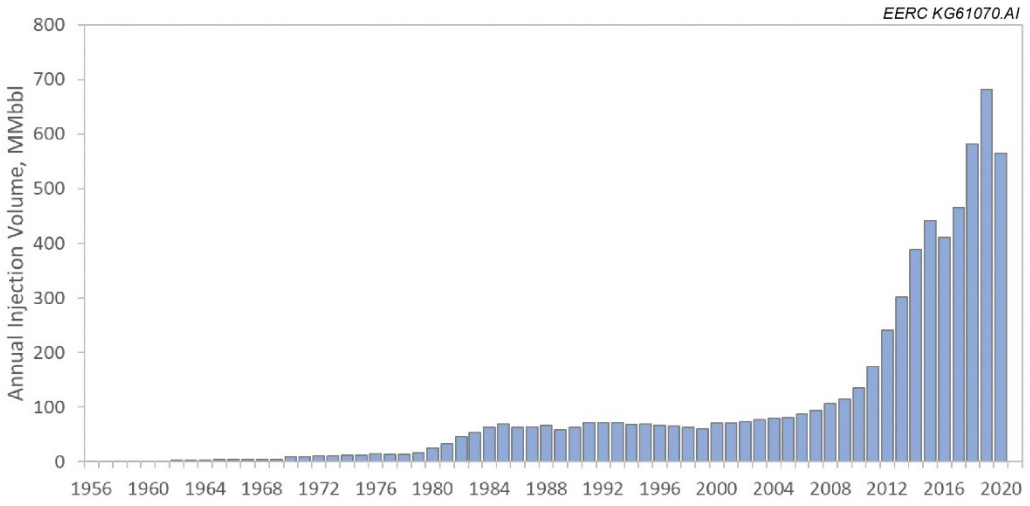


Figure 2-5. Volumes of all water injected into North Dakota SWD wells since 1956 (data source: North Dakota Industrial Commission, 2021).

DocuSign Envelope ID: 2FA9A609-C360-4E53-8B28-BE8B77B6994A

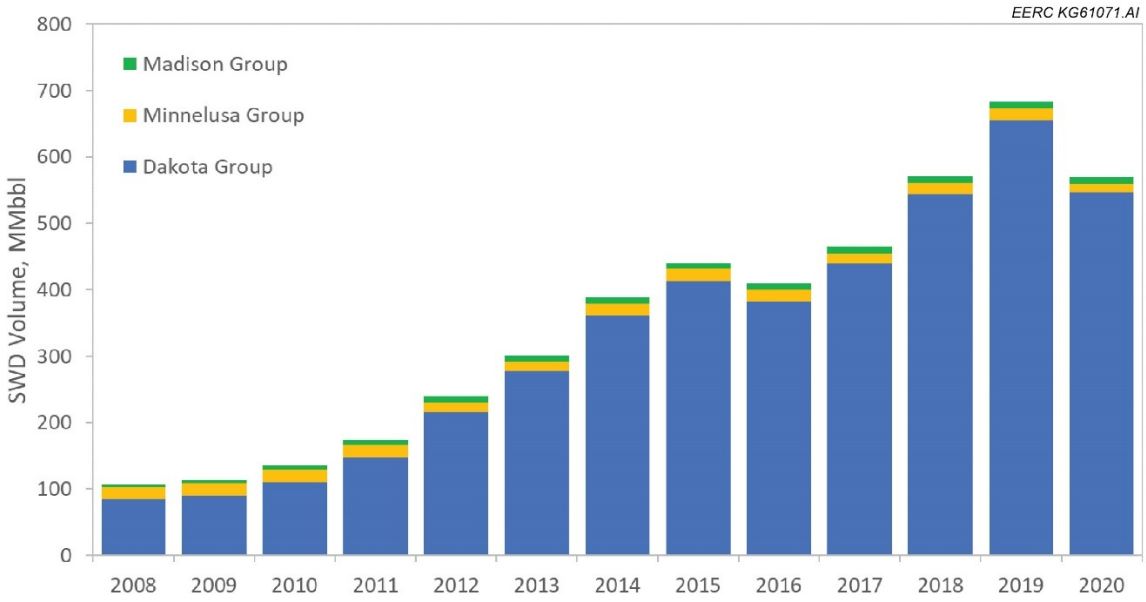


Figure 2-6. Annual SWD injection volume by geologic group from 2008 to 2020 (data source: North Dakota Industrial Commission, 2021).

In addition to SWD well performance, localized areas of pressurization of the Dakota's Inyan Kara Formation in proximity to higher-density areas of SWD wells is resulting in operational changes and added expense for Bakken operators when drilling new production wells. Operators in the region apply the best industry practices when drilling through these pressurized zones. A higher-density drilling fluid is needed when drilling through areas with increased formation pressure.

In some cases, operators need to install an additional casing string (Basu and others, 2019) to manage pressure while drilling by mechanically isolating the Inyan Kara, as illustrated in Figure 2-7. Installation of the additional casing string is reported to increase the impacted cost of Bakken wells by about $500,000–$750,000. At a potential 10%–15% increase in well cost, the additional casing string becomes a factor for operators when considering capital placement, economics, and profitability (Personal Communication, Bakken producers, 2020).

DocuSign Envelope ID: 2FA9A609-C360-4E53-8B28-BE8B77B6994A

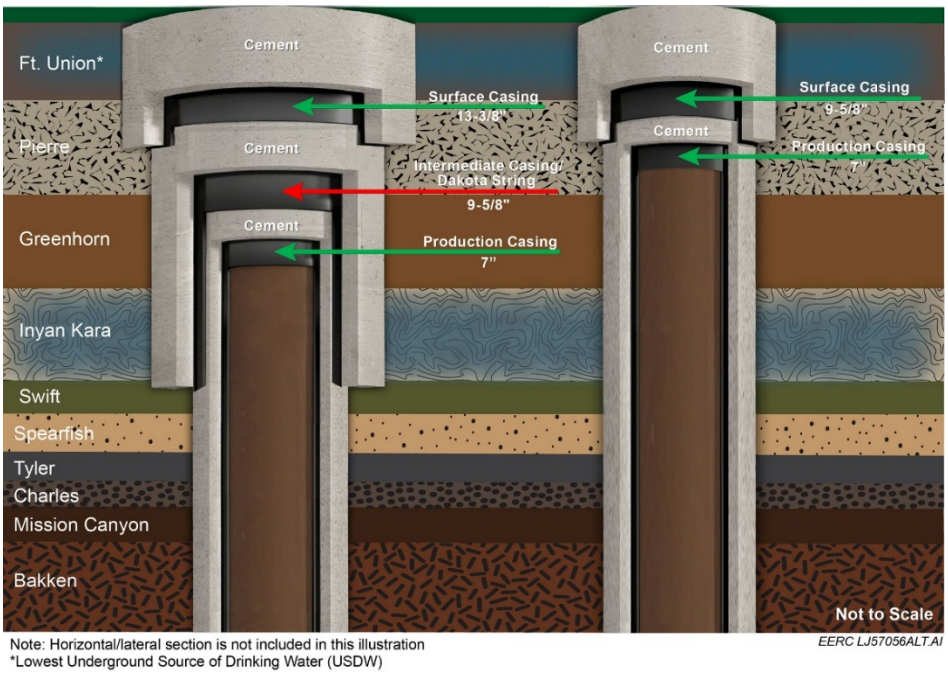


Figure 2-7. Illustrative diagram for a well using an intermediate casing string, or "Dakota string" (left wellbore), and a typical well diagram without the addition of a Dakota string (right wellbore).

2.5 Produced Water Recycling and Reuse Discussion

The general trend associated with oil- and gas-related produced water management in North Dakota has been a sustained increase of freshwater use, increasing water production, and increasing SWD volumes. Tremendous volumes of water are being managed in the region, and the continued trend of increasing volumes may present challenges for SWD into the Inyan Kara Formation. The current approach to water management provides the most cost-efficient means of disposal and limits the amount of handling/processing of produced water, thereby reducing the risk of spills. The Inyan Kara's geographic extent, relatively shallow depth, proper confining zones, and injectability provide a SWD target that is suitable across the entire Bakken producing region in the state. However, should current approaches to SWD in the Inyan Kara ever become technically or economically challenged, then alternative produced water management options for North Dakota may be desirable.

One target for reuse of produced water is as makeup water for hydraulic fracturing fluids. Water volumes for hydraulic fracturing are averaging 200,000 bbl/well for a single well stimulation, resulting in significant logistical hurdles for use to aggregate temporary storage of those volumes of water on-site for a single well stimulation. In regions where this type of reuse is occurring, operators are using a hybrid approach where 50%–70% of the makeup water volume is produced water, while the remaining volumes are made up of freshwater to in part help alleviate the storage challenge.

DocuSign Envelope ID: 2FA9A609-C360-4E53-8B28-BE8B77B6994A

Safely handling high-TDS produced water for recycling poses a risk if not properly contained. Recycling of produced water may result in generation and disposal of technologically enhanced naturally occurring radioactive material (TENORM) and other by-products of the recycling process (e.g., salts, metals). This occurs as solids settle in tanks and concentrate NORM, and if these solids are classified as TENORM, they require compliant disposal with the associated costs and regulations.

While produced water recycling is not yet widespread in North Dakota, commercial operators are making strides in overcoming the technical and regulatory challenges of using high-salinity produced water in completion operations (Marathon Oil, 2020). Despite some of the aforementioned challenges, oil and gas operators are increasingly driven by environmental, social, and governance (ESG) considerations. According to the United Nations Principles for Responsible Investment, ESG integration is defined as "the explicit and systematic inclusion of ESG issues in investment analysis and investment decisions." Put another way, ESG integration is the analysis of all material factors in investment analysis and investment decisions, including environmental, social, and governance (ESG) factors" (United Nations Principles for Responsible Investment, 2018).

While ESG has been around for a while, the topic has been of increasing discussion in recent years. According to an article in Hart Energy's October 2021 Energy ESG Report, many of the drivers regarding ESG in the United States thus far have come from the investment community. What started out as a push from social impact investors and institutional investors has now moved to the mainstream investment community, with the impacts to the oil and gas community being profound. In the last 2 years, ESG penetration in the sector has gone from awareness to all-out disclosure by a significant percentage of publicly traded companies (Hart Energy October 2021 Energy ESG, 2021). While disclosures are currently voluntary (this can likely change pending proposed rules by the Securities and Exchange Commission regarding climate risk disclosure) and vary depending on the company, many companies report voluntary disclosure topics based on the Sustainability Accounting Standards Board (SASB) Index. One of the main topics in the SASB Index regarding the environmental aspect of ESG is water management. This includes items such as the amount of freshwater used, the volume of produced water generated, and percent injected via Class II injection well as well as the amount recycled for use in other wells (Sustainability Accounting Standards Board, 2018).

Given the large amounts of freshwater typically required for oil and gas operations and SASB disclosure metrics, this has become a major focal point for companies when it comes to ESG reporting. For example, some companies track their water intensity, which is defined as the barrels of water used in completions per barrels of oil equivalent produced (Continental Resources, 2020). This gives the ability for companies to track their reduction in freshwater use year over year. As companies are looking to reduce their freshwater use, they are also recognizing the need for innovations that enable the recycling and reuse of flowback and production water for future operations. This is currently being done, with some fracture companies creating custom fluid chemistry such as friction reducers that is compatible with the highly saline production water, allowing operators to use that recycled water for future fracture jobs, thereby displacing freshwater usage with water recycling and reducing the pressure on local freshwater sources (Liberty, 2020). While the variability in water chemistry can be challenging to developing the proper fluid

DocuSign Envelope ID: 2FA9A609-C360-4E53-8B28-BE8B77B6994A

chemistry needed for produced water recycling, a concept like GHCR could result in a more consistent water chemistry and more favorable economics, enabling increased use.

2.6 Produced Water Recycling Approach—GHCR Concept

A component of the NDIC OGRP (NDIC Contract G-051-101) project cofunded by the U.S. Department of Energy (DOE) Fossil Energy (FE) Program awarded to the EERC includes a techno-economic assessment of using a geologic formation to treat produced water for beneficial reuse applications through the GHCR approach. GHCR is a novel produced water management approach that uses a subsurface geologic formation as a natural medium for managing produced water recycling and reuse. Produced water is already injected into the subsurface via SWD wells (Figure 2-8), and the concept seeks to take advantage of the hypothesized natural processes occurring in the subsurface (e.g., filtering, mixing, diluting, etc.) and to extract the water at some distance from the disposal well (Figure 2-9). The extracted water, which is presumably of significantly higher quality (i.e., lower TDS) than the injected produced water, is hypothesized to be more conducive for use in hydraulic fracturing makeup water or other beneficial uses or subsequent treatment, thus reducing oil and gas industry freshwater demand. Additionally, the extraction of water will slow the pressurization of SWD targets, thus extending the life of disposal wells and reducing the need for additional disposal wells in the future.

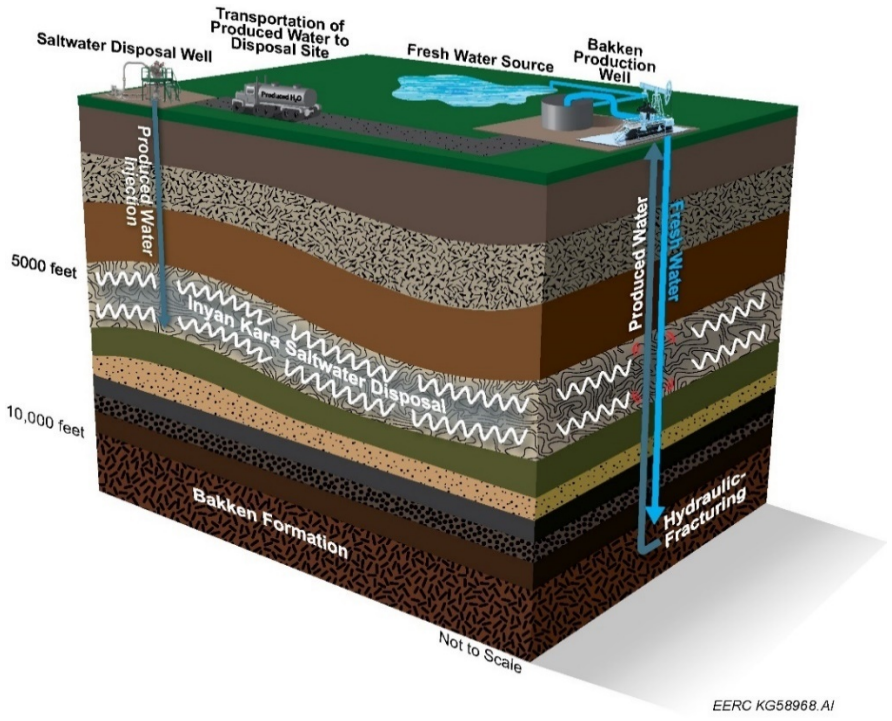


Figure 2-8. Traditional approach to water management.

DocuSign Envelope ID: 2FA9A609-C360-4E53-8B28-BE8B77B6994A

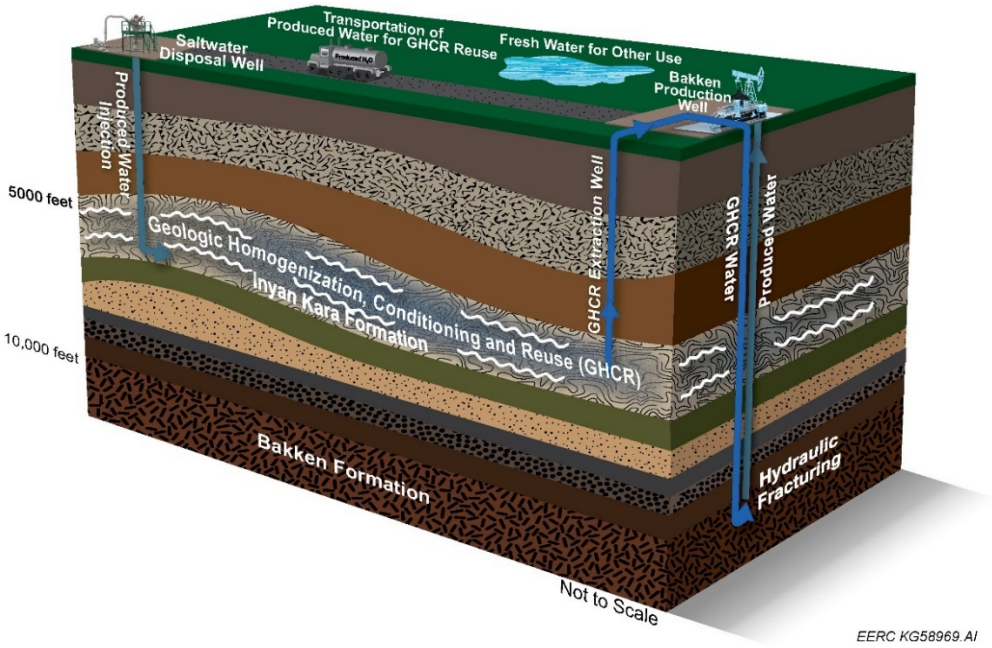


Figure 2-9. GHCR concept involving the addition of an extraction well and utilizing that water as hydraulic fracturing makeup water for Bakken wells.

The GHCR concept could address many of the recycling challenges outlined in the previous section, and the results of the investigation are reported in the subsequent sections of this report. By utilizing existing SWD infrastructure and the geologic formation as a storage container, the concept may provide a starting point to address some economic and environmental challenges surrounding the concept of recycling. This project investigated the techno-economic viability and potential benefits of the GHCR concept including the following:

- By adding an extraction well to existing SWD sites, the implementation of GHCR could be accomplished at a lower price point than installing traditional water-processing/recycling facilities.

- By using the geologic formation in lieu of surface storage and extracting water on demand, the potential for produced water spills is greatly reduced and the approach provides virtually unlimited on-demand storage/supply capacity.

- By using the geologic formation as a natural treatment, GHCR extracted water may have fewer problem constituents and greater consistency in composition, thus reducing or eliminating waste handling.

- Withdrawing water from the formation would slow pressurization.

The EERC, through the State Energy Research Center (SERC), has investigated subsurface pressure management while drilling using temporary brine extraction. The project (Connors and

DocuSign Envelope ID: 2FA9A609-C360-4E53-8B28-BE8B77B6994A

others, 2020) modeled subsurface pressures between a SWD well and an extraction well in the Dakota. Results indicated that brine extraction could theoretically be used to temporarily reduce Dakota pressure while drilling to avoid the need to install a Dakota water string. Results indicated that an extraction well 10,000 feet from a SWD well, temporarily extracting brine between 5000 and 25,000 bbl/day (bpd) and using or reinjecting off-site, could temporarily reduce Dakota pressure to allow drilling a Bakken well(s) in an area impacted by elevated pressure without requiring an intermediate water string.

3.0 LABORATORY AND FIELD EVALUATION OF GHCR CONCEPT

Laboratory column testing and fluid sampling at a commercial SWD site with an associated extraction well helped evaluate the physical processes and efficacy of the GHCR concept. The goal of the testing was to better understand the physical processes that would likely occur in a commercial setting where the GHCR concept would be implemented. The results from the laboratory testing and fluid sampling were used to inform the geologic modeling and numerical simulation efforts described in Section 4.0. The laboratory column testing consisted of three separate column tests, with each designed to understand the interactions occurring between native Inyan Kara Formation chemistry water, Bakken produced water, and Inyan Kara Formation (rock) material. The three column tests are described in Section 3.1. The fluid testing at a commercial SWD site is described in Section 3.2.

3.1 Laboratory Column Testing

The laboratory column testing was designed to replicate Bakken SWD into the Inyan Kara Formation to understand the natural processes that would occur in the subsurface. The column testing aimed to gain insight into the potential water chemistry that could be expected with water extracted from the Inyan Kara Formation if the GHCR concept was implemented. The laboratory column testing was separated into three separate tests, as described in Sections 3.1.1, 3.1.2, and 3.1.3, and were referred to as the sand column, outcrop column, and core column, respectively. The sand and outcrop tests were run in the same system utilizing a glass column. The core column was run in a separate specialized core holder but utilizing the same enclosures and sampling hardware. Column flow rates were chosen to target a 36-day residence time based on minimum residence time observed in the geologic model representing the brine extraction and storage test (BEST) field location discussed in Section 3.2. A temperature of 170°F based on field measurements for the Inyan Kara Formation was initially targeted in the column but had to be reduced to 150°F because of excessive evaporation and gas production in the column. More detailed schematics and preparation methods for both systems are provided in Appendix B.

3.1.1 Sand Column Test

The first laboratory column test was conducted to evaluate injected Bakken produced water with synthetic Inyan Kara Formation water and a quartz sand to replicate Inyan Kara sand filtering. This initial column test acted as a control experiment to evaluate the filtration efficacy of the sand and any reactions that occur through bacteria development in the produced water/formation matrix.

DocuSign Envelope ID: 2FA9A609-C360-4E53-8B28-BE8B77B6994A

The size distribution of the sand is shown in Table 3-1. The size distribution is predominantly larger than 70 mesh (66.5% mass). Table 3-2 shows the initial test conditions of the column using packed and saturated quartz sand. Throughout testing with quartz sand, the flow properties of the column were not impacted significantly.

Table 3-1. Sand Column Test – Pure Quartz Sand Size Distribution

Screen Size (U.S. mesh)	Retained, %
50	33.0
70	33.5
80	16.6
100	10.4
120	3.9
140	1.2
200	0.7
Pan	0.8
Total	100.0

Table 3-2. Sand Column Test – Starting Conditions

Temperature, °F	150
Injection Pressure, psig	1–2
Target Flow Rate, mL/min	0.135
Permeability, mD	6473
Sand Mass, kg	35.424
Sand Density, g/cm^3	2.65
Sand Volume, cm^3	13,368
Column Volume, cm^3	19,635
Sand Volume, %	68
Column Porosity, %	32

Prior to injection of Bakken produced water, the sand column was saturated with synthetic Inyan Kara brine prepared in the laboratory. Both the produced water and synthetic brine were analyzed for key parameters prior to testing, and results are presented in Table 3-3. Injection began on September 23, 2020, and ran through February 16, 2021, for a total of 146 days. The injection rate was set to achieve a flow-through residence time of 36 days to mimic model estimates of field conditions for Bakken produced water being injected into, migrating through, and subsequently extracted from the Inyan Kara Formation at the BEST field site (described in Section 3.2). (Figure 4-20 in the modeling section can be referenced for injection interruptions and rates.) Interruptions and flow reductions were occasionally observed due to system issues such as damaged tubing or clogs.

DocuSign Envelope ID: 2FA9A609-C360-4E53-8B28-BE8B77B6994A

Table 3-3. Sand Column Test – Inyan Kara Synthetic Brine and Bakken Produced Water Analysis

	Inyan Kara Brine	Bakken Produced Water
Date	July 1, 2020	July 16, 2020
pH	6.78	5.66
Conductivity, mS/cm	19.8	246
Density, g/mL	1	1.2
TDS, mg/L	11,400	325,000
Alkalinity, HCO_3, mg/L	NA[1]	109
Sodium, mg/L	4000	93,500
Potassium, mg/L	120	9700
Calcium, mg/L	283	21,200
Magnesium, mg/L	14.6	1140
Strontium, mg/L	NA	1810
Chloride, mg/L	6670	195,000
Bromide, mg/L	NA	966
Sulfate, mg/L	283	209
Iron, mg/L	NA	127
Boron, mg/L	0	580
Barium, mg/L	NA	41.9
Lithium, mg/L	NA	94.6
Manganese, mg/L	NA	15.3
Total Organic Carbon (TOC), mg/L	NA	145
Total Suspended Solids (TSS), mg/L	<10	185

[1] Not analyzed – minor and trace components were not included in the synthetic brine and therefore not analyzed.

Brine samples exiting the column were collected daily, with the exception of weekends. The column was allowed to run continuously over the weekend, and fluid was collected on the next business day. Fluid conductivity analysis was performed on each collected sample, and a complete set of parameters were analyzed for eight samples collected periodically throughout the test. The parameters included pH, TDS, density, sodium, potassium, calcium, magnesium, strontium, chloride, bromide, sulfate, iron, boron, barium, lithium, manganese, zinc, TSS, and TOC. Testing concluded when the concentrations of the parameters evaluated had reached a plateau. Water chemistry results are presented in Appendix A.

DocuSign Envelope ID: 2FA9A609-C360-4E53-8B28-BE8B77B6994A

Conductivity data indicated breakthrough of injected Bakken produced water occurred on Day 18 at the column exit as evidenced by the increase in conductivity (Figure 3-1). Initial observations indicated the GHCR test column was effectively filtering TSS as evidenced by the consistently low (ranging from <10 to 50 mg/L) TSS in the samples collected at the exit of the column relative to the 180 mg/L TSS measured for the Bakken produced water being injected into the column (Figure 3-2). This TSS reduction provides evidence the packing of the column was sufficient and that there were no high-permeability preferential flow pathways present in the column that could contribute to nonrepresentative results.

With the exception of sulfate (Figure 3-3), other major analytes (Appendix A, Figures A-1–A-5) trended with conductivity and TDS (Figure 3-4), providing data on the volumetric (pore-volume basis) efficacy of the GHCR process relative to flow rate. The TDS, conductivity, and sulfate values were used to calibrate reservoir simulation models described in Section 4.0. TOC increased over time but at a lower rate than the other analytes (Figure 3-5). The observed trends in sulfate (Figure 3-3) and TOC are potentially indicative of bacterial activity, and select samples were evaluated for sulfate-reducing bacteria. BART (biological activity reaction test) biodetector test kits were used to evaluate whether sulfate- reducing bacteria were present in samples collected from the laboratory column test. The five samples tested were a blank (deionized water), the synthetic Inyan Kara brine, and three column outlet samples collected at 1-month increments. No presence of these bacteria was found, indicating that sulfate-reducing bacteria were not likely the cause for the reduction in sulfate. The changing chemistry of the injected brines (i.e., reductions in sulfate and other organic constituents) may be from other geochemical reactions.

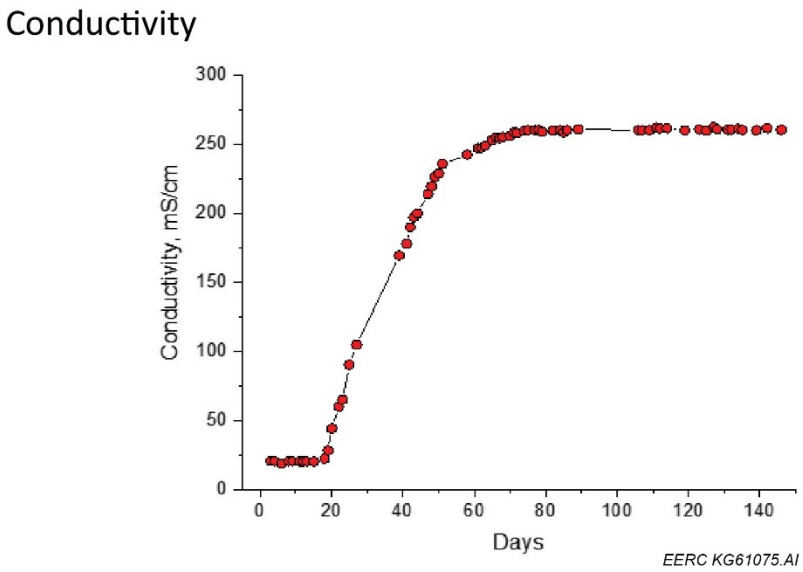


Figure 3-1. Conductivity measurements of laboratory sand column test outlet fluid samples. Results indicate that breakthrough of injected Bakken produced water occurred on Day 18, with a reading of 22.3 mS/cm.

DocuSign Envelope ID: 2FA9A609-C360-4E53-8B28-BE8B77B6994A

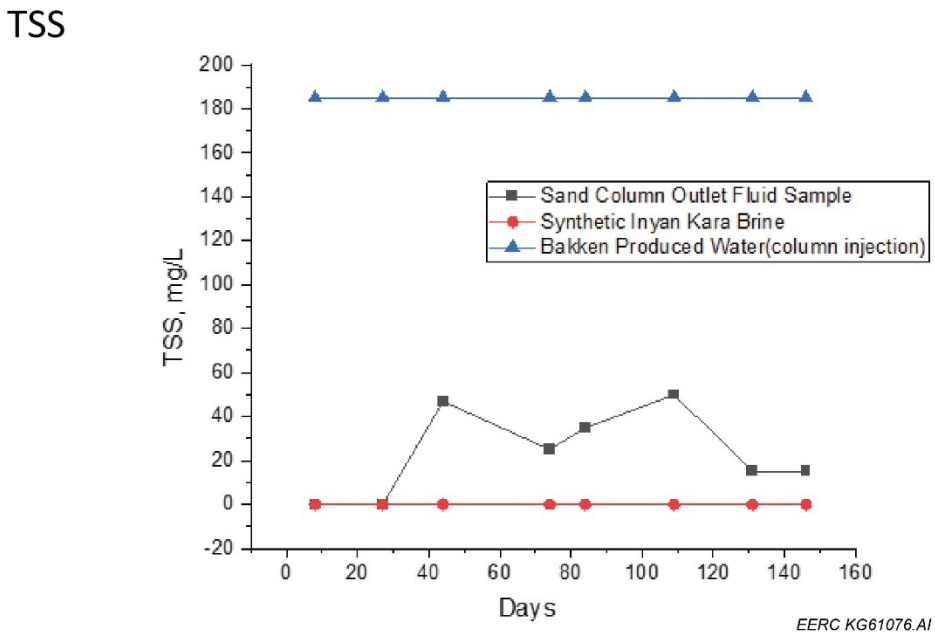


Figure 3-2. TSS measurements of laboratory sand column test outlet fluid samples. Results indicate packing of the column was sufficient and that there were no high-permeability preferential flow pathways present in the column that could contribute to nonrepresentative results.

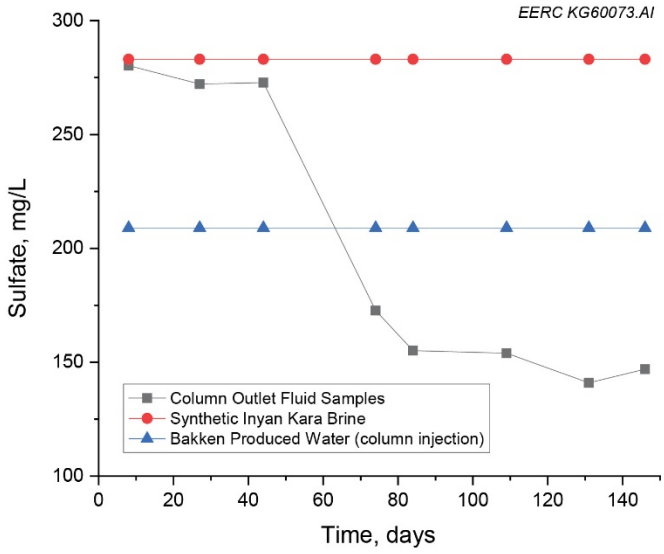


Figure 3-3. Sulfate measurements of laboratory sand column test samples (synthetic Inyan Kara brine used to saturate the column, Bakken produced water injected into the column, and fluid samples collected from the column outlet). Reduction of sulfate over time to levels below those present in the injected Bakken produced water could be indicative of chemical reactions occurring within the system.

DocuSign Envelope ID: 2FA9A609-C360-4E53-8B28-BE8B77B6994A

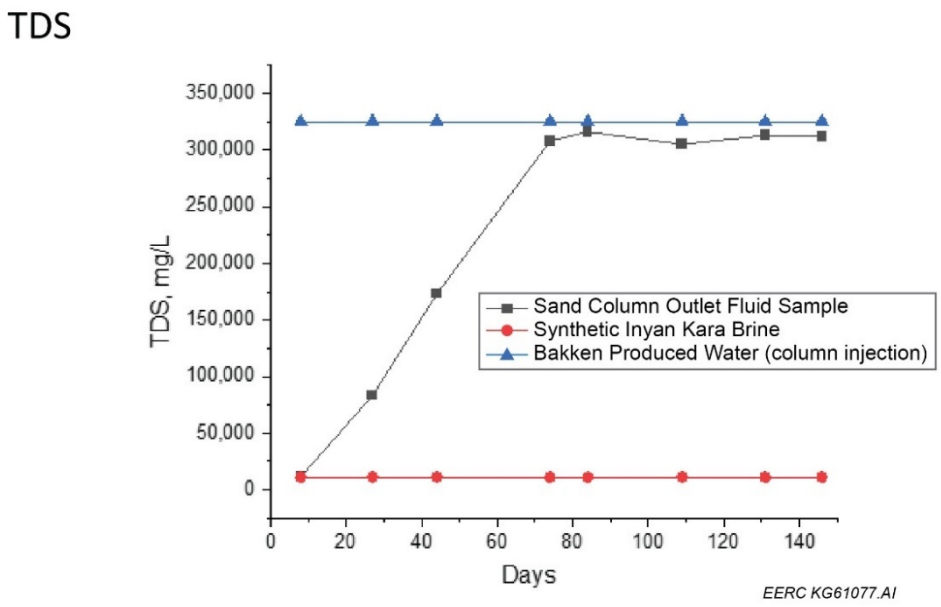


Figure 3-4. TDS measurements of laboratory sand column test samples (synthetic Inyan Kara brine used to saturate the column, Bakken produced water injected into the column, and fluid samples collected from the column outlet). Gradual increase of TDS provides an indication of injected Bakken produced water breakthrough at the column outlet and efficacy of the GHCR process.

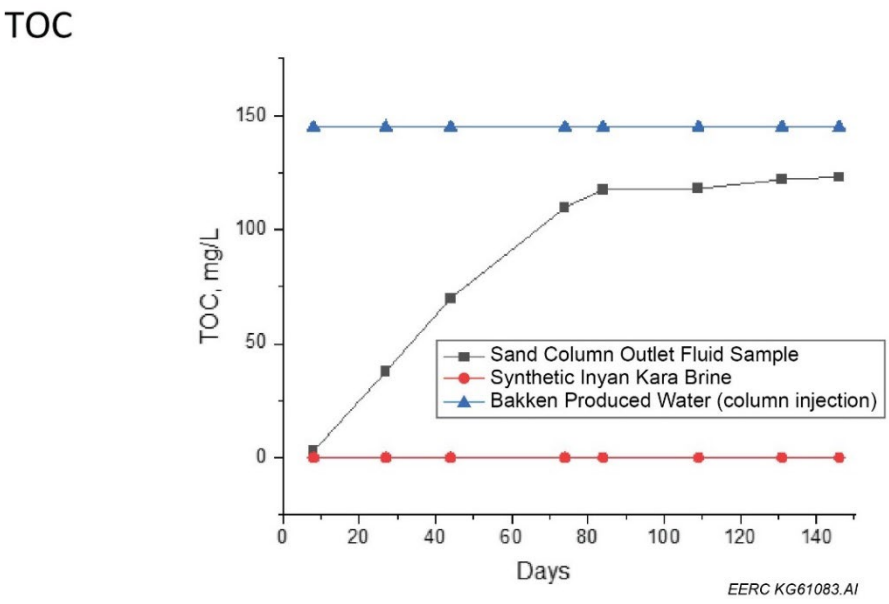


Figure 3-5. TOC measurements of laboratory sand column test samples (synthetic Inyan Kara brine used to saturate the column, Bakken produced water injected into the column, and fluid samples collected from the column outlet). The lower rate of increase in TOC could be indicative of chemical reactions occurring within the system.

DocuSign Envelope ID: 2FA9A609-C360-4E53-8B28-BE8B77B6994A

X-ray fluorescence (XRF) spectroscopy and x-ray diffraction (XRD) analysis were performed on the sand samples pretest and posttest. This analysis helped to identify accumulation of filtered solids, precipitates, and formation of any new mineral phases due to interactions between the injected fluids and/or between the fluids and the quartz sand. Table 3-4 shows the pretest and posttest XRF results, and Table 3-5 shows the posttest XRD results. The pretest XRD was not run because the initial sand was verified to meet a specification of greater than 99.7% silica.

Table 3-4. Sand Column Test – XRF Results for Pretest and Posttest Samples from the Inlet and Outlet of the Column

Oxide	Pretest	Posttest Inlet	Posttest Outlet
SiO_2	99.76	93.36	96.91
Na_2O	0.08	1.74	1.72
Cl	0.00	0.58	0.59
CaO	0.00	0.34	0.27
Fe_2O_3	0.11	0.13	0.17
K_2O	0.00	0.17	0.13
Al_2O_3	0.08	0.07	0.11
SrO	0.00	0.03	0.03
TiO_2	0.02	0.02	0.03
P_2O_5	0.01	0.01	0.01
MnO	0.00	0.00	0.00
SO_3	0.01	0.01	0.03
BaO	0.00	0.01	0.00
MgO	0.01	0.01	0.01
Unknown	0.00	0.50	0.00

Table 3-5. Sand Column Test – XRD Results for Posttest Samples from the Inlet and Outlet of the Column

Phase	Column Inlet, wt%	Column Outlet, wt%
Quartz	96.4	96.3
Halite	3.1	3.2
Brookite	0.4	0.5

XRF results (Table 3-4) show that the initial sand is very clean at 99.7% silica with minor impurities. After testing, samples from the inlet and outlet both showed an accumulation of salts and iron from XRF analysis. The concentration was slightly higher in the inlet versus the outlet, indicating that the column still had some remaining capacity for filtration. XRD analysis (Table 3-5) of the inlet and outlet shows the formation of halite and brookite at similar concentrations. The Total XRF analysis shows approximately a 6% accumulation of solids in the quartz sand at the inlet.

DocuSign Envelope ID: 2FA9A609-C360-4E53-8B28-BE8B77B6994A

3.1.2 Inyan Kara Outcrop Column

The second laboratory column study was conducted to better understand the reactions taking place between the injected Bakken produced water, the native Inyan Kara Formation water, and the actual formation material (rock). The outcrop column used Inyan Kara Formation material collected from a roadside outcrop near Rapid City, South Dakota.

The size distribution of the Inyan Kara outcrop sand was significantly finer than the pure quartz sand used in the previous test, as shown in Table 3-6, with sand primarily smaller than 140 mesh (72.5% mass). The initial conditions for the outcrop column test are presented in Table 3-7.

Table 3-6. Outcrop Column Test – Inyan Kara Outcrop Sand Size Distribution

Screen Size (U.S. mesh)	Retained, %
50	9.9
70	3.3
80	1.5
100	3.7
120	3.3
140	5.9
200	21.5
Pan	51.0
Total	100.0

Table 3-7. Outcrop Column Test – Starting Conditions

Temperature, °F	150
Injection Pressure, psig	2.95
Flow Rate Target, mL/min	0.135
Permeability, mD	36.0
Sand Mass, kg	34.673
Sand Density, g/cm^3	2.677
Sand Volume, cm^3	12,950
Column Length, cm	255
Column Diameter, cm	10
Column Volume, cm^3	19,635
Sand Volume, %	66.0
Column Porosity, %	34.0

DocuSign Envelope ID: 2FA9A609-C360-4E53-8B28-BE8B77B6994A

Since there was not enough Bakken produced water and synthetic brine left from the sand column test to complete the outcrop column test, a new Bakken produced water sample was collected and a new Inyan Kara synthetic brine prepared. Both the produced water and synthetic brine were analyzed for key parameters prior to testing, and results are presented in Table 3-8.

Injection began on June 23, 2021, and ran through September 15, 2021, with a period of 14 days in July and 12 days in August when the column stopped flowing and was down for maintenance. Excluding those days, the test ran for 57 days.

Table 3-8. Outcrop Column Test – Inyan Kara Synthetic Brine and Bakken Produced Water Analysis

	Inyan Kara Brine	Bakken Produced Water
Date	April 22, 2021	June 3, 2021
pH	7.46	5.34
Conductivity, mS/cm	19.5	259
Density, g/mL	1	1.2
TDS, mg/L	10,780	340,000
Alkalinity, HCO_3, mg/L	77	52
Sodium, mg/L	3860	90,100
Potassium, mg/L	105	7570
Calcium, mg/L	279	22,600
Magnesium, mg/L	26.5	1340
Strontium, mg/L	15.8	1710
Chloride, mg/L	6010	213,000
Bromide, mg/L	NA[1]	1070
Sulfate, mg/L	267	185
Iron, mg/L	NA	100
Boron, mg/L	NA	455
Barium, mg/L	NA	41.9
Lithium, mg/L	NA	94.6
Manganese, mg/L	NA	15.3
TOC, mg/L	NA	145
TSS, mg/L	<10	1930

[1] Not analyzed – minor and trace components were not included in the synthetic brine and therefore not analyzed.

As with the sand column test, fluid samples exiting the column were collected regularly. Conductivity analysis was performed on each collected sample, and a complete set of parameters were measured for eight samples selected periodically throughout the test. The parameters measured were the same as those for the sand column test, and testing concluded when the concentrations of the parameters evaluated had reached a plateau. See Appendix A for all water parameter results.

DocuSign Envelope ID: 2FA9A609-C360-4E53-8B28-BE8B77B6994A

Conductivity data indicated breakthrough of injected Bakken produced water occurred on Day 26 as evidenced by the increase in conductivity (Figure 3-6). This was approximately 8 days longer than when breakthrough occurred in the sand column testing. Since the flow rates for both tests were similar, the later breakthrough is likely due to increased reactivity due to the significantly finer Inyan Kara sand resulting in a higher surface area and higher reactivity than the quartz sand (Table 3-1 and Table 3-6).

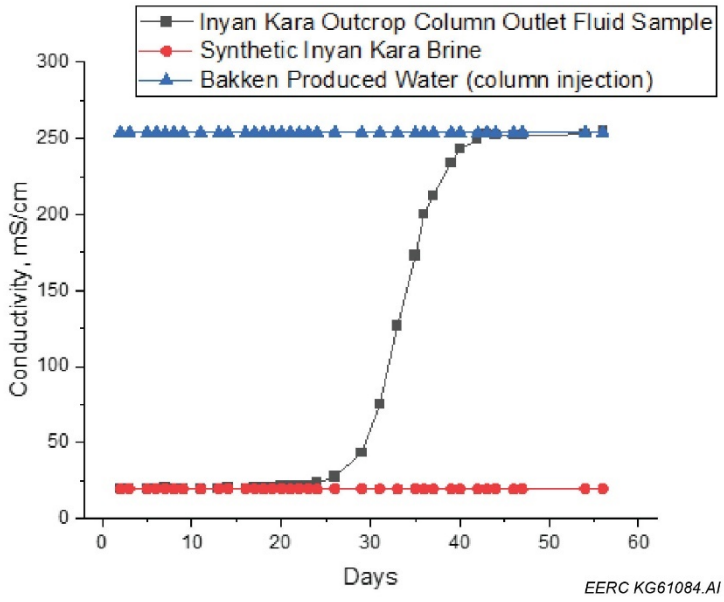


Figure 3-6. Conductivity measurements of laboratory outcrop column test outlet fluid samples. Results indicate that breakthrough of injected Bakken produced water occurred on Day 26, with a reading of 23.3 mS/cm.

Similar to the sand column testing, most analytes followed an increasing trend with the TDS, except for magnesium and sulfate (Figures 3-7, 3-8, and 3-9 and Appendix A Figures A-6–A-9). Between Days 33 and 47, magnesium concentrations at the outlet actually exceeded the original concentration of the Bakken injection brine and then began to decrease to injection brine levels at the end of the test. Sulfate concentrations exceeded the injection brine concentration throughout most of the testing, with levels decreasing the last 7 days.

DocuSign Envelope ID: 2FA9A609-C360-4E53-8B28-BE8B77B6994A

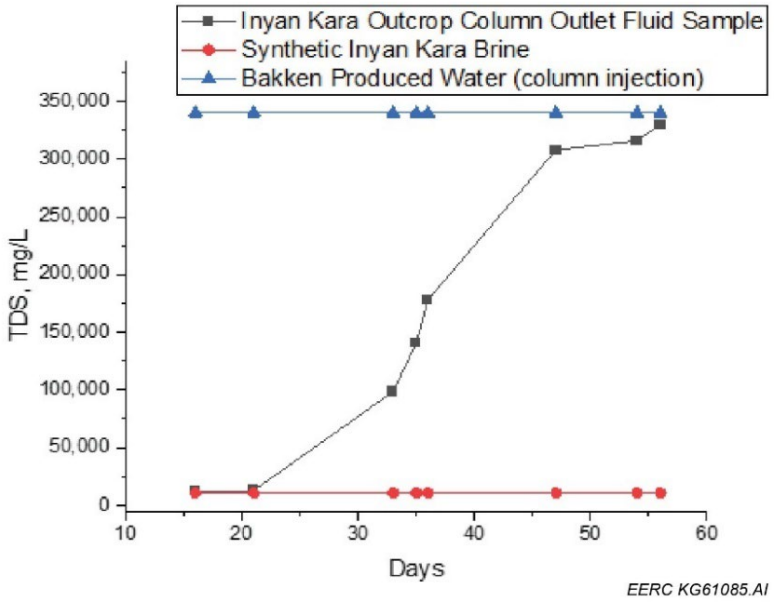


Figure 3-7. TDS measurements of laboratory outcrop column test samples (synthetic Inyan Kara brine used to saturate the column, Bakken produced water injected into the column, and fluid samples collected from the column outlet). Gradual increase of TDS provides an indication of injected Bakken produced water breakthrough at the column outlet and efficacy of the GHCR process.

The TSS concentration of the Bakken injection brine used for the outcrop column testing was significantly higher than that of the brine used in the sand column testing (1930 mg/L versus 185 mg/L), yet results indicate the outcrop material was extremely effective in filtering the solids (Figure 3-10). Levels were reduced from 1930 to 16 mg/L in the first outlet sample tested at Day 17 and remained low throughout the entire test.

The TOC concentrations remained relatively stable throughout the testing, with a few values exceeding the initial brine concentration (Figure 3-11). This could be a result of organic matter present in the native outcrop material and being extracted by the brine.

DocuSign Envelope ID: 2FA9A609-C360-4E53-8B28-BE8B77B6994A

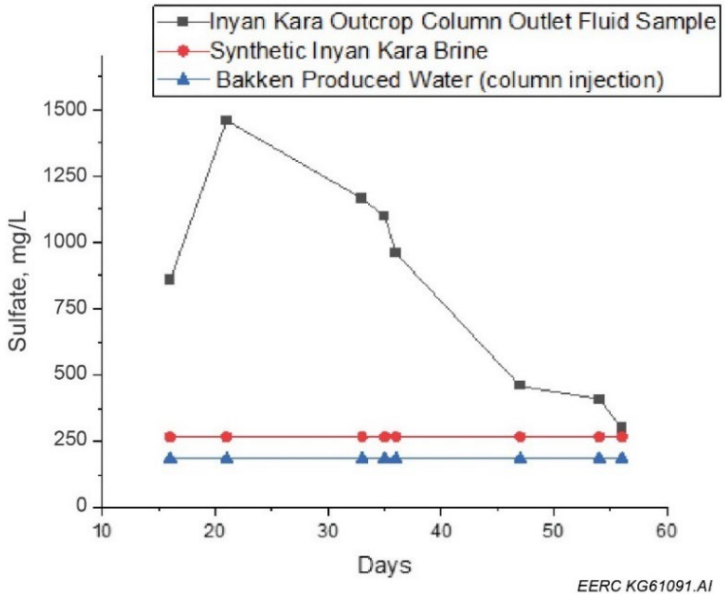


Figure 3-8. Sulfate measurements of laboratory outcrop column test samples (synthetic Inyan Kara brine used to saturate the column, Bakken produced water injected into the column, and fluid samples collected from the column outlet). The source of the elevated initial sulfate content is unknown. The initial concentration of 1200 mg/L represents an approximately 0.017% of the sand column mass. This is a concentration below the detection limits of XRD and also represents the lower detection limit from XRF. It may be due to slight leaching of sulfates from the Inyan Kara outcrop material, a result of sorption and desorption from the media or some other mechanism. Additional testing is required to make a clear determination as to the source of the variation, which was outside the scope of this effort.

DocuSign Envelope ID: 2FA9A609-C360-4E53-8B28-BE8B77B6994A

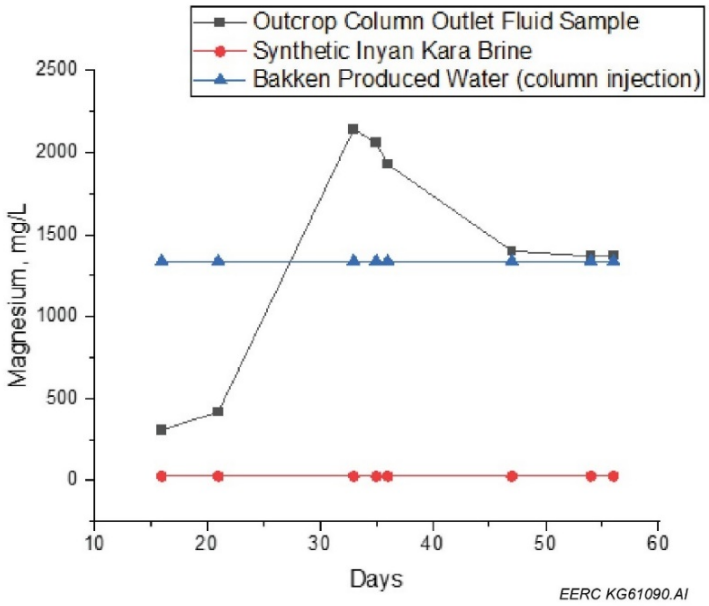


Figure 3-9. Magnesium measurements of laboratory outcrop column test samples (synthetic Inyan Kara brine used to saturate the column, Bakken produced water injected into the column, and fluid samples collected from the column outlet). The spike in magnesium concentrations between Days 33 and 47 may be due to slight leaching of magnesium from the Inyan Kara outcrop material, a result of sorption and desorption from the media or some other mechanism. Additional testing is required to make a clear determination as to the source.

DocuSign Envelope ID: 2FA9A609-C360-4E53-8B28-BE8B77B6994A

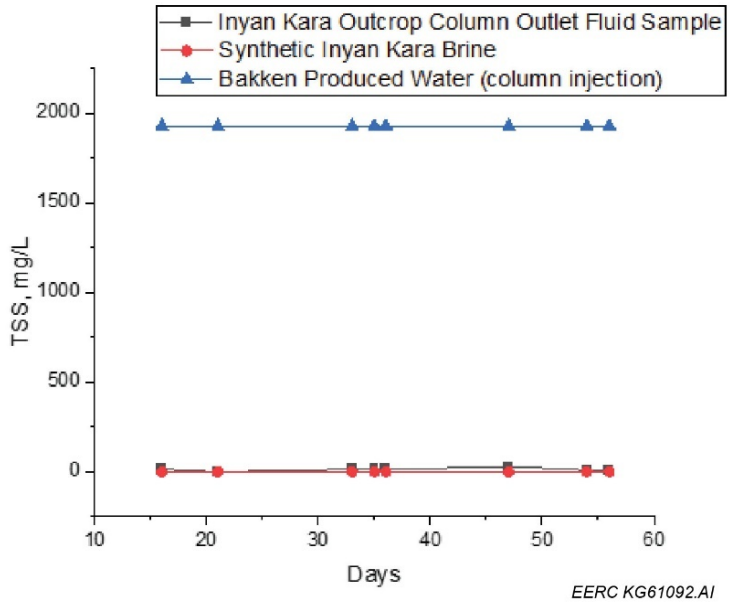


Figure 3-10. TSS measurements of laboratory outcrop column test outlet fluid samples. Results indicate packing of the column was sufficient and that there were no high-permeability preferential flow pathways present in the column that could contribute to nonrepresentative results.

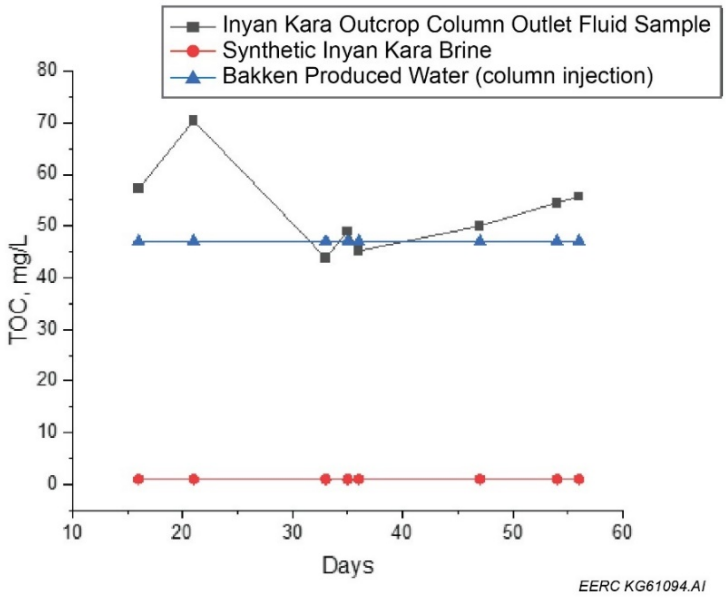


Figure 3-11. TOC measurements of laboratory outcrop column test samples (synthetic Inyan Kara brine used to saturate the column, Bakken produced water injected into the column, and fluid samples collected from the column outlet).

DocuSign Envelope ID: 2FA9A609-C360-4E53-8B28-BE8B77B6994A

XRF and XRD analysis were performed on the Inyan Kara outcrop samples pretest and posttest. This analysis helped to identify accumulation of filtered solids, precipitates, and formulation of any new mineral phases due to interactions between the injected fluids and formation sand for comparison to quartz sand. Table 3-9 shows the pretest and posttest XRF results, and Table 3-10 shows the pretest and posttest XRD results.

Table 3-9. Outcrop Column Test – XRF Results for Pretest and Posttest Samples from the Inlet and Outlet of the Column

Oxide	Pretest	Posttest Inlet	Posttest Outlet
SiO_2	92.00	80.89	86.28
Al_2O_3	3.31	3.91	2.96
Fe_2O_3	2.86	2.97	2.83
TiO_2	0.65	0.59	0.60
K_2O	0.47	0.80	0.57
CaO	0.41	1.14	0.83
SO_3	0.11	0.13	0.10
MgO	0.09	0.12	0.06
P_2O_5	0.04	0.05	0.04
MnO	0.03	0.03	0.03
BaO	0.02	0.01	0.01
V_2O_5	0.01	0.01	0.01
SrO	0.01	0.06	0.04
NiO	0.00	0.00	0.00
Cl	0.00	6.02	3.20
Na_2O	0.00	3.28	2.44

Table 3-10. Outcrop Column Test – XRD Results for Pretest and Posttest Samples from the Inlet and Outlet of the Column

Analysis – Rietveld	Pretest	Post-Column Inlet	Post-Column Outlet
Quartz	86.3	69.1	67.8
Kaolinite	6.9	6.0	5.1
Goethite	4.5	8.1	6.0
Illite/Muscovite	1.2	2.0	0.8
Epsomite	0.4	2.0	1.6
Anhydrite	0.2	0.2	0.5
Halite	0.1	11.5	16.8
Sylvite	0.03	0.1	0.4
Other	0.5	0.9	0.9

DocuSign Envelope ID: 2FA9A609-C360-4E53-8B28-BE8B77B6994A

XRF results (Table 3-9) show that initially the outcrop material contains approximately 92% silicon dioxide. Posttesting samples from the inlet and outlet both showed an accumulation of mainly salts from XRF analysis. Similar to the quartz sand, the concentration was slightly higher in the inlet versus the outlet, indicating that the column still had some remaining capacity for filtration. Iron oxide seems to be mostly saturated near 2.9%, and the XRD analysis (Table 3-10) of the inlet and outlet shows a reduction in kaolinite. This is likely due to clay fines being mobilized and washed from the system during filling and some fines being produced out. This fines migration also likely led to the eventual clogging of the column, which ended the test because of an inability to maintain flow at a safe injection pressure. The Inyan Kara outcrop material was more reactive and better trapped solids than the sand column. The XRF results showed a trapped concentration of solids exceeding 11% versus 6% with pure quartz sand. Similarly, XRD showed a concentration of approximately 17% nonquartz solids retained by the outcrop material compared to less than 4% retained by the pure quartz sand. The increased capacity for filtration is likely because of increased surface area due to fine, smaller-than-200-mesh particles and a higher reactivity due to a more diverse mineral composition. This resulted in accumulation of additional minerals such as goethite, epsomite, and anhydrite and much larger concentrations of halite.

3.1.3 Inyan Kara Core Column

The third and final laboratory column test was conducted using Inyan Kara core sections obtained from NDIC Well 90383 (BEST I1). This core test was performed to look for geochemical changes in the produced output in comparison to the outcrop test. These core samples are unique in that they have been previously exposed to Bakken produced water at the injection site, and the core samples were not exposed to the same weathering as outcrop materials. The contrast between the outcrop and core tests helped identify the similarities and differences between the materials and their GHCR-related performance, and the additional testing better-informed model calibration. Table 3-11 shows the attributes of core plugs that were presaturated with synthetic Inyan Kara brine.

DocuSign Envelope ID: 2FA9A609-C360-4E53-8B28-BE8B77B6994A

Table 3-11. Core Column Test – Data for Core Plugs Used in Core Flood Test

No.	Depth, ft	Mass Dry, g	Mass Sat., g	Diameter, cm	Length, cm	Mass Diff., g	Vol. Pore, mL	Vol. Bulk, mL	Porosity, %
1	5303	124.833	137.82	3	8.93	12.987	12.987	63.1225	20.57
2	5316.7	127.812	139.595	3	8.88	11.783	11.783	62.7690	18.77
3	5302	126.123	138.795	3	8.9	12.672	12.672	62.9104	20.14
4	5314.5	153.234	161.547	3	8.79	8.313	8.313	62.1328	13.38
5	5315.5	127.567	140.49	3	8.92	12.923	12.923	63.0518	20.50
6	5320.7	129.21	140.66	3	8.9	11.45	11.45	62.9104	18.20
7	5322.7	128.326	140.8	3	8.9	12.474	12.474	62.9104	19.83
8	5293.5	128.37	142.875	3	9.1	14.505	14.505	64.3241	22.55
9	5291	120.217	132.824	3	8.57	12.607	12.607	60.5778	20.81
10	5286	123.804	139.415	3	9.03	15.611	15.611	63.8293	24.46
11	5296	124.04	137.055	3	8.98	13.015	13.015	63.4759	20.50
12	5288	116.59	130.706	3	8.53	14.116	14.116	60.2950	23.41
13	5313	139.57	151.194	3	9.26	11.624	11.624	65.4551	17.76
14	5297.5	118.943	130.346	3	8.66	11.403	11.403	61.2139	18.63
						Total	**175.483**	**878.9784**	**19.97**

The Inyan Kara cores were loaded into the core holder in random order and treated as a single composite core section for the purposes of testing. The core test was particularly challenging because extremely low injection rates were required to attempt to hit the same 36-day residence time. The minimum achievable injection rate of 0.007 mL/min represents approximately an 18-day residence time, or about half the desired residence time. The reduced injection rates result in reduced sample volume rates relative to the sand and outcrop columns. The reduced volumes meant that TSS was not analyzed for the column, although based on visual observations, the output water was relatively clear. Again, the goal of this core test was to look at geochemical changes between the core and outcrop material, and the physical filtering of TSS was not imperative for this core test, especially considering the output fluid volumes were limited. Furthermore, XRD/XRF analysis was not performed on the core column as had been done on the two other column tests. This is primarily due to the 14 core sections that were used to fill the core holder, and each individual core would need to undergo XRD/XRF analysis, which was time- and cost-prohibitive.

Table 3-12 shows the conditions at the start of the core flood test and bulk properties of the composite core.

DocuSign Envelope ID: 2FA9A609-C360-4E53-8B28-BE8B77B6994A

Table 3-12. Core Column Test – Starting Conditions

Temperature, °F	150
Injection Pressure, psig	30
Target Flow Rate, mL/min	0.007
Permeability, mD	2.00
Grain Mass, kg	1.789
Grain Density, g/cm^3	2.543
Grain Volume, cm^3	703
Core Length, cm	124.35
Core Diameter, cm	3.00
Core Bulk Volume, cm^3	879
Sand Volume, %	80.0
Core Porosity, %	20.0

The same Bakken produced water and Inyan Kara synthetic brine used for the outcrop column test were used for the core flow-through test; however, another sample of the Bakken brine was collected from the transfer container and analyzed to confirm the concentrations just prior to injection. Another sample was collected and analyzed at the end of the test, since there appeared to be some settling in the transfer container over the course of the testing. The results of TDS and corresponding analytes show a decrease in concentrations from the start of the test to the end of the test. Results are presented in Table 3-13, and both sets of data are included in the figures in this section.

Bakken produced water injection for the core flow-through test began on July 27, 2021, and ran through October 18, 2021, for a total of 83 days.

DocuSign Envelope ID: 2FA9A609-C360-4E53-8B28-BE8B77B6994A

Table 3-13. Core Column Test – Inyan Kara Synthetic Brine and Bakken Produced Water Analysis

	Inyan Kara Brine	Bakken Produced Water – Start	Bakken Produced Water – End
Date	April 22, 2021	July 27, 2021	October 20, 2021
pH	7.46	4.04	3.46
Conductivity, mS/cm	19.5	240	230
Density, g/mL	1	1.2	1.15
TDS, mg/L	10,780	319,000	236,000
Alkalinity, HCO_3, mg/L	77	0	0
Sodium, mg/L	3860	89,400	67,500
Potassium, mg/L	105	8270	5620
Calcium, mg/L	279	21,000	16,700
Magnesium, mg/L	26.5	1230	1010
Strontium, mg/L	15.8	1710	1270
Chloride, mg/L	6010	195,000	142,000
Bromide, mg/L	NA[1]	1020	702
Sulfate, mg/L	267	290	258
Iron, mg/L	NA	71.5	14.8
Boron, mg/L	NA	513	428
Barium, mg/L	NA	13.5	10.5
Lithium, mg/L	NA	98.7	62.5
Manganese, mg/L	NA	21.3	19.9
TOC, mg/L	NA	71	24.7
TSS, mg/L	<10	NA	NA

[1] Not analyzed – minor and trace components were not included in the synthetic brine and therefore not analyzed.

Because the Inyan Kara core material used in this test was significantly smaller in scale than column tests, the injection flow rate was reduced to a minimum achievable flow rate of 0.007 mL/min to maximize residence time. This resulted in samples being collected at the outlet less frequently, ranging from 7 to 10 days between sample collection. When enough volume of water was generated at the column outlet to collect the first sample on Day 10, breakthrough had already occurred based on a conductivity reading of 40.7 mS/cm (Figure 3-12). Although the day of actual breakthrough could not be determined, it was still fewer days than either the sand column test or the outcrop column test (Day 18 and Day 26, respectively). The lower volumes of collected samples resulted in TSS not being measured for the core column.

Although there was a slight decrease in TDS of the Bakken injection brine throughout the testing, the data show trends similar to those in the sand column and outcrop column testing. Most analytes followed an increasing trend with conductivity and TDS, except for sulfate (Figures 3-12–3-15). The sulfate concentration spiked above the injection brine level at the start of the test but leveled off for the remainder of the test.

DocuSign Envelope ID: 2FA9A609-C360-4E53-8B28-BE8B77B6994A

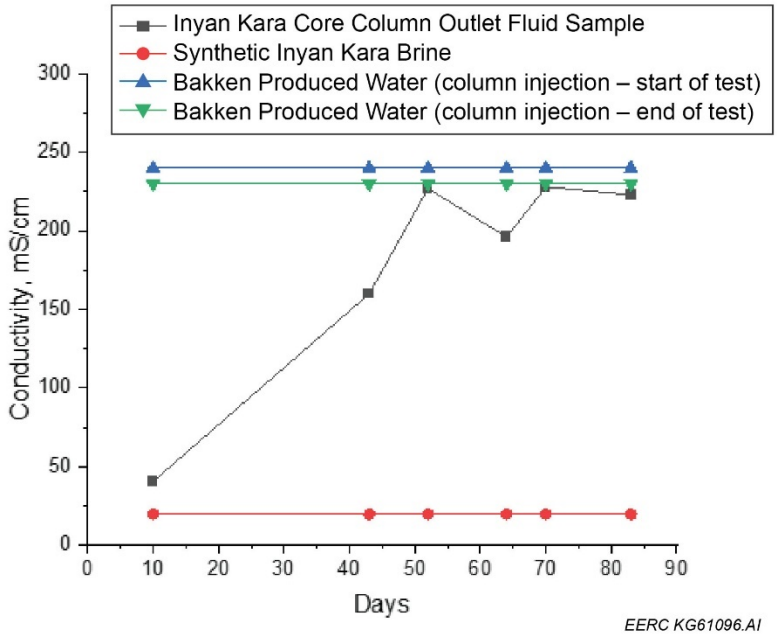


Figure 3-12. Conductivity measurements of laboratory core column test outlet fluid samples. Results indicate that breakthrough had occurred prior to the first outlet sample being collected on Day 10, with a reading of 40.7 mS/cm.

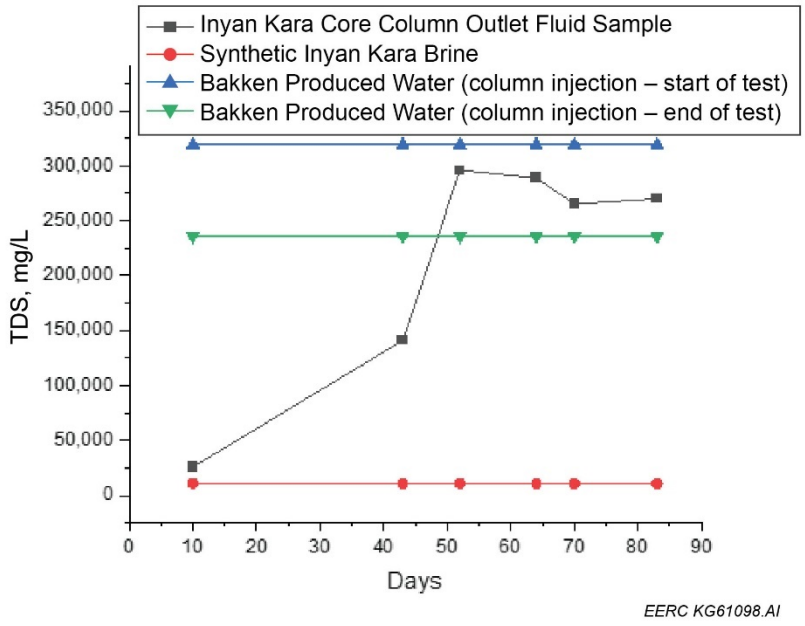


Figure 3-13. TDS measurements of laboratory core column test samples (synthetic Inyan Kara brine used to saturate the column, Bakken produced water injected into the column, and fluid samples collected from the column outlet).

DocuSign Envelope ID: 2FA9A609-C360-4E53-8B28-BE8B77B6994A

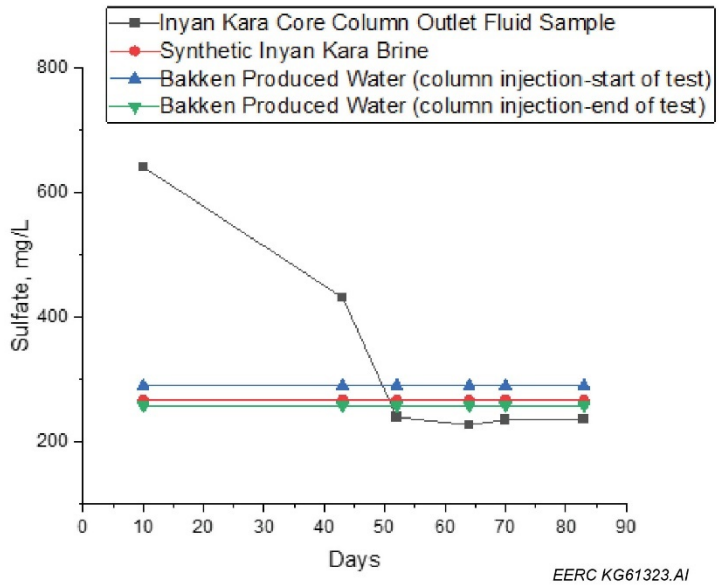


Figure 3-14. Sulfate measurements of laboratory core column test samples (synthetic Inyan Kara brine used to saturate the column, Bakken produced water injected into the column, and fluid samples collected from the column outlet). Similar to the outcrop test, an initial elevated sulfate saturation of 600 mg/L was observed. This represents less than 0.016% of the core material by mass. As with the outcrop test, additional testing is required to determine the source of these initially elevated sulfate levels.

It is worth noting that each of the outlet samples collected throughout the core column test had a distinct hydrocarbon layer on the surface of the sample. Since this was not observed in the previous Inyan Kara outcrop column study, and the fact that the same Bakken produced water was used for injection, it seems reasonable that the hydrocarbons were coming from the core material. This was supported by the TOC measurements, which ranged from 2× to 10× higher than the original Bakken injection brine (Figure 3-15).

DocuSign Envelope ID: 2FA9A609-C360-4E53-8B28-BE8B77B6994A

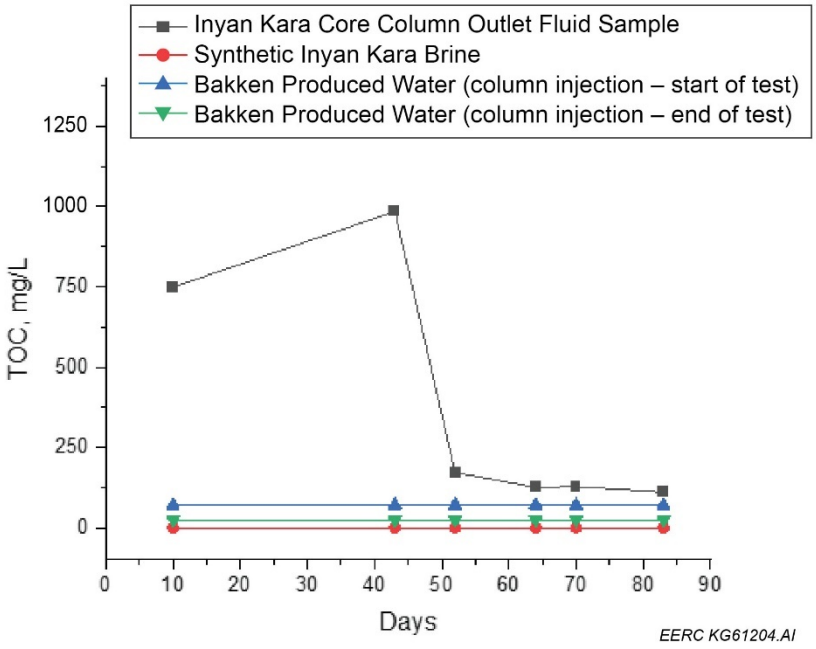


Figure 3-15. TOC measurements of laboratory core column test samples (synthetic Inyan Kara brine used to saturate the column, Bakken produced water injected into the column, and fluid samples collected from the column outlet). The fluid samples collected at the core outlet had a distinct hydrocarbon layer on the surface.

3.1.4 Key Observations for the Three Laboratory Column Tests

- All three column tests were effective in homogenizing the Bakken produced water chemistry to a consistent conductivity and TDS level by the end of the testing.

- Most major ions followed a similar increasing trend and plateau with TDS and conductivity, with the exception of sulfate. Sulfate followed roughly an inverse trend, with a unique pattern depending on which column was tested.

- Magnesium and sulfate in the outcrop column test showed a spike in concentrations in the middle of the test period. Leaching and/or sorption/desorption mechanisms are suspected.

- Both the sand column and outcrop column tests were effective in filtering TSS. Because of reduced sample volumes collected in the core column test, TSS could not be measured at the outlet.

- Because of the possible presence of organic matter in the Inyan Kara outcrop material and visible hydrocarbons being extracted from the Inyan Kara core, it was difficult to evaluate the efficacy of the laboratory GHCR process for TOC.

DocuSign Envelope ID: 2FA9A609-C360-4E53-8B28-BE8B77B6994A

- It is possible that contamination of the BEST core from previous Bakken SWD injection may have led to deposits in the core that leached into the low-TDS Inyan Kara synthetic brine, resulting in an artificially accelerated breakthrough measurement.

- The Inyan Kara outcrop showed a greater efficacy for filtration when compared to the sand column control test. As evidenced by the accumulation of species that were more concentrated in the exposed material compared to the pure quartz. Contributing factors are likely the much higher surface area of the smaller Inyan Kara particles (<200 mesh versus >70 mesh) and the more diverse composition, allowing more opportunities for reaction as evidenced by XRF and XRD analysis of pretest and posttest sand samples.

3.2 Field Evaluation

The GHCR concept involves extracting water from the same geologic formation where SWD is occurring. Typically, there are no wells producing from the same formation in the same area where SWD is occurring. However, the EERC has partnered with Nuverra Environmental Solutions (Nuverra) on a multiyear project to demonstrate new strategies and methods of injection well operation. This project, referred to as BEST, is being conducted at the Nuverra-operated Johnsons Corner site, which was established in 2008 as a commercial SWD facility. The BEST site provides a unique opportunity because there was an extraction well (BEST E1) installed that produces fluids from the Inyan Kara sandstone, which is the SWD injection target for two SWD wells (Rink 1 and 2), as shown in Figure 3-16. The two Rink SWD wells have been injecting since 2008 (Rink 1) and 2010 (Rink 2), and the extraction BEST E1 was installed October 2018, just outside of the expected saltwater plumes, which were estimated based upon geologic model and simulation outputs for the BEST site. While the BEST E1 well was initially installed to evaluate the ability to manage the SWD reservoir, the arrangement of project wells offers the opportunity to evaluate the GHCR concept at a commercially operating SWD location.

DocuSign Envelope ID: 2FA9A609-C360-4E53-8B28-BE8B77B6994A



Figure 3-16. BEST project site. Fluid samples were collected from the BEST E1 well to test the efficacy of the GHCR concept at a commercial SWD site.

3.2.1 Field Sampling Results

Water samples were collected regularly from the BEST E1 well between October 2018 and October 2021 to monitor the water quality for Bakken produced water being injected into, migrated through, and subsequently extracted from the Inyan Kara Formation at the BEST E1 well. As with the laboratory column testing, a complete set of parameters were measured for each collected field

DocuSign Envelope ID: 2FA9A609-C360-4E53-8B28-BE8B77B6994A

sample. The parameters measured were the same as those for the laboratory tests, and testing continued for the duration of this GHCR project.

In the years leading up to this GHCR project work, the Rink SWD wells typically received Bakken produced water for disposal via truck. However, conversations with personnel operating the Rink wells revealed that the continued development of other SWD wells in the area that receive produced water via pipeline delivery resulted in the Rink SWD wells receiving limited Bakken produced water, and, therefore, the SWD wells received primarily gas condensate water from nearby gas-processing facilities over the most recent ~18 months. Oil well operators favor routing their produced waters through pipelines to other SWD locations in the area. The gas condensate waters have significantly lower TDS values (ranging from ~100,000 to 180,000 mg/L) than typical Bakken produced water (~300,000–330,000 mg/L). While this operational change may affect the samples collected, this information was incorporated into the field modeling and simulation efforts to account for any impacts on the evaluation of GHCR efficacy.

Similar to the laboratory column testing, most analytes followed an increasing trend with the TDS (Figure 3-17, Appendix A), except for TOC and sulfate (Figures 3-18 and 3-19). The parameters shown plateaued at values about 15% to 30% below the average values of the Rink injection brine, with the exception of the increases found in TOC and sulfate. The reduced values show the potential of the GHCR concept in a field setting. The fluctuations of the TOC and sulfate may be indicative of geochemical reactions or biological activity occurring in the formation, where bacteria utilize organic carbon to reduce dissolved sulfate in the water to insoluble sulfide species which would precipitate out of solution. If the sulfides were then exposed to injected fluids of differing chemistries, such as brine that contained species that are oxidative to sulfide (such as dissolved oxygen, nitrate, manganese [+4], iron [+3]), the sulfide would oxidize back to sulfate and appear in solution. (Bolles, 1998). The increased reductions of analytes during the most recent 18 months of monitoring may be due to the increased percentage of lower-TDS gas condensate water injection.

DocuSign Envelope ID: 2FA9A609-C360-4E53-8B28-BE8B77B6994A

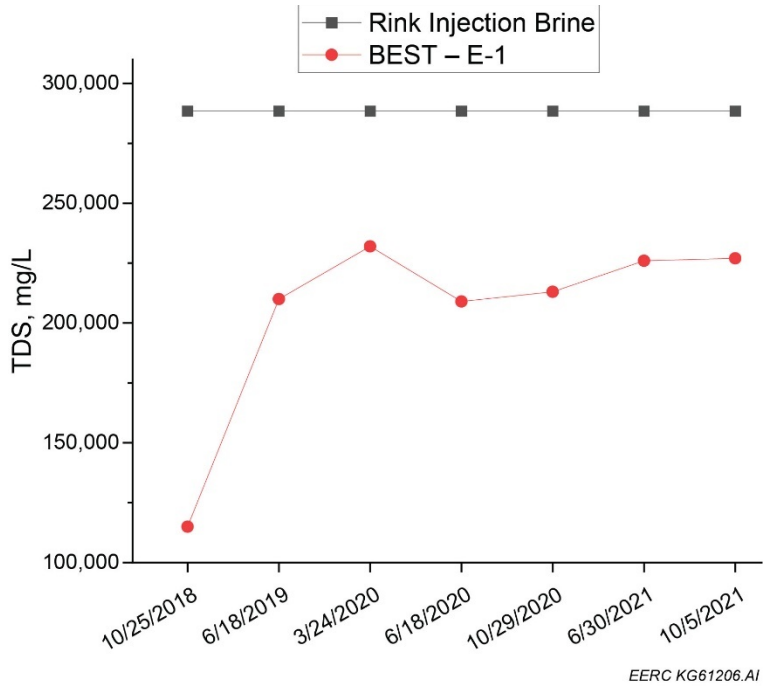


Figure 3-17. TDS measurements collected from the BEST E1 well. Measurements plateau at about 225,000 mg/L.

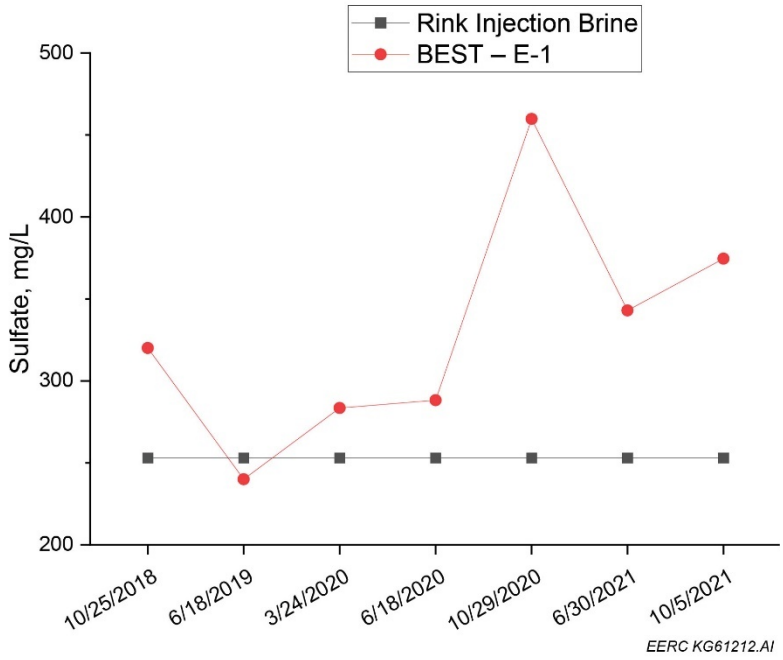


Figure 3-18. Sulfate measurements collected from the BEST E1 well. These concentration fluctuations may be caused by biological activity occurring in the reservoir where injected sulfates are reduced to sulfide by bacterial activity and then subsequently oxidized back to sulfate upon injection of and exposure to water with potential oxidative species, such as oxygen, nitrate, iron, and manganese.

DocuSign Envelope ID: 2FA9A609-C360-4E53-8B28-BE8B77B6994A

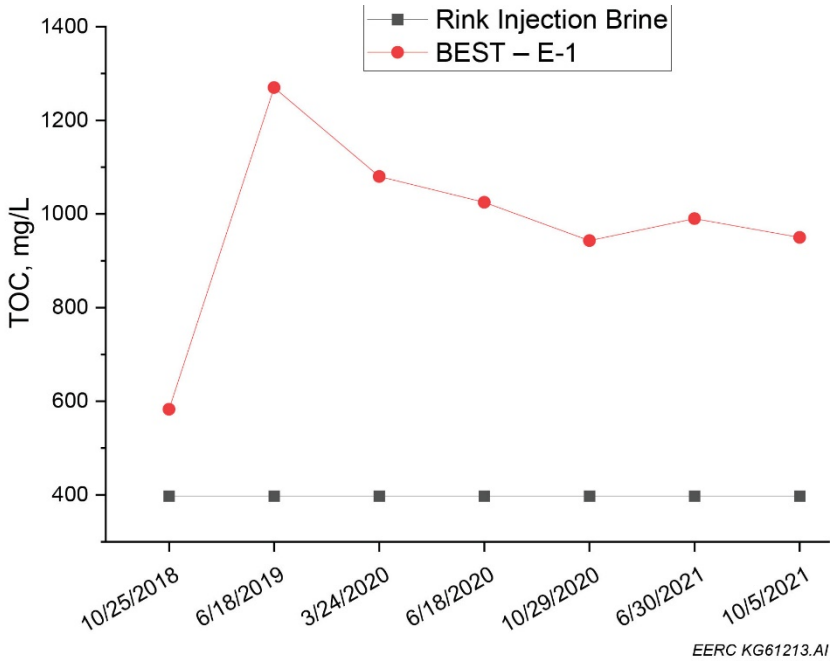


Figure 3-19. TOC measurements collected from the BEST E1 well. The Inyan Kara site has been injecting Bakken produced water over several years, resulting in a significant presence of hydrocarbons. The increased TOC concentration is likely due to the introduction of organics and could possibly be a driving factor for biological activity in the formation.

3.2.2 Key Observations from the Field Sampling and Evaluation

- Significant increases in several parameters measured during the field sampling effort indicate movement of the injected produced water (from Wells Rink 1 and 2) toward the extraction well (BEST E1) within a few months of the commencement of production operations.

- The rapid movement of the injected brine, and ultimate change in extracted water chemistry, was anticipated and confirmed by computer modeling efforts that assessed pressure and water chemistry compositional effects at the injection and extraction wells.

- The fact that the components of the dissolved constituent chemistry (i.e., TDS, sodium, chloride, etc.) leveled off below the injected produced water concentrations may likely be due to interactions with components of the formation that are causing a "buffering" effect of the fluid chemistry.

- Compositional chemistry changes, primarily decreases in concentration, in the recent 18 months of monitoring are likely due to changes in injected water chemistry (i.e., injection of less saline gas condensate water).

- Fluctuations of TOC and sulfate may be indicative of geochemical reactions or biological activity occurring in the formation.

DocuSign Envelope ID: 2FA9A609-C360-4E53-8B28-BE8B77B6994A

- The reduced, and relatively consistent, values of TDS and associated ions show the potential of the GHCR concept in a field setting.

4.0 GEOLOGIC MODELING AND NUMERICAL SIMULATION EVALUATION OF GHCR CONCEPT

The modeling and simulation evaluation involved a field model of the Inyan Kara Formation within the study area and a laboratory-scale simulation model built with information provided from the columns and core holder experiments described in Section 3.0. The subsections within Section 4.0 describe the field simulation model, while the laboratory-scale simulation models are described in Appendix C. Some additional scenarios derived from the field simulation efforts are also shown in Appendix D. The objective of the modeling and simulation activity was to provide enough information to characterize and validate the efficacy and performance of the GHCR concept based on the observed differences in water chemistry, rock mineralogy, and geochemistry. This was achieved by calibrating and matching the numerical laboratory-scale model with the laboratory experiment data. Once the model was developed, it was used to evaluate different operational scenarios to assess the technical feasibility of using the Inyan Kara Formation as a geologic solution for produced water management and recycling of produced water. An additional benefit is to provide a potential solution for pressure control in the formation due to the constant water disposal injection.

Numerical simulation studies for evaluating the GHCR concept used Computer Modelling Group's (CMG's) GEM, a compositional reservoir simulation module. A compositional simulator is one of the most mechanistically accurate methods to solve compositional multiphase fluid flow processes. Compositional simulators utilize cubic equations of state, such as Peng–Robinson, which calculates thermal dynamic properties of fluids within the reservoir, including the resulting mixture of fluids when the disposal water with a higher salinity concentration is injected and dissolved into the native formation brine. During the simulation process, the geochemical model was included in the numerical model to account for the aqueous fractions and mineral precipitation/dissolution through the water injection time. The geochemical modeling allows the simulator to calculate the stoichiometry of chemical equilibrium, dissolution and precipitation, and ion exchange reactions directly from mineral and aqueous reactions introduced into the simulation model.

4.1 Field Numerical Models

Field numerical simulations were conducted using the Inyan Kara Formation geomodel. Simulations were carried out using CMG's GEM 2018.1, a compositional reservoir simulation module, with the addition of the geochemical modeling. The geochemical modeling improves the representation of the native Inyan Kara water and the Bakken produced water injection salinities as well as the rock mineral properties in order to evaluate any potential interactions between the water and the rock. The calculated temperature and pressure, along with a reference datum depth, were used to initialize the reservoir equilibrium conditions for performing numerical simulation (Figure 4.1).

DocuSign Envelope ID: 2FA9A609-C360-4E53-8B28-BE8B77B6994A

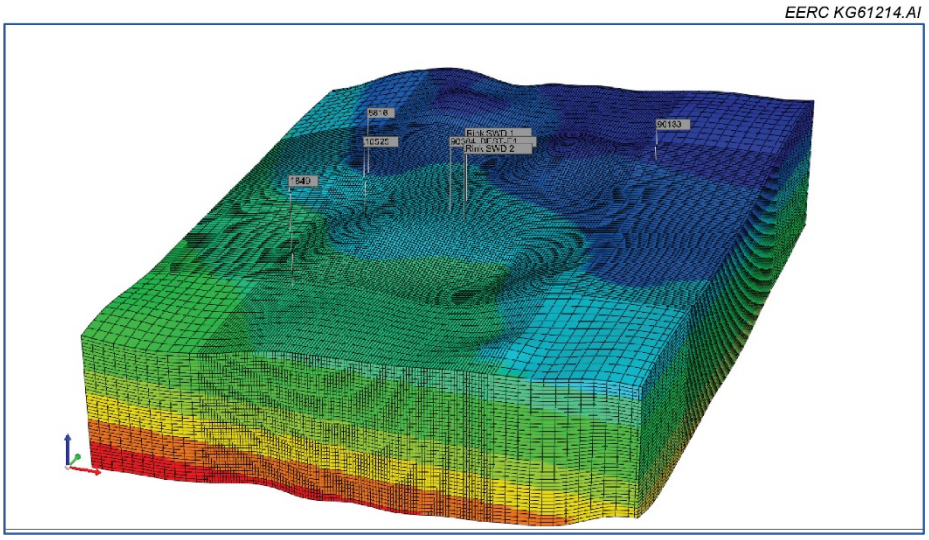


Figure 4-1. Field numerical model for Inyan Kara Formation.

The Inyan Kara geomodel used in the evaluation of the GHCR concept was provided from the BEST project's geologic modeling efforts. The model was previously history-matched using field data from water injector wells within the area of evaluation, including the water injector wells Rink SWD1 and SWD2, injector Well 10525, and Well 90183. The last data available used during the history match were from June 2021. The simulation model boundaries were assigned as an open condition, and the reservoir was assumed to be 100% brine-saturated with an initial formation salinity of 11,700 ppm TDS.

The numerical modeling allowed for simulation of mixing between the water injected from the Rink 1 and Rink 2 SWD wells (salinity of 197,000 ppm TDS) and the formation brine. The salinity value was calculated during the history match process, which matched the simulation's water density results with the data obtained from water samples collected in the field. During the history match, the permeability was regionally tuned by applying a multiplier to match reservoir properties.

The Inyan Kara model was also evaluated and calibrated using the salinity concentrations from different Bakken produced water samples collected at different times for this GHCR project. The model showed a decent calibration with the salinity values from the samples analyzed in the laboratory. For simplicity, the results shown in this report are for the simulation results using a 197,000-mg/L salinity concentration for injected Bakken produced water, which was calculated during the model history match.

DocuSign Envelope ID: 2FA9A609-C360-4E53-8B28-BE8B77B6994A

4.2 Field Simulation Work Descriptions

Different operational scenarios and sensitivities were evaluated during 20 years of injection and production prediction from 2022 to 2042. The scenarios include varied distances between BEST location wells (Rink 1 and Rink 2 SWD wells) and production wells (simulates GHCR water production), number of production wells, and injection and production water rates, with the purpose of evaluating the changes in the GHCR production water volumes and the potential decrease of Inyan Kara formation pressure (Table 4-1).

Table 4-1. Field Numerical Simulation Scenarios

Scenario	Number of Additional Production Wells	Distance Between Water Production Wells and Rink SWD 1 and Rink SWD 2
1	E1 well	
2	E1 + two production wells	0.5 miles
3	E1 + two production wells	1.0 miles
4	E1 + three production wells	0.3 miles
5	E1 + two production wells	0.5 miles
6	E1 + four production wells	0.5 miles
7	E1 + five production wells	0.5 miles
8	E1 + five production wells	0.3 miles

Within the field simulation model, the distance between the BEST E1 well and the Rink SWD 1 was 0.286 miles and BEST E1 and the Rink SWD 2 was 0.254 miles (Figure 4-2). Four injector wells were identified in the area of interest and included in the numerical model: Rink SWD 1, Rink SWD 2, NDIC 10525, and NDIC 90183 (Figure 4-2).

DocuSign Envelope ID: 2FA9A609-C360-4E53-8B28-BE8B77B6994A

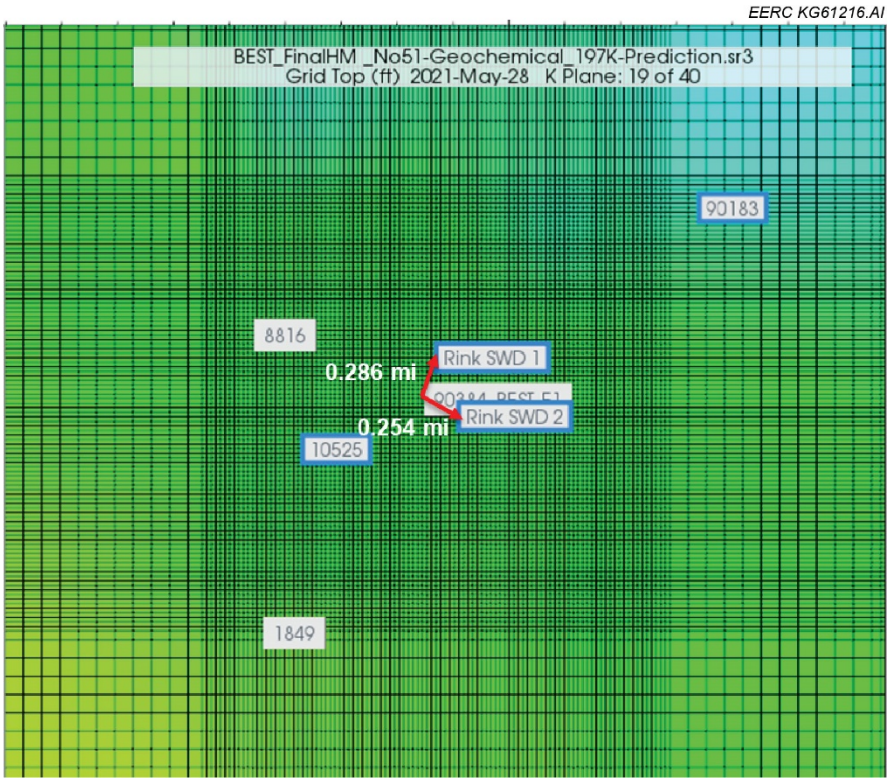


Figure 4-2. Field numerical model showing the distance in miles from the E1 producer well to Rink SWD 1 and SWD 2 – Scenario 1.

The additional production wells were placed at a distance no greater than 1 mile from the Rink SWD 1 and SWD 2 wells. The production water rate for the BEST E1 well was assumed to be the same as the field data at about 4900 bpd. Initially, a 6000-bpd water production rate was assumed for the new production wells. Two to five production wells were incorporated into the model within the BEST study area. The addition of the two to five production wells, along with the evaluation of the varied distances of those wells, helps to evaluate any potential changes in the BEST E1 water salinity while assessing their contribution to better controlling/reducing the pressure in the Inyan Kara Formation.

4.3 Field Numerical Modeling and Simulation Results

The field numerical simulation model for the Inyan Kara Formation around the BEST location allowed for evaluation of different operational scenarios for GHCR implementation (Table 4-1). The scenarios include a sensitivity analysis on the number of production wells to be added near the current BEST location (E1 and Rink SWD wells), the variable distance between the added production wells with respect to the BEST location, and the production and injection water rates for the added production wells.

All the cases were initially evaluated at two different salinity values: 197,000 ppm calculated to history match the simulation result with the brine density from the sample collected in the field and a salinity of 325,000 ppm for the injector wells based upon one of the last Bakken produced

DocuSign Envelope ID: 2FA9A609-C360-4E53-8B28-BE8B77B6994A

water samples collected from the field. For simplicity, and to preserve the history match in the model, the results using a Bakken produced water salinity of 197,000 ppm will be shown in this report.

4.3.1 Sensitivity Analysis – Number of Wells and Distance Between Wells

The sensitivity analysis evaluated the number of production wells that would be implemented as part of GHCR implementation and the distance between these added wells and the BEST location. The minimum number of production wells was two, leading to a total of three producing wells when BEST E1 is considered. Similarly, the maximum number of production wells was five, for a total of six producing wells. The additional wells were placed in an area around the current BEST location with well distances of 0.3 to 1.0 mile between the Rink SWD injector wells and the added production wells, as shown in Figure 4-3. Initially, the production wells were simulated using a water production rate of 6000 bpd to follow similar historical values for the BEST E1 production well. The production rate for the BEST E1 well was kept the same as the latest water production rates observed in the field of around 4900 bpd.

This subsection provides results on two of the scenarios (i.e., Scenarios 1 and 4), while the results for the remaining scenarios are provided in Appendix D. Scenarios 1 and 4 provide contrasting scenarios: Scenario 1 represents the status quo approach to water management continuing to operate in the BEST area and Scenario 4 provides an example of what could happen should multiple GHCR wells be installed in close proximity to the BEST location.

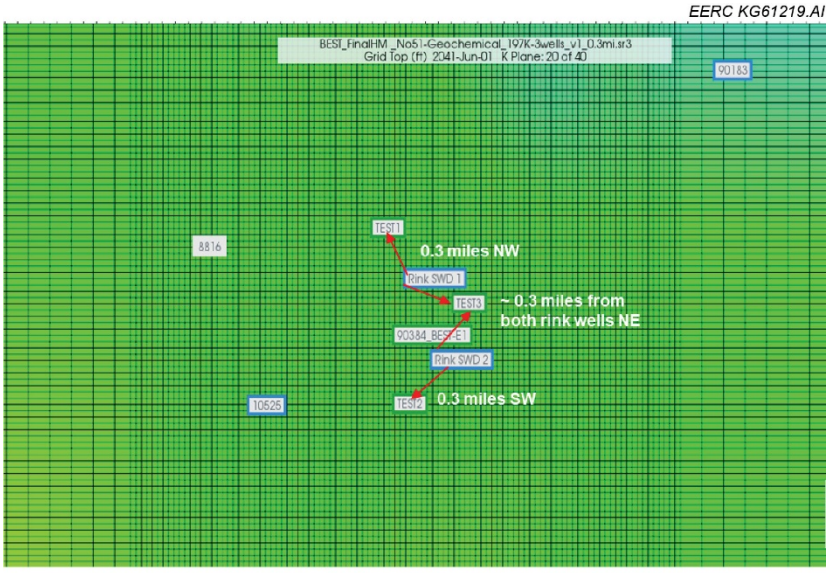


Figure 4-3. Three production wells with a distance between Rink SWD 1 and SWD 2 of 0.3 miles – Scenario 4.

DocuSign Envelope ID: 2FA9A609-C360-4E53-8B28-BE8B77B6994A

In Appendix E, changes in the injection water rates were evaluated by reducing injection volumes by 50% of current (as of June 2021) operational volumes for the SWD wells in the BEST modeling area. A complete shutdown of the water injector wells during the 20-year injection/production predictions was simulated to evaluate injection rate effects on the field's formation pressure. In addition, a case increasing the maximum production rate for the new wells to a value around 30,000 barrels of water per day (bwpd) was evaluated to predict pressure depletion.

Scenario 1

Simulation results have shown that having production from only the BEST E1 well, Scenario 1, under the current injection and production operational conditions, TDS can increase from the initial value of 117,000 mg/L (ppm) at the end of the history match in June 2021, to around 170,000 ppm at the end of the 20 years. The results also indicated a constant pressure increase over 3100 psi under the current operational conditions with no other operational changes within the formation within the model area (Figures 4-4–4-6). This scenario indicates that continued SWD in the area, specifically from the Rink 1 and Rink 2 SWD wells, will result in increasing salinity values as the target reservoir continues to fill with the injected produced waters. Production from the single BEST E1 well is not enough to impact (e.g., reduce) formation pressures within the area.

DocuSign Envelope ID: 2FA9A609-C360-4E53-8B28-BE8B77B6994A

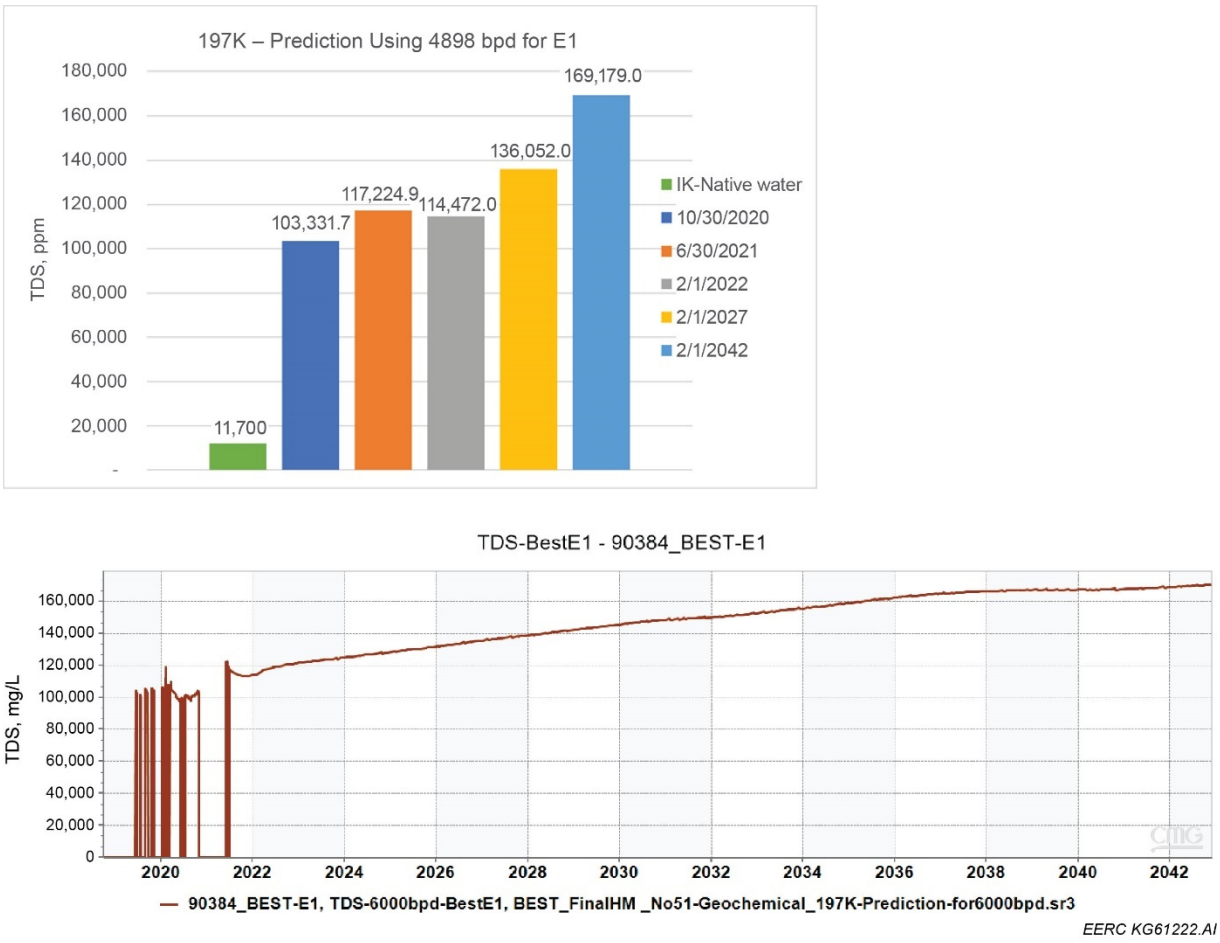


Figure 4-4. Scenario 1 TDS values for BEST E1 producer well during the simulated prediction of 2022 to 2042.

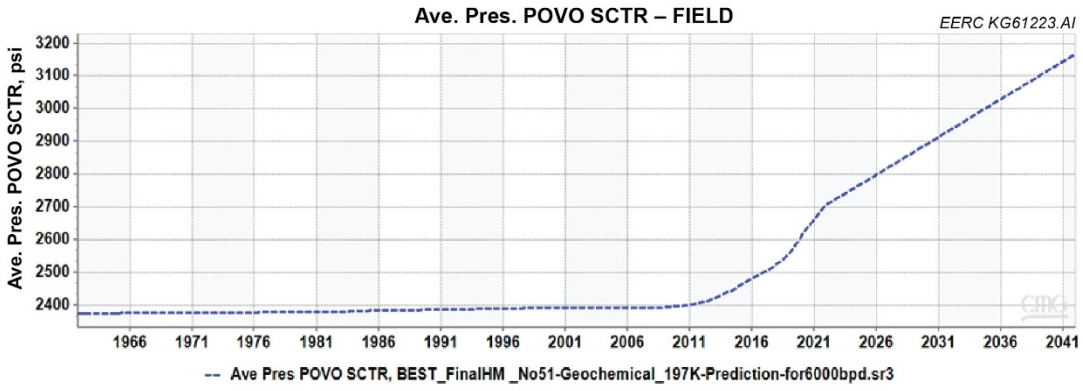


Figure 4-5. Scenario 1 formation pressure with only water production from BEST E1 well.

DocuSign Envelope ID: 2FA9A609-C360-4E53-8B28-BE8B77B6994A

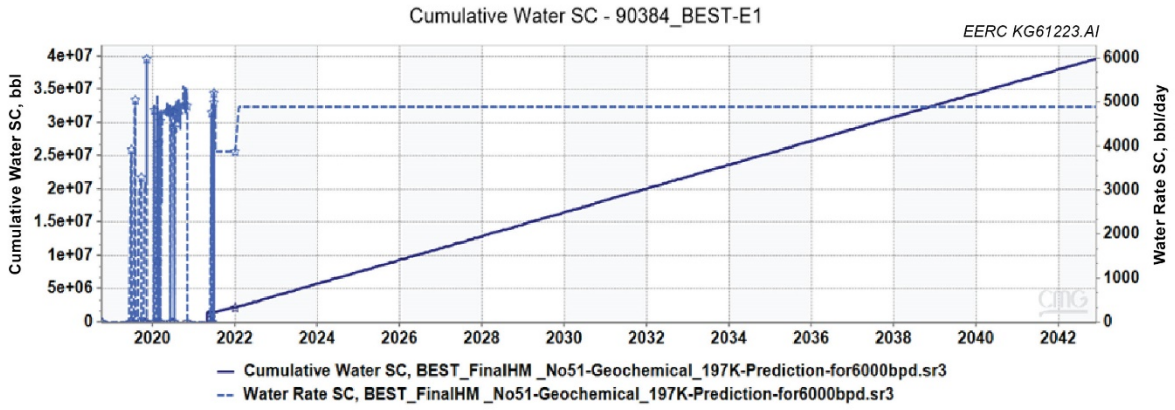


Figure 4-6. Scenario 1 total water produced and water rate for BEST E1 well.

Scenario 4

Adding more production wells into the BEST area can reduce the salinity in the BEST E1 well along the 20 years of predictions and can help control the pressure in the formation. Simulation results for Scenario 4, when three production wells were added in the area with a distance between wells of 0.3 miles and with a water production rate for the additional producer wells of 6000 bpd, showed a decrease in the water salinity for the BEST E1 well from 169,000 to 156,000 mg/L at the end of the 20 years. Also, a decrease in formation pressure was observed, with a reduction of over 400 psi, from about 3100 psi with only the BEST E1 operating to about 2700 psi with the three production wells (Figures 4-7 and 4-8). The additional three production wells also resulted in the total water produced of 177 MMbbl (Figure 4-9). This represents an increase of 347% in comparison with the volume produced by only the BEST E1 well.

This scenario provides an example of changes in the reservoir should the GHCR concept be implemented. The simulation results clearly show that the additional waters extracted from the Inyan Kara Formation would reduce formation pressure at the BEST location. Additionally, a by-product of the removal of fluids is the reduced salinities observed at BEST E1. This reduction at BEST E1 is likely due to the manipulation of the saltwater plumes from the Rink 1 and 2 SWD wells. By extracting water from the formation at simulated production wells (e.g., the GHCR concept wells), the saltwater plumes are drawn toward the production wells, thus keeping the higher-TDS waters from moving directly toward the BEST E1 well as would be seen in Scenario 1.

DocuSign Envelope ID: 2FA9A609-C360-4E53-8B28-BE8B77B6994A

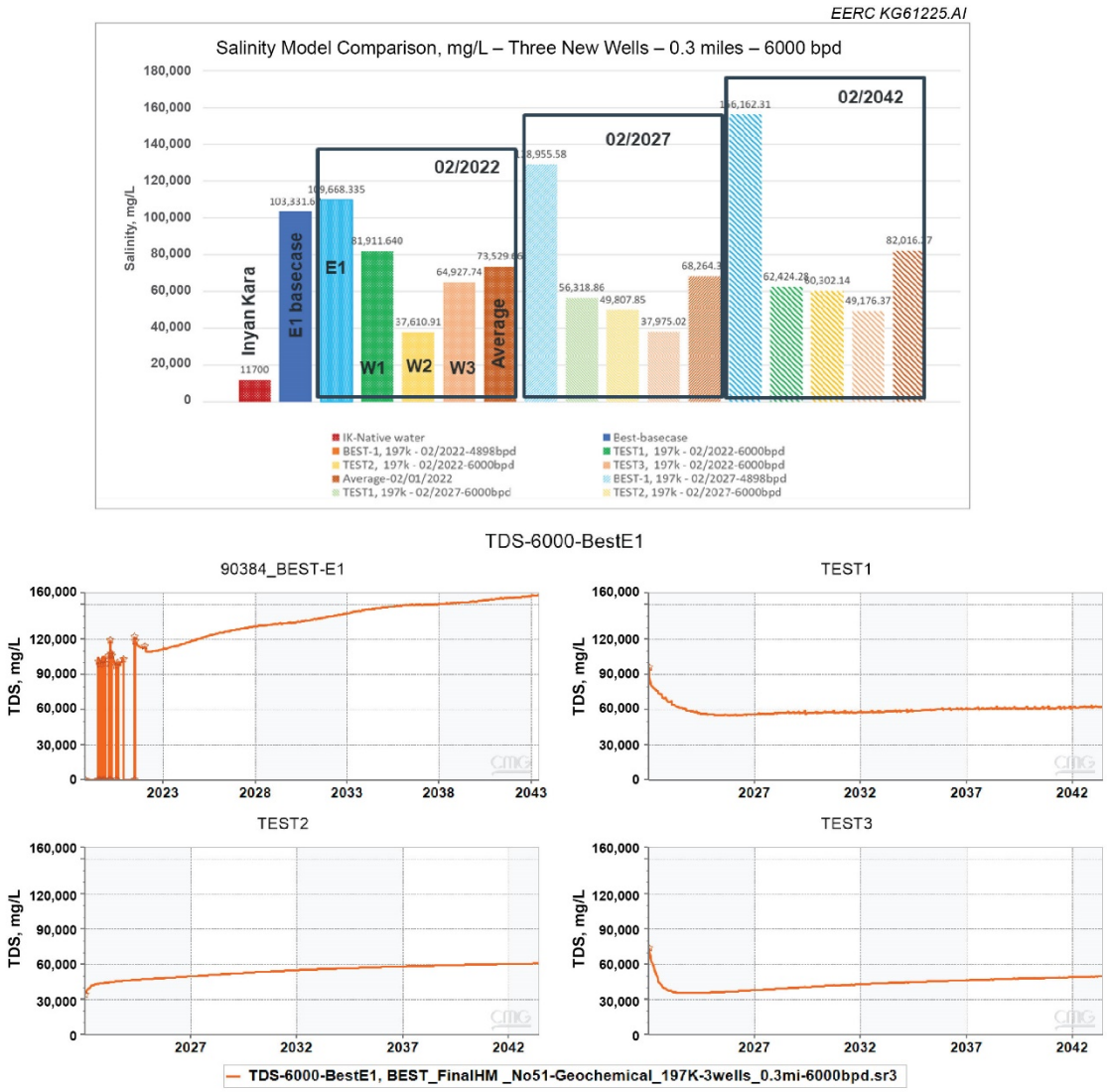


Figure 4-7. Scenario 4 changes in the water salinity (TDS) for each of the four production wells.

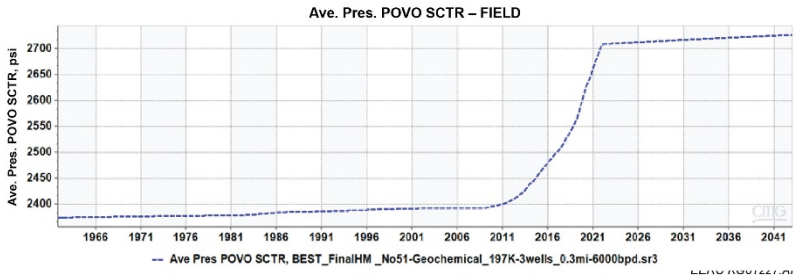


Figure 4-8. Scenario 4 formation pressure with water production from BEST E1 well plus three production wells.

DocuSign Envelope ID: 2FA9A609-C360-4E53-8B28-BE8B77B6994A

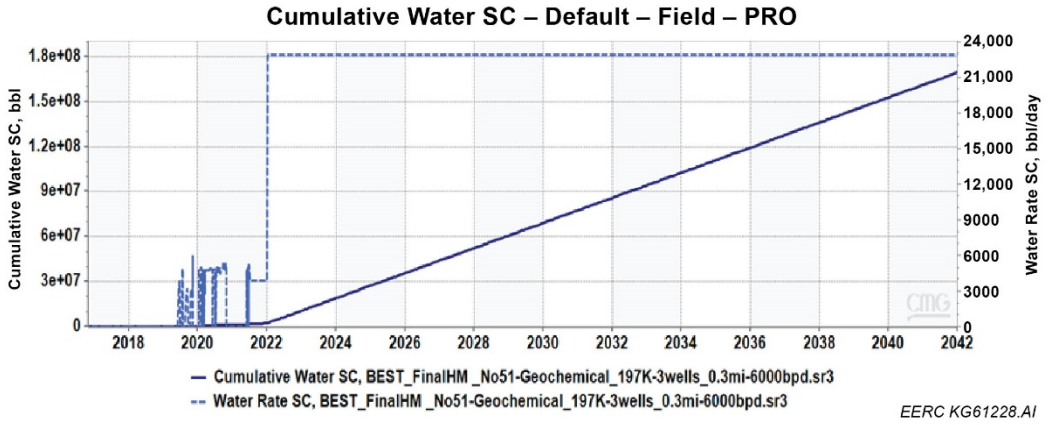


Figure 4-9. Scenario 4 formation pressure with water production from BEST E1 well plus three production wells.

Additional Scenarios

Appendix D shows the simulation results for the additional scenarios. In general, the simulation results for this evaluation showed that adding more production wells to the current BEST E1 well may increase the total water produced from about 39.6 MMbbl up to 267 MMbbl. Also, the pressure in the formation can be reduced and controlled in some cases from over 3100 to about 2400 psi under the operational condition evaluated in these simulations. The constant increase in the pressure currently observed in the BEST area is primarily due to water disposal activity.

The simulation results show that the distance between wells may reduce the water salinity concentration for the water produced and improve the water quality in general. For Scenario 3, where the production wells are placed at 1.0 mile from the BEST location, water salinity concentrations for the production wells were close to native Inyan Kara water of around 11,700 mg/L. The reason for the reduced salinity observed in the simulation results is that the SWD plume at Rink SWD 1 and 2 is not reaching the production wells placed at the 1.0-mile distance, even during the 20 years of SWD injection. Comparing Scenarios 2 and 3 (conditions described in Table 4-1), the formation pressure did not change for the two cases, and only changes in TDS were observed, thus making these scenarios not ideal for GHCR as there was no benefit in formation pressure reduction.

On the other hand, with the production wells at a distance of 0.3–0.5 miles from the BEST location, simulation results showed a decrease in the water salinity for the BEST E1 well and a considerably lower salinity concentration for the new production wells. Simulated cases showed an average water salinity from all the wells (BEST E1 and additional production wells) even lower than 100,000 mg/L, depending on the number of additional wells and the distance between wells. The reduction in the salinity depends on the number of production wells added and their distance from the BEST location. A lower salinity was observed when the production wells were placed at a distance of 0.5 miles from the BEST location, as compared to the values at a well distance of

DocuSign Envelope ID: 2FA9A609-C360-4E53-8B28-BE8B77B6994A

0.3 miles. These values are considerably lower than when only the BEST E1 wells is producing. Figure 4-10 shows the average salinity values from all the production wells in each of the simulated scenarios.

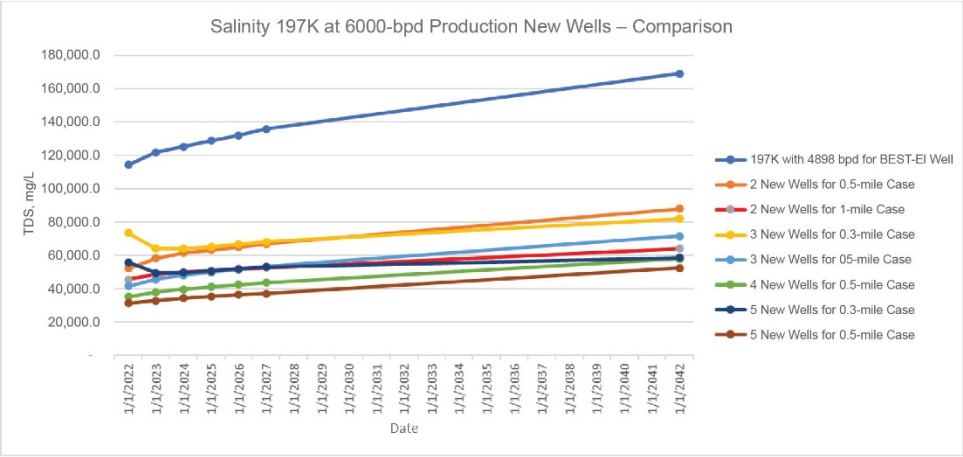


Figure 4-10. Average salinity values calculated from all the producer wells in accordance with each of the scenarios.

Tables 4-3 and 4-4 summarize the field simulation results for the different well layouts and operational conditions evaluated, and the tables show the simulated values at the end of the 20-year simulation. In general, two or more production wells installed as an example of GHCR implementation results in reductions in water salinity and formation pressures across the modeled area, regardless of the given well distances (Table 4-3). Salinity and pressures will vary depending on the number of production wells installed and their distances relative to the BEST location.

Reducing the injection rate of the water injector (i.e., SWD) wells in the area can contribute to greater reductions in water salinity and formation pressures in a GHCR implementation scenario. Table 4-4 summarizes the simulation results when the water injection (i.e., SWD) rates were reduced to half of the current field operation values.

DocuSign Envelope ID: 2FA9A609-C360-4E53-8B28-BE8B77B6994A

Table 4-2. Summary of the Simulation Results for the Number of Wells and Distance Between Wells

Scenario	Conditions	Total Vol. Produced, bbl	Total Produce Rate, bbl/day	Average Salinity at the End of 20 years, mg/L	Field Pressure at the End of 20 years, psi
1	Prediction	39,600,000	4900	169,200	3170
2	Two new wells – 0.5 miles	131,165,000	16,900	87,962	2873
3	Two new wells – 1.0 miles	131,165,000	16,900	64,170	2873
4	Three new wells – 0.3 miles	177,476,000	22,900	82,020	2726
5	Three new wells – 0.5 miles	177,476,000	22,900	71,530	2726
6	Four new wells – 0.5 miles	212,900,000	28,900	54,000	2575
7	Five new wells – 0.5 miles	268,747,000	34,900	50,800	2418
8	Five new wells – 0.3 miles	268,747,000	34,900	54,570	2418

Table 4-3. Summary of the Simulation Results When the Water Injection (SWD) Rate Was Reduced for the Number of Wells and Distance Between Wells

Scenario	Conditions	Total Vol. Produced, bbl	Total Produce Rate, bbl/day	Average Salinity at the End of 20 years, mg/L	Field Pressure at the End of 20 years, psi
1	Prediction	39,600,000	4900	124,200	2885
2	Two new wells – 0.5 miles	131,165,000	16,900	62,895	2606
4	Three new wells – 0.3 miles	177,476,000	22,900	47,904	2417
6	Four new wells – 0.5 miles	212,900,000	28,900	36,096	2273
8	Five new wells – 0.3 miles	268,474,000	34,900	36,560	2117

4.4 Key Observations from Numerical Simulation

- Simulation results have shown that a constant increase in the pressure in the formation and in the water salinity concentration due to the water disposal activity in the area will continue if no operational changes are made and normal SWD operation continues.

- Adding more water production wells in the area with a production rate around 6000–7000 bwpd and with a significant decrease in the injection rate would help to decrease the pressure in the Inyan Kara Formation from an initial pressure of over 2700 psi (where only the BEST E1 well is producing) to 2450–2500 psi.

DocuSign Envelope ID: 2FA9A609-C360-4E53-8B28-BE8B77B6994A

- The addition of more production wells to the current BEST E1 well not only would contribute to a decrease and control of the pressure in the reservoir but would increase the volume and reduce the salinity of the water produced.

- The results have shown a well distance between 0.3 and 0.5 miles from Rink SWD 1 and SWD 2 is favorable for a reduction in the water salinity, thus improving the water quality to be potentially used in other field operations.

- A 50% reduction of the current operational water injection (i.e., SWD) rate in the BEST area resulted in a reduction of the water salinity and reservoir pressure, without diminishing the volume of water produced.

5.0 TECHNO-ECONOMIC ANALYSIS OF GHCR CONCEPT

This activity consisted of a techno-economic analysis (TEA) of GHCR as an approach to Bakken water management. It begins with a review of technical and regulatory drivers that impact how GHCR could be implemented, followed by a study of GHCR implementation costs. All findings are then used to inform a discussion regarding the outlook for GHCR in North Dakota.

GHCR is hypothesized to be a more sustainable water management approach because it couples fluid extraction with disposal injection in the Inyan Kara Formation, which is North Dakota's primary SWD target. After drilling, the extracted fluid is recycled and used for hydraulic fracturing makeup water for new wells which lowers freshwater demand. After the GHCR well is done being used to supply water and during oil production, it can be converted and used for on-site SWD to minimize the cost and risk of transporting produced water. The latter point is significant as produced water management is widely identified as the single largest lease operating expense (LOE) in the Bakken (e.g., Figure 5-1).

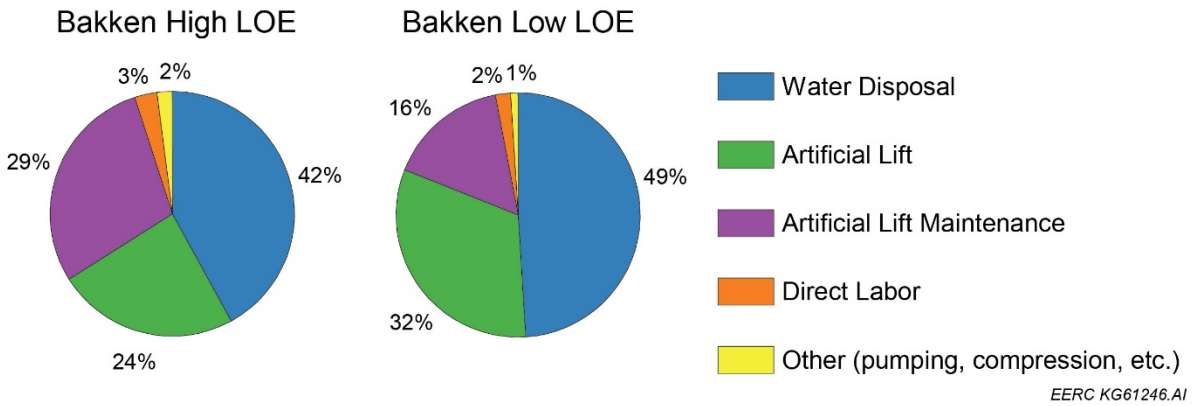


Figure 5-1. Typical Bakken LOE breakdowns (IHS Global Inc., 2015).

DocuSign Envelope ID: 2FA9A609-C360-4E53-8B28-BE8B77B6994A

5.1 TEA Technical Inputs

Several sources of input information were used to create the full-scale model of GHCR performance, including results from other activities under this project, prior studies, and reviewer feedback. The basis and rationale for each key TEA assumption are discussed in this section.

5.1.1 Inyan Kara Pressure Management

One of the benefits of producing fluid from a GHCR well is to locally reduce formation pressure or to slow pressure rise in an area with simultaneous disposal injection. For an active SWD facility, pressure management could extend the useful life of the disposal well and perhaps also reduce the operating power cost to inject fluid. From an injection standpoint, the maximum allowable pressure is 90% of the calculated fracture gradient of the cap rock (Connors and others, 2020). In certain areas of the Williston Basin where SWD injection is high, the Inyan Kara Formation exceeds the standard hydrostatic pore pressure gradient of 0.433 psi/ft and is accommodated for by using an increased drilling mud weight or the use of an additional drill string casing to prevent water influx during drilling of the Inyan Kara interval (Connors and others, 2020). From the standpoint of a Bakken operator, the key benefit of pressure reduction through fluid extraction would likely be the potential to locally reduce formation pressure and avoid the use of extra casing for wells drilled in the affected area.

Data to evaluate the potential magnitude of pressure reduction primarily came from a prior study by Connors and others (2020) that evaluated the impact of Inyan Kara water extraction on localized formation pressure reduction. That study modeled the effects of water production rate and total produced volume on the formation pressure at several distances from the producer well. In order to evaluate the pressure reduction potential of GHCR, a subset of results from Connors and others (2020) were replotted in Figure 5-2 to indicate the affected distances, along with the produced fluid volumes that would be expected in a GHCR application, which were based on a Bakken average value of 200,000 bbl per completion (Energy & Environmental Research Center, 2020). Each curve in Figure 5-2 represents the distance at which formation pressure was reduced by 135 psi, which was one of the threshold scenarios assumed by Connors and others (2020) to avoid using a Dakota string.

With respect to the TEA, Figure 5-2 shows that significant pressure reductions can be achieved from the withdrawal volumes that would be expected from a GHCR production well and that the effect extends a greater distance as the production rate increases. However, the longest affected distance is approximately ¼ mile (~1300 ft), which implies that a GHCR producer would need to be similarly close to the location of the oil wells to provide a beneficial effect. Therefore, a GHCR well might be expected to benefit wells on the same drill spacing unit (DSU) having nominal dimensions of 1 mile by 2 miles, or perhaps adjacent DSUs if the wells were sufficiently close to the border, but likely not any further.

DocuSign Envelope ID: 2FA9A609-C360-4E53-8B28-BE8B77B6994A

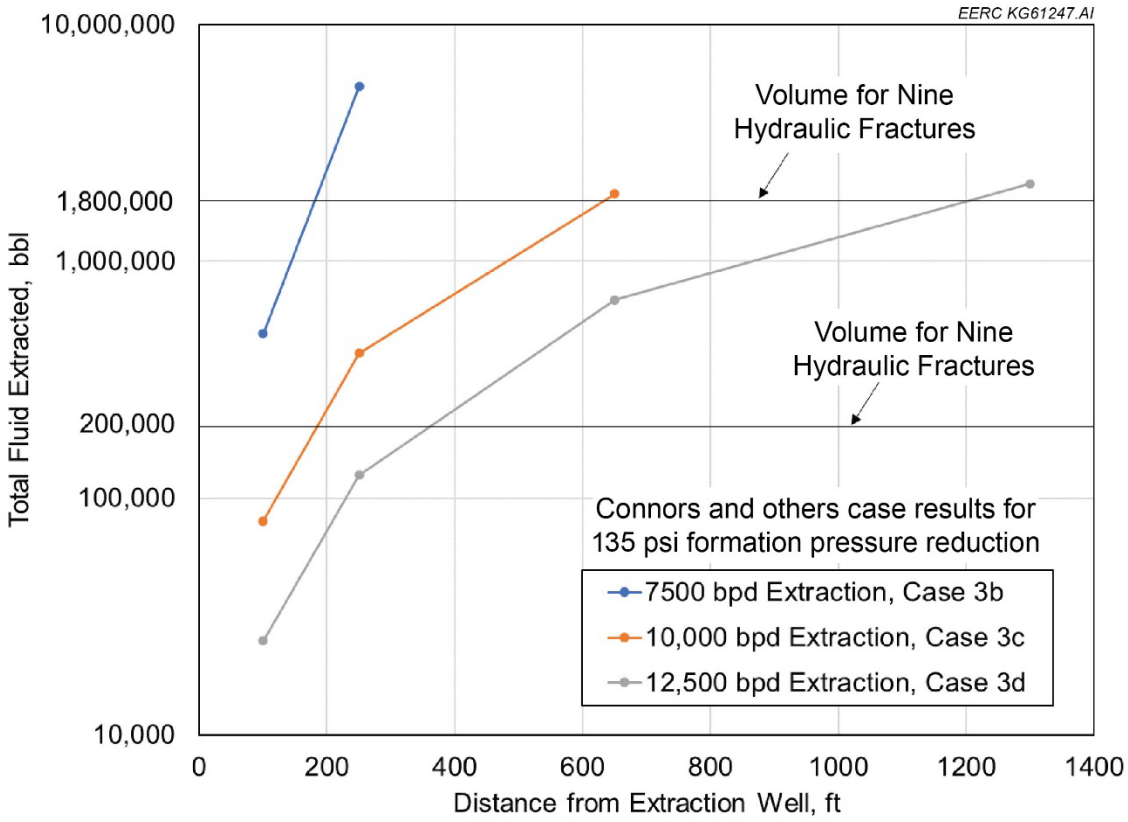


Figure 5-2. Connors and others (2020) model results replotted according to pressure-affected distance.

The size of the pressure-affected zone is one factor that will impact the utility of GHCR pressure management; another is obtaining the proper sequencing of GHCR fluid production and drilling of the oil well(s) that might benefit from pressure reduction. For example, assuming that a series of infill oil wells can be positioned within the pressure-affected zone of a GHCR producer well, the fluid would need to be produced prior to infill drilling to be of any benefit. However, that creates an issue of where the produced fluid should go during drilling, since surface storage of produced water in large, open-top brine tanks, earthen ponds, or liquid waste pits has historically not been allowed in North Dakota. Three hypothetical scenarios were identified that might allow for the proper sequencing.

1. The infill wells on a DSU are drilled and completed sequentially rather than drilled and completed as a group. In this way, the extracted fluid used for completing the first well creates the pressure-affected zone for the second well, and so on.

2. The produced fluid is used for completions on a neighboring DSU, and these occur prior to drilling the DSU that contains the GHCR producer well.

3. Two GHCR wells are drilled: a producer that creates the needed temporary pressure relief zone near the infill wells and an injector that is used to dispose of the produced fluid away from the

DocuSign Envelope ID: 2FA9A609-C360-4E53-8B28-BE8B77B6994A

pressure-affected zone. After infill drilling, one or both of the GHCR wells are used to produce fluid for fracturing, and after completion, one of the wells is converted for SWD.

Of these examples, only Scenarios 2 and 3 appear compatible with the typical pattern of group drilling and completion in the Bakken. In Scenario 2, the produced fluid is simultaneously used for fracturing, while in Scenario 3, the fluid is temporarily stored in the Inyan Kara using an injector well. Given these limitations in matching pressure relief with well drilling, the TEA modeled both outcomes for the GHCR cases, i.e., the oil well costs were calculated both with and without the use of a Dakota string.

5.1.2 GHCR Produced Fluid Characteristics

Another hypothesized benefit of GHCR was that the quality of the produced water would be improved after passage through the Inyan Kara Formation; effectively the formation would serve as a very large filtering and conditioning element. The core flow tests and field site sampling reported under Section 3.0 generally show this to be the case. For example, suspended solids content of the flow-through liquid was largely reduced, thereby demonstrating a filtering function. Based on these positive results, the TEA cases that included produced fluid recycling were assumed to use 100% recycled fluid with no substantive water treatment following production.

Equally important to recycling potential was the produced fluid's consistency i.e., the uniformity in the fluid's chemical composition over the entire volume needed for a completion. Operator feedback suggested that completion fluid chemistries can be tailored to use a wide range of produced water composition; however, consistency was key (Energy & Environmental Research Center, 2020). Consistency is of most concern during breakthrough i.e., when the produced fluid composition changes from being largely formation fluid to a steady-state mixture of formation fluid and injected saltwater since fluid produced prior to and after breakthrough will very likely be suitable for recycling. To evaluate the composition changes during breakthrough, Section 4.0 field modeling results were reviewed for cases that resulted in breakthrough. Based on the observed rates of composition change, it was determined that changes due to breakthrough would likely be insignificant over individual batches of 200,000 bbl, which was assumed to be a typical volume needed for an individual completion.

GHCR water management also requires that a sufficient quantity of fluid is produced before reservoir pressure depletion and that the production rate roughly matches the demand set by hydraulic fracturing, which by design is a short-duration, high-flow process. Field modeling results reported in Section 4.0 and Appendix D were again used to evaluate the potential production under conditions where the formation pressure alone was used to drive fluid to the surface. In general, these results appear to show no significant limitations for GHCR due to the quantity of produced fluid. Likewise, the rate of production could also be supported, but, of course, the actual production potential will be dependent on site-specific reservoir conditions. One trend highlighted by the modeling was that multiple GHCR wells producing in aggregate could supply a target production rate for a longer period compared to using only a single producing well. Therefore, while a single-well GHCR system might be technically possible in pressurized areas of the Inyan Kara, a system based on multiple production wells will likely be adaptable to more Bakken locations and offer a greater range of production rates.

DocuSign Envelope ID: 2FA9A609-C360-4E53-8B28-BE8B77B6994A

5.2 Regulatory Considerations

5.2.1 Review of Regulatory Environment

While understanding the technical and economic feasibility of GHCR is important, additional key regulatory considerations need to be addressed to permit a project of this nature. Produced water management in association with oil and gas production in the state of North Dakota is predominantly regulated by NDIC's Department of Mineral Resources (DMR) Oil and Gas Division. The North Dakota Century Code (NDCC) establishes general authority for NDIC DMR jurisdiction to regulate disposal of saltwater and oilfield wastes (NDCC Section 38-08-04 subsection 1b). NDIC DMR regulates produced water management associated with oil and gas exploration and production. Specifically, NDIC DMR handles the different components of produced water management including the water produced at the wellsite in association with oil and gas production, the transportation of produced water via underground gathering pipeline, saltwater-handling facilities associated with storing and managing produced water at surface facilities, and the disposal of the produced water in a SWD injection well. SWD wells are regulated as Class II injection wells under the federal underground injection control (UIC) program. NDIC DMR received primary regulatory authority over Class II injection well activities (i.e., Class II primacy) from the U.S. Environmental Protection Agency (EPA) in 1983. This regulatory authority applies to all Class II injection well activities in the state of North Dakota, except for Indian Lands where EPA maintains Class II regulatory authority. NDIC DMR began regulating produced water transportation via underground gathering pipelines in 2013. In 2015, the North Dakota Legislature expanded NDIC DMR's authority to include the construction and operation of crude oil and saltwater underground gathering pipelines.

The North Dakota Department of Water Resources, formerly known as the State Water Commission, regulates water appropriation in the state, including groundwater. The State Engineer is charged with managing the use of the state's waters as directed under NDCC Chapter 61-04 and Article 89-03 of the North Dakota Administrative Code (NDAC). This regulatory authority includes water source wells that would be necessary to extract formation fluid if the GHCR concept were implemented. Water source wells used to extract water from geologic formations, including the Inyan Kara Formation, exist today in North Dakota oil and gas operations. These wells provide a working fluid that is injected in the mineral-bearing reservoir for enhanced oil recovery operations. In addition, current water source wells are used to provide water for hydraulic fracturing and other oilfield operations. In North Dakota, there are currently 68 water supply wells used predominantly to supply water for enhanced oil recovery operations (Figure 5-3). The water appropriation permit is issued by the North Dakota Department of Water Resources and identifies the total quantity of water permissible to extract and the maximum withdrawal rate. In addition, the well is permitted and regulated by NDIC DMR in a dual permitting process.

Table 5-1 identifies the regulatory authority and applicable state regulations based on the particular phase of produced water management.

DocuSign Envelope ID: 2FA9A609-C360-4E53-8B28-BE8B77B6994A

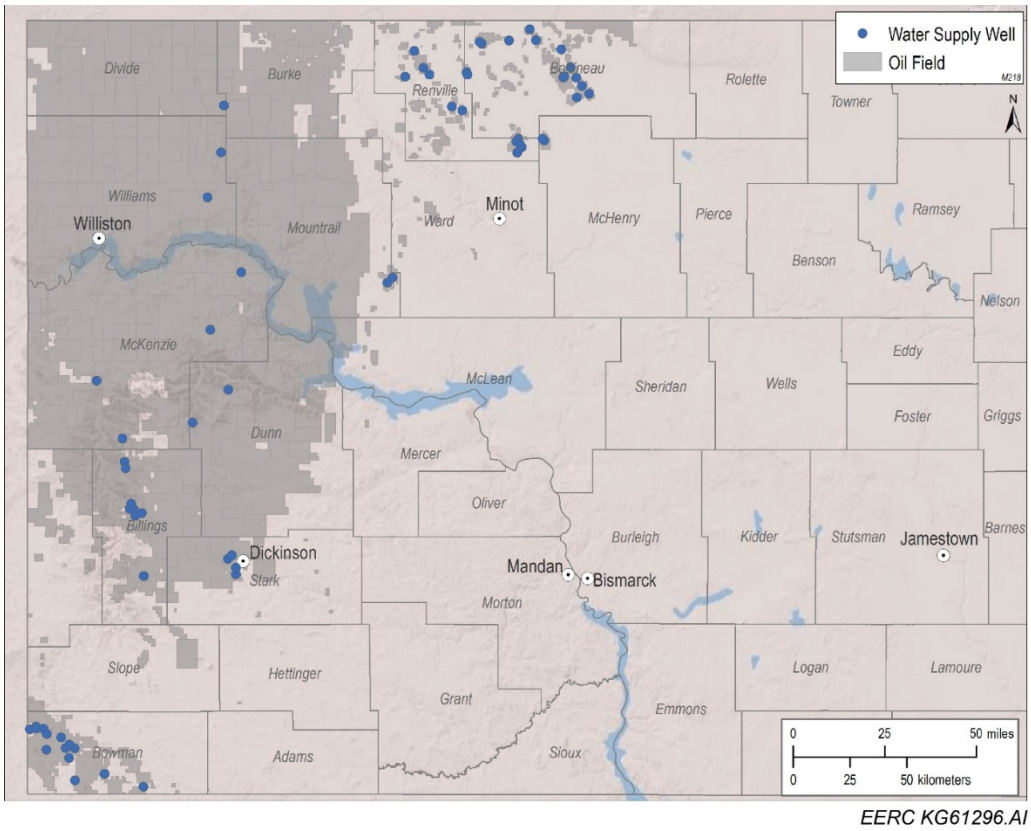


Figure 5-3. Active water supply wells in North Dakota.

DocuSign Envelope ID: 2FA9A609-C360-4E53-8B28-BE8B77B6994A

Table 5-1. Summary of North Dakota Regulations Relevant for GHCR Produced Water Regulatory Jurisdictions and References

Produced Water Management Activity	Regulatory Authority	Regulatory Framework
Produced Water (includes Class II SWD injection wells)	NDIC DMR Oil and Gas Division	(Class II SWD injection wells) NDAC Chapter 43-02-05 Underground Injection Control
Produced Water Pipelines (underground gathering pipelines)	NDIC DMR Oil and Gas Division	NDCC Section 38-08-27 Controls, Inspections, and Engineering Design on Crude Oil and Produced Water Underground Gathering Supplies NDAC Section 43-02-03-29.1 Crude Oil and Produced Water Underground Gathering Pipelines
Saltwater-Handling Facilities	NDIC DMR Oil and Gas Division	NDAC Section 43-02-03-53 Saltwater-Handling Facilities; NDAC Section 43-02-03-53.1 Saltwater-Handling Facilities Requirements; NDAC Section 43-02-03-53.2 Saltwater-Handling Facilities Siting; NDAC Section 43-02-03-53.3 Saltwater-Handling Facilities Construction and Operation Requirements; NDAC Section 43-02-03-53.4 Saltwater-Handling Facilities Abandonment and Reclamation Requirements
Water Source Well	North Dakota Department of Water Resources	NDCC Chapter 61-01 and NDAC Section 89-03-01

From a regulatory standpoint, GHCR water management can be divided into three operational steps, all of which will have to comply with regulatory oversight:

1. Operating a water production well (i.e., water source well) from a deep formation (i.e., Inyan Kara) to produce fluids for industrial use.

2. Transporting produced water either on- or off-pad for use in hydraulic fracturing, maintenance water needs, or other commercial uses.

3. Operating a Class II SWD injection well.

DocuSign Envelope ID: 2FA9A609-C360-4E53-8B28-BE8B77B6994A

Steps 1 and 3 have established frameworks in place, but Step 2 could introduce new scenarios that may require regulatory clarification. Specifically, using produced fluid for hydraulic fracturing will require transporting large volumes of fluid over a relatively short duration of time, and the normal methods of delivering freshwater may not apply to higher-TDS produced fluids, for example, the use of temporary lay-flat hose. Lay-flat hoses are used in the oil fields in North Dakota but have been only permitted to transport freshwater for use in hydraulic fracturing. Regulatory guidance is necessary for the use of temporary hoses to transport produced brine. There is also regulatory uncertainty related to the long-term surface storage of produced fluids, as NDIC DMR has not normally allowed the use of large open-top brine tanks or earthen ponds utilized in oil and gas production operations, specifically in drilling and hydraulic fracturing.

Regulations for saltwater-handling facilities can be found in NDAC Section 43-02-03-53, which outlines the necessary permits and infrastructure required for surface facilities used to manage large volumes of produced water. The main focus of these regulations are the protection of freshwater sources and the near-surface environment as Section 43-02-13-53.2 states that "all saltwater handling facilities must be sited in such a fashion that they are not located in a geologically or hydrologically sensitive area." NDAC Section 43-02-03-53 provides the permitting process for saltwater-handling facilities, including construction standards. NDAC Section 43-02-03-53.3 Saltwater-Handling Facility Construction and Operation Requirements, outlines the necessary safety barriers that need to be erected such as creating a dike around saltwater tanks and the saltwater-handling facility location. "Dikes must be of sufficient dimension to contain the total capacity of the largest tank plus one day's fluid throughput." NDIC DMR regulations for saltwater-handling facilities are specific to facilities that are not colocated with a SWD well.

5.2.2 Review of Various States' Regulation of Produced Water

A produced water regulatory review for the larger oil and gas-related water-producing states was conducted to identify similarities or differences, if any, with the North Dakota regulatory frameworks. During the analysis of state policy and legislation, it was noted that regulation does not currently exist in many states with regard to the reuse or recycle of produced water. States such as Texas and New Mexico have recently enacted bills that have created groups and consortiums to further research and develop methods. However, the language in many of these bills and enacted laws shows an indication for continued research to enhance state knowledge and provide guidance for policy coverage in this industry. Oklahoma has recently engaged an adjusted bonding regulation providing further incentive for oil and gas businesses to reuse and/or recycle produced water.

DocuSign Envelope ID: 2FA9A609-C360-4E53-8B28-BE8B77B6994A

Table 5-2. Produced Water Ownership and Liability Findings in Six States
Disclaimer: This table should not be considered a legal opinion regarding the ownership of or liability for produced water under all circumstances. It is merely a compilation of general research conducted on behalf of the Ground Water Protection Council (GWPC).

State	Groundwater Right Doctrine	Produced Water Ownership		Produced Water Liability	
		Operator	Landowner	Operator	Other Persons
New Mexico	Prior appropriation		X[1]	X	X
North Dakota	Prior appropriation		X[2]	X[3]	X
Oklahoma	Reasonable use	X[4]		X	
Pennsylvania	Reasonable use	[5]	[5]	X	
Texas	Absolute Ownership Rule		X	X	X[6]
Wyoming	Prior appropriation		X[2]	X	

Specific provisions that may apply to or modify the information contained in Table 5-2 include the following:

[1] In New Mexico, the term "possession" is often used because actual water ownership is by contract only.

[2] Water is not owned, but pore space is the property of the surface rights owner.

[3] Operator is immunized from liability if transferred to a commercial oilfield special waste-recycling facility.

[4] Produced water ownership in Oklahoma resides with the oil and gas operator except that landowners have "domestic use" of water flowing across the property (Mack Oil Co. v. Laurence, 389 P.2d 955 [Okla. 1964]).

[5] The Pennsylvania Legislature has not explicitly defined who owns produced water. As a result, produced water is likely owned by either the landowner or the oil and gas operator. However, use of groundwater off of the premises is considered unreasonable and unlawful per se if other users' rights are interfered with (Bishop, 2006; Weston and Burcat, 1990).

[6] Texas limits tort liability for sellers or transferors of recycled produced water (3 Texas Natural Resources Code Annotated § 122.003[a] [2015]).

Texas oil and gas produced water jurisdiction is overseen by the Texas Commission on Environmental Quality. This agency oversees wastewater surface discharge from state oil and gas well production in the industry. The Railroad Commission of Texas has jurisdiction of wastewater from the oil and gas industry if the produced water is used in other methods such as reuse, dust suppression, impoundment maintenance, evaporation, or irrigation (Texas Commission on Environmental Quality, 2021). While both departments oversee water use and dispersant in the state of Texas, there are few guidelines that dictate the industrial use of produced water. There is movement within the state legislature to further knowledge of produced water constituents, reuse, and recycling opportunities. In June 2021, Texas creating the Texas Produced Water Consortium which aims to study the economics and environmental impact of reused produced water (Texas Produced Water Consortium, 2021). With Texas's interest in expanding produced water research, more detailed policy may emerge to give way to a clear path for produced water business.

New Mexico has taken a similar path to Texas. The New Mexico Legislature (2019) adopted the Produced Water Act on July 1, 2019, which defines produced water as "fluid that is an incidental byproduct from drilling for or the production of oil and gas." This act identifies the responsible parties for all aspects of produced water, which include use, handling, disposal, transfer, selling, conveying, transport, recycle, reuse, or treatment of produced water. It also further encourages the research and development of industrial uses of produced water. Although, New Mexico does not have an existing permit process for produced water, as outlined in Section 19.15.34.8 Requirements for Reuse, Recycling or Disposal of Produced Water,

DocuSign Envelope ID: 2FA9A609-C360-4E53-8B28-BE8B77B6994A

Section 19.15.34.8A(1) states that, "No permit registration is required from the division for the re-use of produced water for drilling, completion, production, pressure maintenance, secondary recovery or enhanced recovery of oil or natural gas of wells pursuant to 19.15.34 NMAC." This policy acknowledges the need for continued research into this topic as Section 19.15.34.8A(3) states, "research using produced water is to be encouraged through pilot projects approved by the division."

Oklahoma recently signed into law, Senate Bill 1875 in May 2020, also known as the Oil and Gas Produced Water and Waste Recycling Reuse Act (State of Oklahoma, 2020). This bill clarifies that "produced water and waste is the property of the oil and gas producer until it is officially transferred to another person. It also shields liability from those who process wastewater into recycled water and/or transport this recycled water for further use in oil and gas production" (Oklahoma Senate, 2020). This recent movement demonstrates that Oklahoma is on the path for the advancement of creating guidance and regulations for produced water business.

Regulatory guidance on produced water exists in other states in the form of waste management, but not to the extent that is required for GHCR to become an industrial resource. Oklahoma has paved the way in policy recently, with the realization for the need for additional guidelines. In comparing the rules and regulations to the those from North Dakota, it is evident that produced water is an emerging industry for which many regulators are looking to provide proper policy guidelines.

5.2.3 Regulatory Discussion

Based on the regulatory review, the tasks of drilling into the Inyan Kara for SWD and for producing water for industrial use have precedent in North Dakota, and a workable regulatory solution for GHCR seems likely. However, restrictions in the state regarding surface storage and transport of produced fluids may limit some activities, which will affect how GHCR could ultimately be implemented.

The NDIC DMR Oil and Gas Division has typically not allowed surface storage of large open-top brine tanks or earthen ponds utilized in oil and gas operations, specifically in drilling and hydraulic fracturing. These prohibitions would seem to restrict recycling facilities in North Dakota. On the other hand, GHCR would appear to be allowed under current NDIC DMR precedent, provided it can operate without a large surface storage buffer. The performance impact of a minimal fluid storage buffer is that the production rate of GHCR produced fluid would need to nearly match the rate the fluid is used for hydraulic fracturing.

Lay-flat hose is used in North Dakota for the temporary transport of freshwater, but its application to recycled fluids may run counter to the state's efforts to eliminate produced water spills. An alternative to temporary hose transport is trucking, but this option is more costly.

One possible solution for the temporary transport of recycled fluids is if the GHCR producer and the wells being completed were in close proximity on the same pad. In such a case, it is conceivable that the entire transport line would be within the pad's containment berm to limit regulatory concerns.

DocuSign Envelope ID: 2FA9A609-C360-4E53-8B28-BE8B77B6994A

5.3 GHCR Cost Modeling

All TEA cases were based on the same underlying oil production scenario, which was the infill development of a single DSU that has an existing parent well. Nine infill wells were assumed to be added based on the infill well density observed in areas of the Bakken where infill development has not been completed and where there has been the need to use a Dakota string, e.g., north of Williston, North Dakota (Connors and others, 2020). Specifically, infill density was characterized by units of the Lone Tree Lake and East Fork Fields. Workover of the parent well was not included as part of the TEA.

Four TEA case studies were evaluated to investigate the value proposition of GHCR water management. Details of the studies, one of which was a model of conventional Bakken practice, are summarized in Table 5-3, which is followed by brief descriptions.

- Conventional water management consisted of conventionally sourced freshwater for both hydraulic fracturing and maintenance water needs and off-site produced water disposal at a SWD facility. This case assumed there is a Dakota string that would be required for the oil wells.

Table 5-3. TEA Case Details

Case	Conventional	GHCR 1	GHCR 2	On-Site SWD
Potential to Eliminate Dakota String	No	Yes	Yes	No
Number of GHCR/SWD Wells	0	1	2	1
On/Off-Site SWD	Off-site	On-site	On-site	On-site
Fracture Fluid Water Source	Fresh	Produced	Produced	Fresh
Maintenance Water Source	Fresh	Fresh	Produced	Fresh

- The GHCR 1 case assumed one Inyan Kara well is drilled and used to produce fluid for hydraulic fracturing, either on the same DSU or a nearby unit. Fluid production could lower formation pressure and, if its proximity and timing aligned, may avert the need for a Dakota string on subsequent oil wells drilled nearby. After production, the single GHCR well is converted for on-site SWD, but since it can no longer be used for fluid production, maintenance water needs would be met from a conventional freshwater source.

- The GHCR 2 case assumed drilling two Inyan Kara wells to increase the likelihood of achieving the maximum benefits of GHCR. Initially the two wells would be set up as a producer and injector pair to create a zone of reduced formation pressure where the associated oil wells could be drilled without a Dakota string. After drilling, both GHCR wells are used to produce fracture fluid, and after the completion phase, one of the GHCR wells is converted to on-site SWD while the other continues to produce fluid for maintenance water needs.

DocuSign Envelope ID: 2FA9A609-C360-4E53-8B28-BE8B77B6994A

- The on-site SWD does not include a production phase to support hydraulic fracturing. Instead, the well is only used during oil production for on-site SWD. As with the conventional case, no fluid is produced from the SWD well, and there is no opportunity to reduce Inyan Kara pressure to possibly avoid using a Dakota string on the associated oil wells.

5.3.1 Cost Assumptions

The scope of the TEA included initial investments for the oil well and facilities, along with any GHCR water management investments (e.g., GHCR well or wells and facilities). Oil well completion costs were also counted as initial investments. Future costs included LOEs during the production phase, as categorized in Table 5-4.

Table 5-4. TEA Considered Costs

	Initial Investments		Future Costs
TEA Case	**Drilling**	**Completion**	**Production LOE**
Conventional	Oil well with Dakota string; surface facilities	Freshwater-based fracture fluid	Nonwater LOE, off-site SWD, fresh maintenance water
GHCR 1 and 2	Oil well with/without Dakota string; surface facilities; GHCR wells and surface infrastructure.	Produced fluid-based fracture fluid	Nonwater LOE; on-site SWD; fresh or produced maintenance water
On-Site SWD	Oil well with Dakota string; surface facilities; SWD well and surface infrastructure	Freshwater-based fracture fluid	Nonwater LOE; off-site SWD; fresh maintenance water

Cost values used for the nominal TEA calculations are presented in Table 5-5, along with the basis used to identify them. As noted in the table, several costs were based on typical assumptions noted in well file disclosures or from direct feedback by various operators. These values were used here to be consistent with the general evaluation criteria for Bakken wells and were not based on the detailed analysis of a specific project.

DocuSign Envelope ID: 2FA9A609-C360-4E53-8B28-BE8B77B6994A

Table 5-5. Nominal TEA Costs

TEA Input	Assumed Value	Basis
Oil Well Drilling and Completion	$6,800,000/well	(IHS Global Inc., 2015)
Dakota String Addition	$500,000/well	(Connors and others, 2020)
Oil Production Facilities	$600,000/well	(IHS Global Inc., 2015)
Inyan Kara Well Cost	$1,500,000/well	Feedback about existing SWD facilities
GHCR Facilities	$1,000,000 for initial well; $500,000 for second well	Feedback about existing SWD facilities
Freshwater Cost	$3.00/bbl delivered	(Energy & Environmental Research Center, 2020)
On-Site Produced Water Cost	$0.70/bbl	Typical operating cost for conventional freshwater (Energy & Environmental Research Center, 2020)
Off-Site SWD	$3.00/bbl	(Energy & Environmental Research Center, 2020)
On-Site SWD	$0.55/bbl	Typical operating cost for conventional SWD (Energy & Environmental Research Center, 2020)
Maintenance Chemicals	$0.30/bbl maintenance fluid	Feedback, based on 10% of freshwater charge
Nonwater LOE	$5.00/bbl oil	Nonwater LOE fraction from (IHS Global Inc., 2015)
Wellhead Oil Value	$50.00/bbl	Typical well file value
Wellhead Gas Value	$3.00/MMBtu	Typical well file value
Royalty Assumption	20% oil and gas revenue	Typical well file value
Oil Tax Rate	10% oil revenue	Typical well file value
Gas Tax Rate	$0.10/Mcf gas	Typical well file value

DocuSign Envelope ID: 2FA9A609-C360-4E53-8B28-BE8B77B6994A

5.3.2 Oil and Gas Production Profiles

Oil and gas decline curves were developed from Bakken-average data prepared by the North Dakota Pipeline Authority (Kringstad, 2020). Both profiles are plotted in Figure 5-4. The estimated ultimate recovery based on the profiles was 534 MMbbl for oil and 1594 MMscf for gas after 30 years of production. Given their lesser financial impact, natural gas liquids were not included in the TEA.

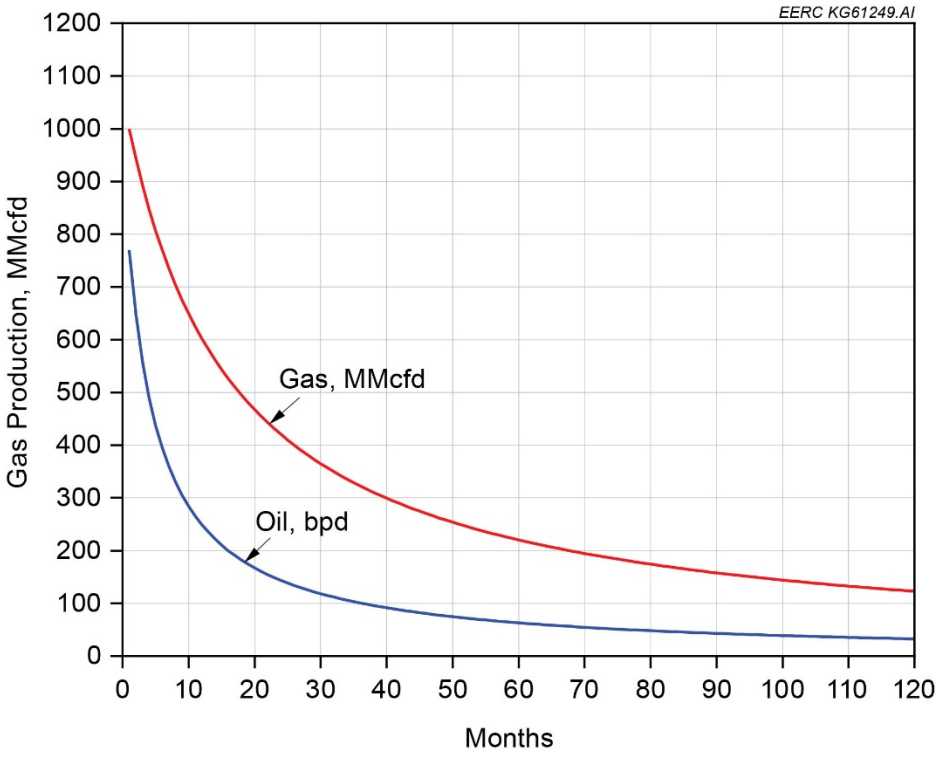


Figure 5-4. Oil and gas decline curves assumed in the TEA.

5.3.3 Water Demand and Disposal Profiles

Similar to oil and gas production, demand and production profiles were developed for the water streams associated with Bakken oil development. These streams included the water demand for hydraulic fracturing, the water produced with oil that needs disposal, and the maintenance water demand.

Hydraulic fracturing water is needed during the completion phase of an oil well and is a relatively short-duration, but high-intensity water demand. For the TEA, a water demand typical of recent slickwater fractures, 200,000 bbl, was assumed (Energy & Environmental Research Center, 2020), and the rate was spread evenly over a typical completion time of 4 days. The other water demand is for maintenance water, which is needed during oil production to dilute the produced water and prevent salt precipitation. Industry guidance identified an average value of

DocuSign Envelope ID: 2FA9A609-C360-4E53-8B28-BE8B77B6994A

35 bpd per well for maintenance water (Energy & Environmental Research Center, 2020). For the TEA, it was assumed that maintenance water would start 12 months after initial oil production, when oil production was estimated to drop to roughly one-third its initial production value. In the GHCR 2 case, produced fluid is used for maintenance; however, it was assumed that more of it would be needed to achieve an equivalent level of dilution compared to fresh maintenance water. In the TEA, it was assumed that 20% more produced water, or a total of 42 bpd, was needed for maintenance purposes. A graphical summary of both water demand streams is presented in Figure 5-5.

Water disposal from the water produced alongside oil production was based on the Bakken-average oil decline curve in Figure 5-4 and the assumption of a 0.58 water cut (Energy & Environmental Research Center, 2020). The total produced water quantity was 738 MMbbl over 30 years. As noted in the SWD profiles of Figure 5-6 for the GHCR cases, the GHCR wells were assumed to be converted to SWD only after the final oil well completion (since the GHCR wells were needed to provide fracture fluid). Therefore, in the TEA, it was assumed that these cases relied on off-site SWD until all hydraulic fracturing was complete.

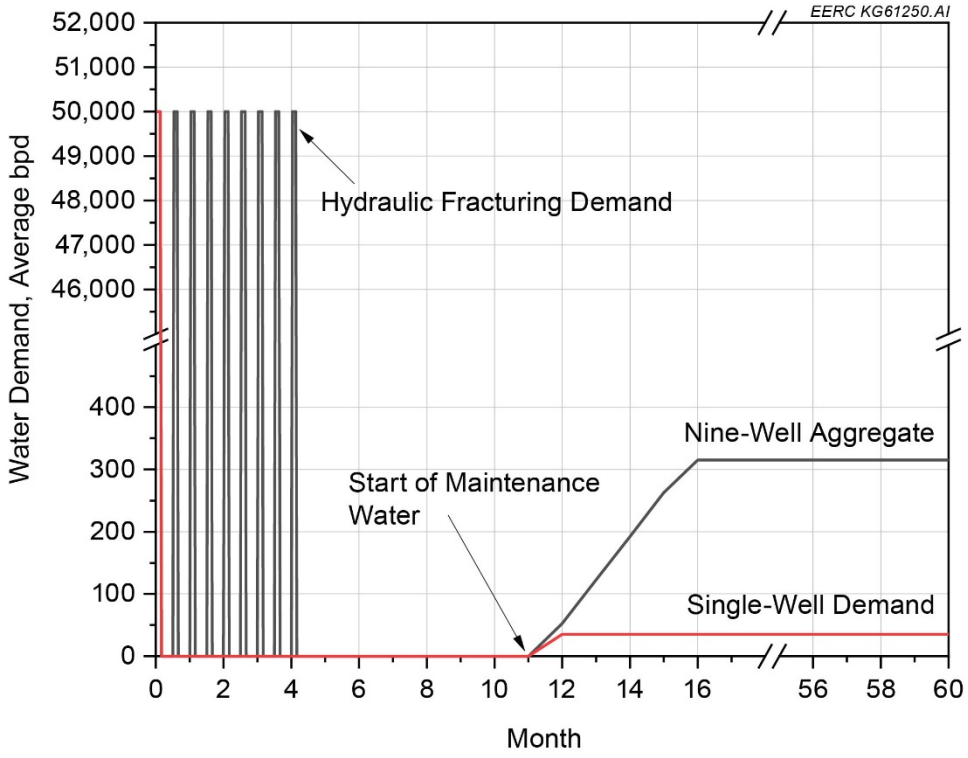


Figure 5-5. Time profiles for water demand assumed in the TEA.

DocuSign Envelope ID: 2FA9A609-C360-4E53-8B28-BE8B77B6994A

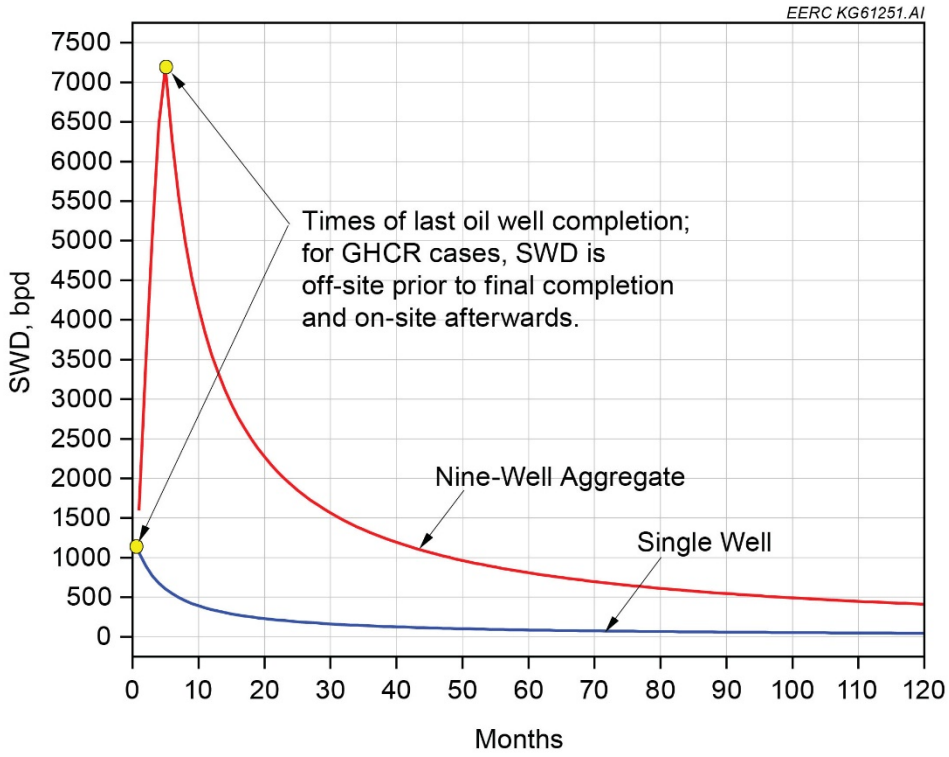


Figure 5-6. SWD profiles assumed in the TEA.

5.4 TEA Results

Summary economic metrics for the TEA cases are presented in Table 5-6 and include commonly used values such as the net present value (NPV), internal rate of return (IRR), simple payback period, and return on investment (ROI). The NPV metric assumed a 10% discount rate, which was the typical value found in well files for various Bakken operators. IRR calculations compute the resulting discount rate for a zero NPV and did not require a rate assumption. The latter two metrics of simple payback and ROI do not incorporate a discount rate.

As for results, economic metrics for the conventional case are somewhat conservative compared to Bakken well files; however, the case does not appear to have an unusually low NPV. The GHCR and SWD options that involved adding an Inyan Kara well (or wells) reflect the appropriation of those costs on a per-oil-well basis, and the nominal TEA assumption was that all nine infill wells could be supported by a single GHCR 1 or on-site SWD well or a single well pair for GHCR 2. Therefore, the NPVs for the GHCR/on-site SWD options spread development costs over nine oil wells.

DocuSign Envelope ID: 2FA9A609-C360-4E53-8B28-BE8B77B6994A

Table 5-6. Economic Evaluation Metrics for the Nominal TEA Case Assumptions

	Conventional	GHCR 1		GHCR 2		On-Site SWD
Dakota String	Yes	Yes	No	Yes	No	Yes
Oil Wells Supported	NA[1]	9	9	9	9	9
10% NPV per Well	$1,843,000	$3,007,000	$3,503,000	$3,067,000	$3,563,000	$2,695,000
IRR	17.4%	22.6%	26.0%	22.2%	25.4%	20.7%
Simple Payback, yr	3.52	2.77	2.44	2.85	2.52	3.00
ROI, No Discount	1.91:1	2.15:1	2.29:1	2.20:1	2.33:1	2.06:1

[1] Not applicable.

Economic metrics for both GHCR and the on-site SWD cases suggest that all of these options could be more competitive than the conventional approach to water management. The GHCR 1 and 2 options produce NPVs similar to each other when comparing cases that have the same Dakota string assumption. For example, both GHCR cases that assumed the use of a Dakota string had NPVs over $3.5MM. However, as discussed in the case descriptions, the GHCR 2 case likely offers a more certain path to eliminating the Dakota string because produced fluid from the first well can be injected in the second, and a tertiary link to completions on a separate DSU does not need to be made. Finally, the on-site SWD case fell between the other options; it was more competitive than the conventional case but less so than any of the GHCR cases.

Insight into the underlying TEA drivers is provided in Figure 5-7, which is a breakout of the cost contributors for each case. In the figure, the NPVs that correspond to those in Table 5-6 are represented as the difference between the net revenue potential, which was the same for all cases since no impacts to hydrocarbon production were assumed, and the top of the TEA cost column as illustrated for the conventional case. As shown, all TEA cases had common values for the cost of the oil well and the nonwater portion of the LOE (e.g., artificial lift maintenance and electricity). Differences exist for the fracture fluid depending on whether freshwater or produced fluid was used; similarly, for the present value (PV) of the maintenance water supply, only the GHCR 2 case could capitalize on lower-cost produced fluid.

Significant differences appear among the present values for SWD, with the most costly being the conventional case since it relied exclusively on off-site SWD. The minor difference between GHCR 1 and 2 and the on-site SWD case is due to the fact that there was no delay in using the SWD well for produced water disposal, whereas with GHCR 1 and 2, the early months of produced water were assumed to be disposed of off-site since the GHCR well(s) was still being used to produce fluid for hydraulic fracturing.

DocuSign Envelope ID: 2FA9A609-C360-4E53-8B28-BE8B77B6994A

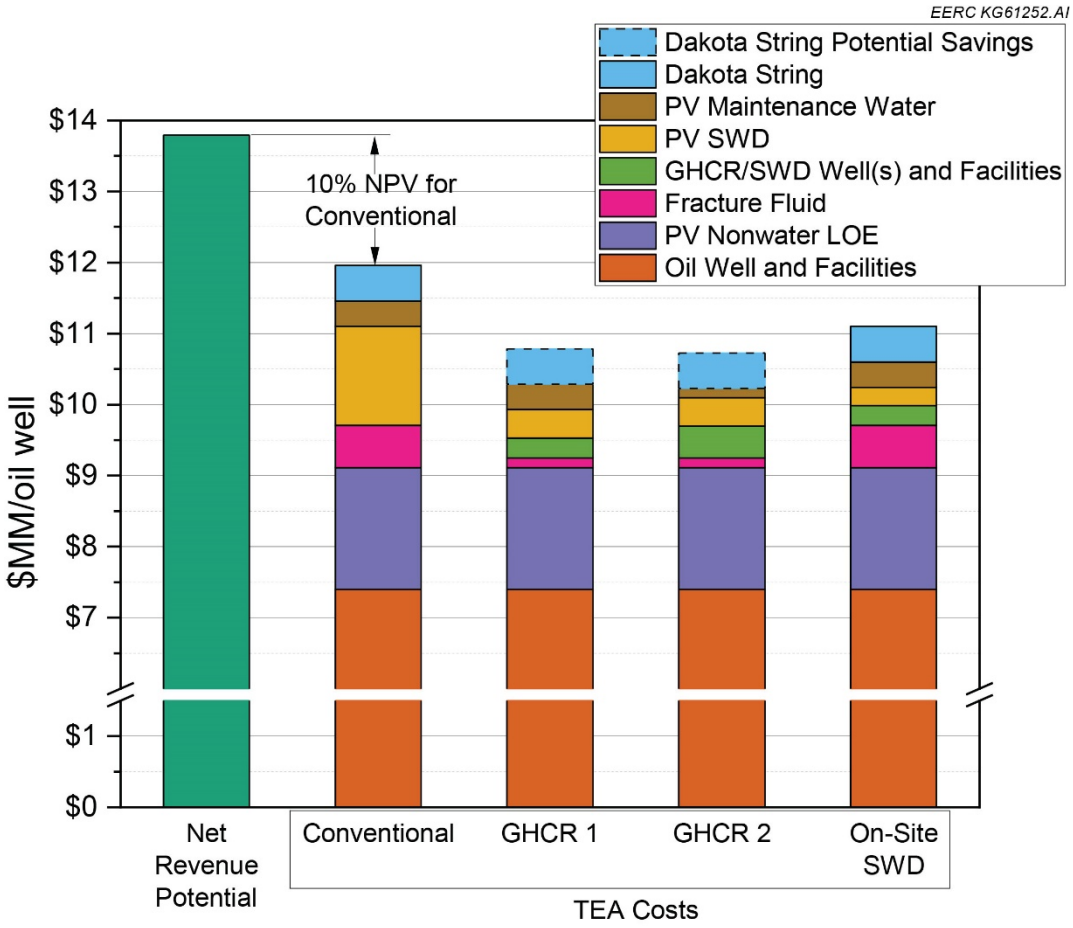


Figure 5-7. NPV cost breakdowns for the nominal-value TEA cases (10% discount rate assumed).

Inspection of Figure 5-7 shows that savings in SWD over the oil well's lifetime is the primary source of cost reduction when applying GHCR or on-site SWD. Lesser but noticeable savings appear possible from using recycled fluid for hydraulic fracturing over freshwater. However, the use of recycled fluid for maintenance water does not appear to be as clear-cut, since the metrics for GHCR 1 and 2 were quite close when comparing cases that had the same Dakota string assumption. These results suggest that the investment cost to develop the second GHCR well has a similar magnitude to the lifetime savings in maintenance water costs. However, if the second GHCR 2 well allows for the Dakota string to be eliminated when it would otherwise be needed under GHCR 1, then the investment seems more favorable.

The previous results in Table 5-6 and Figure 5-7 are only for one set of TEA assumptions. To further evaluate GHCR water management, several sensitivity studies were performed for key parameters that included: off-site SWD cost, freshwater cost, and the number of supported oil wells.

DocuSign Envelope ID: 2FA9A609-C360-4E53-8B28-BE8B77B6994A

Results from the SWD cost study are shown in Figure 5-8, which shows that the conventional case is most impacted by SWD cost since all the others primarily used on-site SWD. As the cost of off-site SWD is reduced, the conventional NPV increases, up to the point that it would equal that for on-site SWD at a fee of approximately $1.15/bbl. However, the fee would need to be reduced to approximately $0.10/bbl for the conventional NPV to match the GHCR cases with a Dakota string. As expected, as off-site SWD increases in cost, the conventional case rapidly loses value. The GHCR cases have a slight sensitivity to off-site SWD cost because they were assumed to use off-site disposal until all hydraulic fracturing was complete.

Freshwater cost is a key parameter for those cases that use it for fracturing and/or maintenance. The sensitivity results are shown in Figure 5-9, and as expected, the GHCR 2 case is unaffected since it did not use any freshwater. The GHCR 1 cases are impacted because of the assumed use of freshwater for maintenance, and the conventional and on-site SWD cases have identical sensitivity because they used freshwater for both fracturing and maintenance. Where freshwater is low-cost (i.e., less than $2/bbl), the NPV advantage of GHCR over on-site SWD erodes to the point that the values begin to converge. Value distinctions grow as freshwater costs increase, including between GHCR 1 and 2 which were previously somewhat inseparable under the nominal TEA assumptions.

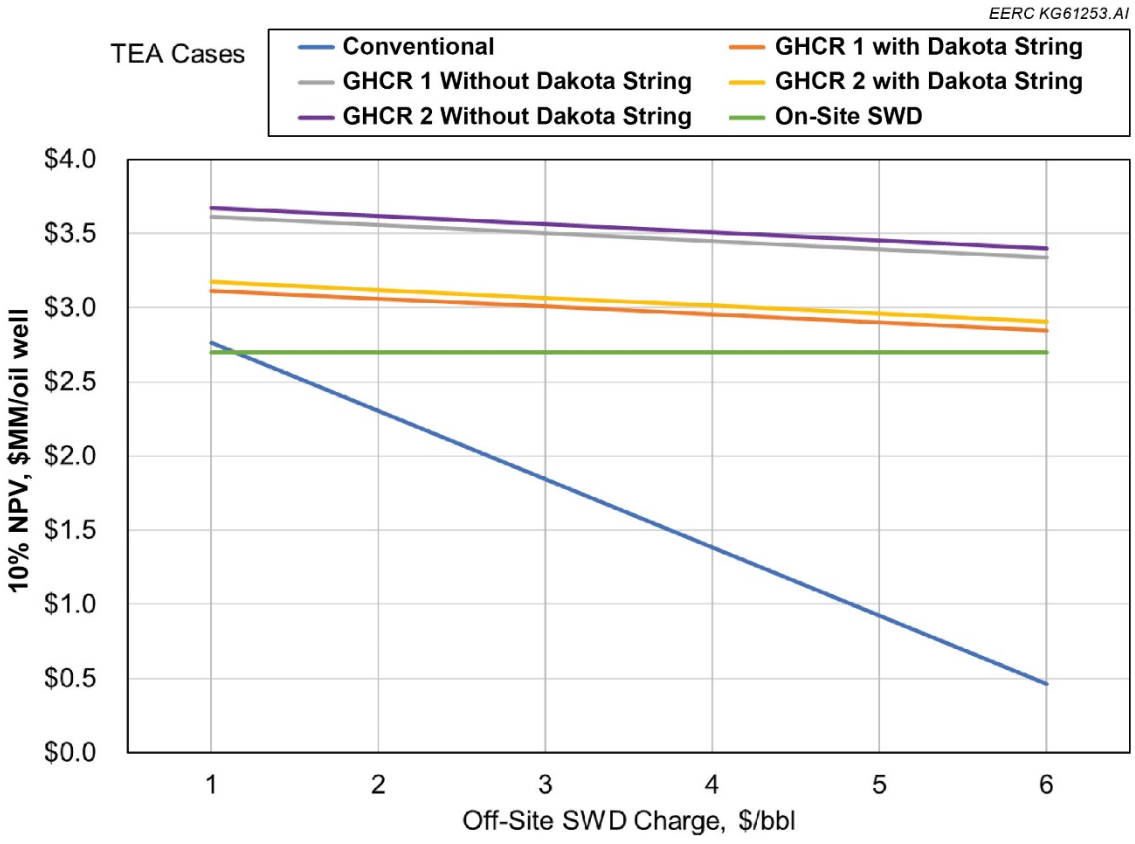


Figure 5-8. NPV sensitivity to off-site SWD cost.

DocuSign Envelope ID: 2FA9A609-C360-4E53-8B28-BE8B77B6994A

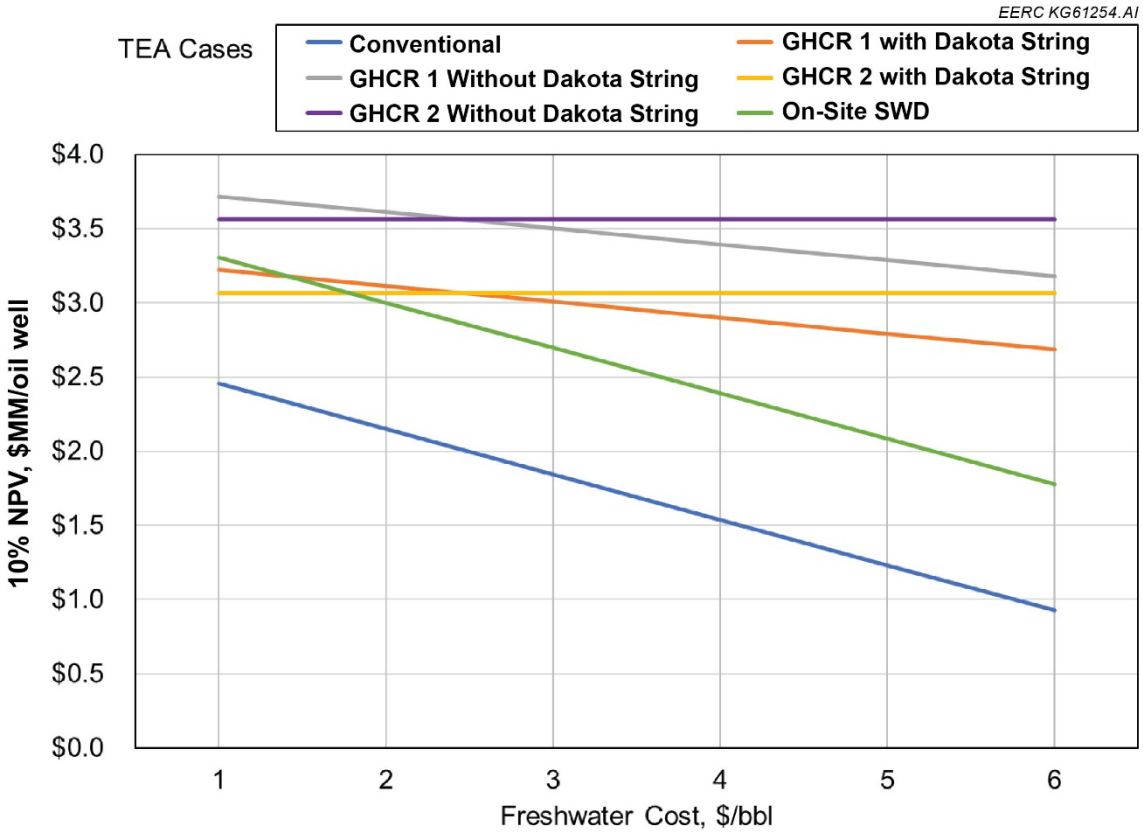


Figure 5-9. NPV sensitivity to freshwater cost.

The final sensitivity study is for the number of oil wells that each GHCR or on-site SWD well is assumed to support. These results are show in Figure 5-10 as a function of the oil well to GHCR/SWD well ratio. This ratio determines how many producing oil wells support the cost of GHCR/SWD well development. At the minimum value of one oil well per GHCR/SWD well (or one well pair for GHCR 2), all of the GHCR/SWD cases appear less competitive than conventional water management. However, NPVs for the GHCR/on-site SWD cases rapidly normalize at six or more oil wells per GHCR/SWD well, which suggests the minimum DSU size target for development.

5.4.1 Centralized GHCR

The TEA results thus far have been based on the local application of GHCR at a single DSU. However, a centralized model of GHCR water management can also be considered that is analogous to siting of the central treatment facilities found in the Permian Basin. Potential advantages of centralization include the following.

- Lower-cost GHCR well development since the cost of GHCR producer and injector wells can be distributed over many more active oil wells compared to those on a single DSU.

DocuSign Envelope ID: 2FA9A609-C360-4E53-8B28-BE8B77B6994A

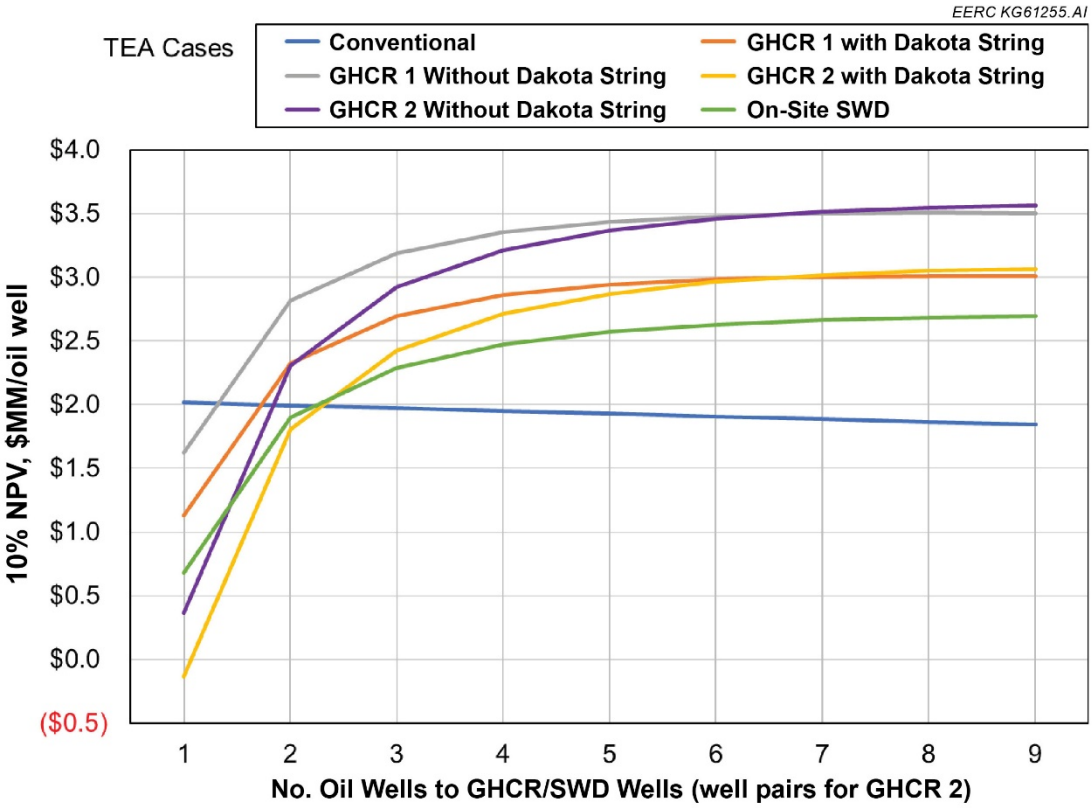


Figure 5-10. NPV sensitivity to the ratio of oil wells to GHCR wells.

- Improved reliability for supplying on-demand fluid for hydraulic fracturing. At a centralized facility, a plurality of producer wells might be used to meet the demand profile of hydraulic fracturing, while simultaneous SWD injections could be used to manage formation pressure and prevent depletion.

- Continued support of a key ESG goal by drastically reducing the demand for freshwater but still offering the potential for third-party operation.

On the other hand, centralized GHCR would apparently undermine the potential savings from reduced transport of recycled fracture fluid and SWD. As the distance between the DSU and the central facility increases, these costs would also increase. Additionally, the increased distance between GHCR water production and oil well placement would likely mean that the localized reduction in formation pressure would be insufficient to eliminate the Dakota string. One final consideration would be the regulatory uncertainty regarding the temporary transport of produced fluids from a central facility to hydraulic fracturing sites.

An overview of central versus local GHCR implementation features is presented in Table 5-7. In summary, centralized GHCR would ultimately be expected to approach the cost and reliability of conventional water management but with the advantage of significantly reducing freshwater demand.

DocuSign Envelope ID: 2FA9A609-C360-4E53-8B28-BE8B77B6994A

Table 5-7. Qualitative Comparison of Cost Drivers Between Local and Central GHCR

Cost Driver	On-DSU GHCR	Centralized GHCR
GHCR Well Development	Rapid price normalization achieved with six or more oil wells.	Costs per oil well expected to decline further as more than one DSU is served.
Dakota String	Possibly avoid extra casing if sequencing of fluid production can occur before drilling.	Unlikely to affect well casing design, given the longer distance to a central GHCR extraction well.
Fracture Fluid	Minimum-cost fluid expected, given close proximity of the on-site producer well.	Higher-cost fluid impacted by transportation from a central facility producer well.
SWD Cost	Minimum-cost disposal, given close proximity.	Higher-cost SWD due to added transport to central facility.
Maintenance Water	Marginally cost effective to produce on-site compared to moderate-cost freshwater.	Likely to be similar to moderate-cost freshwater because of the transport cost from the central facility.
Technical Risk	Risk from producing fracture fluid at a high rate using a small number of wells and no pressure maintenance.	Reduced risk of meeting fracture fluid production targets, given the dedicated facility function and simultaneous pressure maintenance from SWD injections.
Regulatory Risk	Potentially few regulatory complications if the GHCR well and transport line can be entirely within containment.	Regulatory complications may arise from the need to temporarily distribute produced fluids for fracturing, potentially with lay-flat hose as in other basins.
ESG Targets	Supports freshwater reduction targets.	Supports freshwater reduction targets.

5.5 Key Observations from the TEA

5.5.1 Technical Evaluation

- GHCR appears to be capable of providing useful services of fluid storage, homogenization, and limited conditioning for fluid volumes that are typical of hydraulic fracturing operations in the Bakken.

- The conditioning aspect of GHCR does not appear to reach the highest standards that are used elsewhere for produced water recycling (i.e., production of a clear, chloride salt brine) but is not likely to be a limiting factor as to whether the fluid can be fully recycled for completions.

- GHCR appears capable of homogenizing the produced fluid such that changes to fluid composition are gradual, and individual batches of hydraulic fracturing fluid could be considered homogeneous.

DocuSign Envelope ID: 2FA9A609-C360-4E53-8B28-BE8B77B6994A

- Producing fluids from a GHCR well also show the potential to locally reduce Inyan Kara Formation pressure to the point that it might be possible to eliminate the Dakota string on oil wells drilled nearby.
  - For the formation modeling that was analyzed, the pressure-affected distance from the GHCR producing well was approximately ¼ mile, suggesting that a GHCR production well could impact the oil wells on the same DSU, or at most, an adjacent DSU if the wells were placed near a common boundary.
  - In addition to the size of the pressure-affected zone created by GHCR fluid production, sequencing the operation to happen before oil well drilling and having a place to put the fluids must also be considered. Using only a single GHCR well means that the produced fluid might need to be transported off the DSU and perhaps used for the completion of nearby wells. It might be possible to use two GHCR wells on the DSU as a producer–injector pair to create temporary formation pressure relief without transporting fluid off-site.

- A potential risk associated with GHCR appears to be with matching the rate of fluid production to the demand needed by hydraulic fracturing. By design, hydraulic fracturing is a short-duration, high-flow process, and it may prove difficult to produce fluid at the needed rate using a single GHCR well. Increasing the number of GHCR producing wells will likely increase the reliability of providing on-demand produced water for hydraulic fracturing.

- Installing two GHCR wells appears to improve the likelihood of achieving the maximum possible benefits with GHCR.
  - Two wells might be used to lower formation pressure and thus avoid the expense of using a Dakota string without having to transport fluid off-site.
  - Two wells might also be a more reliable way to produce fluid at the rate it is needed for hydraulic fracturing since the flow resistance pressure for two wells is theoretically reduced to one-quarter the value needed with a single well.

5.5.2 Regulatory Considerations

- The tasks of accessing, injecting, and producing Inyan Kara water for industrial uses akin to GHCR appear to have precedent in North Dakota, and it is likely that a workable permitting strategy can be identified.

- GHCR seems to offer an alternative to the centralized produced water recycling facilities that are found in the Permian basin and elsewhere, and which typically store produced fluids above ground in lined ponds. The GHCR approach appears to be consistent with North Dakota's current prohibition of brine storage in surface impoundments.

- Temporary transport of produced fluid from a GHCR well to the hydraulic fracturing site might pose a regulatory challenge for recycling these fluids. Above ground, lay-flat hose appears to be used extensively for this purpose in other shale plays, but given the increased risk of spills, using it in North Dakota with produced fluids will require regulatory review and approval.

- Without off-pad transport, GHCR costs would need to be recouped from benefits accrued on a single DSU, which was the nominal assumption used in this TEA.

DocuSign Envelope ID: 2FA9A609-C360-4E53-8B28-BE8B77B6994A

5.5.3 Economic Analysis

- From an economic standpoint, it appears that GHCR could be a lower-cost option than a conventional water management approach that relies on freshwater and off-site SWD. Using the nominal TEA assumptions, the GHCR cases had a 60% to 90% higher NPV and a 0.7- to 1-year shorter simple payback time than the conventional approach. In general, the up-front investment required to develop GHCR infrastructure was recouped primarily from SWD savings over the life of the project.

- Sites that are potentially attractive for GHCR are those that are located above a pressurized zone of the Inyan Kara, need six or more infill wells, and face high costs for conventional SWD and/or freshwater.

- Adding a second GHCR well to produce maintenance water appeared marginally cost-effective on its own, without accounting for other possible benefits of the second well such as eliminating the Dakota string.

- In comparing on-DSU GHCR and a centralized model, the centralized concept may undermine the key cost savings from on-site, low-cost SWD, and it could face more regulatory restrictions with respect to recycled fluid transport. However, it would likely require less up-front investment (on a per-oil-well basis), and it would still support reductions in freshwater use and possibly help manage Inyan Kara pressure.

6.0 CONCLUSIONS

The general trend associated with oil- and gas-related water management in North Dakota has been a sustained increase of freshwater use, increased water production, and increased SWD volumes. Tremendous volumes of water are being managed in the region, and the continued trend of increasing volumes may present challenges for SWD into the Inyan Kara Formation. The current approach to water management provides the most cost-efficient means of disposal and limits the amount of handling/processing of produced water, thereby reducing the risk of spills. The Inyan Kara's geographic extent, relatively shallow depth, proper confining zones, and injectability provide a SWD target that is suitable across the entire Bakken producing region in the state. However, should current approaches to SWD in the Inyan Kara ever become technically or economically challenged, then alternative produced water management options for North Dakota may be desirable.

Produced water recycling and in-industry reuse is of interest to the state of North Dakota and the oil and gas operators in the state. Recycling of produced water faces regulatory, technical, logistical, and economic challenges that have thus far precluded widespread commercial adoption. Such challenges are associated with large-volume transport, aggregation, and the need for large-scale temporary surface storage of high-TDS brines needed to supply a high-rate 200,000-bbl hydraulic fracture stimulation. However, commercial operators are making strides at overcoming these technical challenges as interest in recycling has grown, and some operators have begun

DocuSign Envelope ID: 2FA9A609-C360-4E53-8B28-BE8B77B6994A

implementing produced water recycling as they aim to reduce their freshwater consumption (Marathon Oil, 2020).

The GHCR concept could address many of the recycling challenges outlined in this report (e.g., large-volume transport, large-scale temporary surface storage of high-TDS fluids, etc.). By utilizing existing SWD infrastructure and the geologic formation as a storage container, the concept can provide an approach to address some of the economic and environmental challenges surrounding recycling of produced water.

The technical evaluation of the GHCR concept consisted of laboratory column flow-through testing, field sampling at a commercial SWD location that has a water production well targeting the same formation, and geologic modeling and numerical simulations. These efforts indicate that the GHCR concept appears to be capable of providing fluid storage, homogenization, and some conditioning for fluid volumes that are typical of hydraulic fracturing operations in the Bakken. Depending on the volumes of water extracted and locations of the relevant wells, implementing the GHCR concept could reduce formation pressure at the DSU level. One potential challenge to the implementation of GHCR is matching the rate of fluid production to the demand needed for hydraulic fracturing. Depending on the site-specific characteristics of the reservoir, more than one GHCR well may be needed to provide sufficient water supply within the short-duration time frame for a well completion.

The regulatory and economic evaluation of the GHCR concept revealed that there are pathways to implementation. There are likely workable permitting strategies that can be identified to implement a GHCR commercial operation. The GHCR approach is consistent with the state of North Dakota's restrictions for brine storage in large, open-top surface impoundments; however, lay-flat hose, while frequently used in other jurisdictions, would require regulatory review and approval in North Dakota. Economically, it appears that GHCR could be a competitive or even lower-cost option over conventional water management approaches. Sites that are potentially attractive for GHCR are those that are located above a pressurized zone of the Inyan Kara, need six or more infill wells, and face higher costs for conventional SWD and/or freshwater.

In summary, this study reveals pursuing GHCR can be a viable approach to water management in North Dakota. The GHCR concept addresses some of the challenges that hinder the more traditional approaches to recycling in the industry. Furthermore, an assessment of the current landscape of water management within the state reveals the ongoing trend of increasing volumes of produced water and SWD. Projections reveal that the volumes of produced water that needs to be managed is expected to double over the next decade (Energy & Environmental Research Center, 2020). With the continued development of the Bakken and continuing driving factors related to ESG initiatives, implementing a practice such as GHCR is a feasible approach to adding recycling of produced water to industry within the state.

7.0 MILESTONES

The completed milestone table can be found in Table 7-1.

DocuSign Envelope ID: 2FA9A609-C360-4E53-8B28-BE8B77B6994A

Table 7-1. Milestones

Milestone Title/ Description	Planned Completion Date	Actual Completion Date	Verification Methods	Comments
M1 – Inyan Kara Outcrop Rock Samples Collected for GHCR Lab Test	6/30/2020	6/30/2020	Reported in subsequent quarterly report	Quartz sand with various grain sizes to replicate Inyan Kara grain distribution and porosity was purchased.
M2 – Laboratory and Field Validation of GHCR Concept Initiated	7/31/2020	7/30/2020	Reported in subsequent quarterly report	
M3 – Produced Water Quality Assessment Completed	10/1/2020	9/30/2020	Reported in subsequent quarterly report and in D4	D4 submitted to DOE Technical Monitor.
M4 – Findings Review with BPOP Member Technical Advisory Group	5/31/2021	5/31/2021	Reported in subsequent quarterly report	
M5 – Techno-Economic Assessment Completed	8/31/2021	11/30/2021	Relevant findings and results presented in the final report	Moved to 11/30/2021 as discussed with DOE Technical Monitor.

8.0 REFERENCES

American Petroleum Institute, 2019, Operations for lay-flat hose in oilfield water applications: API Recommended Practice 15WT, 1st edition, December.

Basu, S., Cross, T., and Skvortsov, S. (ConocoPhillips), 2019, Saltwater disposal modeling of Dakota sand, Williston Basin, to drive drilling decisions: Presented at the Unconventional Resources Technology Conference, Denver, Colorado, July 22–24, 2019, URTeC 488.

Benko, K.L., and Drewes, J.E., 2008, Produced water in the western United States—geographical distribution, occurrence, and composition: Environmental Engineering Science, v. 25, no. 2, DOI: 10.1089/ees.2007.0026.

Bishop, P., 2006, A short review of Pennsylvania water law: Pennsylvania Department of Environmental Protection (PADEP), 4.

Bolles, B.A., 1998, A methodology for studying denitrification by recently formed sulfides: Master's thesis, University of North Dakota, 99 p.

Connors, K.C., Jacobson, L.L., Jiang, T., Klapperich, R.J., Taunton, M.A., and Williamson, C.B., 2020, Subsurface pressure management: managing the Inyan Kara Formation while drilling:

DocuSign Envelope ID: 2FA9A609-C360-4E53-8B28-BE8B77B6994A

Final report for North Dakota State Energy Research Center, EERC Publication 2020-EERC-07-11, Grand Forks, North Dakota, Energy & Environmental Research Center, July.

Continental Resources, 2020, ESG report: www.clr.com/wp-content/uploads/2021/08/Continental-Resources-2020-ESG-Report.pdf (accessed November 2021).

Energy ESG, 2021, Investing in our future: October.

Energy & Environmental Research Center, 2020, Produced water management and recycling options in North Dakota: Final report for North Dakota Legislative Management Energy Development and Transmission Committee and North Dakota Industrial Commission.

Feder, J., 2020, Saltwater disposal optimization drives water midstream sector: Journal of Petroleum Technology, https://jpt.spe.org/saltwater-disposal-optimization-drives-water-midstream-sector (accessed November 2021).

IHS Global Inc., 2015, Oil and gas upstream cost study: Final report for Energy Information Administration: www.eia.gov/analysis/studies/drilling/pdf/upstream.pdf (accessed September 2021).

Journal of Petroleum Technology, 2020, Permian basin produced water recycling facility up and running, October 7: https://jpt.spe.org/permian-basin-produced-water-recycling-facility-and-running (accessed November 2021).

Kringstad, J.J., 2020, Presentation to EmPower ND Commission, February 4, 2020: https://ndpipelines.files.wordpress.com/2020/02/kringstad-empowernd-2-4-2020.pdf (accessed March 2020).

Liberty, 2020, Bettering human lives: 2020 ESG report. www.libertyfrac.com/wp-content/uploads/2021/06/Liberty-ESG-2020-Bettering-Human-Lives.pdf (accessed November 2021).

Marathon Oil, 2020, Sustainability report: https://cdn.sanity.io/files/ghcnw9z2/website/91744eb6ef8fbe59505a911c6b8d2e8dd9a537fa.pdf?dl (accessed November 2021).

Morris, G., 2019, Full immersion industry gets religion on produced water: E&P Magazine, March 1, www.hartenergy.com/exclusives/full-immersion-industry-gets-religion-produced-water-177993 (accessed November 2021).

New Mexico Legislature, 2019, Produced Water Act: New Mexico Statute § 70-13-4, www.nmlegis.gov/Sessions/19%20Regular/final/HB0546.pdf (accessed November 2021).

Nichols, K., Sawyer, J., Bruening, J., Halldorson, B., Madhavan, K., 2017, Development of a large-scale water recycling program for the Delaware Basin, New Mexico: Paper presented at the Society of Petroleum Engineers Health, Safety, Security, Environment, & Social Responsibility Conference, Paper SPE-186086-MS.

North Dakota Department of Mineral Resources, 2020, Director's cut: December 2019 production, www.dmr.nd.gov/oilgas/directorscut/directorscut-2020-02-14.pdf (accessed February 2020).

DocuSign Envelope ID: 2FA9A609-C360-4E53-8B28-BE8B77B6994A

North Dakota Industrial Commission, 2021, October data collection.

North Dakota Department of Mineral Resources, 2021, Directors cut: October 2021, www.dmr.nd.gov/oilgas/directorscut/directorscut-2021-10-13.pdf (accessed November 2021).

Oklahoma Senate, 2020, Governor signs oil and gas produced water and waste recycling and reuse act into law: press release, May, https://oksenate.gov/press-releases/governor-signs-oil-and-gas-produced-water-and-waste-recycling-and-reuse-act-law (accessed November 2021).

Pearson, C.M., Griffin, L., and Wright, C., 2013, Breaking up is hard to do—creating hydraulic fracture complexity in the Bakken central basin: Presented at the Society of Petroleum Engineers Hydraulic Fracturing Technology Conference, The Woodlands, Texas, February 4–6.

Primus Line, 2021, Primus Line overland piping, January: hwww.primusline.com/fileadmin/user_upload/en/applications/downloads/primus-line-overland-piping-flyer-en.pdf (accessed November 2021).

Railroad Commission of Texas, 2021, Notice to oil and gas operators: gardendale seismic response action, September, www.rrc.texas.gov/media/4ryp5kqr/nto-gardendale-seismic-response-action_9-22-2021.pdf (accessed November 2021).

Scanlon, B.R., Reedy, R.C., Xu, P., Engle, M., Nicot, J.P., Yoxtheimer, D., Yang, Q., and Ikonnikova, S., 2020, Can we beneficially reuse produced water from oil and gas extraction in the U.S.?: Science of the Total Environment, v. 717, p. 137085.

State of Oklahoma, 2020, Oil and gas produced water, Bill no. 1875: http://webserver1.lsb.state.ok.us/cf_pdf/2019-20%20ENR/SB/SB1875%20ENR.PDF (accessed November 2021).

Stepan, D.J., Shockey, R.E., Kurz, B.A., Kalenze, N.S., Cowan, R.M., Ziman, J.J., and Harju, J.A., 2010, Bakken water opportunities assessment—Phase 1: Final report summary (June 19, 2009–March 15, 2010) for North Dakota Industrial Commission Contract No. G018-036, EERC Publication 2010-EERC-04-03, Grand Forks, North Dakota, Energy & Environmental Research Center, April.

Sustainability Accounting Standards Board, 2018, Oil & Gas – Services, Sustainability Accounting Standard: www.sasb.org/wp-content/uploads/2018/11/Oil_Gas_Services_Standard_2018.pdf (accessed November 2021).

TETRA Technologies. TETRA Steel Lay-Flat Hose 800 and 1200, August 10, 2020: https://tetratec.com/download/tetra-steel-product-data-sheet/?wpdmdl=1180 (accessed November 2021).

Texas Commission on Environmental Quality, 2021, www.tceq.texas.gov/permitting/wastewater/oilandgas (accessed November 2021).

Texas Produced Water Consortium, 2021, Senate Bill no. 601: https://capitol.texas.gov/tlodocs/87R/billtext/html/SB00601I.htm (accessed November 2021).

DocuSign Envelope ID: 2FA9A609-C360-4E53-8B28-BE8B77B6994A

United Nations Principles for Responsible Investment, 2018, What is ESG integration? April 25: www.unpri.org/fixed-income/what-is-esg-integration/3052.article (accessed November 2021).

Weston, R.T., and Burcat, J.R., 1990, Legal aspects of Pennsylvania water management, *in* Majumdar, S.K. and others (eds.): Water resources in Pennsylvania—availability, quality and management 219, 220.

Wilmoth, A., 2018, Water fight heats up in Kingfisher County: The Oklahoman, July 23, www.oklahoman.com/article/5602102/water-fight-heats-up-in-kingfisher-county (accessed November 2021).

Zartler, B., 2017, Permian Basin produced water trends: Presentation for Produced Water Society, https://producedwatersociety.com/wp-content/uploads/2021/07/00130_Solaris-Midstream-Presentation.pdf (accessed November 2021).

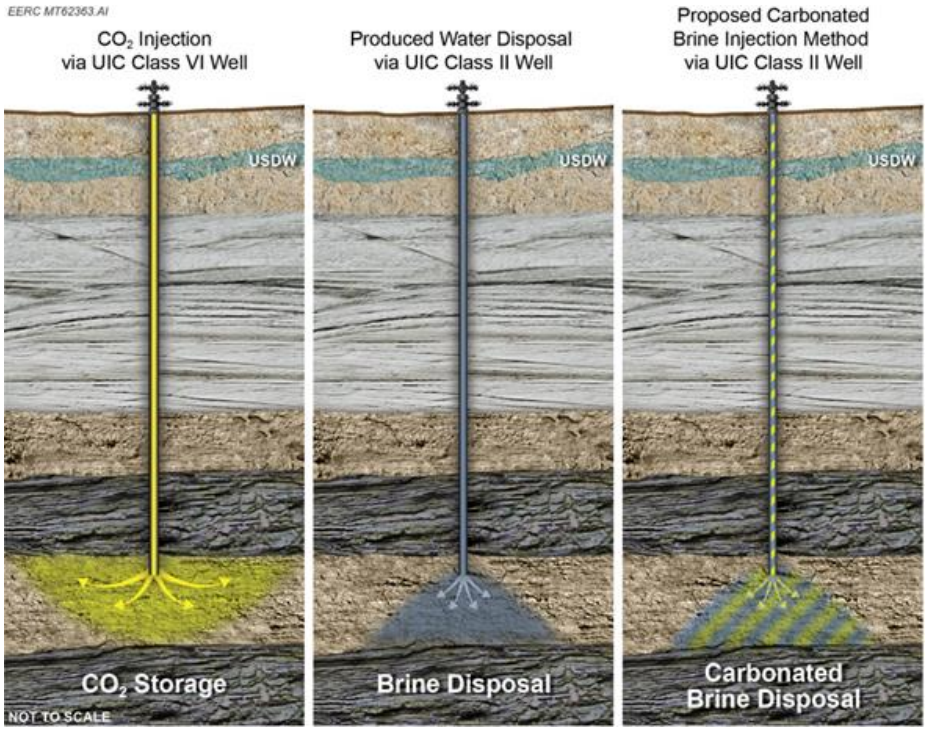
DocuSign Envelope ID: 2FA9A609-C360-4E53-8B28-BE8B77B6994A

APENDIX K

ASSESSMENT OF CARBONATED BRINE INJECTION REPORT – 2023

DocuSign Envelope ID: 2FA9A609-C360-4E53-8B28-BE8B77B6994A

NATIONAL ENERGY TECHNOLOGY LABORATORY



Assessment of Carbonated Brine Injection as Low-risk Strategy for Geologic Carbon Storage

20 October 2023

U.S. DEPARTMENT OF ENERGY | NATIONAL ENERGY TECHNOLOGY LABORATORY

Office of Fossil Energy and Carbon Management

DOE/NETL-2023/4328

DocuSign Envelope ID: 2FA9A609-C360-4E53-8B28-BE8B77B6994A

Disclaimer

This project was funded by the United States Department of Energy, National Energy Technology Laboratory, in part, through a site support contract. Neither the United States Government nor any agency thereof, nor any of their employees, nor the support contractor, nor any of their employees, makes any warranty, express or implied, or assumes any legal liability or responsibility for the accuracy, completeness, or usefulness of any information, apparatus, product, or process disclosed, or represents that its use would not infringe privately owned rights. Reference herein to any specific commercial product, process, or service by trade name, trademark, manufacturer, or otherwise does not necessarily constitute or imply its endorsement, recommendation, or favoring by the United States Government or any agency thereof. The views and opinions of authors expressed herein do not necessarily state or reflect those of the United States Government or any agency thereof.

Cover Illustration: Graphical representation of proposed carbonated brine injection (CBI) method compared to traditional free-phase CO_2 injection via Class VI well and standard produced water disposal via Class II well. As shown in the center image, with the CBI method, the CO_2 remains dissolved into the brine, thereby eliminating the risk of free-phase CO_2 migration and negligible pressure changes when compared to standard Class II operations.

Suggested Citation: Xiong, W.; Belarbi, Z.; Thomas, R.; Crandall, D.; Tesfu, M.; Taunton, M.; Klapperich, R.; Kurz, M. *Assessment of Carbonated Brine Injection as Low-risk Strategy for Geologic Carbon Storage*; DOE.NETL-2023. 4328; NETL Technical Report Series; U.S. Department of Energy, National Energy Technology Laboratory: Pittsburgh, PA, 2023; p 56.
https://doi.org/10.2172/2204489

An electronic version of this report can be found at:

https://netl.doe.gov/energy-analysis/search

DocuSign Envelope ID: 2FA9A609-C360-4E53-8B28-BE8B77B6994A

Assessment of Carbonated Brine Injection as Low-risk Strategy for Geologic Carbon Storage

Wei Xiong[1,2]; Zineb Belarbi[3,4]; Randal Thomas[3]; Dustin Crandall[5]; Merry Tesfu[6]; Meghan Taunton[6]; Ryan Klapperich[6]; Marc Kurz[6]

[1] National Energy Technology Laboratory, 626 Cochran Mill Road, Pittsburgh, PA 15236, USA

[2] NETL Support Contractor, 626 Cochran Mill Road, Pittsburgh, PA 15236, USA

[3] National Energy Technology Laboratory, 1450 SW Queen Avenue, Albany, OR 97321, USA

[4] NETL Support Contractor, 1450 SW Queen Avenue, Albany, OR 97321, USA

[5] National Energy Technology Laboratory, 3610 Collins Ferry Road, Morgantown, WV 26505, USA

[6] University of North Dakota, Energy & Environmental Research Center (EERC), 15 North 23rd Street, Stop 9018, Grand Forks, ND 58202, USA

DOE/NETL-2023/4328

20 October 2023

NETL Contacts:

Randal Thomas and Wei Xiong, Principal Investigators

Dustin Crandall, Technical Portfolio Lead

Bryan Morreale, Associate Laboratory Director for Research & Innovation, Research & Innovation Center

DocuSign Envelope ID: 2FA9A609-C360-4E53-8B28-BE8B77B6994A

This page intentionally left blank.

DocuSign Envelope ID: 2FA9A609-C360-4E53-8B28-BE8B77B6994A

Table of Contents

EXECUTIVE SUMMARY **1**
1. INTRODUCTION **3**
1.1 OVERVIEW OF SALTWATER DISPOSAL 4
1.2 OVERVIEW OF CARBON CAPTURE, UTILIZATION, AND STORAGE 6
1.3 THE CONNECTION BETWEEN SWD AND CCUS: THE CONCEPT OF CBI AND STORAGE 6
1.4 RESEARCH ON CBI AND STORAGE 8
2. METHODS **10**
2.1 RESERVOIR MODEL SETUP 10
2.2 PRODUCED WATER DATA 15
2.3 WELLBORE CORROSION MODEL 15
2.4 REACTIVE TRANSPORT MODEL 17
3. RESULTS **20**
3.1 RESERVOIR SIMULATION 20
3.2 WELLBORE CORROSION MODEL 24
3.3 REACTIVE TRANSPORT MODELING 27
4. DISCUSSIONS **37**
4.1 CO_2 CONCENTRATION FOR CBI 37
4.2 COMPATIBILITY OF EXISTING INFRASTRUCTURE 37
4.3 LONG-TERM STORAGE SAFETY 38
4.4 NANOBUBBLE TECHNOLOGY FOR CO_2 INJECTION 39
5. CONCLUSIONS **42**
6. REFERENCES **43**

DocuSign Envelope ID: 2FA9A609-C360-4E53-8B28-BE8B77B6994A

This page intentionally left blank.

DocuSign Envelope ID: 2FA9A609-C360-4E53-8B28-BE8B77B6994A

List of Figures

Figure 1: Graphical representation of a proposed CBI method compared to traditional free-phase CO_2 injection via a Class VI well and standard produced water disposal via a Class II well. As shown in the center, with the CBI method, the CO_2 remains dissolved into the brine, thereby eliminating the risk of free-phase CO_2 migration and negligible pressure changes when compared to standard Class II operations..... 4
Figure 2: Distribution of active SWD wells in 2019 5
Figure 3: States with large wastewater injection volumes can sequester 53 Mtpa CO_2 using CBI.7
Figure 4: Simulation results showing the amount of CO_2 dissolved in water and the CO_2 remaining in the gas phase at reservoir conditions for all scenarios. At a molality of approximately 0.80, the CO_2 is no longer fully saturated in the reservoir..... 12
Figure 5: 2D Reactive transport model domain schematic. 17
Figure 6: BHP for Scenarios 1 to 12. BHP at the start of injection was approximately 2,300 psi. Stabilized BHP 2 years after injection was approximately 2,585 psi for Scenarios 1 to 8. In Scenarios 9 to 12 a rise in BHP was observed. 21
Figure 7: Illustration of the model results of Scenario 3, showing brine carrying dissolved CO_2 to the base of the reservoir. 22
Figure 8: Result of the side-by-side comparison of the 2,255 psi and 1,500 psi. 23
Figure 9: OLI simulation to predict scaling tendency of produced water with and without adding CO_2. Steam amount = 1L. (a). 0 mole/kg CO_2; (b). 0.2 mole/kg CO_2; (c). 0.6 mole/kg CO_2. 25
Figure 10: OLI simulation to predicted pH and corrosion rates of stainless-steel exposed to injected produced water with and without CO_2. 26
Figure 11: OLI simulation to predicted pH and corrosion rates of carbon steel UNS G10180 exposed to injected produced water with and without CO_2. 27
Figure 12: pH changes in the reservoir during injection period. 28
Figure 13: Dissolved solids changes in the reservoir during injection period. 28
Figure 14. Fluid density changes in the reservoir during injection period. 28
Figure 15: Mineral volume changes in the reservoir during injection period..... 29
Figure 16: Porosity changes in the reservoir during injection period. 29
Figure 17: Dissolved carbon species changes in the reservoir during injection period. 30
Figure 18: Primary minerals saturation and volume during injection period. 31
Figure 19: Secondary precipitations at the end of the 20-year injection period. 32
Figure 20: pH, dissolved solids, and porosity during the shut-in period. 33
Figure 21: Dissolved carbon species during shut-in period. 34
Figure 22: Primary mineral volume percentage and saturation changes during the shut-in period. 35
Figure 23: Secondary mineral precipitates saturation during the shut-in period. 35
Figure 24: Dolomite volume percentage changes after 100 years of the shut-in period. 36
Figure 25: Storage security depends on a combination of physical and geochemical trapping. Over time, the physical process of residual CO_2 trapping and geochemical processes of solubility trapping and mineral trapping increase..... 39
Figure 26: Main mechanism of EOR and geological sequestration by CO_2 injection in the form of micro and nanobubbles..... 40
Figure 27: Schematic diagrams comparing CO_2 geological storage techniques 41

DocuSign Envelope ID: 2FA9A609-C360-4E53-8B28-BE8B77B6994A

This page intentionally left blank.

DocuSign Envelope ID: 2FA9A609-C360-4E53-8B28-BE8B77B6994A

List of Tables

Table 1: Reservoir Simulation Constant Parameters 11
Table 2: Results of Experimental Injection Simulation Scenarios 11
Table 3: Reservoir Performance Scenarios for Experimental Injection 13
Table 4: Results of Nine Predictive Injection Simulation Scenarios 13
Table 5: Simulation Initial Conditions for Additional Simulation Scenarios 14
Table 6: Reservoir Performance Scenarios at 1,500 psi and 2,255 psi 14
Table 7. Produced Water Chemistry for Modeling Input 15
Table 8: Chemical Composition of Produced Water - No Added CO_2; Steam Amount = 1L; Temperature 25 ℃, 1 atm 16
Table 9: Formation Rock-Fluid System and Injection Carbonated Brine Chemistry 18
Table 10: Formation Rock-Fluid System and Injection Carbonated Brine Chemistry 19
Table 11: Result of 12 Long-Term Predictive Injection Simulation Scenarios 20
Table 12: Result of 12 Long-Term Predictive Injection Simulation Scenarios with Low Initial Reservoir Pressure (1,500 psi) 23

DocuSign Envelope ID: 2FA9A609-C360-4E53-8B28-BE8B77B6994A

This page intentionally left blank.

DocuSign Envelope ID: 2FA9A609-C360-4E53-8B28-BE8B77B6994A

Acronyms, Abbreviations, and Symbols

Term	Description
BEST	Brine extraction and storage test
CBI	Carbonated brine injection
CCUS	Carbon capture, utilization, and storage
CMG	Computer Modeling Group
EERC	Energy & Environmental Research Center
EOR	Enhanced oil recovery
GWB	Geochemist's Workbench
IAP	Ion activity product
IRS	Internal Revenue Service
K_{sp}	Solubility Product Constant
PISC	Post-injection site closure
RTM	Reactive Transport Model
$scCO_2$	Supercritical carbon dioxide
SI	Scale Index
ST	Scaling Tendency
SWD	Saltwater disposal
TDS	Total dissolved solids
UIC	Underground injection control
USDW	Underground sources of drinking water
USGS	United States Geological Survey

DocuSign Envelope ID: 2FA9A609-C360-4E53-8B28-BE8B77B6994A

Acknowledgments

This work was performed in support of the National Energy Technology Laboratory's (NETL) ongoing research under Carbon Storage Advanced R&D FWP by NETL's Research and Innovation Center. The authors wish to acknowledge Carbon Storage Advanced R&D FWP for programmatic guidance, direction, and support.

The authors also wish to acknowledge Ryan Hall from NGL Energy Partners for valuable discussions for site-related information. Thanks to James Gardiner for working on early lab and field work prior to this simulation project.

DocuSign Envelope ID: 2FA9A609-C360-4E53-8B28-BE8B77B6994A

EXECUTIVE SUMMARY

Carbonated brine injection (CBI) has the potential for large-scale carbon sequestration throughout the oil and gas industry through its network of already existing Class II saltwater disposal (SWD) wells. Dedicated geological carbon storage typically results in the creation of a continuous phase of supercritical carbon dioxide ($scCO_2$) in the subsurface. Injection of fluid requires raising reservoir pressure above normal hydrostatic pressure for some distance away from the injection well. The existence of free-phase CO_2 at this elevated pressure incurs additional risk of leakage due to the combination of induced geomechanical stresses on the storage formation and the corrosive nature and higher mobility of CO_2. Long-term tracking of free-phase CO_2 is required to identify its migration in the subsurface.

For CBI, CO_2 is first dissolved into produced waters being injected into existing Class II SWD wells. Since the CO_2 is mixed with the produced water prior to subsurface injection, the benefits are predicted to include no migration of free-phase CO_2 and negligible pressure increase when compared to standard SWD injection. This technical report examined the risk profile of this alternative method with the hypothesis that there will be a lower risk profile from the absence of free-phase CO_2, resulting in a smaller area of potential impact compared to free-phase CO_2 injection methods and negligible pressure increase compared to standard SWD operations because of the aqueous-phase injection.

The main objective of this early-phase research was to evaluate the techno-economic feasibility and risk associated with combined brine and CO_2 storage in SWD wells using brine dissolution in the North Dakota portion of the Williston Basin. Three simulation studies were conducted to investigate: (1) CO_2 phases at different conditions, (2) wellbore compatibility, and (3) long-term storage fate in reservoir. (1) A simple reservoir model and injection simulations were created using data to represent the BEST (brine extraction and storage test) site, an operational SWD facility located near Watford City, North Dakota. The pressure evolution caused by CO_2 comingled in produced water injectate in a layer cake reservoir was then modeled while tracking aqueous CO_2 throughout the project. The salinity of the injection water, the salinity of the reservoir brine, and the amount of dissolved CO_2 comingled in the injection water were varied. (2) A wellbore corrosion model was performed using the CO_2 concentrations selected based on the reservoir modeling to examine the carbonated produced water impact on wellbore. (3) Reactive transport modeling was conducted with the optimal CO_2 concentration for this injection site to study the rock-fluid interactions and CO_2 fate in the reservoir.

Results suggest that CO_2 dissolved in produced water can be injected without appreciably increasing subsurface pressure or leakage risks. Pressure buildup was found to vary with salinity but not with CO_2 mass fraction. Simulation results show that lower CO_2 percent mass fraction leads to a higher amount of CO_2 that can be dissolved at a higher injection salinity. Furthermore, the long-term goal of dissolution trapping in a traditional carbon storage project is accomplished from the start, mitigating risks associated with potential migration of buoyant CO_2, so long as the reservoir pressure and temperature are used to determine the maximum mass fraction of the dissolved CO_2. Since pressure equilibrium following injection is not inhibited by two-phase flow, as seen in traditional carbon storage and sequestration, the CO_2 becomes a component of the brine and is stored in the aqueous phase, thereby reducing the CO_2 mobility in the storage reservoir, and results in the carbonated brine densities of the injected fluid similar to that of the native reservoir fluids, greatly reducing the risks associated with vertical and lateral mobility of

DocuSign Envelope ID: 2FA9A609-C360-4E53-8B28-BE8B77B6994A

injected CO_2 and geomechanical stresses on the confining zones. The injection of carbonated produced water into existing SWD wells does not cause significant corrosion at optimal dissolved CO_2 amounts in the injected water.

Lastly, public data concerning produced water injection volumes were used to estimate that at 2% mass fraction, approximately 1 ton of CO_2 could be dissolved into every 198 barrels of brine. Since the volume of CO_2 that can be dissolved into produced water brine is dependent on brine salinity as well as reservoir temperature and pressure, 2% CO_2 mass fraction would likely be a very conservative estimate for basins outside of North Dakota, as the Williston Basin has among the highest produced water salinities in the country, with an average salinity of 300,000 ppm. Lower produced water salinity would result in the ability to dissolve more CO_2. However, using these conservative estimates, approximately 50 million tons of CO_2 could be dissolved into 10.5 billion barrels of produced water currently being injected into existing Class II injection wells in Texas, California, Oklahoma, Wyoming, Kansas, Louisiana, New Mexico, and North Dakota each year. With minimal capital investment and the current Internal Revenue Service 45Q tax credit of $0.425 per barrel of brine (at $85/ton), this represents a critical opportunity to use existing infrastructure and already permitted injection wells to sequester an appreciable amount of CO_2 in the subsurface at no increased risk to current Class II injection projects.

Regulatory considerations for CBI include the regulations surrounding aboveground storage of the produced water on-location and creating a path to approval under Class II injection wells. A pilot field demonstration would aid in answering some of the questions regulators might have surrounding CBI such as whether the wellbore tubing and casing would need to be retrofitted in any form.

DocuSign Envelope ID: 2FA9A609-C360-4E53-8B28-BE8B77B6994A

1. INTRODUCTION

Dedicated geological carbon storage and sequestration typically result in the creation of a continuous phase of supercritical carbon dioxide ($scCO_2$) in the subsurface. Injection of fluid requires raising reservoir pressure above normal lithostatic pressure for some distance away from the injection well. The existence of free-phase CO_2 at this elevated pressure incurs additional risk of leakage due to the combination of induced geomechanical stresses on the storage formation and the corrosive nature and higher mobility of CO_2. Long-term tracking of free-phase CO_2 is required to identify its migration in the subsurface.

In this study, carbonated brine injection (CBI) was investigated as a low-risk CO_2 storage strategy, whereby CO_2 is first dissolved into produced waters being injected into existing Class II saltwater disposal (SWD) wells. Since the CO_2 is mixed with the produced water prior to subsurface injection, the benefits are predicted to include no migration of free-phase CO_2 and negligible pressure increase when compared to standard SWD injection (Figure 1). This project examined the risk profile of this alternative method with the hypothesis that (1) there will be a lower risk profile from the absence of free-phase CO_2, resulting in a smaller area of impact compared to free-phase CO_2 injection methods, and little to no pressure increase compared to standard SWD operations because of the aqueous-phase injection, and (2) CBI is compatible with existing Class II wells without causing significant corrosion issues.

The main objective of this early-phase research was to evaluate the techno-economic feasibility and risk associated with combined brine and CO_2 storage in SWD wells using brine dissolution in the North Dakota portion of the Williston Basin.

DocuSign Envelope ID: 2FA9A609-C360-4E53-8B28-BE8B77B6994A

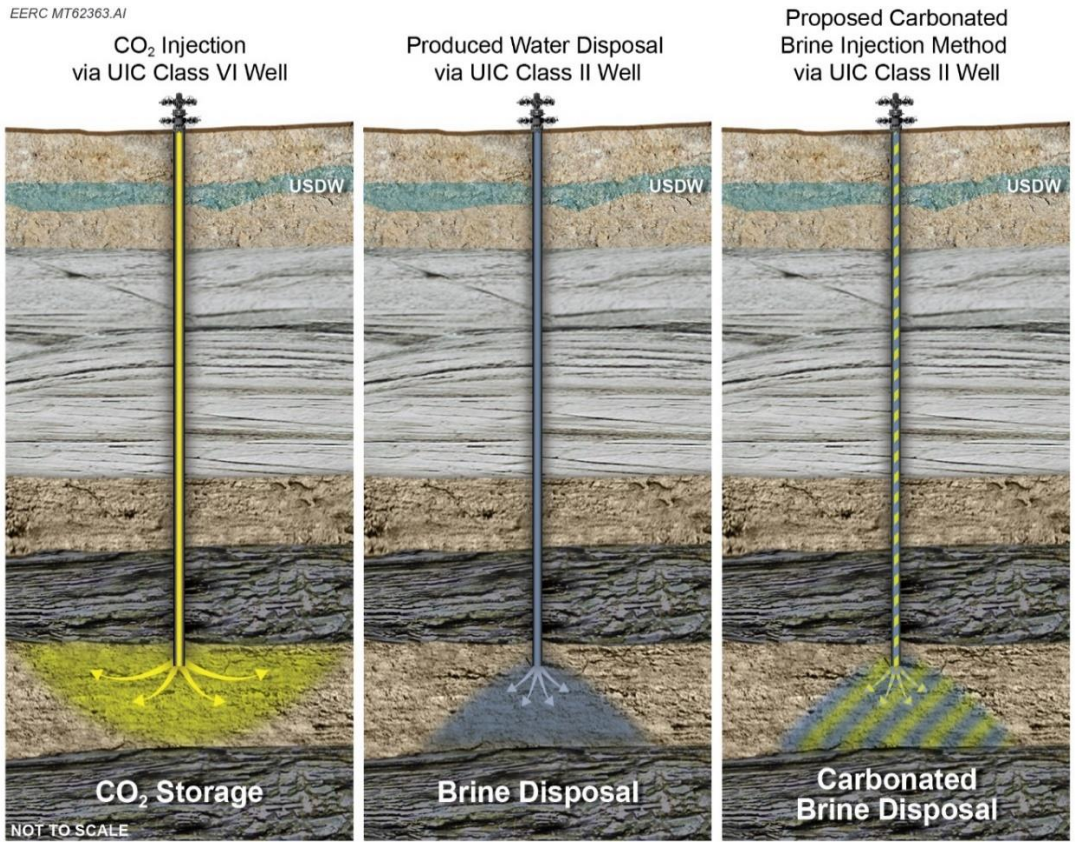


Figure 1: Graphical representation of a proposed CBI method compared to traditional free-phase CO_2 injection via a Class VI well and standard produced water disposal via a Class II well. As shown in the center, with the CBI method, the CO_2 remains dissolved into the brine, thereby eliminating the risk of free-phase CO_2 migration and negligible pressure changes when compared to standard Class II operations.

1.1 OVERVIEW OF SALTWATER DISPOSAL

Significant volumes of saltwater, commonly referred to as "produced water," are coproduced during oil and gas production from wells in unconventional plays such as the Bakken. Water production rate varies by location and geologic formation with Bakken and Three Forks production in the Williston Basin, generating an average of 1–1.5 barrels (bbl) of produced water per barrel of oil (Glazewski et al., 2020). Produced water management represents a significant technical and economic challenge for sustainable oil and gas production. Because of the high salinity and other compounds naturally occurring in the water, produced water needs to be managed in an environmentally safe manner. In North Dakota, for example, the primary means of management of produced water is disposal via subsurface injection, where 95% of produced water volumes are disposed of through injection into the Dakota Group (Figure 2). Since 1956, the Lower Cretaceous Dakota, which includes the Inyan Kara, Skull Creek, Newcastle, and Mowry Formations, has been the primary interval for SWD in North Dakota. Underground injection control (UIC) Class II injection is permitted for the entire Dakota Group; however, lowermost sands of the Inyan Kara Formation are typically the target injection zone for SWD (Bader, 2017). The Dakota Group is prevalent and laterally extensive throughout the Williston

DocuSign Envelope ID: 2FA9A609-C360-4E53-8B28-BE8B77B6994A

Basin, with depths ranging from 1,800 to 6,220 ft and a thickness averaging 700 ft in areas coinciding with use for SWD (North Dakota Geological Survey, 2020). The Dakota Group contains the Mowry and Skull Creek shales and is capped by the shales of the Belle Fourche, Carlile, and ultimately Pierre Formations. The Dakota Group is also underlain by the shales of the Swift and Piper Formations. This package of laterally extensive reservoir and overlying and underlying cap rock makes the Dakota Group an ideal target for both SWD and CO_2 storage, although the Dakota is currently used almost exclusively for SWD. With produced water volumes intrinsically linked to oil and gas production volumes, increased oil and gas production in North Dakota over the past decade has resulted in more produced water needing disposal. In 2008, there were nearly 300 SWD wells distributed throughout the Williston Basin. By 2019, there were over 500 SWD wells, with most of the new wells located within the core of Bakken production (Figure 2).

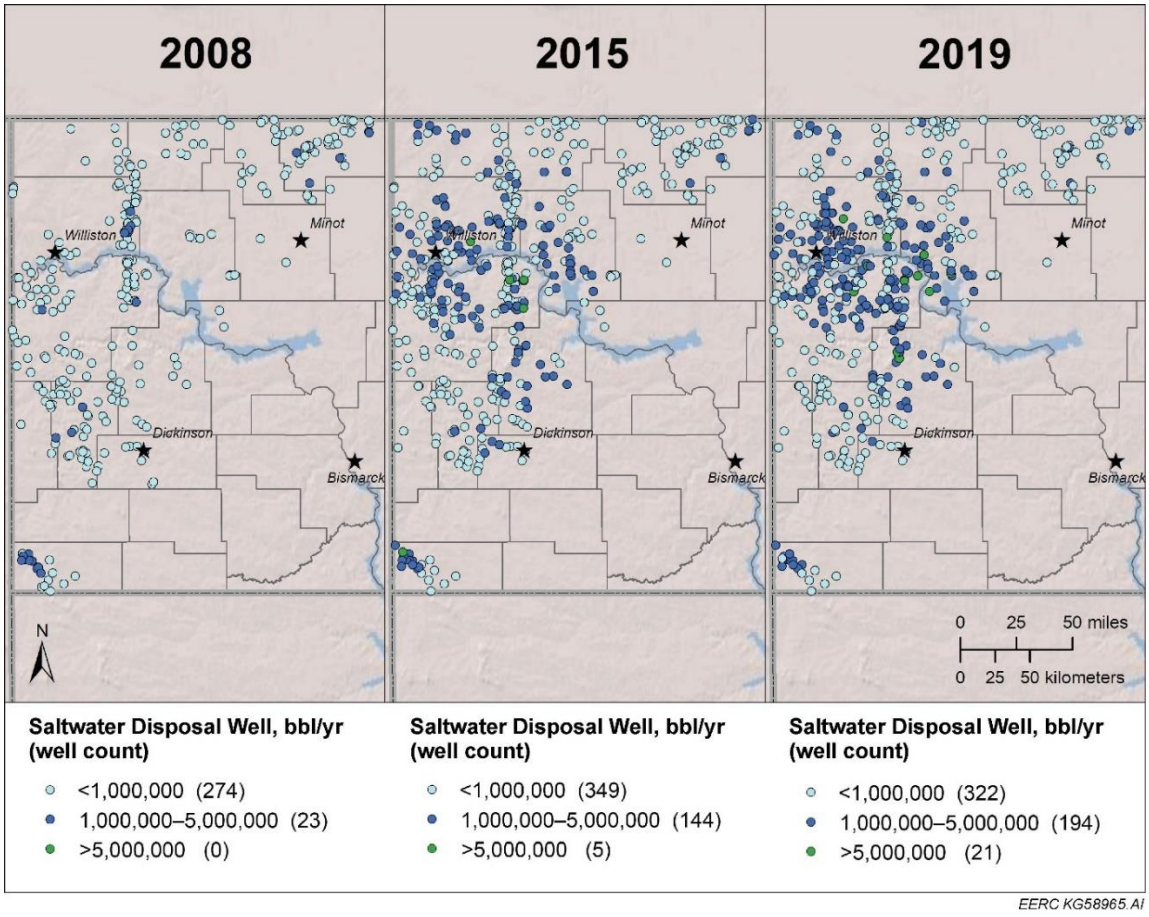


Figure 2: Distribution of active SWD wells in 2019 (data source: North Dakota Industrial Commission, 2020).

DocuSign Envelope ID: 2FA9A609-C360-4E53-8B28-BE8B77B6994A

1.2 OVERVIEW OF CARBON CAPTURE, UTILIZATION, AND STORAGE

Capturing CO_2 emissions from large stationary sources before the CO_2 can be released to the atmosphere is one of the primary approaches to carbon management by which the use of fossil fuels can be maintained to meet increasing energy demands throughout the world. This approach, in conjunction with utilization and/or geologic storage, is termed carbon capture, utilization, and storage (CCUS) and includes a set of technologies that can greatly reduce CO_2 emissions from large point sources such as coal- and gas-fired power plants, natural gas-processing facilities, ethanol plants, and other industrial processes (Metz et al., 2005). CCUS involves the capture of CO_2 by separation from other gases, compression to a liquid or dense fluid state, and then, as with produced water disposal, transportation to an appropriate geological storage location for injection into deep geologic formations, ensuring safe and permanent storage (Metz et al., 2005).

Like produced water disposal, a suitable geologic formation would possess adequate volume, porosity, permeability, and wellbore integrity to safely accept and contain the expected amount of injected CO_2. Typically found in areas with thick accumulations of sedimentary rock known as basins, these formations include porous and permeable layers of rock (reservoirs) that may contain natural fluids, including very salty water (brine), oil, gas, and even CO_2. It is strongly recommended that the chosen formation is at a sufficient depth so that the temperature and pressure are high enough to ensure the injected CO_2 remains in a dense liquid or supercritical state. This greatly increases the storage capacity of the formation. Similar to produced water disposal, the formation must also possess a sealing unit (of sufficient thickness, mechanical integrity, and sufficiently low permeability) that will prevent upward migration of the injected CO_2 and negative impacts to underground sources of drinking water (USDW), defined by the U.S. Environmental Protection Agency UIC Program as water with salinity values of less than 10,000 mg/L.

Depleted hydrocarbon reservoirs are a focus for their storage potential because of their proven ability to store oil and gas for millions of years as well as the possible economic incentives offered through the utilization of the injected CO_2 in enhanced oil recovery (EOR). Deep saline formations, also commonly used for SWD, do not offer traditional economic incentives like those associated with EOR; however, they are more widespread and therefore more likely to be closer to large emission sources, reducing CO_2 transportation costs. Deep saline formations also possess the largest potential capacity because of their size and prevalence. The development of carbon credits such as the Enhancement of Carbon Dioxide Sequestration Credit (a.k.a. Section 45Q) tax program under the Internal Revenue Service (IRS) are also providing new economic incentives for storage in deep saline formations.

1.3 THE CONNECTION BETWEEN SWD AND CCUS: THE CONCEPT OF CBI AND STORAGE

As oil and gas production continues to increase in North Dakota, along with subsequent SWD and produced water management, and with the expansion of Section 45Q tax credits for CO_2 storage, oil and gas operators are looking at alternative ways to both manage SWD costs and reduce carbon footprint. One potential option is the mixing of CO_2 with the produced water prior to injection into Class II SWD wells.

With dissolved CBI, a stream of CO_2 is blended with the brine at the surface as it is injected into the storage formation, so dissolution is intrinsic to the injection process. The blending of CO_2

DocuSign Envelope ID: 2FA9A609-C360-4E53-8B28-BE8B77B6994A

into the produced water stream results in the injection of a higher-density, CO_2-saturated brine that behaves like currently injected brines, sinking into and mixing with native formation fluids. Unlike traditional CO_2 injection methods, there is no mobile free-phase CO_2 plume. As a result, CBI removes differences in fluid compressibility between the brine phase and a sCO_2 phase. With a single, CO_2-saturated aqueous phase, post injection pressure equilibrium is not inhibited by two-phase flow, as this aqueous phase exhibits flow behavior similar to currently disposed brine in the disposal formation. In theory, this behavior would substantially reduce the area of impact and monitoring burden for this type of CO_2 storage compared to traditional CO_2 injection, since the injected CO_2 is already stabilized within the injected fluids. A limitation of this process is that a much smaller volume of CO_2 is likely to be able to be injected compared to typical free-phase CO_2 injection. However, if paired with thousands of existing SWD wells associated with oil and gas production in the U.S., CBI can make a significant contribution to CO_2 mitigation as an economical and low-risk means of CO_2 storage and should open CO_2 storage opportunities to many new participants.

Publicly available data on wastewater volumes in the U.S. show that 10.5 billion barrels of produced water are injected into Class II injection wells in the states of Texas, California, Oklahoma, Wyoming, Kansas, Louisiana, New Mexico, and North Dakota alone (Veil, 2015). Using CBI and assuming a conservative 2% mass fraction of CO_2 is added to each state's wastewater injection volumes, 53 million tons of CO_2 could be sequestered each year into pre-existing, permitted infrastructure. Figure 3 shows a heat map of volumes of CO_2 that could be sequestered using CBI, based on the publicly available data from Veil (2015).

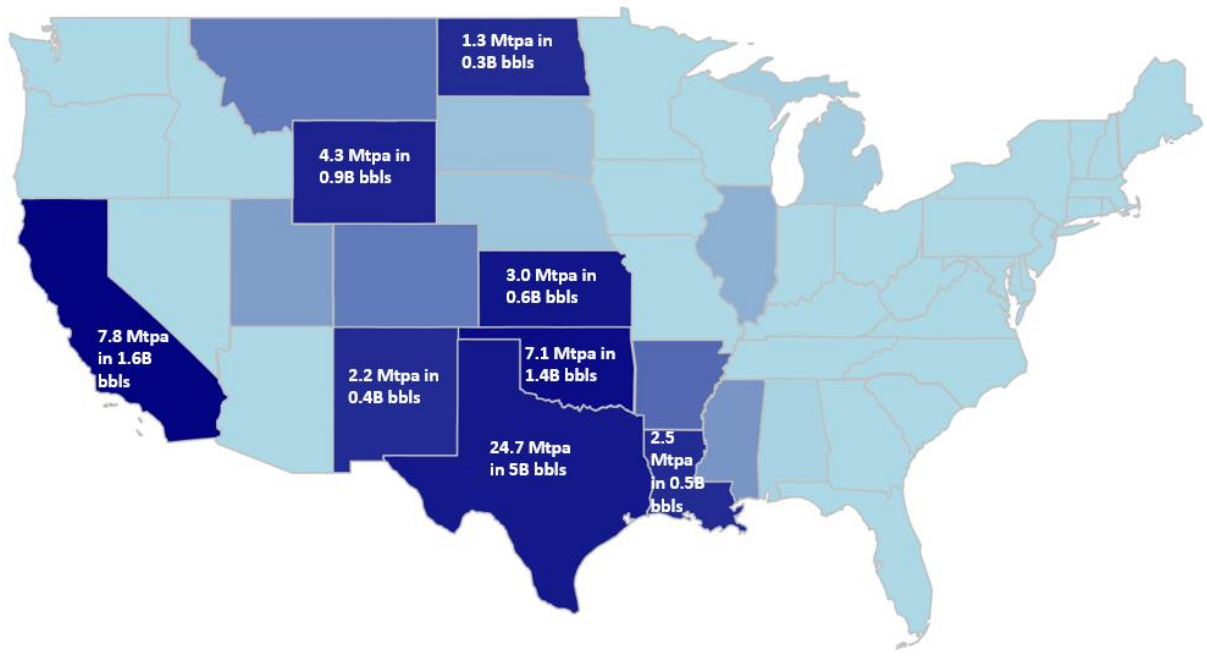


Figure 3: States with large wastewater injection volumes can sequester 53 Mtpa CO_2 using CBI.

DocuSign Envelope ID: 2FA9A609-C360-4E53-8B28-BE8B77B6994A

The pace at which oil and gas operations have been increasing wastewater disposal volumes since 2015 suggests that the amounts shown on Figure 3 are conservative. In the state of North Dakota alone, only an estimated 253 million barrels of wastewater were being injected at that time. However, that volume is now past 800 million barrels of wastewater per year, suggesting over 4 Mtpa of CO_2 could be sequestered in North Dakota using CBI. Oil production in North Dakota increased to over 1.5 million barrels (MMbbl)/day in 2019. While production has decreased due to a downturn in oil prices, as of July 2020, production had recovered to over 1 MMbbl/day. A byproduct of oil and gas production is produced water which refers to the brine that is coproduced with oil. Volumes of produced water vary by location and geologic formation with Bakken production generating an average of 1–1.5 bbl of produced water per barrel of oil.

The existing Class II wellbore compatibility with CBI depends on the extent of chemical reactions and changes to the injection wells because of additional carbonic acid (H_2CO_3) in the produced water. The lowered pH supplies hydrogen as a reducible reactant to fuel the cathodic process, therefore, accelerating the corrosion process. This could lead to corrosion of the wellbore casing, tubing, packer, and surface equipment.

1.4 RESEARCH ON CBI AND STORAGE

While CBI as a method of carbon sequestration is a nascent technology, it was first proposed by Georgescu et al. (2006). CBI provides numerous benefits including immediate dissolution, negative buoyancy, and no free-phase CO_2. If the carbonated brine is denser than the reservoir brine, it will sink to the bottom of the reservoir, reducing the risk of upward CO_2 migration. Carbonated brine occupies only 5% greater volume than unsaturated brine, leading to a smaller displacement volume than bulk CO_2 injection when an equivalent volume of brine is produced (Burton and Bryant, 2009). Compared to CBI, $scCO_2$ injection initially has a smaller areal footprint per unit of CO_2 injected. However, because of high mobility and buoyancy, free CO_2 spreads out along the cap rock and ultimately occupies a larger area than carbonated brine, which sinks to the bottom of the reservoir (Ruprecht and Falta, 2012). Storage volumes are reduced by approximately 50% if CO_2 is dissolved into brine, as opposed to a separate supercritical fluid; additionally, CO_2-saturated brine is denser than undersaturated formation brines, causing CO_2 to migrate downward within a formation, as opposed to upward against the cap rock (Steele-MacInnis et al., 2013).

A few studies have examined CBI in specific regions around the world. Studies in the offshore region of the United Kingdom show that CBI enhances CO_2–brine stability and improves CO_2 sequestration by eliminating the buoyancy force and rapidly immobilizing the CO_2 (Eke et al., 2011). CBI was utilized at the CarbFix site in Iceland to demonstrate the efficacy of the method and to promote rapid mineralization (Sigfusson et al., 2015). Carbonated brine storage has been found to require less pore volume when reservoir brine is used as the dissolution agent (Wu et al., 2017). For example, in the Northeast German Basin, 4.7 billion tons of CO_2 could be stored in solution compared to 1.5 billion tons as free-phase CO_2 (Kühn et al., 2017).

Other studies have looked for methods to improve the process. For example, while surface mixing has been the most studied method of carbonating brine, mixing at depth reduces pressure mixing requirements (Pool et al., 2013). Downhole mixing reduces energy requirements, as the pressure of the formation is used to dissolve the CO_2 (Shariatipour et al., 2016). While mass fractions of dissolved CO_2 will ultimately be controlled by reservoir conditions and energy requirements, silica nanoparticles have been proposed to increase CO_2 concentration in water

DocuSign Envelope ID: 2FA9A609-C360-4E53-8B28-BE8B77B6994A

(Fathollahi and Rostami, 2015). In laboratory studies, core floods with carbonated brine have also been shown to encourage CO_2 trapping via mineralization because of the additional availability of cations (Pearce et al., 2022; Rathnaweera et al., 2016). CBI may alter the wettability of reservoir rock (Motie and Assareh, 2020). Khan et al. (2021) previously proposed CBI through Class II injection wells, pointing out that the infrastructure for produced water disposal is already built and in place. Laboratory observations of CBI in wastewater from oil and gas operations may promote mineralization as another trapping mechanism (Pearce et al., 2021).

DocuSign Envelope ID: 2FA9A609-C360-4E53-8B28-BE8B77B6994A

2. METHODS

This simulation-based research includes: 1) reservoir modeling to investigate CO_2 molality, phase change and pressure change at different salinity; 2) wellbore corrosion modeling to examine the wellbore compatibility with the injection of carbonated produced water; and 3) reactive transport modeling to check rock-fluid interactions in the reservoir during injection and long-term storage. The feasibility and safety of CBI as a low-rick geologic CO_2 sequestration strategy was assessed by analyzing the modeling results.

2.1 RESERVOIR MODEL SETUP

The Computer Modeling Group (CMG) simulation program was utilized in this project to create a reservoir model. Within the CMG launcher, several sub-programs were accessed to derive the desired simulation outcomes. Specifically, the Builder, GEM, and results graph components were employed to execute the simulations and procure the results. For this particular project, the Builder, GEM, and results graph functionalities were sufficient to conduct the simulations and achieve the desired outcomes.

The Builder component of CMG encompasses various aspects of data input, including grid creation, grid property definition, incorporation of production data, fluid properties, rock-fluid interactions, fluid models, and initial conditions. An assessment of CBI was conducted using representative data and properties from typical Williston Basin SWD wells that inject into the Inyan Kara Formation of the Dakota Group. The initial phase involved estimating the quantity of CO_2 that could be injected at specific brine volumes and injection pressures. These parameters were established based on existing SWD operations, adhering to Class II injection regulations.

Numerical simulations of CBI into the targeted formation were carried out across 16 scenarios. The objective was to ascertain the maximum amount of CO_2 that could be dissolved into the formation fluid, leaving no residual undissolved CO_2. A consistent injection rate of 8,000 barrels per day over 5 years was adopted for all scenarios, mirroring the operational practices at SWD sites within the Williston Basin.

To illustrate the process of CBI using a commercial simulator, a stream of injection with dissolved CO_2 molality was defined and utilized as the injection constraint. The reservoir was assumed to be fully saturated with brine (100% brine-saturated), featuring an initial formation salinity of 10,000 parts per million (ppm) and an injection salinity of 10,000 ppm. Molality (m), which expresses solution concentration, along with density and injection volume were the pivotal parameters in calculating the total amount of CO_2 dissolved in the reservoir conditions. To identify the maximal CO_2 dissolution into the injected fluid, scenarios were run with varying molality values ranging from 0.20 to 2.0, while maintaining all other parameters constant. Table 1 and Table 2 provide a breakdown of the simulation parameters and the scenarios that were evaluated. In Table 2, 0.75 mole represents the highest starting concentration at which essentially all of the CO_2 [99.999%] can be dissolved into the brine. At higher molality, not all CO_2 is dissolved.

DocuSign Envelope ID: 2FA9A609-C360-4E53-8B28-BE8B77B6994A

Table 1: Reservoir Simulation Constant Parameters

Constant Parameters	Value
Injection Rate, bbl/day	8,000
Years of Injection	5
Reservoir Pressure, psi	2,255
Reservoir Temperature, °F	165
Injection Temperature, °F	60
Injection Fluid Salinity, ppm	10,000
Reservoir Fluid Salinity, ppm	10,000

Table 2: Results of Experimental Injection Simulation Scenarios

Sc.	Molality, mol/kg	Cumulative Injection of CO_2, gmol	CO_2 Dissolved in Water, gmol	CO_2 Dissolved in Water, tonne	CO_2 in Gas Phase, gmol	CO_2 Dissolved, %	Gas Phase, %	Total, %*
1	2.00	4,332,140,000	3,857,820,000	169,783	475,327,000	89.05	10.97	100.00
2	1.00	2,241,860,000	2,240,980,000	98,625	1,182,910	99.96	0.05	100.00
3	0.85	1,915,640,000	1,915,230,000	84,289	380,447	99.98	0.02	99.99
4	0.80	1,806,130,000	1,805,800,000	79,473	297,109	99.98	0.02	99.99
5	0.75	1,696,230,000	1,695,970,000	74,640	238,336	99.99	0.01	99.99
6	0.70	1,585,950,000	1,585,740,000	69,789	194,658	99.99	0.01	99.99
7	0.65	1,475,280,000	1,475,100,000	64,919	160,893	99.99	0.01	99.99
8	0.60	1,364,210,000	1,363,340,000	60,001	133,932	99.94	0.01	99.95
9	0.55	1,252,750,000	1,251,390,000	55,074	111,907	99.89	0.01	99.90
10	0.50	1,140,890,000	1,138,580,000	50,109	93,522	99.80	0.01	99.81
11	0.45	1,028,630,000	1,026,370,000	45,171	78,003	99.78	0.01	99.79
12	0.40	915,975,000	913,971,000	40,224	64,666	99.78	0.01	99.79
13	0.35	802,913,000	801,620,000	35,279	53,080	99.84	0.01	99.85
14	0.30	689,445,000	688,326,000	30,293	42,857	99.84	0.01	99.84
15	0.25	575,570,000	574,676,000	25,291	33,784	99.85	0.01	99.85
16	0.20	461,285,000	460,723,000	20,276	25,665	99.88	0.01	99.88

* May not equal 100% due to rounding.

DocuSign Envelope ID: 2FA9A609-C360-4E53-8B28-BE8B77B6994A

The simulations encompassed a 1-year pre-injection phase (well shut-in, no injection), followed by 5 years of CBI, and concluded with a 1-year post-injection monitoring phase (well shut-in, no injection). This sequencing aimed to better understand the changes in reservoir conditions prior to and subsequent to the injection. Simulation findings revealed that within the molality range of 0.75 to 0.65, approximately 99.99% of CO_2 would be successfully dissolved into the reservoir fluid (as depicted in Figure 4).

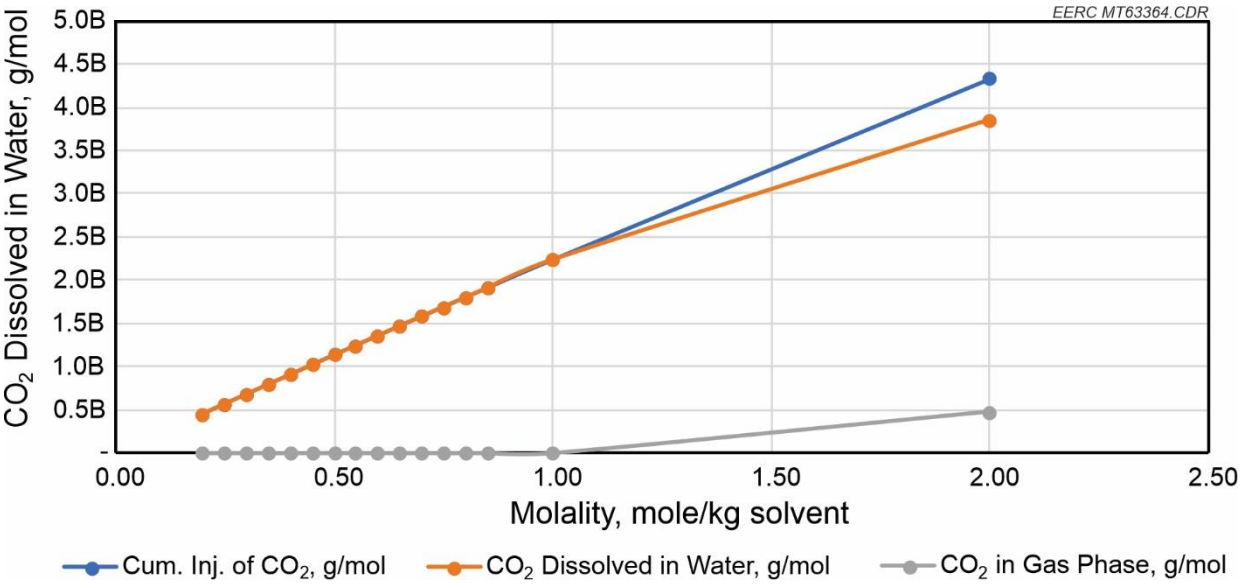


Figure 4: Simulation results showing the amount of CO_2 dissolved in water and the CO_2 remaining in the gas phase at reservoir conditions for all scenarios. At a molality of approximately 0.80, the CO_2 is no longer fully saturated in the reservoir.

Predictive simulations for carbonated brine storage were developed through the scaling up of the existing experimental simulation model to encompass an area around the injection well measuring 1,000 ft by 1,000 ft. A total of nine simulation models were constructed to systematically examine the intricate interplay among injection fluid salinity, reservoir fluid salinity, and CO_2 molality. The specifics of the simulation scenarios can be found in Table 3, while Table 4 provides a comprehensive breakdown of the results achieved for each individual scenario. In the scenarios involving the lowest injected and reservoir brine salinity (Scenarios 1–3), the entirety of the CO_2 volume dissolved into the injected fluid was retained in solution. As the injection brine salinity increased to levels more characteristic of standard SWD fluid salinities, the molality of the injected fluid emerged as a crucial factor. Within Scenarios 4–6, simulating 150,000 ppm TDS (total dissolved solids) injected fluid, the maximum CO_2 dissolution occurred at a concentration of 0.4 molality. In Scenarios 7–9, which represented 300,000 ppm TDS injected fluid, the optimal CO_2 dissolution occurred at a concentration of 0.6 molality.

DocuSign Envelope ID: 2FA9A609-C360-4E53-8B28-BE8B77B6994A

Table 3: Reservoir Performance Scenarios for Experimental Injection

Scenario	Injection Fluid Salinity, ppm	Reservoir Fluid Salinity, ppm	Molality
1	10,000	10,000	0.2
2	10,000	10,000	0.4
3	10,000	10,000	0.6
4	150,000	20,000	0.2
5	150,000	20,000	0.4
6	150,000	20,000	0.6
7	300,000	20,000	0.2
8	300,000	20,000	0.4
9	300,000	20,000	0.6

Table 4: Results of Nine Predictive Injection Simulation Scenarios

Sc.	Molality, mole/kg solvent	Cumulative Injected CO_2, gmol	CO_2 Dissolved in Water, gmol	CO_2 in Gas Phase, gmol	CO_2 Dissolved, %	Gas Phase, %	Total, %*
1	0.2	500,413,000	499,979,000	58,266	99.91	0.012	99.93
2	0.4	544,937,000	544,870,000	54,529	99.99	0.010	99.99
3	0.6	633,511,000	633,433,000	79,993	99.99	0.013	100.00
4	0.2	500,413,000	485,680,000	187,048	97.10	0.037	97.10
5	0.4	544,937,000	544,936,000	347,791	99.99	0.064	100.00
6	0.6	633,511,000	625,504,000	7,795,840	98.74	1.231	99.97
7	0.2	500,413,000	486,711,000	13,389,000	97.26	2.676	99.94
8	0.4	544,937,000	522,326,000	22,048,200	95.85	4.046	99.90
9	0.6	184,272,000	184,261,000	45,575	99.99	0.0247	100.00

* May not equal 100% due to rounding.

While every evaluated scenario demonstrated CO_2 dissolution levels exceeding 95%, a molality of 0.2 might offer the optimal equilibrium between the injected CO_2 volume and the volume of CO_2 that remains in solution. This prompted an examination of the simulation cases to assess the long-term consequences of CO_2 within the reservoir.

Furthermore, supplementary simulations were undertaken to thoroughly assess the long-term consequences of CO_2 within the reservoir. A total of 12 distinct scenarios were examined, encompassing a 1-year pre-injection phase, followed by a 20-year period of CBI, and extending into a 100-year post-injection phase. This comprehensive timeframe was adopted to gain a profound understanding of the enduring effects of the CO_2 plume. The particulars of these additional simulation cases are detailed in Table 5, outlining the initial conditions.

DocuSign Envelope ID: 2FA9A609-C360-4E53-8B28-BE8B77B6994A

Table 5: Simulation Initial Conditions for Additional Simulation Scenarios

Constant Parameters	Value
Injection Rate, bbl/day	8,000
Years of Injection • Pre-injection • Post-injection	20 1 100
Reservoir Pressure, psi	2,255
Reservoir Depth, ft	4,700
Reservoir Temperature, °F	165
Wellhead Temperature, °F	60

These simulation models investigated the dynamic interaction between injection fluid salinity, reservoir fluid salinity, and CO_2 molality. The specifics of the simulation scenarios for each case are presented in Table 6. Furthermore, to comprehend the storage capacity of the reservoir under varying conditions, different initial reservoir pressures were also considered. Specifically, these 12 simulation cases were re-executed utilizing initial reservoir pressures of 1,500 psi and 2,255 psi, enabling a comprehensive assessment of the impact of initial reservoir pressure on storage capacity.

Table 6: Reservoir Performance Scenarios at 1,500 psi and 2,255 psi

Scenario	Injection Fluid Salinity, ppm	Reservoir Fluid Salinity, ppm	Molality
1	100,000	10,000	0.2
2	200,000	10,000	0.2
3	300,000	10,000	0.2
4	400,000	10,000	0.2
5	100,000	20,000	0.4
6	200,000	20,000	0.4
7	300,000	20,000	0.4
8	400,000	20,000	0.4
9	100,000	30,000	0.6
10	200,000	30,000	0.6
11	300,000	30,000	0.6
12	400,000	30,000	0.6

DocuSign Envelope ID: 2FA9A609-C360-4E53-8B28-BE8B77B6994A

2.2 PRODUCED WATER DATA

The produced water data from the region of interest were filtered from the United States Geological Survey (USGS) produced water database (Siefert et al., 2022). The filter was set in the sequence of North Dakota (State), Mckenzie (County), Bakken (Formation). The filtered Bakken produced water data were averaged after removing the data point with a charge imbalance above ±5%. Final data for geochemical related model input is listed in Table 7. Total carbon concentration is the sum of carbonate and bicarbonate concentration.

Table 7. Produced Water Chemistry for Modeling Input

Species	Name	Concentration	Unit
	Density	1.17	g/mL
	pH	5.94	
K+1	Potassium	4483.17	mg/L of K^+
Na+1	Sodium	75341.45	mg/L of Na^+
Ba+2	Barium	34.40	mg/L of Ba^{2+}
Ca+2	Calcium	16674.76	mg/L of Ca^{2+}
Fe+2	Iron II	124.71	mg/L of Fe2+
Mg+2	Magnesium	1091.15	mg/L of Mg^{2+}
Cr+3	Chromium III	0.69	mg/L of Cr^{3+}
Cl-1	Chloride	152006.21	mg/L of Cl^-
CO3-2	Carbonate	1631	mg/L of CO_3^{2-}
HCO3-1	Bicarbonate	341.79	mg/L of HCO_3^-
Total C	Carbon	32.78	mmol/L of total C
NO3-1	Nitrate	151.96	mg/L of NO_3^-
SO4-2	Sulfate	613.46	mg/L of SO_4^{2-}

2.3 WELLBORE CORROSION MODEL

An aqueous chemistry software called OLI Studio was used to model the data from the chosen power plants as streams. This program uses a stream analyzer to perform a variety of functions and water analysis. Stream Analyzer is a comprehensive thermodynamic tool that calculates speciation, scaling tendencies in the systems. The calculation of the aqueous solution speciation, concentrations, activities and transport properties of the reacting species in the brine was performed using the thermophysical module. The corrosion rates were calculated by quantifying the bulk chemistry, transport phenomena, and surface reactions through a thermophysical and electrochemical module using corrosion analyzer. The electrochemical module simulates the electrochemical reactions (oxidation and reduction) occurring on the steel surface were simulated using the electrochemical module.

DocuSign Envelope ID: 2FA9A609-C360-4E53-8B28-BE8B77B6994A

Single-point calculations, determination of water quality properties, and corrosion analysis are some examples of the various useful functions that can be performed using the aqueous chemistry software. For this project, reconciliation and single-point calculations were the main operations used in analyzing the power plant streams. With the produced results from the software, comparisons and an analysis of software performance can be made.

Tubular materials, casing and long string made of carbon steel (API 5CT). API 5CT casing and tubing include grades L80-1, L80 9Cr (Cr 8%-10%), and L80 13Cr (Cr 12%-14%). For corrosion studies, 13Cr stainless-steel, super stainless-steel, and low carbon steel 1010 were considered. Increasing vertical depth of the reservoir means increasing the temperature and the partial pressure of CO_2 in wells. A parametric study was performed to simulate the changes in temperature inside the reservoir. USGS produced water data from North Dakota-McKenzie County-Bakken formation have been selected to perform this study. The chemical composition input for OLI is shown in Table 8. The effects of temperatures, pH, and CO_2 concentration, on corrosion are also investigated. The produced water without adding CO_2 contained 32.78 mmole/ L of HCO_3^- as C. CO_2 partial pressure of produced water with 0.2 mole/kg (8,800 mg/L) CO_2 correspond to 6.415 atm at 25 ^oC, considering a 1 liter of produced water. However, CO_2 partial pressure for produced water with 0.6 mole/kg (26,400 mg/L) CO_2 correspond to 20 atm at 25 ^oC, considering a 1 liter of produced water.

Table 8: Chemical Composition of Produced Water - No Added CO_2; Steam Amount = 1L; Temperature 25 ℃, 1 atm

Physical Parameters/Composition	Values
Density (g/L)	1.18
pH	5.94
K^+ (mg/L)	4483.17
Na^+ (mg/L)	75341.45
Ba^{2+} (mg/L)	34.4
Ca^{2+} (mg/L)	16674.76
Fe^{2+} (mg/L)	124.71
Mg^{2+} (mg/L)	1091.15
Cr^{3+} (mg/L)	0.69
Cl^- (mg/L)	152006.21
HCO_3^- as C (mmol/L)	32.78
NO_3^- (mg/L)	151.96
SO_4^{2-} (mg/L)	613.46

DocuSign Envelope ID: 2FA9A609-C360-4E53-8B28-BE8B77B6994A

2.4 REACTIVE TRANSPORT MODEL

The 2D Reactive Transport Model (RTM) was performed using Geochemist's Workbench (GWB) 10.0 X2t module with the default thermo database. The reservoir setup was similar to the reservoir model. Domain dimension was set at 300 m × 300 m × 100 m. Well location was at x, y = 150 m, 150 m, center of the domain. The fluid discharge rate from the well was 1,280 m^3/day (8,000 bbl/day). In the default domain (Figure 5), the reservoir flow was from left to right. In this model, the reservoir flow rate was 0 and both left and right boundaries were set as open. The Longitudinal dispersivity was 100 cm and the transverse dispersivity was 10 cm. The diffusion coefficient was 10^{-6} cm^2/s. The nodes number was set 29 × 29. The temperature was set at 74 °C (160 °F) for reservoir reactions.

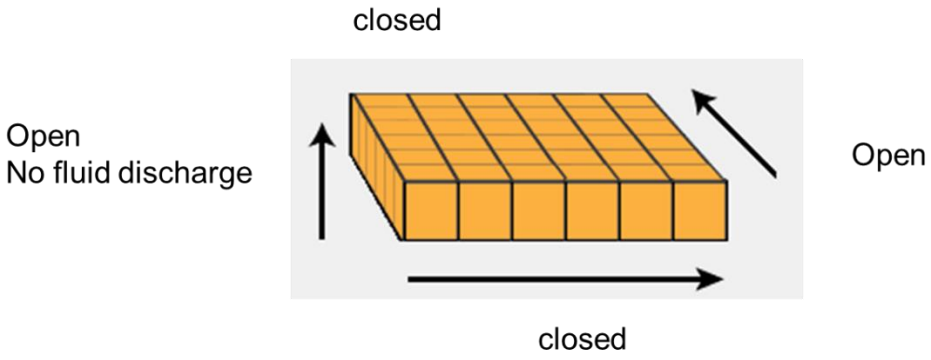


Figure 5: 2D Reactive transport model domain schematic.

From the core analysis conducted by Energy & Environmental Research Center (EERC), the Inyan Kara sandstone contains 70.5 vol% sandstone, 2.7 vol% clay, and 3.8 vol% siderite, resulting in 23% porosity. In the model, muscovite was chosen to represent the clay. The Inyan Kara formation water chemistry was obtained from previous report (Chu, 1991). The initial rock-fluid system data and the injection water data are listed in Table 9. The injection water is composed of the produced water chemistry, replacing the total carbon to the recommended dissolved CO_2 molality (0.2 molal) for carbonated brine.

DocuSign Envelope ID: 2FA9A609-C360-4E53-8B28-BE8B77B6994A

Table 9: Formation Rock-Fluid System and Injection Carbonated Brine Chemistry

Formation	Concentration	Injection water	Concentration
Quartz	70.5 volume %	$SiO_2(aq)$	
Muscovite	2.7 volume %	Al^{+++}	
Siderite	3.8 volume %	Fe^{++}	124.71 mg/L
Mg^{++}	57 mg/L	Mg^{++}	1,091.15 mg/L
pH	6.1	pH	5.94
Ca^{++}	259 mg/L	Ca^{++}	16,674.76 mg/L
Na^{+}	7,114 mg/L	Na^{+}	75,341.45 mg/L
K^{+}	408 mg/L	K^{+}	4,483.17 mg/L
Cl^{-}	10,600 mg/L	Cl^{-}	152,006.21 mg/L
$SO4^{--}$	1,000 mg/L	SO_4^{--}	613.46 mg/L
$HCO3^{-}$	1,086 mg/L	HCO_3^{-} as C	0.2 molal
Ba^{++}		Ba^{++}	34.40 mg/L
NO_3^{-}		NO_3^{-}	151.96 mg/L

Mineral reactants are listed in Table 10. Quartz, muscovite, and siderite are primary minerals in the initial system. All the others are secondary minerals to precipitate. The kinetic rate (k, $mol/cm^2 \cdot s$) and activation energy (E, J/mol) were obtained from literature or set to similar minerals. Surface area of all minerals was assumed to be 1,000 cm^2/g for reservoir rock. Nucleus density was set at 1,000 cm^2/cm^3 for all secondary mineral precipitation. The injection period was set at 20 years with the injection fluid rate (1,280 m^3/day). After 20 years, the injection fluid rate was set at 0 for 100 years as the shut-in period.

DocuSign Envelope ID: 2FA9A609-C360-4E53-8B28-BE8B77B6994A

Table 10: Formation Rock-Fluid System and Injection Carbonated Brine Chemistry

Minerals	k (mol/cm^2·s)	E (J/mol)	Reference
Quartz	1.00E-16	87,500	(Rimstidt and Barnes, 1980)
Muscovite	2.00E-16	64,000	(Nagy, 1995)
Siderite	2.00E-11	55,000	Set to dolomite
Barite	1.26E-12	30,800	(Palandri and Kharaka, 2004)
Calcite	1.58E-10	63,000	(Plummer et al., 1978)
Dolomite	2.00E-11	55,000	(Busenberg and Plummer, 1982)
Witherite	4.47E-12	41,900	Set to strontianite (Sonderegger et al., 1976)
Kaolinite	3.98E-16	64,000	(Sverdrup, 1990)
Dawsonite	1.00E-11	62,800	(Palandri and Kharaka, 2004)
Magnesite	4.57E-14	23,500	(Palandri and Kharaka, 2004)
Aragonite	1.58E-10	63,000	Set to calcite
Huntite	2.00E-11	55,000	Set to dolomite
Monohydrocalcite	1.58E-10	63,000	Set to calcite
Maximum Microcline	1.26E-15	58,000	Set to K-feldspar
K-feldspar	1.26E-15	58,000	(Helgeson et al., 1984)

DocuSign Envelope ID: 2FA9A609-C360-4E53-8B28-BE8B77B6994A

3. RESULTS

3.1 RESERVOIR SIMULATION

3.1.1 High Reservoir Pressure

An experimental simulation was developed to measure the solubility of the injection fluid in the reservoir. A comprehensive experimental characterization was conducted to analyze the influence of molality and salinity on the solubility of CO_2 in brine. The results of the simulation highlight the pivotal role of molality and salinity in CBI. Table 4 presents a snapshot of the simulation outcomes, underscoring how molality and salinity govern the process. Additionally, a series of 12 simulation cases were executed to explore the enduring effects of CO_2 injection into the reservoir. The findings from these simulations are summarized in Table 11.

Table 11: Result of 12 Long-Term Predictive Injection Simulation Scenarios

Sc.	Injection Fluid Salinity (ppm)	Reservoir Fluid Salinity (ppm)	Molality (mole/kg)	CO_2 Dissolved, %	CO_2 Gas Phase, %
1	100,000	10,000	0.2	99.99%	0.01%
2	200,000	10,000	0.2	99.99%	0.01%
3	300,000	10,000	0.2	99.97%	0.02%
4	400,000	10,000	0.2	99.94%	0.04%
5	100,000	20,000	0.4	99.99%	0.01%
6	200,000	20,000	0.4	99.98%	0.02%
7	300,000	20,000	0.4	93.06%	6.93%
8	400,000	20,000	0.4	63.92%	36.07%
9	100,000	30,000	0.6	99.99%	0.01%
10	200,000	30,000	0.6	92.19%	7.80%
11	300,000	30,000	0.6	65.35%	34.64%
12	400,000	30,000	0.6	53.19%	46.79%

The outcomes show that in scenarios featuring lower reservoir brine salinity (Scenarios 1–3), the injected fluid retained the dissolved CO_2 in solution. Similarly, scenarios with lower injected fluid salinity (Scenarios 1, 5, and 9) exhibited successful retention of CO_2 in solution. However, higher salinity levels in both the injected fluid and reservoir brine led to the emergence of CO_2 in the gas phase within the reservoir. This underscores the substantial impact of injected and reservoir brine salinity on the phase behavior of CO_2. For instance, in Scenario 12, with an injected fluid salinity of 400,000 ppm TDS and a reservoir fluid salinity of 30,000 ppm TDS, representing the highest salinity concentration, approximately 35% of the CO_2 transitioned into the gas phase.

DocuSign Envelope ID: 2FA9A609-C360-4E53-8B28-BE8B77B6994A

Molality also plays a crucial role in this context. When considering higher injection brine salinities, which are more representative of typical SWD fluid salinities, the molality of the injected fluid emerged as a key factor. Specifically, in Scenarios 1–4 with a molality of 0.2 mole/kg, the highest level of CO_2 dissolution occurred at lower salinities. This trend persisted in Scenarios 5–8 with a molality of 0.4 and Scenarios 9–12 with a molality of 0.6. Given typical reservoir and injection fluid salinities, a molality of 0.2 appears to strike the optimal balance between the injected CO_2 volume and the volume of CO_2 remaining in solution.

Figure 6 illustrates the model results of Scenario 1 to 12. Bottomhole pressure (BHP) built steadily throughout the simulation period while still remaining well below the maximum BHP for a typical SWD well in the Williston Basin (~3,000–3,300 psi). The the highest BHP observed in these tests came from Scenario 12 which reached 3,010 psi at the end of the injection phase. Scenario 12 represents the case with the highest tested salinity and dissolved CO_2 molality of 0.6.

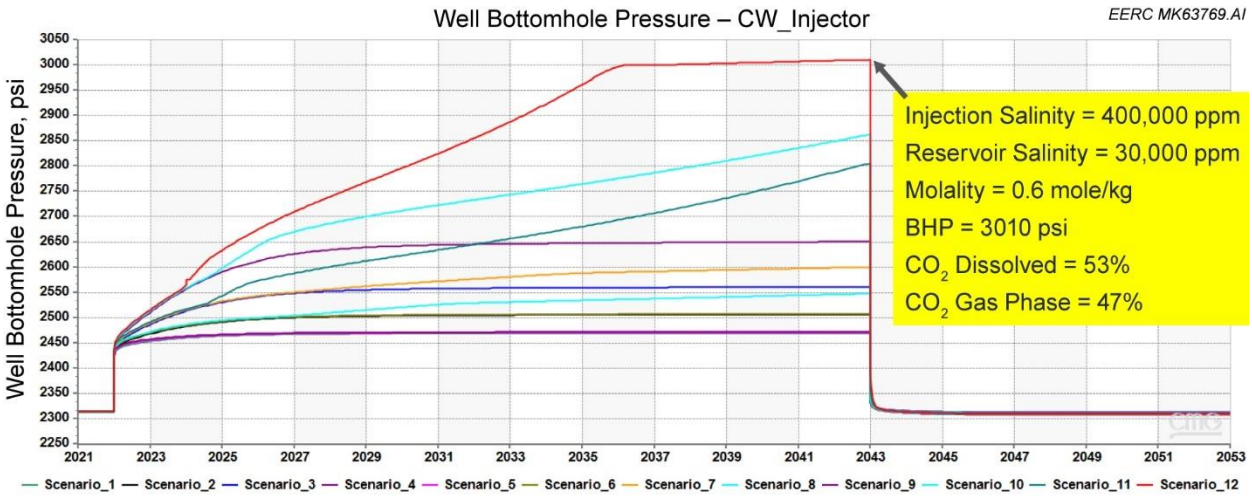


Figure 6: BHP for Scenarios 1 to 12. BHP at the start of injection was approximately 2,300 psi. Stabilized BHP 2 years after injection was approximately 2,585 psi for Scenarios 1 to 8. In Scenarios 9 to 12 a rise in BHP was observed.

In all the injection scenarios where the CO_2 remained fully dissolved, the dissolved CO_2 remains close to the injection well during and after injection as the injected brine with CO_2 tends to sink within the reservoir to below the injection well. As an example, Figure 7 illistrates the results from Scenario 3, 100 years after injection has ceased, showing the distribution of CO_2 molality stabilizing at the bottom of the reservoir. Some mixing diffusion is observed along the edges of the plume but this mixing zone does not extend far beyond the wellbore. This phenomenon suggests that CO_2 migration has a low likelyhood to occur with dissolved CO_2 injection.

DocuSign Envelope ID: 2FA9A609-C360-4E53-8B28-BE8B77B6994A

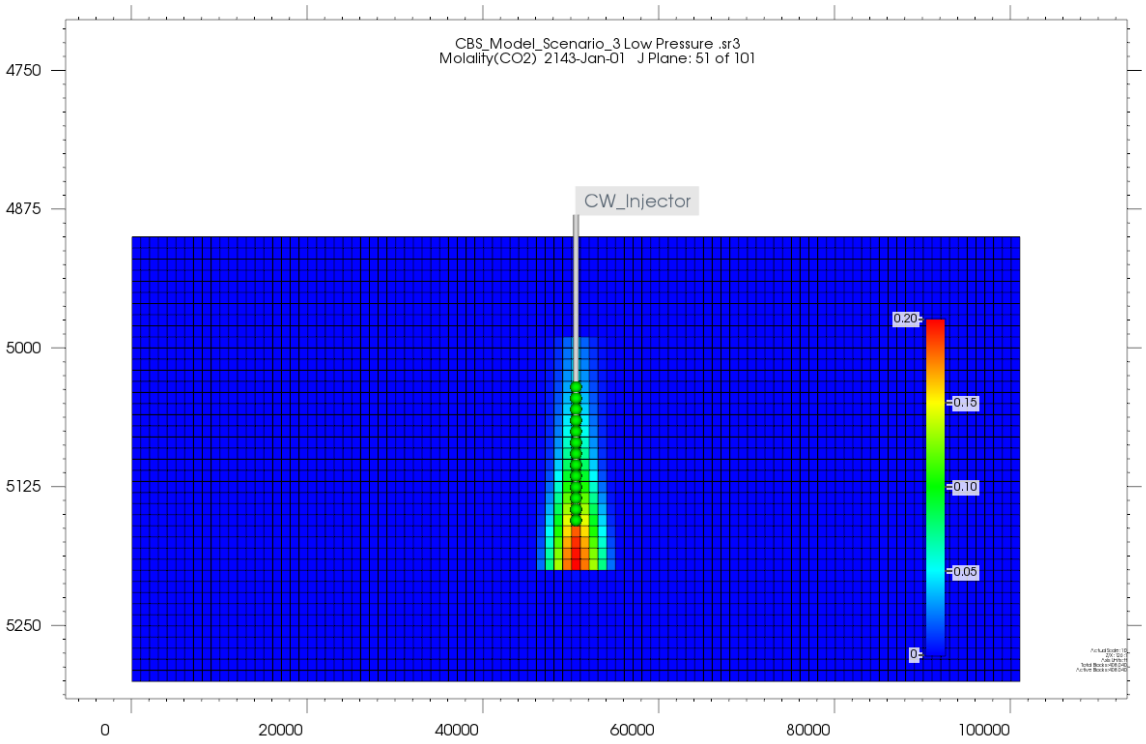


Figure 7: Illustration of the model results of Scenario 3, showing brine carrying dissolved CO_2 to the base of the reservoir.

3.1.2 Low Reservoir Pressure

Table 12 presents the outcomes of the 12 simulations conducted with an initial reservoir pressure of 1,500 psi. These simulations aimed to evaluate the effects of low initial reservoir pressure, although it is important to note that this initial pressure does not accurately represent actual reservoir conditions. The results indicate that CO_2 dissolution was slightly higher with lower initial reservoir pressure. However, the influence of lower initial reservoir pressure is not substantial when considering scenarios with lower reservoir and injection fluid salinities (Scenarios 1 to 6) and the resulting mass of CO_2 disolved was similar to that found with higher initial pressures (Table 11).

DocuSign Envelope ID: 2FA9A609-C360-4E53-8B28-BE8B77B6994A

Table 12: Result of 12 Long-Term Predictive Injection Simulation Scenarios with Low Initial Reservoir Pressure (1,500 psi)

Scenario	Injection Fluid Salinity (ppm)	Reservoir Fluid Salinity (ppm)	Molality (mole/kg)	CO_2 Dissolved, %	CO_2 Gas Phase, %
1	100,000	10,000	0.2	99.99%	0.01%
2	200,000	10,000	0.2	99.99%	0.01%
3	300,000	10,000	0.2	99.98%	0.01%
4	400,000	10,000	0.2	99.96%	0.03%
5	100,000	20,000	0.4	99.99%	0.01%
6	200,000	20,000	0.4	99.99%	0.01%
7	300,000	20,000	0.4	87.04%	12.95%
8	400,000	20,000	0.4	70.31%	29.68%
9	100,000	30,000	0.6	99.99%	0.01%
10	200,000	30,000	0.6	94.72%	5.29%
11	300,000	30,000	0.6	76.15%	23.83%
12	400,000	30,000	0.6	59.85%	40.14%

Figure 8 illustrates side-by-side comparison of the result of the 2,255 psi and 1,500 psi test results. As shown in the Figure 8, the impact of lower initial reservoir pressure is less pronounced for lower injection fluid salinity, particularly for a molality of 0.2, which may represent the best case for maximizing the volume of CO_2 remaining in solution during injection.

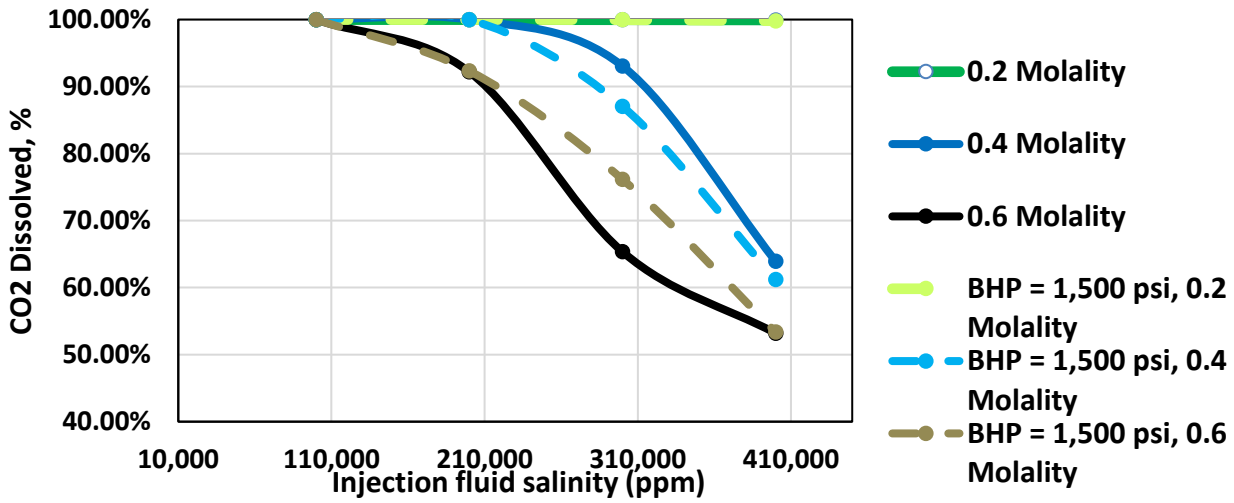


Figure 8: Result of the side-by-side comparison of the 2,255 psi, (solid line) and 1,500 psi, (dashed line).

DocuSign Envelope ID: 2FA9A609-C360-4E53-8B28-BE8B77B6994A

3.2 WELLBORE CORROSION MODEL

3.2.1 Scaling Tendency Prediction of Carbonated Produced Water

Changes in temperature and CO_2 content injected into produced water may initiate pH changes, hence may begin the formation of scales. Scaling tendency (ST) or scale index (SI) can be used to evaluate the scale formation of produced water mixed with CO_2. The ST is the ratio of the ion activity product (IAP) to the solubility product constant (K_{sp}) (Equation 1). The SI is given by Equation 2.

$$Scaling\ tendency = \frac{C}{C_0} = \frac{IAP}{K_{sp}} \qquad \text{(Equation 1)}$$

Where, C: measured concentration, C_0: concentration at equilibrium, IAP: ion activity product and K_{sp}: thermodynamic solubility product constant.

$$SI = log_{10}\left(\frac{IAP}{K_{sp}}\right) = log_{10}\,(scaling\ Tendency) \qquad \text{(Equation 2)}$$

Thus,

- Scaling tendency < 1 or SI < 0: indicates sub-saturation, and the solid is not expected to form.
- Scaling tendency = 1 or SI = 0: indicates saturation, and the solid is in equilibrium with water.
- Scaling tendency > 1 or SI > 0: indicates supersaturation, and the solid is expected to form.

Based on reservoir scenarios discussed earlier, three different concentrations of CO_2 (0, 0.2, and 0.6 mole/kg) were selected for scale tendency evaluation using the OLI software. Figure 5 shows predicted scaling tendency produced water with and without adding CO_2. In the case of produced water without CO_2, the increase in temperature or amount of injected CO_2 did not affect the scaling tendency of barite ($BaSO_4$), Or- dolomite ($CaMg(CO_3)_2$), hematite (Fe_2O_3), and eskolaite (Cr_2O_3). At these conditions, the scaling tendency is equal to 1, which means that the solids are in equilibrium state with produced water, in exception for anhydrite ($CaSO_4$) where the scaling tendency at 25 ^oC is below 1. In this case, no precipitation of $CaSO_4$ is expected. For water with 0.2 mole/kg CO_2, in addition to Cr_2O_3, Fe_2O_3, and $CaSO_4$, calcite ($CaCO_3$) and pyrrhotite (FeS) were in equilibrium state with carbonated produced water. For water with 0.6 mole/kg CO_2, the increase in temperature from 25 to 75 ^oC did not affect the scaling tendency for Fe_2O_3, $CaSO_4$, calcite ($CaCO_3$), and $CaSO_4$. However, at temperatures below 45 ^oC, Cr_2O_3 is not expected to precipitate (scaling tendency <1). Based on the results shown in Figure 9, the amount of CO_2 injected into produced water and temperature are the main factors affecting the chemical composition and the scaling tendency of the deposits.

DocuSign Envelope ID: 2FA9A609-C360-4E53-8B28-BE8B77B6994A

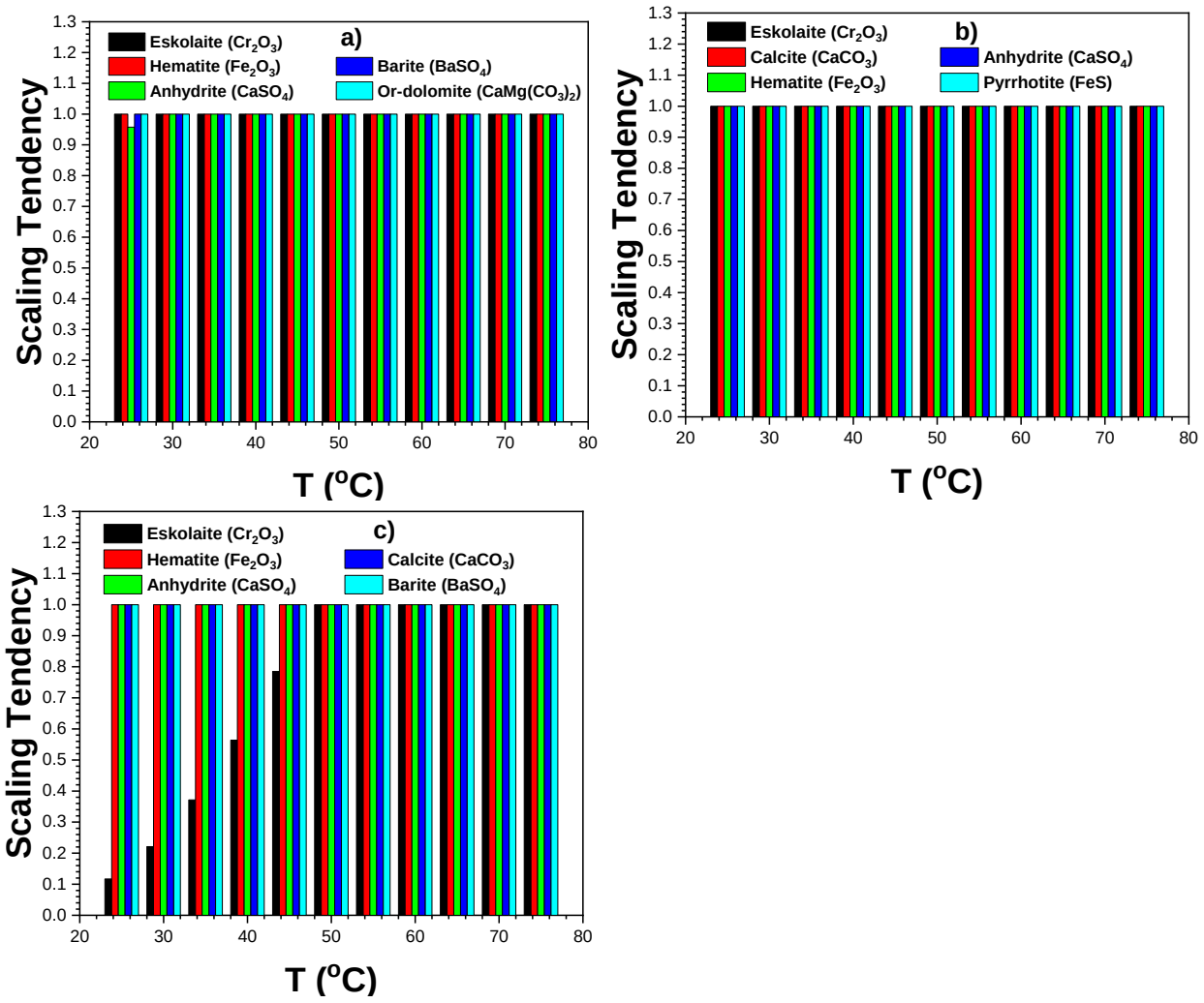


Figure 9: OLI simulation to predict scaling tendency of produced water with and without adding CO_2. Steam amount = 1L. (a). 0 mole/kg CO_2; (b). 0.2 mole/kg CO_2; (c). 0.6 mole/kg CO_2.

3.2.2 Corrosion Prediction of Steels in Carbonated Produced Water

The corrosion behavior of stainless-steel alloys was investigated in simulated CBI reservoir conditions. Corrosion rates and pH were predicted using OLI software. For comparison purposes, carbon steel (UNS G10180) was investigated under the same conditions as stainless-steel alloys. The effect of scaling was not considered during corrosion modeling. Figure 10 shows predicted corrosion rates and pH values calculated as a function of temperature and CO_2 content for the different tested stainless-steels. A higher corrosion rates for 13 Cr stainless-steel was predicted compared to super 13 Cr stainless-steel exposed to produced water with or without CO_2. In general, no significant differences are found between the corrosion rate values of stainless-steel exposed to produced water with or without CO_2. However, for both stainless-steel, corrosion rates increase with temperature, and corrosion rates are below 0.02 mm/y under tested conditions. The results show that stainless-steel alloys (13 Cr and super 13 Cr) have good

DocuSign Envelope ID: 2FA9A609-C360-4E53-8B28-BE8B77B6994A

resistant to CO_2 corrosion due to the higher amount of Cr which can be beneficial for formation of protective scales or passive layer.

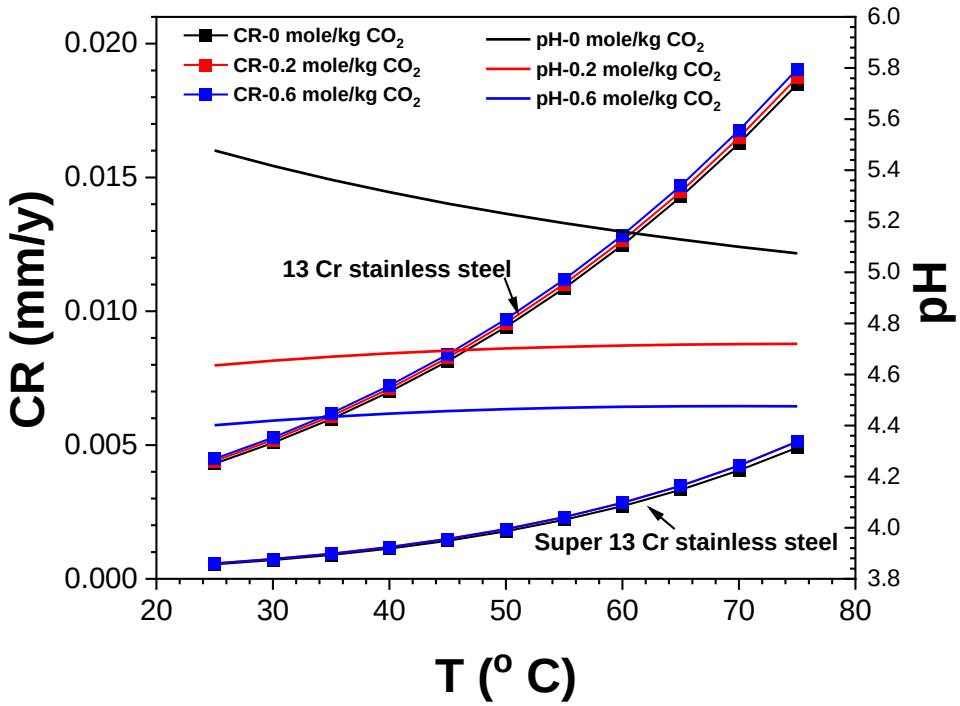


Figure 10: OLI simulation to predicted pH and corrosion rates of stainless-steel exposed to injected produced water with and without CO_2.

Figure 11 shows the corrosion rate of carbon steel as a function of temperature after exposure with produced water with and without CO_2. As shown in the results, the increase of CO_2 amount into produced water or increase in temperature led to a higher corrosion rate. A lower predicted corrosion rate was observed at lower temperatures and at 0 mole/kg CO_2. When dissolved CO_2 is present, the corrosion significantly increases with temperature, suggesting that dissolved CO_2 contributes to accelerating corrosion reaction.

DocuSign Envelope ID: 2FA9A609-C360-4E53-8B28-BE8B77B6994A

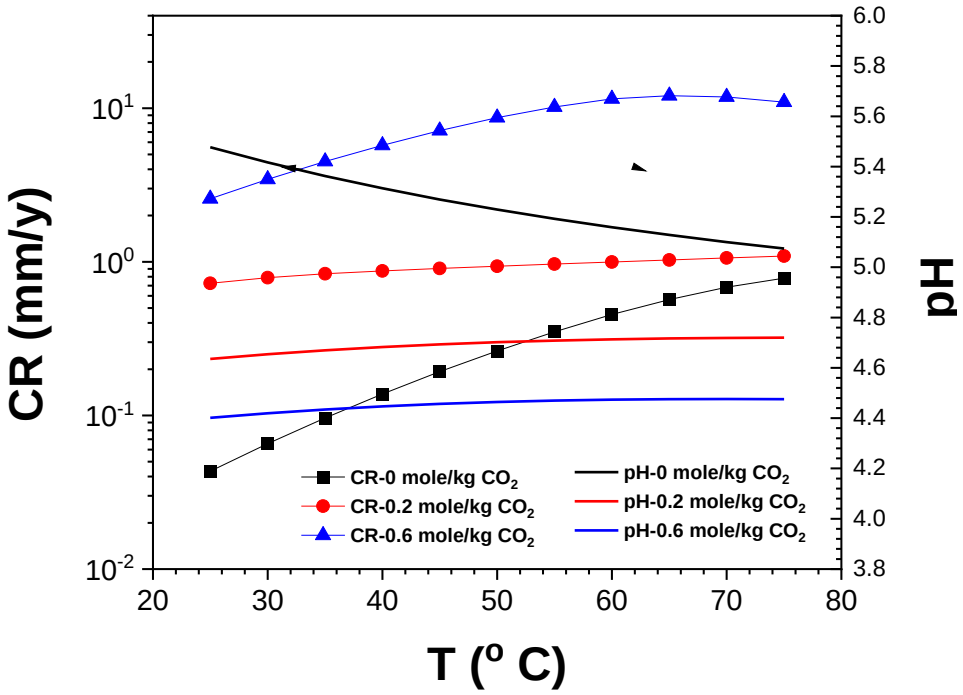


Figure 11: OLI simulation to predicted pH and corrosion rates of carbon steel UNS G10180 exposed to injected produced water with and without CO_2.

3.3 REACTIVE TRANSPORT MODELING

3.3.1 Injection Period (Year 0–20)

In the following figures, the results of the reactive transport modeling are shown as the top view to the reservoir, with the injection well in the center. During the CBI period, the pH change is shown in Figure 12 as a function of time. The initial reservoir pH is 6.1. The injected carbonated water decreases the pH. The central region pH is buffered with mineral dissolution. The dissolved solids (Figure 13) of the entire reservoir after 20 years of injection increases almost 10 times due to the high TDS of the produced water. Fluid density (Figure 14) increases accordingly.

DocuSign Envelope ID: 2FA9A609-C360-4E53-8B28-BE8B77B6994A

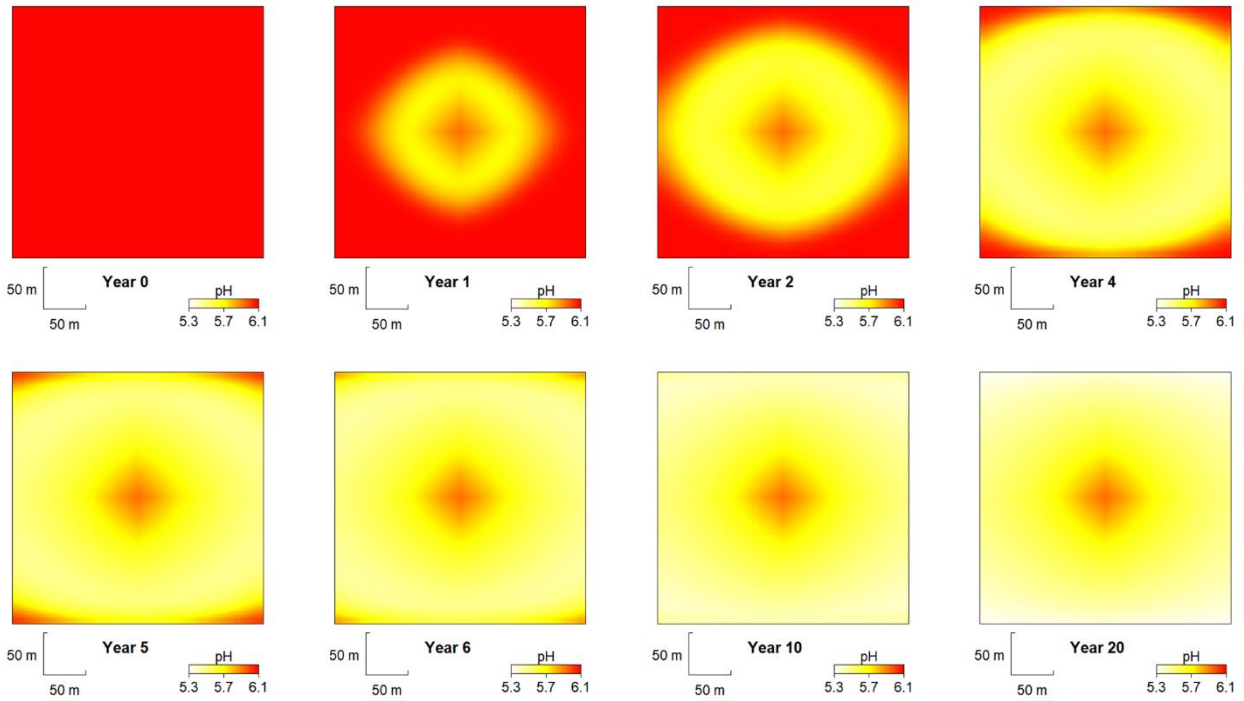


Figure 12: pH changes in the reservoir during injection period.

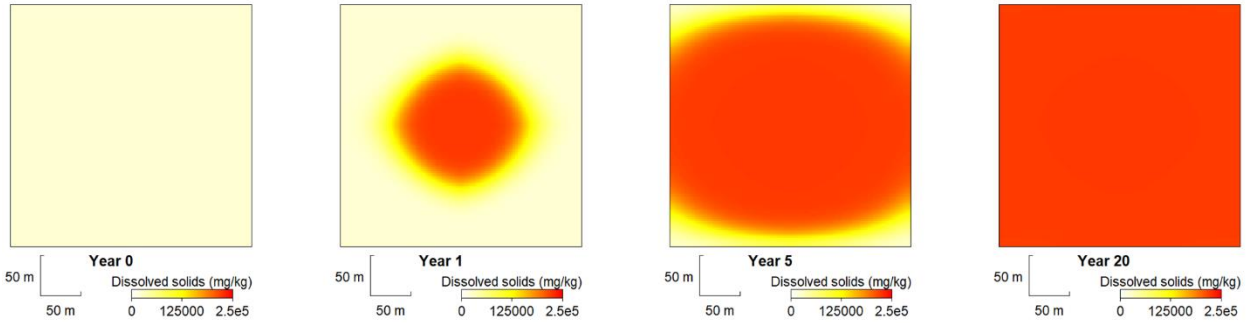


Figure 13: Dissolved solids changes in the reservoir during injection period.

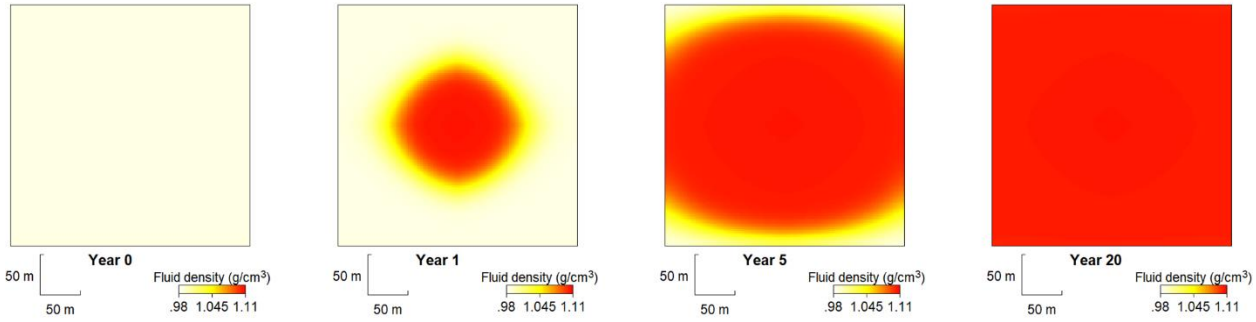


Figure 14. Fluid density changes in the reservoir during injection period.

DocuSign Envelope ID: 2FA9A609-C360-4E53-8B28-BE8B77B6994A

This central region is where most rock-fluid interactions occur. Mineral volume (Figure 15) and porosity (Figure 16) are a result of mineral dissolution and precipitation. Overall, precipitation in the central region outweighs dissolution, resulting in an increased mineral volume, i.e., decreased porosity in this region. As the injected fluid spreads to further regions, the fluids became more geochemically equilibrated. Less mineral precipitation and dissolution are observed outside the central region.

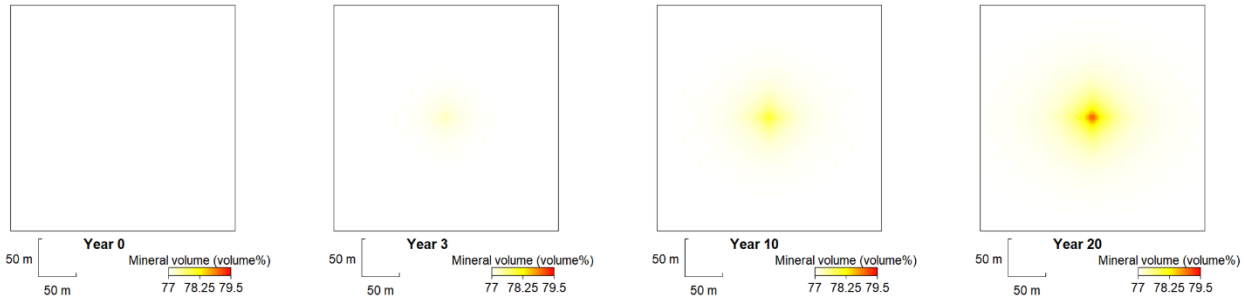


Figure 15: Mineral volume changes in the reservoir during injection period.

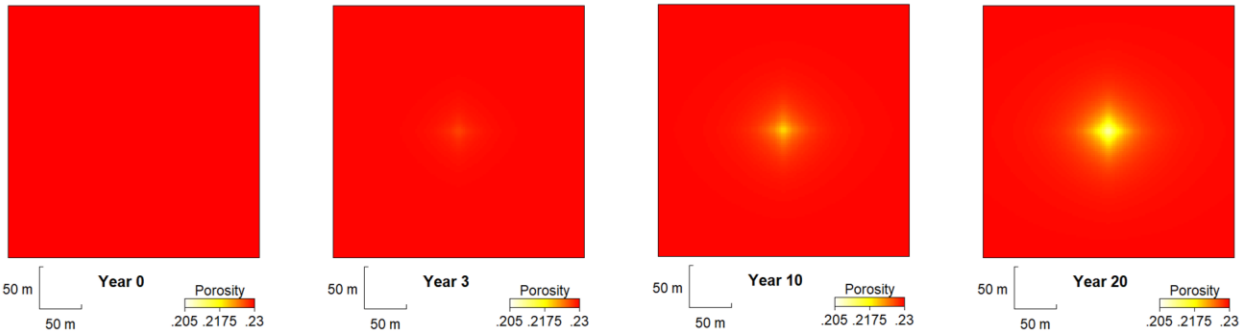


Figure 16: Porosity changes in the reservoir during injection period.

The total dissolved carbon amount increases and spreads to the entire reservoir (Figure 17). Among the dissolved carbon species, CO_2(aq) is the major component. In the central region where rock-fluid interactions are most intense, carbonate and bicarbonate species are present as a result of carbonate mineral dissolution and precipitation. The speciation of dissolved carbon is consistent with the pH changes and distribution (Figure 12).

DocuSign Envelope ID: 2FA9A609-C360-4E53-8B28-BE8B77B6994A

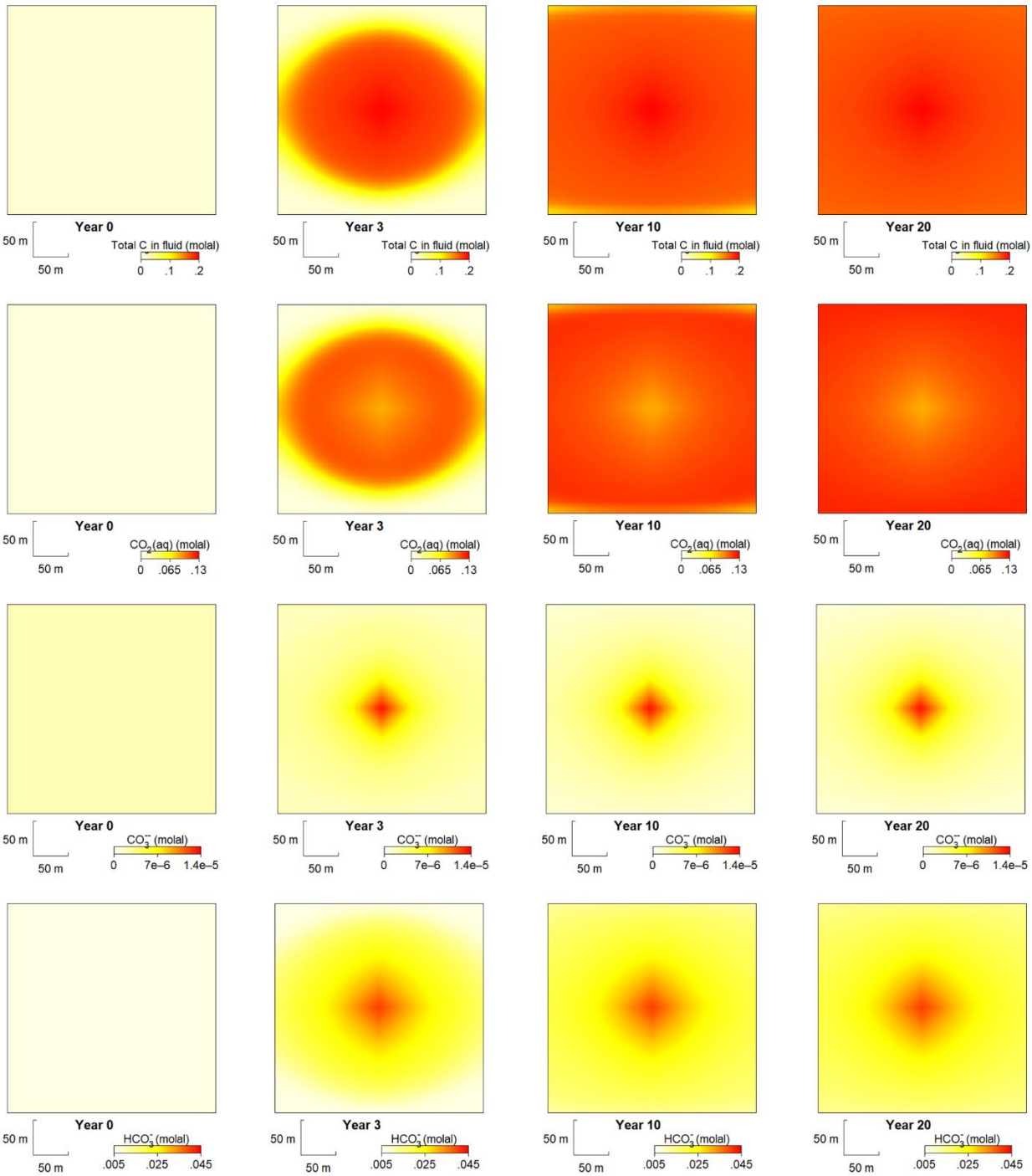


Figure 17: Dissolved carbon species changes in the reservoir during injection period.

For the primary minerals in the reservoir, quartz and muscovite undergo a dissolution-precipitation-redissolution process at the border of the injected fluid as the fluid goes outward from the injection point. This is reflected by the changes of the mineral saturation indices (Figure 18), as the mineral volume changes are not obvious with the large initial percentage. Siderite

DocuSign Envelope ID: 2FA9A609-C360-4E53-8B28-BE8B77B6994A

continues to precipitate in the central region and slowly increases and spreads outwards due to the continuous supply of Fe^{2+} and CO_3^{2-} from the injected carbonated brine.

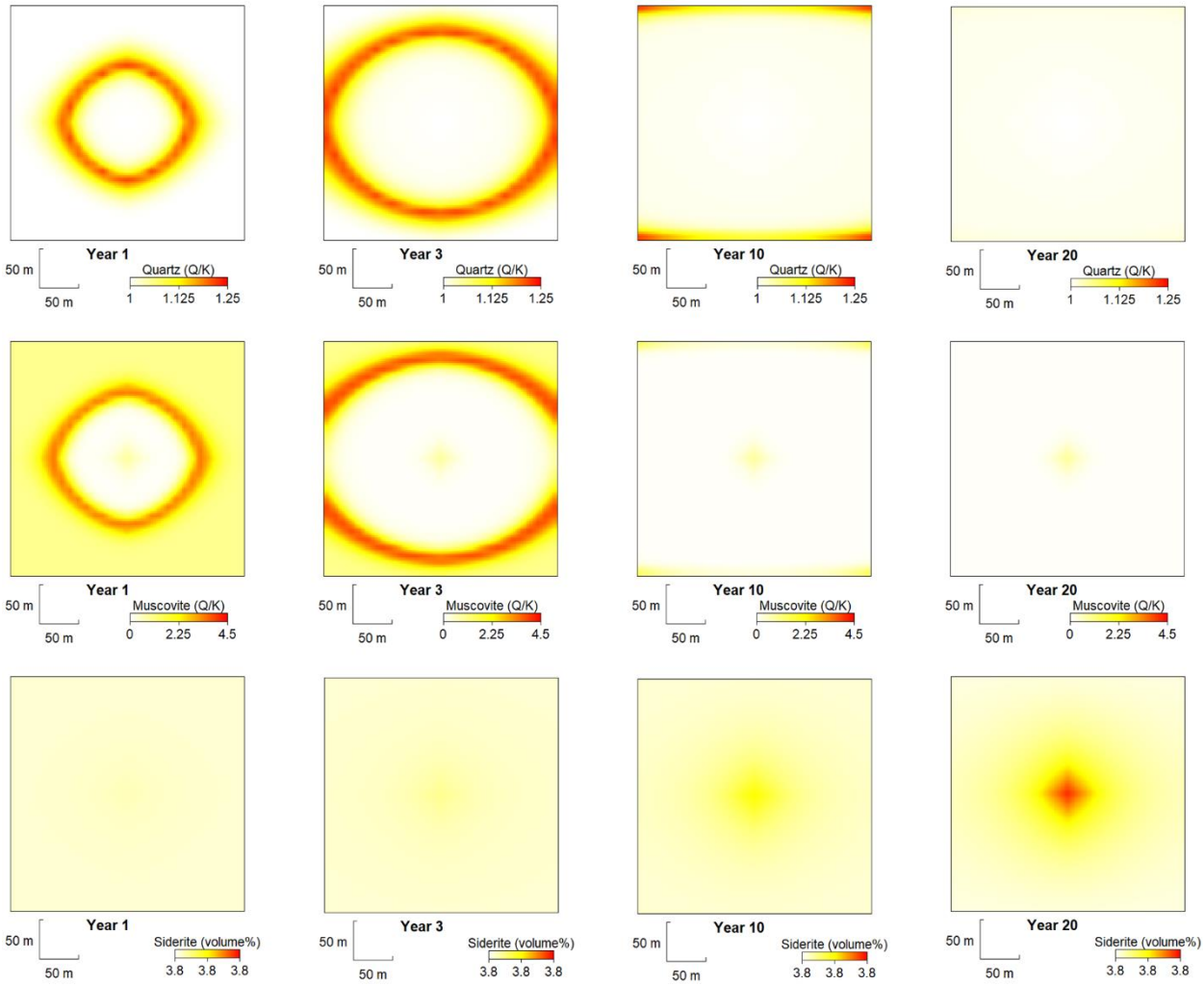


Figure 18: Primary minerals saturation and volume during injection period.

Most secondary precipitations are located in the central region where rock-fluid interactions occur. Figure 19 shows the secondary mineral volume percentage at the end of the 20-year injection period. Secondary precipitates are mostly composed of carbonate minerals (Ca, Mg, Ba carbonates) and some barite.

DocuSign Envelope ID: 2FA9A609-C360-4E53-8B28-BE8B77B6994A

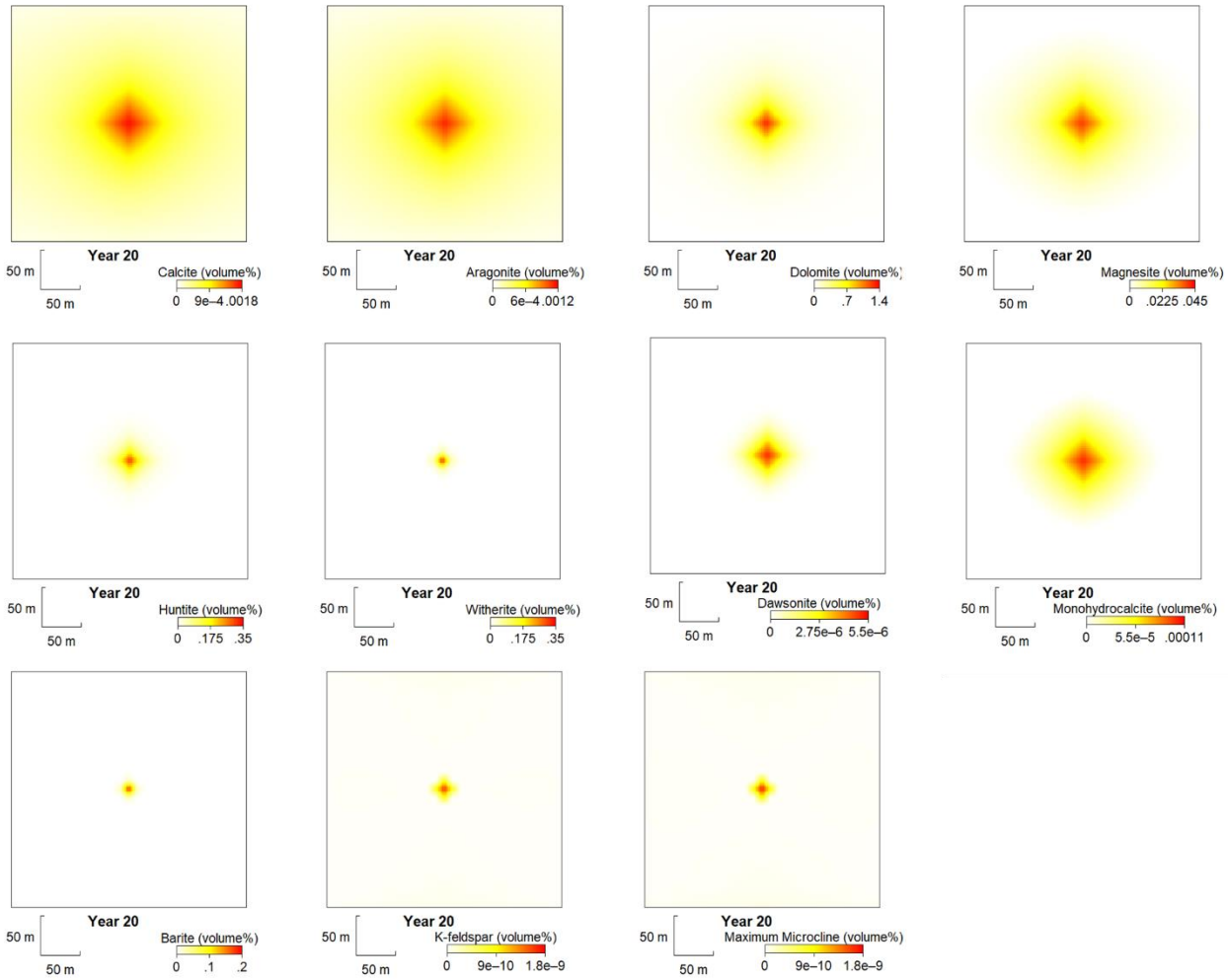


Figure 19: Secondary precipitations at the end of the 20-year injection period.

3.3.2 Shut-in Period (Year 20–120)

The pH continues decreasing slowly over 100 years of the shut-in period (Figure 20). There are no obvious changes for dissolved solids and porosity.

DocuSign Envelope ID: 2FA9A609-C360-4E53-8B28-BE8B77B6994A

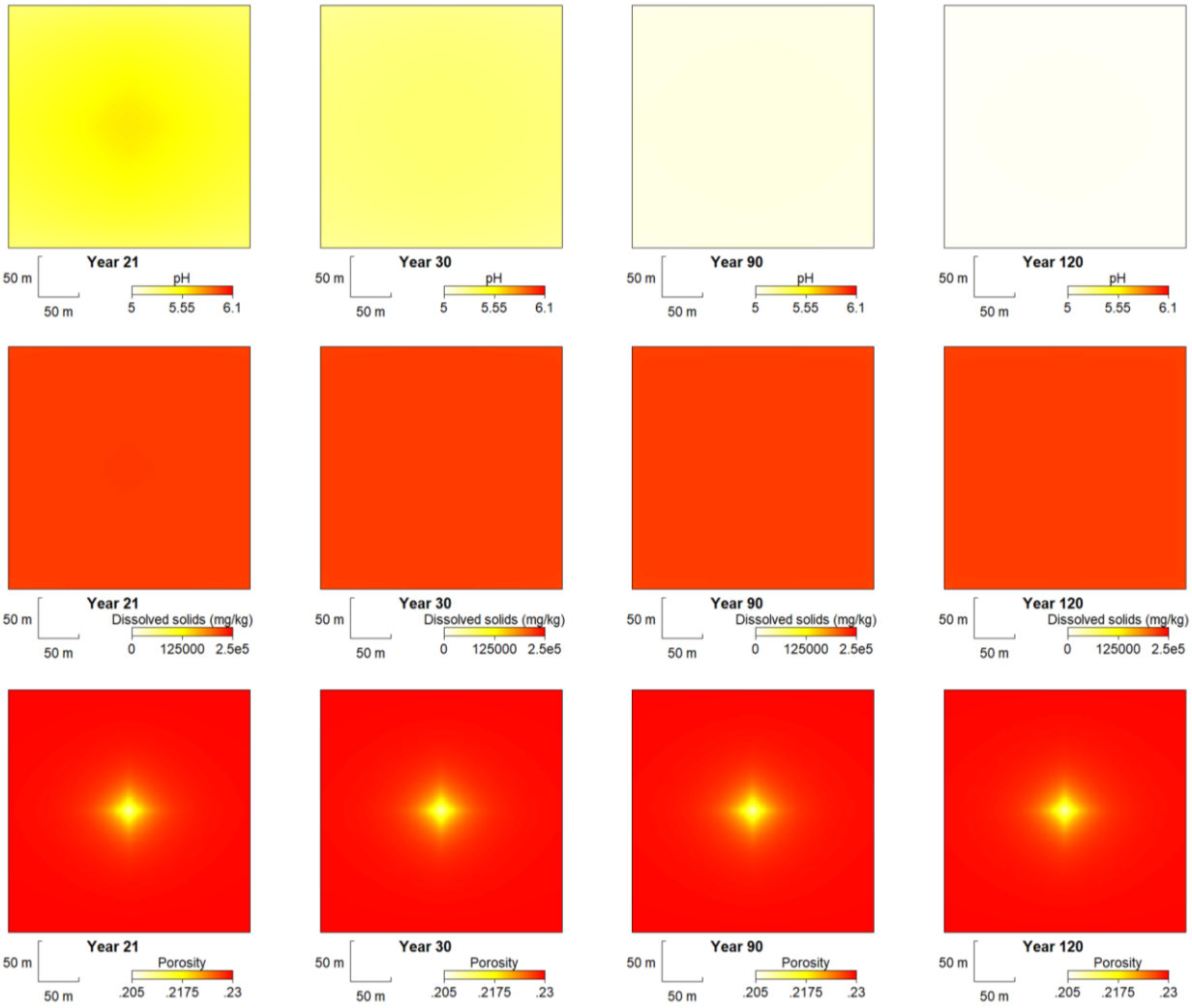


Figure 20: pH, dissolved solids, and porosity during the shut-in period.

The pH change is consistent with dissolved carbon speciation (Figure 21). As pH decreases from 5.5 to 5, CO_2(aq) concentration increases, and HCO_3^- concentration decreases. CO_3^{2-} is minimal in acidic solution, and keeps decreasing with decreased pH. The total dissolved carbon in the solution keeps decreasing slowly, indicating some carbon is sequestered through carbonate mineral precipitation over long-term storage.

DocuSign Envelope ID: 2FA9A609-C360-4E53-8B28-BE8B77B6994A

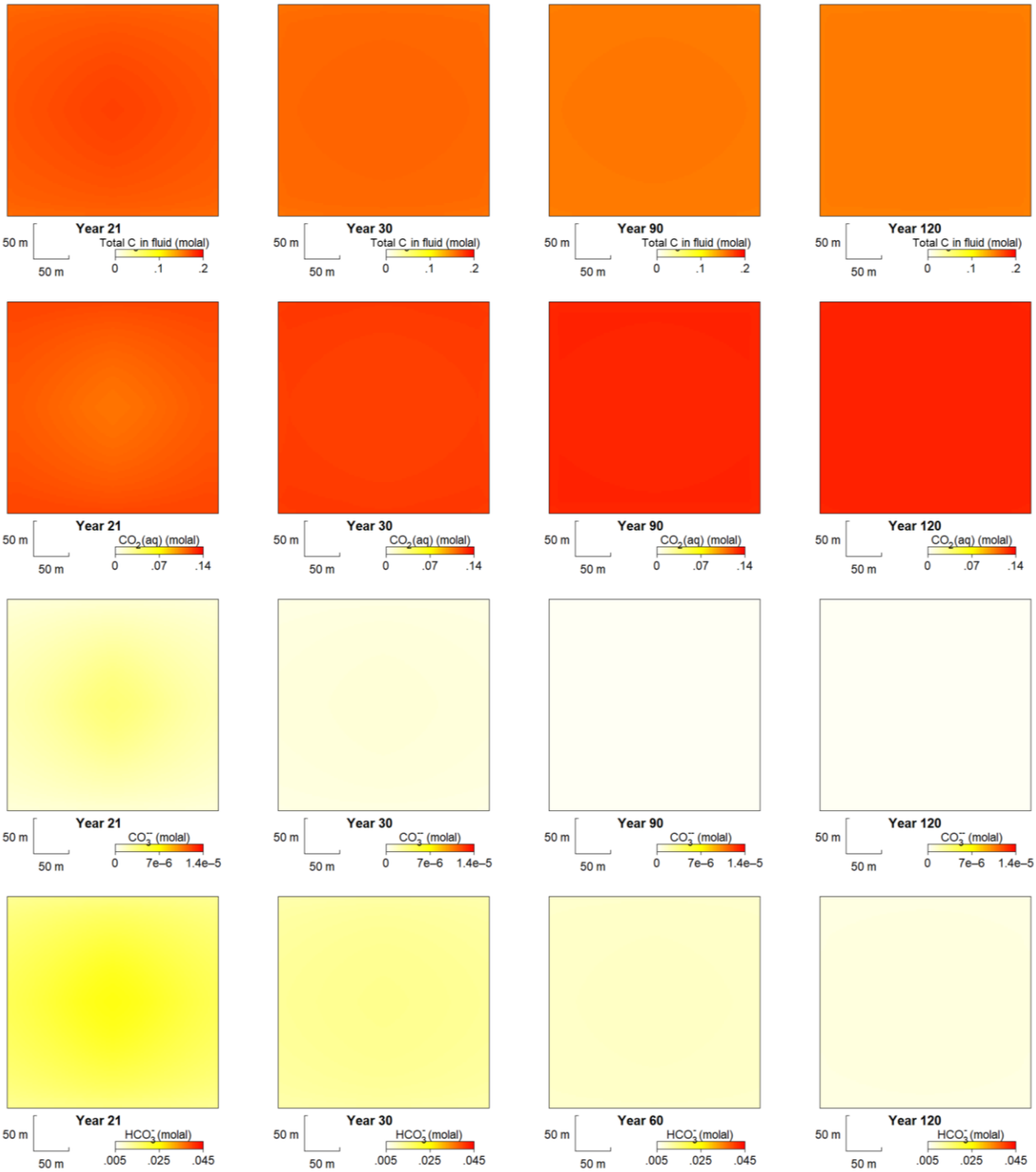


Figure 21: Dissolved carbon species during shut-in period.

For primary minerals in the sandstone, the increased siderite from the injection period keeps precipitating for a short time after injection stops (Figure 22). Then re-dissolves with decreasing pH. This is also reflected by the supersaturation status of siderite at Year 21, followed by undersaturation over the rest of the years. The change in all primary minerals is negligible comparing to their initial volume percentage.

DocuSign Envelope ID: 2FA9A609-C360-4E53-8B28-BE8B77B6994A

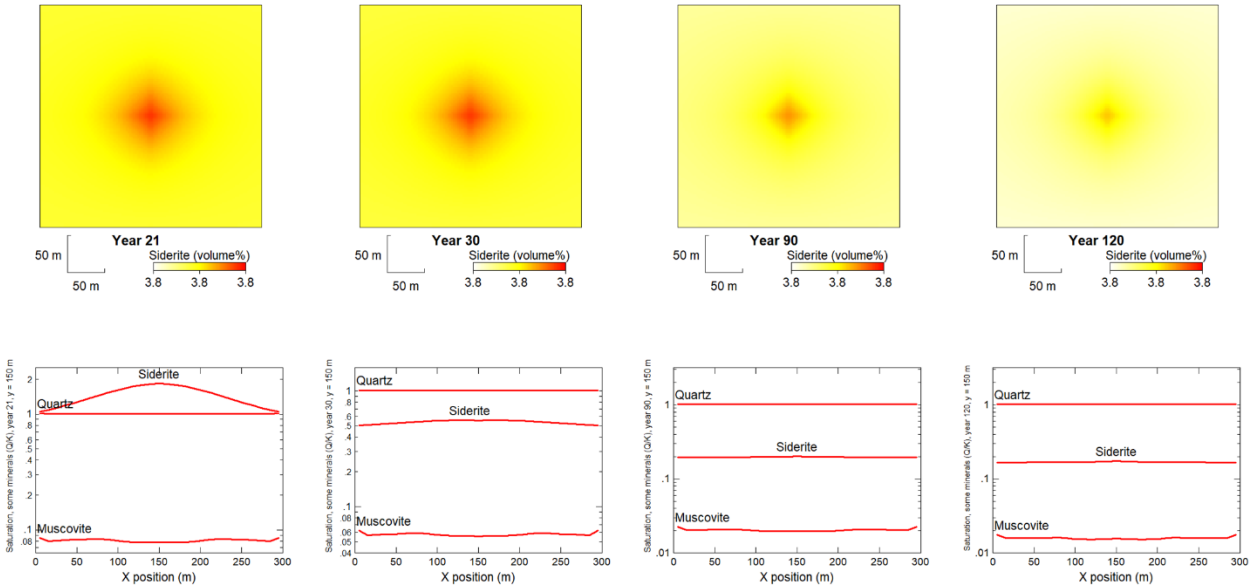


Figure 22: Primary mineral volume percentage and saturation changes during the shut-in period.

Many carbonate minerals are supersaturated when injection just stops. Over decades, only a few carbonate minerals (dolomite, calcite, and aragonite) are still supersaturated and tend to form continuously (Figure 23).

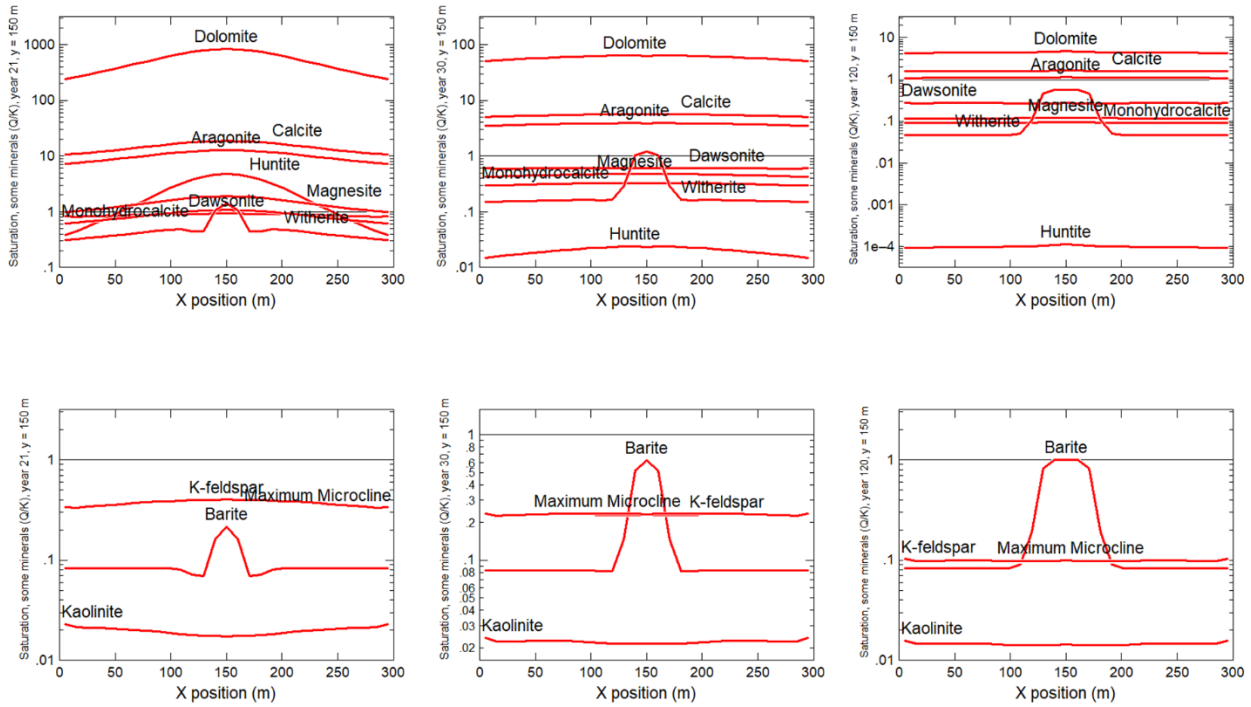


Figure 23: Secondary mineral precipitates saturation during the shut-in period.

DocuSign Envelope ID: 2FA9A609-C360-4E53-8B28-BE8B77B6994A

Although some Ca- and Mg-containing carbonate minerals are supersaturated during the long-term storage, the overall mineral precipitation volume is small across the entire reservoir. Figure 24 shows an example of dolomite volume percentage change from Year 21 to Year 120.

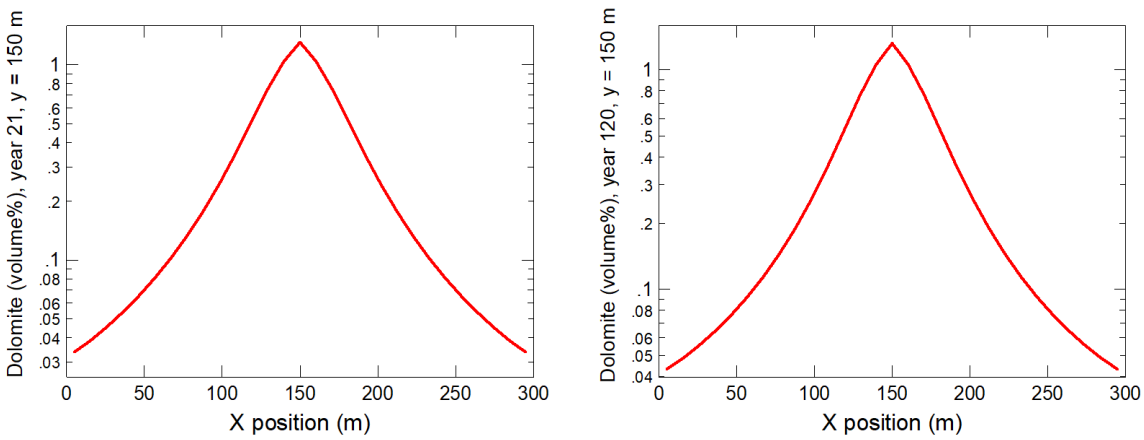


Figure 24: Dolomite volume percentage changes after 100 years of the shut-in period.

DocuSign Envelope ID: 2FA9A609-C360-4E53-8B28-BE8B77B6994A

4. DISCUSSIONS

4.1 CO_2 CONCENTRATION FOR CBI

While the concept of CBI for CO_2 storage is still relatively new, carbonated waterflooding has been used for EOR and represents a critical proxy that produced water operators can borrow from to reduce the learning curve. As there are tens of thousands of disposal wells currently in operation across the U.S., there exists tremendous opportunity to take advantage of pre-existing infrastructure to accelerate deployment of CBI in the future. Pre-dissolving CO_2 into brine has the added benefit of accelerated CO_2 mineralization. As stated above, CarbFix demonstrated rapid mineralization by injecting carbonated water into porous basalts. Future efforts should highlight the mineralization potential of other reservoirs based on mineralogy, pressure, and temperature. Future projects should focus on field demonstration of CBI along with a breakdown of cost considerations.

An important parameter for CBI is CO_2 solubility, the amount of CO_2 that can be fully dissolved into the brine. CO_2 solubility in brine is found to be a function of three parameters: temperature, pressure, and salinity (Burton and Bryant, 2007). In general, CO_2 solubility in brine decreases with increasing temperature, increases with increasing pressure, and decreases with increasing salinity (Burton and Bryant, 2007; Frailey and Finley, 2009). Monovalent salts such as NaCl and KCl are found to inhibit dissolution more than divalent salts such as $CaCl_2$ or $MgCl_2$ (Burton and Bryant, 2007). Different brines have different compositions depending on location, but the dissolved salts in produced water typically consist primarily of sodium chloride (NaCl). Produced water salinity varies among basins, with the Williston Basin having some of the highest TDS concentrations, averaging 300,000 mg/L up to 350,000 mg/L (Glazewski et al., 2020). Previous studies have shown the solubility of CO_2 to be a function of temperature and depth, with depths beyond 2,000 feet showing the solubility of CO_2 in brine to remain nearly constant (Burton and Bryant, 2007). Rising temperature can also reduce fluid viscosity significantly, which can impact the injection capacity of a well (Bisweswar et al., 2020). Surface pump injection pressure and temperature also need to be taken into consideration, with the mixing temperature expected to be bounded by initial reservoir temperature and ambient temperature. The trend in surface dissolution of CO_2 into brine is that less brine is required when the mixing tank operates at higher pressures and lower temperatures (Burton and Bryant, 2009). Future efforts and field demonstration of CBI should include consideration of surface facilities and equipment.

4.2 COMPATIBILITY OF EXISTING INFRASTRUCTURE

The formation of carbonic acid (H_2CO_3) during CBI could lead to corrosion of the wellbore casing, tubing, packer, and surface equipment. When dissolved CO_2 is present, the corrosion is significantly increases with temperature, suggestion that dissolved CO_2 contribute to accelerating corrosion reaction. The rate of corrosion is highly dependent on the amount of CO_2 and temperature (Kahyarian and Nesic, 2020; Nesic, 2007). It was proven in literature that the increase in temperature accelerates electrochemical, chemical reactions, and mass transfer, diffusion of corrosive species to the surface, etc., involved in corrosion process (Kahyarian and Nesic, 2020; Nesic, 2007). Temperature has a strong influence on pH, which has a strong influence on the corrosion rate. The commonly accepted explanation is that with dissolved CO_2, the concentration of H_2CO_3 increases and accelerates the cathodic reaction. CO_2 corrosion might

DocuSign Envelope ID: 2FA9A609-C360-4E53-8B28-BE8B77B6994A

be encountered in carbon steel or stainless-steel due to electrochemical reaction occurring on the steel surface. Dissolved CO_2 reacts with water to form carbonic species according to the following equations (Kahyarian and Nesic, 2020; Nesic, 2007):

$$CO_2 + H_2O \Leftrightarrow H_2CO_3 \qquad \text{(Equation 1)}$$

$$H_2CO_3 \Leftrightarrow HCO_3^- + H^+ \qquad \text{(Equation 2)}$$

$$HCO_3^- \Leftrightarrow CO_3^{2-} + H^+ \qquad \text{(Equation 3)}$$

When the steel surface is in contact with aqueous CO_2, electrochemical processes involving the anodic dissolution of iron (equation 4) and the cathodic evolution of hydrogen (equation 5) are taking place (Kahyarian and Nesic, 2020; Nesic, 2007).

$$Fe \Leftrightarrow Fe^{2+} + 2\,e^- \qquad \text{(Equation 4)}$$

$$2\,H^+ + 2\,e^- \Leftrightarrow H_2 \qquad \text{(Equation 5)}$$

Based on predicted corrosion results, carbon steel is more susceptible to CO_2 corrosion than 13 Cr stainless-steel and super 13 Cr-stainless-steel. Despite predicted corrosion rates, carbon steel can be preferred material because of its low cost. However, additional corrosion control measures, such as corrosion inhibitor injection, are required to control corrosion in wellbore materials. In addition, significant levels of dissolved oxygen can be expected in the BCI water, and while the downhole environment may be anoxic. Care should be taken to prevent the formation of differential aeration cells at the casing steel.

4.3 LONG-TERM STORAGE SAFETY

The success of geologic CO_2 storage depends on a combination of physical and geochemical trapping mechanisms (Figure 25) (Metz et al., 2005). Using CBI directly moves the trapping stage to solubility trapping. Dissolved CO_2 is no longer a separate phase, thereby eliminating the buoyant forces that drive it upwards.

DocuSign Envelope ID: 2FA9A609-C360-4E53-8B28-BE8B77B6994A

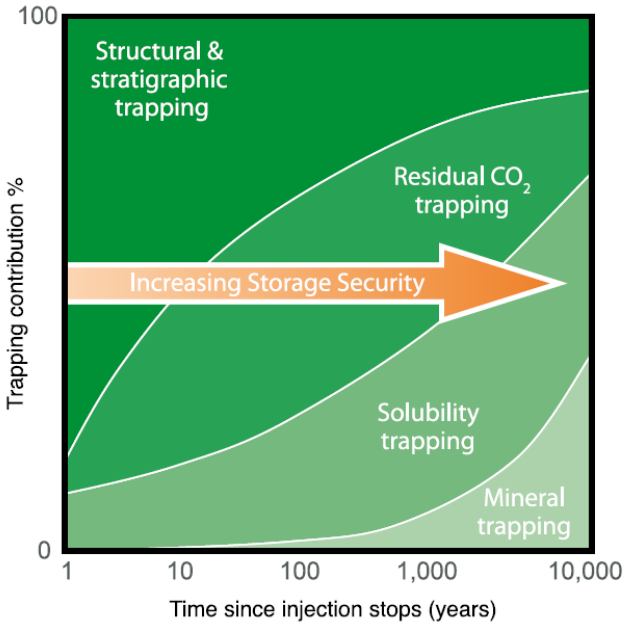


Figure 25: Storage security depends on a combination of physical and geochemical trapping. Over time, the physical process of residual CO_2 trapping and geochemical processes of solubility trapping and mineral trapping increase (Metz et al., 2005).

Using the method of CBI, CO_2 can be safely stored in sandstone reservoirs via solubility trapping. Though small amount of CO_2 converts to carbonate minerals, CO_2 remained in liquid phase in long-term storage. During the injection period, most rock-fluid geochemical interactions are limited in a certain region where the carbonated water is injected. The pH, dissolved carbon speciation, and amount are a result of mineral precipitation and dissolution. The porosity decrease due to mineral precipitation is small. Mineral precipitation due to rock-fluid interactions in the reservoir is unlikely to block flow pathways for injection. Geochemical changes during the long-term shut-in period are not obvious.

4.4 NANOBUBBLE TECHNOLOGY FOR CO_2 INJECTION

The nanobubble technology of dissolving CO_2 in the produced water is a promising application in CO_2 geological storage sites. This technology has been relatively mature. The features of micro and nanobubbles include excellent stability, high internal pressure, extremely large surface-to-volume ratio, and high gas dissolution rate (Figure 26) (Li et al., 2023).

DocuSign Envelope ID: 2FA9A609-C360-4E53-8B28-BE8B77B6994A

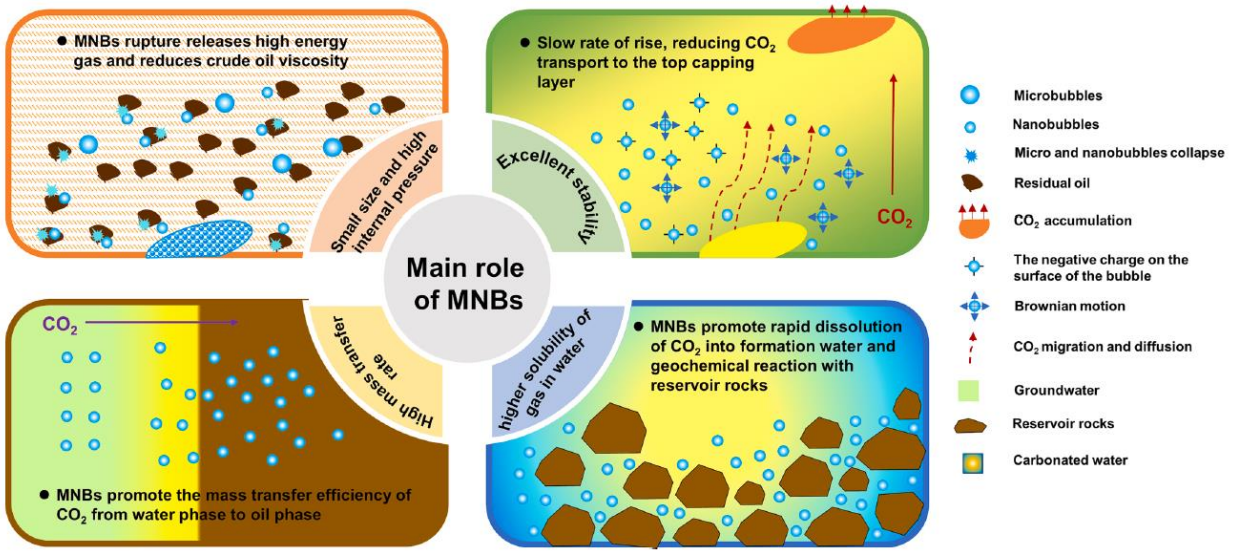


Figure 26: Main mechanism of EOR and geological sequestration by CO_2 injection in the form of micro and nanobubbles (Li et al., 2023).

Dissolving CO_2 nanobubbles in the produced water before or during injection could make it possible to allow all free-phase CO_2 to dissolve before reaching the reservoir (Figure 27) (Uemura et al., 2016). This technology makes CBI a low-risk CO_2 storage method compared to the traditional injection of supercritical CO_2 into the reservoir, where CO_2 needs a long time period to dissolve in groundwater.

DocuSign Envelope ID: 2FA9A609-C360-4E53-8B28-BE8B77B6994A

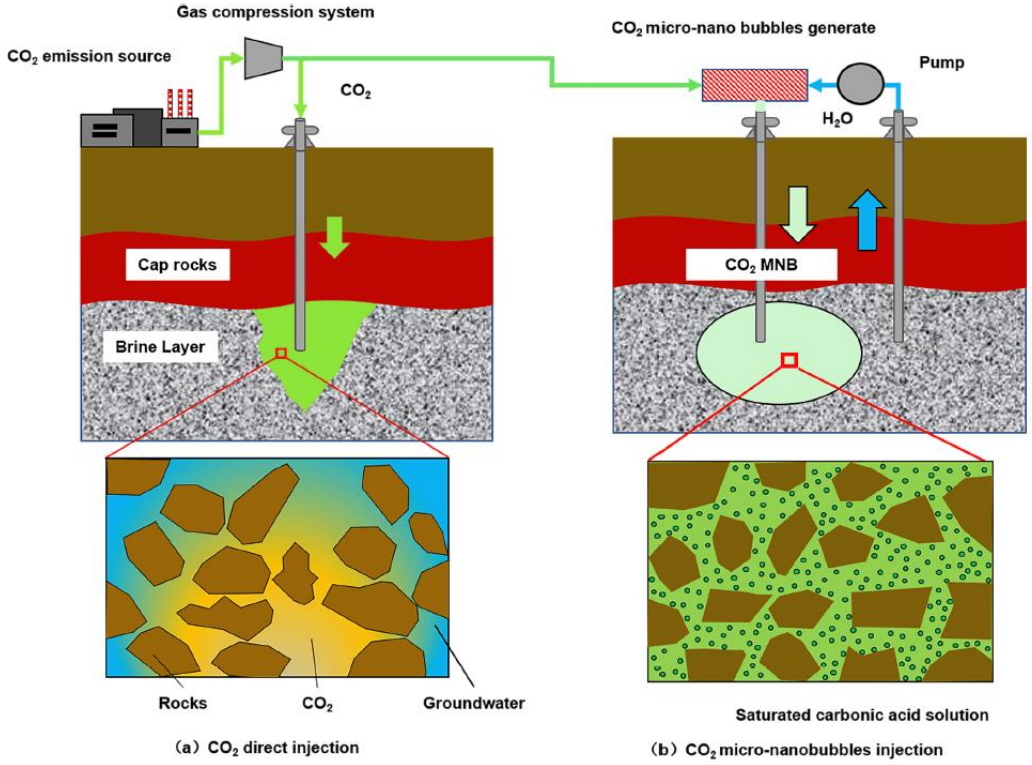


Figure 27: Schematic diagrams comparing CO_2 geological storage techniques (Uemura et al., 2016).

DocuSign Envelope ID: 2FA9A609-C360-4E53-8B28-BE8B77B6994A

5. CONCLUSIONS

Carbonated brine storage is a low-risk geologic CO_2 sequestration strategy. Simulations of CBI at small CO_2 molality (0.2 mol/kg) were found to show no perceivable increases in reservoir pressure or impacts to brine viscosity or density due to the dissolved CO_2. When compared specifically to standard produced water disposal operations, pressure-driven risks such as leakage, induced seismicity, cap rock failure, and migration do not increase because of the inclusion of dissolved CO_2 in the brine injection stream. Since there are no anticipated increased risks, a delineated area of review for a Class II injection well is not anticipated to change with the integration of dissolved CO_2. Wellbore corrosion rates can be anticipated to be at an acceptable range to maintain CBI operations for years. Furthermore, since the pressure equilibrium is identical to the noncarbonated brine standard operations, the length of the post-injection site closure (PISC) period would not be impacted. Oftentimes, the carbonated brine will be denser than the reservoir brine, such that the CO_2-laden brine sinks to the bottom of the reservoir instead of migrating upward because of buoyancy. CO_2 is safely stored via dissolution sequestration in long term storage.

Dissolving CO_2 into produced water disposal streams creates a cash incentive through IRS Section 45Q tax credits. For permanent storage, the tax credit is currently \$85/ton of CO_2 sequestered (Bright, 2022). Given the current reservoir conditions of the Inyan Kara Formation with a reservoir pressure of 2,255 psi, formation temperature of 165 °F, and produced water salinity of 300,000 mg/L, at 2% CO_2 mass fraction, 1 ton of CO_2 could be dissolved into approximately every 200 bbl of Bakken produced water. This equates to approximately \$0.425/bbl of brine, a notable increase in cashflow for a produced water disposal operator. Since CO_2 solubility in brine is found to be a function of temperature, pressure, and salinity, a lower produced water salinity would result in a greater amount of CO_2 that could be dissolved and injected.

While a field demonstration to evaluate the economic impacts is necessary, it is anticipated that the incremental benefit of adding CO_2 to produced water disposal streams may outweigh the incremental costs of transport and pressure mixing under favorable conditions. Compared to new CCUS projects with bulk CO_2 injection, CBI enjoys the benefits of a pre-existing well and infrastructure that has already gone through the necessary permitting process. In the cases where injection rates do not warrant dedicated pipeline investment, trucking CO_2 to the well pad further reduces potential up-front costs. These considerations significantly reduce project capital expenditures and risk, particularly where several years of operating data exist to verify geologic models.

Regulatory considerations for CBI include the regulations surrounding aboveground storage of the produced water on location and creating a path to approval under Class II injection wells. A pilot field demonstration would aid in answering some of the questions regulators might have surrounding CBI such as whether the wellbore tubing and casing would need to be retrofitted in any form.

DocuSign Envelope ID: 2FA9A609-C360-4E53-8B28-BE8B77B6994A

6. REFERENCES

Bader, J. W. Sequence Stratigraphy of the Inyan Kara Formation, Northwestern North Dakota: Extracting the Maximum from Minimal Core and Outcrop Data. AAPG Annual Convention and Exhibition, 2017.

Bisweswar, G.; Al-Hamairi, A.; Jin, S. Carbonated water injection: an efficient EOR approach. A review of fundamentals and prospects. *Journal of Petroleum Exploration and Production Technology* **2020,** *10*, 673–685.

Bright, M. The Inflation Reduction Act creates a whole new market for carbon capture. Clean Air Task Force: Boston, MA, 2022. https://www.catf.us/2022/08/the-inflationreduction-act-creates-a-whole-new-market-for-carbon-capture.

Burton, M.; Bryant, S. L. Eliminating buoyant migration of sequestered CO_2 through surface dissolution: implementation costs and technical challenges. *SPE Reservoir Evaluation & Engineering* **2007,** *12*, 399–407.

Burton, M.; Bryant, S. L. Surface dissolution: minimizing groundwater impact and leakage risk simultaneously. *Energy Procedia* **2009,** *1*, 3707–3714.

Busenberg, E.; Plummer, L. N. The kinetics of dissolution of dolomite in CO 2-H 2 O systems at 1.5 to 65 degrees C and O to 1 atm PCO 2. *American Journal of Science* **1982,** *282*, 45–78.

Chu, M. H. Study of the geothermal production potential in the Williston Basin, North Dakota; 1991.

Eke, P. E.; Naylor, M.; Haszeldine, S.; Curtis, A. CO_2/brine surface dissolution and injection: CO_2 storage enhancement. *SPE Projects, Facilities & Construction* **2011,** *6*, 41–53.

Fathollahi, A.; Rostami, B. Carbonated water injection: Effects of silica nanoparticles and operating pressure. *The Canadian Journal of Chemical Engineering* **2015,** *93*, 1949–1956.

Frailey, S. M.; Finley, R. J. Classification of CO_2 geologic storage: Resource and capacity. *Energy Procedia* **2009,** *1*, 2623–2630.

Georgescu, S.; Lindeberg, E.; Holt, T. Co-injection of CO_2 and water in non-sealed saline aquifers. International Conference on Greenhouse Gas Control Technologies, Trondheim, Norway, 2006.

Glazewski, K. A.; Taunton, M. A.; Wilson, W. I.; Kurz, B. A.; Kovacevich, J.; Azzolina, N. A.; Hamling, J. A.; Sorensen, J. A.; Steadman, E. N.; Harju, J. A.; Gorecki, C. D. Produced water management and recycling options in North Dakota, 2020.

Helgeson, H. C.; Murphy, W. M.; Aagaard, P. Thermodynamic and kinetic constraints on reaction rates among minerals and aqueous solutions. II. Rate constants, effective surface area, and the hydrolysis of feldspar. *Geochimica et Cosmochimica Acta* **1984,** *48*, 2405–2432.

Kahyarian, A.; Nesic, S. On the mechanism of carbon dioxide corrosion of mild steel: Experimental investigation and mathematical modeling at elevated pressures and non-ideal solutions. *Corrosion Science* **2020,** *173*, 108719.

DocuSign Envelope ID: 2FA9A609-C360-4E53-8B28-BE8B77B6994A

Khan, C.; Pearce, J. K.; Golding, S. D.; Rudolph, V.; Underschultz, J. R. Carbon Storage Potential of North American Oil & Gas Produced Water Injection with Surface Dissolution. *Geosciences* **2021,** *11*, 123.

Kühn, M.; Kempka, T.; De Lucia, M.; Scheck-Wenderoth, M. Dissolved CO_2 storage in geological formations with low pressure, low risk and large capacities. *Energy Procedia* **2017,** *114*, 4722–4727.

Li, X.; Peng, B.; Liu, Q.; Liu, J.; Shang, L. Micro and nanobubbles technologies as a new horizon for CO2-EOR and CO_2 geological storage techniques: A review. *Fuel* **2023,** *341*, 127661.

Metz, B.; Davidson, O.; De Coninck, H.; Loos, M.; Meyer, L. *IPCC special report on carbon dioxide capture and storage*; Cambridge: Cambridge University Press, 2005.

Motie, M.; Assareh, M. CO_2 sequestration using carbonated water injection in depleted naturally fractured reservoirs: A simulation study. *International Journal of Greenhouse Gas Control* **2020,** *93*, 102893.

Nagy, K. Dissolution and precipitation kinetics of sheet silicates. *Reviews in Mineralogy and Geochemistry* **1995,** *31*, 173–233.

Nesic, S. Key issues related to modelling of internal corrosion of oil and gas pipelines–A review. *Corrosion Science* **2007,** *49*, 4308–4338.

North Dakota Geological Survey. 2020. https://www.dmr.nd.gov/ndgs/InyanKaraMaps/.

Palandri, J. L.; Kharaka, Y. K. *A Compilation of Rate Parameters of Water-Mineral Interaction Kinetics for Application to Geochemical Modeling*; Open File Report (OF 2004-1068); U.S. Geological Survey; 2004.

Pearce, J.; Khan, C.; Golding, S.; Rudolph, V.; Underschultz, J. Geological storage of CO_2 and acid gases dissolved at surface in production water. *Journal of Petroleum Science and Engineering* **2022,** *210*, 110052.

Pearce, J. K.; Dawson, G. K.; Sommacal, S.; Golding, S. D. Micro CT and experimental study of carbonate precipitation from CO_2 and produced water co-injection into sandstone. *Energies* **2021,** *14*, 6998.

Plummer, L.; Wigley, T.; Parkhurst, D. The kinetics of calcite dissolution in CO 2-water systems at 5 degrees to 60 degrees C and 0.0 to 1.0 atm CO 2. *American Journal of Science* **1978,** *278*, 179–216.

Pool, M.; Carrera, J.; Vilarrasa, V.; Silva, O.; Ayora, C. Dynamics and design of systems for geological storage of dissolved CO2. *Advances in Water Resources* **2013,** *62*, 533–542.

Rathnaweera, T.; Ranjith, P.; Perera, M.; Haque, A. Influence of CO_2–brine co-injection on CO_2 storage capacity enhancement in deep saline aquifers: an experimental study on Hawkesbury sandstone formation. *Energy & Fuels* **2016,** *30*, 4229–4243.

Rimstidt, J. D.; Barnes, H. The kinetics of silica-water reactions. *Geochimica et Cosmochimica Acta* **1980,** *44*, 1683–1699.

DocuSign Envelope ID: 2FA9A609-C360-4E53-8B28-BE8B77B6994A

Ruprecht, C.; Falta, R. Comparison of supercritical and dissolved CO_2 injection schemes. Proceedings of TOUGH Symposium, Lawrence Berkeley National Laboratory, Berkeley, California, 2012.

Shariatipour, S. M.; Mackay, E. J.; Pickup, G. E. An engineering solution for CO_2 injection in saline aquifers. *International Journal of Greenhouse Gas Control* **2016,** *53*, 98–105.

Siefert, N.; Belarbi, Z.; Wenzlick, M. NEWTS USGS Produced Water Database, 2022. https://edx.netl.doe.gov/dataset/newts-usgs-produced-water-database. https://doi.org/10.18141/1890178

Sigfusson, B.; Gislason, S. R.; Matter, J. M.; Stute, M.; Gunnlaugsson, E.; Gunnarsson, I.; Aradottir, E. S.; Sigurdardottir, H.; Mesfin, K.; Alfredsson, H. A. Solving the carbon-dioxide buoyancy challenge: The design and field testing of a dissolved CO_2 injection system. *International Journal of Greenhouse Gas Control* **2015,** *37*, 213–219.

Sonderegger, J. L.; Brower, K.; Lefebre, V. A preliminary investigation of strontianite dissolution kinetics. *American Journal of Science* **1976,** *276*, 997–1022.

Steele-MacInnis, M.; Capobianco, R. M.; Dilmore, R.; Goodman, A.; Guthrie, G.; Rimstidt, J. D.; Bodnar, R. J. Volumetrics of CO_2 storage in deep saline formations. *Environmental Science & Technology* **2013,** *47*, 79–86.

Sverdrup, H. U. *The Kinetics of Base Cation Release due to Chemical Weathering*; University Press: Sweden, 1990.

Uemura, S.; Matsui, Y.; Kondo, F.; Tsushima, S.; Hirai, S. Injection of nanosized CO_2 droplets as a technique for stable geological sequestration. *International Journal of Greenhouse Gas Control* **2016,** *45*, 62–69.

Veil, J. US produced water volumes and management practices in 2012. Groundwater Protection Council, 2015.

Wu, B.; Li, X.; Teng, Y.; Lv, P.; Liu, Y.; Luo, T.; Zheng, J.; Wang, D.; Jiang, L. Characterizing the dissolution rate of CO_2-brine in porous media under gaseous and supercritical conditions. *Applied Sciences* **2017,** *8*, 4.

DocuSign Envelope ID: 2FA9A609-C360-4E53-8B28-BE8B77B6994A





Sean Plasynski
Acting Director
National Energy Technology Laboratory
U.S. Department of Energy

John Wimer
Acting Chief Research Officer
Science & Technology Strategic Plans
& Programs
National Energy Technology Laboratory
U.S. Department of Energy

Bryan Morreale
Associate Laboratory Director for
Research & Innovation
Research & Innovation Center
National Energy Technology Laboratory
U.S. Department of Energy

NETL Technical Report Series

DocuSign Envelope ID: 82FFD83E-5D40-48ED-80BB-7FE5702F5AD5

ACTIVE RESERVOIR MANAGEMENT ENGINEERING AND TREATMENT TECHNOLOGY EVALUATION SUMMARY – BRINE EXTRACTION AND STORAGE TEST LESSONS LEARNED REPORT – PHASE II FINAL REPORT – VOLUME 3

Brine Extraction and Storage Test Phase II Final Report
Task 1 – Deliverable D8

Prepared for:

Andrea McNemar

U.S. Department of Energy
National Energy Technology Laboratory
3610 Collins Ferry Road
PO Box 880, MS P03D
Morgantown, WV 26507-08803

Cooperative Agreement No. DE-FE0026160

Prepared by:

Marc D. Kurz
John A. Hamling
Ryan J. Klapperich
Lonny L. Jacobson
Agustinus Zandy
Timothy M. Shenk
Todd Jiang
Xue Yu
Cody B. Williamson
Nicholas S. Kalenze
Jamie A. Schod

DocuSigned by:
Marc Kurz
4B86FEEEDB3941D...
Marc D. Kurz, Principal Investigator

2024-EERC-07-01

July 3, 2024

DocuSign Envelope ID: 82FFD83E-5D40-48ED-80BB-7FE5702F5AD5

EERC DISCLAIMER

LEGAL NOTICE This research report was prepared by the Energy & Environmental Research Center of the University of North Dakota (UND EERC) as an account of work sponsored by the U.S. Department of Energy (DOE) National Energy Technology Laboratory (SPONSOR). Because of the research nature of the work performed, neither UND EERC nor any of its employees makes any warranty, express or implied, or assumes any legal liability or responsibility for the accuracy, completeness, or usefulness of any information, apparatus, product, or process disclosed, or represents that its use would not infringe privately owned rights. Reference herein to any specific commercial product, process, or service by trade name, trademark, manufacturer, or otherwise does not necessarily constitute or imply its endorsement or recommendation by UND EERC. SPONSOR understands and accepts that this research report and any associated deliverables are intended for a specific project. Any modifications of the report or of any associated deliverables or use or reuse other than for the intended project is at the sole risk of the SPONSOR and without liability or legal exposure to UND EERC or to its directors, officers, or employees.

DOE DISCLAIMER

This report was prepared as an account of work sponsored by an agency of the United States Government. Neither the United States Government, nor any agency thereof, nor any of their employees, makes any warranty, express or implied, or assumes any legal liability or responsibility for the accuracy, completeness, or usefulness of any information, apparatus, product, or process disclosed, or represents that its use would not infringe privately owned rights. Reference herein to any specific commercial product, process, or service by trade name, trademark, manufacturer, or otherwise does not necessarily constitute or imply its endorsement, recommendation, or favoring by the United States Government or any agency thereof. The views and opinions of authors expressed herein do not necessarily state or reflect those of the United States Government or any agency thereof.

DocuSign Envelope ID: 82FFD83E-5D40-48ED-80BB-7FE5702F5AD5

TABLE OF CONTENTS

LIST OF FIGURES ii

EXECUTIVE SUMMARY iv

INTRODUCTION 1

LESSONS LEARNED 3
- Site Selection 3
- Site Infrastructure 5
- Water Treatment Demonstration Facility 12
- Data Analysis and Simulation of ARM 21

DISCUSSION AND CONCLUSIONS 25

REFERENCES 27

DocuSign Envelope ID: 82FFD83E-5D40-48ED-80BB-7FE5702F5AD5

LIST OF FIGURES

1 Location of the BEST project site within North Dakota 2

2 Layout of BEST project site, illustrating the location of the existing saltwater disposal wells and the new project wells and other supporting infrastructure 3

3 Image of Main Street, Watford City, North Dakota 4

4 Drilling rig on location to drill extraction and injections wells 6

5 BEST-I1 T-section of polypropylene pipe flow line was removed to replace fiberglass flow lines and associated fittings 9

6 BEST-I1 polypropylene flow line leading to injection pump was removed to be replaced with fiberglass flow lines with higher temperature ratings 9

7 Yellow fiberglass piping replaced low-temperature polypropylene flow lines to allow high-temperature fluid flow in ARM infrastructure 10

8 Close-up view of the new fiberglass flow line with a higher temperature rating being installed on BEST-I1 injection pump 10

9 Heat trace located on lines into and between brine storage tanks 11

10 Front view of treatment test bed facility 12

11 Back view of treatment facility and associated tanking/infrastructure 13

12 The test bed facility control room houses the SCADA system connected to both the water extraction and injection facilities and the treatment technology test bed facilities 14

13 Virtual interface of Rink SWD #1 and #2 injection system 15

14 Virtual interface of BEST-I1 facility 16

15 DAF unit 18

16 Demonstration bay with blend tank and pretreatment system 18

17 View of technology demonstration activities within the facility 20

Continued . . .

DocuSign Envelope ID: 82FFD83E-5D40-48ED-80BB-7FE5702F5AD5

LIST OF FIGURES (continued)

18 Demonstration personnel with technology equipment at facility..... 20

19 Personnel operating instrumentation during demonstration..... 21

20 3D view of the simulation model and 2D aerial view of the top horizontal layer 22

21 CO_2 plume migration viewed as gas per unit are total in all vertical layers: simulation without brine extraction and simulation with 4:1 ratio of extraction to injection..... 23

22 Raw data and moving average smoothed clean data for dependent variables and independent variables. 24

DocuSign Envelope ID: 82FFD83E-5D40-48ED-80BB-7FE5702F5AD5

ACTIVE RESERVOIR MANAGEMENT ENGINEERING AND TREATMENT TECHNOLOGY EVALUATION SUMMARY – BRINE EXTRACTION AND STORAGE TEST LESSONS LEARNED REPORT – PHASE II FINAL REPORT – VOLUME 3

EXECUTIVE SUMMARY

This document summarizes lessons learned and best practices acquired from nearly a decade of Energy & Environmental Research Center (EERC) work on the North Dakota brine extraction storage test (BEST) project. The EERC performed multiple activities, along with host site operator Select Water, to implement and conduct a field validation of active reservoir management (ARM) engineering strategies for managing formation pressure during CO_2 injection and storage operations. ARM strategies consisted of utilizing extraction well placement and production to manipulate subsurface conditions during CO_2 injection to reduce overall formation pressure and increase storage capacity. The field validation also provided a test bed for evaluation of treatment technologies that were demonstrated and evaluated for treating high total dissolved solid (TDS) brines, extracted from the injection and storage formation, for beneficial use. The work conducted at the BEST facility comprised technical and project management activities, including procuring long-lead items during the drilling and completion of injection and characterization wells, construction of the test bed facility, stakeholder engagement with partners, and decommissioning of site activities.

This lessons learned document provides an opportunity for the EERC to share findings on take-home messages throughout each activity and phase of the project with the public. Significant accomplishments included the demonstration of high TDS (>170,000 parts per million) extracted brine treatment, simulation of large-scale CO_2 injection and brine injection/extraction scenarios, using active reservoir management to enable pressure plume management for neighboring sites, and collaboration with multiple treatment technology vendors to demonstrate a range of water treatment technology techniques.

DocuSign Envelope ID: 82FFD83E-5D40-48ED-80BB-7FE5702F5AD5

ACTIVE RESERVOIR MANAGEMENT ENGINEERING AND TREATMENT TECHNOLOGY EVALUATION SUMMARY – BRINE EXTRACTION AND STORAGE TEST LESSONS LEARNED REPORT – PHASE II FINAL REPORT – VOLUME 3

INTRODUCTION

For nearly a decade, the Energy & Environmental Research Center (EERC) has successfully conducted a 2-phase program to perform a field study of the potential efficacy of formation water extraction during carbon dioxide (CO_2) injection for CO_2 storage as a means of improving CO_2 storage efficiency and/or effectiveness, commonly referred to as active reservoir management (ARM). Phase I was a 15-month study of potential methodologies for a pressure management field study, culminating in site selection and experimental and site design. Phase II was an 8-year effort that involved constructing site facilities, conducting experiments, and evaluating the resulting field data. The experiments were split into two collaborative components, one for ARM and a second component to host and demonstrate potential brine treatment technologies. The results of the overall project are expected to benefit future CO_2 storage projects through validation of techniques that may reduce stress on sealing formations, increase storage capacity, and reduce the area of review of a CO_2 storage facility.

The EERC's brine extraction and storage test (BEST) was sited at a location with active oilfield brine disposal occurring in two existing wells that inject into a regionally expansive brine formation (the Inyan Kara Formation). These two injection wells provided the pressure pulse that acted as a proxy for CO_2 injected for storage and enabled the field testing of various pressure management and plume control strategies without the added complications of injecting a separate CO_2 plume. A new well to extract formation fluid and reduce reservoir pressure was installed downgradient of the two brine disposal wells, and a second well was installed into a deeper saline formation to allow disposal of the extracted formation water without the added interference of reinjecting extracted water into the Inyan Kara Formation. The experiment's host site is operated by project partner Landtech Enterprises, LLC (Landtech), a subsidiary of Select Water (formerly Nuverra Environmental Solutions). The project site location within North Dakota and the overall site layout are shown in Figures 1 and 2, respectively. Drilling of the new wells and installation of the supporting infrastructure (oil–water separator, tanks, flow lines, pumps, downhole pressure sensors, and sensors for safety and control, etc.) and subsequent equipment testing and debugging were conducted over the course of approximately 3 years.

This report analyzes the BEST project's life cycle and breaks down the overall project into three main areas of interest where lessons learned can be derived: site selection, infrastructure, and operations; water treatment demonstration facility; and data analysis and simulation of ARM. Each area is reviewed to highlight the positive elements that contributed to the project's success, the challenges faced, and the lessons learned from both. The findings for ARM simulation and analysis are summarized in the Volume 1 final report (Zandy and others, 2024), and findings for the water treatment demonstrations are summarized in the Volume 2 final report (Kurz and others, 2024). The lessons learned from this study will not only provide a detailed understanding of the project's development but also establish the groundwork for making improved, informative decisions concerning ARM and extracted water treatment.

DocuSign Envelope ID: 82FFD83E-5D40-48ED-80BB-7FE5702F5AD5



Figure 1. Location of the BEST project site within North Dakota.

DocuSign Envelope ID: 82FFD83E-5D40-48ED-80BB-7FE5702F5AD5



Figure 2. Layout of BEST project site, illustrating the location of the existing saltwater disposal (SWD) wells (blue) and the new project wells (yellow) and other supporting infrastructure.

LESSONS LEARNED

Site Selection

The EERC leveraged multiple years of experience working with the geology of the Williston Basin to provide insightful geological characterization to the project. Multiple well logs and other publicly available data assisted in being able to properly characterize and select a suitable site for

DocuSign Envelope ID: 82FFD83E-5D40-48ED-80BB-7FE5702F5AD5

demonstration. The readily available data allowed the EERC to refine the site selection area and populate geologic and simulation models needed for experimental evaluation.

Lessons Learned – Geological Data Availability Vital to Field-Based Monitoring and Modeling Activities
Aligning potential site locations with previously existing wells and associated well log data proved beneficial for subsurface-monitoring activities and developing a robust geologic simulation model for project experimental evaluation.

The BEST project benefited from the ideal location at an active SWD facility and nearby to 24-hour industrial services located in the town of Watford City, North Dakota (highlighted in Figure 3). Access to oil and gas industry-specific services within 20 minutes of the site location provided needed support for miscellaneous equipment rentals, on/off-loading and delivery services, hotel and restaurant accommodations for project personnel and visitors, and parcel shipping services, to name a few.



Figure 3. Image of Main Street, Watford City, North Dakota.

The test bed facility was integrated with ARM and SWD infrastructure and operations, which allowed for access to produced water and extracted brines, with varying salinity concentrations as well as concentrated brine reinjection capabilities. Access to the existing site infrastructure at the disposal facility allowed the EERC to integrate additional equipment and minimize investment in new infrastructure costs overall. Additionally, access to nearby utilities,

DocuSign Envelope ID: 82FFD83E-5D40-48ED-80BB-7FE5702F5AD5

including a freshwater supply line, accommodated the project infrastructure and allowed for the necessary dilution of the brine for the lower-range salinity testing.

Lessons Learned – Active Disposal Facility Was Key to Operations Support for Research
The ability to have project activities integrated with existing industry-specific infrastructure proved extremely valuable. Access to existing injection wells, truck access, building location, and disposal capabilities provided needed support to locate the extraction well, construct the treatment test bed facility, and conduct experimental research.

Lessons Learned – Site Location Vital for Access to Services
Nearby access to services for site and personnel support was an important part of the site selection process. Numerous businesses were able to provide timely support to site needs and room and board options for site personnel and visitors.

The project also benefited from a strong relationship with project partners, particularly the site host partner. The site operator, Landtech, a Select Water company, was a great and dependable partner. Landtech provided staff to supervise and manage site equipment, maintain and update site infrastructure, and operate pumps and equipment when testing started and ended. Landtech/Select Water also provided special equipment when able and helped to find subcontractors when required for site modifications.

Lessons Learned – Good Partnerships Are Important
Building and maintaining a strong partnership can increase the likelihood of success for a field project. Good partners allowed for quick resolution of issues. In this project, a strong partner relationship minimized project delays and enabled maintenance, equipment, and supply needs to be met in a timely manner.

Site Infrastructure

A large component of the BEST project was the drilling and installation of an extraction well in the producing formation (Inyan Kara) and an additional injection well in a separate disposal formation (Amsden/Broom Creek). Figure 4 shows the mobilized drilling rig on location for well-drilling and completion activities.

DocuSign Envelope ID: 82FFD83E-5D40-48ED-80BB-7FE5702F5AD5



Figure 4. Drilling rig on location to drill extraction and injections wells.

The EERC submitted drilling permit applications for both the injection and extraction wells, which were part of the project's field implementation design and were approved within 30 days after submittal. The overall data collection and permit submission process was approximately 6 months. The EERC utilized a thorough permitting process to ensure that all desired information required by the state was included in the application. Communication to state officials before, during, and after the permit application submission was key to ensuring a timely response and approval of the permit.

Recommended Best Practice – Ensure All Information Is Provided for a Timely Permit Review/Issuance Process
A thorough understanding of the desired information and a detail-oriented process to ensure inclusion of all required information are necessary. Any missing information could delay issuance of the permit and impact drilling and construction schedules.

As part of the well-drilling and installation process, a set of formation characterization activities were performed on the injection well, including core, geophysical logs, downhole testing, and fluid sampling in the Inyan Kara and Broom Creek Formations and associated confining layers. 4-in. whole core samples were also collected from the Inyan Kara and Broom Creek Formations. This information was used to populate the geologic and simulation models and provide characterization information for the project evaluation.

DocuSign Envelope ID: 82FFD83E-5D40-48ED-80BB-7FE5702F5AD5

Recommended Best Practice – Well Installation/Geophysical Data Collection
If possible, it is important to take advantage of drilling activities to collect geophysical log data, core formation samples, fluid samples, and drillstem pressure testing to help in the overall characterization of the subsurface and provide lithological and physical data, including pressure, porosity, and permeability to support geologic models and aid with interpretation.

The well-drilling process and associated activities resulted in a significant cost overrun during that phase of project field activities. Several contributing factors led to the overrun and include the following:

- **Geologic Factors**
  - Completion of an additional Amsden interval (BEST-I1 injection well), to ensure adequate injection potential based on findings during the drilling and well completion, were necessary to meet the field implementation plan's anticipated injection rate.

- **Change in Market Conditions**
  - Delay in contracting third-party services (e.g., drilling contractor).
  - Longer-than-anticipated timeline for securing permits and site access agreements.
  - Multiple replans and recompetes of tangibles and services.
  - Variances of planned versus actual costs associated with regional market changes during the development and execution of drilling and completion programs.
    - Availability of services was impacted, including increased wait time leading to a reduction in efficiency.
    - Tangibles and services were increased within the wireline service associated with the borehole-to-surface electromagnetic survey.

- **Operational Factors**
  - Muddy conditions requiring additional site preparation.
  - Cost escalation during the time between the proposal/contracting stage and the implementation of actual drilling activities.
  - Availability of service efficiency increased drilling schedule time (i.e., third-party contractors, major equipment procurement, etc.).
  - Delay in drilling schedule resulting in spring load restrictions requiring overweight permits for drilling rigs.
  - Efficiency of operations including unplanned wiper trips, reduced drilling penetration rates, etc.

The EERC actively managed project activities prior to initiation and took prudent actions to balance the incurred costs with project risks and objectives. The overall cost overrun was ultimately reduced; however, the EERC had to approach the U.S. Department of Energy (DOE) project manager for contractual and funding modifications to keep all project objectives and scope unchanged.

A series of actions were taken to offset the cost variance for field project activities. First, the EERC tracked and regularly discussed variances between estimated costs and cost forecasts with

DocuSign Envelope ID: 82FFD83E-5D40-48ED-80BB-7FE5702F5AD5

the DOE project manager. The EERC managed the project (with concurrence from the DOE project manager) to prioritize completing the infrastructure installation as a priority, as this was a critical path activity necessary for the completion of other field tasks and meeting the technical objectives of the project. The EERC actively managed and took prudent action to balance incurred costs with project risk and objectives. Some examples included reduced on-site supervision, recompeting of tangibles and services for preferred rates where possible and contracting a smaller drilling rig and downsized mud pumps to reduce day rate and mobilization costs.

Lessons Learned – Well Installation/Escalation Costs
Time between project proposals and delays in scheduling can allow for significant escalation in costs, especially in volatile markets such as the oil and gas drilling and equipment sectors.

Recommended Best Practice – Expense Escalation
Projects with large subcontractor activities should budget for unanticipated escalation of costs and negotiate for preferred and/or guaranteed rates where possible.

Recommended Best Practice – Well Installation and Major Project Expenses
For projects with large subcontractor activities, such as drilling, or large-value equipment purchase requirements, it is recommended to diligently monitor and track all expenses and ensure proper and frequent communication with funding agency project management.

The BEST project required significant infrastructure for handling and moving water between the extraction well and new injection well. Design decisions had to be made before the new wells were drilled and were based on the best available information at the time. Unfortunately, this resulted in a condition whereby the downhole temperature proved to be hotter than anticipated, exceeding the capabilities of the polypropylene flow lines that were installed on the site (Figures 5 and 6). These lines were replaced with fiberglass flow lines (Figures 7 and 8) which were able to handle the higher-temperature water.

DocuSign Envelope ID: 82FFD83E-5D40-48ED-80BB-7FE5702F5AD5



Figure 5. BEST-I1 T-section of polypropylene pipe flow line was removed to replace fiberglass flow lines and associated fittings.

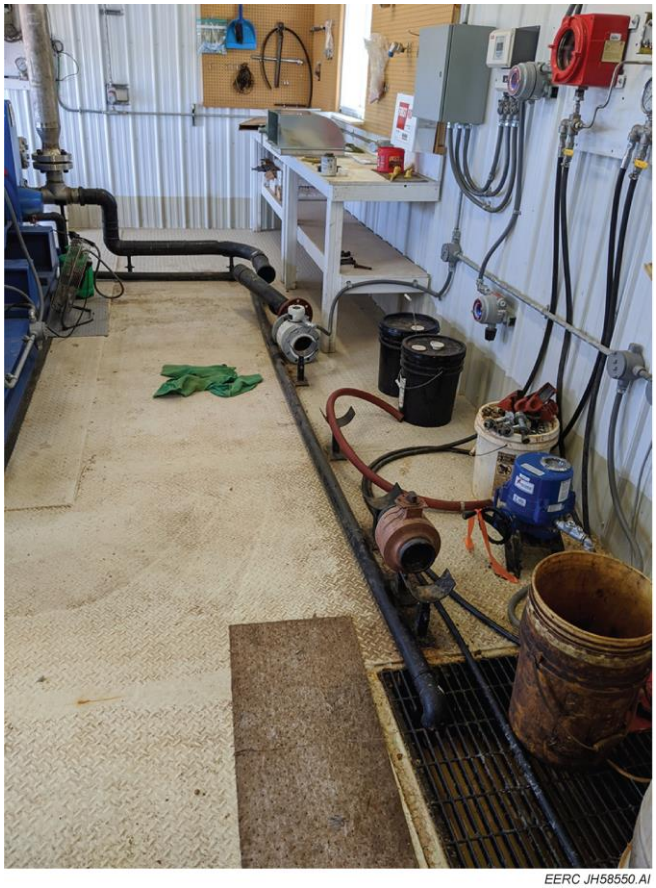


Figure 6. BEST-I1 polypropylene flow line leading to injection pump was removed to be replaced with fiberglass flow lines with higher temperature ratings.

DocuSign Envelope ID: 82FFD83E-5D40-48ED-80BB-7FE5702F5AD5



Figure 7. Yellow fiberglass piping replaced low-temperature polypropylene flow lines to allow high-temperature fluid flow in ARM infrastructure.



Figure 8. Close-up view of the new fiberglass flow line with a higher temperature rating being installed on BEST-I1 injection pump.

DocuSign Envelope ID: 82FFD83E-5D40-48ED-80BB-7FE5702F5AD5

Additionally, the site's location necessitated that pipes, tanks, and flow lines were properly equipped to handle the harsh North Dakota winters. Fluids can freeze in valves or pipes, leading to cracks and eventual failures. It is important to properly inspect valves and flow lines to ensure they are properly winterized, which includes heat-tracing and insulating the exposed surface flow lines and valves. Figure 9 shows insulation and heat traces installed onto flow lines and the bottom of tanks.



Figure 9. Heat trace located on lines into and between brine storage tanks.

Lesson Learned – Ensure Infrastructure Is Compatible with Extreme Temperatures
Thoroughly examine all infrastructure for risks of freezing damage or other weather-related damage. Any temperature-related incident highlights the need for careful planning and preparation to mitigate the effects of extreme weather conditions on the operation of the site. By taking the necessary precautions, such as insulating tanks and lines, covering them with heat tape, and protecting critical valves, future incidents can be prevented, ensuring the smooth operation of the site.

Recommended Best Practice – Plan Ahead for Appropriate Equipment Needs
Careful assessment of possible results and preparation for alternative plans for situations involving expensive, long-term equipment are essential. This involves drilling the well, setting aside the proper amount of time to collect samples, and performing data analysis to thoroughly comprehend well behavior. Assumptions should be strongly challenged to ensure sound decision-making.

DocuSign Envelope ID: 82FFD83E-5D40-48ED-80BB-7FE5702F5AD5

Water Treatment Demonstration Facility

The BEST project included the development of a flexible water treatment demonstration facility intended to provide a demonstration space for novel high-salinity water treatment technologies. This unique facility (shown in Figures 10 and 11) has a 40-ft × 70-ft demonstration bay with a 20-ft-high ceiling capable of hosting skids up the size of full tractor trailer-mounted units. The facility is able to provide up to 25 gpm of pretreated high-saline brine in a wide range of salinities up to 330,000 ppm total dissolved solids (TDS), derived from oilfield produced water. The pretreatment system is designed to knock out any suspended solids and dissolved organics that may be present in the feedwater, but if desired, the raw untreated water can be directly provided. The facility can accommodate continuous or batch flow operation modes, and effluents produced from a demonstration treatment system can be disposed of on-site. Three-phase 440-V power is available on-site and is connected to a data-logging system to monitor and record energy usage during operations. Temporary gas supplies or other energy sources can be provided on-site as needed. The facility includes active air-monitoring systems for methane (CH_4), carbon monoxide (CO), hydrogen sulfide (H_2S), ethylene (C_2H_4), and nitrous oxide (NO_2) and includes a system which automatically vents the building if air quality reaches dangerous levels. Site operations can be monitored remotely, but generally for safety reasons, on-site monitoring of active demonstrations is required. Multiple technologies of varying capacities and capabilities have been successfully demonstrated in the brine treatment demonstration facility as of the writing of this report.



Figure 10. Front view of treatment test bed facility.

DocuSign Envelope ID: 82FFD83E-5D40-48ED-80BB-7FE5702F5AD5



Figure 11. Back view of treatment facility and associated tanking/infrastructure.

BEST project operability was greatly enhanced by a custom-made supervisory control and data acquisition (SCADA) system (Figures 12–14), created by engineers at the EERC and integrated into an existing SCADA system designed by the site host. It facilitated efficient operational control and system-viewing platform, enabled remote viewing and operations, and allowed easy integration of new sensors and equipment. The system's modular design ensured continuous data collection and functionality, with secure data storage and remote visibility. The SCADA system proved to be a strong and low-maintenance solution, enabling continuous and remote site monitoring. A substantial amount of design and configuration work went into the SCADA system before it was fully operational; however, once set up, the system performed up to expectations. The key takeaway is that systems that are designed for a specific purpose can require substantial resources; however, they offer more customized solutions, whereas ready-made, off-the-shelf options may not be optimal for specific project requirements.

DocuSign Envelope ID: 82FFD83E-5D40-48ED-80BB-7FE5702F5AD5

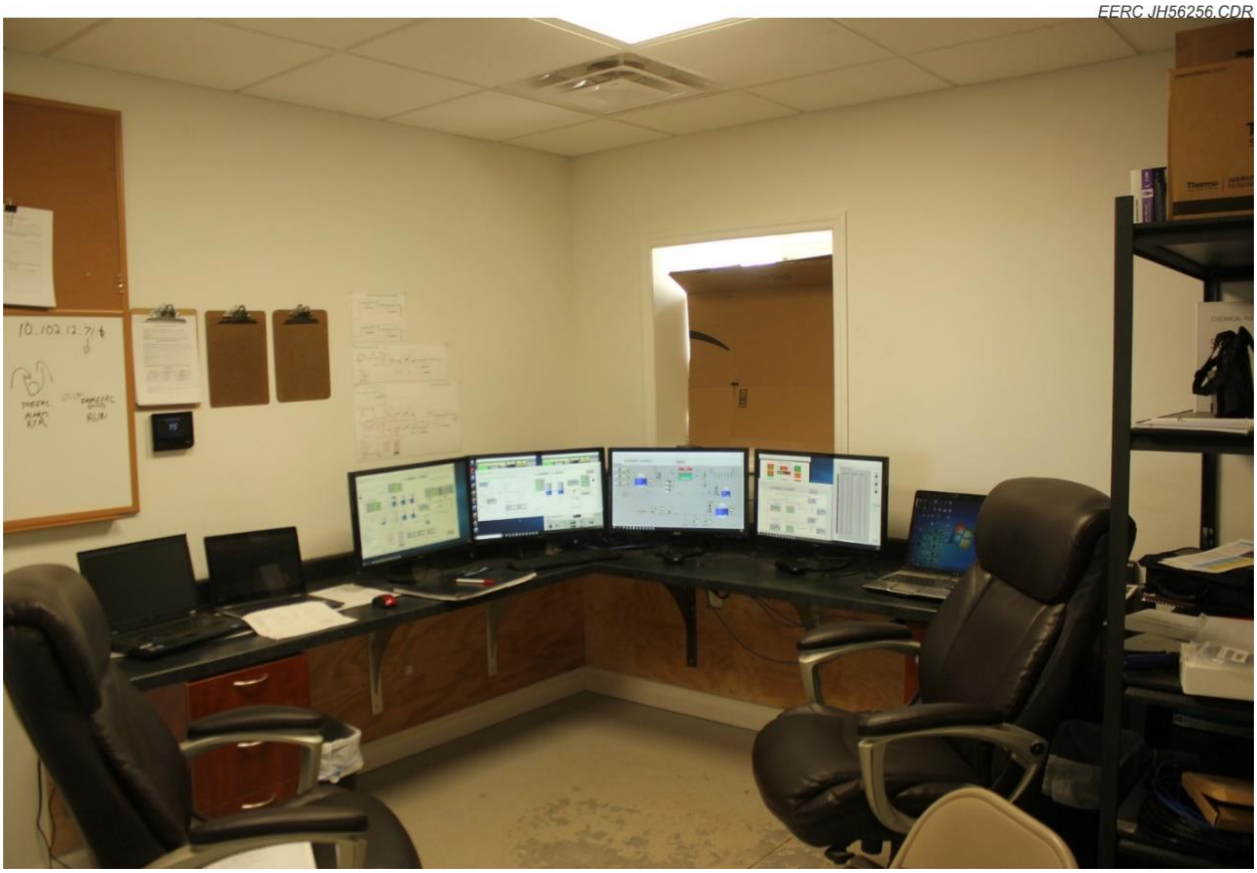


Figure 12. The test bed facility control room houses the SCADA system connected to both the water extraction and injection facilities and the treatment technology test bed facilities. The SCADA system can be monitored remotely by EERC staff.

DocuSign Envelope ID: 82FFD83E-5D40-48ED-80BB-7FE5702F5AD5

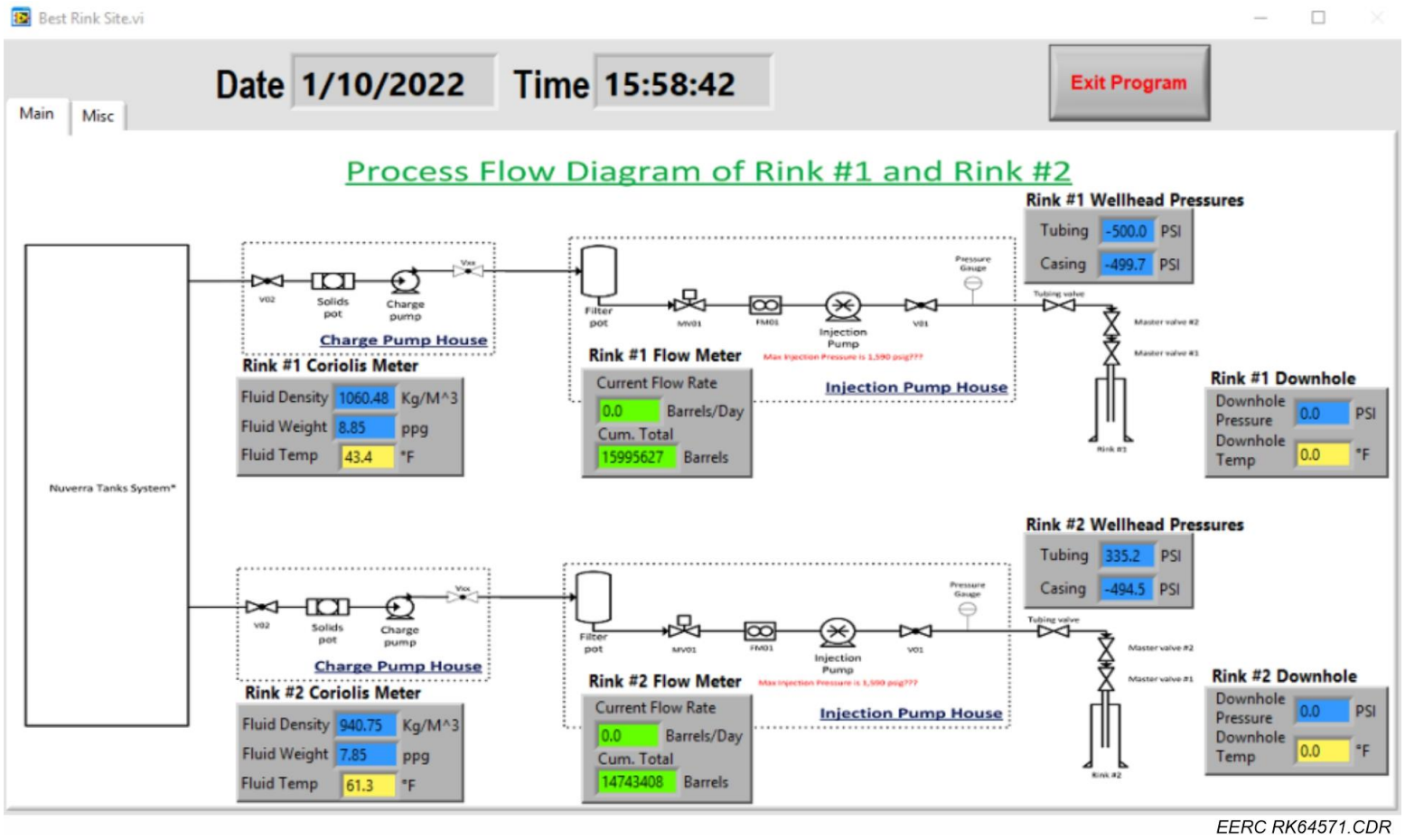


Figure 13. Virtual interface of Rink SWD #1 and #2 injection system.

DocuSign Envelope ID: 82FFD83E-5D40-48ED-80BB-7FE5702F5AD5

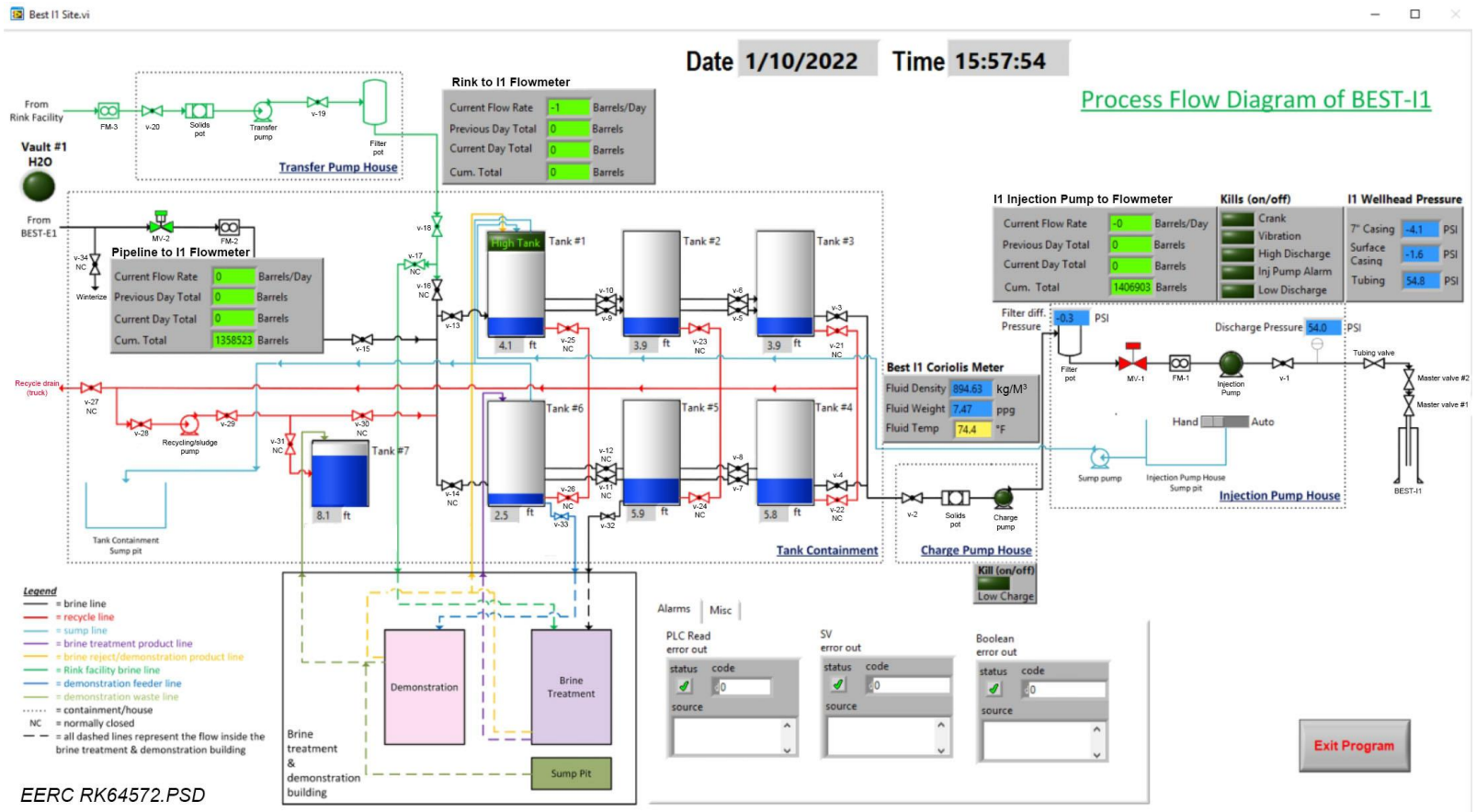


Figure 14. Virtual interface of BEST-I1 facility.

DocuSign Envelope ID: 82FFD83E-5D40-48ED-80BB-7FE5702F5AD5

The SCADA system control computers were located in the office area, which was a nonclassified room adjacent to the demonstration bay. An additional room adjacent to the control room was also set up as a laboratory space that could be used for verification of technology system performance through rapid screening chemical composition analyses. These analytical capabilities included pH, conductivity, total organic carbon, sulfate, and total suspended solids. Additionally, the laboratory space included a sample collection and shipping preparation area where samples for more rigorous chemical analyses were prepared for transportation to an outside laboratory facility.

Recommended Best Practice – Custom-Built Systems Can Accommodate Unique Situations
Custom-built systems that are designed for a specific purpose can require substantial up-front time and resources; however, they offer more customized solutions, whereas ready-made, off-the-shelf options may not be optimal for specific project requirements.

Recommended Best Practice – Analytical Lab Space Availability Is Beneficial to Rapid Chemistry Determinations for Real-Time System Operations Adjustment
An on-site analytical lab space proved to be helpful in the rapid analysis of grab samples from various points in the pretreatment system to ensure consistent-quality brine for treatment technology demonstrations.

Communication is important on any project. The BEST project encountered difficulties with the dissolved air flotation (DAF) system as the unit (Figures 15 and 16) was not suitable and appropriately sized for its intended use on the site. This discrepancy resulted from miscommunications between subcontractors and the vendor. The unit was made of steel that was not an appropriate grade for the application and thus was prone to corrosion. The system was also too large for the flow rate it was intended to handle and had to be significantly modified on-site. The DAF unit was modified by the vendor and eventually worked well enough to finish the project.

DocuSign Envelope ID: 82FFD83E-5D40-48ED-80BB-7FE5702F5AD5



EERC JH56208.AI

Figure 15. DAF unit (right side of image).



EERC JH56210.AI

Figure 16. Demonstration bay with blend tank and pretreatment system.

DocuSign Envelope ID: 82FFD83E-5D40-48ED-80BB-7FE5702F5AD5

Lessons Learned – The Importance of Good Communication
Close supervision and communication with all parties (vendors, subcontractors, etc.) ensures that goals are aligned, project needs are met, and the project can be conducted with minimal issues.

The EERC worked closely with DOE's National Energy Technology Laboratory to evaluate and select high-probability technologies that would potentially be appropriate for the desalination treatment of high-TDS brines. As part of the process, the EERC used various questionnaires and interview processes to determine the most applicable technologies and vendors for demonstration of their technologies. This resulted in the selection of high-quality and professional demonstration partners with technologies appropriate for the anticipated high-salinity application.

Recommended Best Practice – Developing Good Partnerships with Technology Provider
All potential contractors, vendors, and/or project partners should be thoroughly evaluated to determine possible shortcomings and ensure the highest likelihood of achieving project objectives.

Multiple technologies were evaluated throughout the operational period of the test bed facility between 2019 and 2023. Thermal and membrane-assisted thermal technologies were likely to be the most applicable for the targeted high-salinity brines (~180,000 mg/L TDS) and were the focus of the technology selection and resulting evaluations. Overall, each technology demonstrated, with varying degrees of success, the ability to recover relatively fresh distillate water and produce a concentrated brine effluent, with varying inlet salinity ranges and at multiple recovery rates. In addition to the on-site pilot-scale testing, each technology underwent both laboratory and pilot system testing at each respective facility before being mobilized to North Dakota for demonstration. Figures 17–19 are images of actual demonstration activities on-site at the test bed facility.

Lessons Learned – Innovative Technology Scale-Up Issues/Technology Readiness
Both laboratory- and pilot-scale demonstrations were key to determining potential technology shortcomings and scale-up issues as well as individual advantages. Technology readiness levels are subjective determinations that can be verified during performance testing.

DocuSign Envelope ID: 82FFD83E-5D40-48ED-80BB-7FE5702F5AD5



Figure 17. View of technology demonstration activities within the facility.



Figure 18. Demonstration personnel with technology equipment at facility.

DocuSign Envelope ID: 82FFD83E-5D40-48ED-80BB-7FE5702F5AD5



Figure 19. Personnel operating instrumentation during demonstration.

Data Analysis and Simulation of ARM

ARM, or the extraction of formation water from geologic CO_2 storage reservoirs to increase available pore space, manage CO_2 plume migration, and reduce reservoir pressure, has the potential to dramatically increase CO_2 storage performance for both individual projects and projects operating in the same region. The EERC utilized a reservoir model of the project site, using history-matched and processed site data to enable a variety of different ARM scenarios with simulated CO_2 injection (Figure 20). Simulation scenarios included evaluation of operational constraints at reservoir conditions to maintain a large-scale storage estimate (i.e., 1 million metric tons per year) of CO_2 at the reservoir in a single injector with two brine production wells. The water production rate was then modified in each simulation case to represent different CO_2 injection-to-water production ratios. The effectiveness of ARM for controlling pressure and geosteering the injected plume varied with the different scenarios. This work represented some of the first evaluations of ARM with field-calibrated models.

The heterogeneity of the model, or of any geologic storage site, provides challenges in attempting to use generalized approaches for well placement patterns or set injection/extraction ratios. Extraction well placement must be amenable to work around the heterogeneity of permeability fields for optimal positioning to steer the CO_2 plume. In some cases, it may be necessary to extract large amounts of water to see significant influence on the CO_2 plume or reductions in reservoir pressure.

DocuSign Envelope ID: 82FFD83E-5D40-48ED-80BB-7FE5702F5AD5

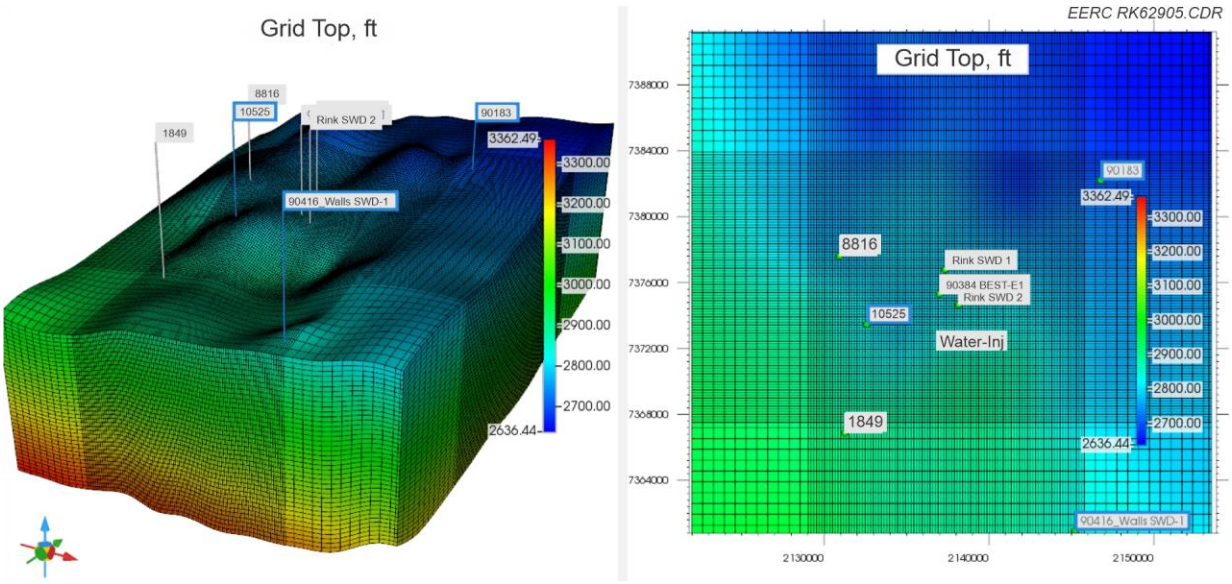


Figure 20. 3D view of the simulation model (left) and 2D aerial view of the top horizontal layer (right). Both images show the grid tops with dark blue regions in the north being the shallower and green/red regions representing deeper depths to the south.

Geosteering was found to be feasible but influenced by several factors in the reservoir and in the simulation model used to design the implementation of ARM. Boundary conditions are one factor that must be considered, as they have a large influence on the simulation. In the cases presented, the model contained open boundaries, where aquifers beyond the modeled area resupply portions of the extracted water, offsetting some of the effectiveness of geosteering. This showed that low extraction rates are likely to have minimal effect on the plume and noticeable changes are only observed when larger extraction rates are used. A maximum case of production well effect on geosteering plume migration was compared to the simulation without production. CO_2 was observed to migrate toward all four extraction wells, reducing the overall concentration of the plume as it spread faster because of the increased hydrodynamic flow within the reservoir (Figure 21). This process increased plume mixing and reduced cap rock stress (by reducing reservoir pressure).

DocuSign Envelope ID: 82FFD83E-5D40-48ED-80BB-7FE5702F5AD5

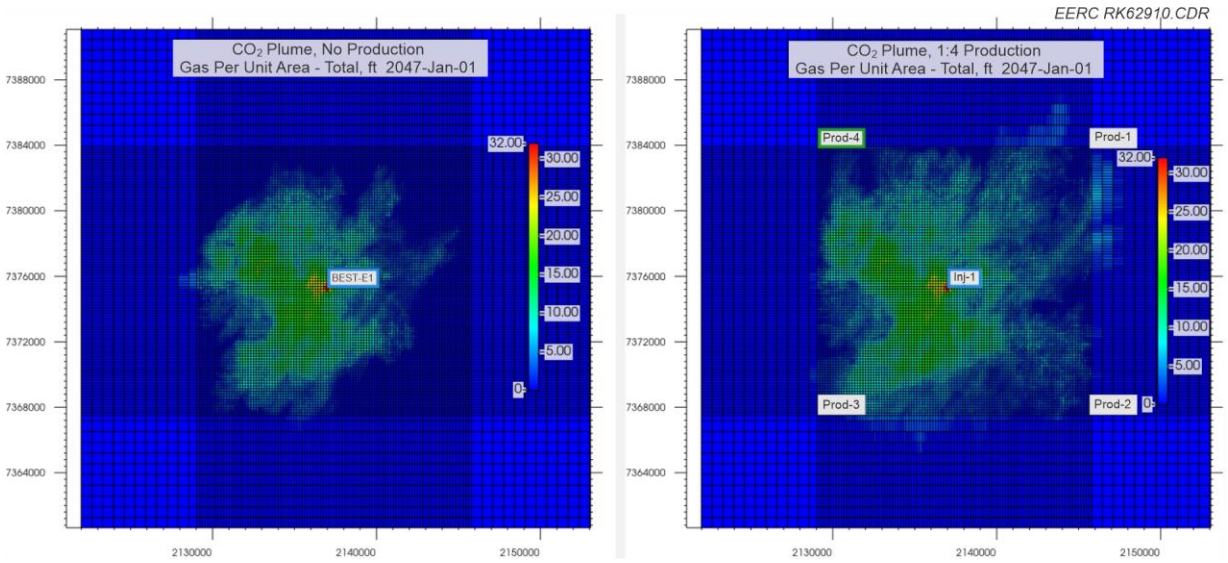


Figure 21. CO_2 plume migration viewed as gas per unit area total in all vertical layers: simulation without brine extraction (left) and simulation with 4:1 ratio of extraction to injection (right).

The results using the model calibrated to ARM field test data suggest that the pattern of extraction well placement and optimizing the timing of extraction and extraction rates are important considerations for optimizing and deploying ARM at geologic CO_2 storage sites, as is an adequate understanding of reservoir, heterogeneity, and boundary conditions.

Lessons Learned – The Influence of Geosteering
The project demonstrated how ARM allowed for geosteering, where the simulated production wells accelerated CO_2 migration toward all four extraction wells, reducing the overall concentration of the plume because the same volume of CO_2 is distributed over a larger reservoir area. The application of geosteering and employing ARM has the potential to enable industrial carbon capture and storage projects that may not otherwise be practical and improve performance of adjacent or neighboring projects within the same region. This would help maximize the geologic CO_2 storage potential of storage sites.

The field test produced a very large volume of data that were hard to handle and interpret during site operation. Data were collected from multiple points every second for multiple months as simulations conducted prior to operating the field site suggested some phenomenon could occur quickly near the wellbores. Over a 2-year period, measurements were collected from three wells: two SWD (injection) wells (RINK SWD 1 and RINK SWD 2) and a brine extraction (production) well (BEST-E1). The injection wells were periodically shut in and reopened, as required by commercial operations at the site. This created discontinuities in the time series data record. The data also had more noise than expected, which added to the difficulty in processing and analyzing. This can be a problem when working with large datasets, as noise can hide important patterns and

DocuSign Envelope ID: 82FFD83E-5D40-48ED-80BB-7FE5702F5AD5

trends, making it difficult to reach valid conclusions. In this case, the project had to find other ways of evaluating the data, and machine learning methods were used to help with data management and interpretation (Figure 22). In particular, outliers in the dataset were detected and removed based on visual inspection using sliding time windows. To reduce the effect of noise in the data, 24-hour centered moving averages were calculated for all variables to smooth the data, and the 24-hour smoothed data were used for all analyses.

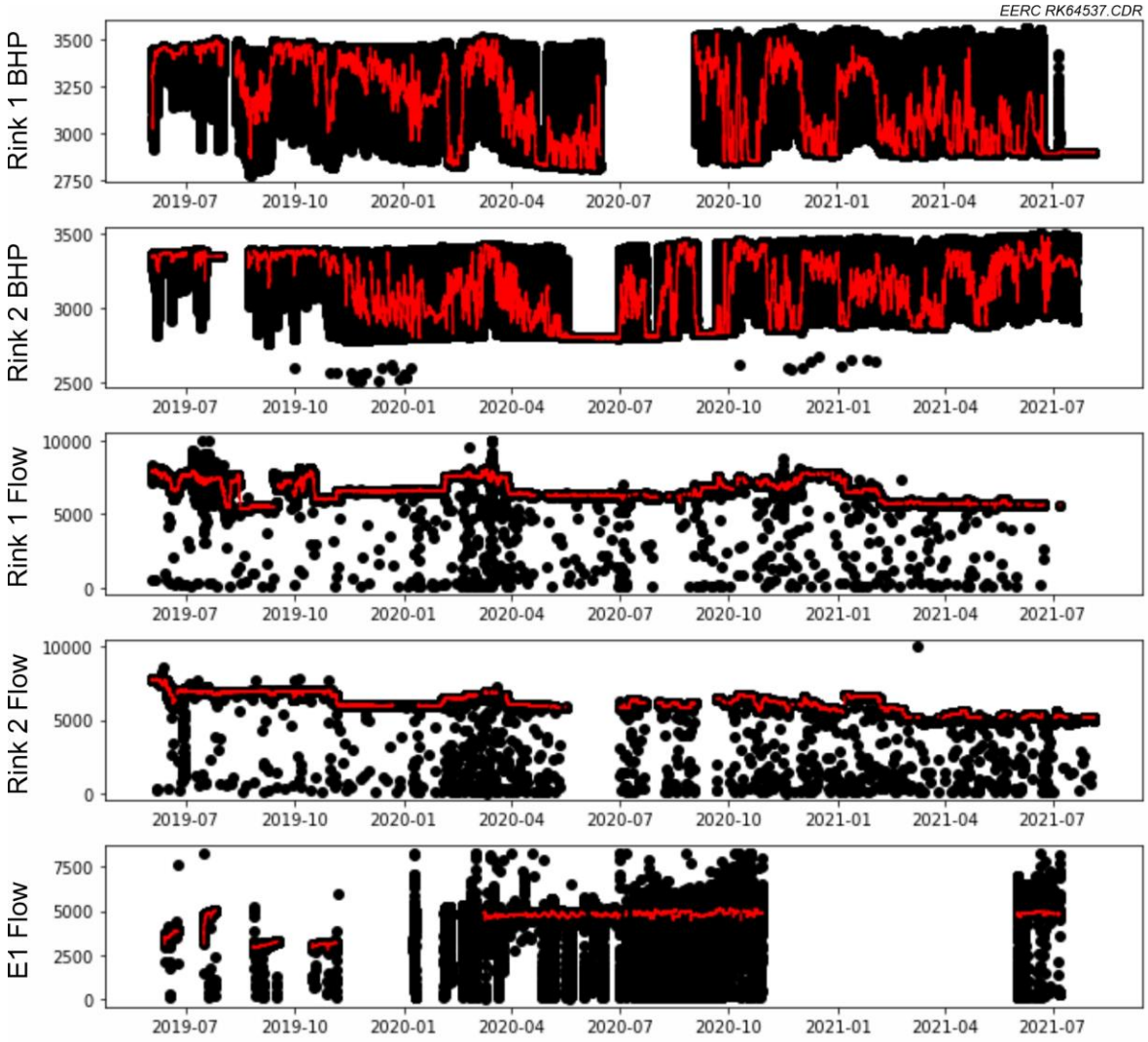


Figure 22. Raw data (black points) and moving average smoothed clean data (red line) for dependent variables (Rink SWD #1 and Rink SWD #2 bottomhole pressures) and independent variables (flow rates at the three wells).

The key takeaway is to try to match data collection with what is needed to evaluate a process. In this case, it was eventually evident that data collected every second was excessive and needed to be adjusted, but before the field tests began, that was a point of uncertainty. Projects should

DocuSign Envelope ID: 82FFD83E-5D40-48ED-80BB-7FE5702F5AD5

carefully consider data collection intervals, possibly looking for dynamic collection models that allow for changing intervals depending on the processes or programs implemented. Projects should also consider plans to account for field data that do not satisfy expectations, because they are too complex, unclear, noisy, or otherwise difficult to use.

Recommended Best Practice – Machine Learning to Interpret Large, Noisy Datasets
Machine learning algorithms work well with noisy data, as they can identify patterns and trends that may not be obvious. When working with large datasets, it is important to have well organized and clear methods to manage and interpret the data and to be ready to be flexible and try different approaches if challenges are encountered.

The BEST project illustrated how variations in porosity and permeability can have significant influence on the behavior of subsurface plumes and the ability to manage them. Zones of increased permeability in particular can have outsized impacts on spreading of injected CO_2 and reduce the ability of ARM to impact that distribution. This emphasizes the need for having a comprehensive knowledge of the geologic formation during the planning phase before any site construction starts. If project wells are selected and installed without this detailed understanding, the ability of ARM to affect the desired results may be significantly impaired, if not rendered wholly ineffective.

Lessons Learned – The Influence of Geologic Properties
Geologic properties have a strong potential influence on the effectiveness of ARM performance. This implies that the study is highly site-specific and that more studies in different geologic settings may be needed to fully understand how to use ARM effectively in varying geologic circumstances.

DISCUSSION AND CONCLUSIONS

Substantial preprogram planning went into the development of the BEST program in an attempt to head off potential challenges, maintain operational flexibility, and enable the ability to adapt to changing conditions. All aspects of the BEST program design were scrutinized for failure points and potential operations and safety risks. As a result, many of the features built in to the BEST facilities performed admirably and contributed to the successful completion of the project.

One such example was a design that enabled the blending of water for the water treatment demonstration facility. Water for the demonstration facility could be provided by any one specific source, or a mix of water sources, such as from the ARM experiment associated BEST-E1 (extraction) well, oilfield produced brine delivered to the site for disposal in Landtech wells, and freshwater provided by the rural water system. This wide range of water qualities enabled custom mixing of water for specific water treatment tests. The connection to the ARM experiment also enabled direct disposal of brine from the demonstration facility into the BEST-I1 (injection) well. These activities were further enabled through maintaining strong communication with partners

DocuSign Envelope ID: 82FFD83E-5D40-48ED-80BB-7FE5702F5AD5

throughout the project life cycle, ensuring extracted or site water was available when needed and that supporting infrastructure was operating properly. This included the use and upkeep of heat tracing along all exposed pipes/valves and tanks, preventing them from freezing in the cold North Dakota winters.

The water treatment demonstration facility also included check valves and manual valves throughout the pretreatment system, enabling flexible operations and bypassing any of the components of the pretreatment system, if needed. For example, the active carbon filtration system could be bypassed if determined not to be necessary for a test. This complemented the existing flexibility built into the water transfer infrastructure between wells and storage tanks, allowing for custom salinity and chemistry derivations. The facility also included a custom-built SCADA system which provided priceless on-site and remote monitoring and control capabilities in a way that no ready-made system could provide.

Water transfer from the BEST-E1 well to the BEST treatment demonstration facility and, ultimately, the BEST-I1 well was accomplished through a double-lined pipe system which included two remotely monitored vaults at low points in the line. Any failure of the inner flow line would be captured by the outer flow line and conveyed to one of the two vaults where it would trip a sensor, indicating a leak. This system was novel technology at the time, reducing the risk of any leaks/spills along the flow line, and performed as expected. Site data were recorded through downhole real-time gauges which enabled data monitoring from beginning to end and captured every experimental event with no issue. Data turnaround was fast and did not require waiting for batch data collection, which may be required with other data-logging systems. The real-time sensors also did not interfere with Landtech's operations; however, it was impossible to properly shut the wells with downhole sensors installed because of the presence of a cable running from the surface through the valve to the real-time gauges downhole. Alternatively, a system of memory gauges could have been installed in the wells, but that would have required shutting in the wells, pulling the gauges to read the data at regular intervals, and then reinstalling the gauges downhole. This type of system would have significantly impacted Landtech's operations.

Multiple important lessons were learned in the course of conducting the BEST program. Some of these lessons were the result of the limitations of project development timelines, some were the result of insufficient data, and some resulted from needing to adapt to unexpected challenges. A future version of this project could be more efficient and effective with some key improvements based on these learnings. Firstly, incorporating an air hookup for blowing all lines dry would help mitigate the risk of freezing, which is a regular operational challenge at the North Dakota site. Careful well drilling, sampling, and data gathering are essential steps to learn about well behavior and test assumptions. Improved communication between subcontractors and vendors about operational limits and anticipated equipment performance is key to avoiding wasteful spending and time delays on equipment that may not be needed or is inappropriately sized.

All the required downhole tests and data collection for a well should be completed prior to making design decisions that should be based on those data. Even if collecting well data includes adding additional time to project installation schedules, doing so will save money by subsequently installing properly designed systems and will prevent unwanted expenditures and lower the

DocuSign Envelope ID: 82FFD83E-5D40-48ED-80BB-7FE5702F5AD5

chances of infrastructure failures. Taking time for data collection and analysis will also enable more precise data analysis and simulation designs by having an early insight into site geology and reservoir performance. Making design choices without site data may result in conditions where data cannot be managed and analyzed effectively and/or efficiently because of the nature or volume of those data.

Improvements to the demonstration facility, by installing equipment that would enable stricter tolerances of tank levels, may have enabled a steadier flow of water through the pretreatment system, thereby reducing the dependence on batch processing. Material selection for the design of the DAF unit was also critical to its long-term utility, but the unit's material as delivered was compromised by the brine's effect on the welds. Improving facility design with automatic doors that activated with the automatic ventilation systems would improve performance if dangerous atmospheres developed and improve the safety of the facility. The use of video monitoring systems would also improve overall site security, which was largely reliant on the presence of Landtech employees.

Overall, the multiyear effort of the BEST project was conducted effectively, and all project objectives were achieved. It is the intent of this compiled "lessons learned" and "recommended best practices" summary to offer valuable insight into project successes and shortcomings for the educational benefit of any potential future similarly scoped projects. These insights have the potential to offer valuable considerations for improving future project applications and executions.

REFERENCES

Hamling, J.A., Klapperich, R.J., Jiang, T., Yu, X., and Williamson, C.B., 2022, Brine extraction and storage test (BEST)—enhancing CO_2 storage through active reservoir management: Presented at the 16th International Conference on Greenhouse Gas Control Technologies, GHGT-16, Lyon, France, October 23–27.

Kurz, M.D., Kalenze, N.S., Martin, C.L., Hamling, J.A., Klapperich, R.J., Jacobson, L.L., and Stevens, B.G., 2024, Brine treatment technology summary – brine extraction and storage test – Phase II final report – Volume 2: Task 5.0 Deliverable 6 final report, 2024-EERC-06-01, Grand Forks, North Dakota, Energy & Environmental Research Center, June 19.

Zandy, A., Williamson, C.B., Jiang, T., Shenk, T.M., Yu, X., Klapperich, R.J., Jacobson, L.L., Pekot, L.J., Kalenze, N.S., Kurz, M.D., and Hamling, J.A., 2024, Active reservoir management engineering and evaluation summary – brine extraction and storage test – Phase II final report – Volume 1: Task 6.0 Deliverable 5 final report, 2024-EERC-04-02, Grand Forks, North Dakota, Energy & Environmental Research Center, April 5.